이학박사 학위논문

Ru-Catalyzed Transfer Hydrogenation for Imine Synthesis and Pd-Catalyzed Direct C–H Functionalization of Unactivated Arene

루테늄 촉매의 이동 수소화를 통한 이민 합성 및 팔라듐 촉매를 이용한 비활성 방향족 화합물의 C–H 결합 기능화

2021 년 2 월

서울대학교 대학원

화학부 유기화학 전공

김 다 은

루테늄 촉매의 이동 수소화를 통한 이민 합성 및 팔라듐 촉매를 이용한 비활성 방향족 화합물의 C–H 결합 기능화

지도교수 최 태 림

이 논문을 이학박사 학위논문으로 제출함
2020 년 11 월

서울대학교 대학원
화학부 유기화학전공
김 다 은

김다은의 이학박사 학위논문을 인준함
2020 년 11 월

위 원 장 김 낙 래 (인)

부위원장 최 태 림 (인)

위 원 이 홍 근 (인)

위 원 이 연 (인)

위 원 홍 승 혁 (인)

Abstract

Ru-Catalyzed Transfer Hydrogenation for Imine Synthesis and Pd-Catalyzed Direct C–H Functionalization of Unactivated Arene

Daeun Kim
Department of Chemistry
The Graduate School
Seoul National University

Transition-metal-catalyzed C–N and C–C bond formation reactions were developed. Part I introduces catalytic imine synthesis utilizing the dehydrogenative alcohol activation strategy. Due to versatile synthetic utilities of imines, many synthetic methods have been developed. The basic strategies and representative examples are discussed in chapter 1. A chemoselective imine synthesis from nitriles and secondary alcohols was achieved with a ruthenium dihydride catalyst (Chapter 2). This reaction offers a simple, convenient, and environmentally benign synthetic method to synthesize versatile imines by applying the hydrogen-transfer strategy.

Part II describes C(sp^2)–H functionalization of arenes mediated by transition-metal catalysis. Direct C–H functionalization of arenes is a central topic in organic synthesis. Recent advances in the transition-metal catalysis enabled the

selective and efficient transformation of unactivated C(sp^2)–H bonds. The C–H functionalization strategies and representative examples in C–C bond-forming reaction through direct C–H arylation and alkylation are introduced in chapter 3. The progress in the photoinduced palladium catalysis and its mechanistic aspects are summarized in chapter 4. The unique properties of photoexcited Pd(0) catalysis have led to the development of novel C–C bond forming reactions. Chapter 5 describes the site-selectivity and mechanism of the Pd-catalyzed C–H arylation of simple arenes. Comprehensive mechanistic investigations including kinetic measurements and stoichiometric experiments provided concrete evidence of a cooperative bimetallic mechanism. The transmetalation step, not the C–H activation step, was identified as the selectivity-determining step in the Pd-catalyzed C–H arylation of simple arenes. Lastly, chapter 6 described the development of catalytic C–H alkylation of simple arenes with alkyl bromides by photoinduced Pd catalysis. Mechanistic investigations clarified that the catalytic turnover process involves a Pd(0)/Pd(I) redox cycle through a Br atom transfer. The distinctive reactivity among alkyl halides originated from the unexpected role of the formate base which reduces the off-cycle $Pd(PPh_3)_2Br_2$ to an active Pd(0) species.

Keywords: imine formation, alcohol activation, transfer hydrogenation, C–H arylation, concerted metalation-deprotonation, C–H alkylation, palladium photocatalysis

Student Number : 2015-20372

Table of Contents

Chapter 6. Direct C(sp^2)–H Alkylation of Unactivated Arenes Enabled by Photoinduced Pd Catalysis

Appendix

List of Tables

Chapter 2

Chapter 5

Chapter 6

List of Schemes

Chapter 1

Chapter 2

Chapter 3

Chapter 4

Chapter 5

Chapter 6

Chapter 1. Imine Synthesis from Alcohol and Amine Using Dehydrogenative Alcohol Activation Strategy

1.1 Introduction

As environmental issues become the primary agenda of the global society, modification of traditional organic transformations into environmentally benign synthetic alternatives has been actively investigated by chemists and chemical industries nowadays. One of the highlighted topics is the atom-economical and catalytic approach to the synthesis of imines. Over the past decades, catalytic alcohol activation has been attracted as a convenient and green method to access various carbonyl derivatives and hydrogenated compounds from non-H_2 hydrogen source. This chapter covers the historical development of transition-metal catalyzed imine formation from alcohols and amines based on the dehydrogenative alcohol activation strategy, and highlights its significance.

1.2 Conventional imine bond synthesis

Imines are versatile intermediates for the synthesis of pharmaceutically and biologically active compounds, and fine chemicals.[1] The C=N double bond in imines is a reactive organic functional group that can perform many organic transformations such as reduction,[2] addition,[2a, 3] and cyclization[4] reactions. Traditionally, imines are synthesized from the condensation of a primary amine with an aldehyde or ketone in the presence of an acid catalyst (Scheme 1.1).[5]

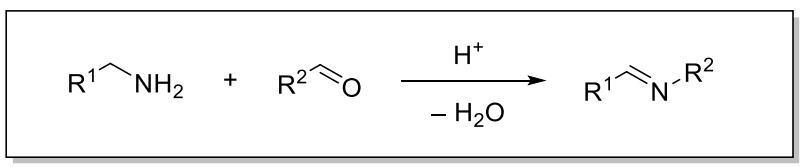

Scheme 1.1 Conventional imine synthetic methods.

Due to their versatile synthetic utility, many alternative methods have been developed including the oxidative dehydrogenation of secondary amines,[6] self-condensation of primary amines,[6f, 6g, 7], and Aza-Wittig reaction (Scheme 1.2).[8] In organic synthesis, recent development of imine-directed C–H activation chemistry makes imine bond not only as a versatile platform to various functional groups but also a useful molecular backbone.[9] For example, the in-situ formation of imines from amines and carbonyls render a transient directing group to activate inert C–H bonds.[10]

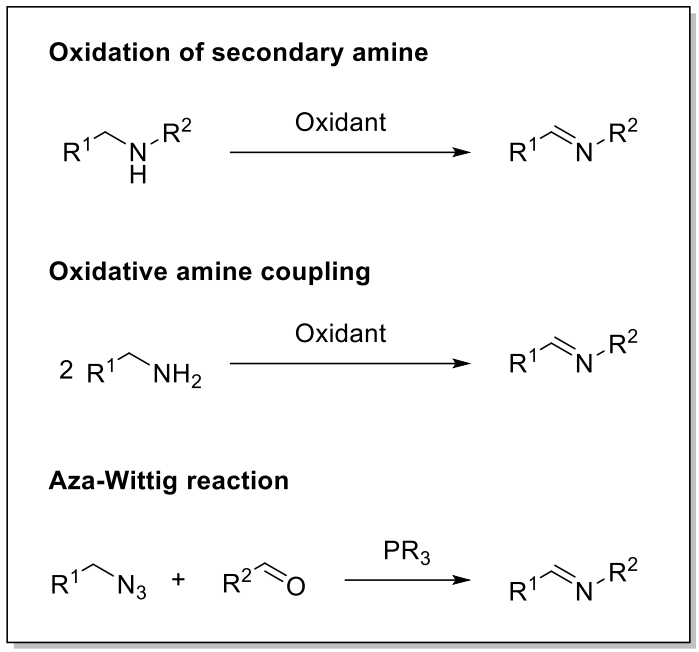

Scheme 1.2 Other imine synthetic methods.

1.3 Dehydrogenative alcohol activation

Alcohols are among the most abundant and cheap feedstocks on Earth because they can be sustainably obtained from nature or raw materials in the chemical industry. Alcohols are common starting materials for chemical reactions; for example, they can be easily oxidized to useful diverse carbonyl compounds and carboxylic acid derivatives. However, traditional alcohol oxidation protocols require a stoichiometric amount of oxidant. An alternative approach of these processes is catalytic alcohol dehydrogenation that uses a catalyst to remove two hydrogen atoms from alcohol, and generates the metal–carbonyl intermediate then undergoes a further transformation.[11] This process provides not only a green and efficient alcohol activation strategy but also a safe and clean method for the utilization of H_2 gas.[12] Therefore, dehydrogenative alcohol activation strategy has been developed

by many researchers in both organic synthesis and sustainable energy.[12b, 12c, 13]

Catalytic alcohol dehydrogenation is categorized into two parts. Hydrogen transfer reaction is a dehydrogenation method with the aid of a sacrificial hydrogen acceptor, which compensates the thermodynamic demands and generates carbonyl product along with the reduced form of the sacrificial hydrogen acceptor (Scheme 1.3A).[14] The concept is also called as transfer hydrogenation when the hydrogenation reaction is more focused on, and alcohols act as sacrificial hydrogen donors in this process. This strategy has been widely applied in organic synthesis in the laboratory because it offers a convenient reduction protocol without a strong reductant or dangerous hydrogen gas. Various transition-metal catalyzed transfer hydrogen reactions with alcohol and unsaturated bonds such as C=C, C=O, or C=N bonds have been reported.[14-15] The typical examples are Meerwein–Ponndorf–Verley reduction and Oppenauer oxidation with aluminum alkoxide catalysts.[16]

Another method is the acceptorless alcohol dehydrogenation, which generates carbonyl compounds from alcohols without a sacrificial hydrogen acceptor (Scheme 1.3B).[11a] Since the first report on Rh-catalyzed acceptorless dehydrogenation of isopropanol by Charman in 1966,[17] the development of new catalysts has dramatically increased the efficiency and expands the substrate scope. Recently, thermodynamically more challenging acceptorless methanol dehydrogenation is realized.[18]

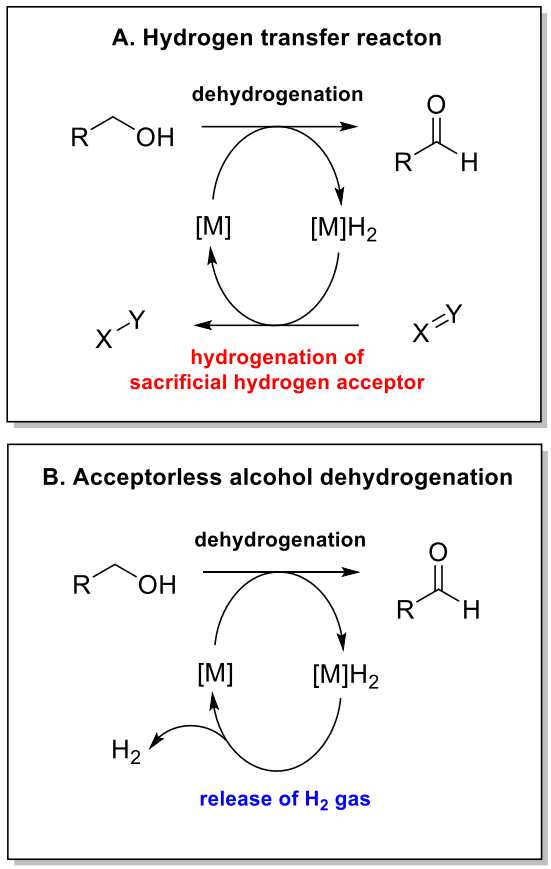

Scheme 1.3 Classification of dehydrogenative alcohol activation mechanisms.

Carbonyl compounds generated from the alcohol dehydrogenation can be further functionalized by reacting with an external nucleophile.[10b] One of the representative examples is the dehydrogenative coupling of primary alcohols with amines to form amides (Scheme 1.4A).[11a, 19] After catalytic dehydrogenation, an amine attacks the carbonyl group to give a hemiaminal intermediate. Finally, dehydrogenation of the hemianimal gives the desired amide product with hydrogen gas as a sole side product. The *N*-alkylation of amine can also be achieved by the dehydration of the hemiaminal intermediate and the catalytic hydrogenation of the imine intermediate.[20] Without external nucleophiles, two primary alcohols

condenses into the corresponding ester product (Scheme 1.4B).[21] In the next section, the imine synthetic approach via the utilization of the dehydrogenative alcohol activation strategy will be discussed in detail.

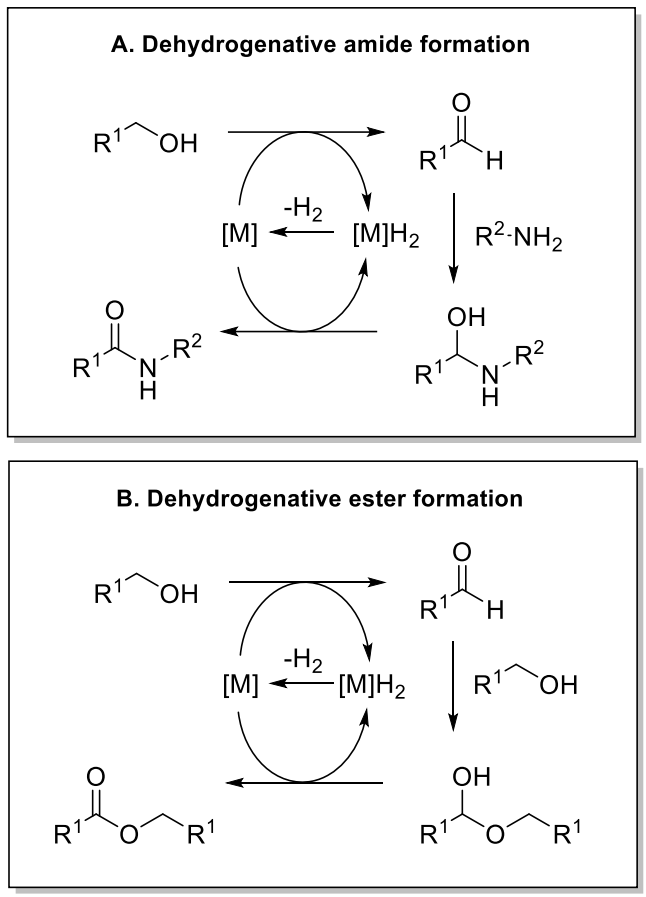

Scheme 1.4 Dehydrogenative coupling of alcohol and nucleophiles.

1.4 Imine synthesis with catalytic dehydrogenative alcohol activation strategy

During the past decade, considerable efforts have been devoted to the direct synthesis of imines, particularly via the catalytic dehydrogenative coupling reaction of amines and alcohols, because alcohols are more readily available and stable than

the aldehydes. This method can reduce energy consumption and purification steps.[6e] A wide variety of catalytic systems have been extensively explored during the past years and bring significant developments to this approach. In this chapter, the outline of these achievements and critical factors that affect the catalytic activity and reaction mechanisms is highlighted.

1.4.1 Imine synthesis with catalytic dehydrogenative alcohol activation: Aerobic oxidative coupling strategy

The aerobic oxidative reactions have been extensively investigated because of the use of oxygen or air as the pollution-free oxidant, and milder reaction conditions, along with the generation of benign water as the byproduct. One of the representative examples is the metal/nitroxyl aerobic systems, which enable the dehydrogenative coupling of alcohols with amines at mild conditions.[22] Reaction mechanism is depicted in Scheme 1.5. Firstly, the coordination of alcohol to the metal complex facilitates the dehydrogenation of alcohol. The metal catalyst is regenerated by nitroxyl catalyst ([N–O]), such as TEMPO. The latter [N–OH] is re-oxidized by oxygen, generating the nitroxyl catalyst with the production of water as a sole byproduct.

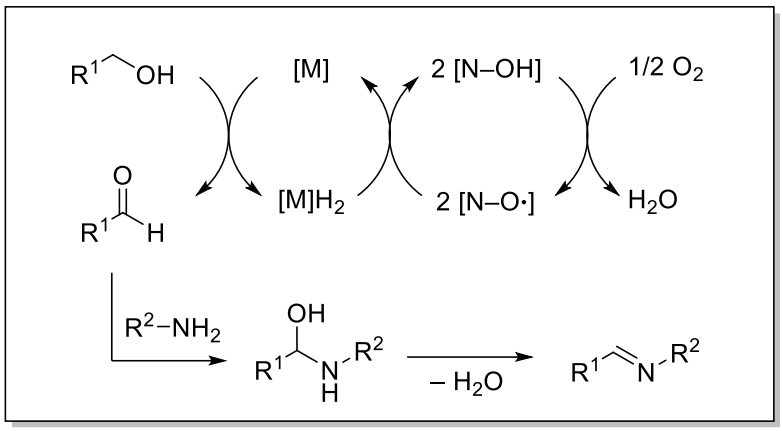

Scheme 1.5 General mechanism of aerobic oxidative imine synthesis from alcohol and amine.

Various transition-metal based catalytic systems have been reported, and representative examples are illustrated. In 2012, the Xu group firstly applied a CuI/TEMPO/bipyridine system for the dehydrogenative coupling of alcohols with amines to synthesize imine at room temperature (Scheme 1.6A). [23] They disclosed that amine substrates worked not only as coupling reagents in the synthesis of imine products but also as promoters to facilitate the alcohol oxidation. Following this work, the Zhao group evaluated various ligands on the efficiency of Cu/TEMPO systems (Scheme 1.6B). It turned out that 4-dimethylaminopyridine (DMAP) ligand is the best for alcohol oxidation and imine synthesis.[24] Considering the fact that iron was an earth-abundant element and also compatible with nitroxyl derivatives, the Xu group reported a $Fe(NO_3)_2$/TEMPO system[6f] where a catalytic amount of base was employed for the dehydrogenative coupling of amine and alcohol (Scheme 1.6C).

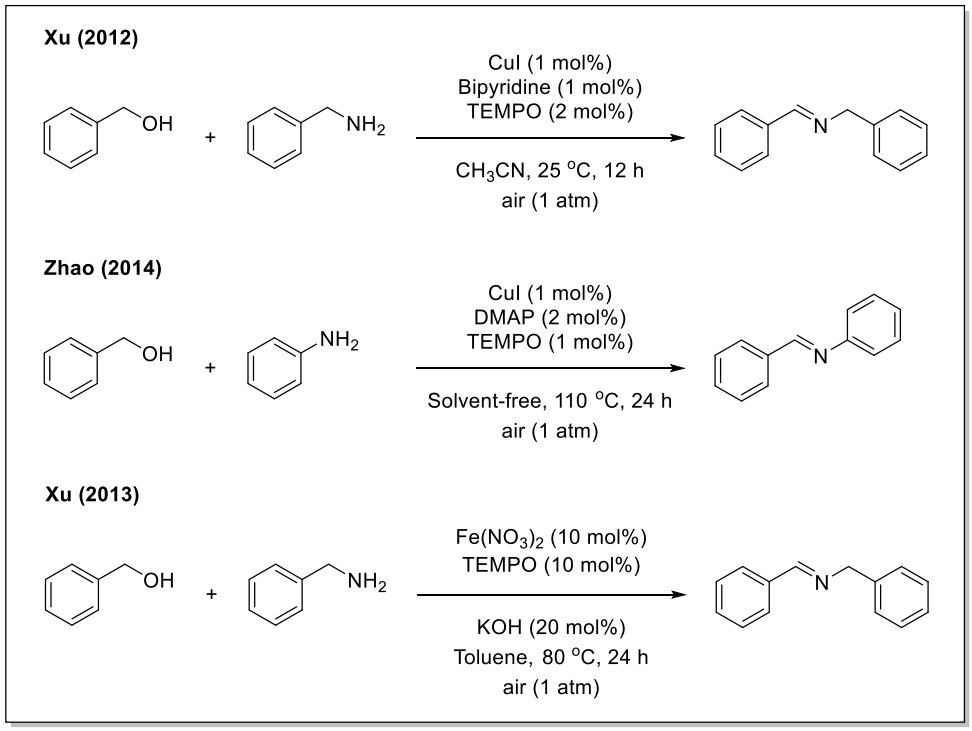

Scheme 1.6 Metal/TEMPO catalyzed dehydrogenative coupling of alcohol with amine for the synthesis of imines.

Furthermore, the development of more active catalyst systems has been widely studied to prevent the use of oxidative reagents such as TEMPO and perform the reaction under mild conditions with good stability. For example, in 2009, Park and co-workers reported that palladium nanoparticles entrapped in boehmite nanofibers (Pd/AlO(OH)) could catalyze the coupling of alcohol and amine without the aid of a nitroxyl catalyst for the first time (Scheme 1.7A)[25]. However, the narrow scope of alcohols and catalytic efficiency limit its applicability. To overcome those limitations, the Yao group developed *N*,*O*-chelated half-sandwich iridium catalyst for this transformation (Scheme 1.7B).[26] The Ir catalytic system showed a broad scope of amine and alcohol, mild reaction

conditions, and excellent catalytic activity.

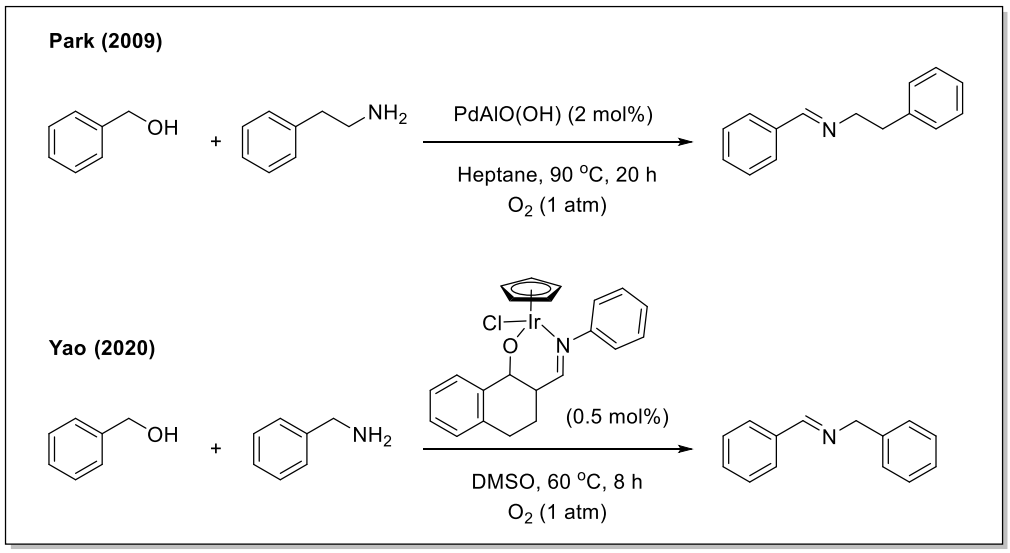

Scheme 1.7 Dehydrogenative coupling of alcohol with amine for the synthesis of imine without nitroxyl additives.

1.4.2 Imine synthesis with catalytic dehydrogenative alcohol activation: Acceptorless dehydrogenative strategy

The catalytic synthesis of imines by acceptorless dehydrogenative coupling of alcohols with amines is an attractive green and sustainable route, in which H_2 is produced as a sole byproduct.[27] Reaction mechanism is depicted in Scheme 1.8. Firstly, an alcohol is dehydrogenated to the carbonyl compound. Condensation of the carbonyl compound with an amine gives the hemiaminal intermediate. Selective dehydration of hemiaminal intermediated finally fives the desired imine product. The metal catalyst is regenerated by direct hydrogen gas evolution.

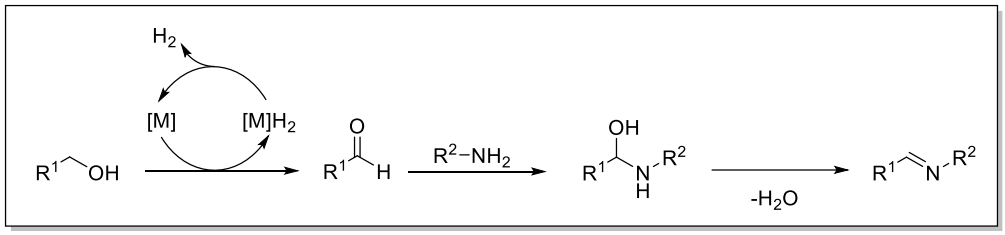

Scheme 1.8 General mechanism of imine synthesis by acceptorless dehydrogenative coupling of alcohol and amine.

In this direction, pioneering work was reported by Milstein and co-workers[27] in 2010, where they used a PNP-Ru pincer complex as the catalyst (Scheme 1.9A). In 2012, Esteruelas groups reported an imine forming reactions catalyzed by the POP-Os pincer complex (Scheme 1.9B).[28] Following those reports, Madsen and co-workers developed an NHC coordinated ruthenium complex as the catalyst for this transformation (Scheme 1.9C).[29] As presented, I*i*Pr (1,3-diisopropylimidazol-2-ylidene) NHC ligand coordinated Ru(II) complex was identified as the active catalytic species.

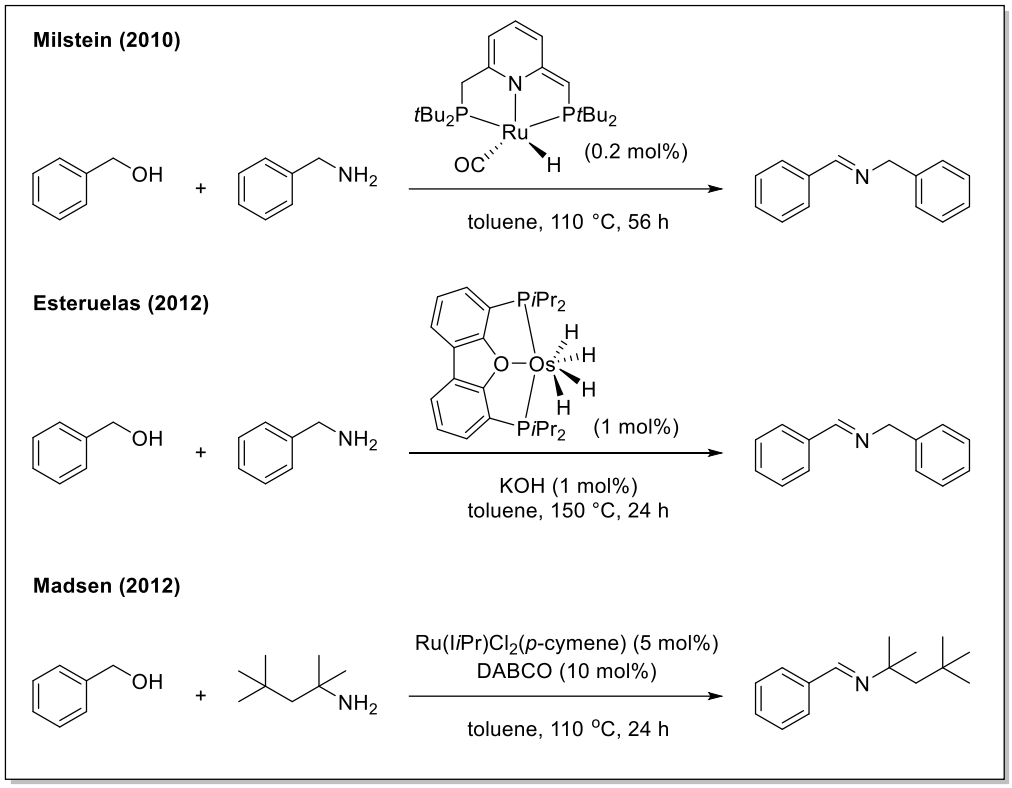

Scheme 1.9 Early development of ruthenium and osmium based catalysts for the acceptorless imine synthesis.

Further modifications towards the use of non-precious metal catalysts have been reported since it is more economical and less toxic. Inspired by the acting mechanism of the PNP-Ru pincer catalyst, Hanson and co-workers introduced the first synthesis of imines catalyzed by a PNP-Co pincer complex.[28] In 2013, Kumar and Singh employed a Fe-phthalocyanine complex as the catalyst.[30] Notably, Milstein and co-workers firstly realized a PNP-Mn pincer complex-mediated imine synthesis in 2016.[31] Subsequently, Kirchner,[32] Kempe[33], and Zhang[34] groups sequentially developed the ligand supported Mn complexes to catalyze this reaction.

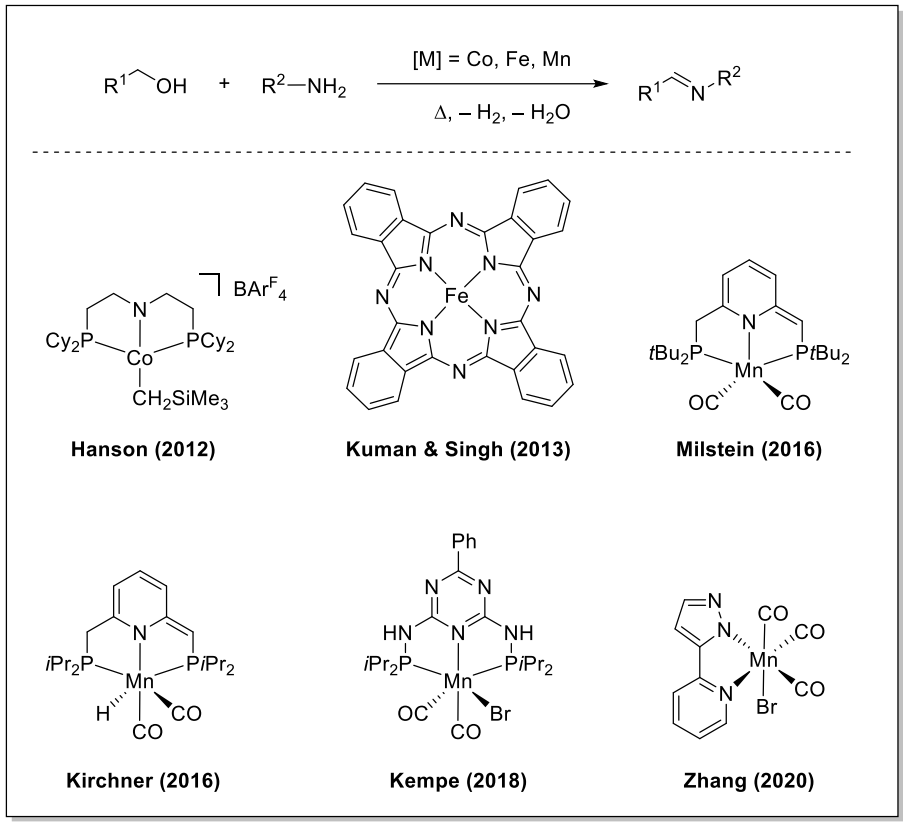

Scheme 1.10 Development of non-precious metal catalysts for the acceptorless imine synthesis.

1.5 Conclusion

During the past decades, remarkable progress has been made in the area of dehydrogenative alcohol activation based on imine synthesis. Utilization of aerobic oxidative and acceptorless dehydrogenative strategies enables atom-economical and eco-friend imine synthesis from alcohol and amine with hydrogen gas and water as byproducts. Hence, earth-abundant metal-based catalytic systems have been recently developed to enhance the practicaly utility of this transformation.

1.6 References

(1) (a) Adams, J. P. *J. Chem. Soc., Perkin Trans. 1* **2000**, 125. (b) Liu, Z.-Y.; Wang, Y.-M.; Li, Z.-R.; Jiang, J.-D.; Boykin, D. W. *Bioorg. Med. Chem. Lett.* **2009**, *19*, 5661.

(2) (a) Xie, J.-H.; Zhu, S.-F.; Zhou, Q.-L. *Chem. Rev.* **2011**, *111*, 1713. (b) Chen, D.; Wang, Y.; Klankermayer, J. *Angew. Chem. Int. Ed.* **2010**, *49*, 9475.

(3) Friestad, G. K.; Mathies, A. K. *Tetrahedron* **2007**, *63*, 2541.

(4) Yao, S.; Saaby, S.; Hazell, R. G.; Jørgensen, K. A. *Chem. Eur. J.* **2000**, *6*, 2435.

(5) (a) Sprung, M. A. *Chem. Rev.* **1940**, *26*, 297. (b) Layer, R. W. *Chem. Rev.* **1963**, *63*, 489. (c) Schiff, H. *Liebigs Annalen* **1864**, *131*, 118.

(6) (a) Murahashi, S.-I.; Naota, T.; Taki, H. *J. Chem. Soc., Chem. Commun.* **1985**, 613. (b) Müller, P.; Gilabert, D. M. *Tetrahedron* **1988**, *44*, 7171. (c) Él l, A. H.; Samec, J. S. M.; Brasse, C.; Bäckvall, J.-E. *Chem. Commun.* **2002**, 1144. (d) Nicolaou, K. C.; Mathison, C. J. N.; Montagnon, T. *Angew. Chem. Int. Ed.* **2003**, *42*, 4077. (e) Sonobe, T.; Oisaki, K.; Kanai, M. *Chem. Sci.* **2012**, *3*, 3249. (f) Zhang, E.; Tian, H.; Xu, S.; Yu, X.; Xu, Q. *Org. Lett.* **2013**, *15*, 2704. (g) Chen, B.; Wang, L.; Gao, S. *ACS. Catal.* **2015**, *5*, 5851.

(7) (a) Zhao, S.; Liu, C.; Guo, Y.; Xiao, J.-C.; Chen, Q.-Y. *J. Org. Chem.* **2014**, *79*, 8926. (b) Huang, B.; Tian, H.; Lin, S.; Xie, M.; Yu, X.; Xu, Q. *Tetrahedron Lett.* **2013**, *54*, 2861. (c) Yuan, Q.-L.; Zhou, X.-T.; Ji, H.-B. *Catal. Commun.* **2010**, *12*, 202. (d) Liu, L.; Zhang, S.; Fu, X.; Yan, C.-H. *Chem. Commun.* **2011**, *47*, 10148. (e) Prades, A.; Peris, E.; Albrecht, M. *Organometallics* **2011**, *30*, 1162. (f) Hu, Z.; Kerton, F. M. *Org. Biomol. Chem.* **2012**, *10*, 1618. (g) Wendlandt, A. E.; Stahl, S. S.

Org. Lett. **2012**, *14*, 2850. (h) Chen, B.; Wang, L.; Dai, W.; Shang, S.; Lv, Y.; Gao, S. *ACS. Catal.* **2015**, *5*, 2788. (i) Largeron, M.; Fleury, M.-B. *Angew. Chem. Int. Ed.* **2012**, *51*, 5409.

(8) (a) Fresneda, P. M.; Molina, P. *Synlett* **2004**, *2004*, 1. (b) Palacios, F.; Alonso, C.; Aparicio, D.; Rubiales, G.; de los Santos, J. M. *Tetrahedron* **2007**, *63*, 523.

(9) (a) Thalji, R. K.; Ahrendt, K. A.; Bergman, R. G.; Ellman, J. A. *J. Am. Chem. Soc.* **2001**, *123*, 9692. (b) Xu, W.; Yoshikai, N. *Chem. Sci.* **2017**, *8*, 5299.

(10) (a) Zhang, F.-L.; Hong, K.; Li, T.-J.; Park, H.; Yu, J.-Q. *Science* **2016**, *351*, 252. (b) Gandeepan, P.; Ackermann, L. *Chem* **2018**, *4*, 199. (c) St John-Campbell, S.; Bull, J. A. *Org. Biomol. Chem.* **2018**, *16*, 4582.

(11) (a) Gunanathan, C.; Milstein, D. *Science* **2013**, *341*, 1229712. (b) Dobereiner, G. E.; Crabtree, R. H. *Chem. Rev.* **2010**, *110*, 681.

(12) (a) Watson, A. J. A.; Williams, J. M. J. *Science* **2010**, *329*, 635. (b) Trincado, M.; Banerjee, D.; Grützmacher, H. *Energy Environ. Sci.* **2014**, *7*, 2464. (c) Zou, Y.-Q.; von Wolff, N.; Anaby, A.; Xie, Y.; Milstein, D. *Nat. Catal.* **2019**, *2*, 415.

(13) Xie, Y.; Milstein, D. *ACS Appl. Energy Mater.* **2019**, *2*, 4302.

(14) Wang, D.; Astruc, D. *Chem. Rev.* **2015**, *115*, 6621.

(15) Wang, C.; Wu, X.; Xiao, J. *Chem. Asian. J.* **2008**, *3*, 1750.

(16) de Graauw, C. F.; Peters, J. A.; van Bekkum, H.; Huskens, J. *Synthesis* **1994**, *1994*, 1007.

(17) Charman, H. B. *Nature* **1966**, *212*, 278.

(18) (a) Nielsen, M.; Alberico, E.; Baumann, W.; Drexler, H.-J.; Junge, H.; Gladiali, S.; Beller, M. *Nature* **2013**, *495*, 85. (b) Andérez-Fernández, M.; Vogt, L. K.;

Fischer, S.; Zhou, W.; Jiao, H.; Garbe, M.; Elangovan, S.; Junge, K.; Junge, H.; Ludwig, R.; Beller, M. *Angew. Chem. Int. Ed.* **2017**, *56*, 559.

(19) Zultanski, S. L.; Zhao, J.; Stahl, S. S. *J. Am. Chem. Soc.* **2016**, *138*, 6416.

(20) Guillena, G.; Ramón, D. J.; Yus, M. *Chem. Rev.* **2010**, *110*, 1611.

(21) Blum, Y.; Shvo, Y. *J. Organomet. Chem.* **1985**, *282*, C7.

(22) Ryland, B. L.; Stahl, S. S. *Angew. Chem. Int. Ed.* **2014**, *53*, 8824.

(23) Tian, H.; Yu, X.; Li, Q.; Wang, J.; Xu, Q. *Adv. Synth. Catal.* **2012**, *354*, 2671.

(24) Guan, M.; Wang, C.; Zhang, J.; Zhao, Y. *RSC Advances* **2014**, *4*, 48777.

(25) Kwon, M. S.; Kim, S.; Park, S.; Bosco, W.; Chidrala, R. K.; Park, J. *J. Org. Chem.* **2009**, *74*, 2877.

(26) Fan, X.-N.; Ou, H.-D.; Deng, W.; Yao, Z.-J. *Inorg. Chem.* **2020**, *59*, 4800.

(27) Gnanaprakasam, B.; Zhang, J.; Milstein, D. *Angew. Chem. Int. Ed.* **2010**, *49*, 1468.

(28) Zhang, G.; Hanson, S. K. *Org. Lett.* **2013**, *15*, 650.

(29) Maggi, A.; Madsen, R. *Organometallics* **2012**, *31*, 451.

(30) Bala, M.; Verma, P. K.; Kumar, N.; Sharma, U.; Singh, B. *Can. J. Chem.* **2013**, *91*, 732.

(31) Mukherjee, A.; Nerush, A.; Leitus, G.; Shimon, L. J. W.; Ben David, Y.; Espinosa Jalapa, N. A.; Milstein, D. *J. Am. Chem. Soc.* **2016**, *138*, 4298.

(32) Mastalir, M.; Glatz, M.; Gorgas, N.; Stöger, B.; Pittenauer, E.; Allmaier, G.; Veiros, L. F.; Kirchner, K. *Chem. Eur. J.* **2016**, *22*, 12316.

(33) Fertig, R.; Irrgang, T.; Freitag, F.; Zander, J.; Kempe, R. *ACS. Catal.* **2018**, *8*, 8525.

(34) Chai, H.; Yu, K.; Liu, B.; Tan, W.; Zhang, G. *Organometallics* **2020**, *39*, 217.

Chapter 2. Ruthenium-Catalyzed Selective Imine Synthesis from Nitriles and Secondary Alcohols under Hydrogen Acceptor- and Base-free Conditions*

2.1 Introduction

Imines are an important functional group in organic chemistry because their versatility and high reactivity facilitate various transformations in laboratory and industrial synthetic processes.[1] Conventionally, imines are synthesized from the condensation of aldehyde or ketone with primary amine in the presence of an acid catalyst.[2] Moreover, imines have been prepared by oxidation of secondary amines,[3] self-condensation of primary amines,[3j, 3l-n, 4] the aza-Wittig reaction,[5] and the dehydrogenative coupling reaction between amines and alcohols.[3m, 3n, 6]

Catalytic methods to convert nitriles to imines have been relatively less explored in organic synthesis. Symmetrical and unsymmetrical imines have been synthesized by coupling nitriles with the corresponding reduced amines or additional amines under hydrogen pressure with liberation of NH_3.[7] Recently, Nikonov and co-workers reported the reaction of nitriles to imines using a cationic Ru complex; however, the alcohol scope was limited

* The majority of this work has been published: Daeun Kim, Byungjoon Kang, and Soon Hyeok Hong*, *Org. Chem. Front.* 2016, *3*, 475–479.

to only 2-propanol and strong basic conditions were required to generate the active catalyst.[8]

We have been working on the development of atom-, step-, and redox-economical C–N bond formation methods for the synthesis of amides, formamides, and imides from nitriles and alcohols through a hydrogen–transfer strategy (Scheme 2.1A).[9] Further, Beller and co-workers reported N-monoalkylation of nitriles using 2-propanol as both the hydrogen source and the coupling partner.[10] As an expansion of these works, we herein report a selective, catalytic imine synthetic method from nitriles and secondary alcohols under base-free and hydrogen acceptor-free conditions (Scheme 2.1B).

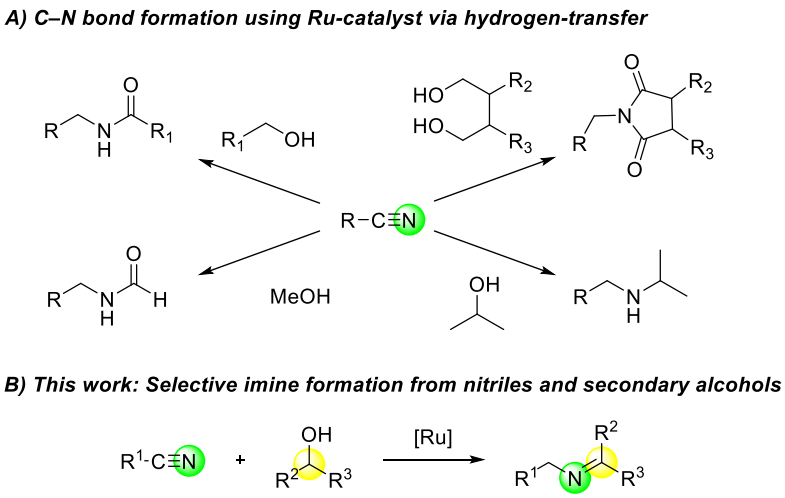

Scheme 2.1 Imine synthesis directly from nitriles and secondary alcohols.

2.2 Results and discussion

2.2.1 Optimization for imine synthesis from nitrile and alcohol

Initially, the reaction between benzonitrile and 2-propanol was selected as a model reaction to investigate the catalytic conditions (Table 2.1 and Table 2.4). Molecular sieves (MS) were added to enable the continuous removal of water during the reaction. We first tested several Ru precatalysts that were known to be active for C–N bond formations from dehydrogenation of alcohols. Milstein catalyst and (NHC)Ru-based dehydrogenation catalytic systems yielded none of the desired imine products; however, *N*-Benzylidenebenzylamine was obtained as a major product (entries 1 and 2).[6k, 7b] When the $RuCl_2(PPh_3)_3$-based catalytic system, which was reported as efficient for the N-alkylation of nitriles using 2-propanol under basic conditions, was applied without any base, it yielded only trace amounts of **4aa** (2%, entry 3).[10] We then found that the Ru(II) dihydride complex $RuH_2(CO)(PPh_3)_3$ (**1**) showed significant activity for the imine synthesis (61%, entry 4). Previously, we reported *N*-heterocyclic carbene (NHC) coordinated Ru(II) dihydride complexes as efficient catalysts for the dehydrogenative amidation of nitriles with primary alcohols.[9] A well-defined Ru dihydride complex, $RuH_2(CO)(PPh_3)_2$(I*i*Pr),[11] gave **4aa** in 60% yield (entry 5). After extensive screening (See experimental section), an increased loading of the readily available precatalyst **1** (10 mol%) accompanied with pyridine as a stabilizing ligand was identified as the most efficient method for the imine synthesis (entry 6).

Table 2.1 Catalyst screening[a]

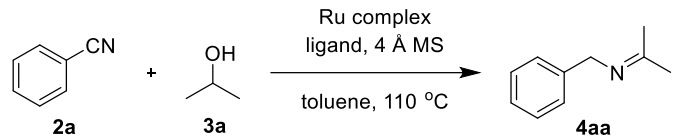

Entry	Catalytic system	Ligand	Time (h)	Yield (%)
1	Mistein Catalyst[c]		18	0
2	$RuCl_2$(I*i*Pr)(p-cymene)[d]		18	0
3	$RuCl_2(PPh_3)_3$		18	2
4	$RuH_2(CO)(PPh_3)_3$		18	61
5	$RuH_2(CO)(PPh_3)_2$(I*i*Pr)[e]		18	60
6	$RuH_2(CO)(PPh_3)_3$ (**1**)[f]	Pyridine	1	84

[a]Reaction conditions: **2a** (0.5 mmol, 1.0 equiv), **3a** (5 equiv), Ru complex (5 mol%), ligand (20 mol%), 4 Å molecular sieves (200 mg), toluene (0.6 mL), and 110 °C. [b]Determined by GC using dodecane as the internal standard. [c]Milstein catalyst: carbonylhydrido[6-(di-tert-butylphosphinomethylene)-2-(*N*,*N*-diethylamino methyl)-1,6-dihydropyridine]ruthenium(II). [d]$RuCl_2$(I*i*Pr)(*p*-cymene) (5 mol%), and 1,4-diazabicyclo[2,2,2]octane (DABCO, 10 mol%). [e]I*i*Pr = 1,3-diisopropylimidazolidene. [f]10 mol% of **1** was used.

2.2.2 Substrate scope of alcohol and nitrile

With the optimized conditions in hand, the substrate scope was then investigated. First, different nitriles were tested with 2-propanol as the coupling partner (Table 2.2). Various aromatic and aliphatic nitriles afforded the corresponding imines in moderate to good yields (entries 1–10). *o*-tolunitrile showed a slightly decreased reactivity and required a longer reaction time than *m*-, and *p*-tolunitrile, presumably because of increased steric hinderance near the reaction center (entry 2). Electron-rich benzonitriles exhibited high reactivity (entries 2–4), whereas electron-deficient nitriles gave diminished yields (entries 5 and 6). Aliphatic nitriles, which are less prone to reduction than aryl nitriles, also gave good yields (entries 7 and 8). However, propionitrile showed poor yield (entry 9). We think that linear alkyl nitrile might coordinate to the catalytically active Ru complex stronger than other nitriles resulting in reduced catalytic activity.[12] Furthermore, a nitrile with a pyridine ring (**2l**) reacted smoothly under the reaction conditions (entry 10).

Table 2.2 Imine synthesis from 2-propanol and nitriles[a]

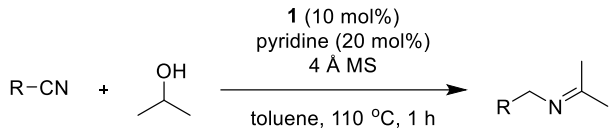

Entry	Nitrile		Product		Yield (%)[b]
1	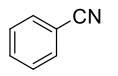	**2a**	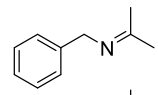	**4aa**	84
2	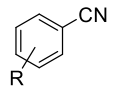	**2b** **2c** **2d**	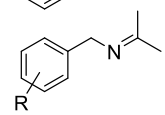	**4ba** **4ca** **4da**	82 82 79[d]
	R = *p*-Me (**2b**) = *m*-Me (**2c**) = *o*-Me (**2d**)		**R** = *p*-Me (**4ba**) = *m*-Me (**4ca**) = *o*-Me (**4da**)		
3	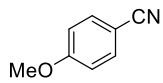	**2e**	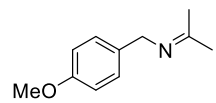	**4ea**	82
4	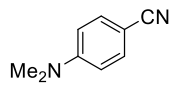	**2f**	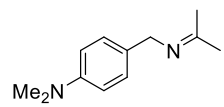	**4fa**	79[c]
5	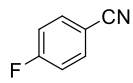	**2g**	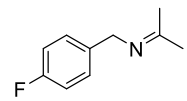	**4ga**	68[c]
6	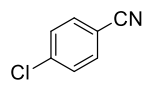	**2h**	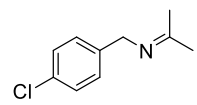	**4ha**	70
7	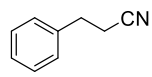	**2i**	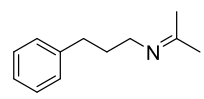	**4ia**	74[d]
8	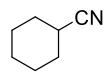	**2j**	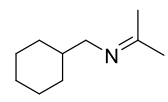	**4ja**	76[e]
9		**2k**	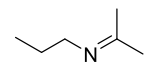	**4ka**	20[e]
10	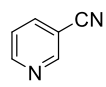	**2l**	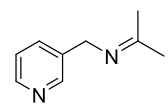	**4la**	88

[a]Reaction conditions: nitrile (0.5 mmol, 1.0 equiv), **3a** (5.0 equiv), **1** (10 mol%), pyridine (20 mol%), 4 Å molecular sieves (200 mg), toluene (0.6 mL), 110 °C, and 1 h reaction time. [b]Determined by ^{1}H NMR with 1,2-dimethoxybenzene as an internal standard. [c]3 h, [d]6 h, and [e]10 h reaction time.

Next, the reactions between benzonitrile and various secondary alcohols were investigated (Table 2.3). Various aliphatic secondary alcohols generated the corresponding imines in moderate to good yields (entries 1–6). Relatively sterically congested secondary alcohols such as 3-pentanol and cyclooctanol could also be used (entries 3 and 6). In the case of 1-phenylethanols, electron-donating 1-(4-methylphenyl)ethanol and 1-(3-methylphenyl)ethanol gave good yields but sterically congested 1-(2-methylphenyl)ethanol exhibited reduced activity (entry 8).

Table 2.3 Imine synthesis from benzonitrile and alcohols[a]

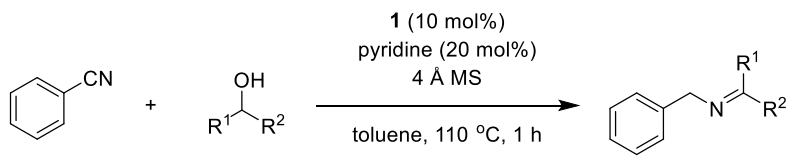

Entry	Alcohol		Product		Yield (%)[b]
1		**3b**	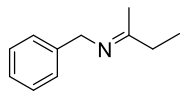	**4ab**	81[c]
2	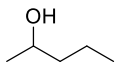	**3c**	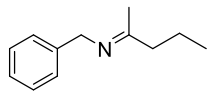	**4ac**	71[c]
3	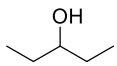	**3d**	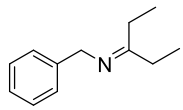	**4ad**	66[c]
4	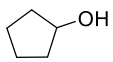	**3e**	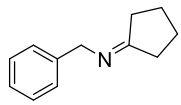	**4ae**	84
5	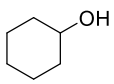	**3f**	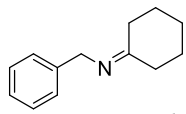	**4af**	85
6	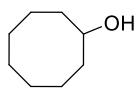	**3g**	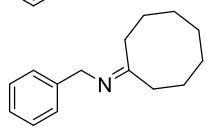	**4ag**	89[c]
7	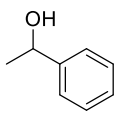	**3h**	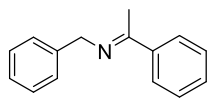	**4ah**	75[d,e]
8	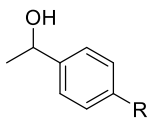	**3i** **3j** **3k**	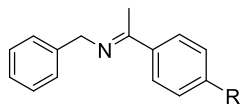	**4ai** **4aj** **4ak**	76[d,e] 73[d,e] 17[d,e]
	R = *p*-Me (**3i**) = *m*-Me (**3j**) = *o*-Me (**3k**)		**R** = *p*-Me (**4ai**) = *m*-Me (**4aj**) = *o*-Me (**4ak**)		

[a]Reaction conditions: **2a** (0.5 mmol, 1.0 equiv), alcohol (5.0 equiv), **1** (10 mol%), pyridine (20 mol%), 4 Å molecular sieves (200 mg), toluene (0.6 mL), 110 ℃, and 1 h reaction time. [b]Determined by ^{1}H NMR with 1,2-dimethoxybenzene as an internal standard. [c]6 h and [d]12 h reaction time. [e]Determined by ^{1}H NMR with nitrobenzene as an internal standard.

2.2.3 Mechanistic studies

To investigate the reaction mechanism, a kinetic study was conducted by monitoring the progress of the reaction between **2a** and **3a** (Scheme 2.2). We found that **2a** was rapidly consumed in 30 min, and benzylamine (**5**) was observed as a major intermediate. The concentration of **5** decreased whereas that of imine (**4aa**) gradually increased and became saturated within 1 h. A small amount of *N*-benzylidenebenzylamine (**7**) was formed from the coupling reaction between **2a** and **5**. Interestingly, we observed very low trace amounts of *N*-isopropylbenzylamine (**6**), which is a further hydrogenated form of **4aa**.

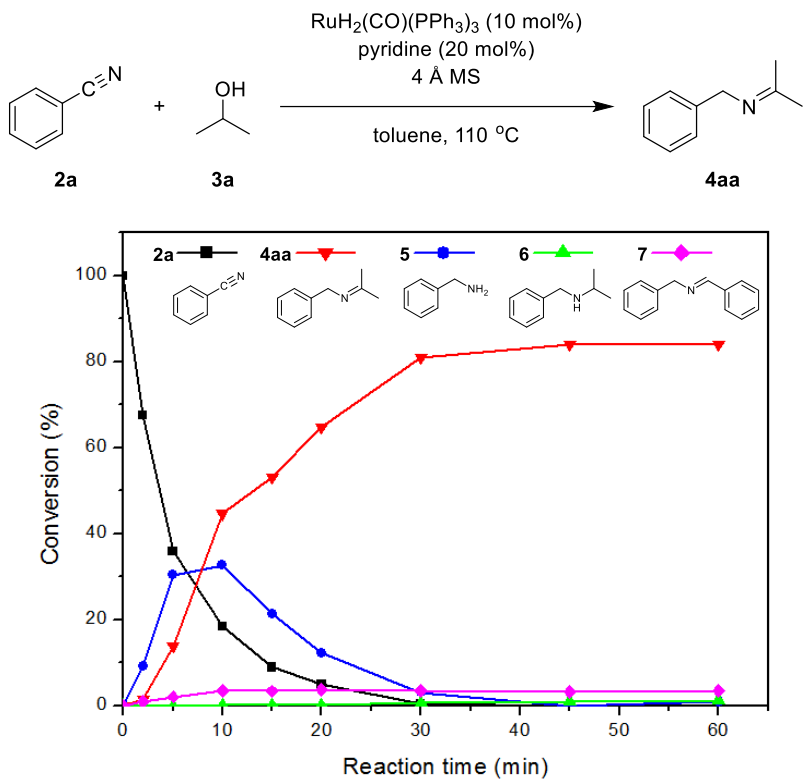

Scheme 2.2 Reaction profiles for the imine synthesis showing the relative amounts of substrates and products. The reaction's progress was monitored by GC analysis using dodecane as an internal standard.

We verified that our catalytic system is not very active for hydrogenation of the *N*-alkyl imine **4aa**, which leads to the selective formation of imine (Scheme 2.3). The results suggest that **1** can hydrogenate nitriles and *N*-protonated imine intermediates, but not *N*-alkylated imines under the reaction conditions used.

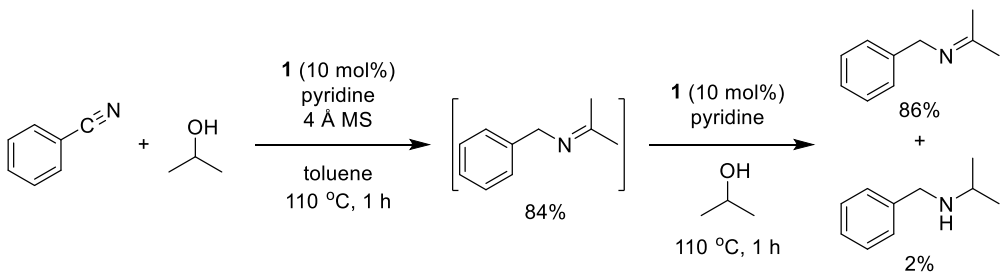

Scheme 2.3 Attempted imine hydrogenation. Reaction conditions: (1) **2a** (0.5 mmol, 1.0 equiv), **3a** (2.5 mmol, 5.0 equiv), **1** (10 mol%), pyridine (20 mol%), 4 Å molecular sieves (200 mg), toluene (0.6 mL), 110 ℃, 1 h. (2) **3a** (2.5 mmol, 5.0 equiv.), **1** (10 mol%), pyridine (20 mol%), 110 ℃, and 1 h reaction time.

A plausible mechanism is proposed on the basis of experimental observations (Scheme 2.4). At the initiation stage, hydrogen transfer from alcohol to nitrile affords the corresponding amine with simultaneous generation of ketone. Then, the generated amine undergoes coupling with ketone to produce the hemiaminal intermediate, which is further dehydrated to imine.

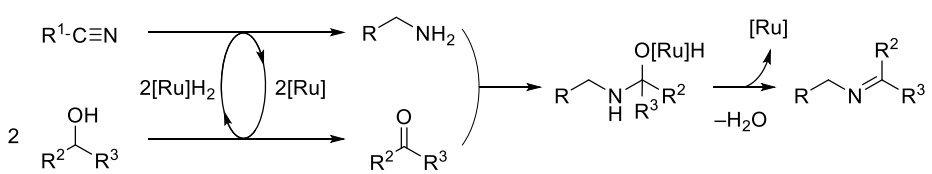

Scheme 2.4 Proposed mechanism.

2.3 Conclusion

We have developed a Ru dihydride-complex-based catalytic system that works without any external base or hydrogen acceptor for the synthesis of imines from nitriles and secondary alcohols. The developed catalytic system can selectively control the pathway to the corresponding imine. This reaction offers a simple, convenient, and environmentally benign synthetic method for the synthesis of versatile imines by applying a hydrogen transfer strategy.

2.4. Experimental section

2.4.1 General information

Unless otherwise noted, all reactions were carried out using standard Schlenk techniques or in an argon-filled glove box. All anhydrous solvents were purchased from commercial suppliers and degassed with dry argon before usage. Deuterated solvents were purchased from Cambridge Isotope Laboratories, Inc. NMR spectra were recorded in $CDCl_3$ or benezene-d_6 using Bruker DPX300, AMX400, Agilent 400-MR, JEOL ECA400, or JEOL ECA400SL spectrometer, and TMS (tetramethylsilane) was used as a reference. Chemical shifts were reported in ppm and coupling constant in Hz. GC analysis was carried out with 7980A GC system from Agilent Technologies, equipped with an HP-5 column and FID detector. $RuH_2(CO)(PPh_3)_3$,[13] NHC precursors,[14] $RuH_2(CO)(PPh_3)_2$(I*i*Pr),[15] and other metal reagents were prepared by literature procedures or purchased from Strem Chemicals, Inc.

2.4.2 General procedure for imine synthesis from nitrile and alcohol

Inside an argon-filled glove box, $RuH_2(CO)(PPh_3)_3$ (46 mg, 0.05 mmol), nitrile (0.50 mmol), alcohol (2.5 mmol), pyridine (8.1 μL, 0.10 mmol), 4 Å Molecular sieve (200 mg), and toluene (0.6 mL) were added to an oven-dried 4 mL vial equipped with septum screw cap. Then, the overall reaction media was stirred at 110 ℃ for 1–12 h before being cooled down to room temperature. Crude mixture was filtered through Celite pad and washed with dichloromethane, and all the volatiles were removed under vacuum.

2.4.3 General procedure for imine reduction

After imine synthesis from above procedure, concentrated mixture was dissolved in 2,2,2-trifluoroethanol (TFE, 2.0 mL). Sodium borohydride ($NaBH_4$, 28 mg, 0.75 mmol) was added and stirred at 40 ℃ for 1–3 h. After completion of the reaction, the mixture was filtered through Celite pad and washed with dichloromethane. All the volatiles were removed under vacuum. Purification of the crude product was performed by flash chromatography (Eluent: dichloromethane and methanol) to afford the corresponding product.

2.4.4 Optimization of reaction conditions

Table 2.4 Screening of catalysts for imine synthesis[a]

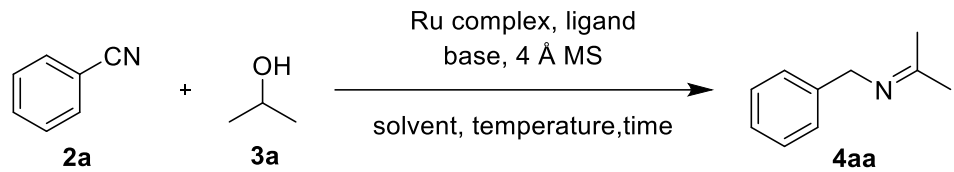

Entry	Ru complex	Ligand (mol%)	Base (mol%)	Solvent (℃)	Time (h)	Yield (%)[b]
1	Shvo's catalyst[c]	-	-	Toluene (110)	18	0
2	Ru-MACHO-BH[d]	-	-	Toluene (110)	18	29
3	$Ru_3(CO)_{12}$	I*i*Pr[e] (5)	NaH (20)	Toluene (110)	18	0
4	$RuHCl(CO)(PPh_3)_3$	I*i*Pr (5)	NaH (20)	Toluene (110)	18	35
5	$RuH_2(PPh_3)_4$	I*i*Pr (5)	NaH (20)	Toluene (110)	18	37
6	$RuH_2(CO)(PPh_3)_3$	I*i*Pr (5)	NaH (20)	Toluene (110)	18	60
7	$RuH_2(CO)(PPh_3)_3$	IMe[f]	NaH (20)	Toluene (110)	18	22
8	$RuH_2(CO)(PPh_3)_3$	IPr[g]	NaH (20)	Toluene (110)	18	27
9	$RuH_2(CO)(PPh_3)_3$	ICy[h]	NaH (20)	Toluene (110)	18	35
10	$RuH_2(CO)(PPh_3)_3$	-	NaH (20)	Toluene (110)	18	27
11	$RuH_2(CO)(PPh_3)_3$	-	NaH (10)	Toluene (110)	18	34
12	$RuH_2(CO)(PPh_3)_3$	-	-	Toluene (110)	18	61
13[i]	$RuH_2(CO)(PPh_3)_3$	-	-	Toluene (110)	18	45
14	$RuH_2(CO)(PPh_3)_3$	-	-	Toluene (100)	18	59
15	$RuH_2(CO)(PPh_3)_3$	-	-	Toluene (120)	18	40
16	$RuH_2(CO)$(I*i*Pr)$(PPh_3)_3$	-	-	Toluene (110)	18	60
17	$RuH_2(CO)(PPh_3)_3$	-	-	Anisole (110)	18	60
18	$RuH_2(CO)(PPh_3)_3$	-	-	CPME (110)[j]	18	55
19	$RuH_2(CO)(PPh_3)_3$			2-propanol (110)	18	27
20	$RuH_2(CO)(PPh_3)_3$	P(*t*Bu)$_3$[k] (5)	-	Toluene (110)	18	73
21	$RuH_2(CO)(PPh_3)_3$	JohnPhos[l] (5)	-	Toluene (110)	18	76
22	$RuH_2(CO)(PPh_3)_3$	CH_3CN (20)	-	Toluene (110)	18	65
23	$RuH_2(CO)(PPh_3)_3$	Pyridine (20)	-	Toluene (110)	18	74

24	$RuH_2(CO)(PPh_3)_3$	Pyridine (10)	-	Toluene (110)	18	57
25	$RuH_2(CO)(PPh_3)_3$	Pyridine (40)	-	Toluene (110)	18	59
26[m]	$RuH_2(CO)(PPh_3)_3$	Pyridine (20)	-	Toluene (110)	18	82
27	$RuH_2(CO)(IiPr)(PPh_3)_2$	Pyridine (20)	-	Toluene (110)	18	60
28[n]	$RuH_2(CO)(PPh_3)_3$	Pyridine (20)	-	Toluene (110)	1	84

[a]Reaction conditions: **2a** (0.5 mmol, 1.0 equiv.), **3a** (5 equiv.), Ru complex (5 mol%), ligand, base, 4 Å molecular sieve (200 mg), solvent (0.6 ml), temperature, time. [b]Determined by GC using dodecane as an internal standard. [c]1-Hydroxytetraphenyl-cyclopentadienyl(tetraphenyl-2,4-cyclopentadien-1-one)-μ-hydrotetracarbonyldiruthenium(II). [d]Carbonylhydrido(tetrahydroborato)[bis(2-diphenylphosphinoethyl)-amino]ruthenium(II). [e]1,3-diisopropylimidazolium bromide. [f]1,3-dimethylimidazolium iodide. [g]1,3-(2,6-(diisopropyl)phenylimidazolium chloride. [h]1,3-dicyclohexylimidazolium chloride. [i]Without 4 Å molecular sieve. [j]cyclopentyl methy ether. [k]tri-*tert*-butyl-phosphine. [l](2-Biphenyl)di-*tert*-butylphosphine. [m]10 equiv. of 2-propanol was used. [n]10 mol% of catalyst was used.

2.4.5 GC analysis for reaction intermediate detection

$RuH_2(CO)(PPh_3)_3$ (46 mg, 0.05 mmol), benzonitrile (51.6 μL, 0.50 mmol), 2-propanol (191.4 μL, 2.5 mmol), pyridine (8.1 μL, 0.10 mmol), 4 Å Molecular sieve (200 mg), and toluene (0.6 mL) were added to an oven-dried 4 mL vial equipped with septum screw cap inside an argon-filled glove box. Dodecane (56.8 μL, 0.25 mmol) as an internal standard was added to the reaction mixture. Then, the overall reaction medias were stirred at 110 ℃ for 2 min, 5 min, 10 min, 15 min, 20 min, 30 min, 45 min, and 60 min, respectively, before being cooled to room temperature. Each sample was diluted with dichloromethane, and filtered with Celite, and analyzed with GC (Scheme 2.2).

2.4.6 Characterization of newly reported compounds

Characterization of newly reported imines, **4ca, 4da**, **4ea**, **4fa**, **4ga**, **4ha**, **4ia**, **4la, 4ac:** the corresponding reduced amine form was provided by imine reduction.

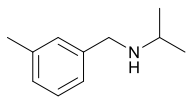

***N*-(3-methylbenzyl)propan-2-amine (4ca):** yellow oil (61.3 mg, 0.375 mmol, 75%); ^{1}H NMR ($CDCl_3$) δ = 1.11 (d, *J* = 6.2 Hz, 6H), 2.34 (s, 3H), 2.87 (septet, *J* = 6.2 Hz, 1H), 3.75 (s, 2H), 7.05 (d, *J* = 7.5 Hz, 1H), 7.11 (d, *J* = 7.5 Hz, 1H), 7.15 (s, 1H), 7.20-7.23 (t, *J* = 7.5 Hz, 1H). NH was not detected; ^{13}C NMR ($CDCl_3$) δ = 138.3, 132.3, 129.2, 128.5, 127.9, 125.5, 51.5, 48.3, 22.8, 21.5; HRMS(ESI) calcd for $C_{11}H_{17}N_1$:163.1361. Found: 163.1360.

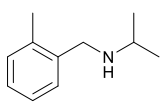

***N*-(2-methylbenzyl)propan-2-amine (4da):**[16] yellow oil (59.8 mg, 0.366 mmol, 73%); ^{1}H NMR ($CDCl_3$) δ = 1.14 (d, *J* = 6.2 Hz, 6H), 2.06 (bs, 1H), 2.38 (s, 3H), 2.92 (septet, *J* = 6.3 Hz, 1H), 3.78 (s, 2H), 7.16-7.19 (m, 3H), 7.32-7.34 (m, 1H).

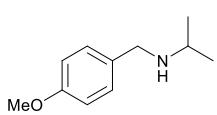

***N*-(4-methoxybenzyl)propan-2-amine (4ea)**:[17] yellow oil (72.0 mg, 0.402 mmol, 80%); ^{1}H NMR ($CDCl_3$) δ = 1.08 (d, *J* = 6.2 Hz, 6H), 1.36 (bs, 1H), 2.84 (septet, *J* = 6.2 Hz, 1H), 3.71 (s, 2H), 3.78 (s, 3H), 6.84 (d, *J* = 8.5 Hz, 2H), 7.22 (d, *J* = 8.5 Hz, 2H).

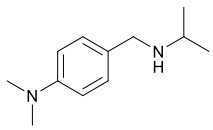

***N*-((isopropylamino)methyl)-N,N-dimethylaniline (4fa):** white crystal (74.4 mg, 0.387 mmol, 77%); ^{1}H NMR ($CDCl_3$) δ = 1.21 (d, *J* = 6.5 Hz, 6H), 2.90 (s, 6H), 2.90-3.01 (m, 1H), 3.74 (s, 2H), 6.68 (d, *J* = 8.7 Hz, 2H), 7.28 (d, *J* = 8.7 Hz, 2H). NH was not detected. ^{13}C NMR ($CDCl_3$) δ = 150.4, 130.2, 124.1, 112.7, 49.6, 48.0, 40.7, 21.4; HRMS(ESI) calcd for $C_{12}H_{20}N_2$: 192.1626. Found: 192.1623.

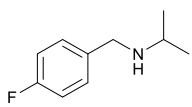

***N*-(4-fluorobenzyl)propan-2-amine (4ga):**[10] yellow oil (51.9 mg, 0.310 mmol, 62%); ^{1}H NMR ($CDCl_3$) δ = 1.11 (d, *J* = 6.2 Hz, 6H), 2.87 (septet, *J* = 6.3 Hz, 1H), 3.78 (s, 2H), 6.99-7.05 (m, 2H), 7.29-7.34 (m, 2H).

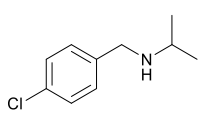

***N*-(4-chlorobenzyl)propan-2-amine (4ha):**[17] yellow solid (60.5 mg, 0.329 mmol, 66%); ^{1}H NMR ($CDCl_3$) δ = 1.08 (d, *J* = 6.3 Hz, 6H), 1.33 (bs, 1H), 2.83 (septet, *J* = 6.2 Hz, 1H), 3.75 (s, 2H), 7.24-7.29 (m, 4H).

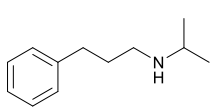

***N*-isopropyl-3-phenylpropan-1-amine (4ia):**[18] white crystal (60.9 mg, 0.344 mmol, 69%); ^{1}H NMR ($CDCl_3$) δ = 1.04 (d, *J* = 6.0 Hz, 6H), 1.79-1.83 (m, 2H),

2.26-2.67 (m, 4H), 2.77 (septet, *J* = 6.4 Hz, 1H), 7.18-7.29 (m, 5H).

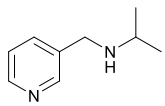

***N*-(pyridine-3-ylmethyl)propan-2-amine (4la):**[19] yellow oil (60.1 mg, 0.400 mmol, 80%); ^{1}H NMR ($CDCl_3$) δ = 1.09 (d, *J* = 6.2 Hz, 6H), 1.46 (bs, 1H), 2.85 (septet, *J* = 6.3 Hz, 1H), 3.80 (s, 2H), 7.23-7.27 (m, 1H), 7.66 (d, *J* = 7.5 Hz, 1H), 8.49 (d, *J* = 4.8 Hz, 1H), 8.56 (s, 1H).

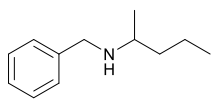

***N*-benzylpentan-2-amine (4ac):**[20] yellow oil (62.9 mg, 0.355 mmol, 71%); ^{1}H NMR ($CDCl_3$) δ = 0.89-0.91 (t, *J* = 7.0 Hz, 3H), 1.09 (d, *J* = 6.4 Hz, 3H), 1.32-1.50 (m, 4H), 1.75 (bs, 1H), 2.70 (heptet, *J* = 6.3 Hz, 1H), 3.74 (d, *J* = 13.1 Hz, 1H), 3.83 (d, *J* = 13.1 Hz, 1H), 7.24-7.33 (m, 5H).

2.5 References

(1) (a) Adams, J. P. *J. Chem. Soc., Perkin Trans. 1* **2000**, 125. (b) Alvaro, G.; Savoia, D. *Synlett* **2002**, 1180. (c) Ma, J. A. *Chem. Soc. Rev.* **2006**, *35*, 630. (d) Erkkila, A.; Majander, I.; Pihko, P. M. *Chem. Rev.* **2007**, *107*, 5416. (e) Friestad, G. K.; Mathies, A. K. *Tetrahedron* **2007**, *63*, 2541. (f) Kobayashi, S.; Mori, Y.; Fossey, J. S.; Salter, M. M. *Chem. Rev.* **2011**, *111*, 2626. (g) Xie, J. H.; Zhu, S. F.; Zhou, Q. L. *Chem. Rev.* **2011**, *111*, 1713.

(2) (a) Sprung, M. M. *Chem. Rev.* **1940**, *26*, 297. (b) Layer, R. W. *Chem. Rev.* **1963**, *63*, 489.

(3) (a) Murahashi, S. I.; Naota, T.; Taki, H. *J. Chem. Soc., Chem. Commun.* **1985**, 613. (b) Muller, P.; Gilabert, D. M. *Tetrahedron* **1988**, *44*, 7171. (c) Ell, A. H.; Samec, J. S. M.; Brasse, C.; Backvall, J. E. *Chem. Commun.* **2002**, 1144. (d) Nicolaou, K. C.; Mathison, C. J. N.; Montagnon, T. *Angew. Chem. Int. Ed.* **2003**, *42*, 4077. (e) Samec, J. S. M.; Ell, A. H.; Backvall, J. E. *Chem. Eur. J.* **2005**, *11*, 2327. (f) Choi, H.; Doyle, M. P. *Chem. Commun.* **2007**, 745. (g) Murahashi, S. I.; Okano, Y.; Sato, H.; Nakae, T.; Komiya, N. *Synlett* **2007**, 1675. (h) Jiang, G.; Chen, J.; Huang, J. S.; Che, C. M. *Org. Lett.* **2009**, *11*, 4568. (i) Aschwanden, L.; Mallat, T.; Maciejewski, M.; Krumeich, F.; Baiker, A. *ChemCatChem* **2010**, *2*, 666. (j) Patil, R. D.; Adimurthy, S. *Adv. Synth. Catal.* **2011**, *353*, 1695. (k) Sonobe, T.; Oisaki, K.; Kanai, M. *Chem. Sci.* **2012**, *3*, 3249. (l) Huang, B.; Tian, H.; Lin, S.; Xie, M.; Yu, X.; Xu, Q. *Tetrahedron Lett.* **2013**, *54*, 2861. (m) Zhang, E.; Tian, H.; Xu, S.; Yu, X.; Xu, Q. *Org. Lett.* **2013**, *15*, 2704. (n) Chen, B.; Wang, L.; Gao, S. *ACS Catal.*

2015, *5*, 5851.

(4) (a) Chu, G.; Li, C. *Org. Biomol. Chem.* **2010**, *8*, 4716. (b) Yuan, Q. L.; Zhou, X. T.; Ji, H. B. *Catal. Commun.* **2010**, *12*, 202. (c) Lang, X.; Ji, H.; Chen, C.; Ma, W.; Zhao, J. *Angew. Chem. Int. Ed.* **2011**, *50*, 3934. (d) Liu, L.; Zhang, S.; Fu, X.; Yan, C.-H. *Chem. Commun.* **2011**, *47*, 10148. (e) Prades, A.; Peris, E.; Albrecht, M. *Organometallics* **2011**, *30*, 1162. (f) Hu, Z.; Kerton, F. M. *Org. Biomol. Chem.* **2012**, *10*, 1618. (g) Largeron, M.; Fleury, M.-B. *Angew. Chem. Int. Ed.* **2012**, *51*, 5409. (h) Wendlandt, A. E.; Stahl, S. S. *Org. Lett.* **2012**, *14*, 2850. (i) Largeron, M.; Fleury, M. B. *Science* **2013**, *339*, 43. (j) Qiu, X.; Len, C.; Luque, R.; Li, Y. *ChemSusChem* **2014**, *7*, 1684. (k) Wang, J.; Lu, S.; Cao, X.; Gu, H. *Chem. Commun.* **2014**, *50*, 5637. (l) Chen, B.; Wang, L.; Dai, W.; Shang, S.; Lv, Y.; Gao, S. *ACS Catal.* **2015**, *5*, 2788.

(5) (a) Fresneda, P. M.; Molina, P. *Synlett* **2004**, 1. (b) Palacios, F.; Alonso, C.; Aparicio, D.; Rubiales, G.; de los Santos, J. M. *Tetrahedron* **2007**, *63*, 523.

(6) (a) Blackburn, L.; Taylor, R. J. K. *Org. Lett.* **2001**, *3*, 1637. (b) Kim, J. W.; He, J.; Yamaguchi, K.; Mizuno, N. *Chem. Lett.* **2009**, *38*, 920. (c) Kwon, M. S.; Kim, S.; Park, S.; Bosco, W.; Chidrala, R. K.; Park, J. *J. Org. Chem.* **2009**, *74*, 2877. (d) Sun, H.; Su, F.-Z.; Ni, J.; Cao, Y.; He, H.-Y.; Fan, K.-N. *Angew. Chem. Int. Ed.* **2009**, *48*, 4390. (e) Gnanaprakasam, B.; Zhang, J.; Milstein, D. *Angew. Chem. Int. Ed.* **2010**, *49*, 1468. (f) Cano, R.; Ramon, D. J.; Yus, M. *J. Org. Chem.* **2011**, *76*, 5547. (g) Esteruelas, M. A.; Honczek, N.; Olivan, M.; Onate, E.; Valencia, M. *Organometallics* **2011**, *30*, 2468. (h) Jiang, L.; Jin, L.; Tian, H.; Yuan, X.; Yu, X.;

Xu, Q. *Chem. Commun.* **2011**, *47*, 10833. (i) Donthiri, R. R.; Patil, R. D.; Adimurthy, S. *Eur. J. Org. Chem.* **2012**, 4457. (j) Kang, Q.; Zhang, Y. *Green Chem.* **2012**, *14*, 1016. (k) Maggi, A.; Madsen, R. *Organometallics* **2012**, *31*, 451. (l) Tian, H. W.; Yu, X. C.; Li, Q.; Wang, J. X.; Xu, Q. *Adv. Synth. Catal.* **2012**, *354*, 2671. (m) Xu, J.; Zhuang, R.; Bao, L.; Tang, G.; Zhao, Y. *Green Chem.* **2012**, *14*, 2384. (n) Soule, J.-F.; Miyamura, H.; Kobayashi, S. *Chem. Commun.* **2013**, *49*, 355. (o) Zhang, G.; Hanson, S. K. *Org. Lett.* **2013**, *15*, 650. (p) Oldenhuis, N. J.; Dong, V. M.; Guan, Z. *Tetrahedron* **2014**, *70*, 4213. (q) Saha, B.; Rahaman, S. M. W.; Daw, P.; Sengupta, G.; Bera, J. K. *Chem. Eur. J.* **2014**, *20*, 6542. (r) Wang, L.; Chen, B.; Ren, L.; Zhang, H.; Lü, Y.; Gao, S. *Chin. J. Catal.* **2015**, *36*, 19.

(7) (a) Reguillo, R.; Grellier, M.; Vautravers, N.; Vendier, L.; Sabo-Etienne, S. *J. Am. Chem. Soc.* **2010**, *132*, 7854. (b) Srimani, D.; Feller, M.; Ben-David, Y.; Milstein, D. *Chem. Commun.* **2012**, *48*, 11853. (c) Chakraborty, S.; Berke, H. *ACS Catal.* **2014**, *4*, 2191. (d) Long, J.; Yin, B.; Li, Y.; Zhang, L. *AlChE J.* **2014**, *60*, 3565. (e) Bagal, D. B.; Bhanage, B. M. *Adv. Synth. Catal.* **2015**, *357*, 883. (f) Choi, J.-H.; Prechtl, M. H. G. *ChemCatChem* **2015**, *7*, 1023.

(8) Lee, S.-H.; Nikonov, G. I. *ChemCatChem* **2015**, *7*, 107.

(9) (a) Kang, B.; Fu, Z.; Hong, S. H. *J. Am. Chem. Soc.* **2013**, *135*, 11704. (b) Kim, J.; Hong, S. H. *Org. Lett.* **2014**, *16*, 4404. (c) Kang, B.; Hong, S. H. *Adv. Synth. Catal.* **2015**, *357*, 834.

(10) Werkmeister, S.; Bornschein, C.; Junge, K.; Beller, M. *Eur. J. Org. Chem.* **2013**, 3671.

(11) Kim, K.; Kang, B.; Hong, S. H. *Tetrahedron* **2015**, *71*, 4565.

(12) Ghosh, S. C.; Muthaiah, S.; Zhang, Y.; Xu, X.; Hong, S. H. *Adv. Synth. Catal.* **2009**, *351*, 2643.

(13) Kakiuchi, F.; Sekine, S.; Tanaka, Y.; Kamatani, A.; Sonoda, M.; Chatani, N.; Murai, S. *Bull. Chem. Soc. Jpn.* **1995**, *68*, 62.

(14) Starikova, O. V.; Dolgushin, G. V.; Larina, L. I.; Ushakov, P. E.; Komarova, T. N.; Lopyrev, V. A. *Russ. J. Org. Chem.* **2003**, *39*, 1467.

(15) Burling, S.; Paine, B. M.; Nama, D.; Brown, V. S.; Mahon, M. F.; Prior, T. J.; Pregosin, P. S.; Whittlesey, M. K.; Williams, J. M. J. *J. Am. Chem. Soc.* **2007**, *129*, 1987.

(16) Jeffrey, J. L.; Bartlett, E. S.; Sarpong, R. *Angew. Chem. Int. Ed.* **2013**, *52*, 2194.

(17) Saidi, O.; Blacker, A. J.; Farah, M. M.; Marsden, S. P.; Williams, J. M. J. *Angew. Chem. Int. Ed.* **2009**, *48*, 7375.

(18) Almena, J.; Foubelo, F.; Yus, M. *Tetrahedron* **1994**, *50*, 5775.

(19) Horn, U.; Mutterer, F.; Weis, C. D. *Helv. Chim. Acta.* **1976**, *59*, 190.

(20) Yu, Z. R.; Alesso, S.; Pears, D.; Worthington, P. A.; Luke, R. W. A.; Bradley, M. *J. Chem. Soc., Perkin Trans. 1* **2001**, 1947.

Chapter 3. Transition Metal-Catalyzed C(sp^2)–H Functionalization of Simple Arenes: Arylation and Alkylation

3.1 Introduction

Direct C–H functionalization is a central topic in organic synthesis as it allows direct conversion of the ubiquitous C−H bonds into valuable compounds. Since the direct C–H functionalization method prevents additional pre-functionalization and purification step, it is regarded as an ideal synthetic strategy in the context of green chemistry. During the past decade, remarkable progress has been achieved in the field of C–C bond forming reaction through direct C–H arylation and C–H alkylation of simple arenes. This chapter introduces several C–H functionalization strategies and historical developments for C−H arylations and alkylations, including mechanistic consideration with an emphasis on simple arene substrates.

3.2 Types of C(sp^2)–H functionalization strategy

Direct C–H bond functionalization has emerged as a powerful tool in organic synthesis, providing original disconnections in retrosynthetic analysis and improving the overall reaction efficiency (Scheme 3.1).[1] "C–H functionalization" is a type of reaction in which a C–H bond is replaced with a C–C or C–X bond (Where X is nitrogen, oxygen, and sulfur, etc.). The term "C–H activation" is defined as a process involving the metal-mediated C–H bond cleavage step that results in a carbon-metal bond.[2]

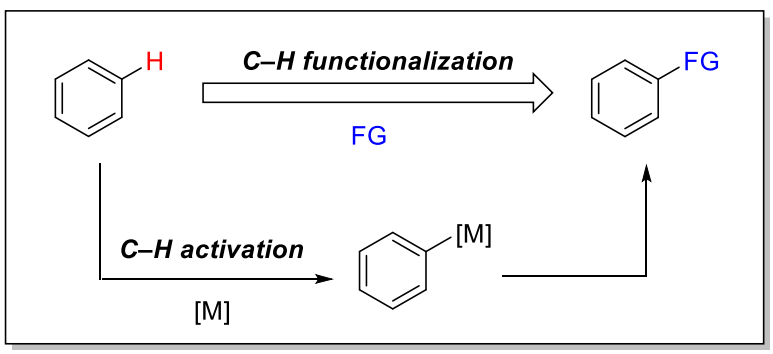

Scheme 3.1 Definition of C–H functionalization and activation.

To achieve the C(sp^2)–H functionalization of arenes, various transition-metal catalyzed strategies have been developed.[3] The type of C–H functionalization can be categorized based on the reaction mechanism. The first type is the oxidative addition of the C–H bond to the metal catalyst to form a metal-hydride intermediate (Scheme 3.2A).[3b, 3c] This process is commonly observed in electron-rich late transition-metal catalysis. The reaction also proceeds in chelation assisted C(sp^2)–H activation or aliphatic C(sp^3)–H activation via agostic interactions.

The second mode is called σ-bond metathesis which involves the concerted exchange of a metal-ligand σ-bond with the substrate. The reaction proceeds via a [2+2] cycloaddition of a metal-ligand bond with a substrate (Scheme 3.2B).[3b, 3c] This reaction mode is typical to early-transition-metal catalysis and lanthanide metallocene compounds with high oxidation states.

The third mode is electrophilic metalation, also called the S_EAr type mechanism (Scheme 3.3B).[3a] This process mainly involves electron-rich arenes as substrates, especially heteroarenes. As in the Friedel-Crafts type process, electrophilic metal catalysts attack the electron-rich arene, affording a Wheland-type intermediate. Subsequent deprotonation completes the C–H activation.

One of the recently investigated C–H activation modes is the concerted metalation-deprotonation (CMD) process (Scheme 3.4B).[3a, 3d] This process is also known as an internal electrophilic substitution (IES) or ambiphilic metal-ligand activation (AMLA). Interaction between the C–H bond of the arene with metal catalyst increases the C–H bond's acidity. Then, a concerted arene metalation and C–H bond cleavage by the coordinated base ligand, such as carboxylate on the metal, occurs with concomitant formation of a C–[M] bond.

Radical addition is the last example of $C(sp^2)$–H functionalization strategy (Scheme 3.2E).[3e, 4] Free radical species (e.g., aryl, alkyl, halogen, and hydroxy, etc.) insert into the arene to generate a radical σ-complex intermediate. This intermediate undergoes single-electron oxidation and rearomatization by base (B)-promoted deprotonation to produce functionalized aromatic compounds. The overall reaction is also called a homolytic aromatic substitution.[5] The representative example is the Minisci reaction that involves the addition of

nucleophilic alkyl radicals to electron-poor heterocycles.[6]

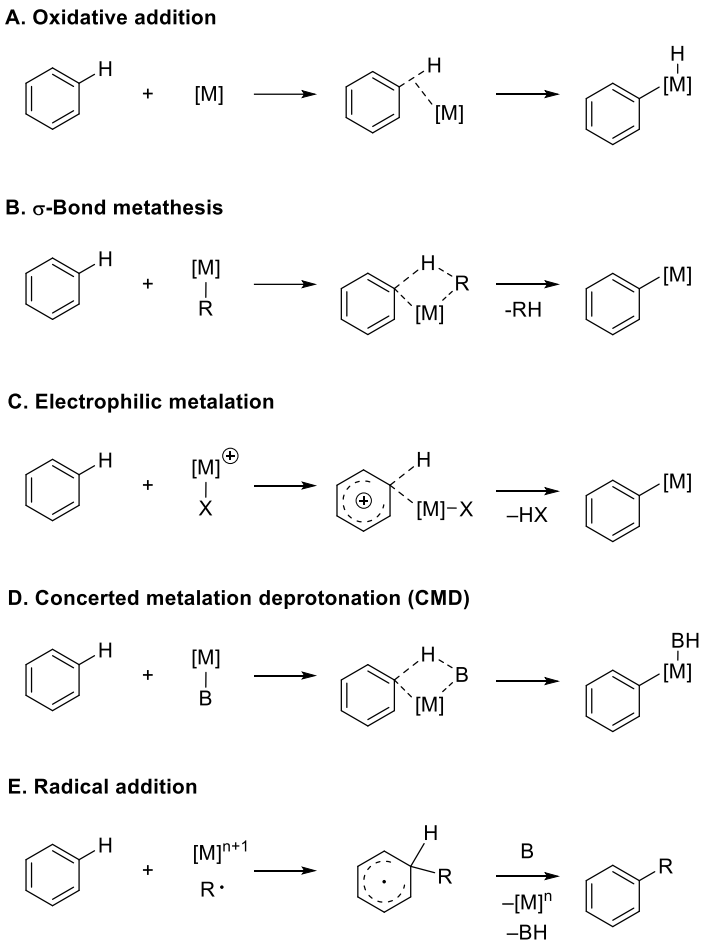

Scheme 3.2 Type of C(sp^2)–H functionalization strategies.

3.3 Substrate-controlled site-selective C(sp^2)–H functionalization strategy

Tremendous development was achieved in C–H functionalization in the past few decades under various mechanisms depending on the substrate, metal catalysts, and the reaction conditions. Apart from identifying the catalytic conditions to activate relatively inert C–H bonds, another challenge is achieving site-selective C–H functionalization of a single C–H bond from the rest of the ubiquitous C–H bonds

within a complex molecule. The site-selective C–H functionalization has been successfully developed by following three types of substrate-controlled strategies.

The most common strategy is the use of substrates that contain a directing group (DG) (Scheme 3.3A).[2, 7] This DG binds to the metal center and drives the catalyst to a proximal C–H bond. Oxidative addition to the C–H bond, as depicted in Scheme 3.2A, results in a metallacycle complex as the key intermediate. This process is also called the chelation-assisted C–H activation or cyclometallation because metallacycle intermediates are produced. In 1993, Murai and co-workers firstly reported a Ru-catalyzed ketone directed *ortho* C–H alkylation of aromatic compounds with alkenes (Scheme 3.3B).[8] Many different DGs have been designed, such as carbonyl derivatives, N-heterocycles, and amino acid groups. Although various site-selective C–H functionalization reactions have been achieved using this DG-assisted strategy, the installation and removal of DGs still limit their applicability.

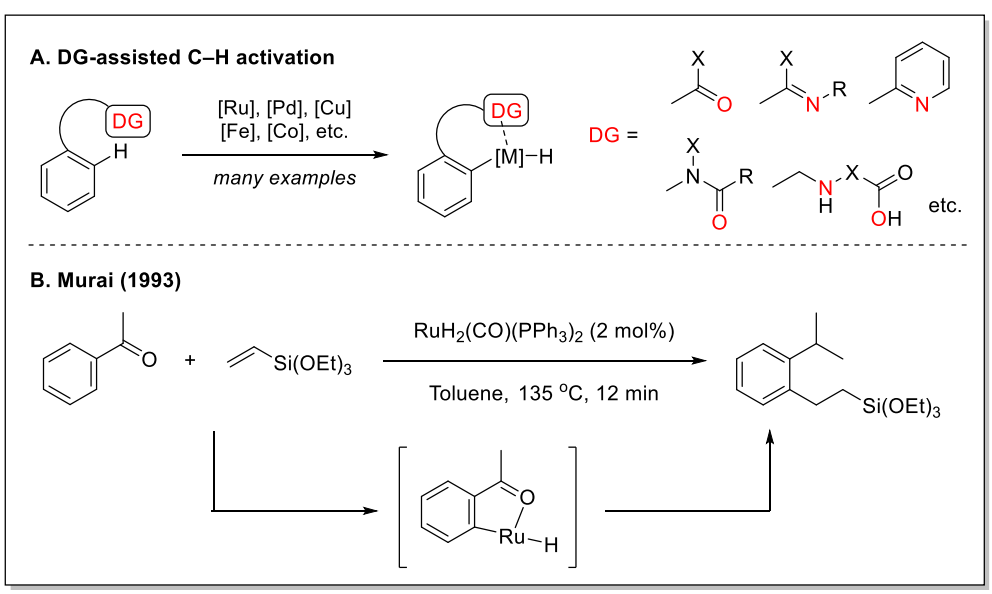

Scheme 3.3 Directing group assisted C–H functionalization.

Electronically activated substrates such as heteroarenes and electron-poor arenes have also been extensively studied to achieve site-selective C–H functionalization (Scheme 3.4A).[9] The introduction of heteroatoms or electron-withdrawing groups (EWGs) in the arene makes the C–H bonds electronically discriminable. The electronic bias dominates the overall reactivity and enables selective C–H activation. For example, electron-deficient arenes can efficiently undergo the CMD process with Pd catalysts, as depicted in Scheme 3.2D. Fagnou and co-workers reported the direct C–H arylation of a diverse set of electron-deficient heteroarenes and perfluoroarenes with aryl bromides (Scheme 3.4B and 3.4C).[10] The computational study of the CMD pathway on each C–H position was in good agreement with experimentally observed site-selectivities.[10a] Arene–metal π-complexation is also utilized to enhance the reactivity of C–H bonds. In 2013, Larrosa and co-workers reported that upon complexation, monofluorobenzenes become nearly as reactive as pentafluorobenzene in the coupling with iodoarenes (Scheme 3.4D).[11]

For decades, tremendous research has been studied in direct C–H functionalization by three substrate-controlled strategies: directing group-assisted, heteroarene-assisted, and electronic activation strategies. However, those strategies are not applicable to simple arenes, so the development of C–H functionalization methods for simple arenes is the current research goal.

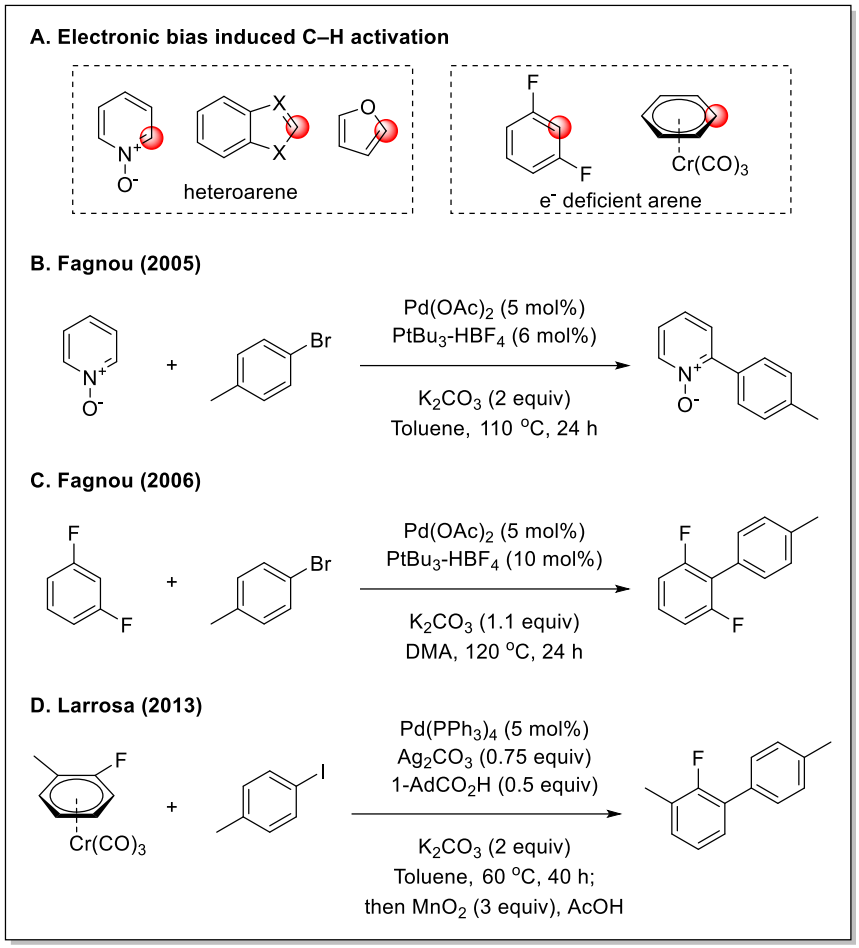

Scheme 3.4 C–H functionalization of electronically activated arenes.

3.4 Transition metal-catalyzed direct C–H arylation of simple arenes

Simple arenes are some of the most fundamental and abundant feedstock chemicals and widely used across all molecular sciences areas. One area of particular interest for organic chemists is the direct C–H arylation of simple arenes to rapidly access value-added biaryl products and complex materials.[12] This section describes the CMD-promoted direct C–H arylation of simple arenes, with experimental and theoretical mechanistic studies.[3d]

3.4.1 C–H arylation of simple arenes by CMD process

Direct C–H arylation, the reaction of aryl halides with arenes to form biaryl products, represents an attractive alternative to traditional cross-coupling reactions because it does not require pre-functionalized organometallic or main group reagents. The general mechanism of the direct C–H arylation with aryl halides is depicted in Scheme 3.5. First, oxidative addition of the aryl halide to the active catalyst (L_nM) generates the metal aryl complex. Ligand exchange with an external base facilitates the C–H bond cleavage following the CMD transition state. Subsequent reductive elimination of the diarylmetal complex furnishes the biaryl product and Pd precatalyst.

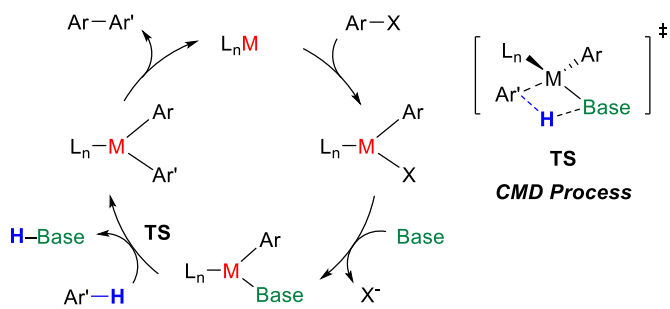

Scheme 3.5 C–H arylation of simple arenes via concerted metalation-deprotonation (CMD) process.

Fagnou group was the first to prove successful in the direct C–H arylation of completely unactivated arene, benzene (Scheme 3.6A).[13] A palladium-pivalate co-catalytic system exhibited unprecedented reactivity to functionalize benzene and other simple arenes efficiently. The pivalate ligands have proved to play a crucial role as a proton shuttle in the C–H bond cleavage step via a CMD pathway.

Computationally, the pivalate ligand's involvement in the transition state of benzene C–H bond cleavage resulted in an energy difference of 1.3 kcal/mol compared to the bicarbonate anion (24.9 vs. 26.2 kcal/mol).[10a]

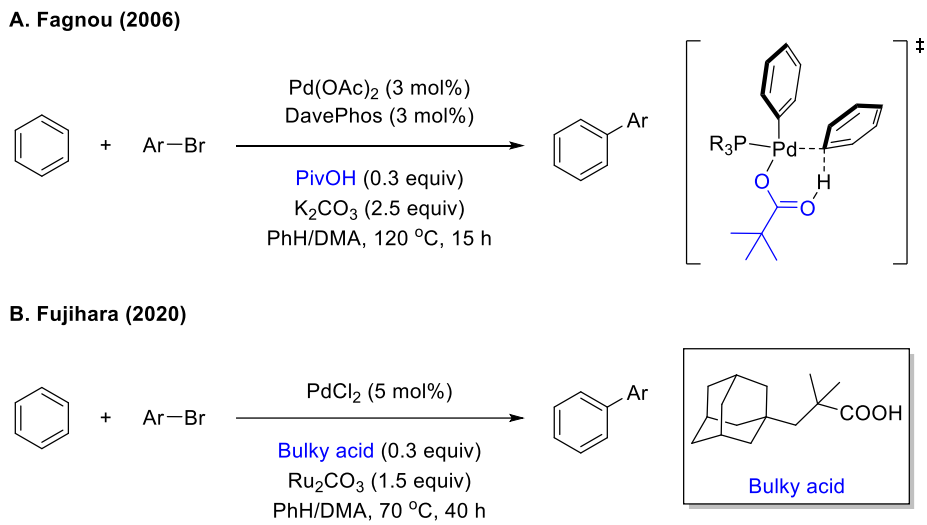

Scheme 3.6 C–H arylation of simple arenes via concerted metalation-deprotonation (CMD) process.

After the Fagnou's initial finding, various transition-metal/acid co-catalytic systems were applied in the intermolecular direct arylation reactions under mild conditions. Ackermann and co-workers applied 2,4,6-trimethylbenzoic acid and 1-adamantylcarboxylic acid as co-catalysts in ruthenium palladium-catalyzed C–H functionalization reactions.[14] Besides, Larrosa and co-workers used *o*-nitrobenzoic acid as an additive in the palladium-catalyzed C2-selective arylation of indoles at room temperature.[15] Recently, Fujihara and co-workers disclosed that the modification of acid co-catalyst could significantly lower the reaction temperature from 120 °C to 70 °C in the direct arylation of benzene without any loss of original reactivity (Scheme 3.6B).[16]

3.4.2 Cooperative bimetallic mechanism in Pd catalytic systems

Since the advent of CMD promoted direct C–H arylation, significant improvements have been achieved in the scope of arenes, reactivity, and selectivity through a better understanding of the metal/carboxylate-promoted CMD mechanism.[3a] In the early stage, most reaction mechanisms have been proposed based on the monometallic mechanism involving one active catalytic species, although several differences existed depending on the catalytic system and coupling partner. Recently, a new cooperative bimetallic mechanism involving two different catalytic species has been suggested.

As depicted in Scheme 3.4B above, the Fagnou group reported the direct C2-arylation of pyridine *N*-oxide (PyO) utilizing a $Pd(OAc)_2$ and P*t*Bu_3 catalytic system through the conventional monometallic mechanism.[10c] After four years, Hartwig and co-workers disclosed that the developed reaction operates via a cooperative bimetallic mechanism based on thorough mechanistic studies (Scheme 3.7).[17] In detail, cyclometalated dimeric complex **2** was generated from the oxidative addition complex **1** as the kinetic studies with complex **2** and stoichiometric experiments between two distinctive palladium–aryl species strongly supported that the complex **2** is responsible for the C−H activation of PyO. Based on the experimental evidence, the authors proposed a cooperative bimetallic mechanism where a single Pd species undergoes oxidative addition with ArBr, and the other cyclometalated Pd species performs C–H activation of PyO. Subsequent transmetalation and reductive elimination would afford the functionalized pyridine *N*-oxide and complete the overall catalytic cycle. This was the first experimental demonstration of cooperative bimetallic catalysis for the C–H arylation of arenes.

Gorelsky computationally supported that the cooperative bimetallic mechanism is favored in the C–H arylation reaction under the phosphine-based Pd catalytic systems.[18]

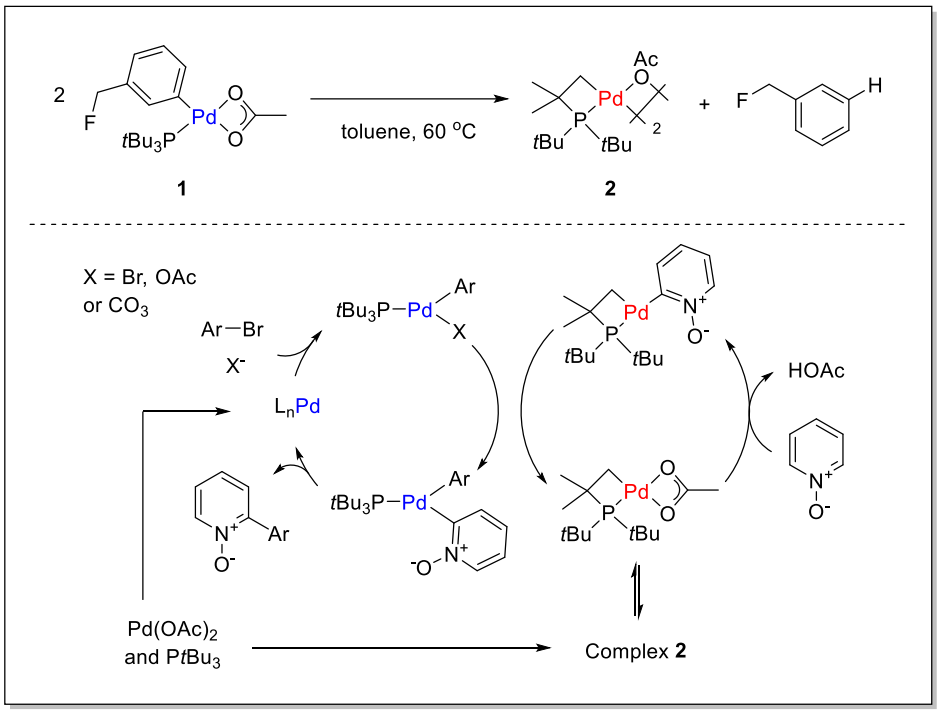

Scheme 3.7 Cooperative bimetallic mechanism of the direct arylation of pyridine *N*-oxide.

In addition to that, Stahl and co-workers revealed that the cooperative bimetallic mechanism is operative in the Pd-catalyzed aerobic oxidative coupling of *o*-xylenes.[19] In the proposed mechanism, parallel C–H activation occurs at two separate Pd species (Scheme 3.8). When the C–H bond cleavage step is the rate-limiting step in the catalytic cycle, first-order dependence on Pd concentration ([Pd]) should be displayed in both monometallic and bimetallic mechanisms. On

the other hand, the transmetalation step could become the rate-limiting step in a sufficiently low [Pd] range in the bimetallic mechanism, where a second-order dependence in [Pd] would be observed. The authors confirmed the first-order dependence at high [Pd] and a second-order dependence at low [Pd], clearly identifying the cooperative bimetallic mechanism being the actual catalytic cycle.

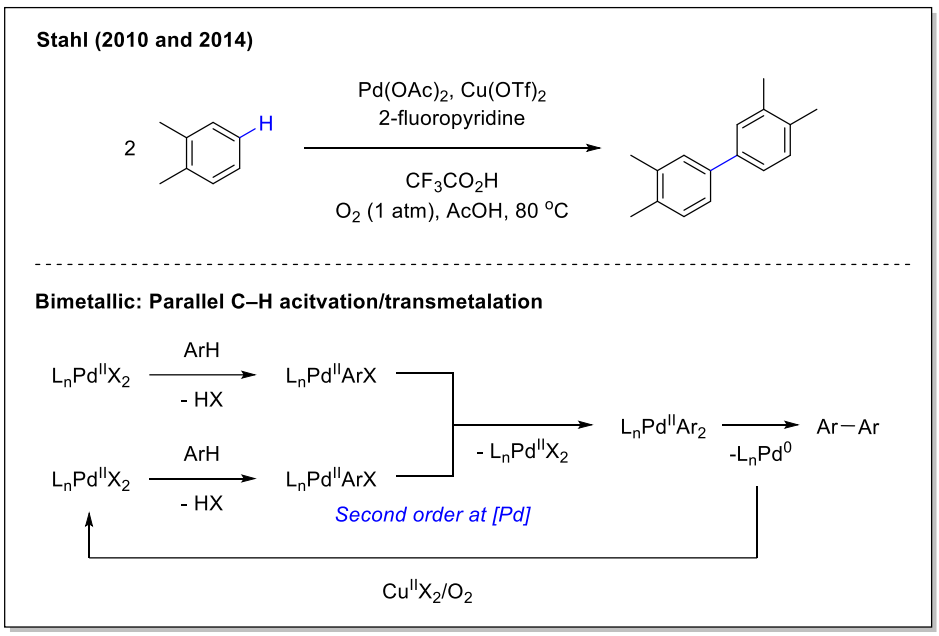

Scheme 3.8 Pd-catalyzed aerobic oxidative coupling of *o*-xylene.

Recently, Hong and co-workers developed a Pd-diimine catalyst to efficiently facilitate the direct C−H arylation of simple arenes with high TONs up to 290. Stoichiometric experiments with Pd oxidative addition complex and observation of the second-order kinetics at [Pd] in low [Pd] range supports the existence of a cooperative bimetallic mechanism for this reaction, consistent with Hartwig's suggestion.[20]

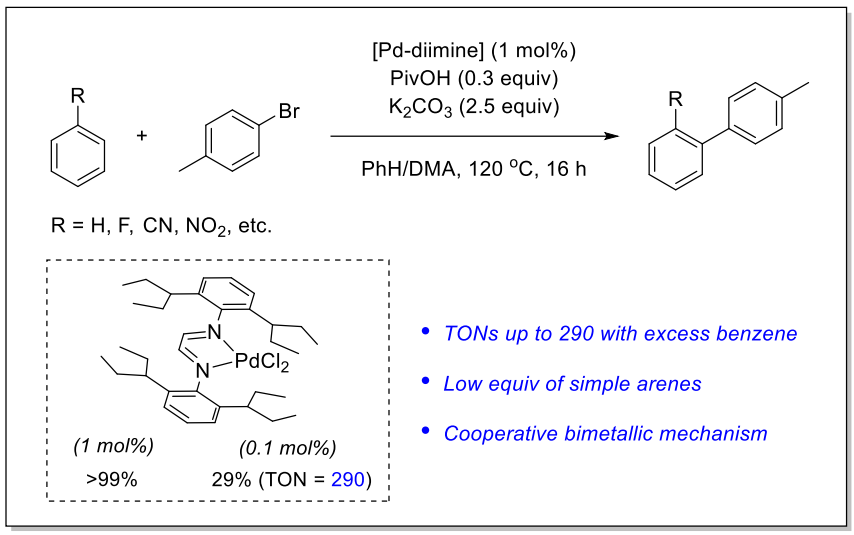

Scheme 3.9 Pd-diimine catalyzed direct C–H arylation of simple arenes.

3.5 Transition metal-catalyzed C–H alkylation of simple arenes

3.5.1 Introduction of C–H alkylation for the synthesis of alkylarenes

Alkylarenes are fundamental motifs in chemistry because they ubiquitously appear in fine chemicals and raw materials, impacting virtually all areas of chemical sciences. Some of these compounds are produced one million tons per year scale for the synthesis of surfactants, lubricants, and heat transfer fluids.[21] Traditionally, alkyl arenes have been synthesized through Friedel–Crafts alkylation reactions of arenes (Scheme 3.10A).[22] However, the restricted scope, the particular electronic requirements of the arene, the usual harsh conditions, and the rearrangement of alkyl fragment often diminish this reaction's utility. An alternative conventional method to prepare alkylarenes is the cross-coupling reaction of aryl (pseudo)halides or arylmetals with appropriate alkylation partners (Scheme 3.10B).[23] However, the atom economy and efficiency of these processes are compromised by the necessity of prefunctionalized arenes that usually require

multi-step sequences to produce.

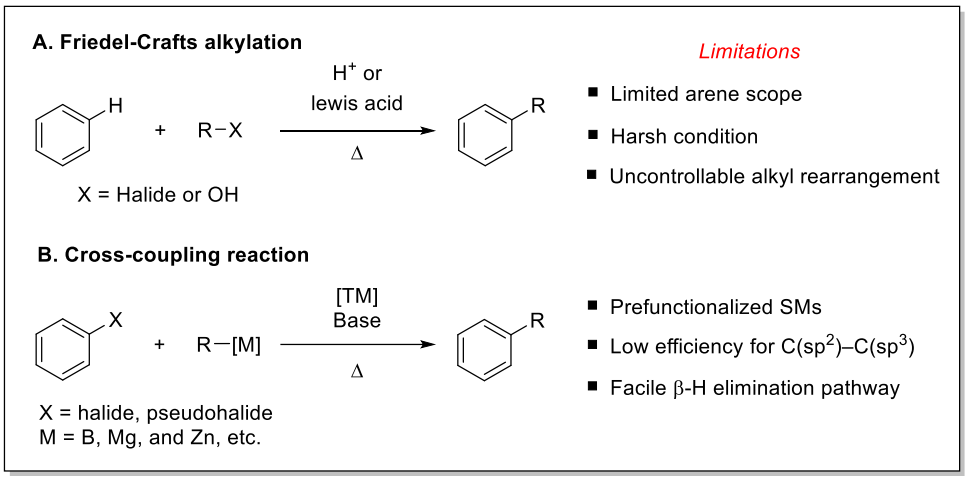

Scheme 3.10 Conventional syntheses of alkylarenes.

3.5.2 Recent progress in the transition metal-catalyzed C–H alkylation of arenes

Since the significant research progress in the field of direct C–H arylation, transition metal-catalyzed direct C–H alkylation of (hetero)arenes with either alkyl (pseudo)halides or alkyl metals (mainly boron or tin derivatives) has emerged as an attractive alternative approach (Scheme 3.11A).[24] This strategy overcomes some of the problems associated with traditional routes, but it still exhibited limited applicability as directing group-implemented arenes,[25] heteroarenes,[26] activated electron-deficient arenes,[27] or intramolecular alkylation systems[28] was essential (Scheme 3.11B). This is due to the challenging oxidative addition to the alkyl electrophile and the high C–H activation barrier of the unactivated arenes (C–H bond dissociation energy, ~110 kcal/mol).[29] Such high reaction barriers inevitably lead to a requirement of harsh reaction conditions, which accompany undesirable

side reactions, such as β–hydride elimination of the intermediary metal-alkyl species. (Scheme 3.11C).

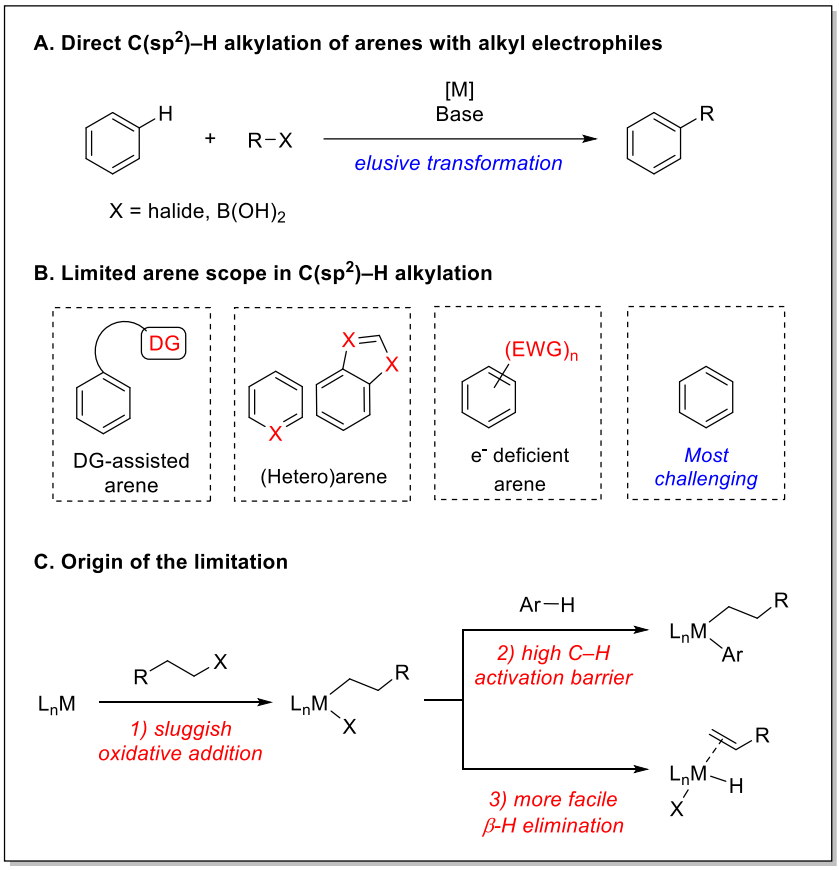

Scheme 3.11 Direct C(sp^2)–H alkylation of arenes with alkyl electrophiles.

Direct alkylation reactions of simple arenes with alkenes are also perfectly atom-economical since no atom is lost throughout the transformation (Scheme 3.12). This reaction is also called the hydroarylation of alkenes with arenes. The reaction involves the direct C–H activation of benzene and a migratory insertion to the olefin, furnishing the corresponding alkylbenzene products. On the other hand, the main issue of this reaction is controlling the selectivity between the branched

and linear isomers. For example, Matsumoto and Periana firstly reported the linear-selective alkylation of benzene with unactivated alkenes by using a well-defined binuclear iridium(III) complex.[30] However, low selectivity (~2:1, linear:branched) was observed due to the difficulties in controlling the migratory insertion process. Since the initial finding, well-defined ruthenium and platinum catalysts were developed by Gunnoe[31] and Goldberg[32] groups for the C–H alkylation of simple arenes with alkenes, but still gave very low regioselectivities. In 2020, Hartwig and Nakao succeeded in the development of linear selective C–H alkylation of benzene by utilizing a nickel system bearing a highly sterically hindered NHC ligand. However, the reaction did not apply to alkenes bearing polar functional groups presumably due to the limited coordination site of the Ni catalyst.[33]

3.5.3 Homolytic aromatic substitution of benzene

Radical-based aromatic C–H functionalizations, so-called homolytic aromatic substitution (HAS) reactions, have emerged as atom-efficient and direct routes to substituted arenes.[5] The number of reports on intermolecular variants of HAS that take advantage of electron transfer induced by the strong base, transition-metal catalysts, and photoredox catalysts has grown significantly. Many successful examples, such as arylation, fluoroalkylation, and alkylation, have been developed.[34] Compared with the Friedel-Craft alkylation reaction, radical-mediated reactions generally give a single constitutional isomer because the rearrangement of carbon-centered radicals is significantly slower than that of their cationic congener.[35]

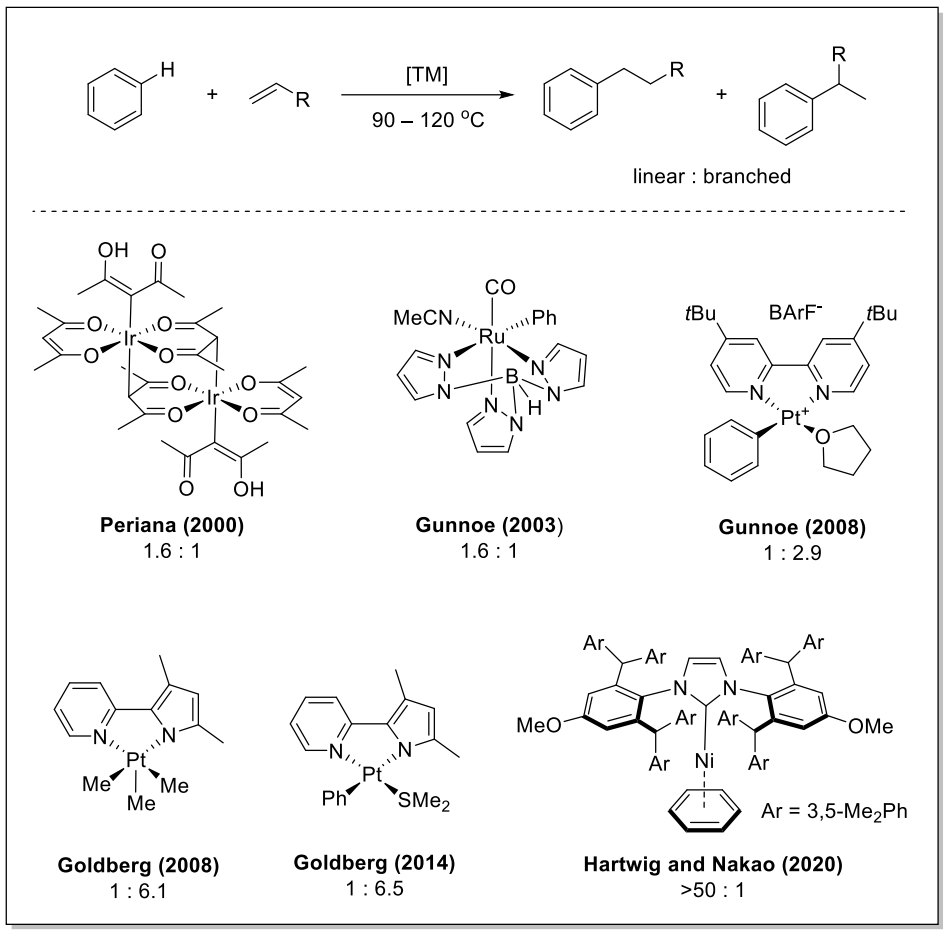

Scheme 3.12 Direct C(sp^2)–H alkylation of arenes with alkenes.

In 1966, Uzelmeier and co-workers investigated the homolytic aromatic cyclohexylation of benzene with cyclohexane utilizing stoichiometric di-*t*-butyl peroxide (DTBP) as the radical initiator (Scheme 3.13).[36] It is a pioneering work in investigating the interaction of secondary alkyl radical with various simple arenes. Because the insertion of nucleophilic alkyl radicals to the electron-rich π-system of arenes is very sluggish, only a low efficiency was observed. The reactive alkyl radical was shown to be more prone to side reactions, such as homodimerization and hydrogen atom transfer (HAT), compared to the desired arene insertion.

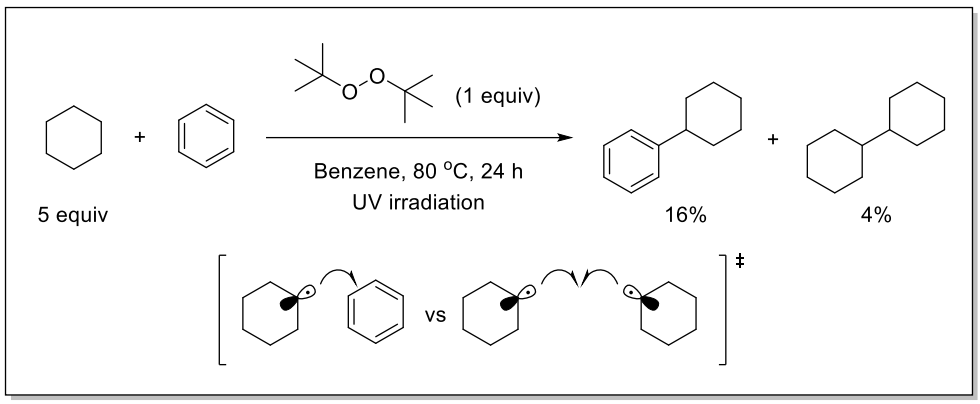

Scheme 3.13 Pioneering work of homolytic aromatic cyclohexylation.

Recently, Adsool and Rossi groups reported the C–H alkylation of benzene with alkyl iodides utilizing a stoichiometric amount of radical initiators such as AIBN and KO*t*Bu (Scheme 3.14A and 3.14B).[37] However, only sterically congested tertiary alkyl iodides can be utilized to rule out side-reactions such as homocoupling and elimination. In 2016, direct C–H alkylation of benzene with alkylboronic acids in the presence of $Mn(OAc)_3$ was developed by Rodriquez and co-workers (Scheme 3.14C).[38] The reaction involves $Mn(OAc)_3$ mediated single-electron oxidation of alkylboronic acids and the σ-complex intermediates.

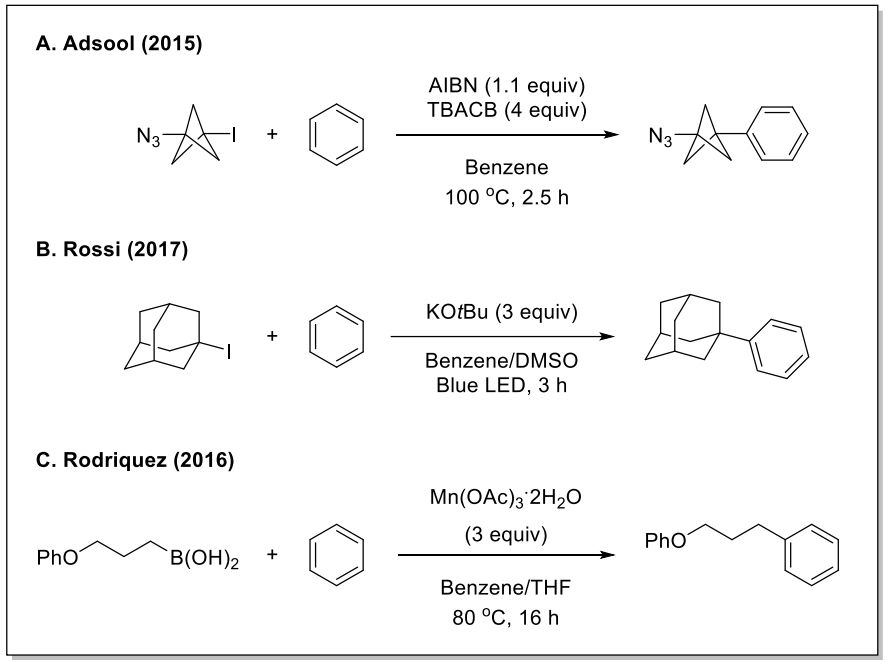

Scheme 3.14 Homolytic aromatic alkylation of benzene.

3.6 Conclusion

This chapter summarizes the historical development in the direct C(sp^2)–H functionalization area. Direct C–C bond formation through C–H arylation and the alkylation of simple arenes is one of the most popular topics in organic chemistry in recent decades, presenting an elegant alternative for the synthesis of biaryls and alkylarenes in a cost-effective and environmentally benign manner. The chemistry of C(sp^2)–H functionalization can be understood in terms of several criteria, such as the type of C–H functionalization mechanism and arene activation strategy. Although the low reactivity of the C–H bond and difficulty of controlling selectivity have made the related transformations challenging, they are envisioned to provide general C–H functionalization methods that contain higher synthetic values.

Despite these advances, the developed strategies bear several limitations. For example, the fundamental mechanistic studies of the direct C–H arylation via the CMD process are still lacking considering the substantial value of this process. Great opportunities remain for developing CMD-promoted new catalytic C–H arylation systems with high reactivity and selectivity. Hence, the scope of C–H alkylation is still minimal due to the facile side reactions and isomerization processes. Therefore, a novel catalytic system operating under versatile and mild reaction conditions is necessary to streamline the synthesis of alkylarenes via the direct alkylation of non-activated C(sp^2)–H bonds.

3.7 References

(1) Hartwig, J. F.; Larsen, M. A. *ACS Cent. Sci.* **2016**, *2*, 281.

(2) Lyons, T. W.; Sanford, M. S. *Chem. Rev.* **2010**, *110*, 1147.

(3) (a) Ackermann, L. *Chem. Rev.* **2011**, *111*, 1315. (b) Lersch, M.; Tilset, M. *Chem. Rev.* **2005**, *105*, 2471. (c) Balcells, D.; Clot, E.; Eisenstein, O. *Chem. Rev.* **2010**, *110*, 749. (d) Lapointe, D.; Fagnou, K. *Chem. Lett.* **2010**, *39*, 1118. (e) Hari, D. P.; König, B. *Angew. Chem. Int. Ed.* **2013**, *52*, 4734.

(4) Gurry, M.; Aldabbagh, F. *Org. Biomol. Chem.* **2016**, *14*, 3849.

(5) Augood, D. R.; Hey, D. H.; Nechvatal, A.; Williams, G. H. *Nature* **1951**, *167*, 725.

(6) Duncton, M. A. J. *MedChemComm* **2011**, *2*, 1135.

(7) Yang, J. *Org. Biomol. Chem.* **2015**, *13*, 1930.

(8) Murai, S.; Kakiuchi, F.; Sekine, S.; Tanaka, Y.; Kamatani, A.; Sonoda, M.; Chatani, N. *Nature* **1993**, *366*, 529.

(9) (a) Rossi, R.; Bellina, F.; Lessi, M.; Manzini, C. *Adv. Synth. Catal.* **2014**, *356*, 17. (b) Ackermann, L.; Vicente, R.; Kapdi, A. R. *Angew. Chem. Int. Ed.* **2009**, *48*, 9792.

(10) (a) Gorelsky, S. I.; Lapointe, D.; Fagnou, K. *J. Am. Chem. Soc.* **2008**, *130*, 10848. (b) Lafrance, M.; Rowley, C. N.; Woo, T. K.; Fagnou, K. *J. Am. Chem. Soc.* **2006**, *128*, 8754. (c) Campeau, L.-C.; Rousseaux, S.; Fagnou, K. *J. Am. Chem. Soc.* **2005**, *127*, 18020.

(11) Ricci, P.; Krämer, K.; Cambeiro, X. C.; Larrosa, I. *J. Am. Chem. Soc.* **2013**, *135*, 13258.

(12) Kuhl, N.; Hopkinson, M. N.; Wencel-Delord, J.; Glorius, F. *Angew. Chem. Int. Ed.* **2012**, *51*, 10236.

(13) Lafrance, M.; Fagnou, K. *J. Am. Chem. Soc.* **2006**, *128*, 16496.

(14) (a) Ackermann, L.; Novák, P. *Org. Lett.* **2009**, *11*, 4966. (b) Ackermann, L.; Vicente, R. *Org. Lett.* **2009**, *11*, 4922.

(15) Lebrasseur, N.; Larrosa, I. *J. Am. Chem. Soc.* **2008**, *130*, 2926.

(16) Tanji, Y.; Hamaguchi, R.; Tsuji, Y.; Fujihara, T. *Chem. Commun.* **2020**, *56*, 3843.

(17) Tan, Y.; Barrios-Landeros, F.; Hartwig, J. F. *J. Am. Chem. Soc.* **2012**, *134*, 3683.

(18) Gorelsky, S. I. *Organometallics* **2012**, *31*, 4631.

(19) (a) Wang, D.; Izawa, Y.; Stahl, S. S. *J. Am. Chem. Soc.* **2014**, *136*, 9914. (b) Izawa, Y.; Stahl, S. S. *Adv. Synth. Catal.* **2010**, *352*, 3223.

(20) Kim, J.; Hong, S. H. *ACS. Catal.* **2017**, *7*, 3336.

(21) (a) Kocal, J. A.; Vora, B. V.; Imai, T. *Appl. Catal. A* **2001**, *221*, 295. (b) Almeida, J. L. G. d.; de Almeida, J. L. G.; Dufaux, M.; Ben Taarit, Y.; Naccache, C. *J. Am. Oil Chem. Soc.* **1994**, *71*, 675.

(22) (a) Gilman, H.; Meals, R. N. *J. Org. Chem.* **1943**, *08*, 126. (b) Sharman, S. H. *J. Am. Chem. Soc.* **1962**, *84*, 2945.

(23) Johansson Seechurn, C. C. C.; Kitching, M. O.; Colacot, T. J.; Snieckus, V. *Angew. Chem. Int. Ed.* **2012**, *51*, 5062.

(24) Ye, S.; Xiang, T.; Li, X.; Wu, J. *Org. Chem. Front.* **2019**, *6*, 2183.

(25) Zhu, R.-Y.; He, J.; Wang, X.-C.; Yu, J.-Q. *J. Am. Chem. Soc.* **2014**, *136*, 13194.

(26) Wu, X.; See, J. W. T.; Xu, K.; Hirao, H.; Roger, J.; Hierso, J.-C.; Zhou, J.

Angew. Chem. Int. Ed. **2014**, *53*, 13573.

(27) Tu, G.; Yuan, C.; Li, Y.; Zhang, J.; Zhao, Y. *Angew. Chem. Int. Ed.* **2018**, *57*, 15597.

(28) Venning, A. R. O.; Bohan, P. T.; Alexanian, E. J. *J. Am. Chem. Soc.* **2015**, *137*, 3731.

(29) Blanksby, S. J.; Ellison, G. B. *Acc. Chem. Res.* **2003**, *36*, 255.

(30) Matsumoto, T.; Taube, D. J.; Periana, R. A.; Taube, H.; Yoshida, H. *J. Am. Chem. Soc.* **2000**, *122*, 7414.

(31) (a) Lail, M.; Arrowood, B. N.; Gunnoe, T. B. *J. Am. Chem. Soc.* **2003**, *125*, 7506. (b) McKeown, B. A.; Prince, B. M.; Ramiro, Z.; Gunnoe, T. B.; Cundari, T. R. *ACS. Catal.* **2014**, *4*, 1607.

(32) (a) Luedtke, A. T.; Goldberg, K. I. *Angew. Chem. Int. Ed.* **2008**, *47*, 7694. (b) Clement, M. L.; Grice, K. A.; Luedtke, A. T.; Kaminsky, W.; Goldberg, K. I. *Chem. Eur. J.* **2014**, *20*, 17287.

(33) Saper, N. I.; Ohgi, A.; Small, D. W.; Semba, K.; Nakao, Y.; Hartwig, J. F. *Nat. Chem.* **2020**, *12*, 276.

(34) (a) Shirakawa, E.; Hayashi, T. *Chem. Lett.* **2012**, *41*, 130. (b) Gao, P.; Gu, Y.-R.; Duan, X.-H. *Synthesis* **2017**, *49*, 3407.

(35) Carey, F. A.; Sundberg, R. J., *Advanced Organic Chemistry: Part A: Structure and Mechanisms*. Springer: 2008; p 1199.

(36) Shelton, J. R.; Uzelmeier, C. W. *J. Am. Chem. Soc.* **1966**, *88*, 5222.

(37) (a) Thirumoorthi, N. T.; Jia Shen, C.; Adsool, V. A. *Chem. Commun.* **2015**, *51*, 3139. (b) Budén, M. E.; Bardagí, J. I.; Puiatti, M.; Rossi, R. A. *J. Org. Chem.* **2017**, *82*, 8325.

Chapter 4. Photoinduced Palladium Catalysis in Organic Transformation

4.1 Introduction

Palladium catalysis is a highly useful and attractive methodology in modern organic chemistry. Although palladium-catalyzed cross-coupling and C–H functionalization reactions have advanced significantly, most of the works have mainly focused on developing and applying the ground-state reactivity of palladium catalysts through the two-electron redox cycle. In contrast to classical palladium catalysis, recently developed photoinduced palladium catalysis operates through single-electron transfer processes, which enable both radical and classical Pd-type coupling chemistry. This unique reactivity has led to the development of many novel transformations that are difficult to achieve through the traditional ground-state Pd(0) catalysis. In this chapter, the progress in the photoinduced palladium catalysis, including the scope and mechanistic aspects, is discussed.

4.2 General concept of photoexcited palladium catalysis

Photoinduced palladium catalysis is an emerging field of catalysis (Scheme 4.1).[1] The photoirradiation of the Pd(0) complex facilitates the single-electron transfer (SET) process under mild conditions.[2] Such processes generate a hybrid Pd/radical species, which exhibit both radical and classical Pd-type reactivities. Besides, the photoexcitation of the Pd(II) complex can also lead to a geometric exchange from square planar to tetrahedral, maintaining the reactivity of hybrid Pd/radical species.[2-3] These unique mechanistic properties can solve the challenging problems in the conventional Pd-catalyzed alkylation chemistry associated with sluggish oxidative addition to alkyl electrophiles and the competitive side reactions such as β-H elimination and protonation of the resulting alkyl palladium intermediates.[4] Since the visible-light induced Pd catalysis area is in its infancy, detailed mechanistic information to construct a complete catalytic turnover cycle is still lacking. Nevertheless, various novel transformations that cannot be achieved through the traditional thermal Pd chemistry have been achieved through photoinduced palladium catalysis.

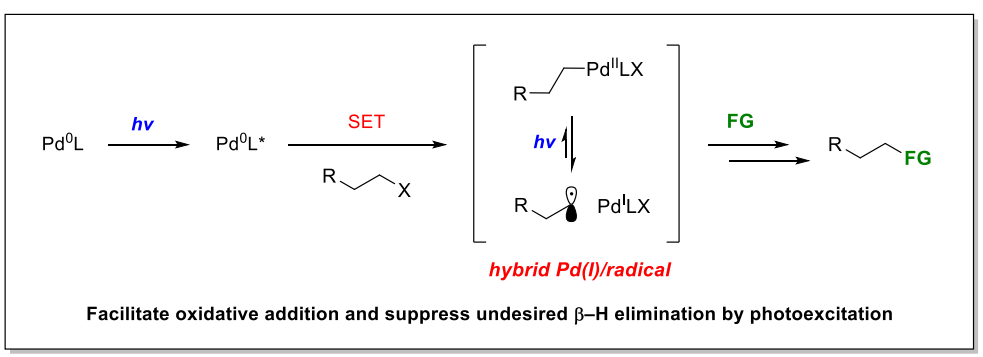

Scheme 4.1 General mechanism of photoexcited palladium catalysis.

4.3 Visible-light induced Pd-catalyzed cross-coupling reactions

4.3.1 Coupling with C(sp^2)–X electrophiles

The first visible-light induced generation of hybrid Pd(I)/radical species was reported by the Gevorgyan group. In 2016, Gevorgyan and co-workers developed the direct desaturation of silyl ethers to silyl enol ethers (Scheme 4.2).[5] The critical hybrid Pd(I)/aryl radical species was generated under the mild photoinduced conditions from an aryl iodide and $Pd(OAc)_2$/bisphosphine catalytic system. Aryl radical undergoes a 1,5-hydrogen atom transfer (HAT) process with respect to the silyl ether substrate to generate thermodynamically more stable α-oxy carboradicals. Four independent pathways were proposed to produce the corresponding silyl enol ether and complete the catalytic cycle: 1) radical recombination with Pd(I) followed by β-H elimination, 2) a direct β-H atom elimination with Pd(I), 3) oxidation by Pd(I) into cationic intermediate followed by deprotonation, and 4) iodine atom-transfer followed by E2 elimination. This strategy was also expanded to the selective remote desaturation of aliphatic amines.[6]

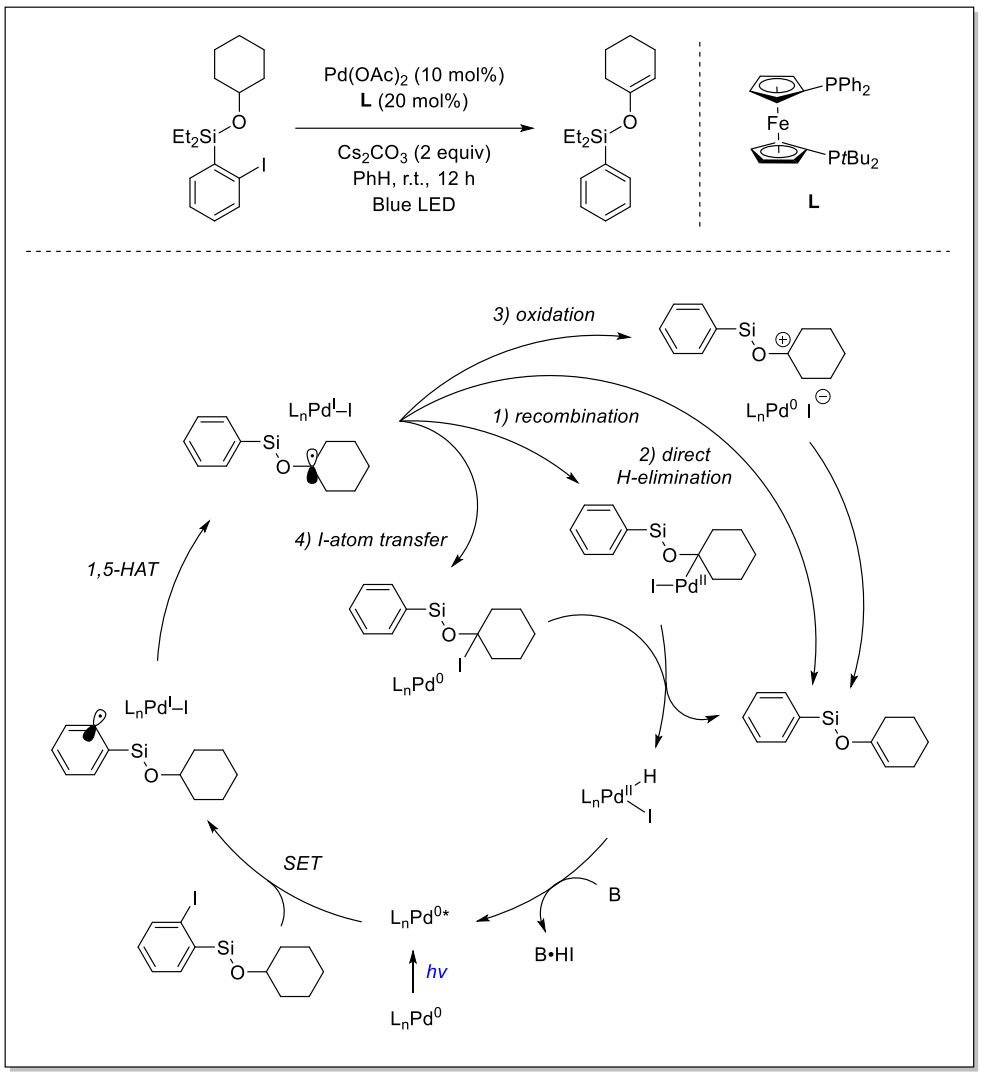

Scheme 4.2 Pioneering work of the photoinduced generation of hybrid Pd(I)/radical: selective oxidation of silyl ethers into silyl enol ethers.

After two years, the same group applied this photoexcited Pd chemistry to 1,5-HAT/iodine atom-transfer radical cyclization, supporting that the fourth iodine atom-transfer followed by E2 elimination pathway is the most plausible mechanism (Scheme 4.3).[7]

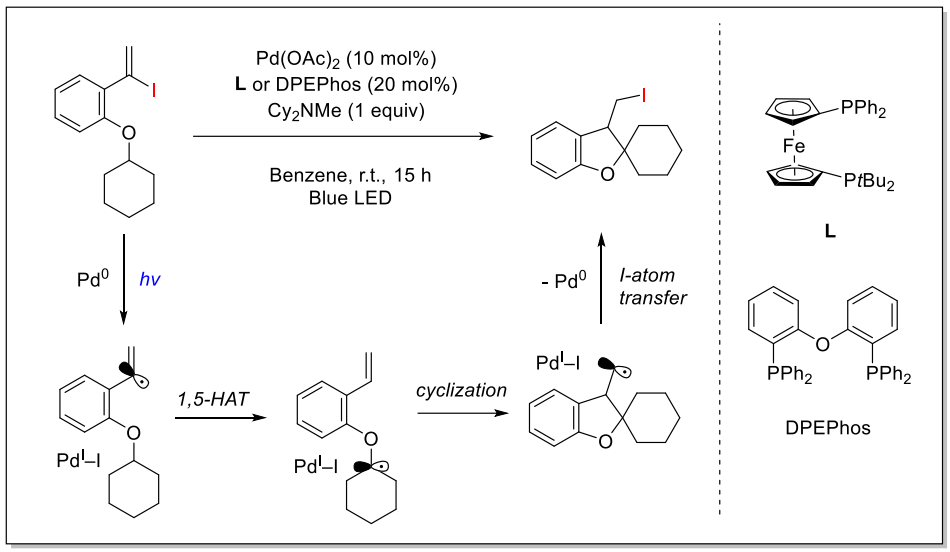

Scheme 4.3 Photoinduced Pd-catalyzed atom-transfer radical cyclization.

Palladium photocatalysis can also dramatically accelerate well-known Pd-catalyzed Heck and Negishi cross-coupling reactions with aryl halides. In 2010, the Köhler group reported a visible-light accelerated the Heck coupling reaction of bromobenzene with styrene (Scheme 4.4A).[8] Instead of the hybrid Pd/radical driven transformation, the author proposed that the light-irradiation might accelerate the reduction of off-cycle Pd(II) complex to an active Pd(0) catalyst. In 2018, the Alcázar group reported a light-accelerated Negishi coupling reaction of aryl bromides and chlorides with organozinc reagents (Scheme 4.4B).[9] Pd(0)-Zn complex absorbs blue light and accelerates the oxidative addition process. Notably, the scope of this light-accelerated Negishi coupling reaction was broader than that under conventional thermal conditions.

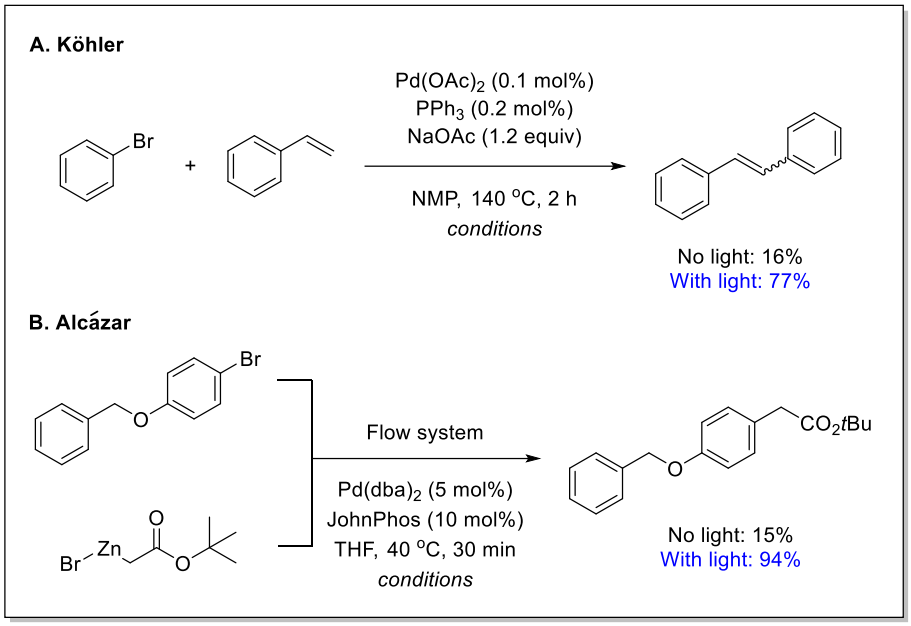

Scheme 4.4 Light-accelerated Pd-catalyzed cross-coupling reactions.

4.3.2 Cross-coupling with alkyl electrophiles

In the traditional Pd-catalyzed cross-coupling reactions, the coupling reaction with alkyl electrophiles is always problematic because of the slow oxidative addition and the facile undesired β-H elimination side reaction. The employment of photoexcited palladium catalysis leads to remarkable progress in the Pd-catalyzed cross-coupling chemistry regarding alkyl electrophiles.

In 2017, the Gevorgyan group reported the first Heck reaction of alkyl halides catalyzed by photoinduced $Pd(OAc)_2$/XantPhos catalytic system at room temperature (Scheme 4.5A).[10] However, the reaction was limited to primary and secondary alkyl halides with vinyl (hetero)arenes. In the same year, the Fu group developed a Heck reaction of vinyl (hetero)arenes,[4] by utilizing a dual phosphine ligand system for the first time, where a broad range of alkyl bromides, even

tertiary alkyl bromides, smoothly engaged in coupling reactions (Scheme 4.5B).

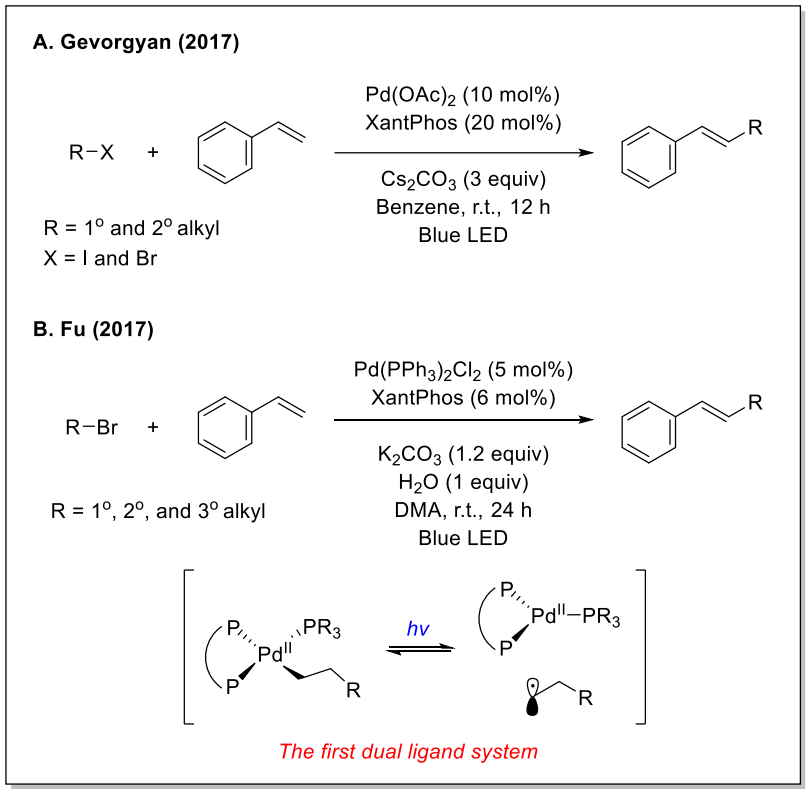

Scheme 4.5 Pioneering work of the photoinduced Pd-catalyzed Heck reaction.

After the pioneering works by the Gevorgyan and Fu groups, redox-active esters (*N*-(acyloxy)phthalimide esters, NHPs) have also been proved to be suitable alkyl coupling partners for photoinduced Pd catalysis by the Glorius[11] and Fu[12] groups. (Scheme 4.6A and 4.6B). In addition to the alkyl coupling partner, the broad scope of olefin coupling partners was explored, such as silyl enol ethers or enamides to afford α-alkylated ketones and α-alkylated N-acyl ketimines (Scheme 4.6C).[13]

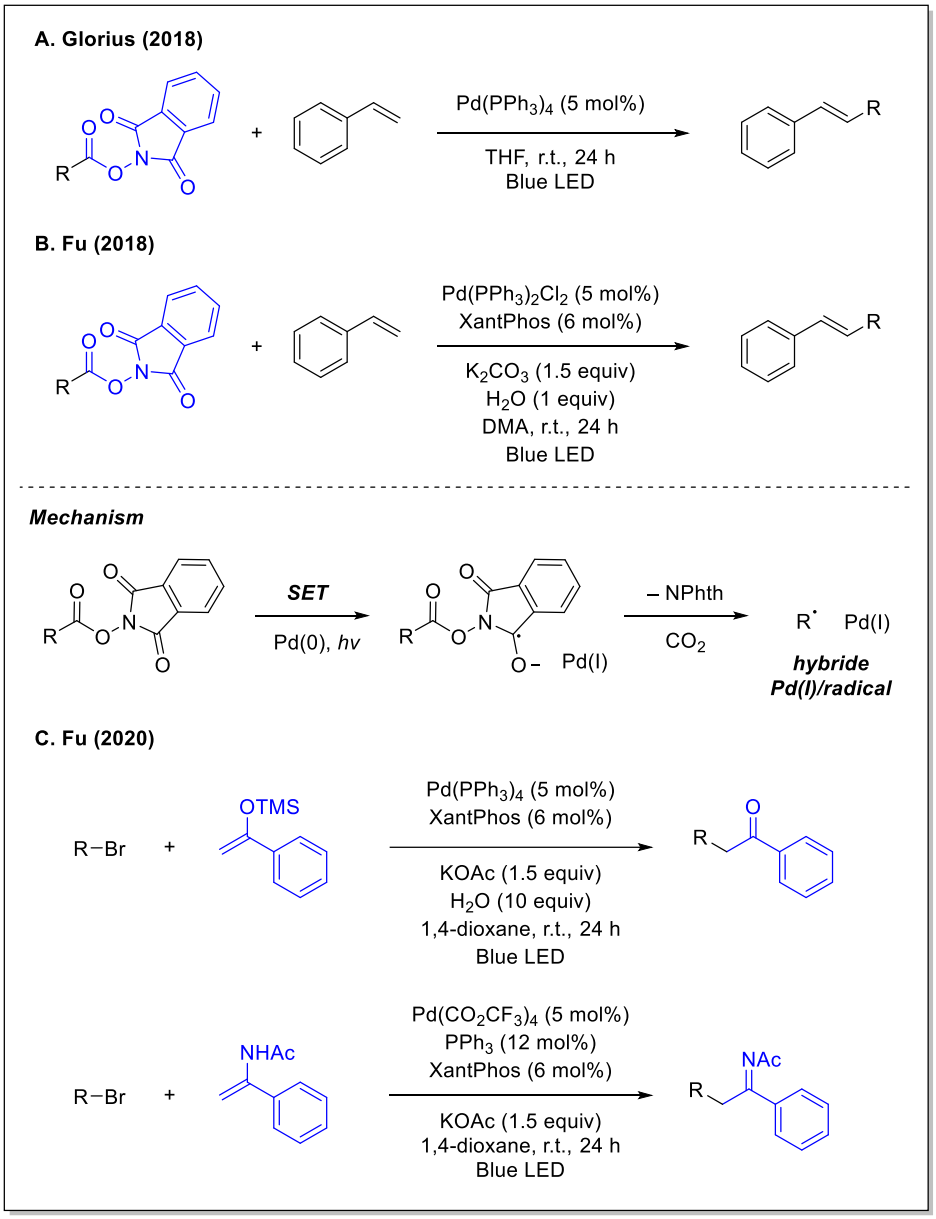

Scheme 4.6 Expansion of coupling substrates.

In 2019, the Rueping group reported the decarboxylative Heck reaction of α,β-unsaturated acids with alkyl bromides (Scheme 4.7).[2] Importantly, through the DFT computational studies, a single-electron reduction of alkyl bromides by photoexcited Pd(0) complex to form alkyl radical was shown barrierless. The

oxidative addition of the alkyl bromides to ground state Pd(0) is highly energy demanding (>40 kcal/mol). Hence, the Rueping group proved that the proposed hybrid Pd(I)/radical mechanism could be theoretically operative.

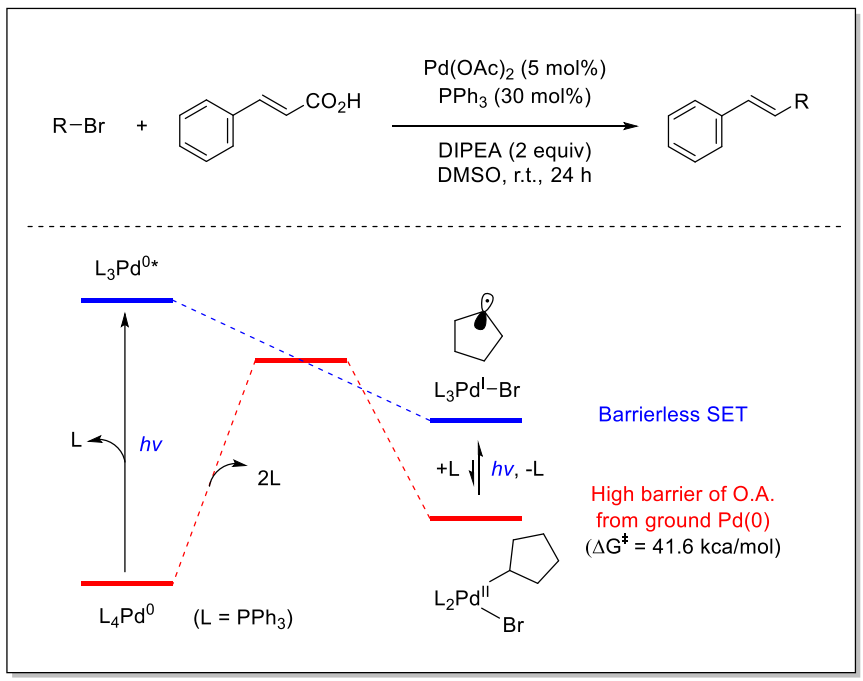

Scheme 4.7 Photoinduced oxidative addition of alkyl halide.

4.4 Visible-light induced Pd-catalyzed C–H alkylation

In 2017, the Yu group reported the first photoinduced Pd-catalyzed α-C(sp^3)–H alkylation of *N*-aryl tetrahydroisoquinolines (Scheme 4.8).[14] The proposed radical-radical coupling mechanism is depicted in Scheme 4.8. Single-electron reduction of an alkyl bromide by photoexcited Pd(0) generates the Pd(I)/alkyl radical hybrid species. After that, single-electron oxidation of the electron-rich tetrahydroisoquinoline by Pd(I) generates a radical cation species and regenerates the Pd(0) catalyst. Deprotonation of radical cation species produces the

corresponding stable α-amino benzylic radical, which eventually undergoes radical-radical coupling with the alkyl radical to afford the desired product.

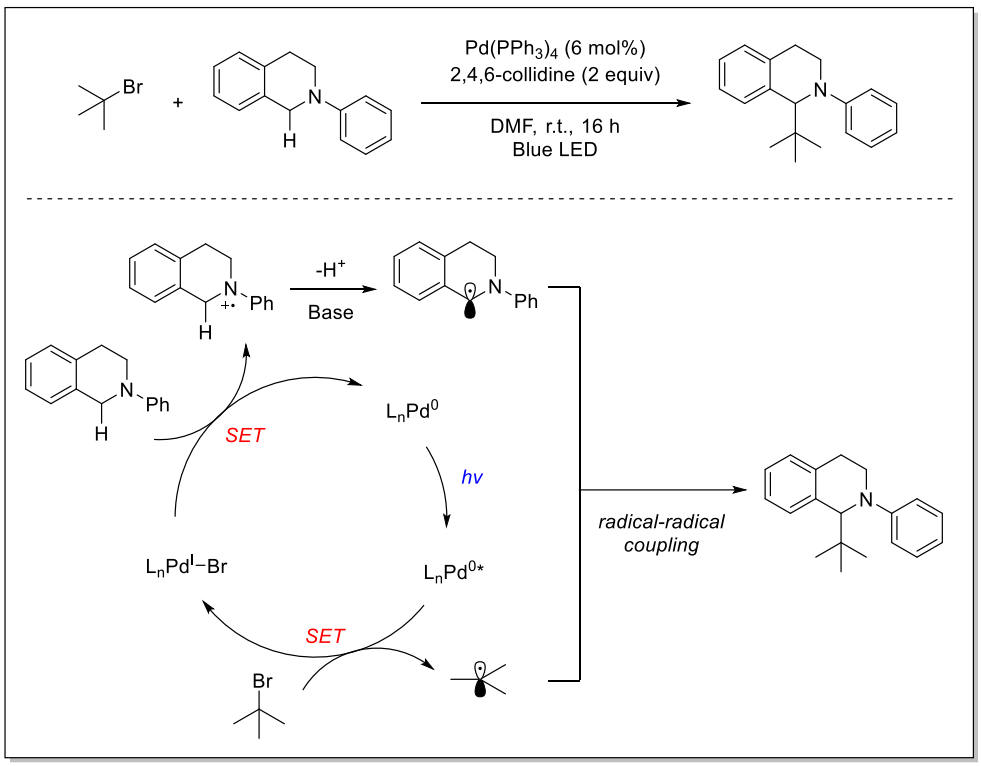

Scheme 4.8 Photoinduced Pd-catalyzed C(sp^3)–H alkylation.

Photoinduced Pd-catalyzed C(sp^2)–H alkylations of heteroarenes were reported by Yu[14], and Fu[15] groups (Scheme 4.9A and 4.9B). The commonly proposed Pd(0)/Pd(I) mechanism for the C(sp^2)–H alkylation reactions is depicted in Scheme 4.9 using thiophene as a representative arene substrate. The SET process as mentioned above generates the Pd(I)/alkyl radical hybrid species. The alkyl radical insertion to arenes produces the corresponding radical σ-complex intermediates. Subsequent single-electron oxidation of the intermediates by Pd(I)

followed by base-assisted deprotonation produces the alkylated arenes and regenerates the Pd(0) catalyst.

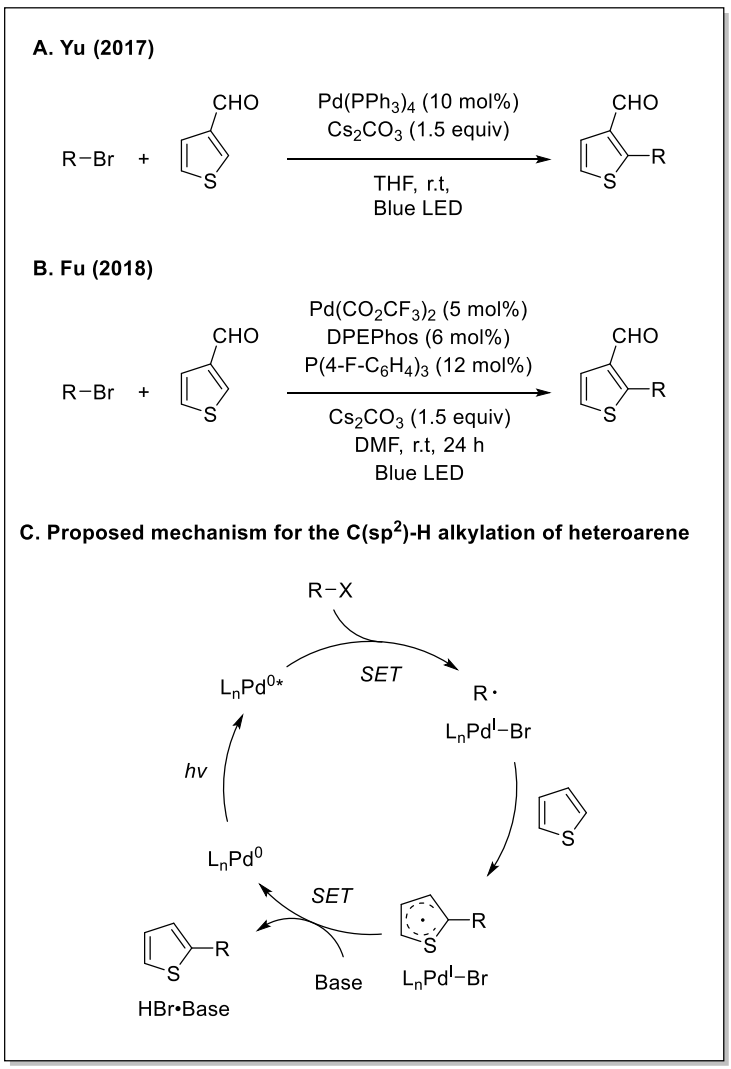

Scheme 4.9 Photoinduced Pd-catalyzed C(sp^2)–H alkylation of heteroarenes.

Meanwhile, the Zhou group reported a *para*-selective C(sp^2)–H alkylation of electron-deficient arenes with alkyl iodides (Scheme 4.10).[16] The abnormal Pd(I)/Pd(II) catalytic turnover cycle involving both Pd(I)- and Pd(II)-mediated SET

was proposed for the first time. Because the detailed mechanism is still not fully unveiled, both Pd(0)/Pd(I) and Pd(I)/Pd(II) mechanisms have been randomly proposed in the reported examples.

4.5 Visible-light induced Pd-catalyzed three-component cascade reaction

Recently, photoinduced Pd catalysis is applied to more advanced three-component cascade reactions to approach more complex architectures. In 2018, the Yu group reported the photoinduced Pd-catalyzed oxy-alkylation of allylamines with alkyl bromides and CO_2 to generate 2-oxazolidinone derivatives (Scheme 4.10).[17] It is noteworthy that the developed methodology was applied to synthesize the patent pharmaceutical, 11β-HSD1 inhibitors.

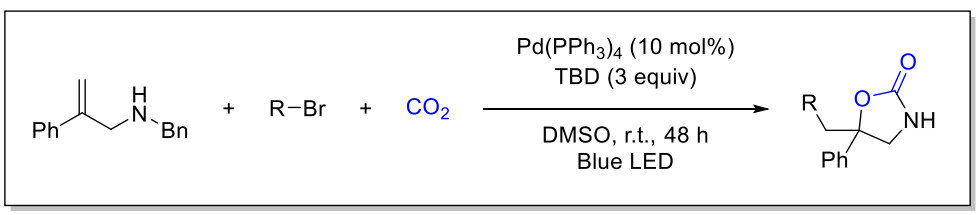

Scheme 4.10 Photoinduced Pd-catalyzed oxy-alkylation of allylamines with CO_2.

The Arndtsen group reported a photoinduced Pd-catalyzed carbonylation reaction under mild conditions (Scheme 4.11).[18] In contrast to thermal Pd catalysis, challenging aryl electrophile and difficult nucleophiles can be utilized to synthesize valuable carbonyl derivatives such as acid chloride, esters, amides, or ketones. Mechanistic studies with well-defined Pd(II) intermediates suggested that the excitation of Pd(0) and Pd(II) intermediates can respectively enhance the rates of both oxidative addition and reductive elimination.

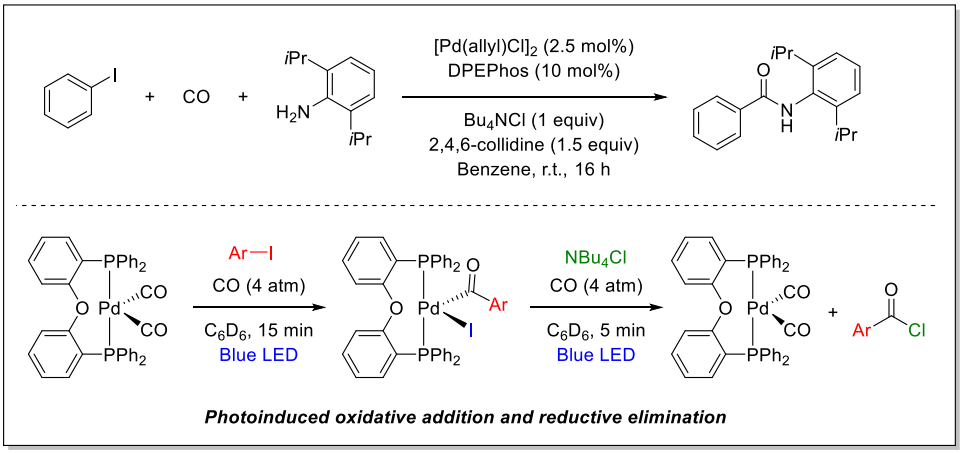

Scheme 4.11 Photoinduced Pd-catalyzed carbonylation.

The Glorius group reported a photoinduced Pd-catalyzed selective 1,4-difunctionalization of unactivated 1,3-diene by employing alkyl electrophiles (alkyl bromides and NHP esters) and various nucleophiles (C, N, O, S-based nucleophiles) (Scheme 4.12A).[19] Through the conceptual combination of the photoinduced Pd-catalyzed Heck reaction and the Tsuji-Trost allylic substitution, the cascade C(sp^3)–C(sp^3) bond and C–N bond formations proceeded selectively in excellent yields with high regio- and diastereoselectivities (mostly >95:5 dr, >20:1 rr). Almost at the same time, the Gevorgyan group reported the selective 1,2-aminoalkylation of dienes with alkyl iodides and various nucleophiles (C, N, O-based nucleophiles), catalyzed by a photoinduced Pd catalytic system (Scheme 4.12B).[20] Subtle differences in the Pd/phosphine ligand conditions resulted in the entirely opposing regioselectivity.

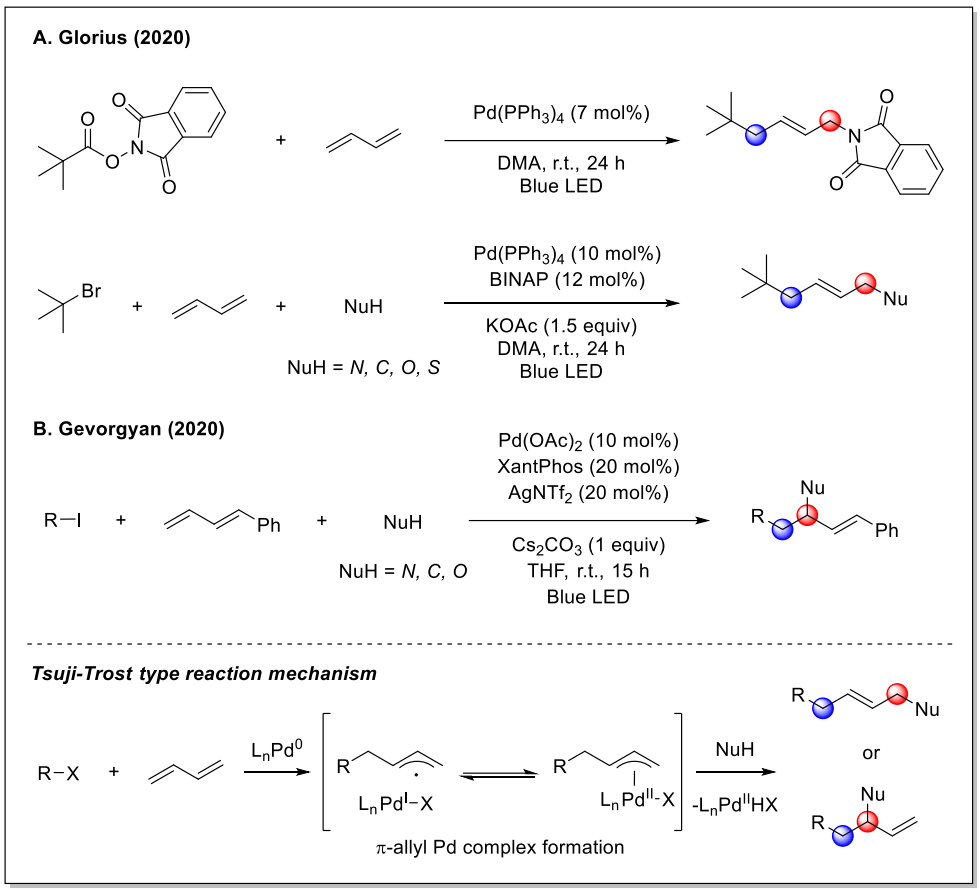

Scheme 4.12 Photoinduced Pd-catalyzed difunctionalization of diene.

4.6 Conclusion

For the recent four years, remarkable progress has been made in the field of visible-light induced Pd catalysis. This chapter introduces the new reactivity regarding photoinduced palladium-catalyzed reactions, such as the remote desaturations by a HAT process, alkyl Heck reactions, photo-accelerated cross-coupling reactions, and challenging three-component coupling reactions. The remarkable reactivity of Pd(I)/radical hybrid species opens a new avenue for the development of novel mild and efficient transformations in this area. However,

more detailed mechanistic studies are highly required to understand the Pd species' behavior, which could guide the development of more novel and useful transformations.

4.7 References

(1) Chuentragool, P.; Kurandina, D.; Gevorgyan, V. *Angew. Chem. Int. Ed.* **2019**, *58*, 11586.

(2) Kancherla, R.; Muralirajan, K.; Maity, B.; Zhu, C.; Krach, P. E.; Cavallo, L.; Rueping, M. *Angew. Chem. Int. Ed.* **2019**, *58*, 3412.

(3) Van Leeuwen, P. W. N. M.; Roobeek, C. F.; Huis, R. *J. Organomet. Chem.* **1977**, *142*, 233.

(4) Wang, G.-Z.; Shang, R.; Cheng, W.-M.; Fu, Y. *J. Am. Chem. Soc.* **2017**, *139*, 18307.

(5) Parasram, M.; Chuentragool, P.; Sarkar, D.; Gevorgyan, V. *J. Am. Chem. Soc.* **2016**, *138*, 6340.

(6) Chuentragool, P.; Parasram, M.; Shi, Y.; Gevorgyan, V. *J. Am. Chem. Soc.* **2018**, *140*, 2465.

(7) Ratushnyy, M.; Parasram, M.; Wang, Y.; Gevorgyan, V. *Angew. Chem. Int. Ed.* **2018**, *57*, 2712.

(8) Fredricks, M. A.; Drees, M.; Köhler, K. *ChemCatChem* **2010**, *2*, 1467.

(9) Abdiaj, I.; Huck, L.; Mateo, J. M.; de la Hoz, A.; Gomez, M. V.; Díaz-Ortiz, A.; Alcázar, J. *Angew. Chem. Int. Ed.* **2018**, *57*, 13231.

(10) Kurandina, D.; Parasram, M.; Gevorgyan, V. *Angew. Chem. Int. Ed.* **2017**, *56*, 14212.

(11) Koy, M.; Sandfort, F.; Tlahuext-Aca, A.; Quach, L.; Daniliuc, C. G.; Glorius, F. *Chem. Eur. J.* **2018**, *24*, 4552.

(12) Wang, G.-Z.; Shang, R.; Fu, Y. *Org. Lett.* **2018**, *20*, 888.

(13) Zhao, B.; Shang, R.; Wang, G.-Z.; Wang, S.; Chen, H.; Fu, Y. *ACS. Catal.* **2020**, *10*, 1334.

(14) Zhou, W.-J.; Cao, G.-M.; Shen, G.; Zhu, X.-Y.; Gui, Y.-Y.; Ye, J.-H.; Sun, L.; Liao, L.-L.; Li, J.; Yu, D.-G. *Angew. Chem. Int. Ed.* **2017**, *56*, 15683.

(15) Wang, G.-Z.; Shang, R.; Fu, Y. *Synthesis* **2018**, *50*, 2908.

(16) Jiao, Z.; Lim, L. H.; Hirao, H.; Zhou, J. S. *Angew. Chem. Int. Ed.* **2018**, *57*, 6294.

(17) Sun, L.; Ye, J.-H.; Zhou, W.-J.; Zeng, X.; Yu, D.-G. *Org. Lett.* **2018**, *20*, 3049.

(18) Torres, G. M.; Liu, Y.; Arndtsen, B. A. *Science* **2020**, *368*, 318.

(19) (a) Huang, H.-M.; Bellotti, P.; Pflüger, P. M.; Schwarz, J. L.; Heidrich, B.; Glorius, F. *J. Am. Chem. Soc.* **2020**, *142*, 10173. (b) Huang, H.-M.; Koy, M.; Serrano, E.; Pflüger, P. M.; Schwarz, J. L.; Glorius, F. *Nat. Catal.* **2020**, *3*, 393.

(20) Shing Cheung, K. P.; Kurandina, D.; Yata, T.; Gevorgyan, V. *J. Am. Chem. Soc.* **2020**, *142*, 9932.

Chapter 5. Site-Selectivity and Mechanism of Pd-Catalyzed C(sp^2)–H Arylation of Simple Arenes*

5.1 Introduction

The functionalization of aromatic compounds is a central topic in organic synthesis, which has great applicability.[1] Among them, electrophilic aromatic substitution (EAS) has been widely used for the functionalization of arenes.[2] Since the pioneering work of Friedel and Crafts,[3] its site-selectivity has been well established, in which an electron-donating group (EDG) or halogen substituent directs an incoming electrophile (E^+) to the *ortho*- and *para*-positions, whereas an electron-withdrawing group (EWG) directs it to the *meta*-position (Scheme 5.1a).[2b]

Biaryls are one of the essential scaffolds found in many types of natural products, pharmaceuticals, and functional materials.[4] Direct C(sp^2)–H arylation is a powerful and attractive tool used to construct the biaryls from arenes in an efficient manner because traditional cross-coupling methods require the preparation of prefunctionalized organometallic or main-group reagents.[1b, 1c, 4a, 4d, 5] To date, significant advances have been achieved in the C–H arylation of heteroarenes[5a, 6] and electronically biased[7] or chelation-assisted[8] arenes to activate certain C–H bonds. However, these approaches limit the applicability of the reaction by requiring electronically activated substrates or additional synthetic operations, such

* The majority of this work has been published: Daeun Kim, Geunho Choi, Woenjeong Kim, Dongwook Kim, Youn K. Kang, and Soon Hyeok Hong*. Chem. Sci. 2020, DOI: 10.1039/D0SC05414C.

as the installation and removal of a directing group to attain the target compound. Therefore, site-selective C–H arylation of unactivated, simple arenes is a fundamental challenge in catalysis to broaden the value of the reaction. Recently, site-selective C–H arylations of simple arenes have been achieved by elaborately designed strategies. For example, *para*-selective arylations of simple arenes have been reported using various arylating reagents such as diaryliodonium salts,[9] arylsilanes,[10] electron-poor arenes,[11] and aryl boronic acids.[4e, 12] Inspired by the Catellani reaction,[13] Yu and co-workers developed a *meta*-selective arylation reaction of simple arenes such as anisole and fluorobenzene with aryl iodide using a Pd/norbornene-based catalytic system to relay the palladium catalyst to the *meta*-position.[14] The Larrosa group also reported a one-pot direct *meta*-selective arylation of simple arenes using a traceless directing group relay strategy utilizing CO_2.[4f, 15] To develop a highly selective and efficient catalytic system, it is crucial to understand the underlying mechanism and factors that control the site-selectivity of the intrinsic palladium catalytic system.

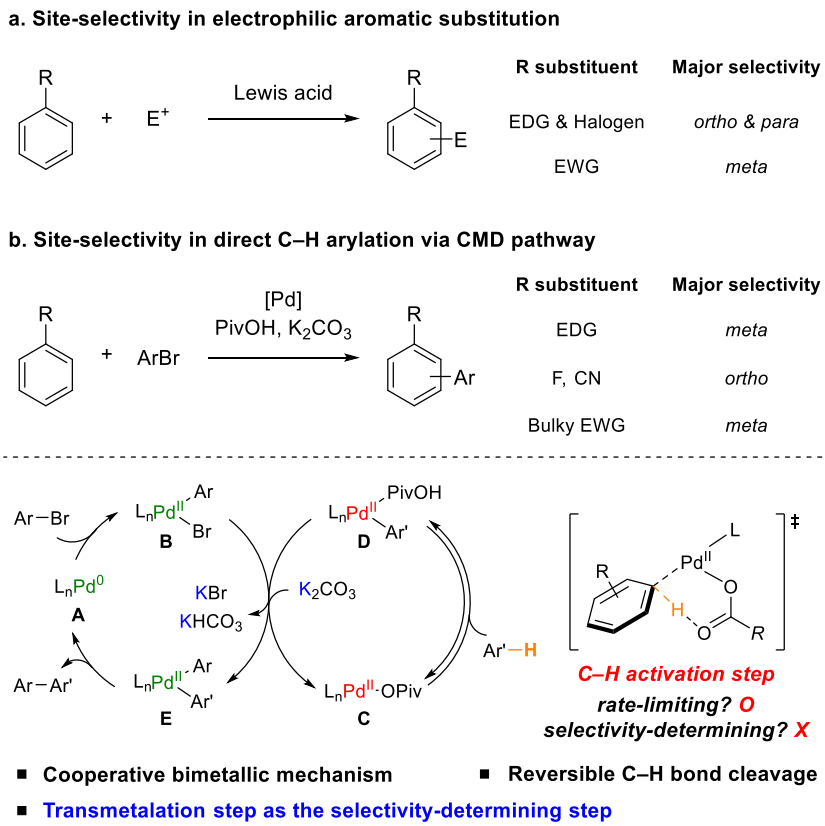

Scheme 5.1 Direct C–H arylation of simple arenes and selectivity.

During the past decades, significant attention has been focused on investigating the underlying mechanism of Pd(II)-catalyzed C(sp^2)–H bond cleavage. In 1985, Ryabov and co-workers proposed an electrophilic palladation pathway in the directed C–H activation of *N*,*N*-dimethylbenzylamine by $Pd(OAc)_2$.[16] Subsequently, Martinez[17], and Davies and Macgregor[18] suggested that the C–H bond cleavage proceeds via a concerted intramolecular proton abstraction by the acetate ligand. This concerted metalation-deprotonation (CMD) is regarded as an elegant system to cleave C–H bonds with the base ligand as the proton shuttle and has been

extensively applied in various catalytic C–H functionalization reactions.[4b, 7d, 19]

In the pioneering work of Pd-catalyzed C–H arylation of arenes by the Fagnou group, the CMD pathway efficiently facilitates the aryl C–H bond activation step operating using the combination of a sub-stoichiometric amount of pivalic acid (PivOH) and K_2CO_3.[20] Both the Brønsted acidity of the C–H bond and distortion-interaction analysis of the CMD transition state using density functional theory (DFT) studies have been adopted to predict the site-selectivity of the Pd-catalyzed C–H arylation of (hetero)arenes.[21] However, the prediction was not well-matched with various simple arenes such as anisole (**1b**) and benzotrifluoride (**1m**). For example, although the *ortho* C–H bonds of **1b** and **1m** are the most acidic and reactive positions based on the current understanding of the CMD mechanism, the *meta*-isomers were observed as the major products in the previously reported studies.[20-21, 22]

After the initial proposition of the Pd(II)-catalyzed monometallic CMD mechanism in the C–H arylation with aryl halide,[17, 23] Hartwig and co-workers experimentally uncovered that a cooperative bimetallic mechanism is operative in the C–H arylation of pyridine *N*-oxide catalyzed by $Pd(OAc)_2$ and P*t*Bu_3.[24] Gorelsky reported that the cooperative bimetallic mechanism involving two palladium species is favored using computational studies with phosphine-based Pd catalytic systems.[25] Our group has also reported that a Pd-diimine catalyst facilitates the direct C–H arylation of benzene via a cooperative bimetallic mechanism with noticeably improved TONs.[26]

However, despite these advances, it is still questionable whether the suggested bimetallic pathway is generally operative even in the absence of a relatively strongly coordinating L-type ligand, such as phosphine or diimine. Moreover, although it is crucial to achieve the site-selective catalytic C–H arylation of simple arenes, there has been no focused study on understanding the site-selectivity of the reaction.

Herein, we investigate the scope and site-selectivity of the Pd-catalyzed C–H arylation reaction of simple arenes with aryl bromides (Scheme 5.1b). Comprehensive mechanistic studies have been conducted using a combination of extensive kinetic measurements and stoichiometric experiments with arylpalladium complexes to address the operating catalytic cycle and factors determining the selectivity. Consequently, it is demonstrated that the applied Pd-based catalytic system works via a cooperative bimetallic mechanism involving two Pd catalytic species, which accounts for the observed counterintuitive site-selectivity trend by disclosing the transmetalation step as the selectivity-determining step.

5.2 Results and discussion

5.2.1 Optimization for C(sp^2)–H arylation

The reaction of ethoxybenzene **1a** with 3-bromotoluene **2a** in DMA was initially chosen to investigate both the reactivity and site-selectivity of the Pd-catalyzed direct C–H arylation (Table 5.1). The use of palladium acetate ($Pd(OAc)_2$) and DavePhos, employed under the Fagnou's condition,[20] afforded the desired biaryl product **3aa** in 54% yield with 69% *meta*-

selectivity (entry 1). When using P*t*Bu$_3$ as a ligand, which is used for the arylation of pyridine *N*-oxide,[24, 27] Pd(OAc)$_2$ exhibits similar reactivity to DavePhos (entry 2). Increased reactivities in the C–H arylation reaction were observed in the absence of a phosphine ligand, as reported by the Hartwig group, along with slightly increased *meta*-selectivity (entries 3 and 4).[28] Changing the Pd precursor to $PdCl_2$ enhanced the reactivity (75%, entry 5). To our delight, the use of $Pd(CH_3CN)_2Cl_2$ further improved the reaction efficiency to 79%, which could be attributed to the improved solubility of the Pd precursor (entry 6). The previously reported Pd–diimine catalyst also displayed good reactivity (81%) with 68% *meta*-selectivity (entry 7).[26] Increasing the catalyst loading (10 mol %) or the use of stoichiometric KOPiv instead of a combination of PivOH and K_2CO_3 resulted in a much lower yield (15% and 32%, respectively) accompanied by the homocoupling and hydrodebromination of **2a** (entries 8 and 9).[20] It is interesting to see that an appropriate choice of acid and base rather than the Pd catalyst or ligand is essential to obtain high efficiency and selectivity (entries 10–12 and Tables 5.7–5.9).[19b, 29] The *meta*-selectivity was noticeably decreased when Rb_2CO_3, NaOPiv, or CsOPiv was used as the base instead of K_2CO_3 or KOPiv, suggesting that there may be a cation effect on the site-selectivity (entries 10–12). The use of other aryl halides including aryl chloride and iodide gave poor reactivities (0% and 4.4%, respectively), suggesting the involvement of halide anion in the catalytic cycle (entries 13 and 14). Control experiments indicated that a source of pivalate is essential for the reaction, which is consistent with previous reports (entry 15).[20, 26, 29a]

Table 5.1 Optimization of the reaction conditions[a]

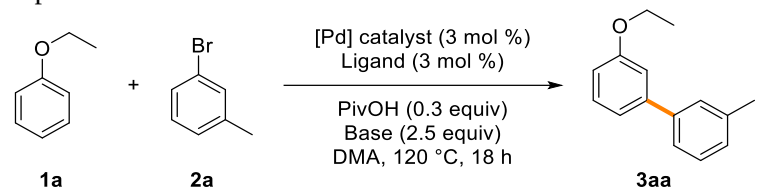

1a **2a** **3aa**

Entry	Catalytic condition	Base	Yield (%)	Selectivity (o / m / p)	% Selectivity (o / m / p)
1	$Pd(OAc)_2$, DavePhos	K_2CO_3	54	1 / 7.2 / 2.3	9 / 69 / 22
2	$Pd(OAc)_2$, P*t*Bu_3-HBF_4	K_2CO_3	57	1 / 6.8 / 2.6	10 / 65 / 25
3	$Pd(OAc)_2$	K_2CO_3	68	1 / 9.7 / 3.1	7 / 70 / 23
4	$Pd(OPiv)_2$	K_2CO_3	67	1 / 10.0 / 3.0	7 / 71 / 22
5	$PdCl_2$	K_2CO_3	75	1 / 10.0 / 3.1	7 / 71 / 22
6	$Pd(CH_3CN)_2Cl_2$	K_2CO_3	79 (76[b])	1 / 10.2 / 3.2	7 / 71 / 22
7	Pd(diimine)Cl_2	K_2CO_3	81	1 / 9.0 / 3.0	7 / 68 / 25
8[c]	$Pd(CH_3CN)_2Cl_2$	K_2CO_3	15	1 / 10.3 / 3.0	7 / 72 / 21
9[d]	$Pd(CH_3CN)_2Cl_2$	KOPiv	32	1 / 6.2 / 2.0	11 / 68 / 21
10	$Pd(CH_3CN)_2Cl_2$	Rb_2CO_3	75	1 / 5.7 / 2.9	10 / 59 / 31
11[d]	$Pd(CH_3CN)_2Cl_2$	NaOPiv	1.3	1 / 1.6 / 1.2	26 / 43 / 31
12[d]	$Pd(CH_3CN)_2Cl_2$	CsOPiv	4.3	1 / 1.4 / 1.8	31 / 45 /24
13[e]	$Pd(CH_3CN)_2Cl_2$	K_2CO_3	0	-	-
14[f]	$Pd(CH_3CN)_2Cl_2$	K_2CO_3	4.4	1 / 2.0 / 4.0	14 / 29 / 57
15[d]	$Pd(CH_3CN)_2Cl_2$	K_2CO_3	0	-	-

[a]Reaction conditions: **2a** (0.2 mmol), **1a** (60 equiv), [Pd] catalyst (3 mol %), ligand (3 mol %), PivOH (0.3 equiv), base (2.5 equiv) and DMA (1.2 mL) at 120 ℃ for 18 h; the total yield and regioselectivity (*ortho* / *meta* / *para*) were determined by GC analysis of the reaction mixture using dodecane as an internal standard. [b]Isolated yield. [c][Pd] catalyst (10 mol %). [d]Without PivOH. diimine=(1*E*,2*E*)-*N*1,*N*2-bis(2,6-di(pentan-3-yl)phenyl)ethane-1,2-diimine. [e]With 3-chlorotoluene. [f]With 3-iodotoluene.

5.2.2 Substrate scope of arenes and aryl bromides

With the optimized conditions in hand, the site-selectivity of the direct C–H arylation of various simple arenes was examined with 1-bromo-3,5-dimethylbenzene **2b** as the coupling partner (Table 5.2). The major isomers are illustrated in Table 5.2 and the observed % site-selectivity reported in the parenthesis as (*ortho* / *meta* / *para*) or (α / β). To gain an idea of the correlation between the C–H bond acidity and site-selectivity in the transformation, the proton affinity at every C-position in the various arenes was calculated (Table 5.22); however, no consistent correlation was observed (Table 5.2). Various monosubstituted electron-rich arenes exhibit good reactivities, counter-intuitively providing the *meta*-isomer as the major product (>60% selectivity). In a similar manner to ethoxybenzene, anisole provided biaryl products **3bb** in 58% yield with 67% *meta*-selectivity. In the case of alkylbenzenes, an almost statistical ratio of the *meta*- and *para*-isomers (~2:1) was observed in excellent yields (**3cb**–**3eb**). *N*-methylacetanilide provided biaryl products **3fb** (>96%) with 62% *meta*-selectivity. Electron-neutral arenes also exhibited good efficiency. Benzene afforded biaryl **3gb** in quantitative yield (>96%). Naphthalene provided **3hb** (70%) in a 1.7:1 ratio favoring the α-arylated product.

Various monosubstituted electron-deficient arenes exhibit higher efficiency even when using a lower amount of the arene (6 equiv) or shorter reaction time (3 h). Fluorobenzene provided biaryl products **3ib** in 96% yield with 88% *ortho*-selectivity when using 6 equiv of arene over 3 h. Similarly, when benzonitrile was subjected to the standard reaction conditions, the

arylated products **3jb** were obtained in 72% yield in favor of the *ortho*-isomer (69% selectivity). The *ortho*-selectivity observed using the electron-deficient arenes has been well acknowledged in the literature and attributed to both the most acidic *ortho* C–H bond and its lower distortion energy in the CMD transition state.[21a, 21c] However, we observed that the steric effect of the substituent can significantly affect the site- selectivity in the CMD catalytic system. Chlorobenzene, which is predicted to exhibit a similar trend to fluorobenzene,[21c] efficiently produced biaryls **3kb** (95%) in favor of the *meta*-isomer (64% selectivity). (Trifluoromethoxy)benzene and benzotrifluoride gave products **3lb** (64%) and **3mb** (86%) with good *meta*-selectivities (61% and 71%, respectively). When using acetophenone as the arene substrate, α-arylation of the ketone occurred exclusively because the α-C(sp^3)–H bond adjacent to the carbonyl group is much more acidic than the aryl C(sp^2)–H bond (Scheme 5.8).[30] When pivalophenone was used to block the undesired C(sp^3)–H arylation, **3nb** was produced in 91% yield with 66% *meta*-selectivity. Nitrobenzene provided biaryl products **3ob** (95%) with decreased *meta*-selectivity (44%) and an almost statistical distribution of regioisomers. The selectivity is significantly dependent on the solvents, as demonstrated in the *ortho*-arylation of nitrobenzene by Fagnou group[29b] and our solvent screening results (Table 5.10). The current method is well suited for disubstituted arenes and displays excellent regioselectivity. *m*-Xylene provided biaryl product **3pb** (53%) as the sole isomer functionalized at the least sterically hindered *meta*-position with respect to the methyl substituent. Fluorotoluene and fluoroanisole resulted in products **3qb**–**3sb**, which were

exclusively functionalized adjacent to the fluoro group. In summary, the C–H arylation of electron-rich arenes exhibits *meta*-selectivity. High *ortho*-selectivity is observed in the case of electron-deficient arenes containing fluoro or cyano groups, as previously reported. However, arenes bearing large electron-withdrawing groups are arylated in favor of the *meta*-isomer rather than at the most acidic *ortho* C–H position.

Next, we explored an array of aryl bromides as the coupling partner in the C–H arylation of ethoxybenzene (Table 5.3). A variety of electron-rich aryl bromides provided their corresponding biaryl products efficiently (61–83%) with good *meta*-selectivities (66–72%). Methyl- and dimethyl-substituted aryl bromides displayed good reactivities (**3aa**–**3ad**). Phenyl and naphthyl groups also gave good product yields (**3ae**–**3ag**). 4-Bromoanisole (**2h**), an aryl ether, exhibited slightly decreased reactivity (61%), but the *meta*-selectivity (70%) was maintained (**3ah**). Electron-deficient aryl bromides bearing trifluoromethyl, chloro, or cyano substituents also provided their corresponding biaryl products (**3ai**–**3al**) in moderate to good yields (44–69%). However, to our surprise, the presence of an electron-withdrawing substituent on the aryl bromide resulted in dramatically decreased *meta*-selectivities (37–53%), contrary to our expectation that the nature of aryl bromide would not significantly affect site-selectivity. Similar results were observed with stoichiometric amounts of ethoxybenzene (Scheme 5.9). The results imply that the electronic property of aryl bromide significantly affects the selectivity-determining step in the catalytic cycle.

Table 5.2 Substrate scope with respect to the arene[a]

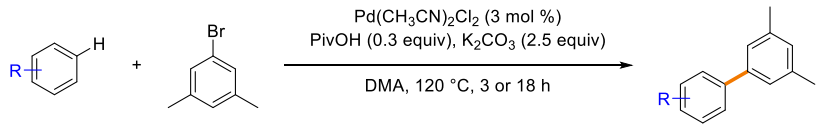

1 **2b** **3**

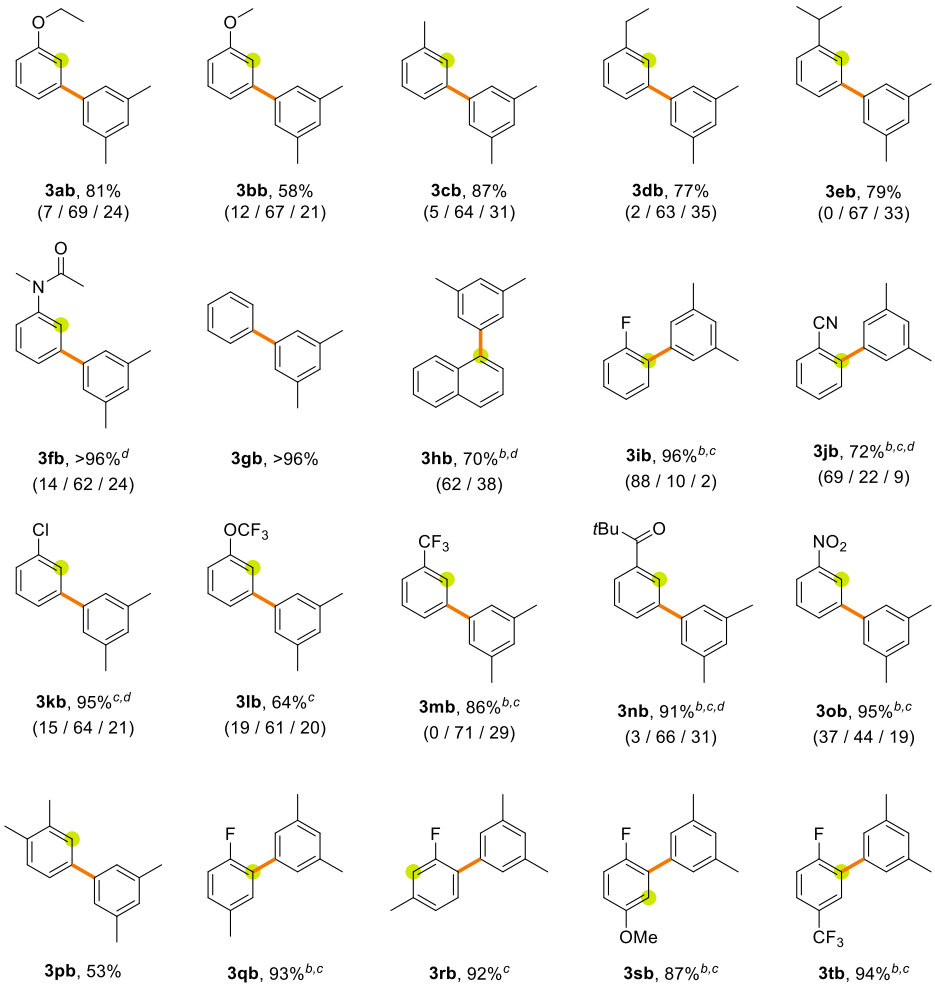

[a]Reaction conditions: **2b** (0.2 mmol), arene (60 equiv), $Pd(CH_3CN)_2Cl_2$ (3 mol %), PivOH (0.3 equiv), K_2CO_3 (2.5 equiv) and DMA (1.2 mL) at 120 °C for 18 h. All yields are isolated yields. The regioselectivity (*ortho* / *meta* / *para* or α / β) was measured by GC analysis of the reaction mixture using dodecane as an internal standard. [b]Arene (6 equiv). [c]3 h. [d]GC yield. [e]The C-position with the lowest proton affinity (calculated using G3MP2; see Table 5.12).

Table 5.3 Substrate scope with respect to the aryl bromide[a]

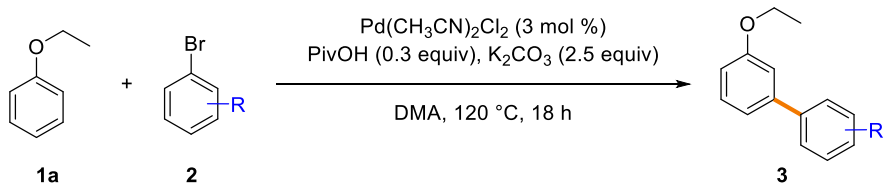

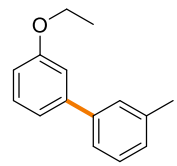

3aa, 75%
(7 / 71 / 22)

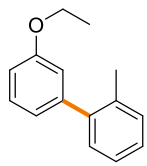

3ac, 78%[b]
(8 / 68 / 24)

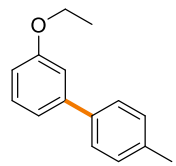

3ad, 83%[b]
(7 / 72 / 21)

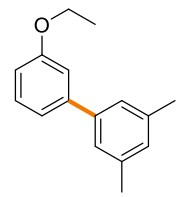

3ab, 81%
(7 / 69 / 24)

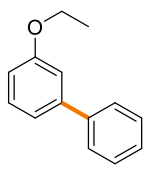

3ae, 81%[b]
(8 / 70 / 22)

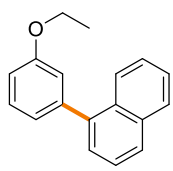

3af, 73%
(12 / 66 / 22)

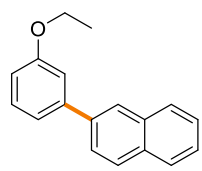

3ag, 82%
(9 / 68 / 23)

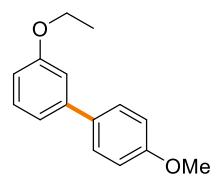

3ah, 61%
(6 / 70 / 24)

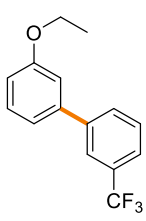

3ai, 54%[b]
(26 / 48 / 26)

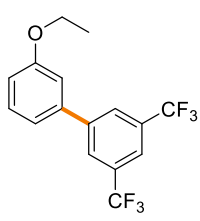

3aj, 69%[b,c]
(35 / 38 / 27)

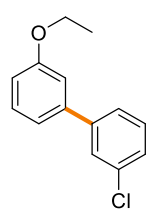

3ak, 49%[c]
(22 / 53 / 25)

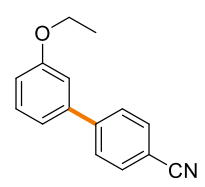

3al, 44%[c]
(37 / 37 / 26)

[a]Reaction conditions: Aryl bromide (0.2 mmol), **1a** (60 equiv), $Pd(CH_3CN)_2Cl_2$ (3 mol %), PivOH (0.3 equiv), K_2CO_3 (2.5 equiv) and DMA (1.2 mL) at 120 ℃ for 18 h; The total yields and regioselectivity (*ortho* / *meta* / *para*) were determined by GC analysis of the reaction mixtures using dodecane as an internal standard. [b]48 h. [c]140 ℃.

5.2.3 Mechanistic studies

To understand the general reactivity and selectivity trends mechanistically, the reaction rates were first compared with a variety of arenes (Scheme 5.2). As rationally expected in the rate-limiting proton-transfer CMD pathway,[2a, 21b, 27] inductively arenes with inductively withdrawing groups reacted faster than electron-rich arenes, which is a reversed tendency to the reactivity profiles obtained for electrophilic aromatic substitution reactions.[2b]

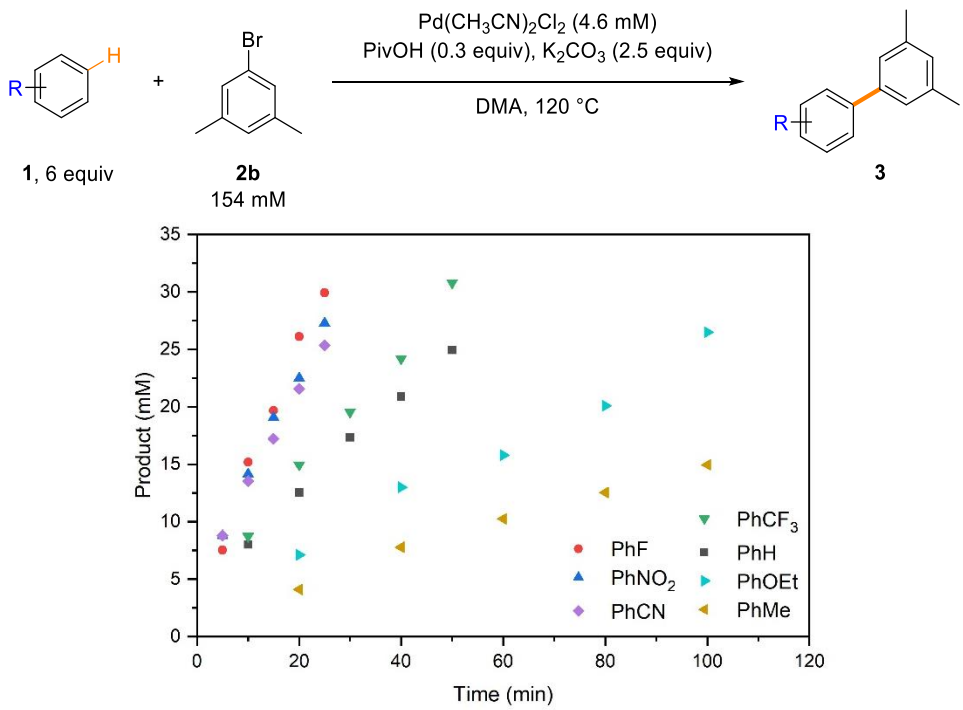

R	F	NO_2	CN	CF_3	H	OEt	Me
Reaction rate (mM/min)	1.1147	0.9066	0.8245	0.2329	0.4223	0.2295	0.1324
k_{rel}	2.6	2.2	1.9	1.3	1	0.54	0.31

Scheme 5.2 Comparision of reaction rates. Combined yields of all isomers, determined by GC using dodecane as an internal standard, were used for kinetic plots. σ_p = Hammett constant. k_{rel} = Relative reaction rate vs $k_{(R=H)}$.

Standard kinetic isotope effect (KIE) experiments were conducted using benzene **1g** and benzene-d_6 **1g-*d*$_6$** to gain additional insight into the rate-limiting step (Scheme 5.3a). The observed large primary KIE (k_H/k_D = 4.4) suggests that the C–H bond cleavage step is involved in the rate-limiting step. This is in agreement with that previously reported,[26-27] implying the involvement of C–H bond cleavage in the rate-limiting step. The dependence of the reaction rate on [Pd], [ArBr], KOPiv and K_2CO_3 was comprehensively investigated (Scheme 5.3b). A first-order dependence with respect to [Pd] and a zero-order with respect to [ArBr] and K_2CO_3 were observed. A positive dependence of the reaction rate on KOPiv was observed,[31] but undesired homocoupling and hydrodebromination of **2b** were observed using higher amounts of pivalate (>0.2 equiv), which retarded the reaction (Table 5.1, entry 9). These results indicate that the C–H bond cleavage step follows the Pd–pivalate-promoted CMD pathway.

Following the initial mechanistic studies, a mechanistic outline involving Pd–pivalate-promoted C–H bond cleavage was constructed. For the Pd-catalyzed C–H arylation reaction, two pathways can be operative: (1) The originally proposed Pd(0/II) monometallic mechanism (Scheme 5.4, top pathway) or (2) a cooperative bimetallic mechanism (Scheme 5.4, bottom pathway), based on the literature precedent.[20, 24-26] As outlined in Scheme 5.4, the most distinguishable difference between the monometallic and cooperative bimetallic processes is the presence of a transmetalation step that only exists in the bimetallic mechanism. Stahl[32] and Hong[26] have previously proposed that a Pd-catalyzed arylation reaction operated by a cooperative

bimetallic pathway can display a first-order dependence at high [Pd], but second-order dependence at low [Pd], where the transmetalation step becomes the rate-limiting step. The second-order dependence can be more pronounced in the deuterated substrate because the slower rate of C–D bond cleavage significantly lowers [Pd–Ar] and thus, further decelerates the rate of the transmetalation step.

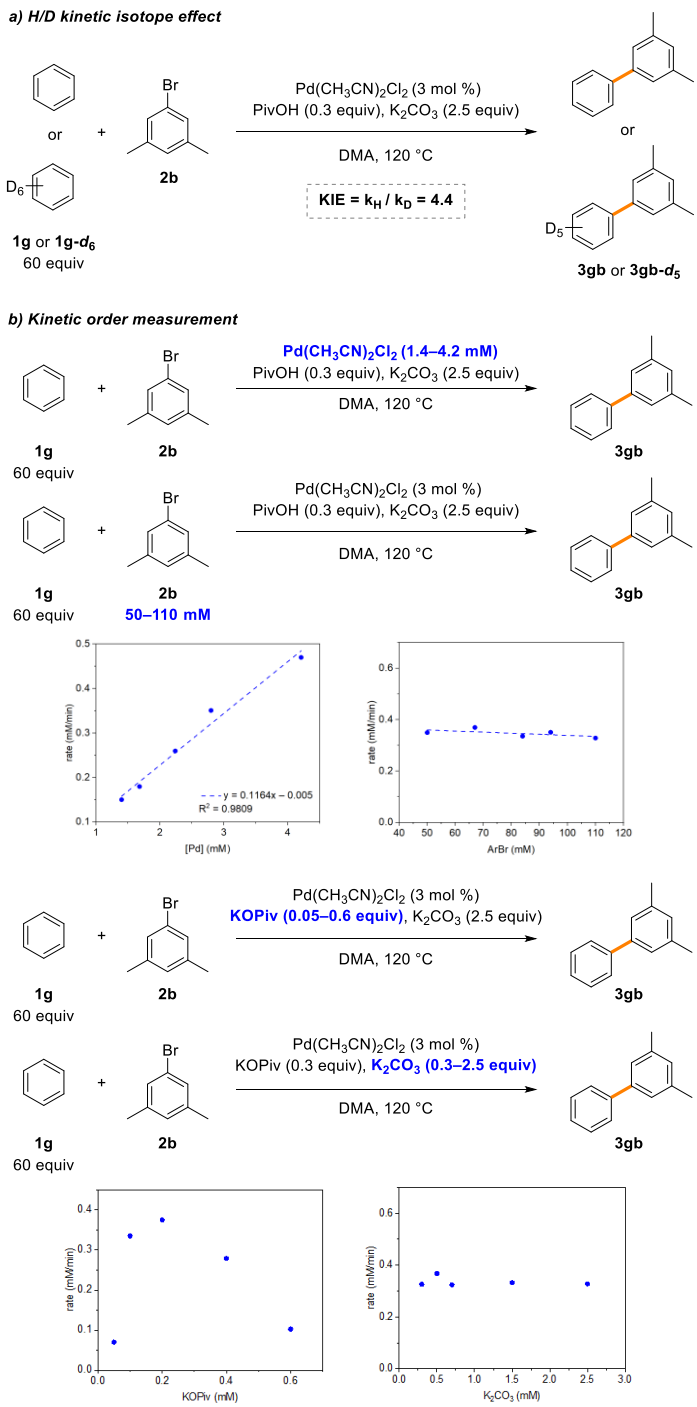

Scheme 5.3 Mechanistic studies.

In previous Pd–diimine catalyzed C–H arylations of simple arenes, we proposed that the rigid bidentate diimine ligand drives the cooperative bimetallic pathway because an open coordination site for the C–H bond of the arene is required to undergo the CMD process for the monometallic pathway to be operative. In regard the current Pd catalytic system, we conjectured a monometallic CMD pathway in operation because there is no strongly coordinating ligand such as a diimine or electron-rich phosphine present. To verify the operative catalytic cycle, we investigated the dependence of the reaction rate at low concentrations of $Pd(CH_3CN)_2Cl_2$ in benzene-d_6 (Scheme 5.4c). To our astonishment, the kinetic study revealed the second-order dependence at very low [Pd], strongly supporting that the reaction follows a cooperative bimetallic mechanism (Scheme 5.4b). Inspired by the results, we performed extensive kinetic to determine whether the cooperative bimetallic mechanism is generally operative. Second-order kinetics were consistently observed at low concentrations of $Pd(OAc)_2$ in the presence of various phosphine ligands (DavePhos, PCy_3, PPh_3, and $P(C_6F_5)_3$) (Scheme 5.24–5.30). Notably, the $Pd(OAc)_2$-based catalytic system without any external ligand (Table 5.1, entry 3) also exhibits second order kinetics at very low concentrations of $Pd(OAc)_2$ (Scheme 5.23), indicating that the cooperative bimetallic pathway is generally working in the Pd-catalyzed arylation of simple arenes with aryl bromides under CMD conditions.

With evidence for the cooperative bimetallic mechanism in hand, we attempted to elucidate the origin of the observed site-selectivity. The *meta*-selectivity observed for many electron-rich and electron-deficient arenes (Table 5.2) was unexpected, counter-intuitive, and contrary to previous

reports suggesting the CMD step is both the rate-limiting and selectivity-determining step based on a monometallic mechanism.[21a, 33] Because the C–H bond cleavage step is independent of the oxidative addition of aryl bromides in the cooperative bimetallic mechanism, the dependence of the selectivity on the electronic effect of aryl bromides with ethoxybenzene (Table 5.3) indicates that the C–H activation step is not the selectivity-determining step. The site-selectivity distribution was further investigated using electron-poor arenes, such as fluorobenzene (**1i**) and chlorobenzene (**1k**), in the C–H arylation with two electronically different aryl bromides (**2b** and **2j**) under stoichiometric conditions (Scheme 5.5). In the case of highly *ortho*-selective fluorobenzene, the site-selectivity slightly changed when using **2b** and **2j**. In the arylation of chlorobenzene, the site-selectivity was significantly varied from 46% *meta*-selectivity with **2b** to 61% *ortho*-selectivity with **2j**, supporting the validity of the hypothesis that the C–H activation step is not the selectivity-determining step.

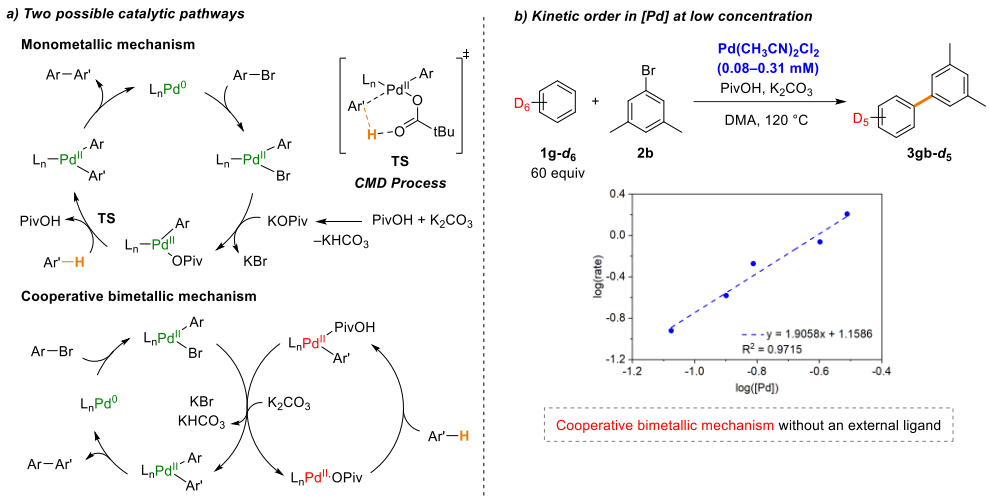

Scheme 5.4 Mechanistic hypothesis and kinetic studies.

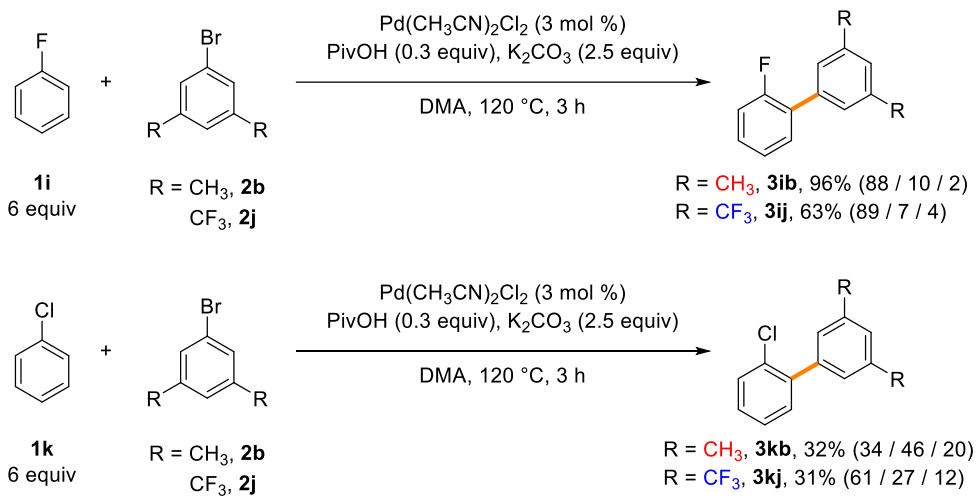

Scheme 5.5 C–H arylation of fluorobenzene and chlorobenzene with two different aryl bromides.

To scrutinize which elementary step is the selectivity-determining step, we first checked the reversibility of the oxidative addition and the C–H cleavage steps. A competition experiment was carried out using electronically different sets of aryl bromides (Scheme 5.6a). The reaction

was conducted using **2e** and electron-rich aryl bromide **2a**, while the other reaction used **2e** and electron-deficient aryl bromide **2i** as the competing substrate. In the former reaction, similar yields of **3ae** and **3aa** were observed in a combined 54% yield. In contrast, only a trace amount of **3ae** was produced in the presence of **2i**, and **3ai** was formed as the dominant product, albeit in a low yield (10%). If the oxidative addition was reversible, the coupling reaction with electron-richer aryl bromide **2e** could occur in a reasonable yield despite the predominant oxidative addition of the electron-poor substrate **2i**.[34] Instead, the observed poor yields indicate that the oxidative addition step is irreversible. We hypothesized that the electron-poor substrates exhibit poor yields, despite the predominant oxidative addition, due to the transmetalation step. The same trend of lower reactivity with electron-poor aryl bromides was observed when examining the substrate scope (Table 5.3, **2i**–**2l**). Subsequently, deuterium exchange reactions were carried out with stoichiometric amounts of ethoxybenzene (**1b**) in the presence of D_2O and benzene-d_6 (**3a-*d*$_6$**), respectively, to confirm the reversibility of the C–H bond cleavage step (Scheme 5.6b). Deuterium incorporations in the aryl group of **3ab** (10.2 and 6.4%, respectively) via H/D scrambling were observed using ^{2}H NMR spectroscopy. If the C–H bond cleavage by the Pd–pivalate species were irreversible, deuterium incorporation into **3ab** would not occur. These results strongly support the reversibility of the C–H activation step. Therefore, the following steps, transmetalation or reductive elimination, may govern the site-selectivity of the reaction.

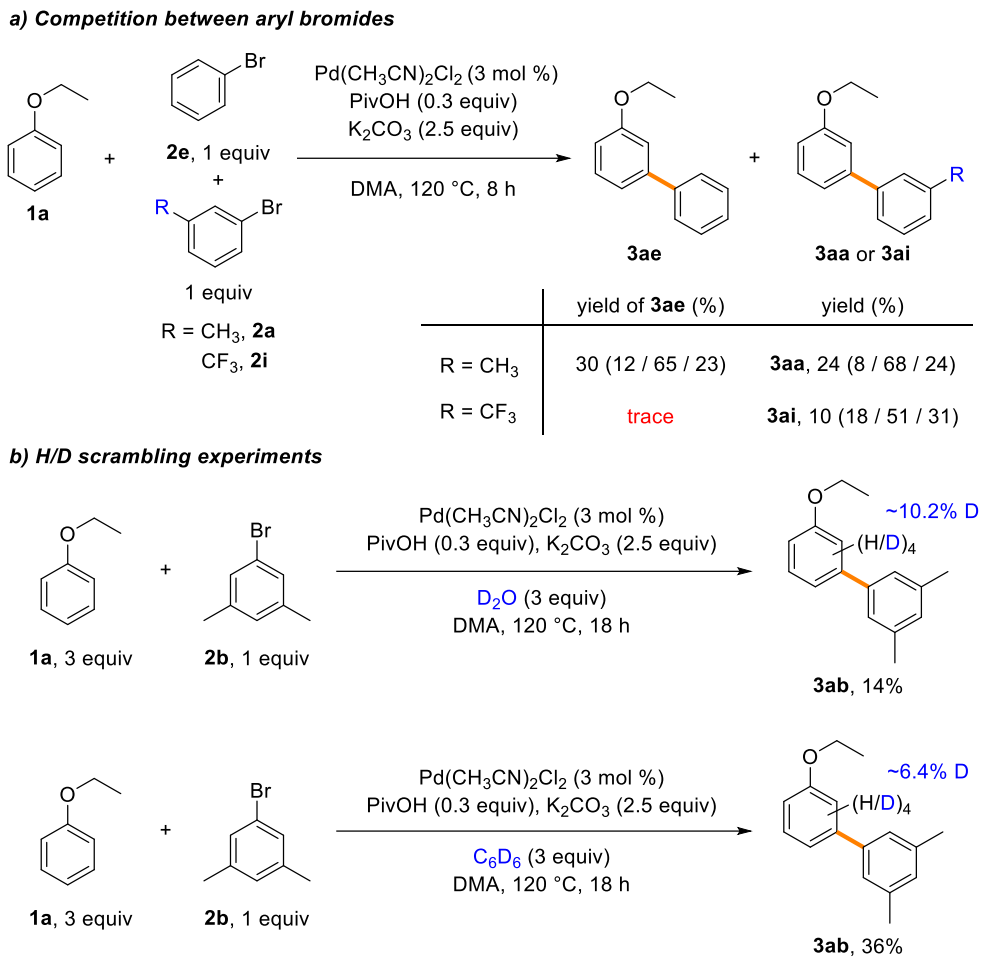

Scheme 5.6 Competition experiments.

Stoichiometric reactions with arylpalladium complexes, which are analogous intermediate, were designed to affirmatively validate the cooperative bimetallic mechanism and further explore the selectivity-determining step. Two different arylpalladium pivalate complexes bearing either electron-rich or electron-poor aryl groups (**4a** and **4b**) were prepared upon the reaction of $Pd(dba)_2$ with P*t*Bu_3[35] in neat aryl iodide, followed by ligand exchange from iodide to pivalate using AgOPiv (Scheme 5.7).[28] The solid-state structure of Pd complex **4b** was confirmed by single-crystal X-ray diffraction analysis (CCDC 2000400).

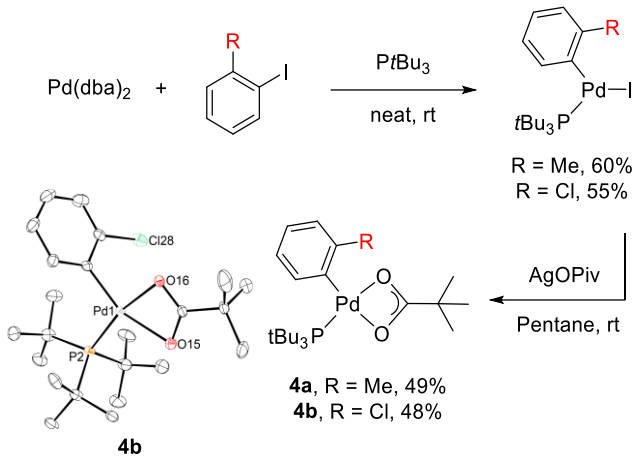

Scheme 5.7 Synthesis of arylpalladium pivalate complexes.

Complex **4a** containing the *o*-tolyl group was subjected to stoichiometric reactions with ethoxybenzene in DMA (Table 5.4). The reaction did not provide the desired product **3ac** in the absence of any additive (entry 1). The addition of PivOH, K_2CO_3, and a bromide source increased the reactivity up to 21%; however, the resulting *meta*-selectivity was significantly low (30 and 35%, entries 2 and 3). In contrast, when an additional Pd source, $Pd(CH_3CN)_2Cl_2$, was added, the *meta*-selectivity increased (24% and 64%, entries 4 and 5) to a level similar to that observed under the standard conditions using P*t*Bu$_3$ (65% *meta*-selectivity, Table 5.1, entry 2). These results strongly suggest that *meta*-selectivity can be only achieved by the cooperative bimetallic mechanism. When complex **4b** containing an *o*-chlorophenyl group was subjected to the stoichiometric reactions, the selectivities observed in the products **3am** were completely different from those observed with **4a**. A high *ortho*-selectivity (84%), albeit in a low yield (7%), was observed in the absence of an additional Pd complex (entry 6). Notably, when an additional Pd source was added, the *ortho*-selectivity significantly decreased (from

84 to 48%) with increased *meta*-selectivity (from 8 to 33%, entry 7). If the reaction would follow a monometallic mechanism, the reaction efficiency and selectivity would not vary significantly, regardless of the addition of an external Pd complex. These results consistently support that the reaction majorly operates via a cooperative bimetallic mechanism and the C–H bond cleavage step was not the selectivity-determining step because the C–H activation is independent of the electronics of the aryl groups of the arylpalladium species under the cooperative bimetallic mechanism.

Table 5.4 Stoichiometric reaction of Pd complexes[a]

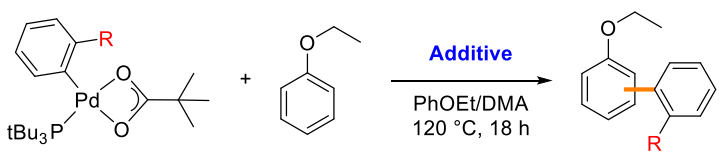

2.1 mM
R = Me, **4a**
= Cl, **4b**

R = Me, **3ac**
= Cl, **3am**

Entry	[Pd]	Additive (equiv)	Yield (%)	Selectivity (o / m / p)	% Selectivity (o / m / p)
1	**4a**	None	0	-	-
2	**4a**	PivOH (20), K_2CO_3 (160)	0.6	1 / 0.7 / 0.7	42 / 30 / 28
3	**4a**	PivOH (20), K_2CO_3 (160), *n*Bu_4NBr (10)	21	1 / 1.3 / 1.4	27 / 35 / 38
4	**4a**	PivOH (20), K_2CO_3 (160), $Pd(CH_3CN)_2Cl_2$ (5)	26	1 / 0.8 / 1.6	29 / 24 / 47
5	**4a**	PivOH (20), K_2CO_3 (160), *n*Bu_4NBr (10), $Pd(CH_3CN)_2Cl_2$ (5)	65	1 / 6.2 / 2.6	10 / 64 / 26
6	**4b**	PivOH (20), K_2CO_3 (160), *n*Bu_4NBr (10)	7	1 / 0.1 / 0.1	84 / 8 / 8
7	**4b**	PivOH (20), K_2CO_3 (160), *n*Bu_4NBr (10), $Pd(CH_3CN)_2Cl_2$ (5)	65	1 / 0.7 / 0.4	48 / 33 / 19

[a]The total yield and regioselectivity (*ortho* / *meta* / *para*) were determined by GC analysis of the reaction mixture using dodecane as an internal standard.

Notably, the effect of the cation in the carbonate base on the site-selectivity of the C–H arylation of ethoxybenzene (**1a**) was observed (Table 5.1, entry 10). The cation effect was further investigated upon the addition of 18-crown-6 under the standard reaction conditions.[36] As the amount of 18-crown-6 increased, the *meta*-selectivity in the C–H arylation of ethoxybenzene gradually decreased (from 71 to 39%, Table 5.5). Same phenomenon was also observed in the C–H arylation of toluene (**1c**), excluding the effect of potential cation-ethoxybenzene interactions on the *meta*-selectivity (Table 5.11). Amatore and Jutand demonstrated that counterion of the base can affect the rate of transmetalation by coordinating the countercation to the Pd intermediate in Pd-catalyzed Suzuki–Miyaura cross-coupling reactions.[37] Although we do not fully understand the Pd species involved in the transmetalation step, the results indicate that a potassium cation can affect the site-selectivity in the transmetalation process rather than the reductive elimination process.

Table 5.5 Impact of crown ether additives on the C–H arylation reaction[a]

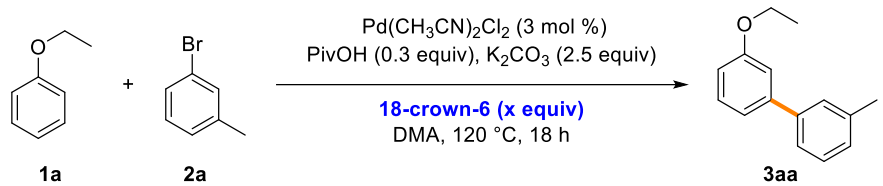

Entry	18-crown-6 (x equiv)	Yield[a] (%)	Selectivity (o / m / p)	% Selectivity (o / m / p)
1	-	79	1 / 10.2 / 3.2	7 / 71 / 22
2	0.3	91	1 / 8.0 / 2.6	9 / 69 / 22
3	1	90	1 / 4.4 / 1.9	14 / 60 / 26
4	2.5	85	1 / 2.8 / 1.5	19 / 53 / 28
5	5	80	1 / 2.0 / 1.4	23 / 47 / 30
6	10	59	1 / 1.4 / 1.2	29 / 39 / 32

[a]Reaction conditions: **2a** (0.2 mmol), **1a** (60 equiv), $Pd(CH_3CN)_2Cl_2$ (3 mol %), PivOH (0.3 equiv), K_2CO_3 (2.5 equiv), 18-crown-6, and DMA (1.2 mL) at 120 °C for 18 h; The total yield and regioselectivity (*ortho* / *meta* / *para*) were determined by GC analysis of the reaction mixture using dodecane as an internal standard.

Reductive elimination is a common process in transition-metal catalysis and its mechanism is well understood.[38] The reductive elimination of [Pd(II)]ArAr' complexes to form biaryls has been thoroughly examined as a facile and irreversible process, particularly at our reaction temperature of 120 °C.[39] It is less likely to be the selectivity-determining step of the reaction. To confirm it further, we conducted DFT modelling of the reductive elimination pathways to check whether the reductive elimination process theoretically produces the experimentally observed site-selectivity. C–H arylations of fluorobenzene and chlorobenzene using **2b** were selected as model reactions for the computational studies. Scheme 5.5 shows

fluorobenzene and chlorobenzene undergo the arylation reaction to produce biaryls **3ib** (96%) with 88% *ortho*-selectivity and **3kb** (32%) with 46% *meta*-selectivity, respectively. To compare with the experimental results, the reductive elimination processes for each isomeric position were calculated (Table 5.6 and Scheme 5.33). The Gibbs free energy changes (ΔG), energy barriers ($\Delta G^{\ddagger}$), and energetic differences ($\Delta\Delta G^{\ddagger}$) are listed in Table 5.6. In the case of fluorobenzene, the reductive elimination at the *meta*-position is preferred over at the *ortho*-position, as indicated by the negative $\Delta\Delta G^{\ddagger}$ value (–1.1 kcal/mol). In the case of chlorobenzene, the *para*-position is the most reactive in the reductive elimination process with a negative $\Delta\Delta G^{\ddagger}$ value of –1.7 kcal/mol. The obtained theoretical selectivities, assuming the reductive elimination step is the selectivity-determining step, are completely different from the experimental results. Therefore, the possibility of the reductive elimination being the site-selectivity determining step is excluded using the computational investigations and the previous studies on the reductive elimination processes occurring in Pd-catalyzed biaryl cross-coupling reactions.[39] Thus, we concluded that the transmetalation step is the selectivity- determining step based on the overall observations and control experiments. Due to the nature of the transition state and intermediate in the transmetalation step still being unknown,[39a, 39b, 40] attempts to predict the site-selectivity using computational studies were unsuccessful.

Table 5.6 Investigation of reductive elimination processes

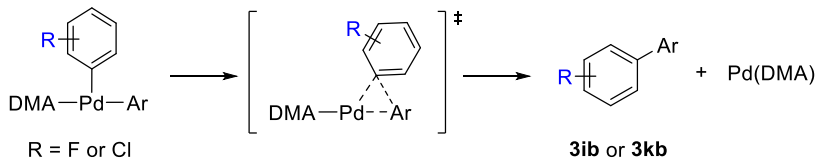

Arylation site	DFT calculated[a]				Experimental	
	ΔG	ΔG‡	ΔΔG‡[b]	%Selectivity (o / m / p)	ΔΔG‡[b]	%Selectivity (o / m / p)
Fluorobenzene						
ortho	−5.0	13.3	0		0	
meta	−8.1	12.2	−1.1	(18 / 70 / 12)	1.3	(88 / 10 / 2)
para	−7.0	13.6	0.3		3.0	
Chlorobenzene						
ortho	−3.3	14.2	0		0	
meta	−5.1	13.9	−0.3	(9 / 14 / 77)	–0.3	(34 / 46 / 20)
para	−6.8	12.5	−1.7		0.4	

[a]Free energies in solution (kcal/mol) obtained at the B3LYP-D3(IEFPCM)/SDD/6-311++G**//B3LYP-D3/LanL2DZ/6-31G** level of theory.[41] [b]The value obtained using ΔG‡(*ortho*) – ΔG‡(position). A negative value indicates the lower energy barrier of the C-position than the *ortho*-position. Ar = 3,5-Dimethylphenyl.

A summary of the investigated mechanism is illustrated in Scheme 5.1. The Pd catalytic system without an external ligand operates via a cooperative bimetallic mechanism. One Pd–Ar species **B** is generated from the irreversible oxidative addition of the aryl bromide (ArBr) to Pd(0) **A**, while another Pd–Ar' species **D** is generated from the rate-limiting C–H bond cleavage of the arene (Ar'H) by Pd(II)–pivalate species **C**. Both Pd species (**B** and **D**) undergo transmetalation to afford Pd(II)ArAr' **E** and regenerate Pd(II)–pivalate species **C**. Importantly, the transmetalation step is disclosed to be the selectivity-determining step with the help of a potassium cation after the reversible C–H activation step. Finally, the reductive

elimination of Pd(II)ArAr' **E** affords the desired biaryl product and the initial Pd(0) species **A**, which then re-enters the catalytic cycle.

5.3 Conclusion

In conclusion, we have comprehensively investigated the scope and site-selectivity of the Pd-catalyzed direct C–H arylation of simple arenes using aryl bromides as a coupling partner. The site-selectivity of the C–H arylation reaction is affected by the steric effect of the substituents on the arene as well as the C–H bond acidity. Generally, electron-rich arenes exhibit meta-selectivity. Although electron-deficient arenes bearing fluoro or cyano groups result in high ortho-selectivity, electron-deficient arenes bearing bulky electron-withdrawing groups produce the meta-isomer as the major product. Thorough mechanistic investigations, including kinetic studies, control experiments, and stoichiometric reactions with arylpalladium complexes, suggest that the reaction follows a cooperative bimetallic mechanism. Notably, the transmetalation step, which is influenced by a cation, is identified as the selectivity determining step, which refutes the previous understanding that the C–H bond cleavage step determines the site-selectivity in the reaction.

5.4 Experimental section

5.4.1 General information

Unless otherwise noted, all reactions were performed under inert conditions. Benzene, ether, pentane and diethyl ether were dried using a PureSolv solvent purification system. All chemicals were purchased from commercial sources (Sigma-Aldrich, Alfa Aesar, TCI, or Strem) and used without further purification. Reactions were monitored by thin-layer chromatography (TLC) on EMD Silica Gel 60 F254 plates, and visualized either using UV light (254 nm) or by staining with potassium permanganate and heating. Nuclear magnetic resonance (NMR) spectra were recorded in $CDCl_3$ and CD_3OD on a Bruker DPX-300 (300 MHz) spectrometer, Varian 400 and 500 NMR (400 and 500 MHz), Bruker AVANCE 300 (300 MHz), Bruker AVANCE 400 (400 MHz), or Bruker AVANCE III HD (400 MHz), and the residual solvent signal was used as a reference. Chemical shifts are reported in ppm and coupling constants are given in Hz. Gas chromatography (GC) was carried out using a 7890A or 7890B GC system (Agilent Technologies) equipped with an HP-5 column and a flame ionization detector (FID). Gas chromatography–mass spectrometry (GC-MS) was carried out using 5977B GC/MSD system (Agilent Technologies) equipped with an HP-5MS column. Elemental analysis was conducted at KAIST Analysis Center for Research Advancement (KARA) using a Flash 1112 elemental analyzer. High-resolution mass spectrometry (HRMS) was performed at the Organic Chemistry Research Center in Sogang University using the ESI method and Korea Basic Science Institute (KBSI) for EI method. X-ray diffraction data of **4b** was collected on a Bruker D8 QUEST coated with Paraton-*N* oil under a stream of N_2 (g) at 173 K

5.4.2 General procedure for the C(sp^2)–H arylation reaction

K_2CO_3 was dried at 120 ℃ in an oven overnight. Inside a glove box, a 10 mL Schlenk tube equipped with a magnetic stirring bar was charged with K_2CO_3 (2.5 equiv, 69 mg, 0.50 mmol), $Pd(CH_3CN)_2Cl_2$ (3.0 mol %, 1.6 mg, 0.0060 mmol), and pivalic acid (0.30 equiv, 6.1 mg, 0.060 mmol). Aryl halide (1.0 equiv, 0.20 mmol) was then added to the Schlenk tube in, followed by DMA (1.2 mL) and arene (60 equiv). The Schlenk tube was sealed and heated to 120 ℃ for 18 h. Upon completion of the reaction, the mixture was cooled down to room temperature. The crude mixture was filtered through Celite® and then analyzed by GC using dodecane as an internal standard and isolated by silica gel flash chromatography using hexane and EtOAc as eluent.

5.4.3 Optimization of reaction conditions

Table 5.7 Evaluation of catalytic condition for the direct C–H arylation of ethoxybenzene[a]

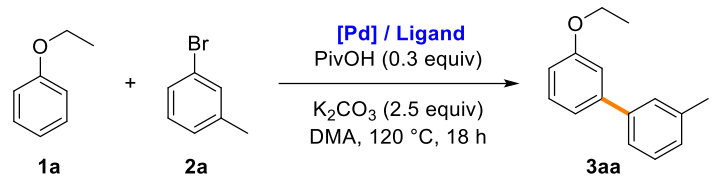

1a 60 equiv **2a** **3aa**

Entry	[Pd] (mol %)	Ligand (mol %)	Temperature (°C)	Yield (%)	Selectivity (o / m / p)	% Selectivity (o / m / p)
1	$Pd(OAc)_2$ (3)	PCy_3 (3)	120	71	1 / 8.2 / 2.9	8 / 68 / 24
2	$Pd(OAc)_2$ (3)	PPh_3 (3)	120	48	1 / 8.5 / 2.8	8 / 69 / 23
3	$Pd(OAc)_2$ (3)	$P(C_6F_5)_3$ (3)	120	14	1 / 6.0 / 2.0	11 / 67 / 22
4	$Pd(OAc)_2$ (3)	1,10-phen (3)	120	0	-	-
5	$Pd(PPh_3)_4$ (3)	-	120	54	1 / 5.3 / 1.9	12 / 65 / 23
6	$Pd(CO_2CF_3)_2$ (3)	-	120	68	1 / 10.0 / 3.1	7 / 71 / 22
7	$Pd(PhCN)_2Cl_2$ (3)	-	120	70	1 / 10.7 / 3.1	7 / 72 / 21
8	$Pd(CH_3CN)_4(BF_4)_2$ (3)	-	120	17	1 / 8.9 / 2.8	8 / 70 / 22
9	$Pd(CH_3CN)_2Cl_2$ (3)	-	120	79	1 / 10.2 / 3.2	7 / 71 / 22
10	$Pd(CH_3CN)_2Cl_2$ (3)	-	100	35	1 / 10.7 / 3.1	7 / 72 / 21
11	$Pd(CH_3CN)_2Cl_2$ (3)	-	140	44	1 / 6.8 / 2.4	8 / 71 / 21
12	$Pd(CH_3CN)_2Cl_2$ (1)	-	120	79	1 / 10.2 / 3.1	7 / 71 / 22
13	$Pd(CH_3CN)_2Cl_2$ (10)	-	120	15	1 / 10.3 / 3.0	7 / 72 / 21
14[b]	$Pd(CH_3CN)_2Cl_2$ (3)	-	120	56	1 / 9.3 / 2.7	8 / 71 / 21

[a]The total yield and regioselectivity (*ortho* / *meta* / *para*) were determined by GC analysis of the reaction mixture using dodecane as an internal standard. [b]With H_2O (2 equiv)

Table 5.8 Acid screening[a]

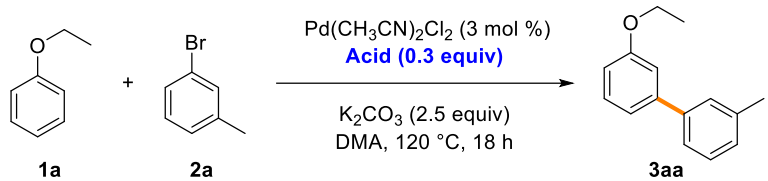

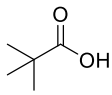	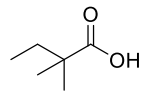	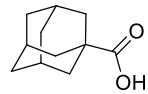	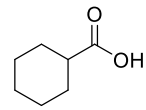	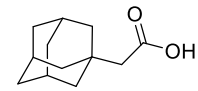
79% (7 / 72 / 22)	22% (8 / 72 / 21)	3% (16 / 48 / 36)	9% (22 / 41 / 37)	11% (21 / 46 / 33)
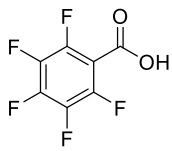	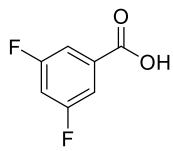	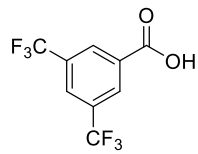	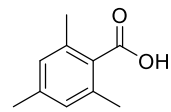	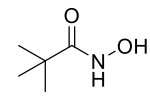
0%	0%	0%	26% (15 / 50 / 35)	2% (38 / 36 / 26)

[a]The total yield and regioselectivity (*ortho* / *meta* / *para*) were determined by GC analysis of the reaction mixture using dodecane as an internal standard.

Table 5.9 Base screening[a]

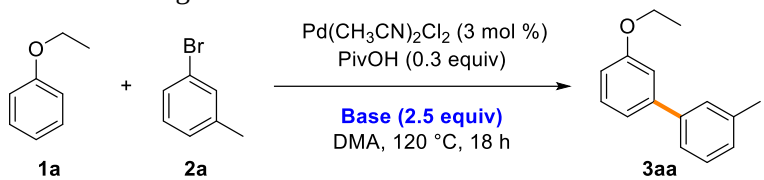

Entry	Base	Yield (%)	Selectivity (o / m / p)	% Selectivity (o / m / p)
1	K_2CO_3	79	1 / 10.2 / 3.2	7 / 71 / 22
2	Na_2CO_3	0	-	-
3	Rb_2CO_3	75	1 / 5.7 / 2.9	10 / 59 / 31
4	Cs_2CO_3	0	-	-
5	K_3PO_4	1.3	1 / 0.7 / 0.8	40 / 30 / 30
6[b]	NaOPiv	1.3	1 / 1.6 / 1.2	26 / 43 / 31
7	KOPiv	25	1 / 5.2 / 1.8	13 / 65 / 22
8[b]	KOPiv	32	1 / 6.2 / 2.0	11 / 68 / 21
9[b]	CsOPiv	4.3	1 / 1.4 / 1.8	31 / 45 /24
10	DABCO	0	-	-
11	Quinuclidine	0	-	-
12	TEA	0	-	-

[a]The total yield and regioselectivity (*ortho* / *meta* / *para*) were determined by GC analysis of the reaction mixture using dodecane as an internal standard. [b]Without PivOH.

Table 5.10 Solvent screening[a]

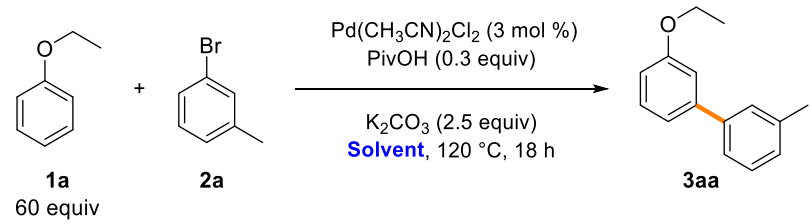

Entry	Solvent	Yield (%)	Selectivity (o / m / p)	% Selectivity (o / m / p)
1	DMA	79	1 / 10.2 / 3.2	7 / 71 / 22
2	DMF	7.3	1 / 3.3 / 1.8	17 / 54 / 30
3	DMSO	3.7	1 / 0.3 / 0.6	51 / 17 / 32
4	CH_3CN	0	-	-
5	Cyclohexane	0	-	-
6	Hexane	0	-	-
7	1,4-Dioxane	0	-	-
8	DCE	0	-	-
9	Mesitylene	0	-	-

[a]The total yield and regioselectivity (*ortho* / *meta* / *para*) were determined by GC analysis of the reaction mixture using dodecane as an internal standard.

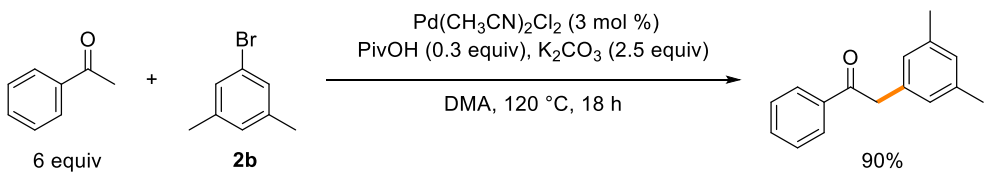

Scheme 5.8 Reaction with acetophenone.

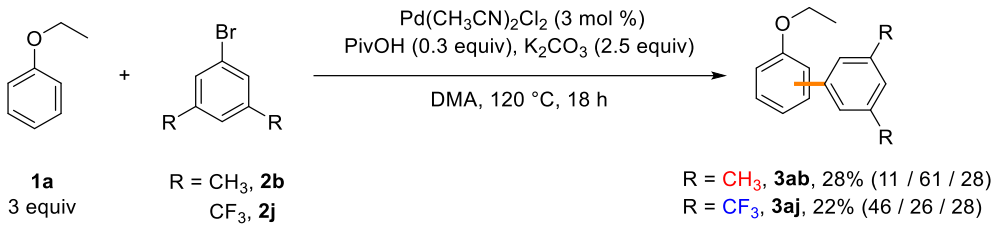

Scheme 5.9 Reactions of ethoxybenzene under the stoichiometric conditions.

5.4.4 Comparison of the reaction rates

Reaction rates of various arenes are compared by obtaining the initial rates of the C–H arylation. Initial rates were analyzed by total yields combining all regioisomers. For accurate comparison of the reaction rates, all arene compounds (99+% purity) were purified by passing through a short pad of activated neutral alumina, and used in a glove box.

All reactions were conducted using the above general procedure with the following modification. Inside a glove box, a 10 mL Schlenk tube equipped with a magnetic stirring bar was charged with K_2CO_3 (2.5 equiv, 69 mg, 0.50 mmol), pivalic acid (0.30 equiv, 6.1 mg, 0.060 mmol, stock solution in DMA). $Pd(CH_3CN)_2Cl_2$ (3.0 mol %, 1.6 mg, 0.0060 mmol, stock solution in DMA) was then added to the Schlenk tube as a solution in DMA, followed by **2b** (28 μL, 0.2 mmol, 1.0 equiv), arene (6.0 equiv) and dodecane (0.044 mmol, 10 μL) as an internal standard. The amount of DMA was varied to maintain the concentration of [Pd] (4.6 mM) and substrate (154 mM). Each tube was sealed and heated to 120 ℃. Aliquots of the reaction mixture were taken as indicated times and analyzed by GC. The same experiment was repeated two more times in each substrates and the average rate values were used to compare the reaction rates.

5.4.5 Kinetic isotope effect (KIE) measurements

The KIE was determined by comparing the initial reaction rates of the C–H arylation with benzene and benzene-d_6. Both reactions were conducted using the above general procedure with the following modification. Inside a glove box, a 10 mL Schlenk tube equipped with a magnetic stirring bar was charged with K_2CO_3 (2.5 equiv, 69 mg, 0.50 mmol), $Pd(CH_3CN)_2Cl_2$ (3.0 mol %, 1.6 mg, 0.0060 mmol), and pivalic acid (0.30 equiv, 6.1 mg, 0.060 mmol). **2b** (28 μL, 0.2 mmol, 1.0 equiv, 91 mM) and dodecane (0.044 mmol, 10 μL) as an internal standard were then added to the Schlenk tube in, followed by DMA (1.2 mL) and benzene or benzene-d_6 (60 equiv, 1.0 mL, 12 mmol). Each tube was sealed and heated to 120 ℃. Aliquots of the reaction mixture were taken every 5 min and analyzed by GC. The observed large primary KIE value (4.43) suggested that the C–H bond cleavage step of the arene is involved in the rate-limiting step.

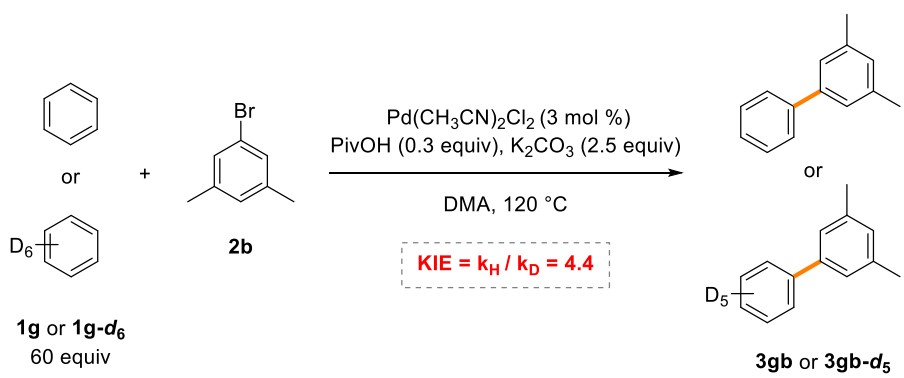

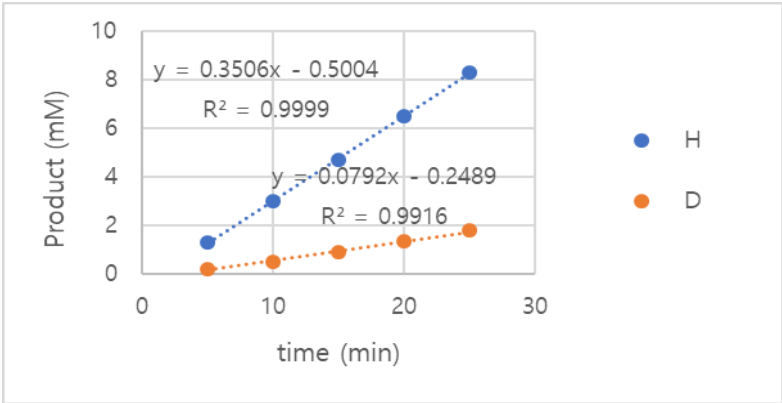

$$KIE = k_H/k_D = 0.3506/0.0792 = 4.43$$

Scheme 5.10 Initial rates of the C–H arylation of benzene and benzene-d_6.

5.4.6 Kinetic data

As shown in Scheme 5.3b, to obtain more information about mechanism of the reaction, kinetic studies were conducted such as the order of [Pd], [ArBr], KOPiv and K_2CO_3. Each kinetic experiment was conducted using the general procedure with the following modification.

5.4.6.1 Order in [Pd]

The order in [Pd] was determined by obtaining the initial rates of the C–H arylation with benzene at differing concentrations of $Pd(CH_3CN)_2Cl_2$ precatalyst. Inside a glove box, a 10 mL Schlenk tube equipped with a magnetic stirring bar was charged with K_2CO_3 (2.5 equiv, 69 mg, 0.50 mmol), pivalic acid (0.30 equiv, 6.1 mg, 0.060 mmol, stock solution in DMA), **2b** (28 μL, 0.2 mmol, 1.0 equiv, 94 mM), and dodecane (0.044 mmol, 10 μL) as an internal standard. Different amount of $Pd(CH_3CN)_2Cl_2$ (stock solution in DMA) was then added to the Schlenk tube in, followed by DMA (1.2 mL) and benzene (60 equiv, 1.0 mL, 12 mmol). Each tube

was sealed and heated to 120 ℃. Aliquots of the reaction mixture were taken every 5 min and analyzed by GC. The same experiment was repeated two more times in each [Pd] concentrations and the average rate values were used.

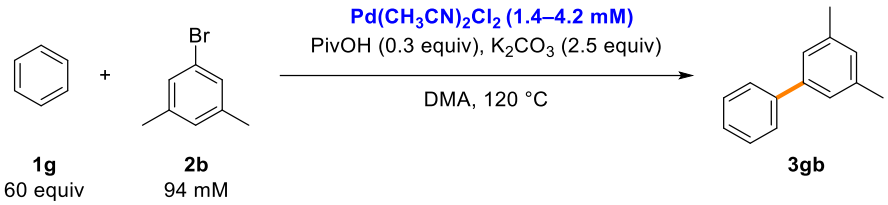

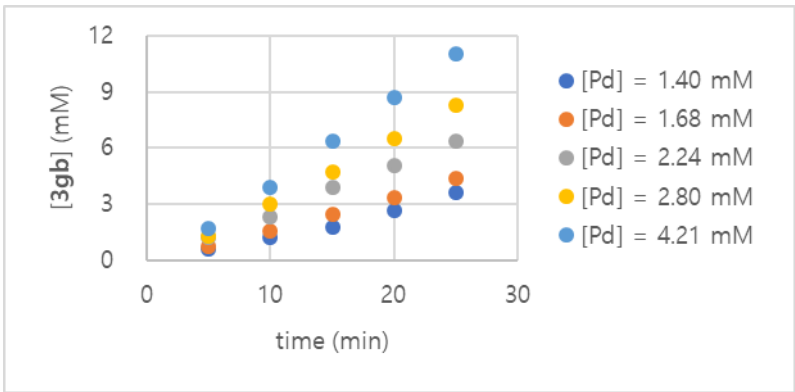

Scheme 5.11 Initial rates with different concentrations of [Pd].

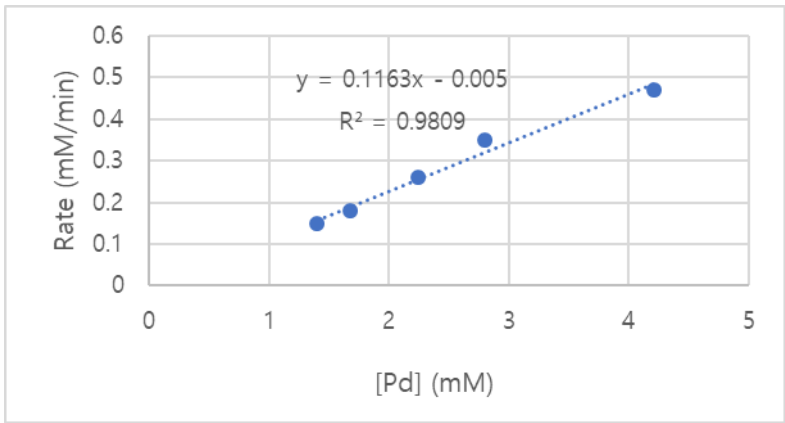

Scheme 5.12 Plot of initial rates with different concentrations of [Pd].

5.4.6.2 Order in [ArBr]

The order in [ArBr] was determined by obtaining the initial rate of the C–H arylation with benzene at differing concentrations of 1-bromo-3,5-dimethylbenzene **2b**. Inside a glove box, a 10 mL Schlenk tube equipped with a magnetic stirring bar was charged with K_2CO_3 (2.5 equiv, 69 mg, 0.50 mmol), pivalic acid (0.30 equiv, 6.1 mg, 0.060 mmol, stock solution in DMA), $Pd(CH_3CN)_2Cl_2$ (3.0 mol %, 1.6 mg, 0.0060 mmol), and dodecane (0.044 mmol, 10 μL) as an internal standard. Different amount of **2b** was then added to the Schlenk tube in, followed by DMA (1.2 mL) and benzene (60 equiv, 1.0 mL, 12 mmol). Each tube was sealed and heated to 120 ℃. Aliquots of the reaction mixture were taken every 5 min and analyzed by GC. The same experiment was repeated two more times in each [ArBr] concentrations and the average rate values were used.

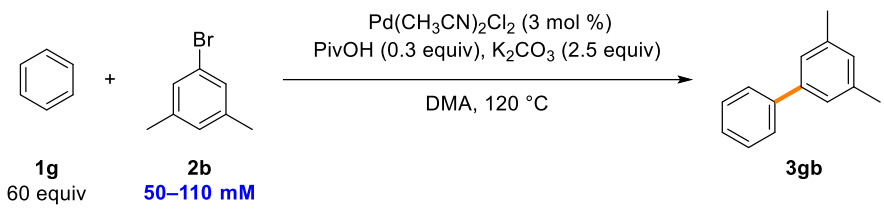

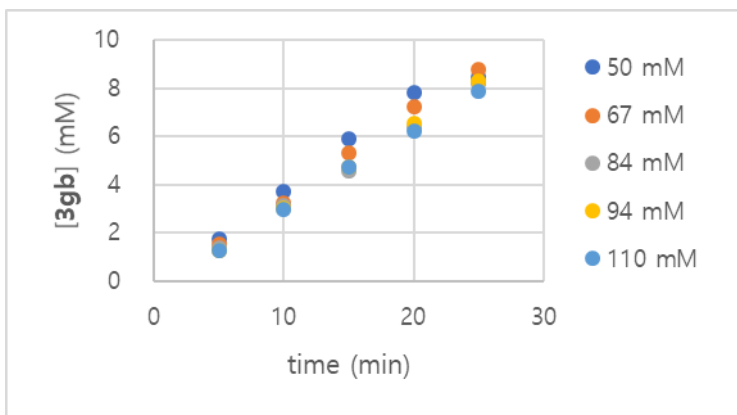

Scheme 5.13 Initial rates with different concentrations of **2b**.

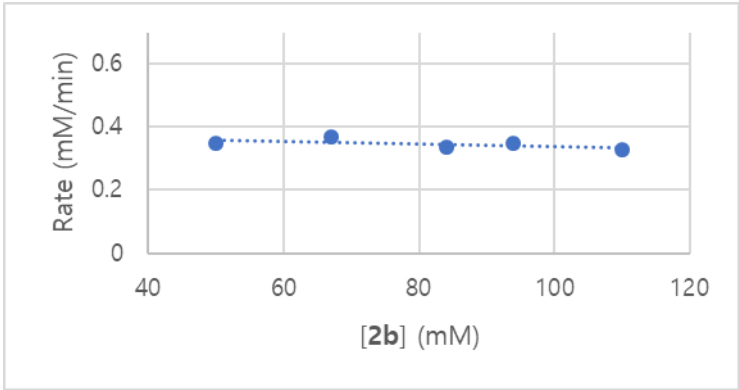

Scheme 5.14 Plot of initial rates with different concentrations of **2b**.

5.4.6.3 Dependence on KOPiv

The dependence on KOPiv was determined by obtaining the initial rate of the C–H arylation with benzene at differing amount of KOPiv. Inside a glove box, a 10 mL Schlenk tube equipped with a magnetic stirring bar was charged with K_2CO_3 (2.5 equiv, 69 mg, 0.50 mmol), $Pd(CH_3CN)_2Cl_2$ (3.0 mol %, 1.6 mg, 0.0060 mmol, stock solution in DMA), 1-bromo-3,5-dimethylbenzene (**2b**, 0.2 mmol, 1.0 equiv, 94 mM), and dodecane (0.044 mmol, 10 μL) as an internal standard. Different amount of KOPiv was the Schlenk tube in, followed by DMA (1.2 mL) and benzene (60 equiv, 1.0 mL, 12 mmol). Each tube was sealed and heated to 120 ℃. Aliquots of the reaction mixture were taken every 5 min and analyzed by GC. The same experiment was repeated in each KOPiv equivalence and the average rate values were used.

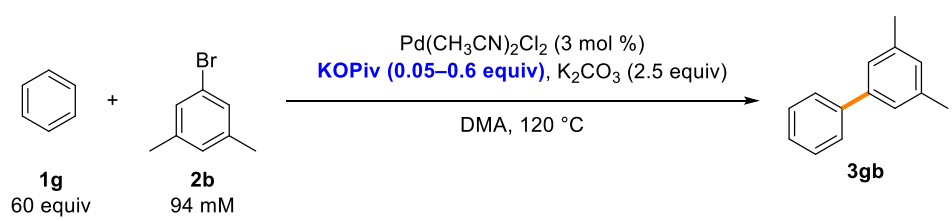

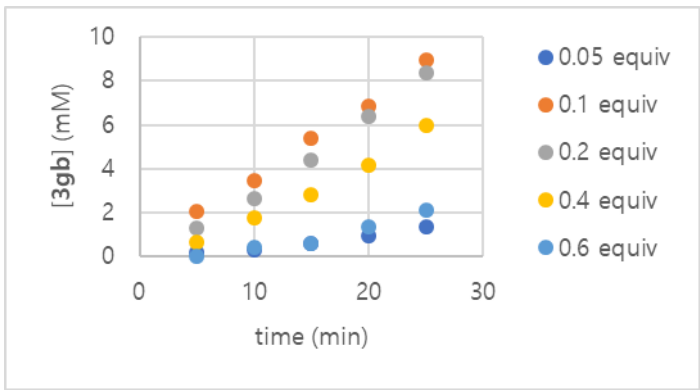

Scheme 5.15 Initial rates of the C–H arylation with different equivalences of KOPiv.

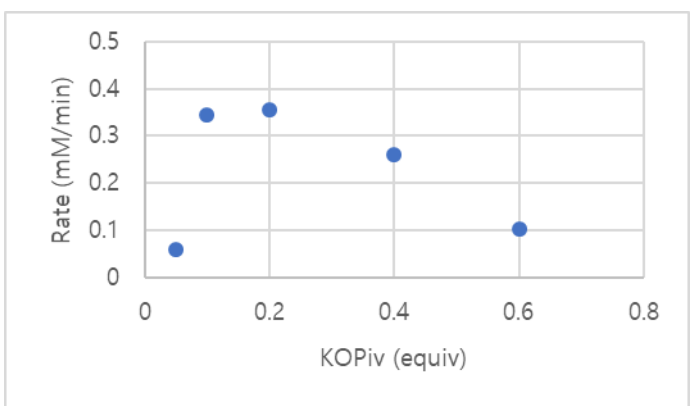

Scheme 5.16 Plot of initial rates with different concentration of KOPiv.

5.4.6.4 Dependence on K_2CO_3

The dependence on K_2CO_3 was determined by obtaining the initial rate of the C–H arylation with benzene at differing amount of K_2CO_3. Inside a glove box, a 10 mL Schlenk tube equipped with a magnetic stirring bar was charged with KOPiv (0.30 equiv, 8.4 mg, 0.060 mmol), $Pd(CH_3CN)_2Cl_2$ (3.0 mol %, 1.6 mg, 0.0060 mmol, stock solution in DMA), 1-bromo-3,5-dimethylbenzene (**2b**, 0.20 mmol, 1.0 equiv,

94 mM), and dodecane (0.044 mmol, 10 μL) as an internal standard. Different amount of K_2CO_3 was the Schlenk tube in, followed by DMA (1.2 mL) and benzene (60 equiv, 1.0 mL, 12 mmol). Each tube was sealed and heated to 120 ℃. Aliquots of the reaction mixture were taken every 5 min and analyzed by GC. The same experiment was repeated two more times in each equivalence of K_2CO_3 and the average rate values were used.

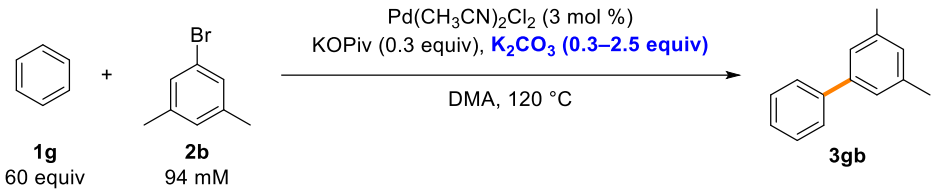

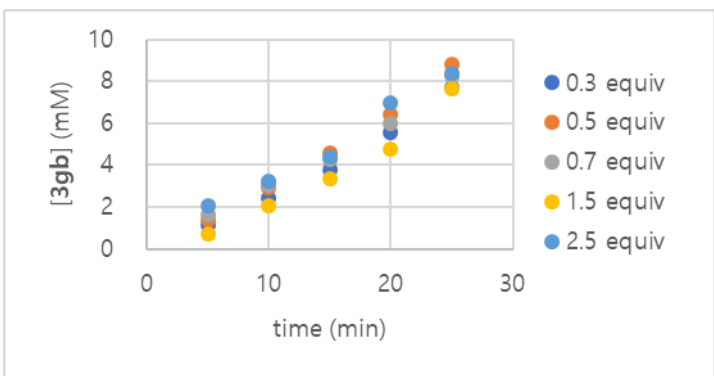

Scheme 5.17 Initial rates of the C–H arylation with different equivalences of K_2CO_3.

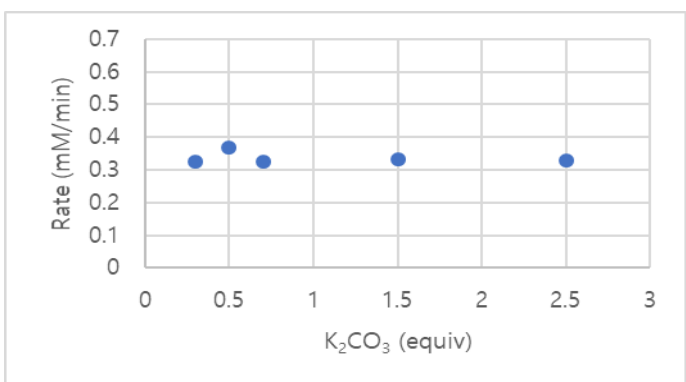

Scheme 5.18 Plot of initial rates with different concentration of K_2CO_3.

5.4.7 Kinetic data in [Pd] at low concentrations in C_6D_6

The order in $Pd(CH_3CN)_2Cl_2$ was determined by obtaining the initial rate of the C–H arylation at low concentration of $Pd(CH_3CN)_2Cl_2$ in benzene-d_6. Inside a glove box, a 10 mL Schlenk tube equipped with a magnetic stirring bar was charged with K_2CO_3 (2.5 equiv, 69 mg, 0.50 mmol), pivalic acid (0.30 equiv, 6.1 mg, 0.060 mmol, stock solution in DMA), 1-bromo-3,5-dimethylbenzene (**2b**, 28 μL, 0.20 mmol, 1.0 equiv, 94 mM), and dodecane (0.044 mmol, 10 μL) as an internal standard. Different amount of $Pd(CH_3CN)_2Cl_2$ (stock solution in DMA) was then added to the Schlenk tube in, followed by DMA (1.2 mL) and benzene-d_6 (60 equiv, 1.0 mL, 12 mmol). Each tube was sealed and heated to 120 ℃. Aliquots of the reaction mixture were taken every 1 h and analyzed by GC. The same experiment was repeated in each [Pd] concentrations and the average rate values were used.

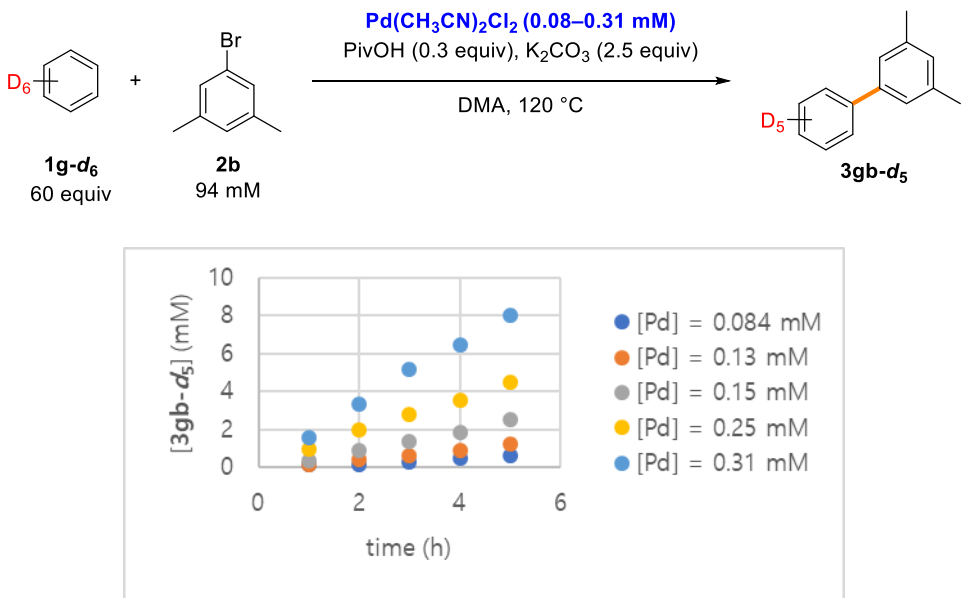

Scheme 5.19 Initial rates of the C–H arylation with different concentrations of $Pd(CH_3CN)_2Cl_2$.

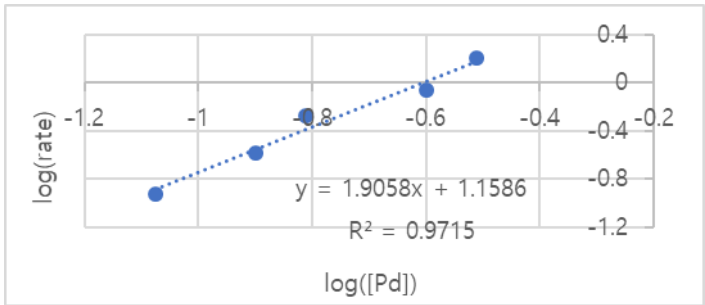

Scheme 5.20 Plot of initial rates with different concentration of $Pd(CH_3CN)_2Cl_2$.

5.4.8 Competition experiments

5.4.8.1 Competition between two different aryl bromides

Experiment A: bromobenzene (**2e**) vs 3-bromotoluene (**2a**)

To a 10 mL Schlenk tube equipped with a magnetic stirring bar were added K_2CO_3 (2.5 equiv, 69 mg, 0.50 mmol), $Pd(CH_3CN)_2Cl_2$ (3.0 mol %, 1.6 mg, 0.0060 mmol), pivalic acid (0.30 equiv, 6.1 mg, 0.060 mmol), DMA (1.2 mL) and ethoxybenzene (60 equiv, 1.52 mL, 12 mmol) followed by **2e** (22 μL, 0.20 mmol, 1.0 equiv) and **2a** (25 μL, 0.20 mmol, 1.0 equiv). The Schlenk tube was sealed and heated to 120 ℃ for 6 h. Upon completion of the reaction, the mixture was cooled to room temperature. The crude mixture was filtered through Celite® and then analyzed by GC using dodecane as an internal standard.

Experiment B: bromobenzene (**2e**) vs 3-bromobenzotrifluoride (**2i**)

The reaction was conducted using **2e** (22 μL, 0.20 mmol, 1.0 equiv) and **2i** (28 μL, 0.20 mmol, 1.0 equiv) as competing substrates followed by the above procedure.

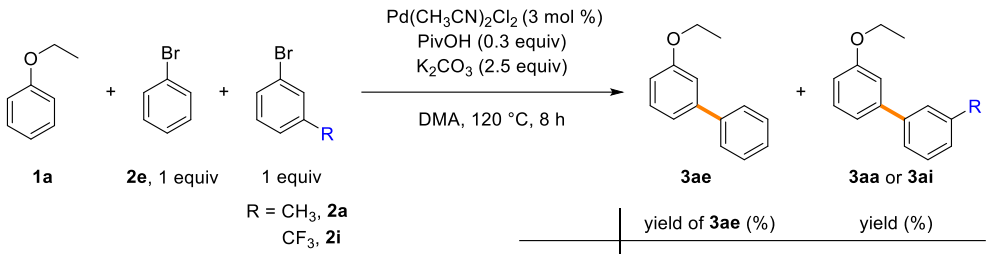

	yield of **3ae** (%)	yield (%)
R = CH_3	30 (12 / 65 / 23)	**3aa**, 24 (8 / 68 / 24)
R = CF_3	trace	**3ai**, 10 (18 / 51 / 31)

5.4.8.2 H/D scrambling experiment with D_2O

H/D scrambling between with D_2O was determined by ^2H NMR analysis of the product **3ab**. The reactions were conducted using the above general procedure with the following modification. To a 4 mL vial equipped with a magnetic stirring bar were added K_2CO_3 (2.5 equiv, 138 mg, 1.0 mmol), $Pd(CH_3CN)_2Cl_2$ (0.030 equiv, 3.1 mg, 0.012 mmol), pivalic acid (0.30 equiv, 12.3 mg, 0.12 mmol). 1-bromo-3,5-dimethylbenzene (**2b,** 1.0 equiv, 56 μL, 0.40 mmol) and ethoxybenzene (3.0 equiv, 152 μL, 1.2 mmol) were then added to the vial in, followed by DMA (1.2 mL) and D_2O (3.0 equiv, 22 μL, 1.2 mmol). The reaction vial was sealed and heated to 120 ℃ for 18 h. Upon completion of the reaction, the mixture was cooled down to room temperature. The crude mixture was filtered through Celite® and then the yield was analyzed by GC using dodecane as internal standard. The product was isolated by flash column chromatography and preparative TLC (PTLC) using hexane/ether eluent. The isolated product **3ab** was further analyzed by ^2H NMR spectroscopy in CH_2Cl_2 solvent with CD_3CN (1.93 ppm) as an internal standard.

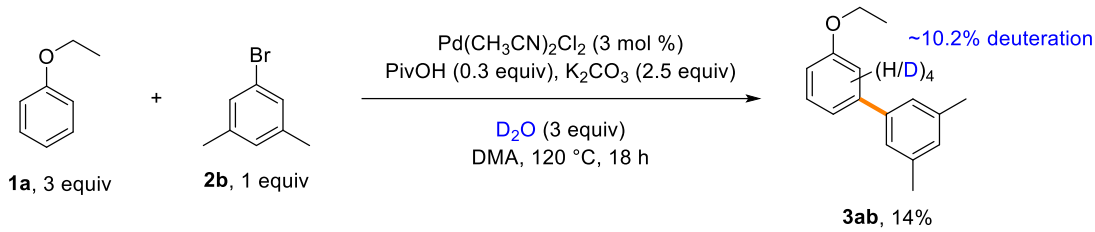

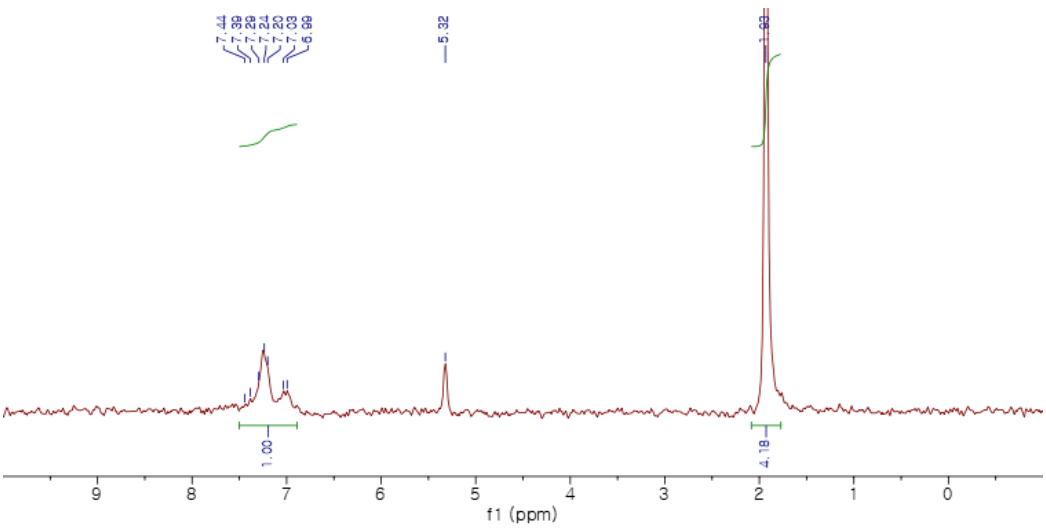

5.4.8.3 H/D scrambling experiment between ethoxybenzene and benzene-d_6

H/D scrambling between two arene substrates was determined by ^{2}H NMR analysis of the product **3ab**. The reactions were conducted using the above general procedure with the following modification. To a 4 mL vial equipped with a magnetic stirring bar were added K_2CO_3 (2.5 equiv, 138 mg, 1.0 mmol), $Pd(CH_3CN)_2Cl_2$ (0.030 equiv, 3.1 mg, 0.012 mmol), pivalic acid (0.30 equiv, 12.3 mg, 0.12 mmol), DMA (1.2 mL), ethoxybenzene (3.0 equiv, 152 μL, 1.2 mmol) and benzene-d_6 (3.0 equiv, 107 μL, 1.2 mmol) followed by **2b** (56 μL, 0.40 mmol, 1.0 equiv). The reaction vial was sealed and heated to 120 ℃ for 18 h. Upon completion of the reaction, the mixture was cooled down to room temperature. The crude mixture was filtered through Celite® and then the yield was analyzed by gas

chromatography using dodecane as internal standard. The product was isolated by flash column chromatography and preparative TLC (PTLC) using hexane/ether eluent. The isolated product **3ab** was further analyzed by ^{2}H NMR spectroscopy in CH_2Cl_2 solvent with CD_3CN (1.93 ppm) as an internal standard. H/D scrambling on the aryl group was clearly detected suggesting that the C–H bond cleavage facilitated by CMD process is reversible.

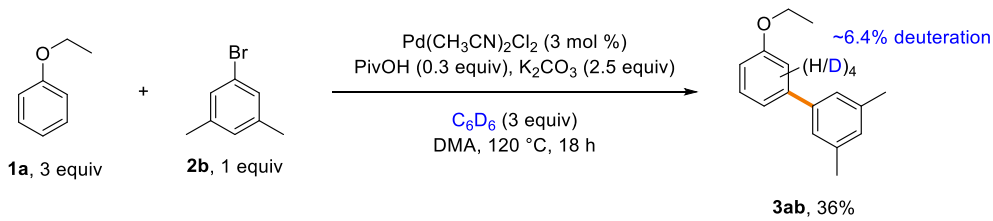

1a, 3 equiv + **2b**, 1 equiv → **3ab**, 36%

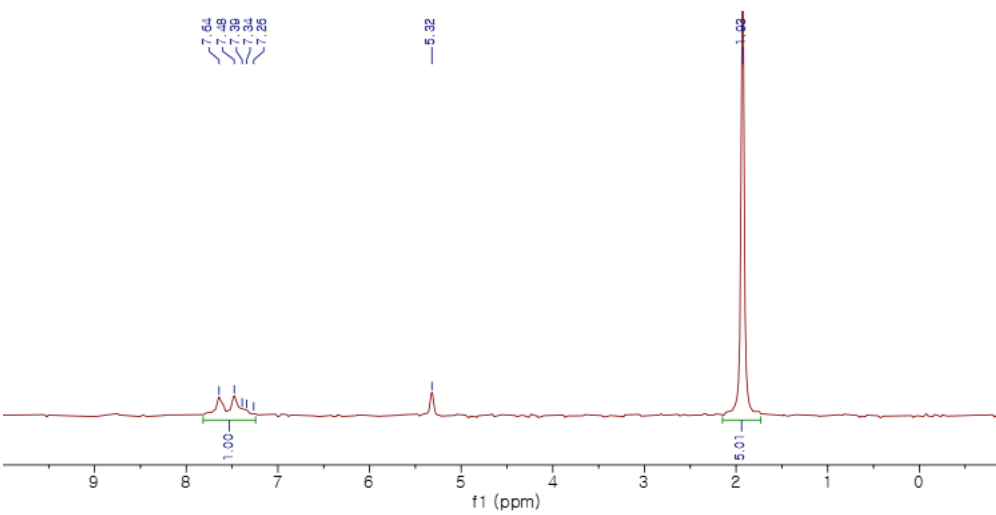

5.4.9 Synthesis of Pd complex 4a and 4b

AgOPiv and Pd complex **4a** were synthesized by literature procedures.[42]

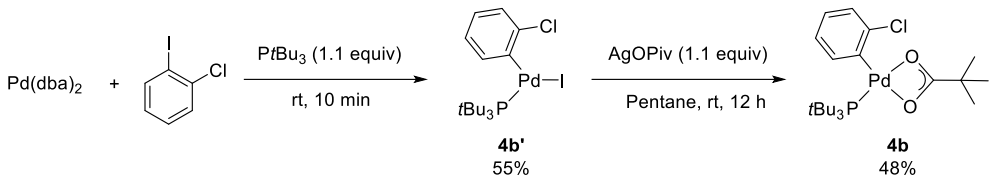

5.4.9.1 Synthesis of intermediate Pd complex 4b'

Inside a glove box, to a stirred solution of P*t*Bu$_3$ (45 mg, 1.1 equiv, 0.22 mmol) and 1-chloro-2-iodobenzene (1.0 mL) was added Pd(dba)$_2$ (115 mg, 1.0 equiv, 0.2 mmol). The reaction mixture was stirred at room temperature for 10 min. Pentane (20 mL) was added and the resulting mixture was stirred for 1 min and then cooled at -20 ℃ for 1 h. The solid was filtered, washed with ether until the filtrate contained no free dba, as judged by ^{1}H NMR spectroscopy. The solid was dried under reduced pressure to obtain the title compound as an orange color solid (60 mg, 55%).

^{1}H NMR (400 MHz, C_6D_6) δ 7.21 (d, J = 7.5 Hz, 1H), 6.98 – 6.95 (m, 1H), 6.61 (t, *J* = 7.4 Hz, 1H), 6.53 (t, *J* = 7.2 Hz, 1H), 1.03 (d, *J* = 12.6 Hz, 27H); ^{13}C NMR (151 MHz, CD_2Cl_2) δ 138.02 (d, *J* = 5.0 Hz), 137.66 (d, *J* = 2.0 Hz), 129.34, 128.73, 125.67, 125.27 (d, *J* = 2.3 Hz), 41.50 (d, *J* = 8.1 Hz), 31.88 (d, *J* = 2.8 Hz); ^{31}P NMR (162 MHz, C_6D_6) δ 53.9; Anal. calc'd for $C_{18}H_{31}ClIPPd$: C, 39.51; H, 5.71. Found: C, 38.3; H, 5.49.

5.4.9.2 Synthesis of Pd complex 4b

Inside a glove box, to a stirred solution of **4b'** (60 mg, 0.11 mmol, 1.0 equiv) and AgOPiv (25 mg, 0.12 mmol, 1.1 equiv) was added pentane (5 mL). The reaction mixture was stirred at room temperature for 12 h. The resulting mixture was filtered through Celite® and concentrated under reduced pressure. Recrystallization from pentane at -20 ℃ produced the Pd complex **4b** as yellow crystals which is suitable for X-ray diffraction analysis. Further filtration and drying afforded the title compound as a yellow solid (30 mg, 48%).

^{1}H NMR (400 MHz, C_6D_6) δ 7.42 (dt, *J* = 7.3, 2.1 Hz, 1H), 7.07 – 7.03 (m, 1H), 6.71 – 6.60 (m, 2H), 1.32 (d, *J* = 12.7 Hz, 27H), 1.28 (s, 9H); ^{13}C NMR (101 MHz, C_6D_6) δ 194.8, 141.1 (d, *J* = 3.0 Hz), 140.5, 138.6 (d, *J* = 3.2 Hz), 128.7, 125.4, 124.6 (d, *J* = 1.5 Hz), 40.6 (d, *J* = 11.8 Hz), 40.4, 32.2 (d, *J* = 3.2 Hz), 27.5; ^{31}P NMR (162 MHz, C_6D_6) δ 76.1; Anal. calc'd for $C_{23}H_{40}ClO_2PPd$: C, 52.98; H, 7.73. Found: C, 52.7; H, 7.82.

5.4.10 Stoichiometric reaction of Pd complex

Inside a glove box, a 10 mL Schlenk tube equipped with a magnetic stirring bar was charged with Pd complex (0.0060 mmol, 1.0 equiv) and the corresponding additives followed by DMA (1.2 mL) and ethoxybenzene (1.5 mL). The Schlenk tube was sealed and heated to 120 ℃ for 18 h. Upon the completion of the reaction, the mixture was cooled down to room temperature. The crude mixture was filtered through Celite® and then analyzed by gas chromatography for **3ac** or GC-MS for **3am** using dodecane (3.0 μL) as an internal standard.

5.4.11 Effect of crown ethers

Inside a glove box, a 10 mL Schlenk tube equipped with a magnetic stirring bar was charged with K_2CO_3 (2.5 equiv, 69 mg, 0.50 mmol), $Pd(CH_3CN)_2Cl_2$ (3.0 mol %, 1.6 mg, 0.0060 mmol), and pivalic acid (0.30 equiv, 6.1 mg, 0.060 mmol). Aryl bromide (1.0 equiv, 0.20 mmol) and crown ether additive were then added to the Schlenk tube, followed by DMA (1.2 mL) and arene (60 equiv, 12 mmol). The Schlenk tube was sealed and heated to 120 ℃ for 18 h. Upon completion of the reaction, the mixture was cooled down to room temperature. The crude mixture was filtered through Celite® and then analyzed by gas chromatography using dodecane as an internal standard.

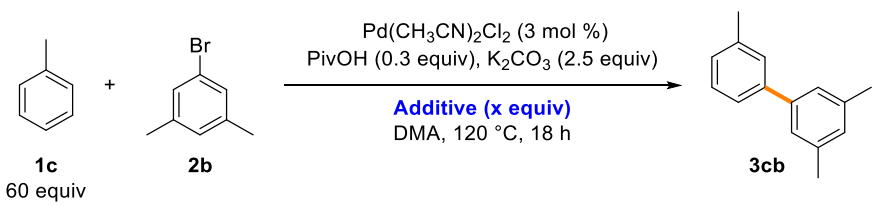

Table 5.11 Impact of crown ether additives in the C–H arylation of toluene[a]

Entry	Additive (x equiv)	Yield (%)	Selectivity (o / m / p)	% Selectivity (o / m / p)
1	-	87	1 / 13.0 / 6.1	5 / 64 / 31
2	18-Crown-6 (0.3)	91	1 / 10.1 / 4.9	6 / 63 / 31
3	18-Crown-6 (1)	90	1 / 5.5 / 2.9	11 / 58 / 31
4	18-Crown-6 (2.5)	85	1 / 3.0 / 1.9	17 / 51 / 32
5	18-Crown-6 (5)	80	1 / 2.1 / 1.5	22 / 46 / 32

5.4.12 Characterization of newly reported compounds

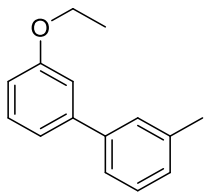

3-Ehoxy-3'-methyl-1,1'-biphenyl (3aa)

A modification of general procedure was employed for the reaction of 3-bromotoluene (**2a**, 0.2 mmol). The isomeric mixture of compound was obtained as a pale yellow oil (76% yield) and its identity was confirmed by comparison with NMR and GC spectra of authentic samples. ^{1}H NMR (500 MHz, $CDCl_3$) δ 7.44 – 7.37 (m, 2H), 7.37 – 7.30 (m, 2H), 7.17 (dd, *J* = 7.6, 1.3 Hz, 2H), 7.13 (t, *J* = 2.1 Hz, 1H), 6.89 (dd, *J* = 8.2, 2.6 Hz, 1H), 4.11 (q, *J* = 6.9 Hz, 2H), 2.42 (s, 3H), 1.45 (t, *J* = 7.0 Hz, 3H); ^{13}C NMR (126 MHz, $CDCl_3$) δ 159.4, 143.0, 141.3, 138.4, 129.8, 128.8, 128.2, 128.1, 124.4, 119.7, 113.6, 113.3, 63.6, 21.7, 15.1; HRMS-EI (m/z) $[M]^+$ calcd for $C_{15}H_{16}O$, 212.1201; found, 212.1200. The *ortho*-isomer; ^{1}H NMR (500 MHz, $CDCl_3$) δ 7.43 – 7.38 (m, 2H), 7.35 (dd, *J* = 7.5, 1.7 Hz, 1H), 7.34 – 7.28 (m, 2H), 7.15 (d, *J* = 7.3 Hz, 1H), 7.03 (t, *J* = 7.4 Hz, 1H), 6.99 (d, *J* = 8.2 Hz, 1H), 4.06 (q, *J* = 7.0 Hz, 2H), 2.42 (s, 3H), 1.37 (t, *J* = 7.0 Hz, 3H); ^{13}C NMR (126 MHz, $CDCl_3$) δ 156.0, 138.7, 137.5, 131.1, 131.0, 130.4, 128.5, 127.9, 127.6, 126.9, 120.9, 112.8, 64.2, 21.7, 14.9; HRMS-EI (m/z) $[M]^+$ calcd for $C_{15}H_{16}O$, 212.1201; found, 212.1199. The *para*-isomer; ^{1}H NMR (500 MHz, $CDCl_3$) δ 7.53 (d, *J* = 8.7 Hz, 2H), 7.38 (d, *J* = 10.8 Hz, 2H), 7.32 (t, *J* = 7.5 Hz, 1H), 7.14 (d, *J* = 7.4 Hz, 1H), 6.98 (d, *J* = 8.7 Hz, 2H), 4.10 (q, *J* = 7.0 Hz, 2H), 2.43 (s, 3H), 1.46 (t, *J* = 7.0 Hz, 3H); ^{13}C NMR (126 MHz, $CDCl_3$) δ 158.6, 141.0,

138.4, 133.9, 128.8, 128.3, 127.7, 127.5, 124.0, 114.8, 77.4, 77.2, 76.9, 63.7, 21.7, 15.0; HRMS-EI (m/z) $[M]^+$ calcd for $C_{15}H_{16}O$, 212.1201; found, 212.1203.

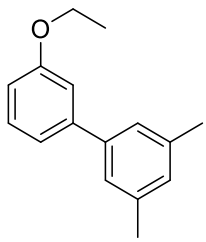

3'-Ethoxy-3,5-dimethyl-1,1'-biphenyl (3ab)

A modification of general procedure was employed for the reaction of 1-bromo-3,5-dimethylbenzene (**2b**, 0.2 mmol). The isomeric mixture of compound was obtained as a pale yellow oil (81% yield) and its identity was confirmed by comparison with NMR and GC spectra of authentic samples. ^{1}H NMR (300 MHz, $CDCl_3$) δ 7.47 – 7.40 (m, 1H), 7.35 (s, 2H), 7.32 – 7.25 (m, 2H), 7.11 (s, 1H), 6.99 (dd, *J* = 7.7, 2.1 Hz, 1H), 4.18 (q, *J* = 7.0 Hz, 2H), 2.50 (s, 6H), 1.55 (t, *J* = 7.0 Hz, 3H); ^{13}C NMR (75 MHz, $CDCl_3$) δ 159.3, 143.0, 141.2, 138.2, 129.7, 129.1, 125.2, 119.6, 113.5, 113.1, 63.4, 21.4, 15.0; HRMS-EI (m/z) $[M]^+$ calcd for $C_{15}H_{18}O$, 226.1358; found, 226.1361. The *ortho*-isomer; ^{1}H NMR (300 MHz, $CDCl_3$) δ 7.45 (dd, *J* = 7.5, 1.8 Hz, 1H), 7.38 (ddd, *J* = 8.1, 7.5, 1.8 Hz, 1H), 7.32 (s, 2H), 7.15 – 7.03 (m, 3H), 4.13 (q, *J* = 7.0 Hz, 2H), 2.48 (s, 6H), 1.46 (t, *J* = 7.0 Hz, 3H); ^{13}C NMR (75 MHz, $CDCl_3$) δ 156.0, 138.6, 137.3, 131.2, 131.0, 128.5, 128.4, 127.5, 120.9, 112.8, 64.1, 21.5, 14.9; HRMS-EI (m/z) $[M]^+$ calcd for $C_{15}H_{18}O$, 226.1358; found, 226.1360. The *para*-isomer; ^{1}H NMR (300 MHz, $CDCl_3$) δ 7.62 (d, *J* = 8.5 Hz, 2H), 7.30 (s, 2H), 7.12 – 7.01 (m, 3H), 4.18 (q, *J* = 7.0 Hz, 2H), 2.49 (s, 6H), 1.55 (t, *J* = 7.0 Hz, 3H); ^{13}C NMR (75 MHz, $CDCl_3$) δ 158.5, 141.0, 138.3, 134.0,

128.4, 128.3, 124.8, 114.8, 63.6, 21.5, 15.0; HRMS-EI (m/z) $[M]^+$ calcd for $C_{15}H_{18}O$, 226.1358; found, 226.1359.

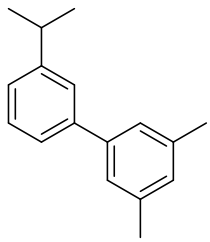

3'-Isopropyl-3,5-dimethyl-1,1'-biphenyl (3eb)

A modification of general procedure was employed for the reaction of 1-bromo-3,5-dimethylbenzene (**2b**, 0.2 mmol) and cumene (**1e**, 60 equiv). The isomeric mixture of compound was obtained as a colorless oil (79% yield) and its identity was confirmed by comparison with NMR and GC spectra of authentic samples. ^{1}H NMR (300 MHz, $CDCl_3$) δ 7.45 – 7.34 (m, 3H), 7.24 – 7.22 (m, 3H), 7.02 (s, 1H), 3.00 (hept, *J* = 6.9 Hz, 1H), 2.42 (s, 6H), 1.34 (d, *J* = 6.9 Hz, 6H); ^{13}C NMR (75 MHz, $CDCl_3$) δ 149.4, 141.8, 141.7, 138.3, 128.9, 128.7, 125.6, 125.3, 125.3, 124.9, 77.6, 77.2, 76.7, 34.4, 24.2, 21.6.; HRMS-EI (m/z) $[M]^+$ calcd for $C_{17}H_{20}$, 224.1565; found, 224.1564. The *ortho*-isomer; ^{1}H NMR (300 MHz, $CDCl_3$) δ 7.44 – 7.31 (m, 2H), 7.24 – 7.17 (m, 2H), 7.02 (s, 1H), 6.94 (s, 2H), 3.10 (hept, *J* = 6.9 Hz, 1H), 2.39 (s, 6H), 1.20 (d, *J* = 6.9 Hz, 6H); ^{13}C NMR (75 MHz, $CDCl_3$) δ 146.5, 142.2, 141.5, 137.5, 130.0, 128.4, 127.6, 127.3, 125.6, 125.3, 77.6, 77.2, 76.8, 29.5, 24.5, 21.5; found, 224.1565. The *para*-isomer; ^{1}H NMR (300 MHz, $CDCl_3$) δ 7.54 (d, *J* = 8.2 Hz, 2H), 7.32 (d, *J* = 8.1 Hz, 2H), 7.24 (s, 2H), 7.01 (s, 1H), 2.98 (hept, *J* = 6.9 Hz, 1H), 2.41 (s, 6H), 1.33 (d, *J* = 6.9 Hz, 6H); ^{13}C NMR (75 MHz, $CDCl_3$) δ 147.9, 141.4, 139.1, 138.3, 128.8, 127.2, 126.9, 125.1, 77.6, 77.2, 76.7, 33.9, 24.2,

21.6; HRMS-EI (m/z) $[M]^+$ calcd for $C_{17}H_{20}$, 224.1565; found, 224.1563.

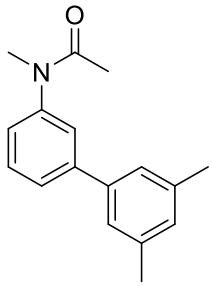

***N*-(3',5'-Dimethyl-[1,1'-biphenyl]-3-yl)-*N*-methylacetamide (3fb)**

A modification of general procedure was employed for the reaction of 1-bromo-3,5-dimethylbenzene (**2b**, 0.2 mmol) and *N*-methylacetanilide (**1f**, 60 equiv). The isomeric mixture of compound was obtained and its identity was confirmed by comparison with NMR and GC spectra of authentic samples. ^{1}H NMR (400 MHz, CD_3OD) δ 7.15 – 6.93 (m, 3H), 6.75 (s, 2H), 6.71 (d, *J* = 7.6 Hz, 1H), 6.57 (s, 1H), 2.81 (s, 3H), 1.92 (s, 6H), 1.42 (s, 3H); ^{13}C NMR (75 MHz, CD_3OD) δ 172.9, 146.0, 144.8, 141.0, 139.6, 132.1, 131.3, 130.5, 127.7, 126.6, 125.9, 37.6, 22.4, 21.5; HRMS-ESI (m/z) $[M+Na]^+$ calcd for $C_{17}H_{19}NNaO$, 276.1359; found, 276.1367. The *ortho*-isomer; ^{1}H NMR (300 MHz, $CDCl_3$) δ 7.41 – 7.34 (m, 3H), 7.23 – 7.19 (m, 1H), 6.99 (s, 1H), 6.88 (s, 2H), 3.02 (s, 3H), 2.33 (s, 6H), 1.80 (s, 3H); ^{13}C NMR (126 MHz, $CDCl_3$) δ 170.6, 142.1, 140.3, 138.8, 138.2, 131.6, 129.5, 128.7, 128.5, 128.3, 126.3, 37.2, 22.4, 21.5; HRMS-ESI (m/z) $[M+Na]^+$ calcd for $C_{17}H_{19}NNaO$, 276.1359; found, 276.1368. The *para*-isomer; ^{1}H NMR (300 MHz, CD_3OD) δ 7.65 (d, *J* = 8.3 Hz, 2H), 7.31 (d, *J* = 8.4 Hz, 2H), 7.22 (s, 2H), 7.00 (s, 1H), 3.25 (s, 3H), 2.35 (s, 6H), 1.88 (s, 3H); ^{13}C NMR (75 MHz, CD_3OD) δ 173.0, 144.5, 142.6, 141.1, 139.6, 130.31, 129.4, 128.4, 125.9, 37.6, 22.4, 21.5; HRMS-ESI (m/z) $[M+Na]^+$ calcd for $C_{17}H_{19}NNaO$, 276.1359; found,

276.1362.

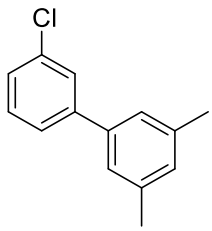

3'-Chloro-3,5-dimethyl-1,1'-biphenyl (3kb)

A modification of general procedure was employed for the reaction of 1-bromo-3,5-dimethylbenzene (**2b**, 0.2 mmol) and chlorobenzene (**1k**, 60 equiv). The isomeric mixture of compound was obtained and its identity was confirmed by comparison with NMR and GC spectra of authentic samples. ^{1}H NMR (300 MHz, $CDCl_3$) δ 7.56 (t, *J* = 1.8 Hz, 1H), 7.45 (dt, *J* = 7.4, 1.6 Hz, 1H), 7.37 – 7.28 (m, 2H), 7.18 (s, 2H), 7.02 (s, 1H), 2.39 (s, 6H). The *ortho*-isomer; ^{1}H NMR (300 MHz, $CDCl_3$) δ 7.53 (dd, *J* = 6.8, 1.3 Hz, 1H), 7.42 – 7.28 (m, 3H), 7.14 (s, 2H), 7.11 (s, 1H), 2.46 (s, 6H); ^{13}C NMR (75 MHz, $CDCl_3$) δ 140.9, 139.5, 137.6, 132.6, 131.5, 130.0, 129.4, 128.4, 127.3, 126.8, 21.5; HRMS-EI (m/z) $[M]^+$ calcd for $C_{14}H_{13}Cl$, 216.0706; found, 216.0707. The *para*-isomer; ^{1}H NMR (500 MHz, $CDCl_3$) δ 7.54 (d, *J* = 8.5 Hz, 2H), 7.42 (d, *J* = 8.5 Hz, 2H), 7.21 (s, 2H), 7.05 (s, 1H), 2.42 (s, 6H); ^{13}C NMR (126 MHz, $CDCl_3$) δ 140.1, 140.0, 138.5, 133.3, 129.4, 128.9, 128.5, 125.0, 21.50; HRMS-EI (m/z) $[M]^+$ calcd for $C_{14}H_{13}Cl$, 216.0706; found, 216.0703. Identity of the *meta*-isomer was confirmed by comparison with reported data.[43]

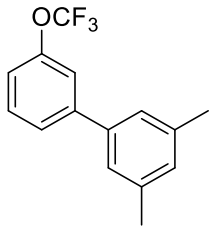

3,5-Dimethyl-3'-(trifluoromethoxy)-1,1'-biphenyl (3lb)

A modification of general procedure was employed for the reaction of 1-bromo-3,5-dimethylbenzene (**2b**, 0.2 mmol) and (trifluoromethoxy)benzene (**1l**, 60 equiv). The isomeric mixture of compound was obtained as a colorless oil (64% yield) and its identity was confirmed by comparison with NMR and GC spectra of authentic samples. ^{1}H NMR (300 MHz, $CDCl_3$) δ 7.54 – 7.45 (m, 2H), 7.37 (t, *J* = 7.9 Hz, 1H), 7.21 (s, 3H), 7.05 (s, 1H), 2.40 (s, 6H); ^{13}C NMR (75 MHz, $CDCl_3$) δ 150.0, 144.0, 139.9, 138.7, 130.1, 129.9, 125.7, 125.3, 121.1 (q, *J* = 257.7 Hz), 120.0, 119.5, 21.3; ^{19}F NMR (376 MHz, $CDCl_3$) δ -57.7; HRMS-EI (m/z) $[M]^+$ calcd for $C_{15}H_{13}F_3O$, 266.0918; found, 266.0920. The *ortho*-isomer; ^{1}H NMR (300 MHz, $CDCl_3$) δ 7.48 – 7.40 (m, 1H), 7.38 – 7.26 (m, 3H), 7.13 (s, 2H), 7.04 (s, 1H), 2.38 (s, 6H); ^{13}C NMR (75 MHz, $CDCl_3$) δ 146.5, 137.9, 137.0, 135.8, 131.7, 129.5, 128.5, 127.2, 127.0, 121.3, 120.8 (q, *J* = 259.2 Hz), 21.4; ^{19}F NMR (376 MHz, $CDCl_3$) δ -57.0; HRMS-EI (m/z) $[M]^+$ calcd for $C_{15}H_{13}F_3O$, 266.0918; found, 266.0918. The *para*-isomer; ^{1}H NMR (300 MHz, $CDCl_3$) δ 7.54 (dt, *J* = 8.7, 2.6 Hz, 2H), 7.27 (d, *J* = 8.0 Hz, 2H), 7.18 (s, 2H), 7.04 (s, 1H), 2.40 (s, 6H); ^{13}C NMR (75 MHz, $CDCl_3$) δ 148.8, 140.6, 140.1, 138.7, 129.6, 128.6, 125.3, 121.1 (q, *J* = 257.0 Hz), 121.3, 21.3; ^{19}F NMR (376 MHz, $CDCl_3$) δ -57.9; HRMS-EI (m/z) $[M]^+$ calcd for $C_{15}H_{13}F_3O$, 266.0918; found, 266.0915.

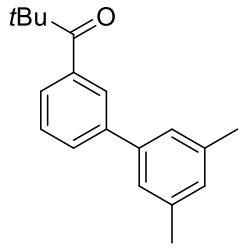

1-(3',5'-Dimethyl-[1,1'-biphenyl]-3-yl)-2,2-dimethylpropan-1-one (3nb)

A modification of general procedure was employed for the reaction of 1-bromo-3,5-dimethylbenzene (**2b**, 0.2 mmol) and pivalophenone (**1n**, 6 equiv). The isomeric mixture of compound was obtained and its identity was confirmed by comparison with NMR and GC spectra of authentic samples. ^{1}H NMR (300 MHz, $CDCl_3$) δ 7.85 (t, *J* = 1.6 Hz, 1H), 7.64 (t, *J* = 8.6 Hz, 2H), 7.44 (t, *J* = 7.7 Hz, 1H), 7.21 (s, 2H), 7.02 (s, 1H), 2.39 (s, 6H), 1.38 (s, 9H); ^{13}C NMR (75 MHz, $CDCl_3$) δ 209.7, 141.6, 140.6, 139.3, 138.6, 129.6, 129.4, 128.4, 126.8, 126.4, 125.2, 44.5, 28.2, 21.5; HRMS-EI (m/z) $[M]^+$ calcd for $C_{19}H_{22}O$, 266.1671; found, 266.1672. The *ortho*-isomer; ^{1}H NMR (300 MHz, $CDCl_3$) δ 7.45 – 7.42 (m, 2H), 7.39 – 7.34 (m, 1H), 7.17 (d, *J* = 7.8 Hz, 1H), 7.03 (s, 2H), 7.01 (s, 1H), 2.37 (s, 6H), 0.94 (s, 9H); ^{13}C NMR (75 MHz, $CDCl_3$) δ 217.0, 141.2, 141.0, 138.3, 138.1, 129.6, 129.3, 128.8, 127.4, 126.7, 125.9, 45.0, 27.5, 21.4; HRMS-EI (m/z) $[M]^+$ calcd for $C_{19}H_{22}O$, 266.1671; found, 266.1673. The *para*-isomer; ^{1}H NMR (300 MHz, $CDCl_3$) δ 7.85 (d, *J* = 8.4 Hz, 2H), 7.65 (d, *J* = 8.4 Hz, 2H), 7.27 (s, 2H), 7.07 (s, 1H), 2.43 (s, 6H), 1.44 (s, 9H); ^{13}C NMR (75 MHz, $CDCl_3$) δ 208.5, 144.1, 140.2, 138.5, 136.8, 129.7, 128.8, 126.8, 125.2, 44.3, 28.3, 21.5; HRMS-EI (m/z) $[M]^+$ calcd for $C_{19}H_{22}O$, 266.1671; found, 266.1673.

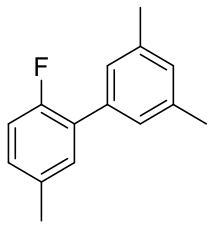

2-Fluoro-3',5,5'-trimethyl-1,1'-biphenyl (3qb)

A modification of general procedure was employed for the reaction of 1-bromo-3,5-dimethylbenzene (**2b**, 0.2 mmol) and 4-fluorotoluene (**1q**, 6 equiv). The title compound was obtained as a colorless oil (93% yield). ^{1}H NMR (300 MHz, $CDCl_3$) δ 7.35 (dd, *J* = 7.5, 2.1 Hz, 1H), 7.30 (s, 2H), 7.21 – 7.10 (m, 3H), 2.51 (s, 4H), 2.48 (s, 2H); ^{13}C NMR (75 MHz, $CDCl_3$) δ 158.1 (d, *J* = 244.7 Hz), 137.94, 136.0 (d, *J* = 1.0 Hz), 133.6 (d, *J* = 3.7 Hz), 131.3 (d, *J* = 3.4 Hz), 129.3, 129.2 (d, *J* = 8.0 Hz), 129.0 (d, *J* = 13.8 Hz), 127.0 (d, *J* = 2.7 Hz), 115.8 (d, *J* = 23.0 Hz), 21.5, 20.8; ^{19}F NMR (376 MHz, $CDCl_3$) δ -123.1; HRMS-EI (m/z) $[M]^+$ calcd for $C_{15}H_{15}F$, 214.1158; found, 214.1156.

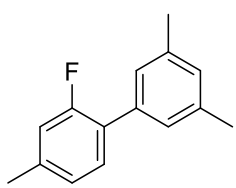

2-Fluoro-3',4,5'-trimethyl-1,1'-biphenyl (3rb)

A modification of general procedure was employed for the reaction of 1-bromo-3,5-dimethylbenzene (**2b**, 0.2 mmol) and 3-fluorotoluene (**1r**, 60 equiv). The title compound was obtained as a colorless oil (92% yield). ^{1}H NMR (300 MHz, $CDCl_3$) δ 7.48 (t, *J* = 8.2 Hz, 1H), 7.40 – 7.35 (m, 2H), 7.17 – 7.10 (m, 3H), 2.55 (s, 6H), 2.53 (s, 3H); ^{13}C NMR (75 MHz, $CDCl_3$) δ 159.7 (d, *J* = 247.2 Hz), 139.3 (d,

J = 8.0 Hz), 137.9, 135.9, 130.5 (d, *J* = 4.1 Hz), 129.2, 126.9 (d, *J* = 2.8 Hz), 126.4 (d, *J* = 13.6 Hz), 125.1 (d, *J* = 3.2 Hz), 116.6 (d, *J* = 22.7 Hz), 21.4, 21.0 (d, *J* = 1.4 Hz); ^{19}F NMR (376 MHz, $CDCl_3$) δ -118.8; HRMS-EI (m/z) $[M]^+$ calcd for $C_{15}H_{15}F$, 214.1158; found, 214.1158.

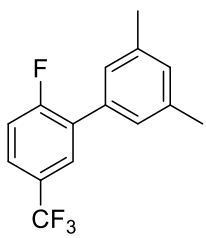

2-Fluoro-3',5'-dimethyl-5-(trifluoromethyl)-1,1'-biphenyl (3tb)

A modification of general procedure was employed for the reaction of 1-bromo-3,5-dimethylbenzene (**2b**, 0.2 mmol) and 4-fluorobenzotrifluoride (**1t**, 6 equiv) for 3 h. The title compound was obtained as a colorless oil (94% yield). ^{1}H NMR (400 MHz, $CDCl_3$) δ 7.71 (dd, *J* = 6.9, 2.2 Hz, 1H), 7.61 – 7.55 (m, 1H), 7.25 (t, *J* = 9.2 Hz, 1H), 7.17 (s, 2H), 7.08 (s, 1H), 2.40 (s, 6H); ^{13}C NMR (101 MHz, $CDCl_3$) δ 161.49 (d, *J* = 251.2 Hz), 138.4, 134.3, 130.4, 130.2, 128.7 – 128.3 (m), 126.9 (d, *J* = 2.6 Hz), 126.2 – 125.9 (m), 125.3, 122.6, 116.80 (d, *J* = 24.4 Hz), 21.5; ^{19}F NMR (376 MHz, $CDCl_3$) δ -61.9, -112.2; HRMS-EI (m/z) $[M]^+$ calcd for $C_{15}H_{12}F_4$, 268.0875; found, 268.0873.

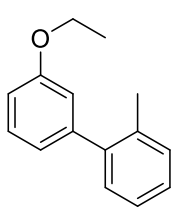

3'-Ethoxy-2-methyl-1,1'-biphenyl (3ac)

A modification of general procedure was employed for the reaction of 2-bromotoluene (**2c**, 0.2 mmol). The isomeric mixture of compound was obtained as a pale-yellow oil (78% yield) and its identity was confirmed by comparison with NMR and GC spectra of authentic samples. ^{1}H NMR (500 MHz, $CDCl_3$) δ 7.35 (t, *J* = 7.8 Hz, 1H), 7.32 – 7.26 (m, 4H), 6.95 – 6.88 (m, 3H), 4.10 (q, *J* = 7.0 Hz, 2H), 2.32 (s, 3H), 1.47 (t, *J* = 7.0 Hz, 3H); ^{13}C NMR (126 MHz, $CDCl_3$) δ 158.8, 143.5, 142.0, 135.5, 130.4, 129.8, 129.2, 127.4, 125.8, 121.7, 115.5, 113.1, 77.4, 77.2, 76.9, 63.6, 20.6, 15.0; HRMS-EI (m/z) $[M]^+$ calcd for $C_{15}H_{16}O$, 212.1201; found, 212.1198. The *ortho*-isomer; ^{1}H NMR (500 MHz, $CDCl_3$) δ 7.35 (t, *J* = 7.8 Hz, 1H), 7.27 – 7.18 (m, 5H), 7.03 (t, *J* = 7.4 Hz, 1H), 6.99 (d, *J* = 8.2 Hz, 1H), 4.04 (q, *J* = 7.0 Hz, 2H), 2.20 (s, 3H), 1.29 (t, *J* = 7.0 Hz, 3H). ^{13}C NMR (126 MHz, $CDCl_3$) δ 156.1, 139.0, 136.9, 131.6, 131.3, 130.2, 129.6, 128.6, 127.2, 125.4, 120.6, 112.3, 64.0, 20.1, 14.9; HRMS-EI (m/z) $[M]^+$ calcd for $C_{15}H_{16}O$, 212.1201; found, 212.1201. The *para*-isomer; ^{1}H NMR (500 MHz, $CDCl_3$) δ 7.30 – 7.24 (m, 6H), 6.97 (d, *J* = 8.6 Hz, 2H), 4.11 (q, *J* = 7.0 Hz, 2H), 2.31 (s, 3H), 1.48 (t, *J* = 7.0 Hz, 3H); ^{13}C NMR (126 MHz, $CDCl_3$) δ 158.0, 141.7, 135.6, 134.3, 130.4, 130.4, 130.0, 127.1, 125.9, 114.1, 63.6, 20.7, 15.1; HRMS-EI (m/z) $[M]^+$ calcd for $C_{15}H_{16}O$, 212.1201; found, 212.1202.

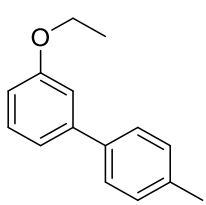

3-Ethoxy-4’-methyl-1,1’-biphenyl (3ad)

A modification of general procedure was employed for the reaction of 4-bromotoluene (**2d**, 0.2 mmol). The isomeric mixture of compound was obtained as a pale-yellow solid (83% yield) and its identity was confirmed by comparison with NMR and GC spectra of authentic samples. ^{1}H NMR (500 MHz, $CDCl_3$) δ 7.53 (d, *J* = 7.9 Hz, 2H), 7.37 (t, *J* = 7.9 Hz, 1H), 7.29 (d, *J* = 8.0 Hz, 2H), 7.20 (d, *J* = 7.6 Hz, 1H), 7.16 (s, 1H), 6.91 (dd, *J* = 8.3, 2.6 Hz, 1H), 4.14 (q, *J* = 7.0 Hz, 2H), 2.44 (s, 3H), 1.49 (t, *J* = 7.0 Hz, 3H); ^{13}C NMR (126 MHz, $CDCl_3$) δ 159.4, 142.8, 138.4, 137.3, 129.8, 129.6, 127.2, 119.5, 113.5, 113.1, 63.6, 21.3, 15.1; HRMS-EI (m/z) $[M]^+$ calcd for $C_{15}H_{16}O$, 212.1201; found, 212.1198. The *ortho*-isomer; ^{1}H NMR (300 MHz, $CDCl_3$) δ 7.49 (d, *J* = 8.0 Hz, 2H), 7.37 – 7.30 (m, 2H), 7.25 (t, *J* = 7.9 Hz, 2H), 7.08 – 6.96 (m, 2H), 4.07 (q, *J* = 7.0 Hz, 2H), 2.42 (s, 3H), 1.38 (t, *J* = 7.0 Hz, 3H); ^{13}C NMR (126 MHz, $CDCl_3$) δ 156.0, 147.4, 136.5, 135.8, 131.0, 129.5, 128.8, 128.4, 120.9, 112.8, 64.1, 21.4, 14.9; HRMS-EI (m/z) $[M]^+$ calcd for $C_{15}H_{16}O$, 212.1201; found, 212.1202. The *para*-isomer; ^{1}H NMR (300 MHz, $CDCl_3$) δ 7.55 (d, *J* = 8.7 Hz, 2H), 7.50 (d, *J* = 8.1 Hz, 2H), 7.27 (d, *J* = 8.0 Hz, 2H), 7.00 (d, *J* = 8.7 Hz, 2H), 4.10 (q, *J* = 7.0 Hz, 2H), 2.43 (s, 3H), 1.48 (t, *J* = 7.0 Hz, 3H); Identity of the *para*-isomer was confirmed by comparison with reported data.[44]

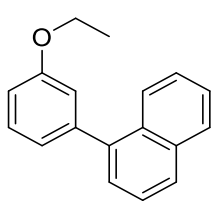

1-(3-Ethoxyphenyl)naphthalene (3af)

A modification of general procedure was employed for the reaction of 1-bromonaphthalene (**2f**, 0.2 mmol). The isomeric mixture of compound was obtained as a yellow oil (73% yield) and its identity was confirmed by comparison with NMR and GC spectra of authentic samples. ^{1}H NMR (500 MHz, $CDCl_3$) δ 8.11 (d, *J* = 8.4 Hz, 1H), 7.97 (d, *J* = 8.1 Hz, 1H), 7.92 (d, *J* = 7.9 Hz, 1H), 7.62 – 7.44 (m, 5H), 7.20 (d, *J* = 7.3 Hz, 2H), 7.07 (dd, *J* = 7.6, 1.9 Hz, 1H), 4.10 (q, *J* = 7.0 Hz, 2H), 1.50 (t, *J* = 7.0 Hz, 3H); ^{13}C NMR (126 MHz, $CDCl_3$) δ 158.9, 142.2, 140.3, 133.9, 131.7, 129.3, 128.3, 127.7, 126.8, 126.1, 126.1, 125.8, 125.4, 122.5, 116.2, 113.5, 63.4, 14.9; HRMS-EI (m/z) $[M]^+$ calcd for $C_{18}H_{16}O$, 248.1201; found, 248.1198. The *ortho*-isomer; ^{1}H NMR (500 MHz, $CDCl_3$) δ 7.91 (d, *J* = 8.1 Hz, 1H), 7.88 (d, *J* = 8.2 Hz, 1H), 7.73 (d, *J* = 8.4 Hz, 1H), 7.56 (d, *J* = 7.5 Hz, 1H), 7.52 – 7.46 (m, 2H), 7.46 – 7.40 (m, 2H), 7.37 (dd, *J* = 7.4, 1.5 Hz, 1H), 7.11 (dt, *J* = 7.4, 1.0 Hz, 1H), 7.05 (d, *J* = 8.3 Hz, 1H), 4.03 – 3.90 (m, 2H), 1.10 (t, *J* = 7.0 Hz, 3H); ^{13}C NMR (126 MHz, $CDCl_3$) δ 156.6, 137.3, 133.5, 132.2, 132.1, 130.1, 129.0, 128.1, 127.6, 127.4, 126.7, 125.5, 125.5, 125.4, 120.6, 112.5, 63.9, 14.6; HRMS-EI (m/z) $[M]^+$ calcd for $C_{18}H_{16}O$, 248.1201; found, 248.1199. The *para*-isomer; ^{1}H NMR (500 MHz, $CDCl_3$) δ 8.00 (d, *J* = 8.4 Hz, 1H), 7.94 (d, *J* = 8.1 Hz, 1H), 7.88 (d, *J* = 8.2 Hz, 1H), 7.59 – 7.42 (m, 6H), 7.07 (d, *J* = 8.5 Hz, 2H), 4.16 (q, *J* = 7.0 Hz, 2H), 1.52 (t, *J* = 7.0 Hz, 3H). Identity of the *para*-isomer was confirmed by comparison with reported data.[45]

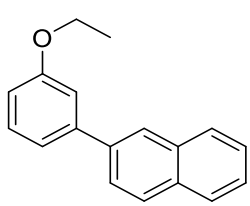

2-(3-Ethoxyphenyl)naphthalene (3ag)

A modification of general procedure was employed for the reaction of 2-bromonaphthalene (**2g**, 0.2 mmol). The isomeric mixture of compound was obtained as a pale-yellow solid (82% yield) and its identity was confirmed by comparison with NMR and GC spectra of authentic samples. ^{1}H NMR (300 MHz, $CDCl_3$) δ 8.07 (s, 1H), 7.95 – 7.87 (m, 3H), 7.77 (dd, *J* = 8.5, 1.8 Hz, 1H), 7.56 – 7.48 (m, 2H), 7.42 (t, *J* = 7.8 Hz, 1H), 7.34 – 7.28 (m, 2H), 6.95 (ddd, *J* = 8.1, 2.5, 1.0 Hz, 1H), 4.16 (q, *J* = 7.0 Hz, 2H), 1.50 (t, *J* = 7.0 Hz, 3H); ^{13}C NMR (75 MHz, $CDCl_3$) δ 159.5, 142.7, 138.6, 133.8, 132.8, 130.0, 128.5, 128.3, 127.8, 126.4, 126.1, 126.0, 125.7, 120.0, 113.9, 113.4, 63.7, 15.1; HRMS-EI (m/z) $[M]^+$ calcd for $C_{18}H_{16}O$, 248.1201; found, 248.1199. The *ortho*-isomer; ^{1}H NMR (500 MHz, $CDCl_3$) δ 8.03 (s, 1H), 7.93 – 7.86 (m, 3H), 7.78 (dd, *J* = 8.5, 1.6 Hz, 1H), 7.54 – 7.46 (m, 3H), 7.36 (td, *J* = 8.2, 1.7 Hz, 1H), 7.10 (t, *J* = 7.4 Hz, 1H), 7.04 (d, *J* = 8.2 Hz, 1H), 4.09 (q, *J* = 7.0 Hz, 2H), 1.37 (t, *J* = 7.0 Hz, 3H); ^{13}C NMR (75 MHz, $CDCl_3$) δ 156.2, 136.5, 133.6, 132.5, 131.3, 131.0, 128.8, 128.4, 128.3, 128.2, 127.7, 127.1, 126.0, 125.8, 121.1, 112.9, 64.2, 14.9; HRMS-EI (m/z) $[M]^+$ calcd for $C_{18}H_{16}O$, 248.1201; found, 248.1198. The *para*-isomer; ^{1}H NMR (300 MHz, $CDCl_3$) δ 8.00 (s, 1H), 7.91 – 7.84 (m, 3H), 7.73 (dd, *J* = 8.5, 1.8 Hz, 1H), 7.68 – 7.63 (m, 2H), 7.48 (pd, *J* = 6.8, 3.4 Hz, 2H), 7.02 (d, *J* = 8.7 Hz, 2H), 4.11 (q, *J* = 7.0 Hz, 2H), 1.47 (t, *J* = 7.0 Hz, 3H). Identity of the *para*-isomer was confirmed by comparison with reported data.[46]

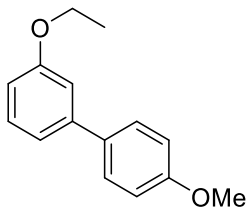

3-Ethoxy-4'-methoxy-1,1'-biphenyl (3ah)

A modification of general procedure was employed for the reaction of 4-bromoanisole (**2h**, 0.2 mmol). The isomeric mixture of compound was obtained as a white solid (61% yield) and its identity was confirmed by comparison with NMR and GC spectra of authentic samples. ^{1}H NMR (300 MHz, $CDCl_3$) δ 7.53 (d, *J* = 8.3 Hz, 2H), 7.32 (t, *J* = 7.8 Hz, 1H), 7.14 – 7.09 (m, 2H), 6.97 (d, *J* = 8.3 Hz, 2H), 6.85 (dd, *J* = 8.2, 2.5 Hz, 1H), 4.10 (q, *J* = 7.0 Hz, 2H), 3.85 (s, 3H), 1.45 (t, *J* = 7.0 Hz, 3H). The *ortho*-isomer; ^{1}H NMR (300 MHz, $CDCl_3$) δ 7.51 (d, *J* = 8.8 Hz, 2H), 7.32 (dd, *J* = 7.5, 1.8 Hz, 1H), 7.29 – 7.23 (m, 1H), 7.03 – 6.93 (m, 4H), 4.04 (q, *J* = 7.0 Hz, 2H), 3.85 (s, 3H), 1.36 (t, *J* = 7.0 Hz, 3H); ^{13}C NMR (75 MHz, $CDCl_3$) δ 159.2, 155.8, 140.0, 130.8, 130.6, 128.8, 128.7, 122.0, 120.8, 115.1, 112.6, 112.6, 63.9, 55.1, 14.8; HRMS-EI (m/z) $[M]^+$ calcd for $C_{15}H_{16}O_2$, 228.1150; found, 228.1147. The *para*-isomer; ^{1}H NMR (300 MHz, $CDCl_3$) δ 7.49 (d, *J* = 3.7 Hz, 2H), 7.46 (d, *J* = 3.7 Hz, 2H), 6.97 (d, *J* = 2.9 Hz, 2H), 6.94 (d, *J* = 2.7 Hz, 2H), 4.07 (q, *J* = 7.0 Hz, 2H), 3.84 (s, 3H), 1.44 (t, *J* = 7.0 Hz, 3H). Identity of the *meta* and *para*-isomers was confirmed by comparison with reported data.[47]

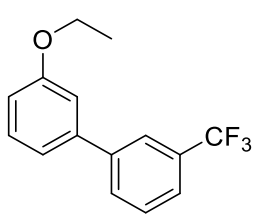

3-Ethoxy-3'-(trifluoromethyl)-1,1'-biphenyl (3ai)

A modification of general procedure was employed for the reaction of 3-bromobenzotrifluoride (**2i**, 0.2 mmol). The isomeric mixture of compound was obtained as a pale-yellow oil (54% yield) and its identity was confirmed by comparison with NMR and GC spectra of authentic samples. ^{1}H NMR (300 MHz, $CDCl_3$) δ 7.86 (s, 1H), 7.75 (d, *J* = 7.6 Hz, 1H), 7.61 (d, *J* = 7.7 Hz, 1H), 7.52 (t, *J* = 7.7 Hz, 1H), 7.37 (t, *J* = 7.9 Hz, 1H), 7.20 – 7.12 (m, 2H), 6.98 – 6.90 (m, 1H), 4.10 (q, *J* = 7.0 Hz, 2H), 1.46 (t, *J* = 7.0 Hz, 3H); ^{13}C NMR (75 MHz, $CDCl_3$) δ 159.6, 142.1, 141.3, 131.2 (q, *J* = 32.4 Hz), 130.6, 130.1, 129.3, 124.4 (q, *J* = 272.4 Hz), 124.1 (m), 119.6, 113.9, 113.8, 63.7, 14.9; ^{19}F NMR (376 MHz, $CDCl_3$) δ -62.5; HRMS-EI (m/z) $[M]^+$ calcd for $C_{15}H_{13}F_3O$, 266.0918; found, 266.0917. The *ortho*-isomer; ^{1}H NMR (300 MHz, $CDCl_3$) δ 7.94 (s, 1H), 7.75 (d, *J* = 7.6 Hz, 1H), 7.58 (d, *J* = 7.8 Hz, 1H), 7.50 (t, *J* = 7.7 Hz, 1H), 7.41 – 7.28 (m, 2H), 7.04 (td, *J* = 7.5, 1.0 Hz, 1H), 6.99 (d, *J* = 8.1 Hz, 1H), 4.05 (q, *J* = 7.0 Hz, 2H), 1.36 (t, *J* = 7.0 Hz, 3H); ^{13}C NMR (75 MHz, $CDCl_3$) δ 156.0, 139.5, 132.9, 130.8, 130.3 (q, *J* = 31.9 Hz), 129.5, 129.2, 128.4, 126.7 (q, *J* = 3.9 Hz), 124.6 (q, *J* = 271.79 Hz), 123.5 (q, *J* = 3.8 Hz), 121.1, 112.6, 64.1, 14.7; ^{19}F NMR (376 MHz, $CDCl_3$) δ -62.5; HRMS-EI (m/z) $[M]^+$ calcd for $C_{15}H_{13}F_3O$, 266.0918; found, 266.0917. The *para*-isomer; ^{1}H NMR (300 MHz, $CDCl_3$) δ 7.84 (s, 1H), 7.70 (d, *J* = 7.6 Hz, 1H), 7.60 – 7.45 (m, 4H), 6.99 (d, *J* = 8.7 Hz, 2H), 4.06 (q, *J* = 7.0 Hz, 2H), 1.46 (t, *J* = 7.0 Hz, 3H); ^{13}C NMR (101 MHz, CDCl) δ 159.1, 141.6, 132.0, 131.1 (q, *J* = 31.5 Hz), 129.9, 129.2, 128.2, 124.3 (q, *J* = 217.6 Hz), 123.3 (q, *J* = 3.8 Hz), 123.2 (q, *J* = 3.8 Hz), 115.0, 63.5, 14.8; ^{19}F NMR (376 MHz, $CDCl_3$) δ -62.6; HRMS-EI (m/z) $[M]^+$ calcd for $C_{15}H_{13}F_3O$, 266.0918; found, 266.0917.

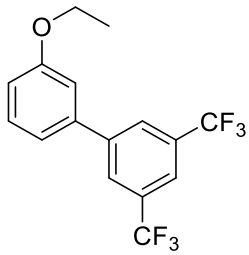

3'-Ethoxy-3,5-bis(trifluoromethyl)-1,1'-biphenyl (3aj)

A modification of general procedure was employed for the reaction of 1-bromo-3,5-bis(trifluoromethyl)benzene (**2j**, 0.2 mmol). The isomeric mixture of compound was obtained as a pale-yellow oil (69% yield) and its identity was confirmed by comparison with NMR and GC spectra of authentic samples. ^{1}H NMR (500 MHz, $CDCl_3$) δ 8.01 (s, 2H), 7.86 (s, 1H), 7.41 (t, *J* = 8.0 Hz, 1H), 7.18 (d, *J* = 8.4 Hz, 1H), 7.12 (t, *J* = 2.1 Hz, 1H), 6.98 (dd, *J* = 8.3, 2.4 Hz, 1H), 4.12 (q, *J* = 7.0 Hz, 2H), 1.47 (t, *J* = 7.0 Hz, 3H); ^{13}C NMR (126 MHz, $CDCl_3$) δ 159.8, 143.4, 139.8, 132.2 (q, *J* = 33.2 Hz), 130.5, 127.4 (m), 123.6 (q, *J* = 272.2 Hz), 121.2 (m), 119.6, 114.6, 114.0, 63.9, 15.0; ^{19}F NMR (376 MHz, $CDCl_3$) δ -62.9; HRMS-EI (m/z) $[M]^+$ calcd for $C_{16}H_{12}F_6O$, 334.0792; found, 334.0789. The *ortho*-isomer; ^{1}H NMR (500 MHz, $CDCl_3$) δ 8.05 (s, 2H), 7.81 (s, 1H), 7.39 – 7.35 (m, 2H), 7.07 (td, *J* = 7.6, 0.8 Hz, 1H), 7.01 (d, *J* = 8.2 Hz, 1H), 4.08 (q, *J* = 7.0 Hz, 2H), 1.37 (t, *J* = 7.0 Hz, 3H). ^{13}C NMR (126 MHz, $CDCl_3$) δ 155.9, 140.6, 131.2 (q, *J* = 33.0 Hz), 130.6, 130.4, 129.9 (m), 127.5, 123.7(d, *J* = 272.7 Hz), 121.2, 120.5 (q, *J* = 4.1 Hz), 112.6, 64.2, 14.7. ^{19}F NMR (376 MHz, $CDCl_3$) δ -62.9; HRMS-EI (m/z) $[M]^+$ calcd for $C_{16}H_{12}F_6O$, 334.0792; found, 334.0795. The *para*-isomer; ^{1}H NMR (500 MHz, $CDCl_3$) δ 7.96 (s, 2H), 7.79 (s, 1H), 7.54 (d, *J* = 8.8 Hz, 2H), 7.01 (d, *J* = 8.8 Hz, 2H), 4.10 (q, *J* = 7.0 Hz, 2H), 1.46 (t, *J* = 7.0 Hz, 3H). Identity of

the *para*-isomer was confirmed by comparison with reported data.[22b]

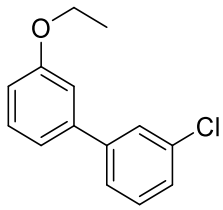

3-Chloro-3'-ethoxy-1,1'-biphenyl (3ak)

A modification of general procedure was employed for the reaction of 1-bromo-3-chlorobenzene (**2k**, 0.2 mmol). The isomeric mixture of compound was obtained as a pale-yellow oil (49% yield) and its identity was confirmed by comparison with NMR and GC spectra of authentic samples. ^{1}H NMR (300 MHz, $CDCl_3$) δ 7.64 – 7.63 (m, 1H), 7.52 – 7.49 (m, 1H), 7.41 – 7.36 (m, 3H), 7.20 – 7.15 (m, 2H), 6.96 (ddd, *J* = 8.3, 2.4, 0.8 Hz, 1H), 4.12 (q, *J* = 7.0 Hz, 2H), 1.50 (t, *J* = 7.0 Hz, 3H); ^{13}C NMR (75 MHz, $CDCl_3$) δ 159.5, 143.1, 141.3, 134.7, 130.0, 129.9, 127.4, 127.4, 125.4, 119.5, 113.9, 113.5, 63.6, 14.9; HRMS-EI (m/z) $[M]^+$ calcd for $C_{14}H_{13}ClO$, 232.0655; found, 232.0658. The *ortho*-isomer ^{1}H NMR (300 MHz, $CDCl_3$) δ 7.72 (s, 1H), 7.63 – 7.49 (m, 1H), 7.47 – 7.33 (m, 4H), 7.12 (t, *J* = 7.1 Hz, 1H), 7.06 (d, *J* = 8.3 Hz, 1H), 4.12 (q, *J* = 7.0 Hz, 2H), 1.46 (t, *J* = 7.0 Hz, 3H); ^{13}C NMR (75 MHz, $CDCl_3$) δ 155.8, 140.5, 133.7, 130.8, 129.8, 129.4, 129.2, 129.2, 127.8, 126.8, 120.9, 112.6, 64.1, 14.7; HRMS-EI (m/z) $[M]^+$ calcd for $C_{14}H_{13}ClO$, 232.0655; found, 232.0656. The *para*-isomer; ^{1}H NMR (300 MHz, $CDCl_3$) δ 7.60 (t, *J* = 1.6 Hz, 1H), 7.52 (dt, *J* = 8.8, 3.0 Hz, 2H), 7.46 (dt, *J* = 7.3, 1.7 Hz, 1H), 7.39 – 7.29 (m, 2H), 7.00 (dt, *J* = 8.8, 2.7 Hz, 2H), 4.09 (q, *J* = 7.0 Hz, 2H), 1.49 (t, *J* = 7.0 Hz, 3H); ^{13}C NMR (75 MHz, $CDCl_3$) δ 159.0, 142.8, 134.7, 132.1, 130.0,

128.2, 126.8, 126.6, 124.8, 114.9, 63.6, 14.9; HRMS-EI (m/z) $[M]^+$ calcd for $C_{14}H_{13}ClO$, 232.0655; found, 232.0655.

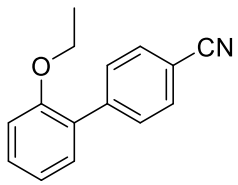

2'-Ethoxy-[1,1'-biphenyl]-4-carbonitrile (3al)

A modification of general procedure was employed for the reaction of 4-bromobenzonitrile (**2l**, 0.2 mmol). The isomeric mixture of compound was obtained as a colorless oil (44% yield) and its identity was confirmed by comparison with NMR and GC spectra of authentic samples. ^{1}H NMR (400 MHz, $CDCl_3$) δ 7.68 (s, 4H), 7.37 (ddd, *J* = 8.2, 7.4, 1.8 Hz, 1H), 7.32 (dd, *J* = 7.6, 1.8 Hz, 1H), 7.05 (td, *J* = 7.5, 1.1 Hz, 1H), 7.00 (dd, *J* = 8.3, 1.1 Hz, 1H), 4.07 (q, *J* = 7.0 Hz, 2H), 1.37 (t, *J* = 7.0 Hz, 3H); ^{13}C NMR (101 MHz, $CDCl_3$) δ 155.8, 143.6, 131.7, 130.7, 130.3, 130.0, 128.7, 121.0, 119.3, 112.5, 110.3, 64.0, 14.8; HRMS-EI (m/z) $[M]^+$ calcd for $C_{15}H_{13}NO$, 223.0997; found, 223.0999. The *meta*-isomer; ^{1}H NMR (400 MHz, $CDCl_3$) δ 7.72 – 7.63 (m, 4H), 7.38 (t, *J* = 8.0 Hz, 1H), 7.15 (ddd, *J* = 7.7, 1.7, 0.9 Hz, 1H), 7.11 – 7.09 (m, 1H), 6.95 (ddd, *J* = 8.3, 2.5, 1.0 Hz, 1H), 4.09 (q, *J* = 7.0 Hz, 2H), 1.45 (t, *J* = 7.0 Hz, 3H); ^{13}C NMR (101 MHz, $CDCl_3$) δ 159.6, 145.6, 140.6, 132.6, 130.2, 127.8, 119.6, 119.0, 114.5, 113.8, 111.1, 63.7, 14.9; ; HRMS-EI (m/z) $[M]^+$ calcd for $C_{15}H_{13}NO$, 223.0997; found, 223.0998. The *para*-isomer; ^{1}H NMR (400 MHz, $CDCl_3$) δ 7.71 – 7.60 (m, 4H), 7.53 (d, *J* = 8.9 Hz, 2H), 6.99 (d, *J* = 8.9 Hz, 2H), 4.09 (q, *J* = 7.0 Hz, 2H), 1.45 (t, *J* = 7.0 Hz, 3H); ^{13}C NMR (101 MHz, $CDCl_3$) δ 159.7, 145.3, 132.7, 131.4, 128.4, 127.2, 119.3,

115.1, 110.1, 63.7, 14.9; HRMS-EI (m/z) $[M]^+$ calcd for $C_{15}H_{13}NO$, 223.0997; found, 223.0998.

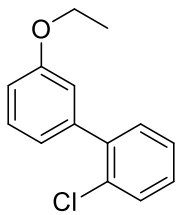

2-Chloro-3'-ethoxy-1,1'-biphenyl (3am)

^{1}H NMR (300 MHz, $CDCl_3$) δ 7.47 – 7.42 (m, 1H), 7.35 – 7.23 (m, 4H), 7.02 – 6.95 (m, 2H), 6.90 (ddd, *J* = 8.3, 2.6, 1.0 Hz, 1H), 4.05 (q, *J* = 7.0 Hz, 2H), 1.41 (t, *J* = 7.0 Hz, 4H); ^{13}C NMR (101 MHz, $CDCl_3$) δ 158.6, 140.7, 140.5, 131.3, 129.9, 129.1, 128.6, 126.8, 121.7, 115.6, 113.8, 63.5, 14.9; HRMS-EI (m/z) $[M]^+$ calcd for $C_{15}H_{13}ClO$, 232.0652; found, 232.0656. The *ortho*-isomer; ^{1}H NMR (300 MHz, $CDCl_3$) δ 7.45 – 7.38 (m, 1H), 7.36 – 7.29 (m, 1H), 7.28 – 7.20 (m, 3H), 7.19 – 7.13 (m, 1H), 6.99 (dt, *J* = 7.4, 1.0 Hz, 1H), 6.94 (d, *J* = 8.3 Hz, 1H), 4.00 (q, *J* = 6.9 Hz, 2H), 1.24 (t, *J* = 7.0 Hz, 3H); ^{13}C NMR (101 MHz, $CDCl_3$) δ k 131.9, 131.1, 129.4, 129.3, 129.0, 128.5, 126.4, 120.4, 112.3, 64.1, 14.8; HRMS-EI (m/z) $[M]^+$ calcd for $C_{15}H_{13}ClO$, 232.0655; found, 232.0656. The *para*-isomer; ^{1}H NMR (400 MHz, $CDCl_3$) δ 7.44 (dd, *J* = 7.5, 1.7 Hz, 1H), 7.36 (d, *J* = 8.2 Hz, 2H), 7.31 (dd, *J* = 7.6, 2.0 Hz, 1H), 7.30 – 7.25 (m, 1H), 7.25 – 7.20 (m, 1H), 6.94 (d, *J* = 8.2 Hz, 2H), 4.07 (q, *J* = 7.0 Hz, 2H), 1.43 (t, *J* = 7.0 Hz, 3H); ^{13}C NMR (101 MHz, $CDCl_3$) δ 158.6, 140.3, 132.7, 131.8, 131.5, 130.7, 130.1, 128.3, 126.9, 114.1, 63.6, 15.0; HRMS-EI (m/z) $[M]^+$ calcd for $C_{15}H_{13}ClO$, 232.0655; found, 232.0654.

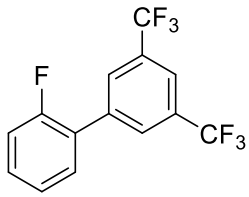

2-Fluoro-3',5'-bis(trifluoromethyl)-1,1'-biphenyl (3ij)

A modification of general procedure was employed for the reaction of 1-bromo-3,5-trifluoromethylbenzene (**2j**, 0.2 mmol) and fluorobenzene (**1i**, 6 equiv) for 3 h. The isomeric mixture was analyzed by ^{19}F NMR and GC. Its identity was confirmed by comparison with NMR and GC spectra of authentic samples. ^{1}H NMR (600 MHz, $CDCl_3$) δ 8.00 (s, 2H), 7.89 (s, 1H), 7.47 (td, *J* = 7.7, 1.7 Hz, 1H), 7.45 – 7.41 (m, 1H), 7.29 (td, *J* = 7.6, 1.2 Hz, 1H), 7.22 (ddd, *J* = 10.7, 8.3, 1.2 Hz, 1H); ^{19}F NMR (376 MHz, $CDCl_3$) δ -62.9, -118.0. The *meta*-isomer; ^{1}H NMR (400 MHz, $CDCl_3$ δ 8.00 (s, 2H), 7.90 (s, 1H), 7.49 (td, *J* = 8.0, 5.8 Hz, 1H), 7.40 (ddd, *J* = 7.7, 1.8, 1.0 Hz, 1H), 7.31 (ddd, *J* = 9.7, 2.5, 1.7 Hz, 1H), 7.16 (tdd, *J* = 8.3, 2.5, 1.0 Hz, 1H); ^{13}C NMR (101 MHz, $CDCl_3$) δ 163.5 (d, *J* = 247.5 Hz), 142.2 (d, *J* = 2.3 Hz), 140.6 (d, *J* = 7.7 Hz), 132.5 (q, *J* = 33.4 Hz), 131.1 (d, *J* = 8.4 Hz), 127.4 (d, *J* = 2.4 Hz), 123.5 (q, *J* = 273.1 Hz), 123.1 (d, *J* = 3.0 Hz), 121.7 (m), 116.0 (d, *J* = 21.1 Hz), 114.5 (d, *J* = 22.6 Hz); ^{19}F NMR (376 MHz, $CDCl_3$) δ -63.0, -111.8; HRMS-EI (m/z) $[M]^+$ calcd for $C_{14}H_7F_7$, 308.0436; found, 308.0433. The *para*-isomer; ^{1}H NMR (600 MHz, $CDCl_3$) δ 7.98 (s, 2H), 7.87 (s, 1H), 7.62 – 7.56 (m, 2H), 7.23 – 7.17 (m, 2H); ^{19}F NMR (376 MHz, $CDCl_3$) δ -62.9, -112.8. Identity of the ortho and *para*-isomers were confirmed by comparison with reported data.[48]

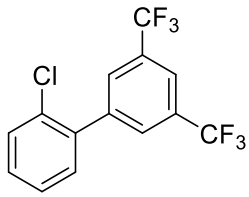

2-Chloro-3',5'-bis(trifluoromethyl)-1,1'-biphenyl (3kj)

A modification of general procedure was employed for the reaction of 1-bromo-3,5-trifluoromethylbenzene (**2j**, 0.2 mmol) and chlorobenzene (**1k**, 60 equiv) for 3 h. The isomeric mixture was analyzed by GC. Its identity was confirmed by comparison with NMR and GC spectra of authentic samples. ^{1}H NMR (400 MHz, $CDCl_3$) δ 7.95 (s, 3H), 7.58 – 7.53 (m, 1H), 7.44 – 7.37 (m, 3H); ^{13}C NMR (101 MHz, $CDCl_3$) δ 141.4, 137.7, 132.5, 131.7 (q, *J* = 33.9 Hz), 131.3, 130.5, 130.2, 129.9 (m), 127.5, 123.5 (q, *J* = 273.7 Hz), 121.7 (m); ^{19}F NMR (376 MHz, $CDCl_3$) δ -62.9; HRMS-EI (m/z) $[M]^+$ calcd for $C_{14}H_7ClF_6$, 324.0140; found, 324.0142. The *meta*-isomer; ^{1}H NMR (400 MHz, $CDCl_3$) δ 7.99 (s, 2H), 7.90 (s, 1H), 7.60 – 7.58 (m, 1H), 7.51 – 7.46 (m, 1H), 7.46 – 7.43 (m, 2H); ^{13}C NMR (101 MHz, $CDCl_3$) δ 142.1, 140.2, 135.5, 132.5 (q, *J* = 37.4 Hz), 130.7, 129.1, 127.6, 127.4 (m), 125.6, 123.4 (q, *J* = 276.0 Hz), 121.7 (m); ^{19}F NMR (376 MHz, $CDCl_3$) δ -62.9; HRMS-EI (m/z) $[M]^+$ calcd for $C_{14}H_7ClF_6$, 324.0140; found, 324.0142.. The *para*-isomer; ^{1}H NMR (400 MHz, $CDCl_3$) δ 7.98 (s, 2H), 7.88 (s, 1H), 7.55 (dt, *J* = 8.7, 2.3 Hz, 2H), 7.48 (dt, *J* = 8.7, 2.3 Hz, 2H); ^{13}C NMR (101 MHz, $CDCl_3$) δ 142.1, 136.6, 135.3, 132.3 (q, *J* = 32.7 Hz), 129.5, 128.5, 127.0 (m), 123.3 (q, *J* = 273.5 Hz), 121.2 (m); ^{19}F NMR (376 MHz, $CDCl_3$) δ -62.9; HRMS-EI (m/z) $[M]^+$ calcd for $C_{14}H_7ClF_6$, 324.0140; found, 324.0140.

5.5 DFT computations

5.5.1 Calculation of proton affinities of arenes

5.5.1.1 General methods

The calculations were performed using the Gaussian 09 (DFT) and Gaussian 16 (G3MP2 and G4MP2) program packages. The gas-phase geometries of thirteen aromatic compounds (Scheme 5.21) and their deprotonated counterparts have been fully optimized using a spin-restricted formalism at the density functional theory (DFT) using the B3LYP hybrid functional and the 6-31++G(d,p) basis sets.[49] Single point frequency calculations were then performed to characterize the minimum-energy stationary points. Thermodynamic parameters that include the zero-point energies (ZPE) and thermal corrections at 298.15K were obtained from frequency calculations. G3MP2[50] and G4MP2[51] calculations were followed with the geometries obtained from the DFT calculations. Proton affinities (PAs) were calculated by the following relation.

$AH(g) \rightarrow A^-(g) + H^+(g)$ $\qquad PA(A^-) = \Delta H°(A^-) + \Delta H°(H^+) - \Delta H°(AH)$

The value of $\Delta H°(H^+)$ was calculated as $5/2RT$ according to an ideal gas expression. The calculated PAs are listed in Table 5.12.

5.5.1.2 Calculational results of proton affinities

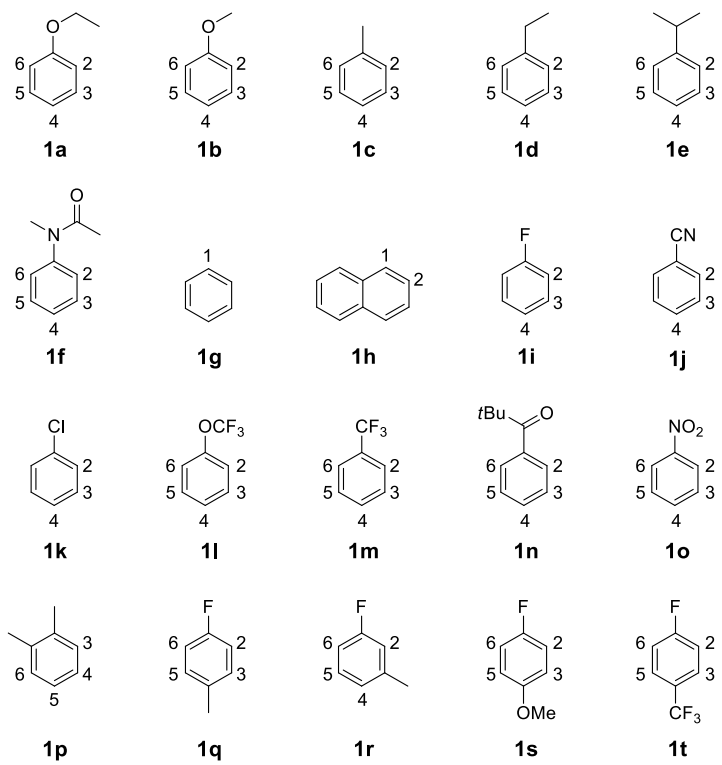

Scheme 5.21 Schematic representation of substituted benzenes and naphthalene with the numbering of deprotonation position.

Table 5.12 The calculated proton affinities of arenes with the numbering of deprotonation position

Compound		**DFT**[a]	**G3MP2**	**G4MP2**
Ethoxybenzene	**1a**			
	1a$_2$	391.9138	391.5291	390.2271
	1a$_3$	399.6899	399.1603	398.2309
	1a$_4$	401.7651	401.2260	400.3268
	1a$_5$	400.5596	399.9823	399.0480
	1a$_6$	397.5783	396.9841	396.0748
Anisole	**1b**			
	1b$_2$	391.7519	391.3861	390.2710
	1b$_3$	399.6253	399.0486	398.2040
	1b$_4$	401.6327	401.0710	400.2352
	1b$_5$	400.4297	399.8549	398.9733
	1b$_6$	397.4930	396.9458	396.0861
Toluene	**1c**			
	1c$_2$	400.1906	400.0507	400.1555
	1c$_3$	401.3214	400.8150	400.1254
	1c$_4$	401.4043	400.9838	400.6098
	1c$_5$	401.3214	400.8200	400.1254
	1c$_6$	400.1906	400.0507	400.1555
Ethylbenzene	**1d**			
	1d$_2$	399.0392	397.7402	398.1054
	1d$_3$	400.7981	399.6491	399.5895
	1d$_4$	400.7654	399.8411	399.8505
	1d$_5$	400.7981	399.6378	399.5895
	1d$_6$	400.8671	400.0049	398.1048
Isopropylbenzene	**1e**			
	1e$_2$	397.7070	397.0575	396.6371
	1e$_3$	400.6098	399.8650	399.3761
	1e$_4$	400.5395	399.9961	399.5707
	1e$_5$	400.3268	399.7081	399.1371
	1e$_6$	398.7869	397.8990	396.9395
N-Methylacetanilide	**1f**			

	1f$_2$	384.9930	385.1254	385.4009
	1f$_3$	389.5060	389.6887	389.6485
	1f$_4$	390.1499	389.9020	390.4925
	1f$_5$	389.5060	389.6887	389.6485
	1f$_6$	384.9930	385.1248	385.1863
Benzene	**1g**			
	1g$_1$	400.8031	400.4486	398.3464
Naphthalene	**1h**			
	1h$_1$	394.1251	393.4656	392.7076
	1h$_2$	395.4429	395.0614	394.3109
Fluorobenzene	**1i**			
	1i$_2$	387.8544	388.3891	387.1999
	1i$_3$	393.9074	394.2149	393.1977
	1i$_4$	395.8822	396.1934	395.5941
Benzonitrile	**1j**			
	1j$_2$	382.9624	382.8017	382.2665
	1j$_3$	384.8349	385.2741	384.7577
	1j$_4$	384.4427	385.0018	385.0702
Chlorobenzene	**1k**			
	1k$_2$	386.2411	387.3010	387.2263
	1k$_3$	390.6713	391.1658	390.6600
	1k$_4$	393.1186	393.1098	392.7013
Trifluoromethoxybenzene	**1l**			
	1l$_2$	381.6936	383.4951	380.7052
	1l$_3$	388.4437	389.3197	389.6014
	1l$_4$	389.9679	390.7931	391.4858
	1l$_5$	388.4437	389.3165	389.5293
	1l$_6$	381.9615	383.5133	383.3853
Trifluoromethylbenzene	**1m**			
	1m$_2$	386.1332	387.4309	385.0627
	1m$_3$	388.9614	390.3218	389.0637
	1m$_4$	388.3935	389.3046	388.8522
	1m$_5$	388.9614	389.7232	389.2387
	1m$_6$	386.1351	386.7563	386.6113
Pivalophenone	**1n**			

	1n$_2$	383.9250	385.3218	385.1737
	1n$_3$	393.1952	393.3646	393.2755
	1n$_4$	390.1323	391.5825	391.1966
	1n$_5$	390.7328	391.4664	391.4720
	1n$_6$	383.9250	385.3287	385.1725
Nitrobenzene	**1o**			
	1o$_2$	380.1913	380.1631	379.6397
	1o$_3$	382.5382	384.6636	384.2714
	1o$_4$	381.0654	383.4970	383.2404
1,2-Dimethylbenzene	**1p**			
	1p$_3$	400.7849	400.2622	399.5795
	1p$_4$	401.9966	401.4752	400.9104
	1p$_5$	401.9966	401.4758	400.9104
	1p$_6$	400.7849	400.1831	399.5795
1-Fluoro-4-methylbenzene	**1q**			
	1q$_2$	388.4907	389.5186	389.3034
	1q$_3$	393.5516	394.0975	392.9429
	1q$_5$	393.5516	393.6796	392.9103
	1q$_6$	388.4907	388.9200	387.3763
1-Fluoro-3-methylbenzene	**1r**			
	1r$_2$	387.5865	388.3226	387.5488
	1r$_4$	395.5389	395.7391	395.5753
	1r$_5$	394.6585	395.4341	394.8901
	1r$_6$	388.8139	389.7815	390.0206
1-Fluoro-4-anisole	**1s**			
	1s$_2$	387.5702	387.9034	386.8027
	1s$_3$	390.8332	390.8922	389.9861
	1s$_5$	385.2992	385.5691	384.4314
	1s$_6$	386.9847	387.3267	386.2204
1-Fluoro-4-trifluoromethylbenzene	**1t**			
	1t$_2$	375.4009	378.2837	378.1964
	1t$_3$	379.3322	381.3240	380.2151
	1t$_5$	379.3322	380.6331	380.2158
	1t$_6$	375.4009	377.6894	376.9559

[a]B3LYP/6-31++G(d,p).

5.5.2 Calculation of reductive elimination process

5.5.2.1 General methods

All calculations were carried out using DFT[52] as implemented in the Gaussian 09 program packages. Gas phase geometry optimizations were conducted with the B3LYP hybrid functional[41a, 53] including Grimme's D3 dispersion correction[41b] and the 6-31G**/LanL2DZ(Pd)[54] basis set. The energies of the optimized structures were reevaluated by additional single point calculations using the B3LYP hybrid functional including Grimme's D3 dispersion correction and the 6-311++G**/SDD(Pd) basis set. The integral equation formalism variant of the Polarizable Continuum Model (IEFPCM) was employed as implemented to account for the solvation effects for *N*,*N*-dimethylacetamide (ε=37.781). Analytical vibrational frequencies within the harmonic approximation were computed with the 6-31G**/LanL2DZ(Pd) basis set to confirm proper convergence to well-defined minima (no imaginary frequency) or saddle points (one and only one imaginary frequency) on the potential energy surface. All thermal corrections from the vibrational frequency calculations were performed at 120 ℃ (393.15 K).

5.5.2.2 Comparison of the reductive elimination processes

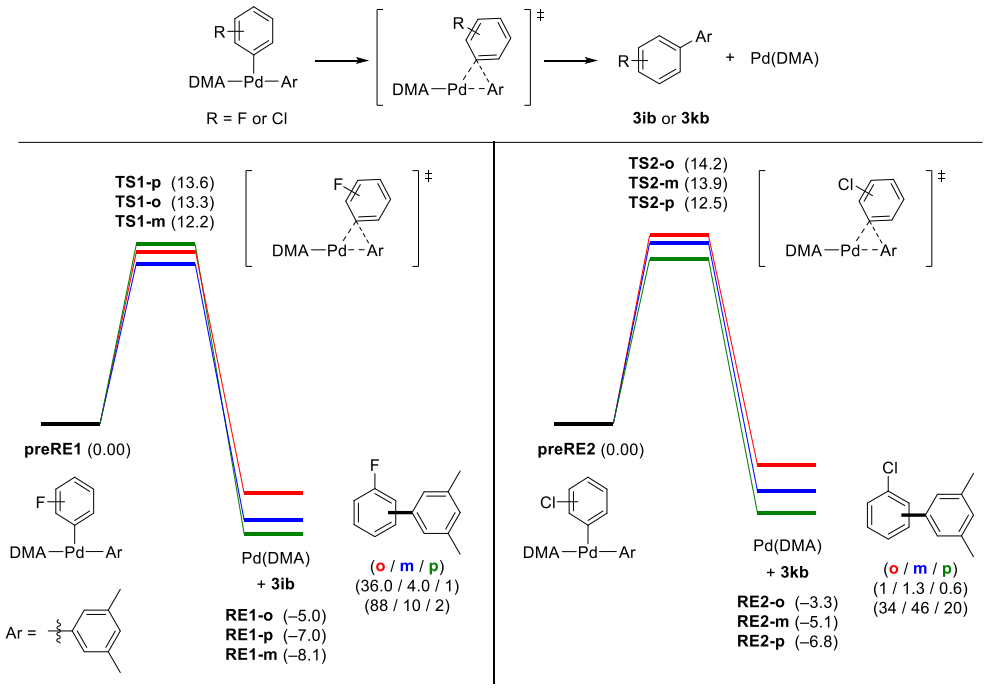

Scheme 5.22 DFT computed energy profiles for reductive elimination processes

5.5.2.3 DFT-optimized structures' energy components

	E(SCF)/(Hartree)	Thermal correction to G /(Hartree)	G(sol)/(kcal/mol)
	6-311++G**/SDD	6-31G**/LanL2DZ	
Pd(DMA)	-415.8457	0.076136	-260899.1356
3ib-o	-641.3715	0.167356	-402361.3459
3ib-m	-641.3735	0.167588	-402362.4893
3ib-p	-641.3731	0.167591	-402362.2454
preRE1-o	-1057.2379	0.272236	-663255.4423
preRE1-m	-1057.2353	0.272717	-663253.5480
preRE1-p	-1057.2338	0.269789	-663254.4133
TS1-o	-1057.2183	0.273792	-663242.1698
TS1-m	-1057.2170	0.273833	-663241.3466
TS1-p	-1057.2151	0.272729	-663240.8479
3kb-o	-1001.7259	0.165703	-628488.0099
3kb-m	-1001.7288	0.165247	-628490.1478
3kb-p	-1001.7286	0.164811	-628490.3188
preRE2-o	-1417.5943	0.269898	-889383.8271
preRE2-m	-1417.5929	0.267948	-889384.1840
preRE2-p	-1417.5906	0.268002	-889382.6549
TS2-o	-1417.5718	0.269988	-889369.6284
TS2-m	-1417.5737	0.270864	-889370.2970
TS2-p	-1417.5723	0.269735	-889370.1230

5.6 References

(1) (a) Hassan, J.; Sévignon, M.; Gozzi, C.; Schulz, E.; Lemaire, M. *Chem. Rev.* **2002**, *102*, 1359. (b) Constable, D. J. C.; Dunn, P. J.; Hayler, J. D.; Humphrey, G. R.; Leazer, J. L., Jr.; Linderman, R. J.; Lorenz, K.; Manley, J.; Pearlman, B. A.; Wells, A.; Zaks, A.; Zhang, T. Y. *Green Chem.* **2007**, *9*, 411. (c) Alberico, D.; Scott, M. E.; Lautens, M. *Chem. Rev.* **2007**, *107*, 174.

(2) (a) Taylor, R., *Electrophilic aromatic substitution*. J. Wiley: Chichester, West Sussex, England; New York, 1990. (b) Carey, F. A.; Sundberg, R. J., *Advanced Organic Chemistry: Part B: Reaction and Synthesis*. 5th edition ed.; Springer: 2010; p 1321.

(3) Friedel, C.; Crafts, J. *J. Chem. Soc.* **1877**, *32*, 725.

(4) (a) Johansson Seechurn, C. C. C.; Kitching, M. O.; Colacot, T. J.; Snieckus, V. *Angew. Chem. Int. Ed.* **2012**, *51*, 5062. (b) Bohra, H.; Wang, M. *J. Mater. Chem. A* **2017**, *5*, 11550. (c) Horton, D. A.; Bourne, G. T.; Smythe, M. L. *Chem. Rev.* **2003**, *103*, 893. (d) McGlacken, G. P.; Bateman, L. M. *Chem. Soc. Rev.* **2009**, *38*, 2447. (e) Chen, X.-Y.; Nie, X.-X.; Wu, Y.; Wang, P. *Chem. Commun.* **2020**, *56*, 5058. (f) Font, M.; Spencer, A. R. A.; Larrosa, I. *Chem. Sci.* **2018**, *9*, 7133.

(5) (a) Verrier, C.; Lassalas, P.; Théveau, L.; Quéguiner, G.; Trécourt, F.; Marsais, F.; Hoarau, C. *Beilstein J. Org. Chem.* **2011**, *7*, 1584. (b) Chen, X.; Engle, K. M.; Wang, D.-H.; Yu, J.-Q. *Angew. Chem. Int. Ed.* **2009**, *48*, 5094. (c) Fu, G. C. *Acc. Chem. Res.* **2008**, *41*, 1555.

(6) (a) Joucla, L.; Djakovitch, L. *Adv. Synth. Catal.* **2009**, *351*, 673. (b) Ackermann, L.; Vicente, R.; Kapdi, A. R. *Angew. Chem. Int. Ed.* **2009**, *48*, 9792. (c) Phipps, R. J.; Grimster, N. P.; Gaunt, M. J. *J. Am. Chem. Soc.* **2008**, *130*, 8172. (d) Wang, L.;

Carrow, B. P. *ACS Catal.* **2019**, *9*, 6821.

(7) (a) Whitaker, D.; Burés, J.; Larrosa, I. *J. Am. Chem. Soc.* **2016**, *138*, 8384. (b) René, O.; Fagnou, K. *Org. Lett.* **2010**, *12*, 2116. (c) Zhou, L.; Lu, W. *Organometallics* **2012**, *31*, 2124. (d) Simonetti, M.; Perry, G. J. P.; Cambeiro, X. C.; Juliá-Hernández, F.; Arokianathar, J. N.; Larrosa, I. *J. Am. Chem. Soc.* **2016**, *138*, 3596. (e) Cambeiro, X. C.; Ahlsten, N.; Larrosa, I. *J. Am. Chem. Soc.* **2015**, *137*, 15636.

(8) (a) Wang, P.; Farmer, M. E.; Huo, X.; Jain, P.; Shen, P.-X.; Ishoey, M.; Bradner, J. E.; Wisniewski, S. R.; Eastgate, M. D.; Yu, J.-Q. *J. Am. Chem. Soc.* **2016**, *138*, 9269. (b) Lyons, T. W.; Sanford, M. S. *Chem. Rev.* **2010**, *110*, 1147. (c) Aihara, Y.; Chatani, N. *Chem. Sci.* **2013**, *4*, 664. (d) Rej, S.; Ano, Y.; Chatani, N. *Chem. Rev.* **2020**, *120*, 1788. (e) Kalyani, D.; McMurtrey, K. B.; Neufeldt, S. R.; Sanford, M. S. *J. Am. Chem. Soc.* **2011**, *133*, 18566. (f) Phipps, R. J.; Gaunt, M. J. *Science* **2009**, *323*, 1593.

(9) (a) Wagner, A. M.; Hickman, A. J.; Sanford, M. S. *J. Am. Chem. Soc.* **2013**, *135*, 15710. (b) Ciana, C.-L.; Phipps, R. J.; Brandt, J. R.; Meyer, F.-M.; Gaunt, M. J. *Angew. Chem. Int. Ed.* **2011**, *50*, 458.

(10) Ball, L. T.; Lloyd-Jones, G. C.; Russell, C. A. *Science* **2012**, *337*, 1644.

(11) Kalkhambkar, R. G.; Laali, K. K. *Tetrahedron Lett.* **2011**, *52*, 5525.

(12) Luan, Y.-X.; Zhang, T.; Yao, W.-W.; Lu, K.; Kong, L.-Y.; Lin, Y.-T.; Ye, M. *J. Am. Chem. Soc.* **2017**, *139*, 1786.

(13) (a) Martins, A.; Mariampillai, B.; Lautens, M. *Top. Curr. Chem.* **2010**, *292*, 1. (b) Wang, J.; Dong, G. *Chem. Rev.* **2019**, *119*, 7478. (c) Catellani, M.; Frignani, F.; Rangoni, A. *Angew. Chem., Int. Ed.* **1997**, *36*, 119.

(14) (a) Liu, L.-Y.; Qiao, J. X.; Yeung, K.-S.; Ewing, W. R.; Yu, J.-Q. *Angew. Chem. Int. Ed.* **2020**, *59*, 13831. (b) Liu, L.-Y.; Qiao, J. X.; Yeung, K.-S.; Ewing, W. R.; Yu, J.-Q. *J. Am. Chem. Soc.* **2019**, *141*, 14870.

(15) Luo, J.; Preciado, S.; Larrosa, I. *J. Am. Chem. Soc.* **2014**, *136*, 4109.

(16) Ryabov, A. D.; Sakodinskaya, I. K.; Yatsimirsky, A. K. *J. Chem. Soc., Dalton Trans.* **1985**, 2629.

(17) Gómez, M.; Granell, J.; Martinez, M. *Organometallics* **1997**, *16*, 2539.

(18) Davies, D. L.; Donald, S. M. A.; Macgregor, S. A. *J. Am. Chem. Soc.* **2005**, *127*, 13754.

(19) (a) Walsh, A. P.; Jones, W. D. *Organometallics* **2015**, *34*, 3400. (b) Tanji, Y.; Mitsutake, N.; Fujihara, T.; Tsuji, Y. *Angew. Chem. Int. Ed.* **2018**, *57*, 10314. (c) Lapointe, D.; Fagnou, K. *Chem. Lett.* **2010**, *39*, 1118. (d) Engle, K. M.; Wang, D.-H.; Yu, J.-Q. *J. Am. Chem. Soc.* **2010**, *132*, 14137.

(20) Lafrance, M.; Fagnou, K. *J. Am. Chem. Soc.* **2006**, *128*, 16496.

(21) (a) Gorelsky, S. I.; Lapointe, D.; Fagnou, K. *J. Org. Chem.* **2012**, *77*, 658. (b) Lafrance, M.; Rowley, C. N.; Woo, T. K.; Fagnou, K. *J. Am. Chem. Soc.* **2006**, *128*, 8754. (c) Gorelsky, S. I. *Coord. Chem. Rev.* **2013**, *257*, 153.

(22) (a) Wang, Y.-N.; Guo, X.-Q.; Zhu, X.-H.; Zhong, R.; Cai, L.-H.; Hou, X.-F. *Chem. Commun.* **2012**, *48*, 10437. (b) Zhou, Q.; Wang, Y.-N.; Guo, X.-Q.; Zhu, X.-H.; Li, Z.-M.; Hou, X.-F. *Organometallics* **2015**, *34*, 1021.

(23) (a) García-Cuadrado, D.; Braga, A. A. C.; Maseras, F.; Echavarren, A. M. *J. Am. Chem. Soc.* **2006**, *128*, 1066. (b) García-Cuadrado, D.; de Mendoza, P.; Braga, A. A. C.; Maseras, F.; Echavarren, A. M. *J. Am. Chem. Soc.* **2007**, *129*, 6880.

(24) Tan, Y.; Barrios-Landeros, F.; Hartwig, J. F. *J. Am. Chem. Soc.* **2012**, *134*,

3683.

(25) Gorelsky, S. I. *Organometallics* **2012**, *31*, 4631.

(26) Kim, J.; Hong, S. H. *ACS Catal.* **2017**, *7*, 3336.

(27) Campeau, L.-C.; Rousseaux, S.; Fagnou, K. *J. Am. Chem. Soc.* **2005**, *127*, 18020.

(28) Tan, Y.; Hartwig, J. F. *J. Am. Chem. Soc.* **2011**, *133*, 3308.

(29) (a) Tanji, Y.; Hamaguchi, R.; Tsuji, Y.; Fujihara, T. *Chem. Commun.* **2020**, *56*, 3843. (b) Caron, L.; Campeau, L.-C.; Fagnou, K. *Org. Lett.* **2008**, *10*, 4533.

(30) Culkin, D. A.; Hartwig, J. F. *Acc. Chem. Res.* **2003**, *36*, 234.

(31) The kinetic order could not be precisely determined due to the solubility issue of KOPiv.

(32) Wang, D.; Izawa, Y.; Stahl, S. S. *J. Am. Chem. Soc.* **2014**, *136*, 9914.

(33) Gorelsky, S. I.; Lapointe, D.; Fagnou, K. *J. Am. Chem. Soc.* **2008**, *130*, 10848.

(34) Colletto, C.; Islam, S.; Juliá-Hernández, F.; Larrosa, I. *J. Am. Chem. Soc.* **2016**, *138*, 1677.

(35) Attempts to synthesize the aryl–Pd complex with acetonitrile or DMA ligands were unsuccessful, presumably due to limited stability of the resulting Pd complexes.

(36) Sha, S.-C.; Tcyrulnikov, S.; Li, M.; Hu, B.; Fu, Y.; Kozlowski, M. C.; Walsh, P. J. *J. Am. Chem. Soc.* **2018**, *140*, 12415.

(37) (a) Amatore, C.; Jutand, A.; Le Duc, G. *Chem. Eur. J.* **2012**, *18*, 6616. (b) Amatore, C.; Le Duc, G.; Jutand, A. *Chem. Eur. J.* **2013**, *19*, 10082.

(38) (a) Brown, J. M.; Cooley, N. A. *Chem. Rev.* **1988**, *88*, 1031. (b) Ananikov, V. P.; Musaev, D. G.; Morokuma, K. *J. Am. Chem. Soc.* **2002**, *124*, 2839.

(39) (a) Sherwood, J.; Clark, J. H.; Fairlamb, I. J. S.; Slattery, J. M. *Green Chem.* **2019**, *21*, 2164. (b) Veerakumar, P.; Thanasekaran, P.; Lu, K.-L.; Lin, K.-C.; Rajagopal, S. *ACS Sustainable Chem. Eng.* **2017**, *5*, 8475. (c) Pérez-Rodríguez, M.; Braga, A. A. C.; Garcia-Melchor, M.; Pérez-Temprano, M. H.; Casares, J. A.; Ujaque, G.; de Lera, A. R.; Alvarez, R.; Maseras, F.; Espinet, P. *J. Am. Chem. Soc.* **2009**, *131*, 3650.

(40) (a) Nilsson, P.; Puxty, G.; Wendt, O. F. *Organometallics* **2006**, *25*, 1285. (b) Casado, A. L.; Espinet, P. *J. Am. Chem. Soc.* **1998**, *120*, 8978. (c) Casado, A. L.; Espinet, P.; Gallego, A. M. *J. Am. Chem. Soc.* **2000**, *122*, 11771.

(41) (a) Lee, C.; Yang, W.; Parr, R. G. *Phys. Rev. B Condens. Matter* **1988**, *37*, 785. (b) Grimme, S.; Antony, J.; Ehrlich, S.; Krieg, H. *J. Chem. Phys.* **2010**, *132*, 154104.

(42) (a) Tan, Y.; Hartwig, J. F. *J. Am. Chem. Soc.* **2011**, *133*, 3308. (b) Endo, K.; Grubbs, R. H. *J. Am. Chem. Soc.* **2011**, *133*, 8525.

(43) Cornella, J.; Righi, M.; Larrosa, I. *Angew. Chem. Int. Ed.* **2011**, *50*, 9429.

(44) Li, X.; Zhang, J.; Zhao, Y.; Zhao, X.; Li, F.; Li, T.; Li, H. L.; Chen, L. *J. Mater. Chem. A* **2015**, *3*, 6265.

(45) Mohan, A.; Ramkumar, V.; Sankararaman, S. *J. Organomet. Chem.* **2015**, *799-800*, 115.

(46) Minami, H.; Saito, T.; Wang, C.; Uchiyama, M. *Angew. Chem. Int. Ed.* **2015**, *54*, 4665.

(47) (a) Lan, P.; Berta, D.; Porco, J. A.; South, M. S.; Parlow, J. J. *J. Org. Chem.* **2003**, *68*, 9678. (b) Keesara, S.; Parvathaneni, S.; Dussa, G.; Mandapati, M. R. *J. Organomet. Chem.* **2014**, *765*, 31.

(48) Yamamoto, K.; Li, J.; Garber, J. A. O.; Rolfes, J. D.; Boursalian, G. B.; Borghs, J. C.; Genicot, C.; Jacq, J.; van Gastel, M.; Neese, F.; Ritter, T. *Nature* **2018**, *554*, 511.

(49) (a) Becke, A. D. *J. Chem. Phys.* **1993**, *98*, 5648. (b) Lee, C.; Yang, W.; Parr, R. G. *Phys. Rev. B* **1988**, *37*, 785. (c) Stephens, P. J.; Devlin, F. J.; Chabalowski, C. F.; Frisch, M. J. *J. Phys. Chem.* **1994**, *98*, 11623.

(50) Baboul, A. G.; Curtiss, L. A.; Redfern, P. C.; Raghavachari, K. *J. Chem. Phys.* **1999**, *110*, 7650.

(51) (a) Curtiss, L. A.; Redfern, P. C.; Raghavachari, K. *J. Chem. Phys.* **2007**, *126*, 084108. (b) Curtiss, L. A.; Redfern, P. C.; Raghavachari, K. *J. Chem. Phys.* **2007**, *127*, 124105.

(52) Calais, J.-L. *Int. J. Quantum Chem.* **1993**, *47*, 101.

(53) (a) Slater, J. C.; Phillips, J. C. *Phys. Today* **1974**, *27*, 49. (b) Vosko, S. H.; Wilk, L.; Nusair, M. *Can. J. Phys.* **1980**, *58*, 1200. (c) Becke, A. D. *Phys. Rev. A Gen. Phys.* **1988**, *38*, 3098. (d) Becke, A. D. *J. Chem. Phys.* **1993**, *98*, 5648.

(54) (a) Wadt, W. R.; Hay, P. J. *J. Chem. Phys.* **1985**, *82*, 284. (b) Hay, P. J.; Wadt, W. R. *J. Chem. Phys.* **1985**, *82*, 299.

Chapter 6. Direct C(sp^2)–H Alkylation of Unactivated Arenes Enabled by Photoinduced Pd Catalysis*

6.1 Introduction

Alkylarenes are essential scaffolds in a wide range of commodity chemicals, including surfactants and detergents, and some biologically active molecules.[1] The Friedel-Crafts alkylation is a textbook reaction for the synthesis of alkylarenes; however, this traditional approach has a number of drawbacks including the requirement for a strong acid catalyst, harsh reaction conditions, and the generation of undesired Wagner-Meerwein rearrangement products, which lead to complex isomeric mixtures (Scheme 6.1a).[2] Therefore, the development of an efficient and selective synthetic method for alkylarenes is a longstanding challenge in catalysis.

In this context, the direct catalytic C–H alkylation of unactivated arenes is an ideal synthetic method to prepare alkylarenes, maximizing atom- and step-economies. For example, the transition metal-catalyzed C(sp^2)–H alkylation of unactivated arenes with alkenes, namely the hydroarylation of alkenes, is one such approach;[3] however, this usually requires regioselective control and harsh reaction conditions, which limit the utility of the reaction (Scheme 6.1a). Recently, Hartwig and Nakao succeeded in the development of a hydroarylation reaction of unactivated arenes with alkenes in high linear/branched selectivities (>50:1). This reaction was catalyzed by a Ni complex bearing a highly sterically bulky *N*-

* The majority of this work has been published: Daeun Kim, Geun Seok Lee, Dongwook Kim, and Soon Hyeok Hong*. *Nat. Commun.* **2020**, *11*, 5266.

heterocyclic carbene (NHC) ligand.[4] However, the reaction is not applicable to polar functional groups, such as nitriles and esters, due to limited functional group tolerance.[5] Although they demonstrated the high selectivity for the linear products, limited examples of the hydroarylation of unactivated arenes with a high selectivity for the branch products have been reported.[6]

The C(sp^2)–H alkylation of arenes with an alkyl electrophile could be an ideal synthetic method for the construction of alkylarenes, as it would avoid the regioselectivity issues associated with the olefin hydroarylation reactions. However, despite significant advances in the field of C–H alkylation, the majority of the reported transition metal-catalyzed C(sp^2)–H alkylation reactions using alkyl electrophiles require directing groups,[7] or have a limited applicability to heteroarenes,[8] activated electron-deficient arenes,[9] and intramolecular alkylation systems.[8b, 10] This significantly limited scope is due to the challenging oxidative addition to the alkyl electrophile and the high C–H activation barrier of the unactivated arenes (C–H bond dissociation energy, ~110 kcal/mol).[11] Such high reaction barriers inevitably lead to a requirement for harsh reaction conditions, which are often accompanied by undesirable side reactions, such as β–hydride elimination. Therefore, a catalytic system operating under versatile and mild reaction conditions is necessary to streamline the synthesis of alkylarenes via the direct alkylation of non-activated C(sp^2)–H bonds.

To address the challenges, we envisioned that a controlled radical-mediated reaction could afford a high activity and selectivity because the rearrangement of reactive carbon-centered radicals is significantly slower than that of their cationic counterparts.[12] Although homolytic aromatic substitution (HAS),

the radical analog of the electrophilic aromatic substitution, has been well developed,[13] the insertion of nucleophilic alkyl radicals to the electron-rich π-system of arenes is significantly more sluggish and the alkyl radicals are prone to undergo side reactions, such as homodimerization and hydrogen atom transfer (HAT).[12, 14] To control the reaction pathways, the recently reported photoinduced Pd catalysis approach was identified as an attractive activation mode to generate alkyl radicals from alkyl halides, since it operates under mild conditions while controlling the concentration of free radical species to suppress undesired side reactions.[8b, 9, 15] Applying the photoinduced Pd catalysis, Gevorgyan and co-workers first succeeded in developing the photoinduced Pd-catalyzed Heck reaction of alkyl halides by utilizing Pd(I)/alkyl radical hybrid species generated by single-electron transfer (SET) activation.[16,17] Further elegant achievements have been reported for various synthetically useful reactions, including Heck reaction,[15a, 15g, 18] desaturation,[15d] hydrodehalogenation,[19] C–H alkylation of (hetero)arenes,[8b, 9] carbonylation,[15i] and 1,4-difunctionalization of conjugated dienes,[15e, 20] exploring the Pd catalysis under visible light irradiation.

Herein we report the catalytic C(sp^2)–H alkylation of benzene with readily available alkyl bromides without any rearrangement enabled by photoinduced Pd catalysis (Scheme 6.1b). Exclusive chemoselectivity and excellent functional group tolerance are demonstrated by synthesizing various linear and branched alkylbenzenes including the late-stage phenylation of bioactive molecule derivatives and an orthogonal one-pot sequential Pd-catalyzed C–C bond formation reaction. Comprehensive mechanistic investigations are conducted with a combination of experimental and computational studies to construct the complete

catalytic cycle. Consequently, it clarifies the catalytic turnover mechanism involving a Pd(0)/Pd(I) redox cycle through the reciprocal exchange of a bromine atom between the Pd catalyst and the alkylating species. It also accounts for the distinctive reactivity of alkyl bromides compared to other halides by disclosing the unexpected role of the formate base which reduces the off-cycle Pd(II) dibromide complex $Pd(PPh_3)_2Br_2$ to an active Pd(0) species.

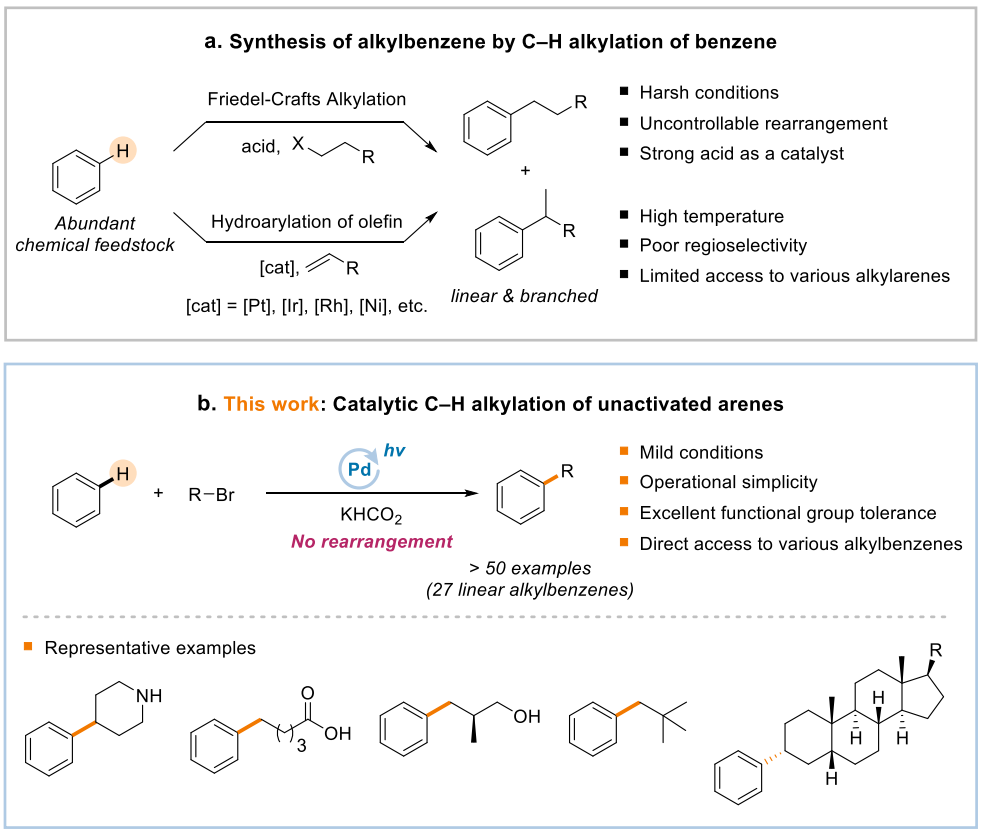

Scheme 6.1 Synthesis of alkylbenzenes.

6.2 Results and discussion

6.2.1 Optimization for C(sp^2)–H alkylation

To examine the photoinduced Pd-catalyzed C–H alkylation of unactivated arenes with alkyl halides, benzene (**1a**) was selected as an ideal aromatic substrate (Table 6.1). The reaction of benzene with bromocyclohexane (**2a**) in the presence of $Pd(PPh_3)_4$ and potassium formate ($KHCO_2$) gave phenylcyclohexane (**3a**) in 76% yield under irradiation with 40 W blue LED (entry 1). Among the other palladium sources investigated, $Pd(PPh_3)_2Cl_2$ and the combination of $Pd(OAc)_2$ and PPh_3 gave comparable yields of 74 and 71%, respectively (entries 2 and 3). We found that dual phosphine ligand systems, containing both monodentate and bidentate phosphines, which were frequently utilized in previously reported photoinduced Pd catalytic processes,[9, 15d, 21] exhibited significantly lower efficiencies (entries 4 and 5), leading to undesired β-H elimination as the major side reaction (Table 6.6). The use of other bases did not improve the yield (entries 6–8). In addition, a decreased product yield was observed when the reaction was carried out at room temperature (entry 9). Therefore, both a mild base and a warm temperature (50±5 ^oC) were found to be crucial to obtaining high conversions and yields. Among the alkyl halides tested, the alkyl bromide was found to be more reactive than the alkyl chloride and the alkyl iodide (RBr >> RCl > RI, entries 10 and 11). The addition of KBr did not exhibit any increased reactivity, but that of nBu$_4$NBr increased the reactivity to 17% and 36% for chlorides and iodides, respectively (Table 6.7). Furthermore, halving the Pd catalyst loading led to a slight increase in yield up to 80%, presumably due to the lowered concentration of alkyl radicals that could suppress the possible side reactions (entry 12). Further lowering the amount of Pd

catalyst resulted in the incomplete conversion of **2a** and a diminished yield (47%, entry 13). The use of less amount of benzene or another solvent with 10 equiv benzene gave diminished yields accompanying undesired debromination and elimination of the alkyl bromide (Tables 6.8 and 6.9). No product formation was observed when the reaction was carried out at 100 ^{o}C without visible light irradiation (entry 14). Finally, control experiments revealed that all components were necessary to complete the alkylation reaction (entry 15).

Table 6.1 Optimization of the Pd-catalyzed C(sp^2)–H alkylation of benzene[a]

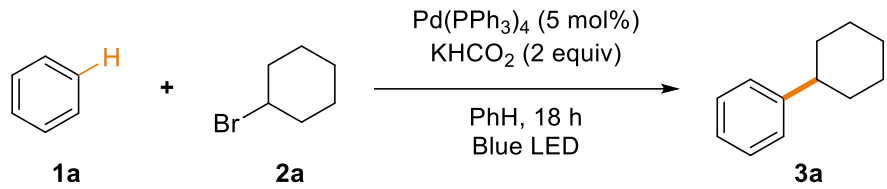

1a **2a** **3a**

Entry	Variation from standard conditions	Yield[b] (%)
1	no deviation	76
2	$Pd(PPh_3)_2Cl_2$ instead of $Pd(PPh_3)_4$	74
3	$Pd(OAc)_2/PPh_3$ (1:4) instead of $Pd(PPh_3)_4$	71
4	$Pd(PPh_3)_2Cl_2$/XantPhos (1:1.2) instead of $Pd(PPh_3)_4$	52
5	$Pd(PPh_3)_4$/DPEPhos (1:1.2) instead of $Pd(PPh_3)_4$	28
6	KOAc instead of $KHCO_2$	74
7	K_2CO_3 instead of $KHCO_2$	32
8	KHMDS instead of $KHCO_2$	44
9	25 ^oC with fan cooling	27
10	with CyCl instead of CyBr	10
11	with CyI instead of CyBr	5
12	2.5 mol% of $Pd(PPh_3)_4$	**82 (80[c])**
13	1 mol% of $Pd(PPh_3)_4$	47
14	at 100 ^oC, in the absence of light irradiation	0
15	without $Pd(PPh_3)_4$ or $KHCO_2$ or light irradiation	0

[a]Reaction conditions: **2a** (0.1 mmol, 0.033 M), $Pd(PPh_3)_4$ (5 mol%), $KHCO_2$ (2 equiv), and benzene (3 mL) under 40 W blue LED irradiation without fan cooling (50±5 ^oC). [b]GC yields using dodecane as an internal standard. [c]Isolated yield.

6.2.2 Substrate scope of alkyl bromides and arenes

With the optimized conditions in hand, we investigated the scope of the reaction with respect to the alkyl bromides (Table 6.2). Various unfunctionalized primary alkyl bromides underwent efficient alkylation (**3b**–**3d**). Excellent compatibility was observed with a diverse set of primary alkyl bromides bearing ether, fluoro, ester, cyano, and trifluoromethyl functional groups (**3e**–**3j**). To our delight, even free alcohol (**3k**) and carboxylic acid (**3l**) functional groups were well-tolerated thanks to the mildness of the Pd photocatalytic system. Completely chemoselective functionalizations of the alkyl bromides were also observed in the presence of alkyl and aryl boronates (**3m** and **3n**) or chlorides (**3o** and **3p**), thereby opening avenues to further synthetic utilizations. The presence of functionalities neighboring the alkyl bromide was also tolerated (**3q** and **3r**), and no detrimental effect stemming from sterics was observed when β,β-disubstituted bromoalkanes (**3s** and **3t**) and even neopentyl bromide (**3u**) were employed. Noticeably, the alkyl fragment bearing an α-chiral center was retained in the obtained product (**3v**).

Six- and five-membered cyclic alkyl bromides reacted smoothly to form the desired alkylated products in good to excellent yields. The transformation was also effective for heterocyclic bromides such as tetrahydropyran (**3w**) and protected piperidines (**3x** and **3y**), both of which are common motifs in medicinal chemistry. The reaction was proven to be easily scalable, producing the product **3x** in 58% yield on a 4.0 mmol scale (1.1 g of **2x**). Notably, piperidine, bearing a free secondary amine moiety, could be efficiently introduced into benzene using KOAc (**3z**) as the base, consistently demonstrating the exceptional functional group tolerance of the developed reaction. *N*-formylated products were obtained (78%)

when $KHCO_2$ was used. A pyrrolidine scaffold could also be readily constructed on benzene (**3ab**). Norbornane (**2ac**) underwent the alkylation exclusively at the *exo* face (**3ac**).[15a] Both secondary and tertiary adamantyl groups were well-tolerated (**3ae**–**3ag**). However, the reaction was less effective with linear secondary alkyl bromides (**3ad**) and no product was observed with tertiary bromides such as *tert*-butyl bromide. The excellent functional group tolerance of this methodology was further confirmed by additive-based robustness screening experiments (Table 6.11).[22]

It should be noted that no isomeric mixture caused by an alkyl radical rearrangement was observed in any case. Indeed, the conventional Friedel-Crafts alkylation is not applicable to the synthesis of linear alkylarenes (**3b**–**3v**) due to rearrangement of the alkylating group.[2] Furthermore, it is noteworthy that a range of products derived from alkyl bromides are inaccessible by the hydroarylation of alkenes since suitable alkenes do not exist for the hydroarylation reaction (**3u, 3v,** and **3ae**–**3ag**), and in other cases, the hydroarylation of internal alkenes furnishes a complex mixture of regioisomers through undesired isomerization processes (**3w**–**3z**).[23]

Table 6.2 Substrate scope of alkyl bromides[a]

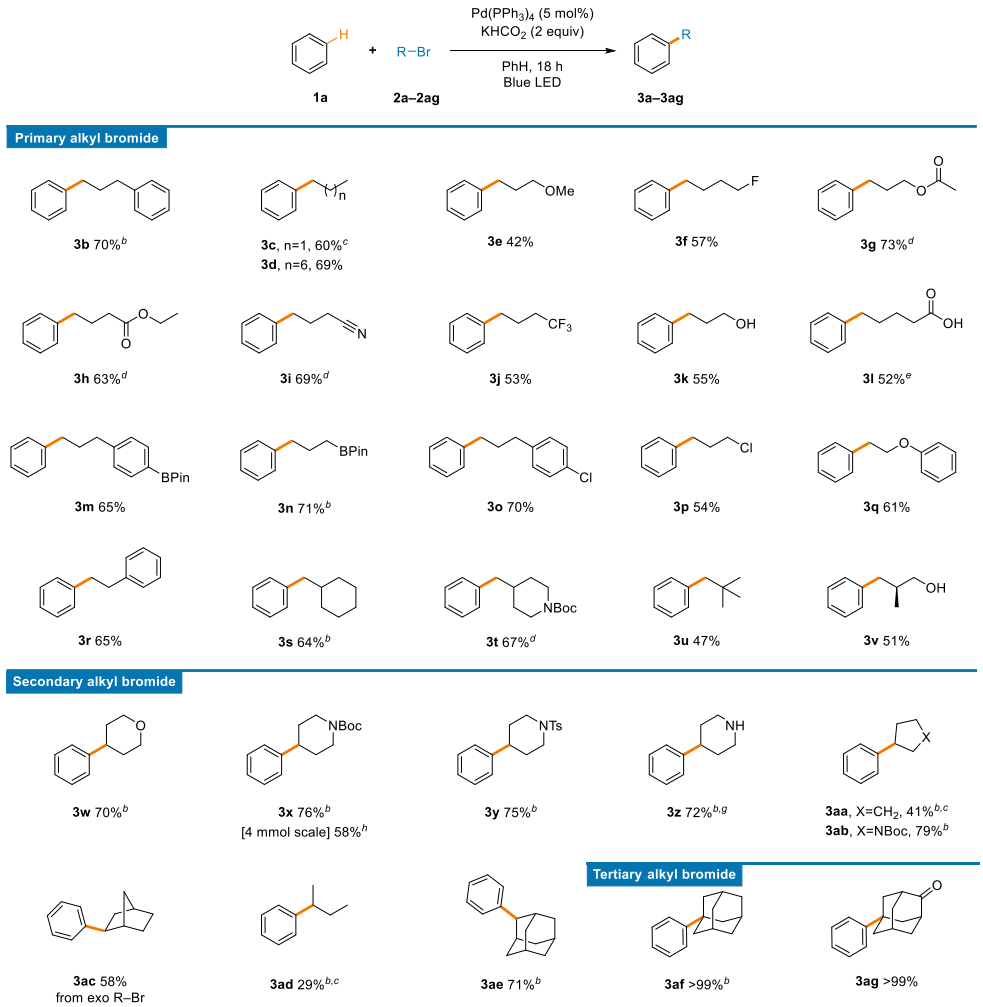

[a]Alkyl bromide (0.1 mmol, 0.033 M), $Pd(PPh_3)_4$ (5 mol%), $KHCO_2$ (2 equiv), and benzene (3 mL) under 40 W blue LED irradiation without fan cooling (50±5 °C). All yields are isolated yields. [b]$Pd(PPh_3)_4$ (2.5 mol%). [c]GC yields using dodecane as an internal standard. [d]$Pd(PPh_3)_4$ (10 mol%). [e]Isolation after methylation with $TMSCH_2N_2$. [f]48 h. [g]KOAc instead of $KHCO_2$. [h]4 mmol scale.

Taking advantage of the excellent functional group tolerance, operative simplicity, and mild reaction conditions of the C–H alkylation protocol, the late-stage phenylations of a wide array of biologically relevant molecules were conducted (Table 6.3). Specifically, the phenylations of various drug derivatives, originated from aceclofenac (**3ah**), probenecid (**3ai**), indomethacin (**3aj**), and febuxostat (**3ak**), were achieved in moderate to good yields. Reactions with alkyl bromides derived from bioactive natural products, such as hippuric acid and biotin, also proceeded smoothly to afford the desired products (**3al** and **3am**). In addition, steroid derivatives, **3an** and **3ao**, were efficiently synthesized as exclusive single diastereomers from the axial alkyl bromides of androsterone and lithocholic acid, demonstrating the potential applicability of the reaction to access diverse structures originating from native complex molecules. The stereochemistry of **3ao** was unambiguously confirmed by X-ray diffraction analysis (CCDC 1952541). These results highlight the practical utility of the reaction for the late-stage phenylation of complex molecules in the presence of biologically relevant functional groups, such as anilines, sulfonamides, electron-rich thiazoles, indoles, ureas, and steroids.

Table 6.3 Synthetic applications[a]

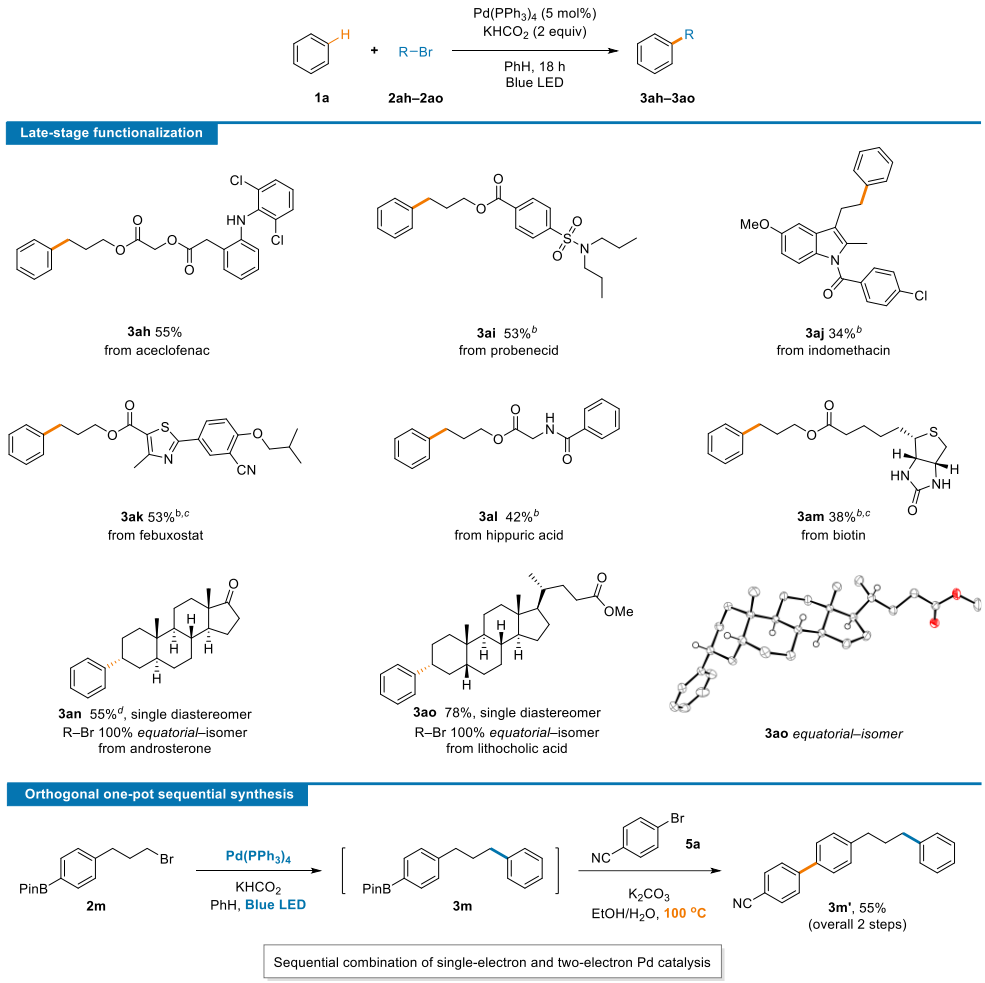

[a]Alkyl bromide (0.1 mmol, 0.033 M), $Pd(PPh_3)_4$ (5 mol%), $KHCO_2$ (2 equiv), and benzene (3 mL) under 40 W blue LED irradiation without fan cooling (50±5 °C). All yields are isolated yields. [b]$Pd(PPh_3)_4$ (10 mol%). [c]48 h. [d]$Pd(PPh_3)_4$ (2.5 mol%).

Inspired by the superb role of Pd catalysis in cross-coupling reactions[24] and the exceptional chemoselectivity of the developed reactions to alkyl bromides (e.g., **3m**–**3p**), an orthogonal one-pot sequential synthesis was proposed whereby the Pd complex obtained after the photoinduced reaction could adopt the additional role of a catalyst for traditional cross-coupling reactions. To our delight, following the photoinduced phenylation of **2m**, the sequential Suzuki-Miyaura cross-coupling reaction smoothly afforded the corresponding arylated product **3m′** in 55% yield by simply introducing a solution of aryl bromide **5a** and K_2CO_3 in a mixture of EtOH/H_2O followed by heating at 100 ^oC. These one-pot, sequential, Pd-catalyzed reactions using this single Pd source, driven by visible light irradiation and thermal energy, respectively, are an intriguing combination of single-electron and two-electron catalysis, which can provide an operationally simple protocol to form two C–C bonds consecutively.

The scope of the arene (C–H) coupling partners was then investigated using **2x** under the optimized conditions (Table 6.4). Reactions employing electronically diverse arenes efficiently afforded the desired products in a regioisomeric mixture. The observed regioselectivities are in good accordance with those previously reported for homolytic aromatic substitution (HAS) reactions.[13b, 14a, 21, 25] More specifically, reaction with anisole and halobenzenes produced compounds **4b**–**4d** in yields of 64–88%, favoring the *ortho*-product, which could be rationalized by considering the inductive effect.[14a] Benzonitrile also exhibited a good reactivity, favoring *ortho*- and *para*-isomers (**4e**) due to the resonance effect of the nitrile group.[14a] In addition, when 1,1,1-trifluorotoluene **1f** was employed as the coupling partner, the *para*-isomer dominated (**4f**). Hyperconjugation of the

fluorine atom, which favors the formation of a positive charge in the *ortho*- and *para*-positions, could drive the unusual *para*- preferred functionalization of **1f** due to steric repulsion at the *ortho*-position.[14a] A lower reactivity was observed with 1,3-benzodioxole (**4g**) due to an increased electron density. When toluene or aniline was employed as the arene substrate, poor reactivity was observed, producing a large amount of debromination byproducts, presumably due to undesired HAT reactions from benzylic C–H and N–H bonds. In terms of disubstituted arene substrates, couplings to the most electron-deficient position were dominant. For example, when 4-fluoroanisole **1h** was used, the *ortho*-coupling product relative to the fluorine atom was observed as the major isomer (**4h**), and for 1,3-difluorobenzene (**1i**), the most electronically favored 2-position was majorly alkylated (**4i**). However, to our surprise, 1,3,5-trifluorobenzene (**4k**) and 1,3,4,5-tetrafluorobenzene (**4l**) exhibited lower reactivities, while pentafluorobenzene **1m** gave no reaction, despite the fact that electrophilic polyfluoroarenes should be more reactive in HAS-type reactions, providing a further distinctive mechanistic insight of the developed reaction which will be discussed below.

Table 6.4 Substrate scope of arenes[a]

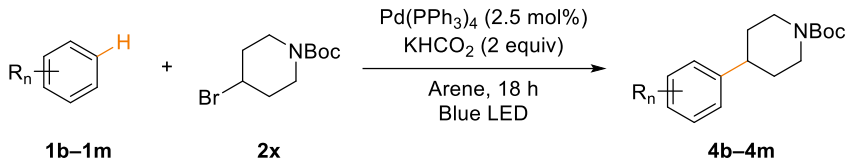

1b–1m **2x** **4b–4m**

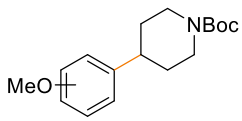

4b 81% (10.5 / 2.8 / 1)

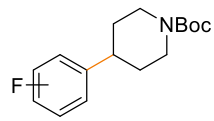

4c 73%[d] (11.2 / 7.6 / 1)

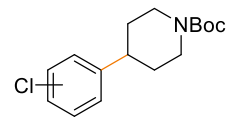

4d 88%[d] (5.6 / 1.8 / 1)

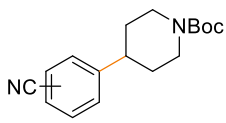

4e 73%[b,c] (19.2 / 1 / 8.8)

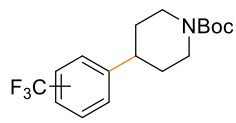

4f 77%[d] (1 / 2.4 / 3.1)

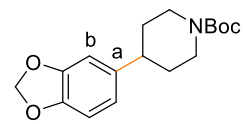

4g 42%[b] (2.0 / 1)

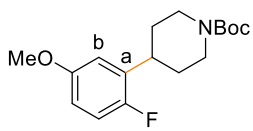

4h 81%[b,d] (3.0 / 1)

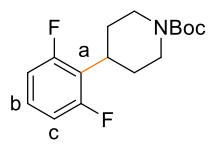

4i 51%[d,e] (9.5 / 3.1 / 1)

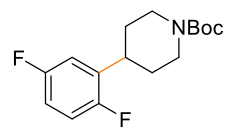

4j 77%[b,d]

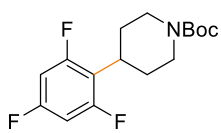

4k 32%[d,e]

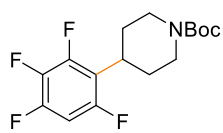

4l <10%[e]

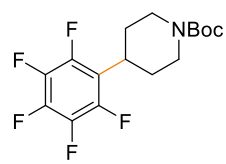

4m N.D.

[a]**2x** (0.1 mmol, 0.033 M), $Pd(PPh_3)_4$ (2.5 mol%), $KHCO_2$ (2 equiv), and arene (3 mL) under 40 W blue LED irradiation without fan cooling (50±5 °C). All yields are isolated yields. Regioselectivity (*ortho*/*meta*/*para*, a/b, a/b/c) is measured by GC or NMR and given in the parenthesis. [b]$Pd(PPh_3)_4$ (5 mol%). [c]1:1 mixture of arene and veratrole as solvent. [d]48 h. [e]NMR yield.

6.2.3 Mechanistic studies

To understand the reaction mechanism, a radical clock substrate (**2ap**) was first employed and the ring-opening product (**3ap**) was exclusively observed, indicating the involvement of a cyclopropylmethyl radical (Scheme 6.2a). The involvement of an alkyl radical was further confirmed by another radical scavenging experiment with TEMPO, where a cyclohexyl-TEMPO adduct (**3a′**) was formed (Scheme 6.2b). To gain additional insight in the rate-limiting step, standard kinetic isotope effect (KIE) experiments were conducted using benzene (**1a**) and benzene-d_6 (**1a-*d*$_6$**) (Scheme 6.2c). The observed inverse secondary KIE (k_H/k_D = 0.88) strongly suggests that the rate-limiting step involves a change in hybridization of the carbon atom from C(sp^2) to C(sp^3).[26]

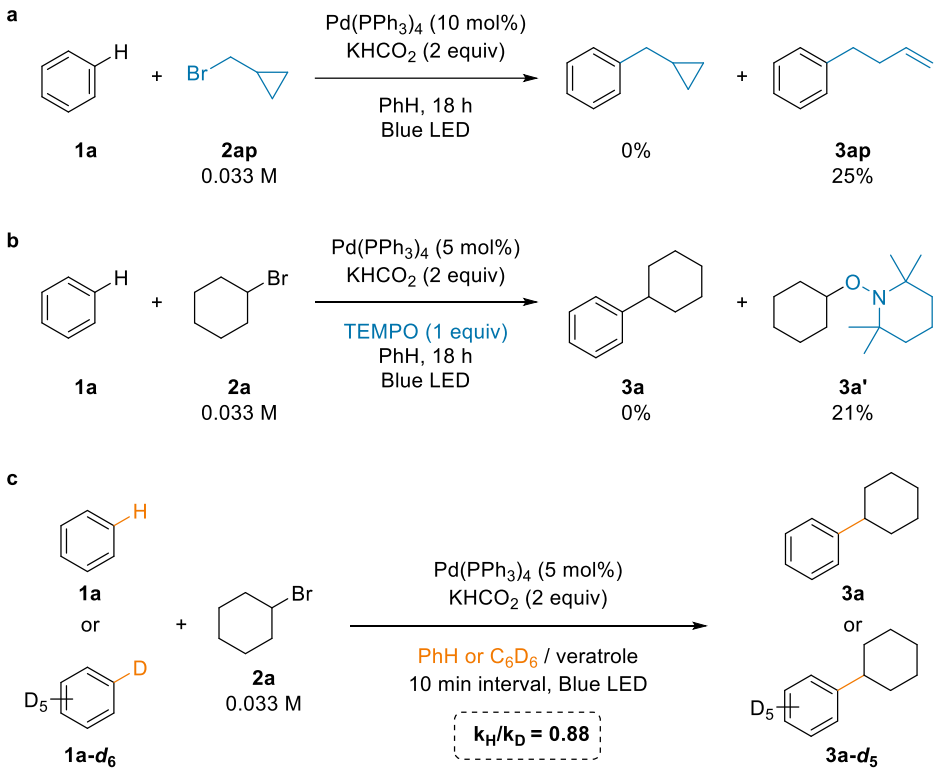

Scheme 6.2 Mechanistic studies. **a**, Radical clock experiment. **b**, Radical scavenger experiment. **c**, Kinetic isotope effect measurement.

Following the initial mechanistic experiments, a mechanistic outline involving a Pd-mediated single-electron reduction of the alkyl bromide to generate an alkyl radical, which subsequently undergoes radical addition to the arene was constructed. To scrutinize the catalytic turnover process, i.e., regeneration of the Pd(0) species upon the formation of the desired product from the radical σ-complex (**I**), two possible pathways were proposed–(1) a single-electron oxidation of the radical σ-complex (**I**) mediated by either a Pd(I) or a Pd(II) species followed by base-assisted rearomatization (Scheme 6.3a, top pathway), or (2) β-hydride elimination from an Pd(II)–alkyl intermediate (**IV**) generated by the reaction

between the radical σ-complex (**I**) and a Pd(I) species (Scheme 6.3a, bottom pathway)–based on the preceding literatures suggesting that both could be operative in photo-excited Pd catalysis.[8b, 15a, 15g, 18a, 27] While the formation of intermediate **IV** through spin recombination of Pd(I) species and **I** could be facile, it should be noted that the resulting Pd(II)–alkyl species could undergo triplet excitation under visible light irradiation to cleave the Pd–alkyl bond, forming a Pd(I)/alkyl radical hybrid.[15a, 18c] This is also the case of the first step involving an alkyl bromide, as under the optimized reaction conditions, only <10% of the eliminated olefin side-products were generated albeit the generation of a Pd(I) species and the alkyl radical intermediate. Therefore, we believe that the intermediate **IV** might not undergo the β-hydride elimination effectively, allowing the reaction to go through the oxidative pathway involving **II** or **III**. To verify the photochemical behaviors of the Pd(II)–alkyl intermediates, computational analyses using time-dependent density functional theory (TD-DFT) were performed with model Pd–alkyl complexes and **IV**. The results indicated clear transitions into the Pd–C antibonding orbitals in the blue light energy region (Table 6.11). Hence, although the β-hydride elimination could be thermodynamically facile, this pathway shall be kinetically inhibited by reversible formation/scission of the Pd–C bond under the visible light irradiation conditions.

Noticeably, a gradual decrease in reactivity was observed in the reactions of polyfluorinated arenes upon increasing the number of fluorine substituents (Table 6.4). For quantitative analysis, the calculated reduction potentials of the Wheland intermediates of the investigated polyfluorinated arenes and the related product yields are summarized in Scheme 6.3b. A negative correlation was

observed between the reduction potential ($E^{o}_{red}[R^{+}/R^{\cdot}]$) and the product yield, and the reactivity was completely shut down in the case of pentafluorobenzene. This illustrates that the formation of less reducing radical σ-complexes, which suppress single-electron transfer to the Pd intermediate, apparently results in lowered reaction efficiencies. This observation is in clear contrast to the photoinduced Pd-catalyzed Heck reaction of alkyl bromides with styrenes recently reported by the Fu group,[15a] which proposed β-hydride elimination as the product forming step, and where the electronic nature of the styrene substrate was insignificant. Possible HAT reactions from the pentafluorobenzene, which may intervene in the productive reaction pathway, were also ruled out by comparing the bond dissociation energies (BDEs) of the related C–H bonds[11, 28] and DFT computations of the HAT barrier (Scheme 6.16).

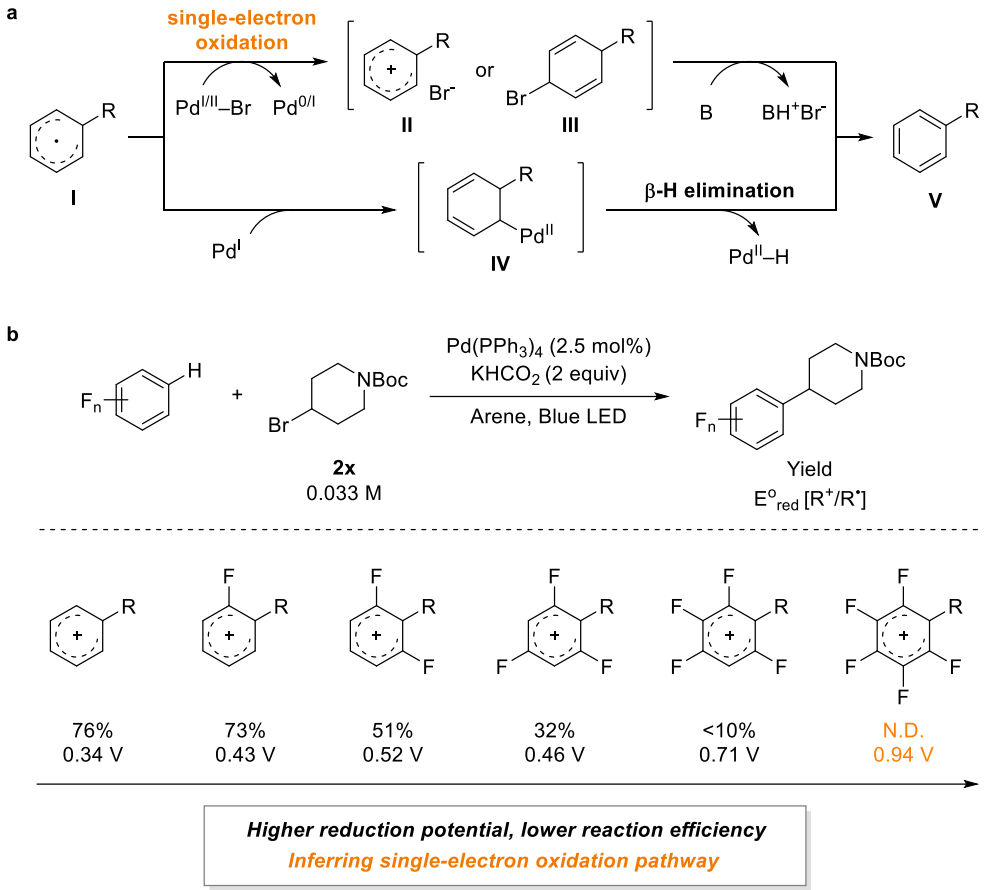

Scheme 6.3 Investigation on the catalytic turnover process. **a**, Two possible catalytic turnover processes. **b**, Reactivity difference among polyfluoroarenes.

With the indirect evidence of an oxidative process, we attempted to discriminate between a direct single-electron transfer (SET), to yield a cationic arenium intermediate (**II**), and a mass transfer-assisted SET[29] to form a transient cyclohexadienyl bromide intermediate (**III**) (Scheme 6.3a, top pathway). To gain more information regarding the former process, we compared the DFT-calculated redox potentials of the Pd(I) bromide species and the radical σ-complexes (Scheme 6.17). It revealed that the direct formation of an arenium cation intermediate (**II**) by

SET without the aid of a bromine atom transfer would be highly disfavored in such nonpolar solvents, thereby indicating that a bromine atom transfer mechanism is more plausible. A similar mechanism proposed by the Zhou group, whereby single-electron oxidation occurs in a deprotonated radical anionic σ-complex (**K** to **K-anion**), was also excluded by DFT computations (Scheme 6.19). While the deprotonation of the electron-poor radical σ-complexes (**K**) was feasible, deprotonation of the corresponding σ-complex derived from benzene (**E** to **E-anion**) was thermodynamically not plausible.

To provide a more concrete experimental evidence for the bromine atom transfer process, a kinetic experiment was designed using benzene-1,3,5-d_3 as the arene substrate (Scheme 6.4). Depending on the position of alkyl radical insertion to benzene-1,3,5-d_3, the generated radical character selectively resides on the C–H or the C–D positions and produces $\mathbf{P_H}$ and $\mathbf{P_D}$. Here, we expect significantly different KIEs as C–H bond cleavage is more involved in the β-hydride elimination pathway. The expected KIEs were first computed through DFT and was determined to be 0.98 and 2.80 for bromine atom transfer and β-hydride elimination, respectively (Table 6.12). The primary KIE for β-hydride elimination is in good agreement with the C–H bond scission process. The small inverse KIE for the bromine atom transfer process could be explained because a C(sp^2) (planar) to C(sp^3) (tetrahedral) hybridization change is involved in the process. Moreover, the bromine atom significantly increases the reduced mass of the relevant vibrational modes, leading to a lower vibrational frequency, and hence a flat energy surface. This would result in only a small difference in the ground state zero-point energies between the protiated and deuterated substrates, thus exhibiting a negligible KIE

value. An intramolecular KIE ([$\mathbf{P_H}$]/[$\mathbf{P_D}$] = ~1) was experimentally determined using benzene-1,3,5-d_3, indicating that the bromine atom transfer is highly likely operating in the catalytic turnover process rather than the β-hydride elimination.

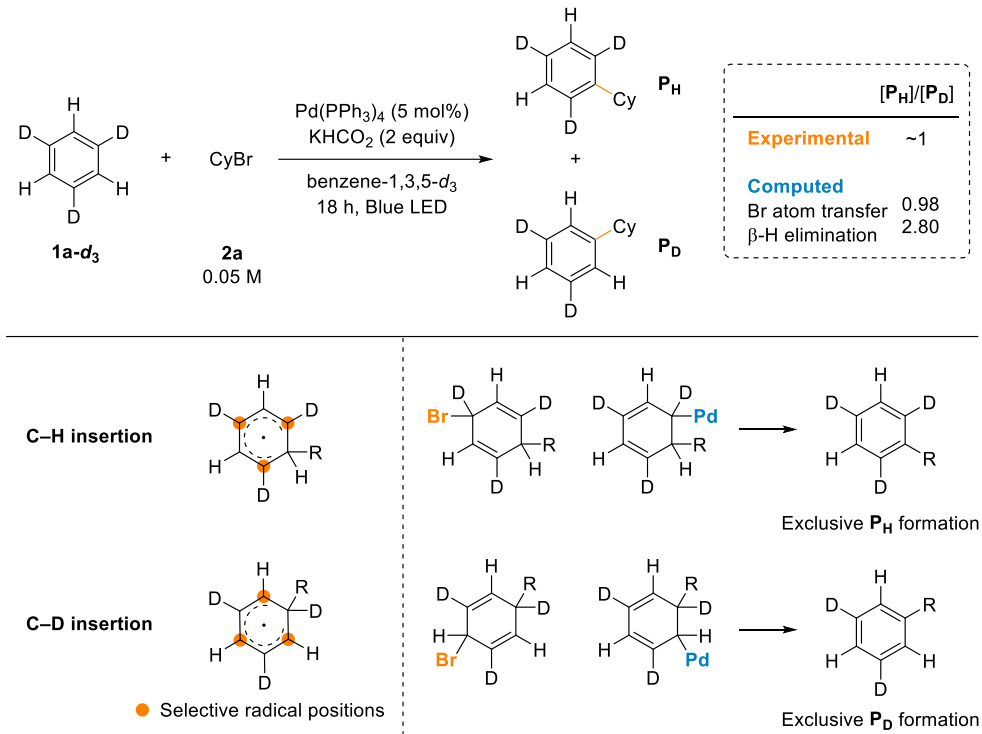

Scheme 6.4 Kinetic isotope effect study with benzene-1,3,5-d_3.

Following the development of an understanding of the catalytic turnover process, we attempted to elucidate why only alkyl bromides prevailed in our reaction (Scheme 6.5a). In particular, the unsuitability of alkyl iodides was unexpected, since alkyl iodides are well-known common radical precursors in the reported photoexcited Pd catalysis.[9, 15g] The generation of alkyl radicals from alkyl chlorides was likely not as facile as from alkyl bromides and iodides, as the

reduction potential of alkyl chlorides is significantly higher,[30] and this was confirmed by a Stern-Volmer quenching experiments of the photoexcited $Pd(PPh_3)_4$ with the alkyl halides under our catalytic conditions (Scheme 6.5b). Compared to the quenching rates of bromocyclohexane and iodocyclohexane, that of chlorocyclohexane was more sluggish with no observation of effective quenching. DFT modeling of the single-electron reduction process of the alkyl halides by a triplet excited $Pd(PPh_3)_3$ catalyst ^{3}**B**, following the reported protocols by Cavallo and Rueping,[18c] was also in good agreement with the experimental results (Scheme 6.5c). The reduction of alkyl chlorides was found to be associated with an energy barrier of 6.7 kcal/mol (^{3}**B-TS**), while the reductions of alkyl bromides and iodides were barrierless. Although the reduction barrier with alkyl chlorides is not significantly high and is nearly diffusion-controlled, this reduction process is an intermolecular reaction in competition with the facile relaxation of the excited Pd(0) species ^{3}**B**, accounting for the dramatically reduced quenching rate observed.

In contrast to the alkyl chlorides, we were puzzled as to why the alkyl iodides failed to furnish any product despite exhibiting a stronger quenching of the catalyst compared to the alkyl bromides (Scheme 6.5b). Since the reaction with alkyl iodides did not yield the desired product exceeding the amount of catalyst loaded (entry 11 in Table 6.1, and Scheme 6.5f), we speculated that a problem may arise in the catalytic turnover process when an alkyl iodide is subjected to the reaction. Hence, the identification of the related Pd species involved in the reaction was attempted by ^{31}P NMR spectroscopy (Scheme 6.5d). The reaction between $Pd(PPh_3)_4$ and bromocyclohexane (10 equiv) generated $Pd(PPh_3)_2Br_2$ (Scheme 6.5d), which could be readily reduced to a Pd(0) species that could re-enter the

catalytic cycle with $KHCO_2$ under blue light irradiation (Scheme 6.5e). While the formation of $Pd(PPh_3)_2I_2$ was also observed in the reaction of $Pd(PPh_3)_4$ with iodocyclohexane (Scheme 6.5d), the reduction of $Pd(PPh_3)_2I_2$ was not facile under the identical conditions (Scheme 6.5e), suggesting that $Pd(PPh_3)_2I_2$ is not involved in the productive catalytic cycle. Such a Pd(II) dihalide intermediate could potentially be generated from a second single-electron transfer between a photoexcited doublet Pd(I) species and an alkyl halide, as suggested by Zhao[27a] and Zhou.[9] Moreover, the DFT-computed transition states of the second single-electron reduction showed a 7.0 kcal/mol lower barrier for propyl iodide compared to propyl bromide, indicating that the inactive $Pd(PPh_3)_2X_2$ complex can be more rapidly formed with alkyl iodides than alkyl bromides (Scheme 6.20).

For further confirmation, a stoichiometric experiment between $Pd(PPh_3)_4$ and **2af** or **2af′** was performed inspired by the studies reported by Zhao and co-workers (Scheme 6.5f).[27a] In their Pd-catalyzed difluoromethylation of aromatic ketones with bromodifluoroacetate (**2ar**) using $Pd(PPh_3)_4$ as the precatalyst, the desired product was not observed when the reaction was performed with a 1:1 ratio of $Pd(PPh_3)_4$ and **2ar**. The reaction only proceeded when 2 equiv of **2ar** vs $Pd(PPh_3)_4$ was used, indicating a Pd(II)-mediated SET mechanism where the generation of Pd(II) species by two consecutive single-electron reductions of the alkyl halide is critical. In clear contrast, the desired product (**3af**) was obtained in 68% yield even with 1 equiv of **2af** vs $Pd(PPh_3)_4$ under our reaction conditions (Scheme 6.5f). This experiment, along with the observations made by ^{31}P NMR spectroscopy, therefore consistently supports that the Pd(II) species is not a catalytic intermediate, but a dormant species in our case.

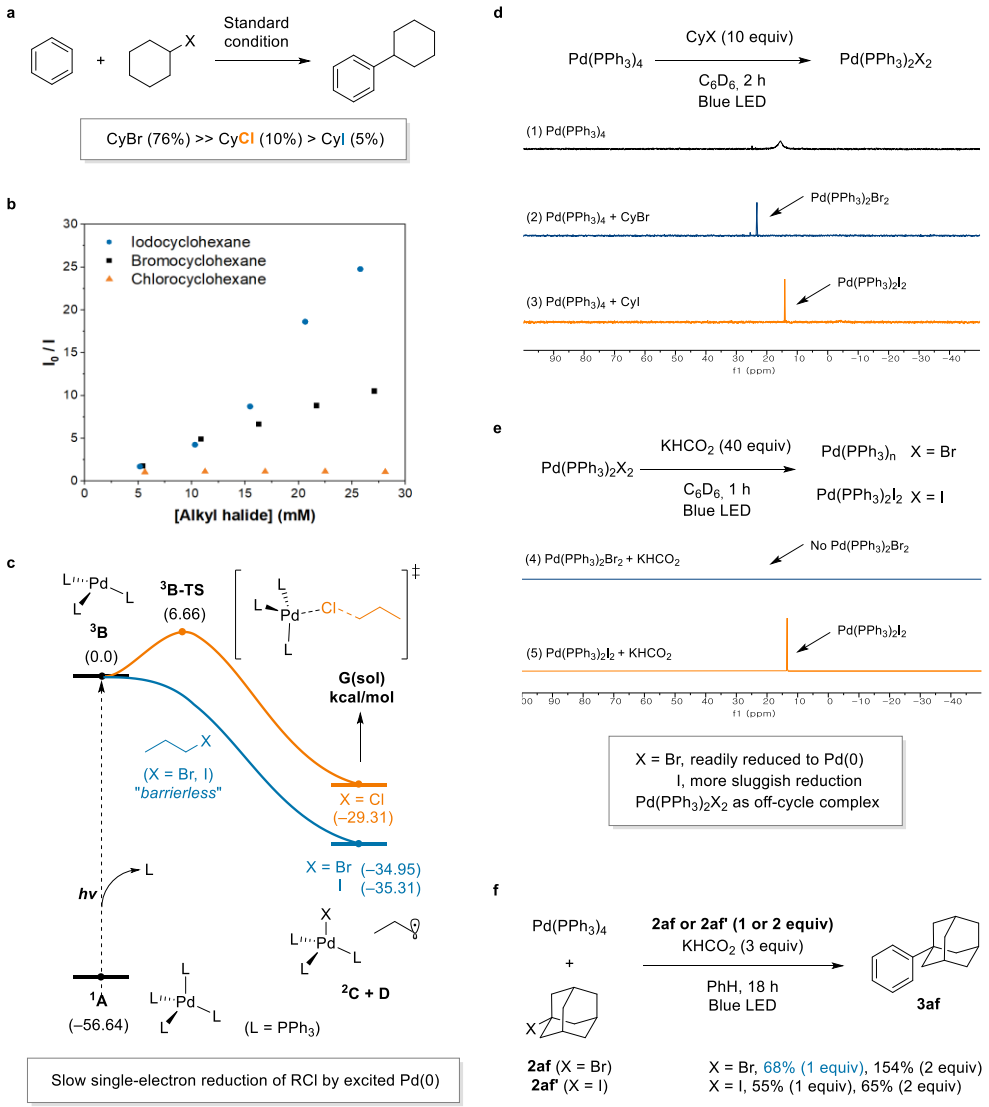

Scheme 6.5 Single-electron reduction of alkyl halides by photoexcited Pd(0). **a**, Reactivity difference among alkyl halides. **b**, Stern-Volmer experiment. **c**, DFT modeling of single-electron reduction. **d**, Formation of $Pd(PPh_3)_2X_2$ from $Pd(PPh_3)_4$ and CyX. **e**, Distinguished reactivity of $Pd(PPh_3)_2Br_2$. f, Reactions with stoichiometric amount of $Pd(PPh_3)_4$.

Lastly, a comprehensive DFT modeling of the overall reaction pathway was performed to verify the feasibility of the proposed mechanism using the B3LYP-D3(IEFPCM)/SDD/6-311++G**//B3LYP-D3/LanL2DZ/6-31G**[31] level of theory (Scheme 6.6). The single-electron oxidative addition of propyl bromide to the excited Pd species ^{3}**B**, which has 56.6 kcal/mol higher energy than the initial catalyst ^{1}**A**, was shown to be barrierless. The generated propyl radical exists as a Pd(I)/alkyl radical hybrid species ^{2}**C + D** with an energy of –35.0 kcal/mol relative to ^{3}**B**. From the hybrid species ^{2}**C + D**, an activation barrier of 21.3 kcal/mol was calculated for the transition state of the propyl radical inserting into benzene, **D-TS**. The resulting radical σ-complex **E** reacts with Pd(I)–Br species ^{2}**C** through bromine atom transfer with a barrier of 17.3 kcal/mol to furnish the transient dearomatized cyclohexadienyl bromide **F** and the initial Pd(0) species ^{1}**B**, which re-enters the catalytic cycle. These two elementary steps comprise the overall activation barrier of the reaction, 23.5 kcal/mol, identifying the bromine atom transfer step as the rate-limiting step, which is in good accordance with our observation that a slight warming of the reaction mixture by turning off the fan cooling was favorable to produce high conversions and yields (entry 9, Table 6.1). The final re-aromatization via an E2-type elimination assisted by the formate anion is highly exergonic with a downhill energy of 45.5 kcal/mol.

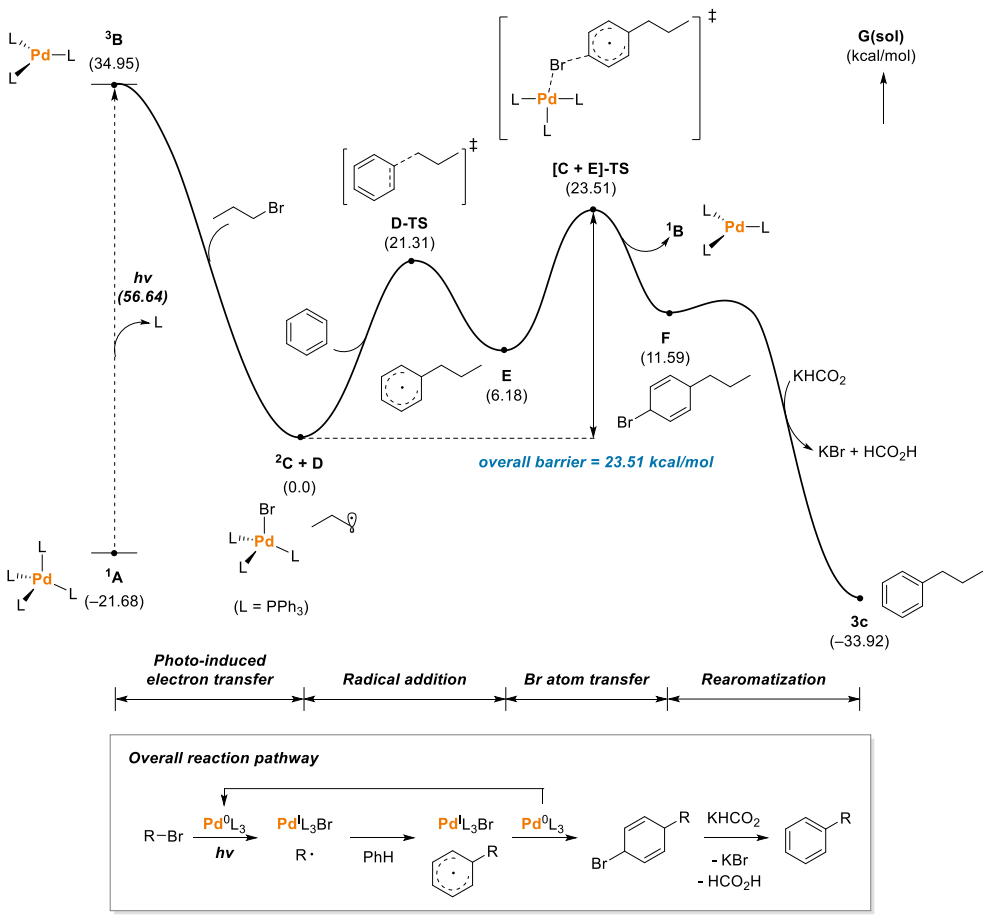

Scheme 6.6 Computed energy profile of the proposed mechanism. Free energies in solution (in kcal/mol) at the B3LYP-D3(IEFPCM)/SDD/6-311++G**//B3LYP-D3/LanL2DZ/6-31G** level are displayed.

6.3 Conclusion

In conclusion, C(sp^2)–H alkylation of unactivated arenes which selectively produces various linear and branched alkylarenes was developed through the use of a photoinduced Pd catalysis. The single-electron-mediated Pd catalysis controls the reactivity of the alkyl radicals generated from alkyl bromides under mild conditions, allowing the installation of various alkyl groups on arenes without the

occurrence of alkyl rearrangements. This operatively simple reaction proceeds efficiently with excellent functional group tolerance, enabling the late-stage functionalization of complex molecules and a one-pot sequential Pd-catalyzed C–C bond forming reaction. A complete Pd(0)/Pd(I) catalytic cycle was constructed with the elucidation of the origin of the counterintuitive reactivity sequence of alkyl halides through comprehensive experimental and computational studies. The developed method will streamline the synthesis of fundamentally useful alkylbenzenes.

6.4 Experimental section

6.4.1 General information

Unless otherwise noted, all reactions were performed under inert conditions. Benzene was dried using a PureSolv solvent purification system. All chemicals were purchased from commercial sources (Sigma-Aldrich, Alfa Aesar, TCI, or Strem) and used. All photocatalytic reactions were conducted under irradiation by 40 W Blue LED lamps purchased from Kessil (Kessil A160WE) using a maximum light intensity and shortest wavelength setup. Reactions were monitored by thin-layer chromatography (TLC) on EMD Silica Gel 60 F254 plates and visualized either using UV light (254 nm) or by staining with potassium permanganate and heating. Nuclear magnetic resonance (NMR) spectra were recorded in $CDCl_3$, CD_2Cl_2 and C_6D_6 on a Bruker DPX-300 (300 MHz) spectrometer, Varian 400 and 500 NMR (400 and 500 MHz), Bruker AVANCE 300 (300 MHz), Bruker AVANCE 400 (400 MHz), or Bruker AVANCE III HD (400 MHz), and the residual solvent signal was used as a reference. Chemical shifts are reported in ppm, and coupling

constants are given in Hz. Gas chromatography (GC) was carried out using a 7890A or 7890B GC system (Agilent Technologies) equipped with an HP-5 column and a flame ionization detector (FID). High-resolution mass spectrometry (HRMS) was performed at the Organic Chemistry Research Center in Sogang University using the ESI method. Stern-Volmer quenching experiments were conducted using an RF-6000 spectrofluorophotometer with LabSolutions RF software. X-ray diffraction data of **3ao** was collected on a Bruker D8 QUEST APEX III coated with Paraton-*N* oil under a stream of N_2 (g) at 173 K.

6.4.2 General procedure for the C(sp^2)–H alkylation reaction

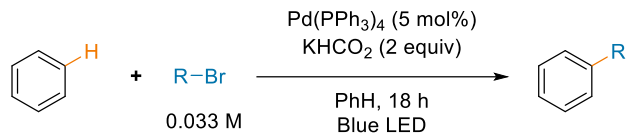

To a 4 mL vial equipped with a PTFE-coated stirrer bar were added the corresponding alkyl bromide (0.10 mmol, 1.0 equiv), $Pd(PPh_3)_4$ (5.8 mg, 0.0050 mmol, 0.050 equiv), $KHCO_2$ (16.8 mg, 0.20 mmol, 2.0 equiv), and benzene (3.0 mL). The resulting mixture was stirred for 18 h at ambient temperature under 40 W blue LED irradiation without fan cooling (measured reaction temperature = 50±5 ^oC). The reaction mixture was filtered through a short pad of Celite®, eluted with CH_2Cl_2, and concentrated under reduced pressure. The resulting residue was purified by flash column chromatography (silica gel, hexanes/EtOAc gradient elution) to afford the desired product.

6.4.3 Optimization of reaction conditions

Table 6.5 Optimization of reaction conditions

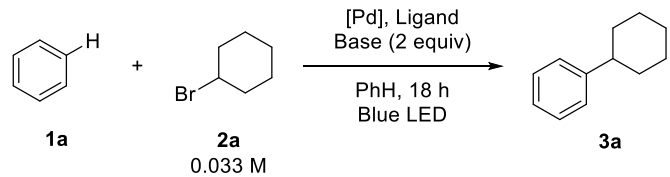

Entry	[Pd] (mol%)	Ligand (mol%)	Base	Yield[a] (%)
1	$Pd(PPh_3)_4$ (5)	-	$KHCO_2$	76
2	$Pd(OAc)_2$ (5)	PPh_3 (20)	$KHCO_2$	70
3	$Pd(OAc)_2$ (5)	Xantphos (10)	Cs_2CO_3	18
4	$Pd(OAc)_2$ (5)	Xantphos (6)	$KHCO_2$	17
5	$Pd(OAc)_2$ (5)	dppp (6)	$KHCO_2$	25
7	$Pd(PPh_3)_4$ (5)	DPEPhos (6)	Cs_2CO_3	26
8	$Pd(PPh_3)_4$ (5)	DPEPhos (6)	$KHCO_2$	28
9	$Pd(PPh_3)_2Cl_2$ (5)	Xantphos (6)	KOAc	22
10	$Pd(PPh_3)_2Cl_2$ (5)	Xantphos (6)	$KHCO_2$	52
11	$Pd(PPh_3)_2Cl_2$ (5)	-	$KHCO_2$	74
12	$Pd(PPh_3)_2Br_2$ (5)	-	$KHCO_2$	70
13	$Pd(PPh_3)_2I_2$ (5)	-	$KHCO_2$	70
14	$Pd(dppf)Cl_2$ (5)	-	$KHCO_2$	0
15	$Pd(PPh_3)_4$ (5)	-	$KHCO_2$	1[b]
16	$Pd(PPh_3)_4$ (5)	-	$KHCO_2$	5[c]

[a]Yields were measured by GC using dodecane as an internal standard. [b]under air. [c]with H_2O (2 equiv).

Table 6.6 Reactivities with dual phosphine ligand systems

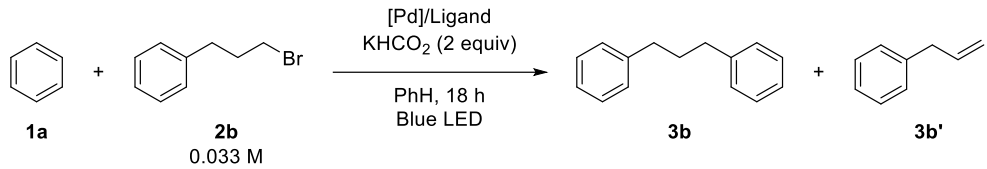

Entry	[Pd] (mol%)	Ligand (mol%)	Yield of 3b[a] (%)	Yield of 3b'[a] (%)
1	$Pd(PPh_3)_4$ (5)	DPEPhos (6)	14	83
2	$Pd(PPh_3)_2Cl_2$ (5)	XantPhos (6)	22	50

[a]Yields were measured by GC using mesitylene as an internal standard.

Table 6.7 The effect of Br^- additives in other alkyl halides

Entry	X	Br^- additive	Yield[a] (%)
1	Cl	-	10
2	Cl	*n*-Bu_4NBr	17
3	Cl	KBr	8
4	I	-	5
5	I	*n*-Bu_4NBr	36
6	I	KBr	4

[a]Yields were measured by GC using dodecane as an internal standard.

Table 6.8 The effect of arene equivalences

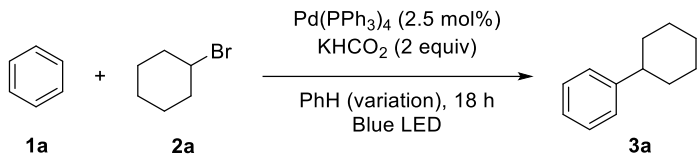

Entry	PhH	Yield[a] (%)
1	1.5 mL	57
2	0.75 mL	41
3	0.30 mL	24
4	90 µL (10 equiv)	18

[a]Yields were measured by GC using dodecane as an internal standard.

Table 6.9 The effect of solvents

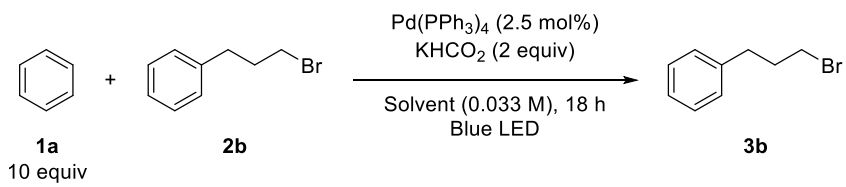

Entry	Solvent	Yield[a] (%)
1	EA	7
2	DCM	6
3	DMA	6
4	Dioxane	9
5	Veratrole	2
6	CH_3CN	12

[a]Yields were measured by GC using mesitylene as an internal standard.

6.4.4 Synthetic applications

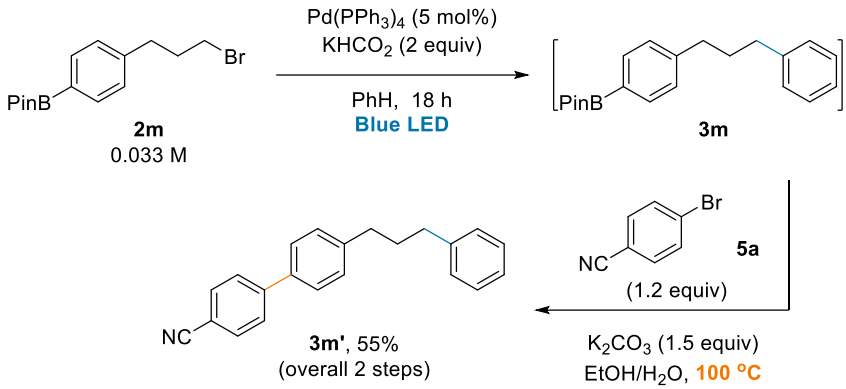

To a 4 mL vial equipped with a PTFE-coated stirrer bar were added the corresponding alkyl bromide **2m** (32.5 mg, 0.10 mmol, 1.0 equiv), $Pd(PPh_3)_4$ (5.8 mg, 0.0050 mmol, 0.050 equiv), $KHCO_2$ (16.8 mg, 0.20 mmol, 2.0 equiv), and benzene (3.0 mL). The resulting mixture was stirred for 18 h at ambient temperature under 40 W blue LED irradiation without fan cooling (measured reaction temperature = 50±5 ^oC). The solution of 4-bromobenzonitrile **5a** (21.9 mg, 0.12 mmol, 1.2 equiv), K_2CO_3 (20.7 mg, 0.15 mmol, 1.5 equiv) in $EtOH/H_2O$ (1:1, 0.6 mL) was then added in the reaction vial. The resulting mixture was stirred for further 18 h at 100 ^oC. The reaction mixture was then diluted with 1 M $NaHCO_3$ (10 mL), extracted with CH_2Cl_2 (3 x 10 mL), dried (anhydrous Na_2SO_4), filtered, and concentrated under reduced pressure. The resulting residue was purified by flash column chromatography (silica gel, hexanes/EtOAc gradient elution) to afford the desired product (16.4 mg, 55%) as a white solid.

6.4.5 Kinetic isotope effect (KIE) measurements

6.4.5.1 KIE determined from rate comparision of two parallel reactions

To obtain the information about the rate-limiting step of the reaction, KIE experiments were conducted. The following procedure was employed for the parallel reactions with benzene (**1a**) and benzene-d_6 (**1a-*d*$_6$**).

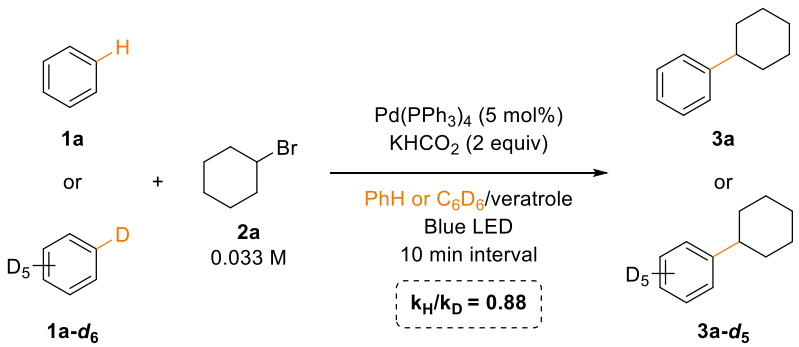

A 4 mL reaction vial equipped with a PTFE-coated stirrer bar was charged with **2a** (13 µl, 0.10 mmol, 1.0 equiv), $Pd(PPh_3)_4$ (5.8 mg, 0.0050 mmol, 0.050 equiv), $KHCO_2$ (17 mg, 0.2 mmol, 2.0 equiv), benzene or benzene-d_6 (0.50 mL), dodecane (internal standard, 5.0 µl), and veratrole (2.5 mL) in a glovebox. The vial was closed with a Teflon-lined septum-cap and taken out of the glovebox. Argon balloon was attached to the septum with a needle to maintain the inert atmosphere. The resulting mixture was stirred under 40 W blue LED lamp irradiation. Aliquots of the reaction mixture were taken every 10 min and analyzed by gas chromatography to determine the product (**3a** or **3a-*d*$_5$**) yields. The initial rates were compared and kinetic isotope effect (KIE) was measured. The same experiment was repeated two more times and the average KIE value of 0.88 was obtained. The observed inverse KIE value suggested that the rate-limiting step involves a change in hybridization of the carbon atom from C(sp^2) to C(sp^3).

6.4.5.2 KIE determined from an intramolecular competition with benzene-1,3,5-d_3

To a 4 mL vial equipped with a PTFE-coated stirrer bar were added **2a** (6.5 µL, 0.050 mmol, 1.0 equiv), $Pd(PPh_3)_4$ (2.9 mg, 0.0025 mmol, 0.050 equiv), $KHCO_2$ (8.4 mg, 0.10 mmol, 2.0 equiv), and benzene-1,3,5-d_3 (1.0 mL). The resulting mixture was stirred for 18 h at ambient temperature under 40 W blue LED irradiation without fan cooling (measured reaction temperature = 50±5 °C). The reaction mixture was filtered through a short pad of Celite®, eluted with CH_2Cl_2, and concentrated under reduced pressure. The resulting residue was purified by flash column chromatography (silica gel, pentane elution) to afford the desired products. The ratio of the products was compared by ^{1}H NMR analysis and intramolecular KIE ([$\mathbf{P_H}$]/[$\mathbf{P_D}$] ~ 1) was determined.

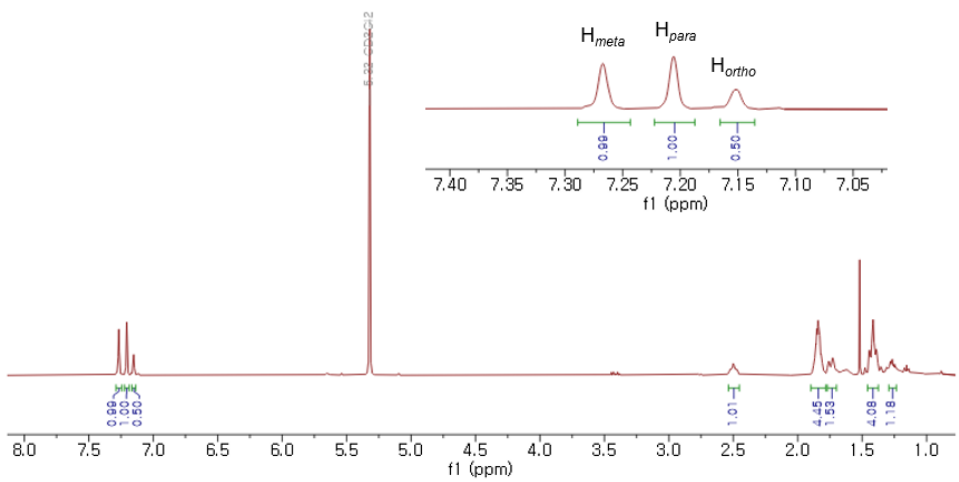

Scheme 6.7 ^{1}H-NMR spectra (300 MHz, CD_2Cl_2) of a mixture of $\mathbf{P_H}$ and $\mathbf{P_D}$.

6.4.6 Stern-Volmer quenching experiments

All emission spectra of the samples were collected under an argon atmosphere. A solution of $Pd(PPh_3)_4$ (1.0×10^{-3} M) was prepared in a cuvette. Chlorocyclohexane (CyCl), bromocyclohexane (CyBr), and iodocyclohexane (CyI) were used as quenchers. The prepared solutions were excited at 420 nm and the emission intensity at 650 nm was observed. As shown in Scheme 6.8 to 6.10, Stern-Volmer quenching experiments resulted in positive dependence between I_0/I and the concentration of quenchers. The results indicate that CyBr and CyI quench the excited state of $Pd(PPh_3)_4$, where it engages in a single-electron transfer (SET) event with the photoexcited Pd(0) complex. Compared to those of CyBr and CyI, the quenching rate of CyCl was extremely sluggish.

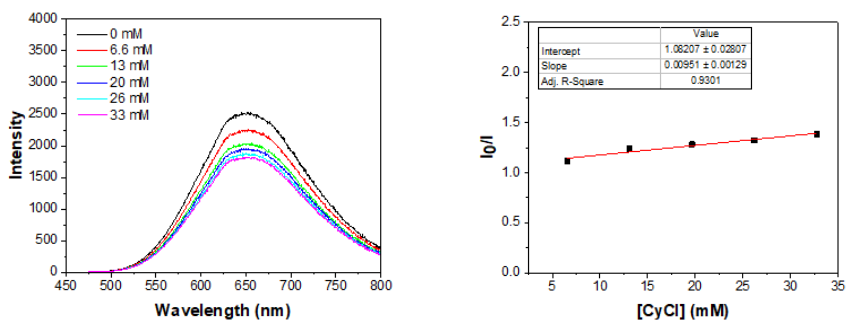

Scheme 6.8 Stern-Volmer quenching study with chlorocyclohexane.

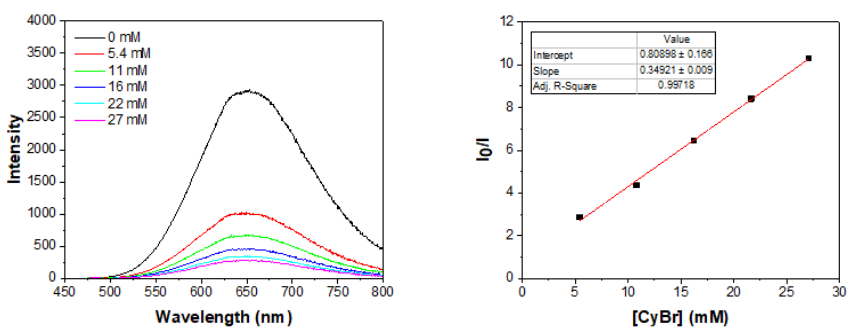

Scheme 6.9 Stern-Volmer quenching study with bromocyclohexane.

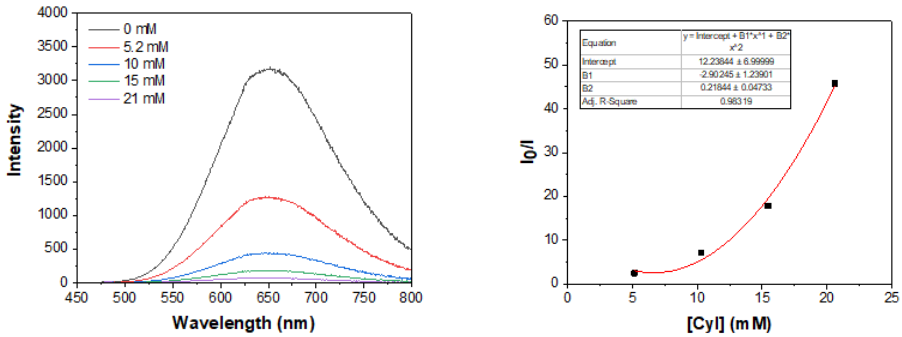

Scheme 6.10 Stern-Volmer quenching study with iodocyclohexane.

6.4.7 In-situ ^{31}P NMR experiments

^{31}P NMR spectroscopic experiments were carried out to analyze the palladium intermediates in benzene-d_6 (1.0 mL). ^{31}P NMR spectra were taken under the below conditions, respectively.

$Pd(PPh_3)_4$ exhibited a broad signal at 15.6 ppm in benzene-d_6 (**1**). New signals analyzed as $Pd(PPh_3)_2Br_2$ and $Pd(PPh_3)_n$ appeared at 23.3 ppm and 6.7 ppm under the standard reaction condition (**2**). $Pd(PPh_3)_2Br_2$ or $Pd(PPh_3)_2I_2$ was formed when CyBr (10 equiv) or CyI (10 equiv) was mixed with $Pd(PPh_3)_4$ under the blue light irradiation (**3** and **4**).

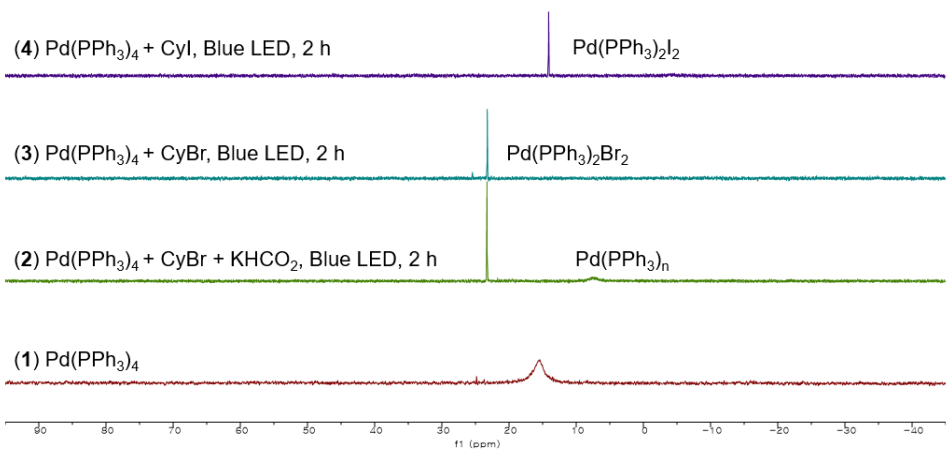

Scheme 6.11 Formation of $Pd(PPh_3)_2X_2$ from $Pd(PPh_3)_4$ and CyX.

While we equally observed the formation of Pd(II) dihalide species with CyBr or CyI, only $Pd(PPh_3)_2Br_2$ can be readily reduced to a Pd(0) species with $KHCO_2$ (40 equiv) under blue light irradiation (**5**). In contrast, the reduction of $Pd(PPh_3)_2I_2$ was extremely sluggish under identical conditions (**6**).

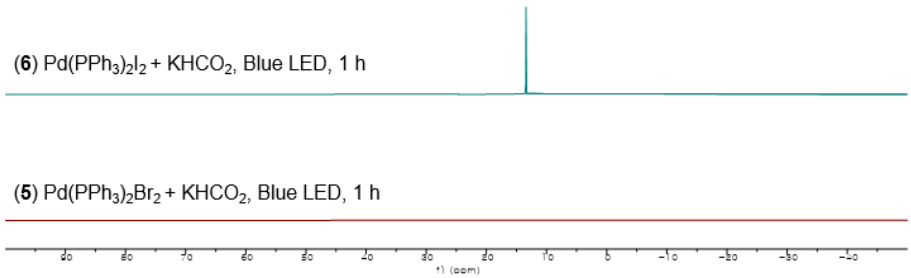

Scheme 6.12 Distinguished reactivity of $Pd(PPh_3)_2Br_2$.

6.4.8 Reactions with stoichiometric amount of $Pd(PPh_3)_4$

To a 4 mL reaction vial equipped with a PTFE-coated stirrer bar were added $Pd(PPh_3)_4$ (57.8 mg, 0.050 mmol, 1.0 equiv), alkyl halide **2af** or **2af'** (1.0 or 2.0 equiv), $KHCO_2$ (13.4 mg, 0.15 mmol, 3.0 equiv), and benzene (3.0 mL). The resulting mixture was stirred for 18 h at ambient temperature under 40 W blue LED irradiation without fan cooling (measured reaction temperature = 50±5 ^oC). The reaction mixture was filtered through a short pad of Celite®, eluted with CH_2Cl_2, and analyzed by gas chromatography using dodecane as an internal standard to obtain the yield of the product **3af**.

6.4.9 Additive-based robustness screen

The robustness of the C–H alkylation of arenes was investigated by applying an intermolecular additive-based screen. This simplified robustness screen method, reported by the Glorius group,[22] evaluates both a functional group tolerance and the stability of additives to the reaction conditions. For the analysis, the standard reaction was carried out in the presence of the equimolar additive. The calibration of the additives and the product of the reaction was conducted using GC to analyze the yields of the additives and the product. According to the general procedure, 20 reactions were conducted with 20 different additives (0.1 mmol, 1.0 equiv, see table below). After the reaction, the amount of remaining additive and the yield of the product was determined by GC using dodecane as an internal standard. Table 6.11 shows the effect of a given additives on the standard reaction condition. The yields of product **3a** and the remaining additive after the reaction are given in the table. Color-coding helps the assessment of the data: green (above 66%), yellow (33-66%), and red (below 33%)

Table 6.10 Robustness screening results

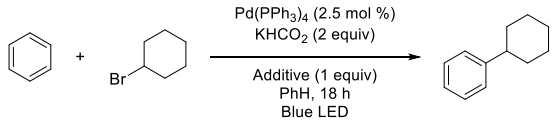

Entry		Additive remaining %	Yield of **Product** %	Entry		Additive remaining %	Yield of **Product** %
1		✓ 104	✓ 75	11	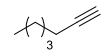	− 58	X 14
2		✓ 90	✓ 73	12	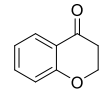	✓ 85	− 55
3		✓ 87	X 6	13	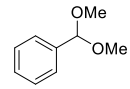	✓ 92	✓ 73
4	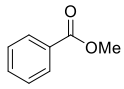	✓ 97	✓ 73	14	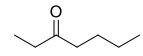	✓ 104	✓ 73
5	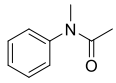	✓ 94	✓ 80	15	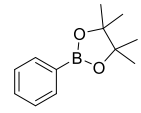	✓ 100	✓ 71
6		✓ 71	− 38	16	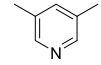	✓ 101	✓ 78
7		X 0	− 64	17		✓ 88	✓ 67
8		✓ 102	✓ 75	18	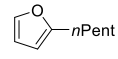	✓ 98	✓ 68
9		✓ 93	✓ 72	19		✓ 90	✓ 73
10		✓ 70	− 66	20		✓ 85	X 5

6.4.10 Characterization of newly reported compounds

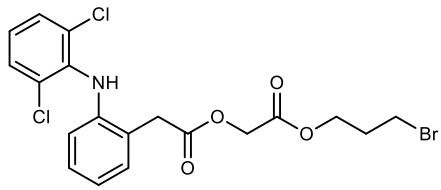

2-(3-Bromopropoxy)-2-oxoethyl 2-(2-((2,6-dichlorophenyl)amino)phenyl)acetate (2ah)

White solid, 386 mg (0.81 mmol, 81% yield); ^{1}H NMR (400 MHz, $CDCl_3$) δ 7.34 (d, *J* = 8.1 Hz, 2H), 7.27 (d, *J* = 5.3 Hz, 1H), 7.14 (t, *J* = 7.7 Hz, 1H), 7.03 – 6.94 (m, 2H), 6.72 (brs, 1H), 6.56 (d, *J* = 8.0 Hz, 1H), 4.69 (s, 2H), 4.27 (t, *J* = 6.1 Hz, 2H), 3.93 (s, 2H), 3.33 (t, *J* = 6.4 Hz, 2H), 2.09 (p, *J* = 6.2 Hz, 2H); ^{13}C NMR (101 MHz, $CDCl_3$) δ 171.6, 167.5, 142.9, 137.9, 131.1, 129.7, 129.0, 128.4, 124.3, 123.9, 122.3, 118.6, 63.3, 61.4, 38.2, 31.5, 29.1; HRMS-ESI (m/z) $[M+Na]^+$ calcd for $C_{19}H_{18}BrCl_2NNaO_4$, 495.9689; found: 495.9688.

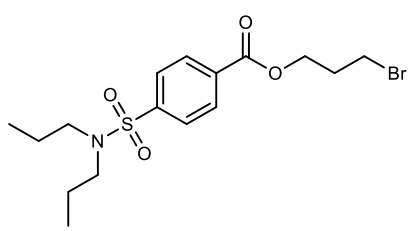

3-Bromopropyl 4-(*N*,*N*-dipropylsulfamoyl)benzoate (2ai)

White solid, 297 mg (0.73 mmol, 73% yield); ^{1}H NMR (400 MHz, $CDCl_3$) δ 8.15 (dt, *J* = 8.6, 1.9 Hz, 1H), 7.88 (dt, *J* = 8.7, 1.8 Hz, 1H), 4.51 (t, *J* = 6.0 Hz, 1H), 3.55 (t, *J* = 6.5 Hz, 1H), 3.13 – 3.06 (m, 2H), 2.34 (p, *J* = 6.3 Hz, 1H), 1.55 (h, *J* = 7.4 Hz, 3H), 0.87 (t, *J* = 7.4 Hz, 3H); ^{13}C NMR (101 MHz, $CDCl_3$) δ 165.2, 144.6,

133.4, 130.4, 127.2, 63.5, 50.1, 31.8, 29.3, 22.1, 11.3; HRMS-ESI (m/z) $[M+Na]^+$ calcd for $C_{16}H_{24}BrNNaO_4S$, 428.0502; found: 428.0502.

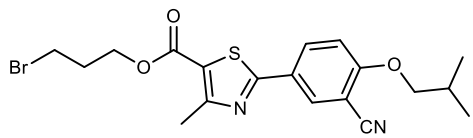

3-Bromopropyl 2-(3-cyano-4-isobutoxyphenyl)-4-methylthiazole-5-carboxylate (2ak)

White solid, 332 mg (0.76 mmol, 76% yield); ^{1}H NMR (400 MHz, $CDCl_3$) δ 8.16 (d, *J* = 2.3 Hz, 1H), 8.07 (dd, *J* = 8.8, 2.3 Hz, 1H), 7.00 (d, *J* = 8.9 Hz, 1H), 4.44 (t, *J* = 6.0 Hz, 2H), 3.89 (d, *J* = 6.5 Hz, 2H), 3.53 (t, *J* = 6.5 Hz, 2H), 2.75 (s, 3H), 2.30 (p, *J* = 6.3 Hz, 2H), 2.18 (dq, *J* = 13.3, 6.7 Hz, 1H), 1.08 (d, *J* = 6.7 Hz, 6H); ^{13}C NMR (101 MHz, cdcl$_3$) δ 167.5, 162.6, 161.9, 161.6, 132.7, 132.2, 126.0, 121.4, 115.5, 112.7, 103.1, 75.8, 63.1, 31.7, 29.4, 28.2, 19.2, 17.6; HRMS-ESI (m/z) $[M+H]^+$ calcd for $C_{19}H_{22}BrN_2O_3S$, 437.0529; found: 437.0529.

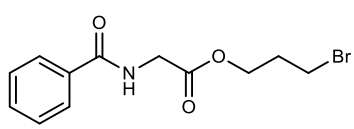

3-Bromopropyl benzoylglycinate (2al)

White solid, 240 mg (0.80 mmol, 80% yield); ^{1}H NMR (400 MHz, $CDCl_3$) δ 7.80 (d, *J* = 7.7 Hz, 2H), 7.51 (t, *J* = 7.3 Hz, 1H), 7.43 (t, *J* = 7.5 Hz, 2H), 6.77 (s, 1H), 4.34 (t, *J* = 6.0 Hz, 2H), 4.24 (d, *J* = 5.1 Hz, 2H), 3.46 (t, *J* = 6.4 Hz, 2H), 2.21 (p, *J* = 6.2 Hz, 2H); ^{13}C NMR (101 MHz, $CDCl_3$) δ 170.1, 167.7, 133.7, 132.0, 128.8,

127.2, 63.4, 41.9, 31.5, 29.2; HRMS-ESI (m/z) $[M+Na]^+$ calcd for $C_{12}H_{14}BrNNaO_3$, 322.0049; found: 322.0049.

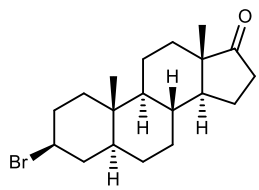

(3S,5S,8R,9S,10S,13S,14S)-3-bromo-10,13-dimethylhexadecahydro-17*H*-cyclopenta[a]phenanthren-17-one (2an)

White solid, 318 mg (0.90 mmol, 90% yield); ^{1}H NMR (400 MHz, $CDCl_3$) δ 4.08 – 3.96 (m, 1H), 2.43 (dd, *J* = 19.2, 8.3 Hz, 1H), 2.19 – 1.76 (m, 8H), 1.73 (dt, *J* = 13.4, 3.7 Hz, 1H), 1.66 – 1.44 (m, 3H), 1.38 – 1.13 (m, 6H), 1.09 – 0.91 (m, 2H), 0.86 (d, *J* = 9.5 Hz, 6H), 0.75 – 0.65 (m, 1H); ^{13}C NMR (101 MHz, $CDCl_3$) δ 221.3, 54.5, 52.3, 51.5, 48.1, 47.9, 40.6, 39.9, 36.0, 35.7, 35.1, 34.2, 31.6, 30.9, 28.2, 21.9, 20.5, 13.9, 12.4; HRMS-ESI (m/z) [M+Na]+ calcd for $C_{19}H_{29}BrNaO$, 375.1294, 375.1294.

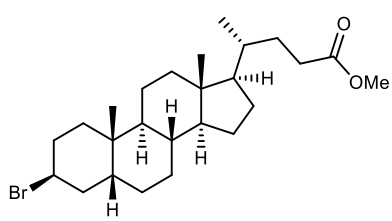

Methyl (R)-4-((3S,5R,8R,9S,10S,13R,14S,17R)-3-bromo-10,13-dimethylhexadecahydro-1*H*-cyclopenta[a]phenanthren-17-yl)pentanoate (2ao)

White solid, 399 mg (0.88 mmol, 88% yield); ^{1}H NMR (400 MHz, $CDCl_3$) δ 4.79 (p, *J* = 2.9 Hz, 1H), 3.66 (s, 3H), 2.40 – 2.30 (m, 1H), 2.29 – 2.16 (m, 2H), 2.00 –

1.74 (m, 7H), 1.66 – 1.52 (m, 5H), 1.49 – 1.03 (m, 13H), 1.00 (s, 3H), 0.90 (d, *J* = 6.4 Hz, 3H), 0.65 (s, 3H); ^{13}C NMR (101 MHz, $CDCl_3$) δ 174.9, 57.2, 56.8, 56.1, 51.6, 42.9, 41.0, 40.3, 37.5, 35.8, 35.5, 35.5, 35.5, 31.2, 31.1, 31.0, 29.8, 28.3, 26.8, 26.5, 24.3, 23.8, 21.1, 18.4, 12.2.; HRMS-ESI (m/z) $[M+Na]^+$ calcd for $C_{25}H_{41}BrNaO_2$, 475.2182; found: 475.2182.

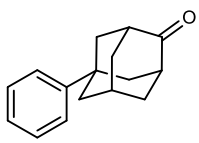

5-Phenyladamantan-2-one (3ag)

White solid, 22.7 mg (0.10 mmol, <99% yield); ^{1}H NMR (400 MHz, $CDCl_3$) δ 7.38 – 7.31 (m, 4H), 7.25 – 7.20 (m, 1H), 2.67 (s, 2H), 2.27 (d, *J* = 11.8 Hz, 3H), 2.24 – 2.15 (m, 4H), 2.14 – 2.01 (m, 4H); ^{13}C NMR (101 MHz, $CDCl_3$) δ 218.1, 148.1, 128.5, 126.4, 124.9, 46.8, 44.5, 42.1, 38.7, 36.2, 28.3; HRMS-ESI (m/z) $[M+Na]^+$ calcd for $C_{16}H_{18}NaO$, 249.1252; found: 249.1252.

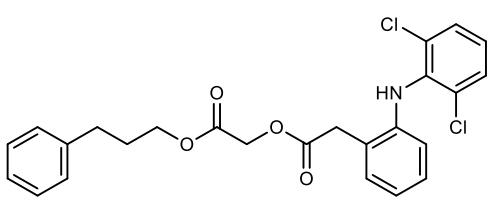

2-Oxo-2-(3-phenylpropoxy)ethyl 2-(2-((2,6-dichlorophenyl)amino)phenyl)acetate (3ah)

Colorless liquid, 26.0 mg (0.055 mmol, 55% yield); ^{1}H NMR (500 MHz, $CDCl_3$) δ 7.35 (d, *J* = 8.1 Hz, 2H), 7.31 – 7.24 (m, 3H), 7.20 (t, *J* = 7.3 Hz, 1H), 7.17 – 7.11

(m, 3H), 7.02 – 6.95 (m, 2H), 6.75 (brs, 1H), 6.56 (d, *J* = 8.0 Hz, 1H), 4.69 (s, 2H), 4.17 (t, *J* = 6.5 Hz, 2H), 3.96 (s, 2H), 2.63 (t, *J* = 7.6 Hz, 2H), 1.97 – 1.87 (m, 2H); ^{13}C NMR (75 MHz, $CDCl_3$) δ 171.6, 167.6, 142.9, 141.0, 138.0, 131.1, 129.7, 129.0, 128.6, 128.5, 128.3, 126.2, 124.2, 124.0, 122.3, 118.6, 65.0, 61.4, 38.2, 32.1, 30.1; HRMS-ESI (m/z) $[M+Na]^+$ calcd for $C_{25}H_{23}Cl_2NNaO_4$, 494.0896; found: 494.0896.

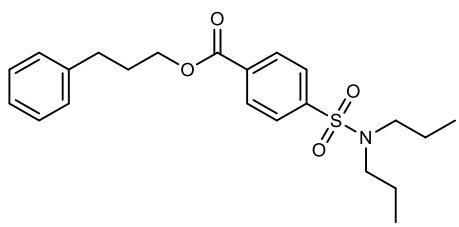

3-Phenylpropyl 4-(*N*,*N*-dipropylsulfamoyl)benzoate (3ai)

White solid, 21.4 mg (0.053 mmol, 53% yield); ^{1}H NMR (300 MHz, $CDCl_3$) δ 8.12 (d, *J* = 8.5 Hz, 2H), 7.87 (d, *J* = 8.5 Hz, 2H), 7.35 – 7.26 (m, 2H), 7.25 – 7.16 (m, 3H), 4.38 (t, *J* = 6.5 Hz, 2H), 3.10 (t, *J* = 7.6 Hz, 4H), 2.80 (t, *J* = 7.5 Hz, 2H), 2.22 – 2.04 (m, 2H), 1.63 – 1.47 (m, 4H), 0.87 (t, *J* = 7.4 Hz, 6H); ^{13}C NMR (75 MHz, $CDCl_3$) δ 186.2, 165.4, 144.3, 141.1, 133.7, 130.3, 128.7, 128.5, 127.1, 126.3, 65.1, 50.1, 32.5, 30.3, 22.1, 11.3; HRMS-ESI (m/z) $[M+Na]^+$ calcd for $C_{22}H_{29}NNaO_4S$, 426.1710; found: 426.1710.

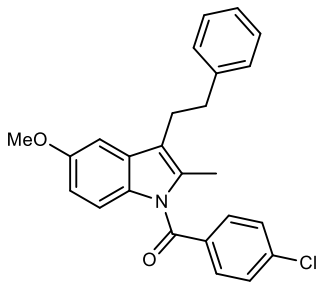

(4-Chlorophenyl)(5-methoxy-2-methyl-3-phenethyl-1*H*-indol-1-yl)methanone (3aj)

Yellow solid, 13.7 mg (0.034 mmol, 34% yield); ^{1}H NMR (400 MHz, $CDCl_3$) δ 7.57 (d, *J* = 8.4 Hz, 2H), 7.44 (d, *J* = 8.4 Hz, 2H), 7.22 (dd, *J* = 15.5, 8.4 Hz, 3H), 7.13 (d, *J* = 6.9 Hz, 1H), 7.04 (d, *J* = 9.0 Hz, 1H), 6.91 (d, *J* = 2.4 Hz, 1H), 6.69 (dd, *J* = 8.9, 2.4 Hz, 1H), 3.84 (s, 3H), 2.99 – 2.87 (m, 4H), 1.97 (s, 3H); ^{13}C NMR (101 MHz, $CDCl_3$) δ 168.4, 156.1, 141.7, 139.1, 134.4, 131.3, 131.2, 131.1, 129.3, 129.1, 128.8, 128.5, 126.2, 118.9, 115.2, 111.2, 101.5, 55.9, 35.9, 26.4, 13.2; HRMS-ESI (m/z) $[M+Na]^+$ calcd for $C_{25}H_{22}ClNNaO_2$, 426.1231; found: 426.1231.

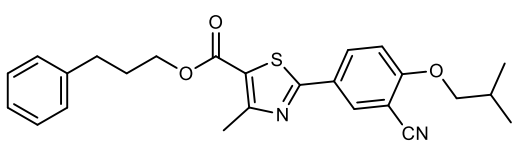

3-Phenylpropyl 2-(3-cyano-4-isobutoxyphenyl)-4-methylthiazole-5-carboxylate (3ak)

White solid, 23.0 mg (0.053 mmol, 53% yield); ^{1}H NMR (400 MHz, $CDCl_3$) δ 8.18 (d, *J* = 2.3 Hz, 1H), 8.10 (dd, *J* = 8.9, 2.4 Hz, 1H), 7.30 (t, *J* = 7.0 Hz, 2H), 7.22 (d, *J* = 7.3 Hz, 3H), 7.01 (d, *J* = 8.8 Hz, 1H), 4.31 (t, *J* = 6.4 Hz, 2H), 3.90 (d, *J* = 6.4

Hz, 2H), 2.85 – 2.70 (m, 5H), 2.25 – 2.16 (m, 1H), 2.14 – 2.01 (m, 2H), 1.09 (d, *J* = 6.7 Hz, 6H); ^{13}C NMR (101 MHz, $CDCl_3$) δ 167.4, 162.7, 162.2, 161.3, 141.1, 132.7, 132.3, 128.7, 128.6, 126.3, 126.1, 121.9, 115.5, 112.8, 103.1, 75.8, 64.8, 32.4, 30.3, 28.3, 19.2, 17.6; HRMS-ESI (m/z) $[M+Na]^+$ calcd for $C_{25}H_{26}N_2NaO_3S$, 457.1556; found: 457.1556.

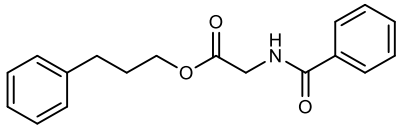

3-Phenylpropyl benzoylglycinate (3al)

White solid, 12.5 mg (0.042 mmol, 42% yield); ^{1}H NMR (300 MHz, $CDCl_3$) δ 7.82 (d, *J* = 7.8 Hz, 2H), 7.53 (t, *J* = 6.7 Hz, 1H), 7.45 (t, *J* = 7.6 Hz, 2H), 7.34 – 7.26 (m, 2H), 7.20 (t, *J* = 7.5 Hz, 3H), 6.61 (brs, 1H), 4.31 – 4.16 (m, 4H), 2.71 (t, *J* = 7.6 Hz, 2H), 2.10 – 1.94 (m, 2H); ^{13}C NMR (75 MHz, $CDCl_3$) δ 170.3, 167.5, 141.0, 133.9, 132.0, 128.8, 128.6, 128.5, 127.2, 126.3, 65.1, 42.0, 32.2, 30.2; HRMS-ESI (m/z) $[M+Na]^+$ calcd for $C_{18}H_{19}NNaO_3$, 320.1257; found: 320.1257.

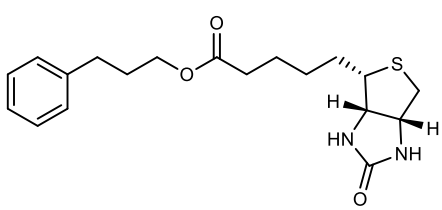

3-Phenylpropyl 5-((3aS,4S,6aR)-2-oxohexahydro-1*H*-thieno[3,4-d]imidazol-4-yl)pentanoate (3am)

White solid, 13.8 mg (0.038 mmol, 38% yield); ^{1}H NMR (400 MHz, $CDCl_3$) δ 7.32 – 7.26 (m, 2H), 7.19 (t, *J* = 7.3 Hz, 3H), 5.76 (s, 2H), 4.53 – 4.47 (m, 1H), 4.34 – 4.27 (m, 1H), 4.09 (t, *J* = 6.5 Hz, 2H), 3.19 – 3.12 (m, 1H), 2.91 (dd, *J* = 12.7, 4.4 Hz, 1H), 2.74 (d, *J* = 12.8 Hz, 1H), 2.71 – 2.64 (m, 2H), 2.33 (t, *J* = 7.4 Hz, 2H), 1.95 (p, *J* = 14.0, 6.7 Hz, 2H), 1.68 (tt, *J* = 14.0, 7.6 Hz, 4H), 1.52 – 1.40 (m, 2H); ^{13}C NMR (101 MHz, $CDCl_3$) δ 173.9, 163.5, 141.3, 128.6, 128.5, 126.1, 63.9, 62.2, 60.5, 55.5, 40.6, 34.0, 32.3, 30.3, 28.5, 28.4, 24.9; HRMS-ESI (m/z) $[M+Na]^+$ calcd for $C_{19}H_{26}N_2NaO_3S$, 385.1556; found: 385.1557.

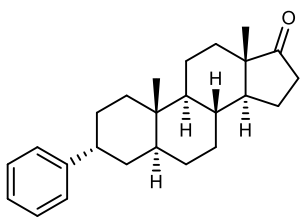

(3R,5R,8R,9S,10S,13S,14S)-10,13-Dimethyl-3-phenylhexadecahydro-17*H*-cyclopenta[a]phenanthren-17-one (3an)

White solid, 19.3 mg (0.055 mmol, 55% yield); ^{1}H NMR (300 MHz, $CDCl_3$) δ 7.34 – 7.26 (m, 2H), 7.25 – 7.13 (m, 3H), 2.62 – 2.50 (m, 1H), 2.45 (dd, *J* = 19.0, 8.9 Hz, 1H), 2.09 (dd, *J* = 18.5, 9.4 Hz, 1H), 2.02 – 1.89 (m, 1H), 1.87 – 1.63 (m, 6H), 1.62 – 1.47 (m, 4H), 1.39 – 1.24 (m, 6H), 1.11 (td, *J* = 12.7, 4.2 Hz, 1H), 1.06 – 0.94 (m, 1H), 0.89 (d, *J* = 8.1 Hz, 6H), 0.84 – 0.73 (m, 1H); ^{13}C NMR (75 MHz, $CDCl_3$) δ 221.6, 147.7, 128.4, 126.9, 126.0, 54.9, 51.7, 48.0, 47.2, 44.9, 39.0, 36.7, 36.1, 36.0, 35.3, 31.8, 31.1, 29.9, 28.7, 21.9, 20.5, 14.0, 12.6; HRMS-ESI (m/z) $[M+Na]^+$ calcd for $C_{25}H_{34}NaO$, 373.2502; found: 373.2502.

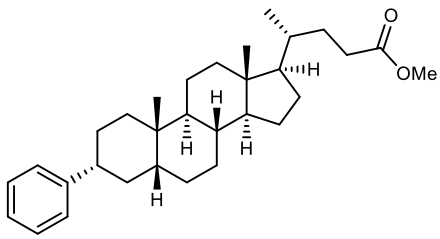

Methyl (R)-4-((3R,5R,8R,9S,10S,13R,14S,17R)-10,13-dimethyl-3-phenylhexadecahydro-1*H*-cyclopenta[a]phenanthren-17-yl)pentanoate (3ao)

White solid, 35.2 mg (0.078 mmol, 78% yield); ^{1}H NMR (300 MHz, $CDCl_3$) δ 7.35 – 7.27 (m, 2H), 7.26 – 7.14 (m, 3H), 3.67 (s, 3H), 2.65 – 2.49 (m, 1H), 2.36 (ddd, *J* = 15.2, 10.2, 5.0 Hz, 1H), 2.30 – 2.15 (m, 1H), 2.02 – 1.73 (m, 6H), 1.63 – 1.02 (m, 22H), 0.99 (s, 3H), 0.93 (d, *J* = 6.3 Hz, 3H), 0.66 (s, 3H); ^{13}C NMR (75 MHz, $CDCl_3$) δ 175.0, 148.0, 128.4, 127.0, 125.9, 56.7, 56.1, 51.6, 45.2, 44.1, 42.9, 40.9, 40.4, 37.8, 36.1, 35.5, 35.4, 35.0, 31.2, 31.2, 28.6, 28.4, 27.6, 26.7, 24.4, 24.2, 21.0, 18.4, 12.2; HRMS-ESI (m/z) $[M+Na]^+$ calcd for $C_{31}H_{46}NaO_2$, 473.3390; found: 473.3390.

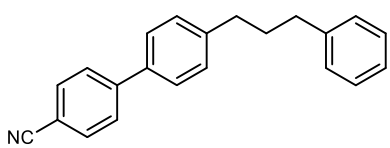

4'-(3-phenylpropyl)-[1,1'-biphenyl]-4-carbonitrile (3m')

White solid, 16.4 mg (0.055 mmol, 55% yield). ^{1}H NMR (300 MHz, $CDCl_3$) δ 7.76 – 7.64 (m, 4H), 7.52 (d, *J* = 8.1 Hz, 2H), 7.33 – 7.27 (m, 4H), 7.24 – 7.16 (m, 3H), 2.70 (q, *J* = 7.7 Hz, 4H), 2.00 (p, *J* = 7.7, 7.3 Hz, 2H); ^{13}C NMR (101 MHz, $CDCl_3$) δ 145.7, 143.3, 142.2, 136.8, 132.7, 129.4, 128.6, 128.5, 127.6, 127.3,

126.0, 119.2, 110.7, 35.6, 35.2, 33.0; HRMS-ESI (m/z) $[M+Na]^+$ calcd for $C_{22}H_{19}NNa$, 320.1410; found: 320.1411.

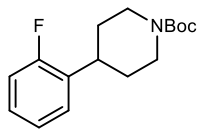

***tert*-Butyl 4-(2-fluorophenyl)piperidine-1-carboxylate (4c)**

The isomeric mixture of compound was obtained as a colorless liquid (20.4 mg, 0.073 mmol, 73% yield). Its identity was confirmed by comparison with NMR and GC spectra of authentic samples. ^{1}H NMR (300 MHz, $CDCl_3$) δ 7.26 – 7.16 (m, 2H), 7.11 (t, *J* = 6.9 Hz, 1H), 7.07 – 6.98 (m, 1H), 4.27 (d, *J* = 12.4 Hz, 2H), 3.02 (tt, *J* = 12.1, 3.4 Hz, 1H), 2.84 (t, *J* = 12.0 Hz, 2H), 1.82 (d, *J* = 12.7 Hz, 2H), 1.75 – 1.57 (m, 2H), 1.50 (s, 9H); ^{13}C NMR (75 MHz, $CDCl_3$) δ 160.7 (d, *J* = 244.7 Hz), 155.0, 132.4 (d, *J* = 14.3 Hz), 127.8 (d, *J* = 8.5 Hz), 127.6 (d, *J* = 5.0 Hz), 124.3 (d, *J* = 3.5 Hz), 115.5 (d, *J* = 22.7 Hz), 79.6, 44.5, 35.6 (d, *J* = 2.3 Hz), 31.9, 28.6; ^{19}F NMR (376 MHz, $CDCl_3$) δ -119.4; HRMS-ESI (m/z) $[M+Na]^+$ calcd for $C_{16}H_{22}FNNaO_2$, 302.1527; found: 302.1525. The meta-isomer; ^{1}H NMR (300 MHz, $CDCl_3$) δ 7.32 – 7.21 (m, 1H), 6.99 (d, *J* = 7.8 Hz, 1H), 6.95 – 6.86 (m, 2H), 4.26 (d, *J* = 13.2 Hz, 2H), 2.80 (td, *J* = 13.2, 2.2 Hz, 2H), 2.66 (tt, *J* = 12.1, 3.4 Hz, 1H), 1.83 (d, *J* = 12.9 Hz, 2H), 1.70 – 1.54 (m, 2H), 1.52 (2, 9H); ^{13}C NMR (75 MHz, $CDCl_3$) δ 163.1 (d, *J* = 245.4 Hz), 154.9, 148.5 (d, *J* = 6.8 Hz), 130.0 (d, *J* = 8.3 Hz), 122.5 (d, *J* = 2.7 Hz), 113.7 (d, *J* = 21.2 Hz), 113.2 (d, *J* = 21.1 Hz), 79.6, 44.3, 42.5 (d, *J* = 1.8 Hz), 33.1, 28.6; ^{19}F NMR (376 MHz, $CDCl_3$) δ -113.3; HRMS-ESI (m/z) $[M+Na]^+$ calcd for $C_{16}H_{22}FNNaO_2$, 302.1527; found: 302.1528.

The para-isomer; ^{1}H NMR (300 MHz, $CDCl_3$) δ 7.21 – 7.07 (m, 2H), 6.97 (t, *J* = 8.7 Hz, 2H), 4.23 (d, *J* = 13.2 Hz, 2H), 2.78 (td, *J* = 13.1, 2.4 Hz, 2H), 2.61 (tt, *J* = 12.1, 3.5 Hz, 1H), 1.79 (d, *J* = 12.8 Hz, 2H), 1.65 – 1.52 (m, 2H), 1.47 (s, 9H). The compound (**4c-p**) was identified by spectral comparison with literature data. [32]

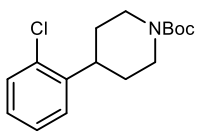

***tert*-Butyl 4-(2-chlorophenyl)piperidine-1-carboxylate (4d)**

The isomeric mixture of compound was obtained as a colorless liquid (26.0 mg, 0.088 mmol, 88% yield). Its identity was confirmed by comparison with NMR and GC spectra of authentic samples. ^{1}H NMR (400 MHz, $CDCl_3$) δ 7.35 (d, *J* = 8.6 Hz, 1H), 7.24 – 7.20 (m, 2H), 7.16 – 7.10 (m, 1H), 4.26 (dt, *J* = 13.3, 2.4 Hz, 2H), 3.16 (tt, *J* = 12.1, 3.4 Hz, 1H), 2.84 (td, *J* = 13.2, 2.6 Hz, 2H), 1.83 (d, *J* = 13.4 Hz, 2H), 1.56 (qd, *J* = 12.8, 4.2 Hz, 2H), 1.48 (s, 10H); ^{13}C NMR (101 MHz, $CDCl_3$) δ 155.0, 142.7, 133.6, 129.7, 128.6, 127.5, 127.2, 79.6, 44.5, 38.9, 31.9, 28.6; HRMS-ESI (m/z) $[M+Na]^+$ calcd for $C_{16}H_{22}ClNNaO_2$, 318.1231; found: 318.1232. The meta-isomer; ^{1}H NMR (400 MHz, $CDCl_3$) δ 7.29 – 7.16 (m, 3H), 7.09 (d, *J* = 7.5 Hz, 1H), 4.25 (d, *J* = 13.2 Hz, 2H), 2.79 (td, *J* = 12.9, 2.6 Hz, 2H), 2.63 (tt, *J* = 12.2, 3.6 Hz, 1H), 1.82 (d, *J* = 13.9 Hz, 2H), 1.60 (qd, *J* = 12.6, 4.2 Hz, 2H), 1.49 (s, 9H); ^{13}C NMR (101 MHz, $CDCl_3$) δ 154.9, 147.9, 134.4, 129.9, 127.2, 126.6, 125.1, 44.4, 42.6, 33.1, 28.6; HRMS-ESI (m/z) $[M+Na]^+$ calcd for $C_{16}H_{22}ClNNaO_2$, 318.1231; found: 318.1233. The para-isomer; ^{1}H NMR (400 MHz, $CDCl_3$) δ 7.26 (d, *J* = 8.5 Hz, 2H), 7.12 (d, *J* = 8.4 Hz, 2H), 4.23 (d, *J* = 13.4 Hz, 2H), 2.78 (td, *J* = 13.0, 2.6 Hz, 2H), 2.61 (tt, *J* = 12.2, 3.6 Hz, 1H), 1.79 (d, *J* = 14.3 Hz, 2H), 1.64

– 1.51 (m, 2H), 1.47 (s, 9H). The compound (**4d-p**) was identified by spectral comparison with literature data. [33]

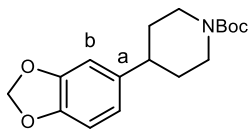

***tert*-Butyl 4-(benzo[d][1,3]dioxol-4-yl)piperidine-1-carboxylate (4g)**

The isomeric mixture of compound was obtained as a pale yellow oil (12.8 mg, 0.042 mmol, 42% yield). Its identity was confirmed by comparison with NMR and GC spectra of authentic samples. ^{1}H NMR (400 MHz, $CDCl_3$) δ 6.79 (t, *J* = 7.8 Hz, 1H), 6.71 (dd, *J* = 7.8, 1.3 Hz, 1H), 6.67 (dd, *J* = 7.7, 1.3 Hz, 1H), 5.93 (s, 2H), 4.23 (d, *J* = 13.2 Hz, 2H), 2.79 (tt, *J* = 12.1, 3.6 Hz, 3H), 1.81 (d, *J* = 12.8 Hz, 2H), 1.70 (qd, *J* = 12.6, 4.4 Hz, 2H), 1.48 (s, 9H); ^{13}C NMR (101 MHz, $CDCl_3$) δ 155.0, 147.3, 144.9, 127.4, 121.8, 119.9, 106.9, 100.6, 79.6, 44.3, 37.4, 31.4, 28.6; HRMS-ESI (m/z) $[M+Na]^+$ calcd for $C_{17}H_{23}NNaO_4$, 328.1519; found: 328.1521. The b-isomer; ^{1}H NMR (400 MHz, $CDCl_3$) δ 6.74 (d, *J* = 8.0 Hz, 1H), 6.69 (d, *J* = 1.7 Hz, 1H), 6.64 (dd, *J* = 8.0, 1.8 Hz, 1H), 5.92 (s, 2H), 4.22 (d, *J* = 13.1 Hz, 2H), 2.76 (td, *J* = 12.9, 2.6 Hz, 2H), 2.56 (tt, *J* = 12.2, 3.6 Hz, 1H), 1.77 (d, *J* = 13.8 Hz, 2H), 1.55 (qd, *J* = 12.5, 4.3 Hz, 2H), 1.47 (s, 9H); ^{13}C NMR (101 MHz, $CDCl_3$) δ 155.0, 147.8, 146.0, 140.0, 119.7, 108.3, 107.4, 101.0, 79.6, 44.5, 42.6, 33.6, 28.6; HRMS-ESI (m/z) $[M+Na]^+$ calcd for $C_{17}H_{23}NNaO_4$, 328.1519; found: 328.1520.

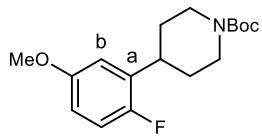

***tert*-Butyl 4-(2-fluoro-5-methoxyphenyl)piperidine-1-carboxylate (4h)**

The isomeric mixture of compound was obtained as a white solid (25.0 mg, 0.081 mmol, 81% yield). Its identity was confirmed by comparison with NMR and GC spectra of authentic samples. ^{1}H NMR (400 MHz, $CDCl_3$) δ 6.93 (t, *J* = 9.3 Hz, 1H), 6.72 – 6.64 (m, 2H), 4.24 (d, *J* = 13.1 Hz, 2H), 3.76 (s, 3H), 2.96 (tt, *J* = 12.2, 3.5 Hz, 1H), 2.81 (td, *J* = 13.0, 2.6 Hz, 2H), 1.79 (d, *J* = 13.5 Hz, 2H), 1.61 (qd, *J* = 12.6, 4.3 Hz, 2H), 1.48 (s, 9H); ^{13}C NMR (101 MHz, $CDCl_3$) δ 155.9 (d, *J* = 1.9 Hz), 155.7 (d, *J* = 237.5 Hz), 155.0, 133.3 (d, *J* = 16.2 Hz), 115.8 (d, *J* = 24.8 Hz), 113.3 (d, *J* = 4.7 Hz), 111.9 (d, *J* = 8.4 Hz), 79.6, 55.8, 44.5, 35.8, 31.9, 28.6; ^{19}F NMR (376 MHz, $CDCl_3$) δ -130.0; HRMS-ESI (m/z) $[M+Na]^+$ calcd for $C_{17}H_{24}FNNaO_3$, 332.1632; found: 332.1635. The b-isomer; ^{1}H NMR (400 MHz, $CDCl_3$) δ 6.88 – 6.81 (m, 2H), 6.77 (dd, *J* = 9.7, 4.7 Hz, 1H), 4.23 (d, *J* = 13.1 Hz, 2H), 3.80 (s, 3H), 3.06 (tt, *J* = 12.1, 2.8 Hz, 1H), 2.81 (td, *J* = 13.0, 2.6 Hz, 2H), 1.77 (d, *J* = 13.3 Hz, 2H), 1.58 – 1.46 (m, 11H); ^{13}C NMR (101 MHz, $CDCl_3$) δ 157.4 (d, *J* = 237.8 Hz), 155.0, 152.98 (d, *J* = 2.0 Hz), 135.87 (d, *J* = 6.6 Hz), 113.75 (d, *J* = 23.5 Hz), 112.75 (d, *J* = 22.8 Hz), 111.27 (d, *J* = 8.3 Hz), 79.5, 56.0, 44.6, 35.5, 31.8, 28.6; ^{19}F NMR (376 MHz, $CDCl_3$) δ -123.6; HRMS-ESI (m/z) $[M+Na]^+$ calcd for $C_{17}H_{24}FNNaO_3$, 332.1632; found: 332.1634.

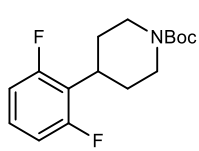

***tert*-Butyl 4-(2,6-difluorophenyl)piperidine-1-carboxylate (4i-a)**

White solid. ^{1}H NMR (400 MHz, $CDCl_3$) δ 7.11 – 7.01 (m, 1H), 6.76 (t, *J* = 8.4 Hz, 2H), 4.17 (d, *J* = 13.6 Hz, 2H), 3.06 (tt, *J* = 12.5, 3.7 Hz, 1H), 2.71 (t, *J* = 12.7 Hz, 2H), 1.95 (qd, *J* = 12.2, 3.4 Hz, 2H), 1.61 (d, *J* = 13.4 Hz, 2H), 1.42 (s, 9H); ^{13}C NMR (101 MHz, $CDCl_3$) δ 161.6 (dd, *J* = 247.1, 9.1 Hz), 155.0, 127.9 (t, *J* = 10.7 Hz), 120.5 (t, *J* = 17.7 Hz), 111.8 (d, *J* = 26.8 Hz), 79.6, 44.7, 33.3, 30.1, 28.6; ^{19}F NMR (376 MHz, $CDCl_3$) δ -113.7; HRMS-ESI (m/z) $[M+Na]^+$ calcd for $C_{16}H_{21}F_2NNaO_2$, 320.1433; found: 320.1432.

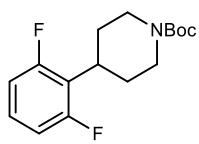

***tert*-butyl 4-(3,5-difluorophenyl)piperidine-1-carboxylate (4i-b)**

Colorless oil. ^{1}H NMR (400 MHz, $CDCl_3$) δ 6.68 – 6.61 (m, 2H), 6.57 (tt, *J* = 8.9, 2.3 Hz, 1H), 4.17 (d, *J* = 13.2 Hz, 2H), 2.71 (td, *J* = 13.3, 2.6 Hz, 2H), 2.56 (tt, *J* = 12.2, 3.6 Hz, 1H), 1.74 (d, *J* = 13.6 Hz, 2H), 1.49 (qd, *J* = 12.5, 4.3 Hz, 2H), 1.41 (s, 9H); ^{13}C NMR (101 MHz, $CDCl_3$) δ 163.2 (dd, *J* = 247.9, 13.0 Hz), 154.9, 149.9 (t, *J* = 8.5 Hz), 109.7 (dd, *J* = 18.6, 6.5 Hz), 101.8 (t, *J* = 25.4 Hz), 79.8, 42.6, 32.9, 28.6; ^{19}F NMR (376 MHz, $CDCl_3$) δ -110.1; HRMS-ESI (m/z) $[M+Na]^+$ calcd for $C_{16}H_{21}F_2NNaO_2$, 330.1433; found: 330.1436.

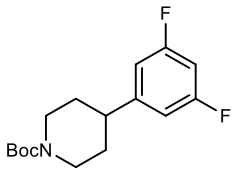

***tert*-butyl 4-(2,4-difluorophenyl)piperidine-1-carboxylate (4i-c)**

Colorless oil. ^{1}H NMR (400 MHz, $CDCl_3$) δ 7.11 – 7.03 (m, 1H), 6.80 – 6.66 (m, 2H), 4.17 (dt, *J* = 13.3, 2.4 Hz, 2H), 2.88 (tt, *J* = 12.2, 3.6 Hz, 1H), 2.74 (td, *J* = 13.2, 2.6 Hz, 2H), 1.71 (d, *J* = 13.5 Hz, 2H), 1.54 (qd, *J* = 12.8, 4.3 Hz, 2H), 1.41 (s, 9H); ^{13}C NMR (101 MHz, $CDCl_3$) δ 162.3 (dd, *J* = 89.6, 11.9 Hz), 159.8 (dd, *J* = 90.4, 11.9 Hz), 155.0, 128.5 – 128.2 (m), 111.3 (dd, *J* = 20.8, 3.7 Hz), 103.9 (dd, *J* = 26.9, 25.1 Hz), 79.7, 44.5, 35.3, 32.0, 28.6; ^{19}F NMR (376 MHz, $CDCl_3$) δ -114.4 (dd, *J* = 685.2, 6.8 Hz); HRMS-ESI (m/z) $[M+Na]^+$ calcd for $C_{16}H_{21}F_2NNaO_2$, 330.1433; found: 330.1434.

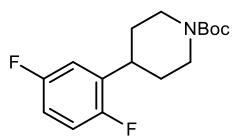

***tert*-butyl 4-(2,5-difluorophenyl)piperidine-1-carboxylate (4j)**

White solid, 22.9 mg (0.077 mmol, 77% yield). ^{1}H NMR (400 MHz, $CDCl_3$) δ 6.99 (td, *J* = 9.2, 4.6 Hz, 1H), 6.95 – 6.82 (m, 2H), 4.27 (d, *J* = 13.4 Hz, 2H), 3.00 (tt, *J* = 12.2, 3.6 Hz, 1H), 2.84 (t, *J* = 11.6 Hz, 2H), 1.82 (d, *J* = 13.3 Hz, 2H), 1.60 (qd, *J* = 12.8, 4.4 Hz, 3H), 1.50 (s, 9H); ^{13}C NMR (101 MHz, $CDCl_3$) δ 159.0 (dd, *J* = 241.7, 2.2 Hz), 156.6 (dd, *J* = 240.6, 2.5 Hz), 154.9, 134.2 (dd, *J* = 17.0, 7.2 Hz), 116.4 (dd, *J* = 25.8, 8.7 Hz), 114.3 (dd, *J* = 23.9, 2.3 Hz), 114.0 (dd, *J* = 24.1, 4.8 Hz), 79.7, 44.3, 35.6, 31.8, 28.6; ^{19}F NMR (376 MHz, $CDCl_3$) δ -118.74 (d, *J* =

17.7 Hz), -125.40 (d, J = 17.2 Hz); HRMS-ESI (m/z) $[M+Na]^+$ calcd for $C_{16}H_{21}F_2NNaO_2$, 320.1433; found: 320.1433.

6.5 DFT computations

6.5.1 General methods

All calculations were carried out using DFT[34] as implemented in the Gaussian 09[35] program packages. Gas phase geometry optimizations were conducted with the B3LYP hybrid functional[31a, 36] including Grimme's D3 dispersion correction[31b] and the 6-31G**/LanL2DZ(Pd, Br, I)[37] basis set. The energies of the optimized structures were reevaluated by additional single point calculations using B3LYP hybrid functional including Grimme's D3 dispersion correction and the 6-311++G**/SDD(Pd, Br, I) basis set. The integral equation formalism variant of the Polarizable Continuum Model (IEFPCM) was employed as implemented to account for the solvation effects for benzene (ε = 2.284) unless noted otherwise. Analytical vibrational frequencies within the harmonic approximation were computed with the 6-31G**/LanL2DZ(Pd, Br, I) basis set to confirm proper convergence to well-defined minima (no imaginary frequency) or saddle points (one and only one imaginary frequency) on the potential energy surface. All thermal corrections from the vibrational frequency calculations were performed at 50 ^{o}C (323.15 K).

The free energy in solution phase G(sol) has been calculated as follows:

$$G(sol) = H(sol) - TS(gas) \quad (1)$$

$$H(sol) = E(SCF,sol) + ZPE \quad (2)$$

$$\Delta G(sol) = \Sigma G(sol) \text{ for products} - \Sigma G(sol) \text{ for reactants} \quad (3)$$

Time-dependent density functional theory (TD-DFT) calculations were carried out as implemented in the Gaussian 09 program package using the hybrid exchange/correlation CAM-B3LYP[38] functional with long-range corrections and the 6-311++G**/SDD(Pd, Br) basis set. The solvation effects for benzene (ε = 2.284) were accounted for using the integral equation formalism variant of the Polarizable Continuum Model (IEFPCM) as implemented.

6.5.2 Computational studies of alkyl–Pd(II) species

While the formation of an alkyl–Pd(II) is expected in the presence of a Pd(I) species and an alkyl radical, photoirradiation conditions serve to cleave the alkyl–Pd(II) bond through triplet excitation, regenerating the initial Pd(I) species and the alkyl radical. We believe that this is a key feature of the photoexcited Pd catalysis which prevents β-hydride elimination through the formation of a Pd(I)/alkyl radical hybrid. Therefore, although the β-hydride elimination may exhibit a lower computed energy barrier, this pathway shall be kinetically inhibited by reversible formation/scission of the Pd–C bond with visible light.

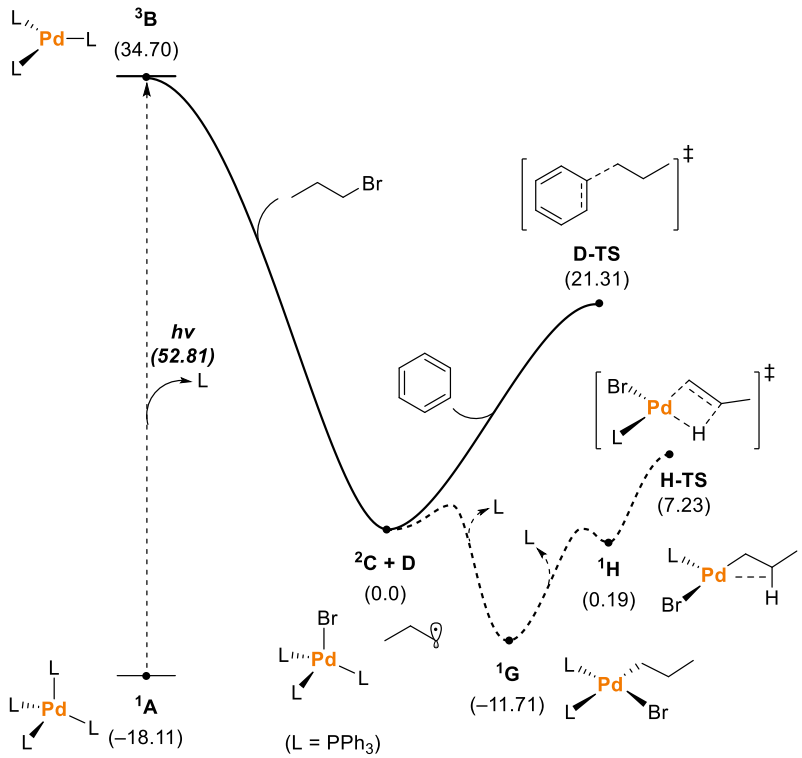

Scheme 6.13 Completing β-hydride elimination of starting alkyl bromide.

This feature can be demonstrated with the first alkyl radical addition step as shown above. Although the binding of propyl radical **D** to the Pd(I) center to form **^{1}G** followed by β-hydride elimination is a facile process (energy barrier of 18.9 kcal/mol), this process is efficiently prohibited through light irradiation, allowing the reaction to proceed towards the desired radical insertion pathway (energy barrier of 21.3 kcal/mol). Similarly, as shown below, although the energy barrier is meaningfully lower for the β-hydride elimination pathway, only <10% elimination product was detected under our optimized conditions performing the desired alkylation reaction majorly. Similarly, we think that the β-hydride elimination of the Pd(II)–alkyl adduct **^{1}I** could also be kinetically disfavored,

guiding the reaction to the bromine atom transfer pathway via **[C + E]-TS**.

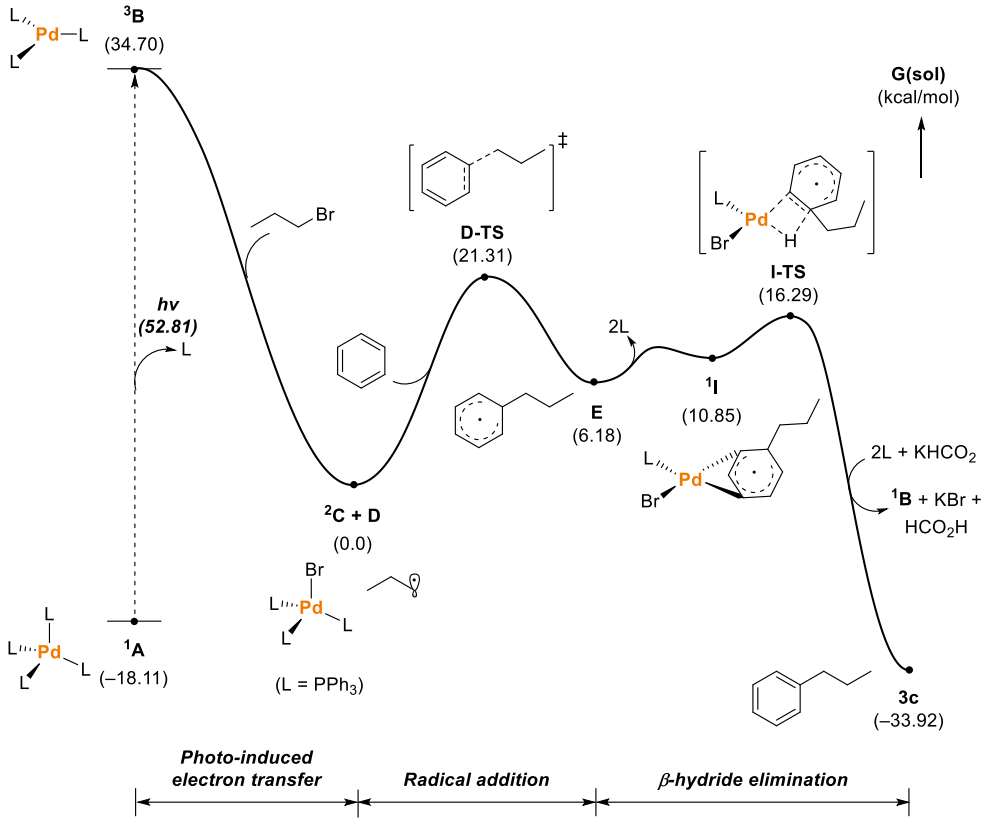

Scheme 6.14 Energy diagram for the β-hydride elimination pathway.

Table 6.11 TD-DFT computations of alkyl–Pd(II) species.[a]

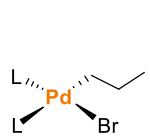

^{1}G

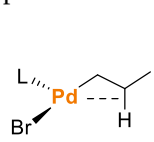

^{1}H

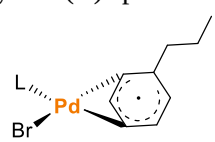

^{1}I

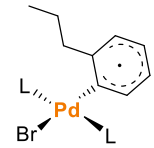

^{1}J

State	Wavelength (nm)	f	Transitions
			^{1}G
1 (3)	366.72	0.0216	HOMO–16 → LUMO (7.9%) HOMO–10 → LUMO (2.3%) HOMO–4 → LUMO (9.7%) HOMO–3 → LUMO (3.3%) HOMO–1 → LUMO (32.8%) HOMO → LUMO (20.7%)
			^{1}H
1 (4)	400.49	0.0352	HOMO–8 → LUMO (8.7%) HOMO–3 → LUMO (39.6%) HOMO–2 → LUMO (13.7%) HOMO → LUMO (23.6%)
2 (10)	362.15	0.0113	HOMO–10 → LUMO (24.6%) HOMO–2 → LUMO (36.7%) HOMO → LUMO (21.6%)
			^{1}I
1 (5)	404.86	0.0471	HOMO–13 → LUMO (2.4%) HOMO–4 → LUMO (3.6%) HOMO–3 → LUMO (39.7%) HOMO–1 → LUMO (22.8%) HOMO → LUMO (19.5%)
2 (6)	375.50	0.0596	HOMO–14 → LUMO (5.5%) HOMO–12 → LUMO (5.4%) HOMO–3 → LUMO (4.9%) HOMO–2 → LUMO (2.1%) HOMO–1 → LUMO (49.6%) HOMO → LUMO (20.8%)
			^{1}J
1 (9)	453.40	0.0059	HOMO–13 → LUMO (2.5%) HOMO–5 → LUMO (3.0%) HOMO–4 → LUMO (3.7%) HOMO–2 → LUMO (78.9%)
2 (15)	408.47	0.0164	HOMO–4 → LUMO (2.4%) HOMO–1 → LUMO+1 (6.5%) HOMO → LUMO+1 (23.9%) HOMO → LUMO+2 (50.3%) HOMO → LUMO+3 (3.0%)
3 (17)	401.69	0.0109	HOMO–13 → LUMO (4.1%) HOMO–11 → LUMO (5.2%) HOMO–5 → LUMO (4.0%) HOMO–4 → LUMO (6.9%) HOMO–3 → LUMO (66.3%)
4 (19)	383.80	0.0710	HOMO–7 → LUMO (4.0%) HOMO–6 → LUMO (4.8%) HOMO–5 → LUMO (5.5%) HOMO–4 → LUMO (38.3%) HOMO–3 → LUMO (6.7%) HOMO–2 → LUMO (3.5%) HOMO–1 → LUMO+1 (2.5%) HOMO → LUMO+3 (7.5%)

[a]Only relevant transitions into the Pd–C antibonding orbitals (LUMO) with oscillator strength f > 0.0025 are shown.

In addition, attempts to optimize a triplet Pd(II)–alkyl species led to the scission of the Pd–C bond (>3.3 Å Pd–C bond lengths) as shown below, also indirectly indicating that the absorbed energy serves to weaken the Pd–C bond through vibrational relaxation.

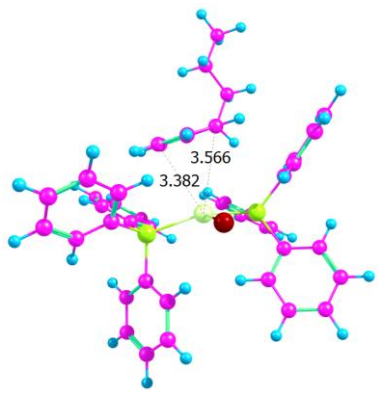

Scheme 6.15 Optimized geometry of ^{3}**I**.

6.5.3 Computations involving polyfluoroarenes

The reduction potentials of the Wheland intermediates derived from various polyfluoroarenes were assessed by DFT calculations. The standard reduction potentials, E_{red}^{o} were obtained from the electron attachment energy in the solution phase, ΔG^{EA}(sol), and subsequent application of the following relationships, where n is the number of electrons and F is the Faraday constant. ΔG^{EA}(sol) was computed by extracting the Gibbs free energies of the cationic species (denoted **cat**) from those of the radical/anionic species (denoted **rad/anion**).

$$\Delta G^{EA}(sol) = -nFE^{o}$$

$$E_{red}^{o} = -E^{o} - E^{o}(N.H.E.) = -E^{o} - 4.43\ V$$

Here, we employed the absolute potential that has been measured to be 4.43 V

for the normal hydrogen electrode.[39] For the computation of ΔG^{EA}(sol), all methods were identical to the general procedure with the exception of the solvation energy being computed at ε = 37.5 for acetonitrile.

6.5.4 Computation of the hydrogen atom transfer barrier for pentafluorobenzene

The hydrogen atom transfer (HAT) barrier of pentafluorobenzene by a propyl radical was computed to clarify whether this type of side reaction pathway may hinder the formation of **4m**. However, due to the high barrier of 26.2 kcal/mol associated with the HAT pathway, this type of side reaction pathway was excluded.

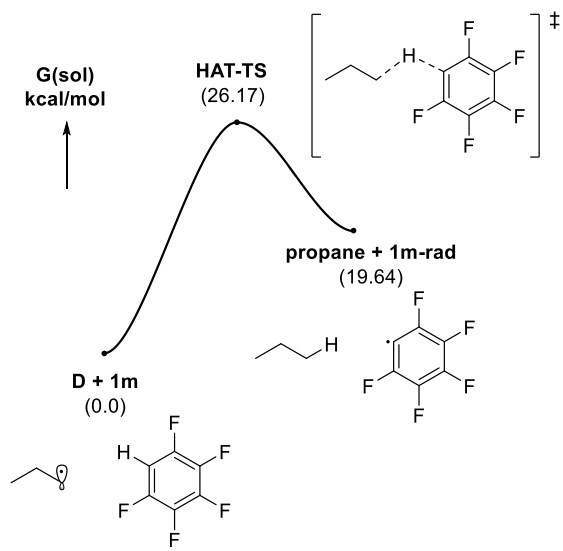

Scheme 6.16 Hydrogen atom transfer barrier in pentafluorobenzene.

6.5.5 Direct single-electron transfer

The standard reduction potentials of the Pd(I) and Pd(II) species were computed using the method described above. The electron attachment energies of the following equations were evaluated and converted to reduction potentials for the Pd(I)–Br and Pd(II)–Br_2 species. This value was compared with the reduction potentials of the Wheland intermediates to verify the feasibility of direct SET processes.

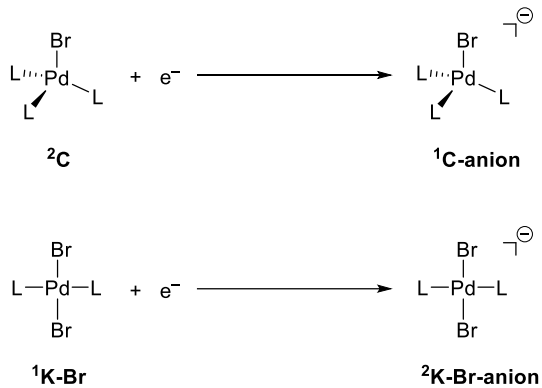

Scheme 6.17 The standard reduction potentials of Pd(I) and Pd(II) species.

Using the aforementioned method, the computed standard reduction potentials of the above species are shown below, whereby a significant mismatch of the redox potentials can be seen. This indicates that the direct oxidation of the radical adduct to the cation is not feasible with either a Pd(I) or a Pd(II) species.

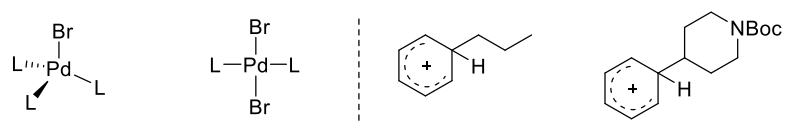

¹C	¹K-Br	E-cat	3x-cat
E^o_{red} = –0.77V	E^o_{red} = –0.46V	E^o_{red} = 0.21V	E^o_{red} = 0.34V

Scheme 6.18 DFT-computed redox potentials of the Pd species and radical σ-complexes.

6.5.6 Deprotonation of the radical σ-complexes

The Zhou group reported a *para*-selective alkylation via Pd photocatalysis and proposed a mechanism involving a deprotonation of the radical σ-complex (**L**).[9] The deprotonation of the electron-deficient radical (**L**) by a strong phosphate base, as used by the Zhou group, was calculated to be extremely exergonic, with anisole as the solvent (ε = 4.2247) under the identical solvation model. In clear contrast, due to the weak basicity of the formate anion and the electron-rich nature of benzene, deprotonation of the radical σ-complex (**E**) was highly disfavored with a large mismatch of pK_a values, indicating that the operating mechanism of the developed reaction should be different to that reported in Zhou's case.

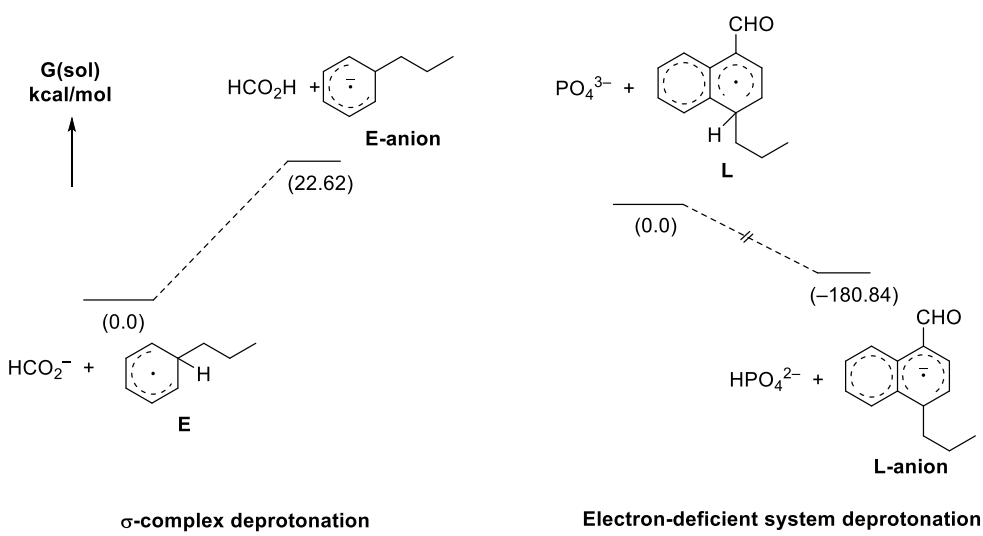

Scheme 6.19 Deprotonation of the radical σ-complexes.

6.5.7 Kinetic isotope effect computations

Kinetic isotope effects were computed using the (Iso=2) keyword after the hydrogen atom of interest and performing additional frequency calculations while maintaining the identical electronic energy. The barriers of the protiated and deuterated pathways were compared and the KIEs were computed from the Boltzmann distribution factor at 323.15 K. The obtained energy barriers are shown below (Table 6.12). The transition states are denoted as **I-TS-d_3-H**, **I-TS-d_3-D**, **[C+E]-TS-d_3-H**, **[C+E]-TS-d_3-D** and their exact energy components are given in section 12.11. The **H** and **D** indicates the hydrogen and the deuterium on the 1-position (*ipso* to the propyl substituent)

Table 6.12 Kinetic isotope effect computations.

	$\Delta\Delta G^{\ddagger}$	**KIE (calc)**
β-H elimination	0.66	2.80
Br atom transfer	–0.013	0.98

6.5.8 Single-electron reduction of alkyl halides by photoexcited Pd(0)

The reduction of chloropropane is associated with an energy barrier of 6.7 kcal/mol, while those of bromopropane and iodopropane were found to be barrierless. Although the reduction barrier with alkyl chlorides is not significantly high and is nearly diffusion-controlled, this reduction process is an intermolecular reaction in competition with the facile relaxation of the excited Pd(0) species ^{3}**B**, accounting for the dramatically reduced quenching rate observed.

6.5.9 Second single-electron reduction of alkyl halides by Pd(I) complexes

The second reduction barrier by ^{2}**M** was assessed by DFT. It is noted here that the reaction should proceed via a photoexcited Pd(I) species generated from ^{2}**M**, which cannot be modeled using a classical DFT method. However, the transition state, ^{2}**M-TS**, could be modeled, and the reduction barrier of the iodopropane was therefore calculated to be 6.2 kcal/mol lower than that of bromopropane, suggesting that alkyl iodides are more prone to form Pd(II) ^{1}**K-I**, an off-cycle Pd species.

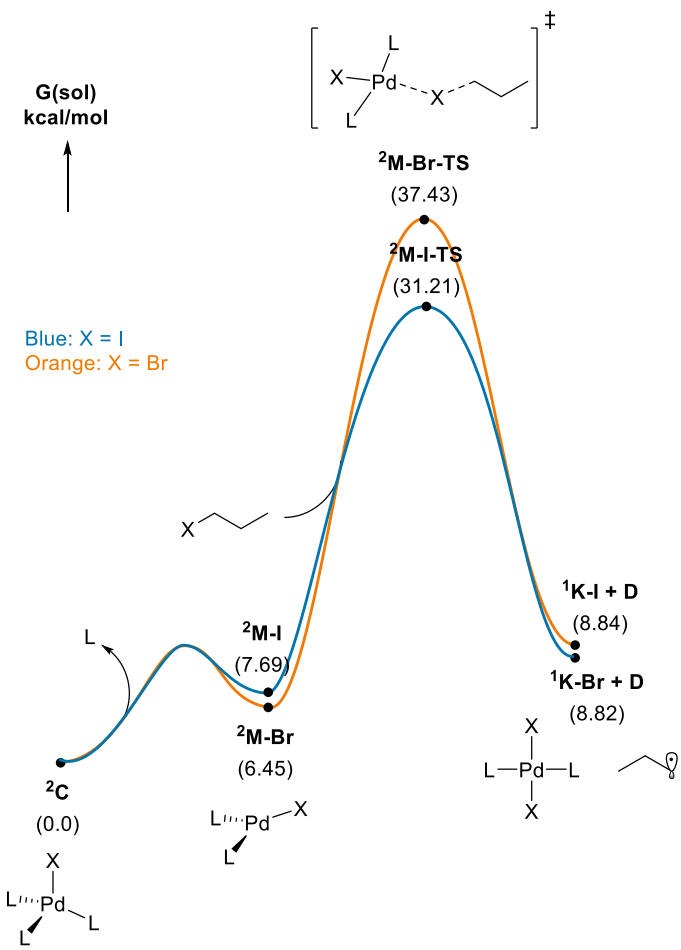

Scheme 6.20 Second single-electron reduction of alkyl halides by Pd(I) complexes.

6.5.10 DFT-optimized structures' energy components

Table 6.13 DFT-optimized structures' energy components.

	E(SCF)/(Hartree)	**ZPE/(kcal/mol)**	**S(gas)/(cal/mol·K)**	**G(sol)/(kcal/mol)**
	6-311++G**/SDD	6-31G**/LanL2DZ	6-31G**/LanL2DZ	
PPh_3	-1036.532687	171.9437	133.268	-650304.7117
^{1}A	-4274.254017	692.91878	376.136	-2681561.493
^{1}B	-3237.671997	518.90685	311.198	-2031249.974
^{3}B	-3237.594485	518.03216	304.807	-2031200.144
2c	-131.9637197	59.51467	76.166	-82773.52018
^{2}C	-3251.097663	520.6847	314.527	-2039673.998
D	-118.5127618	55.65388	69.461	-74334.6171
benzene	-232.3175689	63.14956	66.841	-145739.8154
D-TS	-350.818809	120.35117	97.507	-220053.1182
E	-350.8473951	122.12532	94.328	-220068.2548
[C + E]-TS	-3601.945771	644.41216	358.784	-2259724.917
F	-364.2610516	124.4754	104.969	-228486.5336
$KHCO_2$	-789.2551169	14.02191	70.698	-495273.5133
HCO_2H	-189.8321928	21.31861	59.319	-119119.2598
KBr	-613.4348604	0.28146	60.099	-384955.0354
3c	-350.302646	116.57183	92.133	-219731.264
2a-rad	-235.2904975	97.90471	77.116	-147573.9201
2a-TS	-467.5960563	162.51781	103.202	-293291.5656
3a-rad	-467.6192446	163.83739	103.098	-293304.7633
2ad-rad	-157.8456021	73.4861	77.489	-99001.09042
2ad-TS	-390.1512784	138.45927	101.982	-244717.9348
3ad-rad	-390.1745087	139.88649	100.445	-244730.5881
2aq-rad	-157.8517718	73.35423	77.188	-99004.99654
2aq-TS	-390.1579275	138.05939	99.966	-244721.8556

3aq-rad	-390.1756923	139.67444	97.804	-244730.6894
1m	-728.6279089	37.37254	91.886	-457212.8909
D-TS'	-847.1345042	94.64834	121.611	-531529.1759
E'	-847.1659945	96.82905	119.508	-531546.076
^{1}G	-2333.09778	406.67063	255.091	-1463715.617
^{1}H	-1296.512567	232.13736	178.97	-813399.009
H-TS	-1296.497538	229.29232	177.568	-813391.9625
^{1}I	-1528.838075	297.93317	205.592	-959128.1553
I-TS	-1528.826531	294.38098	200.177	-959122.7137
^{1}J	-2565.400946	471.42653	284.497	-1609432.691
3x-rad	-829.6181049	236.97024	144.191	-520402.4525
4c-*o*-rad	-928.8903817	232.03472	148.299	-582702.9626
4i-rad	-1028.160663	227.00604	152.214	-645002.2515
4k-rad	-1127.426678	221.86673	156.809	-707299.1931
4l-rad	-1226.68197	216.79914	161.576	-769589.3905
4m-rad	-1325.93579	211.65319	166.969	-831878.9445
3x-cat	-829.4454484	238.10955	142.756	-520292.5059
4c-o-cat	-928.7148695	233.21614	146.165	-582590.9561
4i-cat	-1027.982171	228.26492	149.346	-644888.0602
4k-cat	-1127.250462	223.24897	153.965	-707186.3148
4l-cat	-1226.496964	218.07406	158.024	-769470.8749
4m-cat	-1325.742172	212.75086	163.378	-831755.1895
HAT-TS	-847.1161485	92.66103	126.843	-531521.3355
propane	-119.1855585	65.17338	65.342	-74745.95251
1m-rad	-727.9275579	29.44679	93.665	-456781.915
HCO_2^-	-189.3311832	12.64185	58.336	-118813.2309
E-anion	-350.3042256	110.78509	96.982	-219739.6089
L (anisole)	-617.9118329	158.47746	116.467	-387624.3952

L-anion (anisole)	-617.4299412	149.55968	116.079	-387330.7962
PO_4^{3-} **(anisole)**	-642.5238955	8.67881	69.464	-403203.2956
HPO_4^{2-} **(anisole)**	-643.2903783	15.93337	71.681	-403677.7323
I-TS-d_3-H	-1528.826531	288.21915	201.701	-959129.368
I-TS-d_3-D	-1528.826531	288.90675	201.839	-959128.725
[C+E]-TS-d_3-H	-3601.945771	638.22991	360.341	-2259731.603
[C+E]-TS-d_3-D	-3601.945771	638.17174	360.202	-2259731.616
E-d_3-H	-350.8473951	116.10981	96.081	-220074.8368
E-d_3-D	-350.8473951	115.93854	95.755	-220074.9027
chloropropane	-578.8129224	59.95649	73.079	-363173.9771
iodopropane	-130.0014968	59.27615	78.003	-81543.03977
^{3}B-TS	-3816.417625	578.08946	337.754	-2394367.463
^{2}C-Cl	-3697.937878	520.9505	310.882	-2320068.811
^{2}C-I	-3249.137437	520.87668	314.932	-2038443.878
^{2}M-Br	-2214.520055	347.04104	239.437	-1389361.598
^{2}M-I	-2212.561379	347.05584	240.128	-1388132.72
^{2}M-Br-TS	-2346.441418	404.68938	276.52	-1472097.776
^{2}M-I-TS	-2342.529511	404.11579	279.49	-1469644.552
^{1}K-Br	-2227.948708	347.71917	252.3	-1397791.678
^{1}K-I	-2224.02846	347.56268	253.715	-1395332.3
^{2}C (MeCN)	-3251.112723	520.6847	314.527	-2039683.449
^{2}C-anion (MeCN)	-3251.244899	519.00151	313.576	-2039767.766
^{1}K-Br (MeCN)	-2227.962335	347.71917	252.3	-1397800.228
^{2}K-Br-anion (MeCN)	-2228.102461	345.99238	258.216	-1397891.797
E-cat (MeCN)	-350.6801094	123.3022	94.118	-219962.0368
E (MeCN)	-350.8488024	122.12532	94.328	-220069.1379

6.6 References

(1) (a) Kocal, J. A.; Vora, B. V.; Imai, T. *Appl. Catal. A* **2001**, *221*, 295. (b) Almeida, J. L. G. d.; de Almeida, J. L. G.; Dufaux, M.; Ben Taarit, Y.; Naccache, C. *J. Am. Oil Chem. Soc.* **1994**, *71*, 675.

(2) (a) Carey, F. A.; Sundberg, R. J., *Advanced Organic Chemistry: Part B: Reaction and Synthesis*. Springer: 2010; p 1321. (b) Sharman, S. H. *J. Am. Chem. Soc.* **1962**, *84*, 2945. (c) Roberts, R. M.; Shiengthong, D. *J. Am. Chem. Soc.* **1964**, *86*, 2851.

(3) (a) Yang, L.; Huang, H. *Chem. Rev.* **2015**, *115*, 3468. (b) Dong, Z.; Ren, Z.; Thompson, S. J.; Xu, Y.; Dong, G. *Chem. Rev.* **2017**, *117*, 9333.

(4) Saper, N. I.; Ohgi, A.; Small, D. W.; Semba, K.; Nakao, Y.; Hartwig, J. F. *Nat. Chem.* **2020**, *12*, 276.

(5) Boerner, L. K. https://cen.acs.org/synthesis/catalysis/Straightforward-path-linear-alkylbenzenes-identified/98/web/2020/02.

(6) (a) McKeown, B. A.; Prince, B. M.; Ramiro, Z.; Gunnoe, T. B.; Cundari, T. R. *ACS Catal.* **2014**, *4*, 1607. (b) Luedtke, A. T.; Goldberg, K. I. *Angew. Chem. Int. Ed.* **2008**, *47*, 7694. (c) Crisenza, G. E. M.; McCreanor, N. G.; Bower, J. F. *J. Am. Chem. Soc.* **2014**, *136*, 10258.

(7) (a) Zhu, R.-Y.; He, J.; Wang, X.-C.; Yu, J.-Q. *J. Am. Chem. Soc.* **2014**, *136*, 13194. (b) Zhao, Y.; Chen, G. *Org. Lett.* **2011**, *13*, 4850.

(8) (a) Ackermann, L. *Chem. Commun.* **2010**, *46*, 4866. (b) Zhou, W.-J.; Cao, G.-M.; Shen, G.; Zhu, X.-Y.; Gui, Y.-Y.; Ye, J.-H.; Sun, L.; Liao, L.-L.; Li, J.; Yu, D.-G. *Angew. Chem. Int. Ed.* **2017**, *56*, 15683. (c) Wu, X.; See, J. W. T.; Xu, K.; Hirao, H.; Roger, J.; Hierso, J.-C.; Zhou, J. S. *Angew. Chem. Int. Ed.* **2014**, *53*, 13573. (d)

Xiao, B.; Liu, Z.-J.; Liu, L.; Fu, Y. *J. Am. Chem. Soc.* **2013**, *135*, 616.

(9) Jiao, Z.; Lim, L. H.; Hirao, H.; Zhou, J. S. *Angew. Chem. Int. Ed.* **2018**, *57*, 6294.

(10) (a) Venning, A. R. O.; Bohan, P. T.; Alexanian, E. J. *J. Am. Chem. Soc.* **2015**, *137*, 3731. (b) Beaulieu, L.-P. B.; Sustac Roman, D.; Vallée, F.; Charette, A. B. *Chem. Commun.* **2012**, *48*, 8249.

(11) Blanksby, S. J.; Ellison, G. B. *Acc. Chem. Res.* **2003**, *36*, 255.

(12) Carey, F. A.; Sundberg, R. J., *Advanced Organic Chemistry: Part A: Structure and Mechanisms*. Springer: 2008; p 1199.

(13) (a) Gurry, M.; Aldabbagh, F. *Org. Biomol. Chem.* **2016**, *14*, 3849. (b) Sun, C.-L.; Li, H.; Yu, D.-G.; Yu, M.; Zhou, X.; Lu, X.-Y.; Huang, K.; Zheng, S.-F.; Li, B.-J.; Shi, Z.-J. *Nat. Chem.* **2010**, *2*, 1044.

(14) (a) Shelton, J. R.; Uzelmeier, C. W. *J. Am. Chem. Soc.* **1966**, *88*, 5222. (b) Budén, M. E.; Bardagí, J. I.; Puiatti, M.; Rossi, R. A. *J. Org. Chem.* **2017**, *82*, 8325.

(15) (a) Wang, G.-Z.; Shang, R.; Cheng, W.-M.; Fu, Y. *J. Am. Chem. Soc.* **2017**, *139*, 18307. (b) Sun, S.; Zhou, C.; Yu, J.-T.; Cheng, J. *Org. Lett.* **2019**, *21*, 6579. (c) Chuentragool, P.; Kurandina, D.; Gevorgyan, V. *Angew. Chem. Int. Ed.* **2019**, *58*, 11586. (d) Cheng, W.-M.; Shang, R.; Fu, Y. *Nat. Commun.* **2018**, *9*, 5215. (e) Huang, H.-M.; Koy, M.; Serrano, E.; Pflüger, P. M.; Schwarz, J. L.; Glorius, F. *Nat. Catal.* **2020**, *3*, 393. (f) Ye, S.; Xiang, T.; Li, X.; Wu, J. *Org. Chem. Front.* **2019**, *6*, 2183. (g) Kurandina, D.; Rivas, M.; Radzhabov, M.; Gevorgyan, V. *Org. Lett.* **2018**, *20*, 357. (h) Kwiatkowski, M. R.; Alexanian, E. J. *Acc. Chem. Res.* **2019**, *52*, 1134. (i) Torres, G. M.; Liu, Y.; Arndtsen, B. A. *Science* **2020**, *368*, 318.

(16) Parasram, M.; Chuentragool, P.; Sarkar, D.; Gevorgyan, V. *J. Am. Chem. Soc.*

2016, *138*, 6340.

(17) Kurandina, D.; Parasram, M.; Gevorgyan, V. *Angew. Chem. Int. Ed.* **2017**, *56*, 14212.

(18) (a) Wang, G.-Z.; Shang, R.; Fu, Y. *Org. Lett.* **2018**, *20*, 888. (b) Koy, M.; Sandfort, F.; Tlahuext-Aca, A.; Quach, L.; Daniliuc, C. G.; Glorius, F. *Chem. Eur. J.* **2018**, *24*, 4552. (c) Kancherla, R.; Muralirajan, K.; Maity, B.; Zhu, C.; Krach, P. E.; Cavallo, L.; Rueping, M. *Angew. Chem. Int. Ed.* **2019**, *58*, 3412.

(19) Zhou, Z.-Z.; Zhao, J.-H.; Gou, X.-Y.; Chen, X.-M.; Liang, Y.-M. *Org. Chem. Front.* **2019**, *6*, 1649.

(20) (a) Huang, H.-M.; Bellotti, P.; Pflüger, P. M.; Schwarz, J. L.; Heidrich, B.; Glorius, F. *J. Am. Chem. Soc.* **2020**, *142*, 10173. (b) Shing Cheung, K. P.; Kurandina, D.; Yata, T.; Gevorgyan, V. *J. Am. Chem. Soc.* **2020**, *142*, 9932.

(21) Yu, F.; Wang, T.; Zhou, H.; Li, Y.; Zhang, X.; Bao, H. *Org. Lett.* **2017**, *19*, 6538.

(22) Collins, K. D.; Glorius, F. *Nat. Chem.* **2013**, *5*, 597.

(23) (a) Bair, J. S.; Schramm, Y.; Sergeev, A. G.; Clot, E.; Eisenstein, O.; Hartwig, J. F. *J. Am. Chem. Soc.* **2014**, *136*, 13098. (b) Clement, M. L.; Grice, K. A.; Luedtke, A. T.; Kaminsky, W.; Goldberg, K. I. *Chemistry* **2014**, *20*, 17287.

(24) Johansson Seechurn, C. C. C.; Kitching, M. O.; Colacot, T. J.; Snieckus, V. *Angew. Chem. Int. Ed.* **2012**, *51*, 5062.

(25) (a) Testaferri, L.; Tiecco, M.; Spagnolo, P.; Zanirato, P.; Martelli, G. *J. Chem. Soc. Perkin Trans. 2* **1976**, *0*, 662. (b) Pryor, W. A.; Davis, W. H.; Gleaton, J. H. *J. Org. Chem.* **1975**, *40*, 2099. (c) Volovik, S. V.; Dyadyusha, G. G.; Staninets, V. I. *Theor. Exp. Chem.* **1988**, *23*, 380.

(26) Sharma, K. K.; Patel, D. I.; Jain, R. *Chem. Commun.* **2015**, *51*, 15129.

(27) (a) Tu, G.; Yuan, C.; Li, Y.; Zhang, J.; Zhao, Y. *Angew. Chem. Int. Ed.* **2018**, *57*, 15597. (b) Ratushnyy, M.; Kvasovs, N.; Sarkar, S.; Gevorgyan, V. *Angew. Chem. Int. Ed.* **2020**, *59*, 10316.

(28) Namazian, M.; Coote, M. L. *J. Fluorine Chem.* **2009**, *130*, 621.

(29) Yamamoto, K.; Li, J.; Garber, J. A. O.; Rolfes, J. D.; Boursalian, G. B.; Borghs, J. C.; Genicot, C.; Jacq, J.; van Gastel, M.; Neese, F.; Ritter, T. *Nature* **2018**, *554*, 511.

(30) Isse, A. A.; Lin, C. Y.; Coote, M. L.; Gennaro, A. *J. Phys. Chem. B* **2011**, *115*, 678.

(31) (a) Lee, C.; Yang, W.; Parr, R. G. *Phys. Rev. B Condens. Matter* **1988**, *37*, 785. (b) Grimme, S.; Antony, J.; Ehrlich, S.; Krieg, H. *J. Chem. Phys.* **2010**, *132*, 154104.

(32) Barré, B.; Gonnard, L.; Campagne, R.; Reymond, S.; Marin, J.; Ciapetti, P.; Brellier, M.; Guérinot, A.; Cossy, J. *Org. Lett.* **2014**, *16*, 6160.

(33) Wang, J.; Qin, T.; Chen, T.-G.; Wimmer, L.; Edwards, J. T.; Cornella, J.; Vokits, B.; Shaw, S. A.; Baran, P. S. *Angew. Chem. Int. Ed.* **2016**, *55*, 9676.

(34) Calais, J.-L. *Int. J. Quantum Chem.* **1993**, *47*, 101.

(35) Gaussian 09, Revision D.01, M. J. Frisch, G. W. Trucks, H. B. Schlegel, G. E. Scuseria, M. A. Robb, J. R. Cheeseman, G. Scalmani, V. Barone, B. Mennucci, G. A. Petersson, H. Nakatsuji, M. Caricato, X. Li, H. P. Hratchian, A. F. Izmaylov, J. Bloino, G. Zheng, J. L. Sonnenberg, M. Hada, M. Ehara, K. Toyota, R. Fukuda, J. Hasegawa, M. Ishida, T. Nakajima, Y. Honda, O. Kitao, H. Nakai, T. Vreven, J. A. Montgomery, Jr., J. E. Peralta, F. Ogliaro, M. Bearpark, J. J. Heyd, E. Brothers, K.

N. Kudin, V. N. Staroverov, T. Keith, R. Kobayashi, J. Normand, K. Raghavachari, A. Rendell, J. C. Burant, S. S. Iyengar, J. Tomasi, M. Cossi, N. Rega, J. M. Millam, M. Klene, J. E. Knox, J. B. Cross, V. Bakken, C. Adamo, J. Jaramillo, R. Gomperts, R. E. Stratmann, O. Yazyev, A. J. Austin, R. Cammi, C. Pomelli, J. W. Ochterski, R. L. Martin, K. Morokuma, V. G. Zakrzewski, G. A. Voth, P. Salvador, J. J. Dannenberg, S. Dapprich, A. D. Daniels, O. Farkas, J. B. Foresman, J. V. Ortiz, J. Cioslowski, and D. J. Fox, Gaussian, Inc., Wallingford CT, 2013.

(36) (a) Slater, J. C.; Phillips, J. C. *Phys. Today* **1974**, *27*, 49. (b) Vosko, S. H.; Wilk, L.; Nusair, M. *Can. J. Phys.* **1980**, *58*, 1200. (c) Becke, A. D. *Phys. Rev. A Gen. Phys.* **1988**, *38*, 3098. (d) Becke, A. D. *J. Chem. Phys.* **1993**, *98*, 5648.

(37) (a) Wadt, W. R.; Hay, P. J. *J. Chem. Phys.* **1985**, *82*, 284. (b) Hay, P. J.; Wadt, W. R. *J. Chem. Phys.* **1985**, *82*, 299.

(38) Yanai, T.; Tew, D. P.; Handy, N. C. *Chem. Phys. Lett.* **2004**, *393*, 51.

(39) Trasatti, S. *J. Macromol. Sci. Part A Pure Appl. Chem.* **1986**, *58*, 955.

Appendix − NMR Spectra

Chapter 2

^{1}H NMR (**4ca**) ($CDCl_3$)

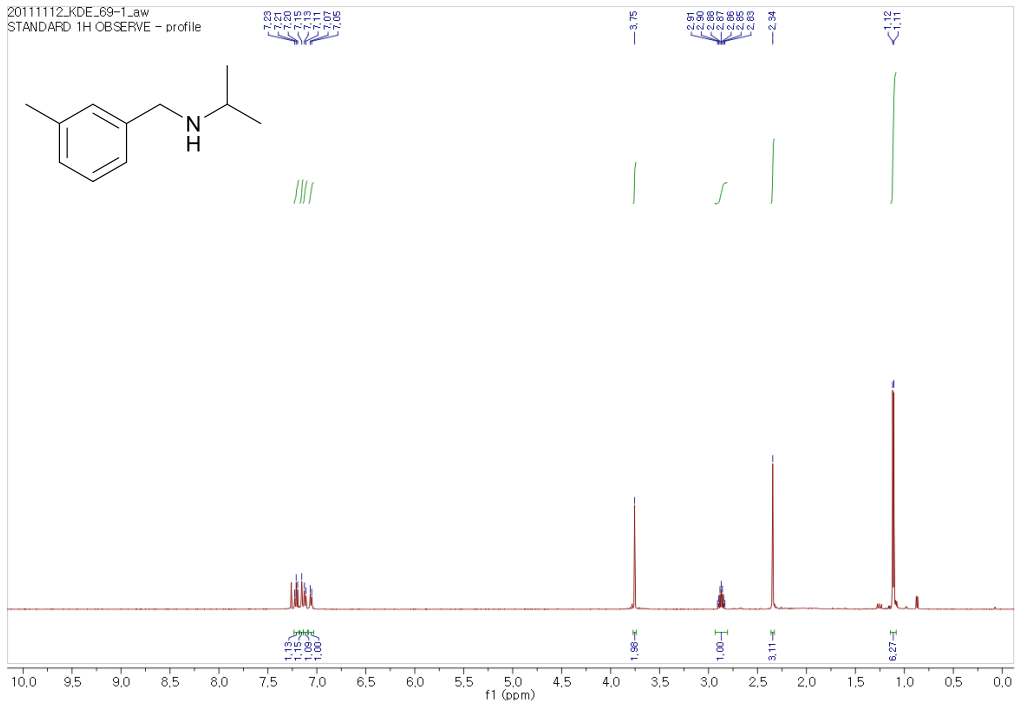

^{13}C NMR (**4ca**) ($CDCl_3$)

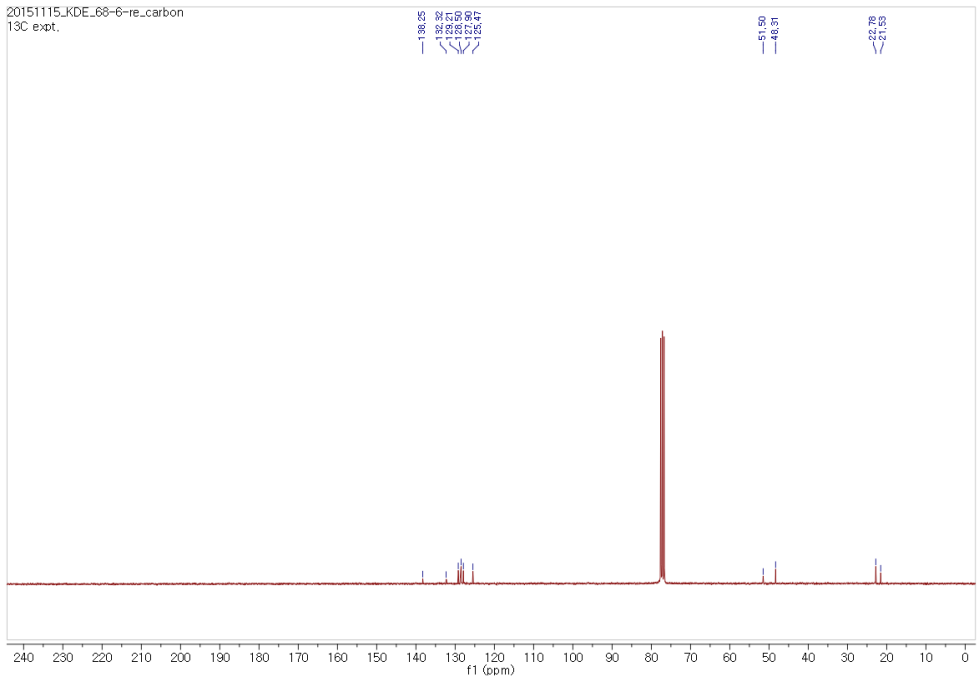

^{1}H NMR (**4da**) ($CDCl_3$)

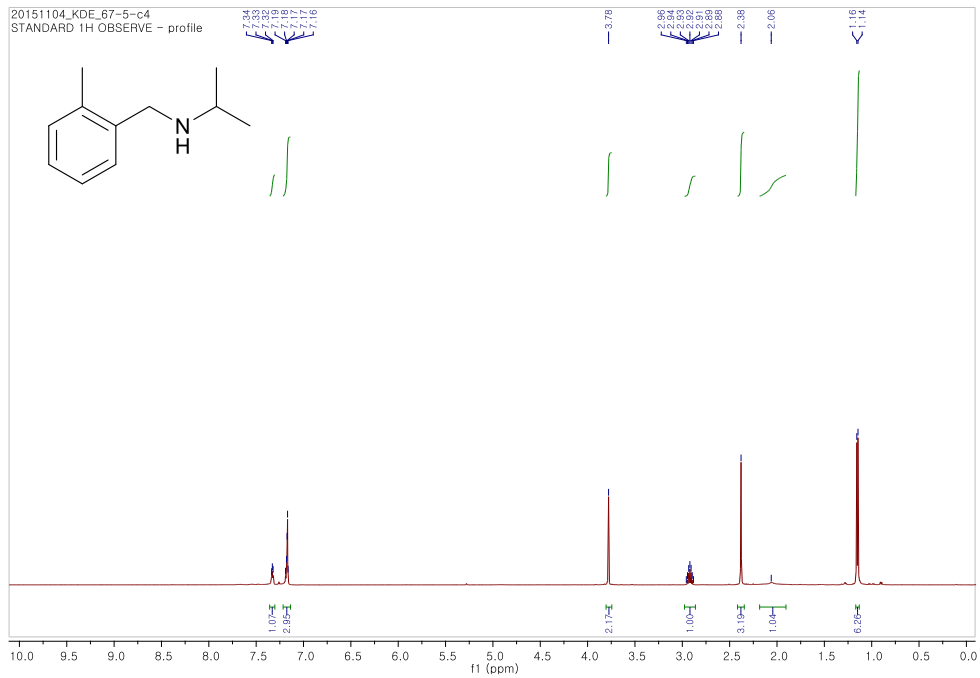

^{1}H NMR (**4ea**) ($CDCl_3$)

^{1}H NMR (**4fa**) ($CDCl_3$)

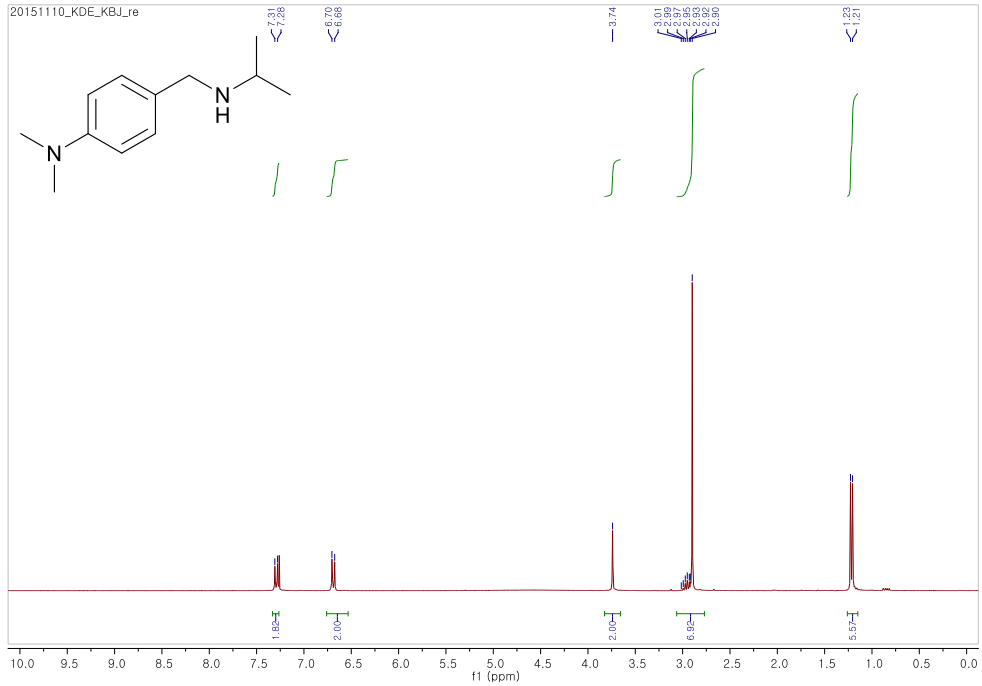

^{13}C NMR (**4fa**) ($CDCl_3$)

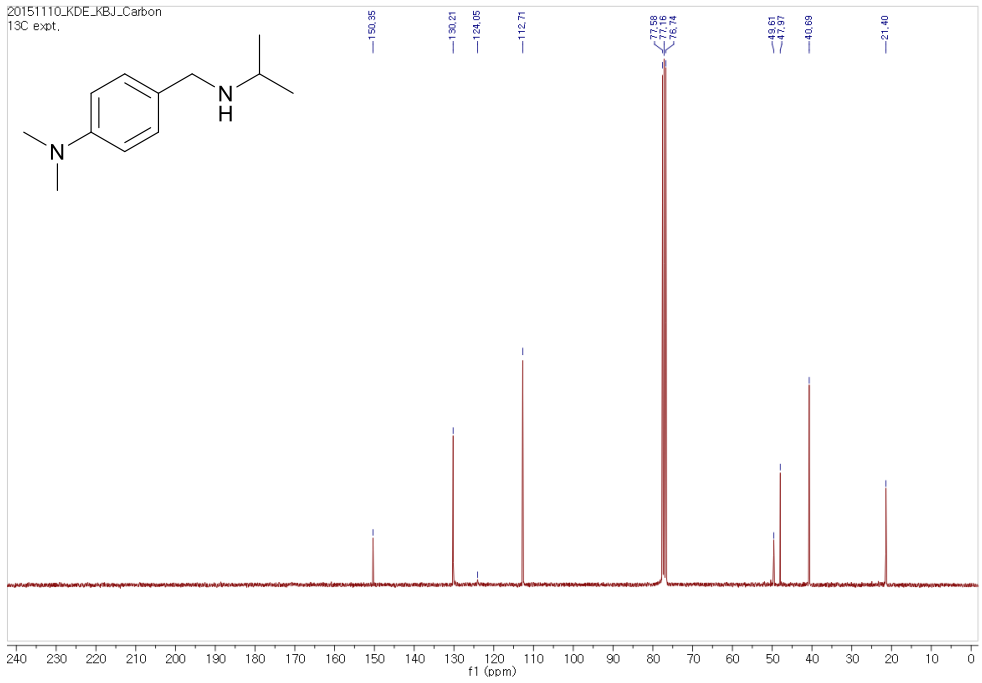

^{1}H NMR (**4ga**) ($CDCl_3$)

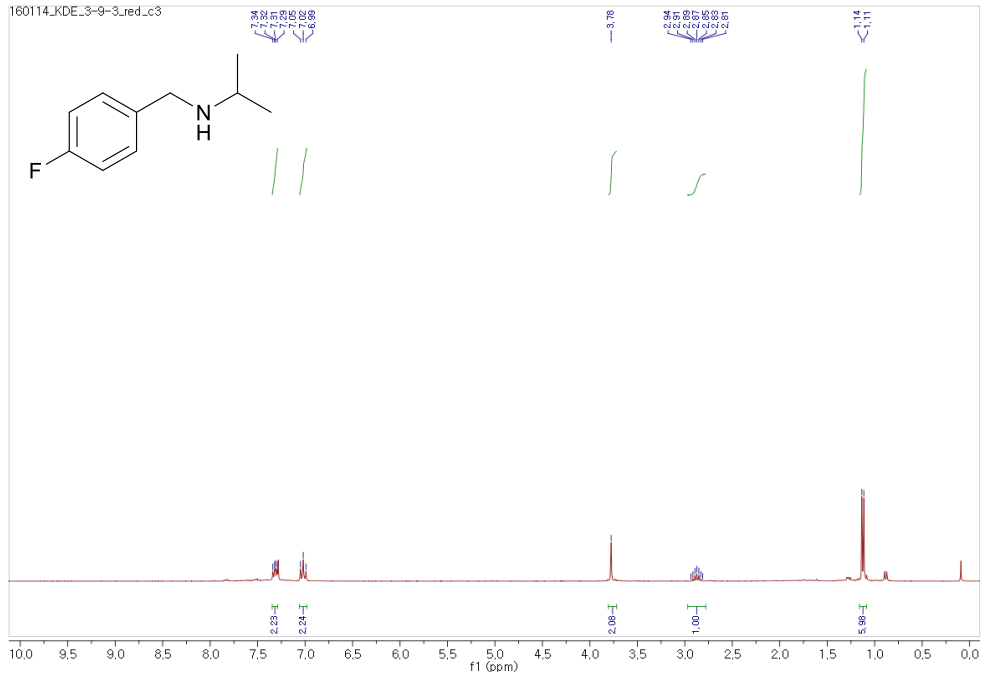

^{1}H NMR (**4ha**) ($CDCl_3$)

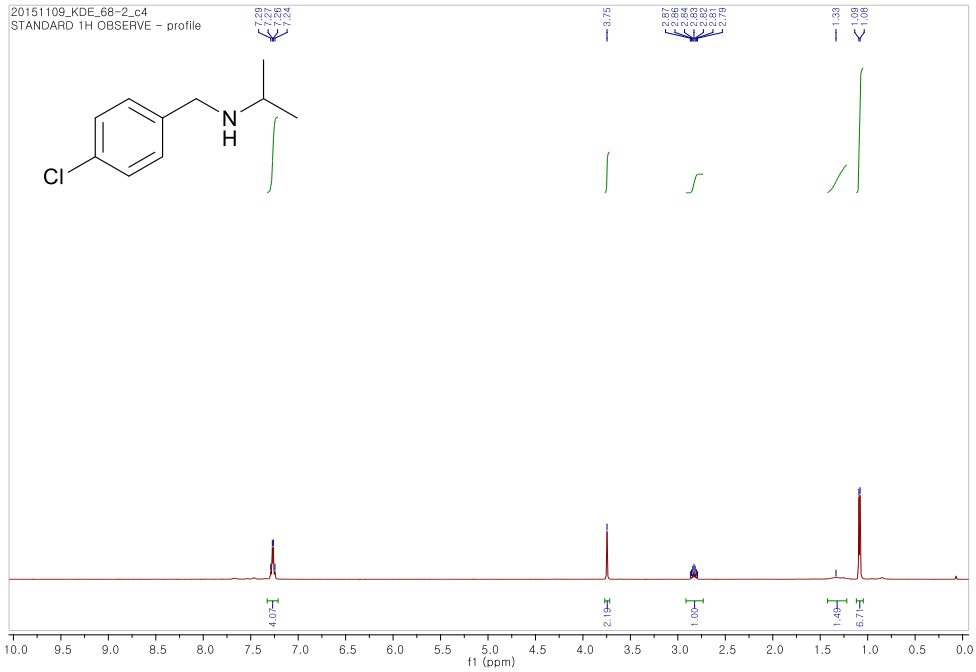

^{1}H NMR (**4ia**) ($CDCl_3$)

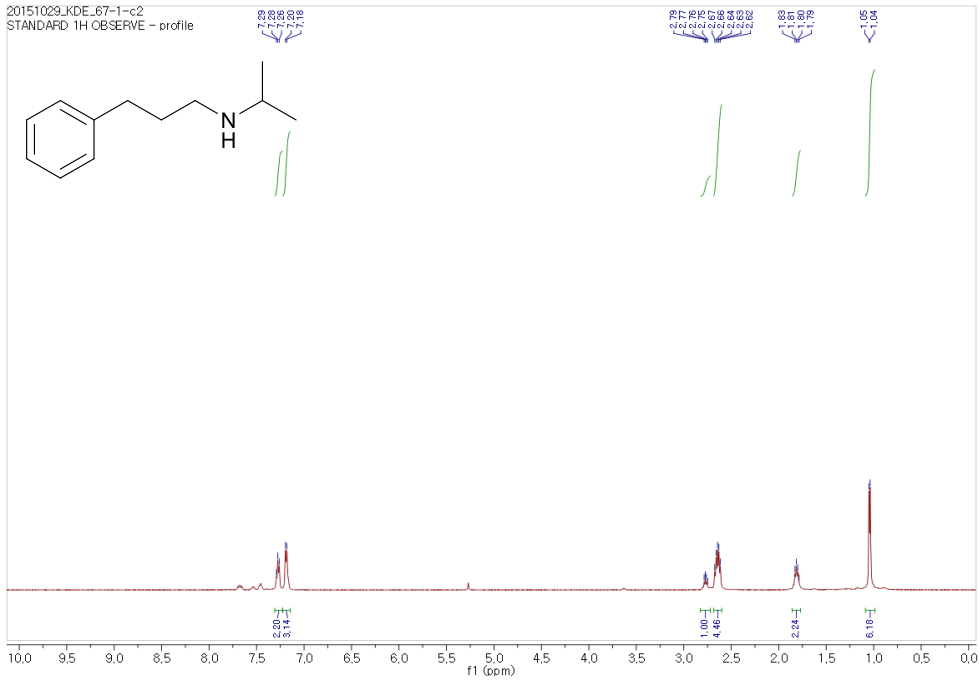

^{1}H NMR (**4la**) ($CDCl_3$)

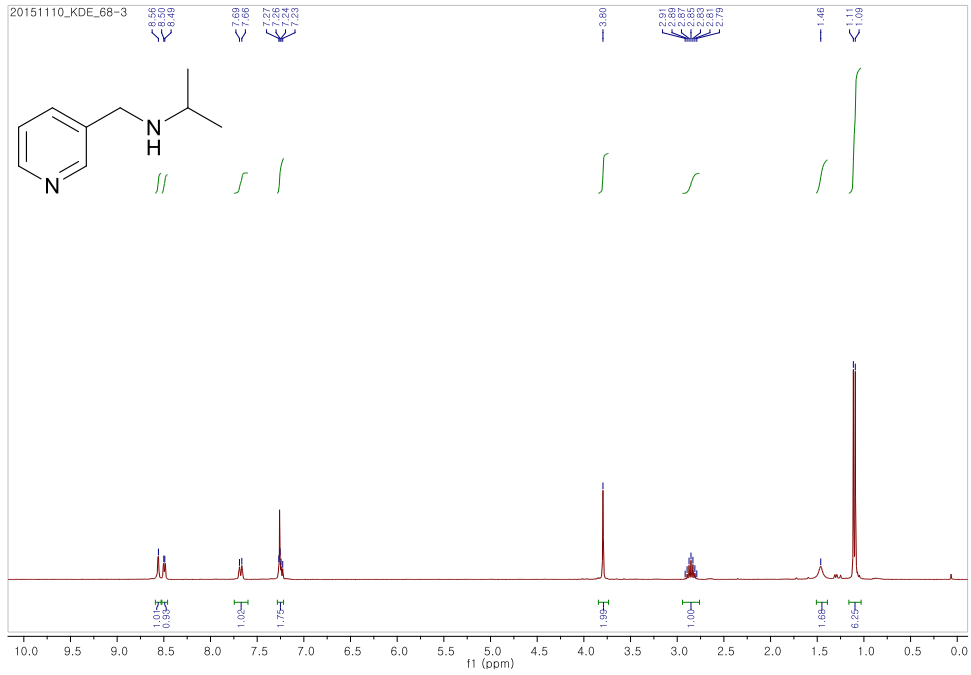

^{1}H NMR (**4ac**) ($CDCl_3$)

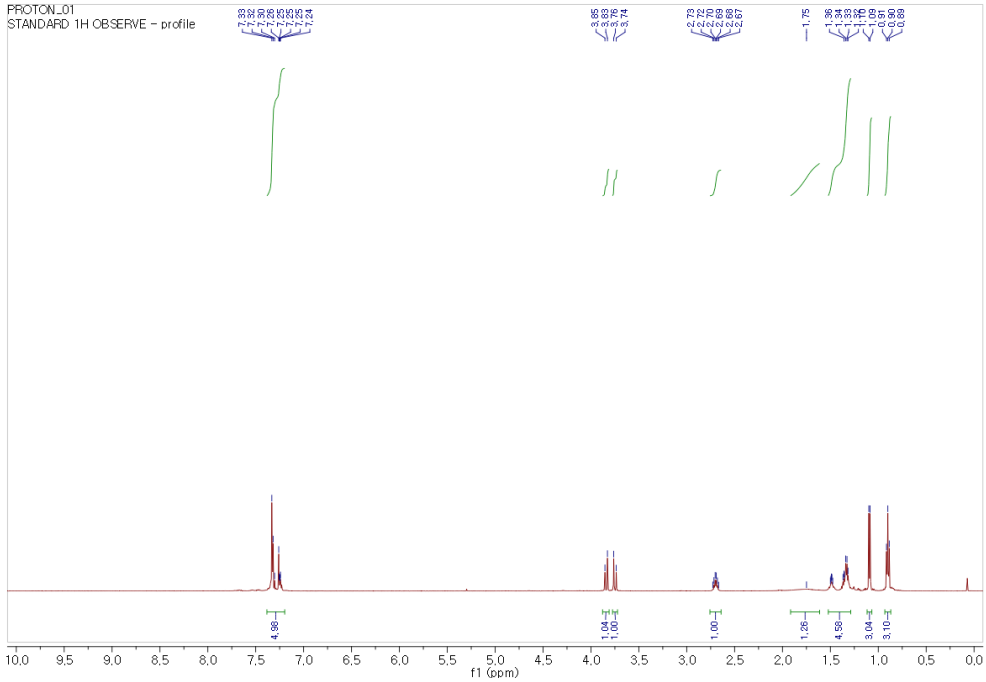

Chapter 5

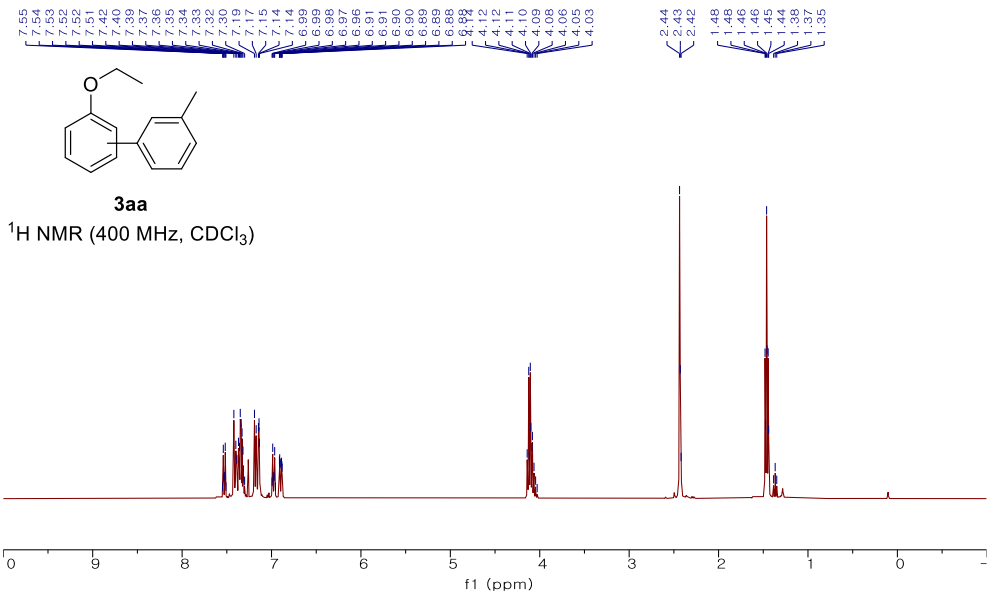
7.55 7.54 7.53 7.52 7.52 7.51 7.42 7.40 7.39 7.37 7.36 7.35 7.34 7.33 7.32 7.30 7.19 7.17 7.15 7.14 7.14 6.99 6.98 6.97 6.96 6.91 6.91 6.90 6.90 6.89 6.89 6.88 6.88 4.13 4.12 4.12 4.11 4.10 4.09 4.08 4.06 4.05 4.03
2.44 2.43 2.42
1.48 1.48 1.46 1.46 1.45 1.44 1.38 1.37 1.35
O
3aa
^{1}H NMR (400 MHz, $CDCl_3$)
0 9 8 7 6 5 4 3 2 1 0
f1 (ppm)

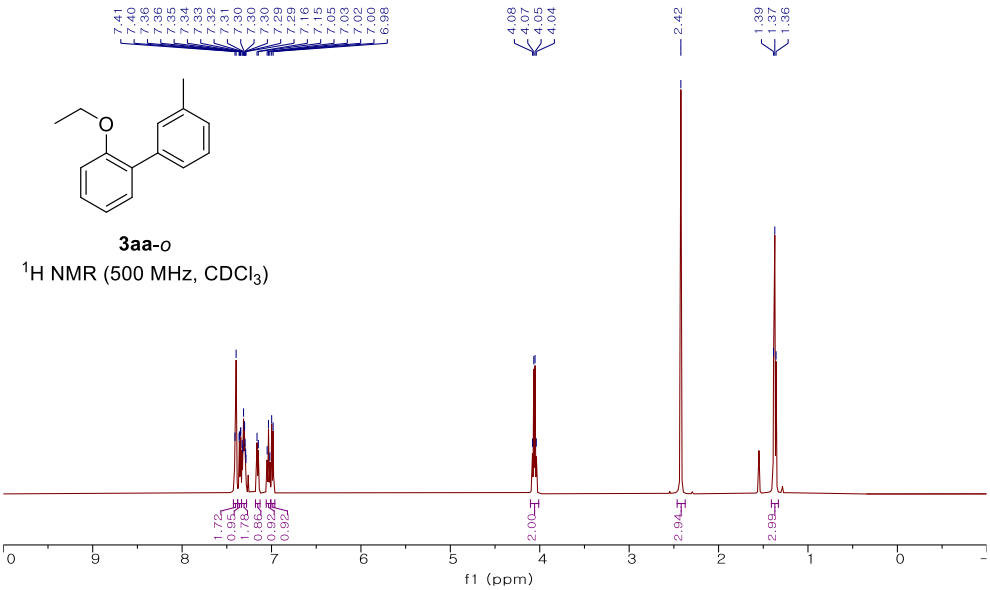
7.41 7.40 7.36 7.36 7.35 7.34 7.33 7.32 7.31 7.30 7.30 7.30 7.29 7.29 7.16 7.15 7.05 7.03 7.02 7.00 6.98
4.08 4.07 4.05 4.04
2.42
1.39 1.37 1.36
O
3aa-o
^{1}H NMR (500 MHz, $CDCl_3$)
1.72 0.95 1.78 0.86 0.92 0.92
2.00
2.94
2.99
0 9 8 7 6 5 4 3 2 1 0
f1 (ppm)

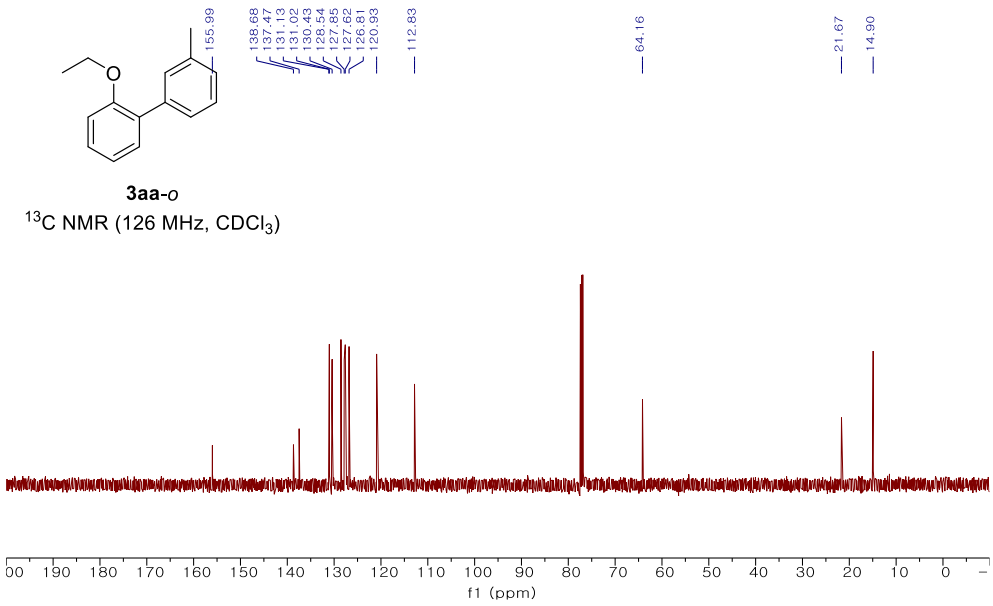

3aa-*o*

^{13}C NMR (126 MHz, $CDCl_3$)

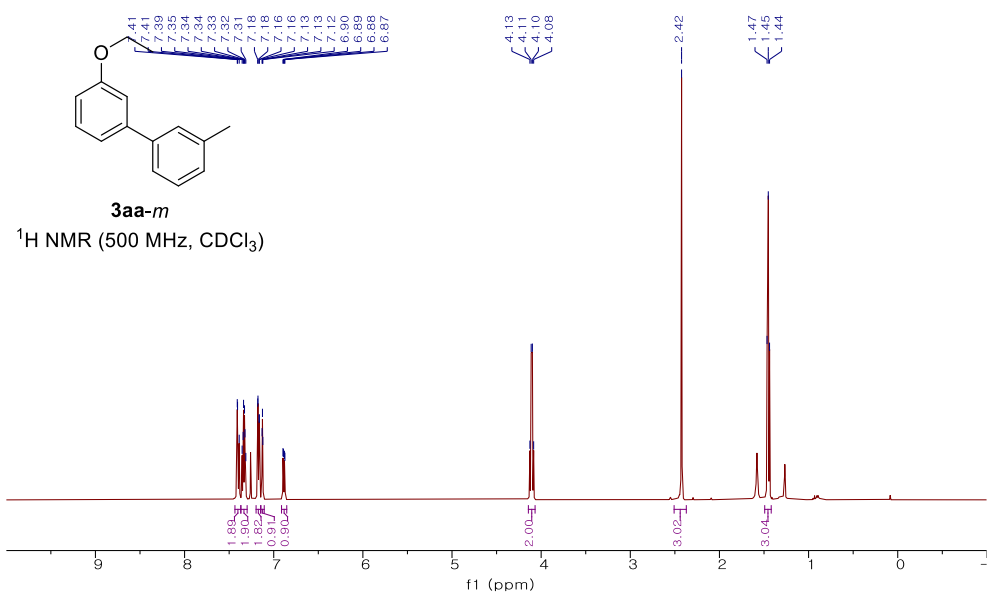

3aa-*m*

^{1}H NMR (500 MHz, $CDCl_3$)

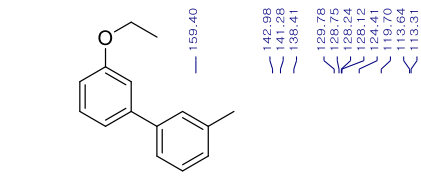

3aa-*m*

^{13}C NMR (126 MHz, $CDCl_3$)

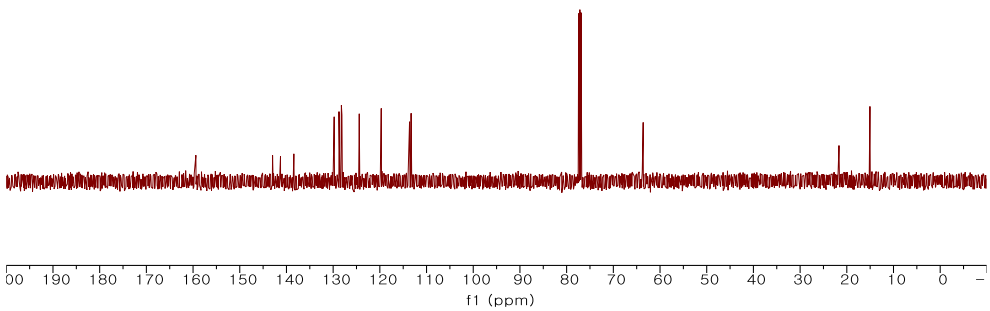

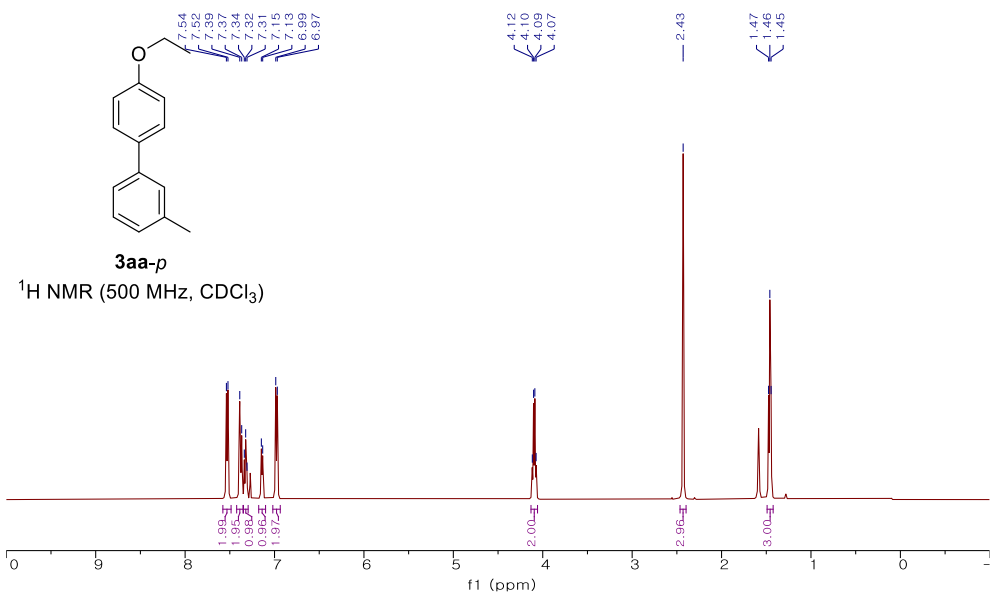

3aa-*p*

^{1}H NMR (500 MHz, $CDCl_3$)

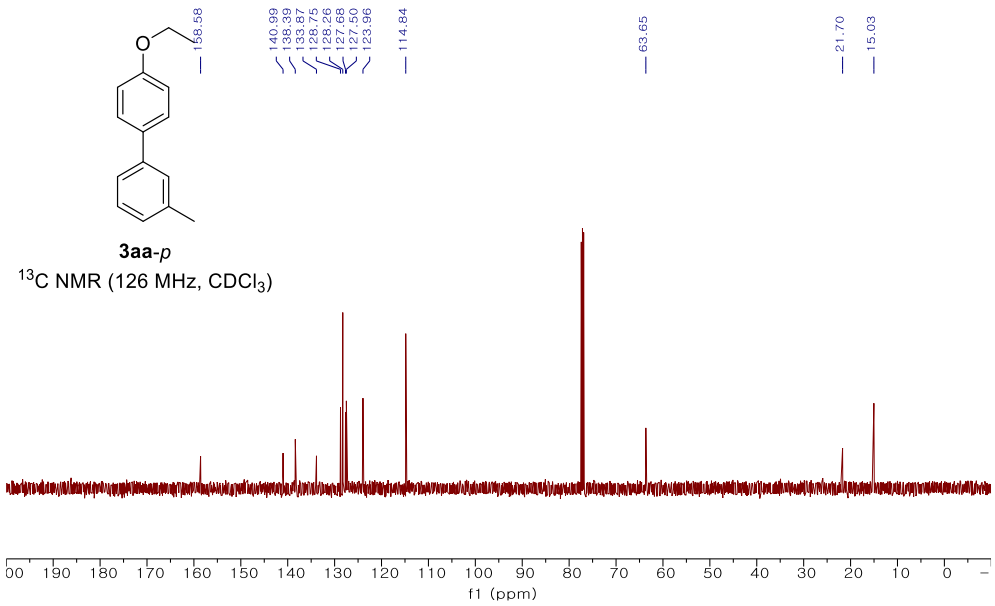

3aa-*p*

^{13}C NMR (126 MHz, $CDCl_3$)

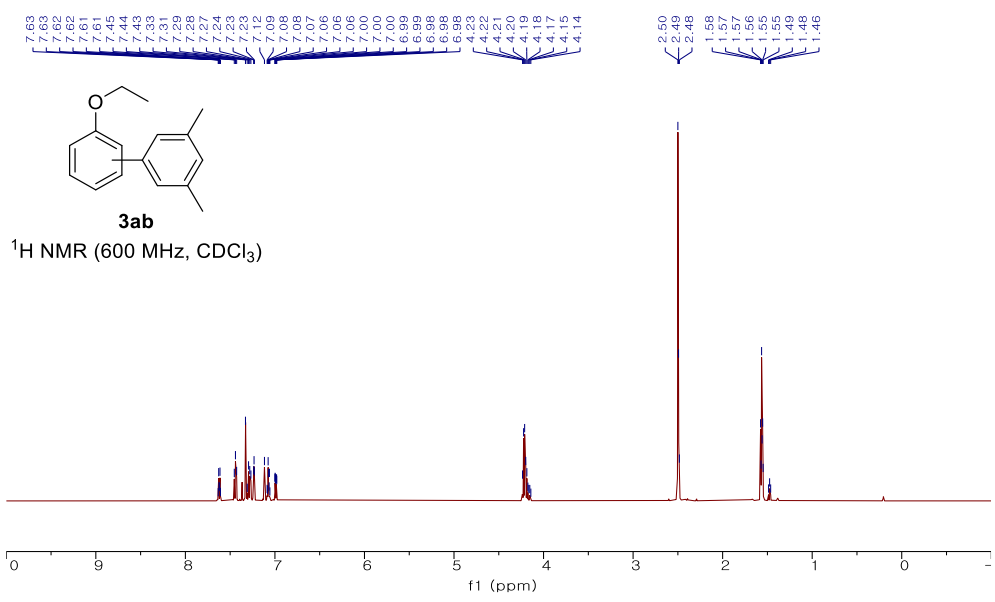

3ab

^{1}H NMR (600 MHz, $CDCl_3$)

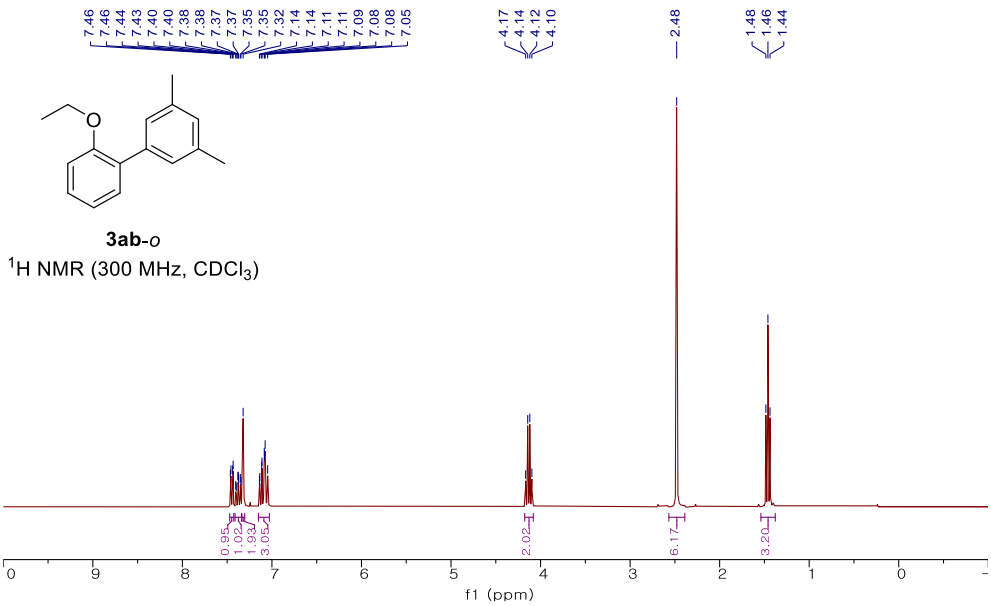

3ab-*o*

^{1}H NMR (300 MHz, $CDCl_3$)

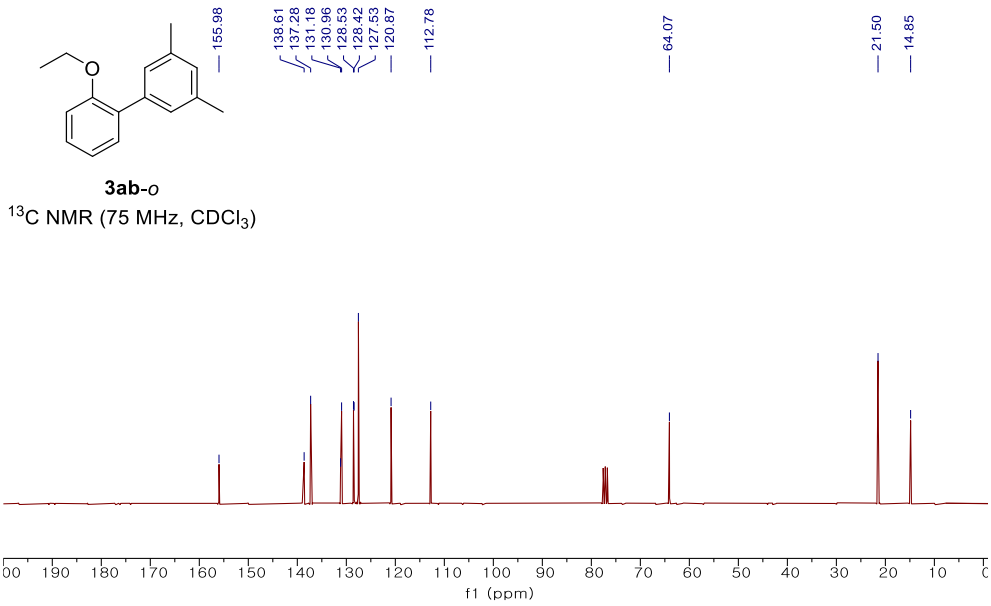

3ab-*o*

^{13}C NMR (75 MHz, $CDCl_3$)

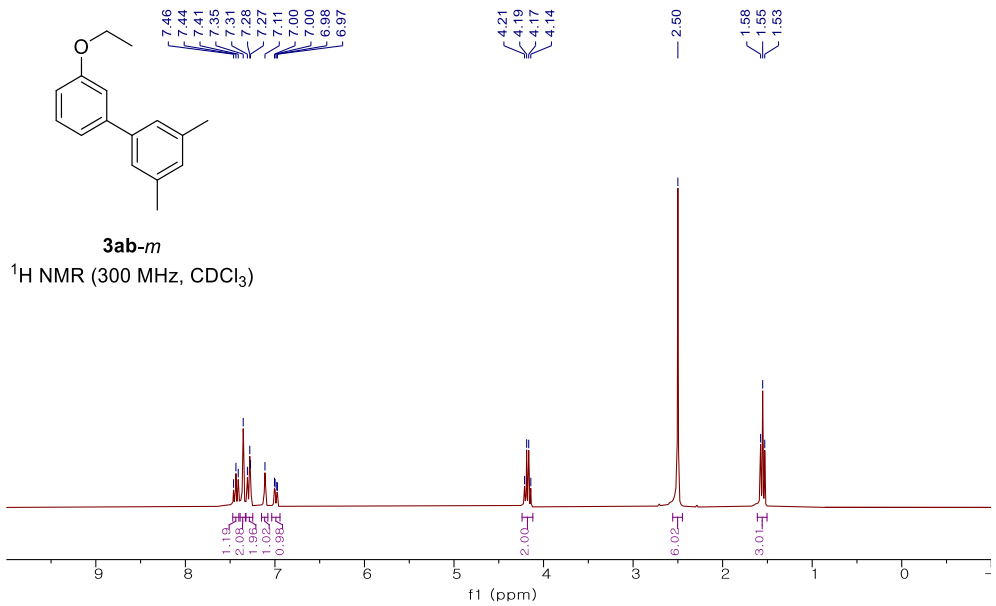

3ab-*m*

^{1}H NMR (300 MHz, $CDCl_3$)

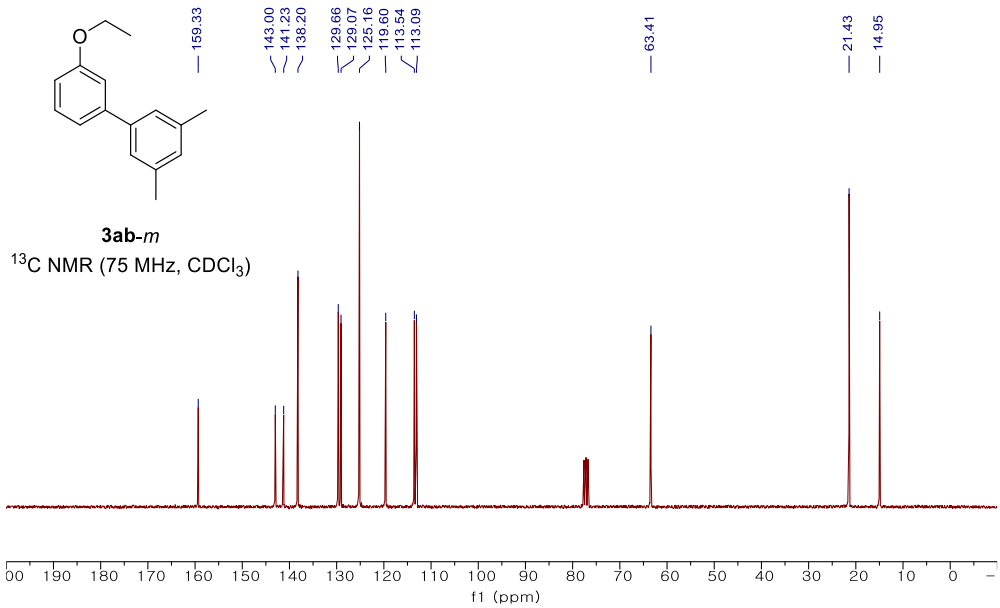

3ab-*m*

^{13}C NMR (75 MHz, $CDCl_3$)

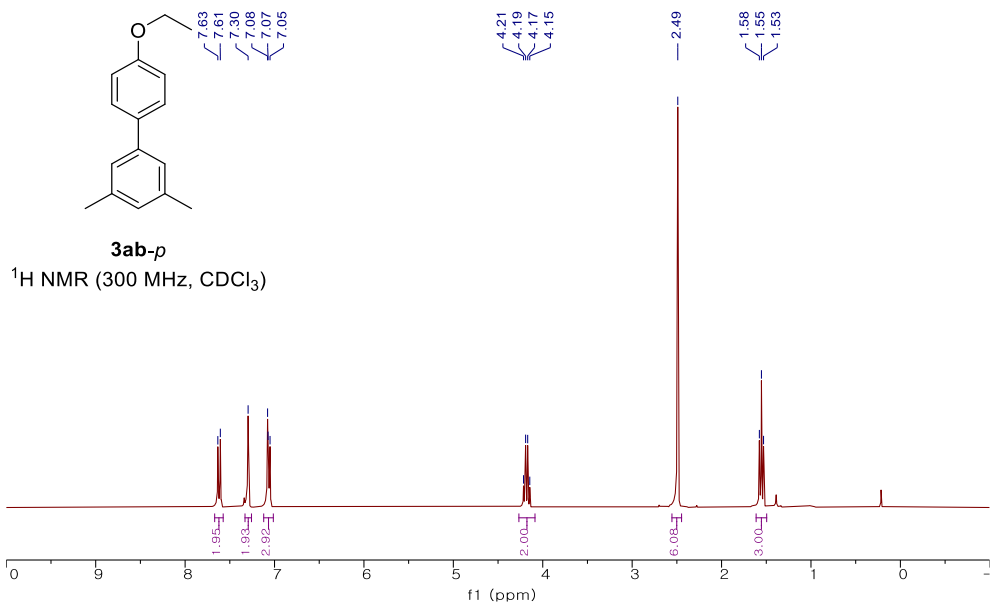

3ab-*p*

^{1}H NMR (300 MHz, $CDCl_3$)

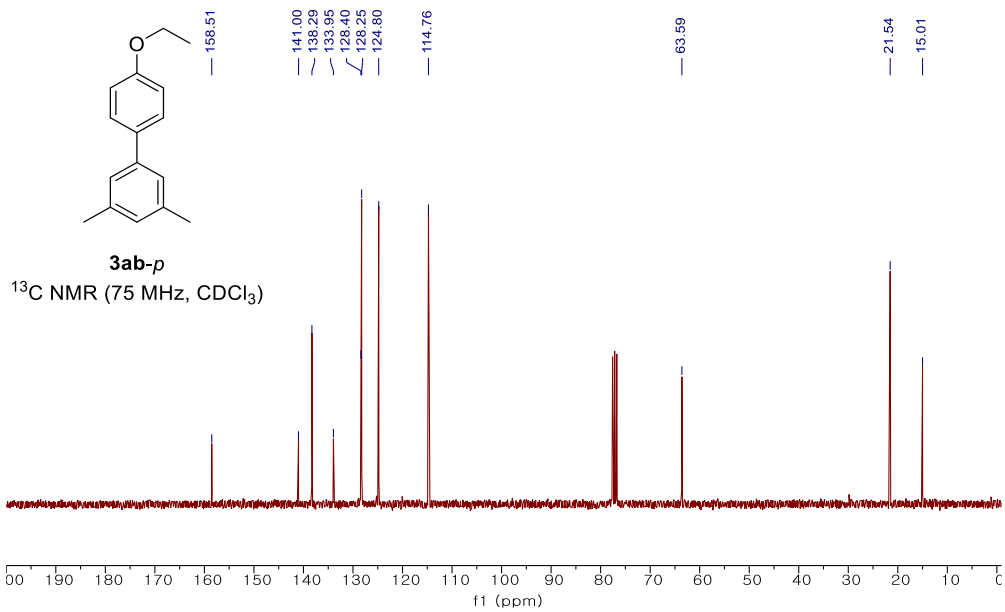

3ab-*p*

^{13}C NMR (75 MHz, $CDCl_3$)

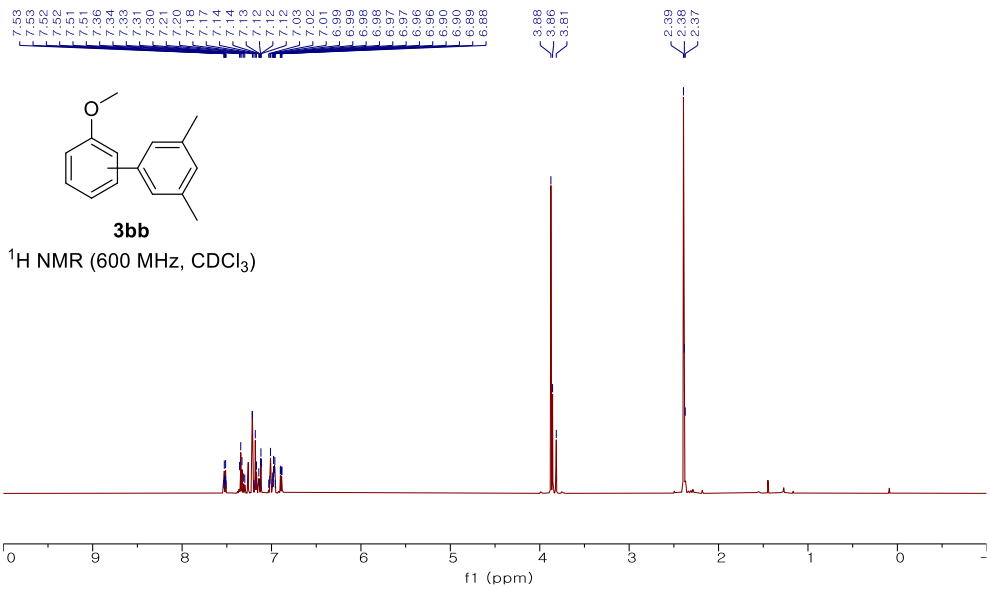

3bb

^{1}H NMR (600 MHz, $CDCl_3$)

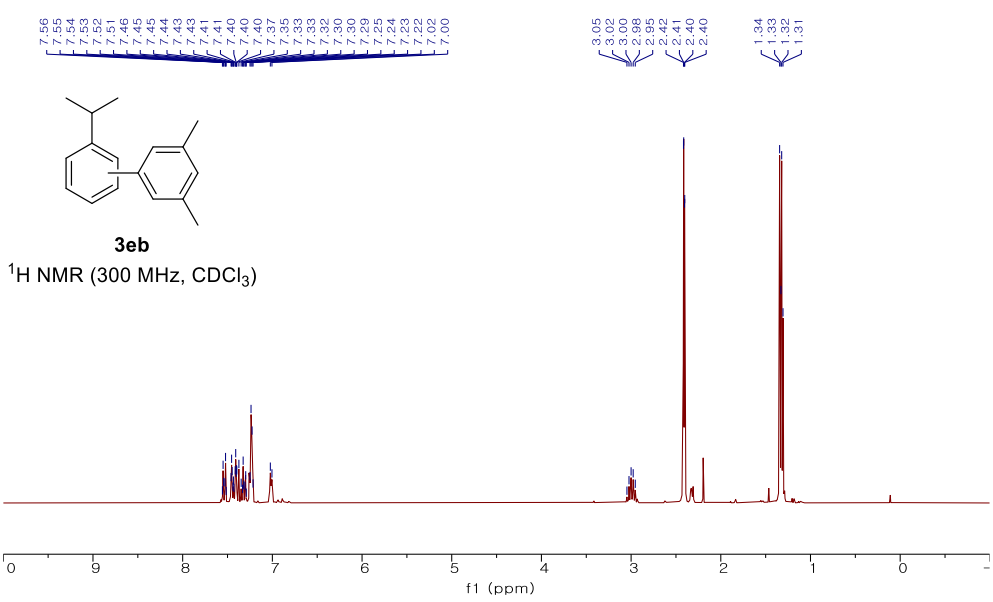

3eb

^{1}H NMR (300 MHz, $CDCl_3$)

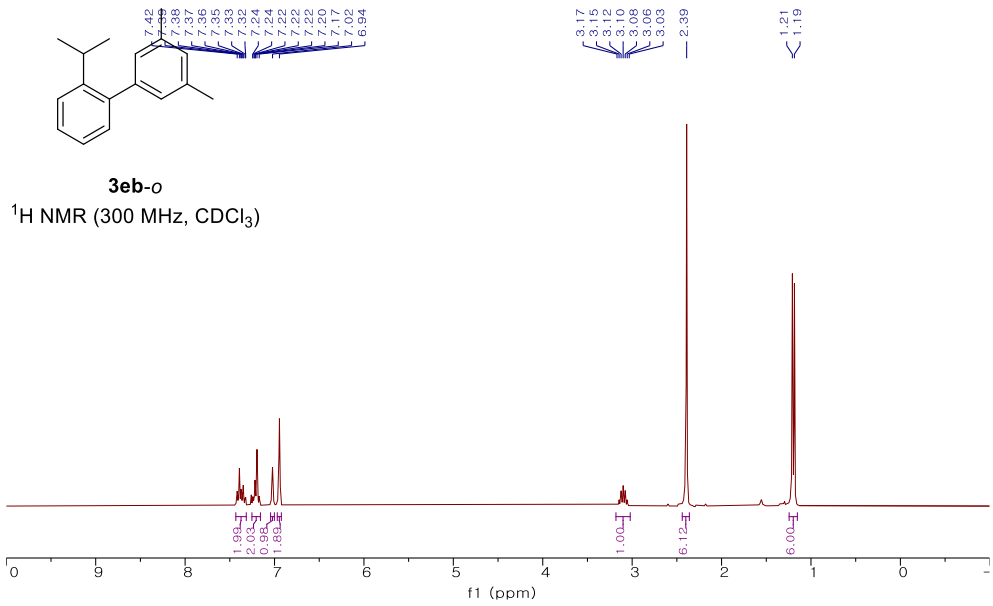

3eb-*o*

^{1}H NMR (300 MHz, $CDCl_3$)

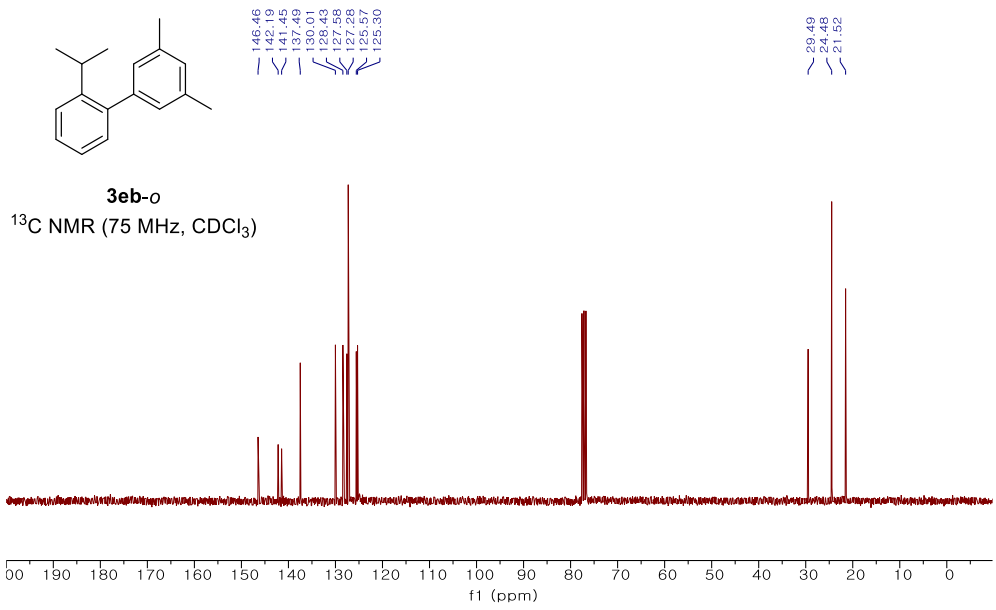

3eb-*o*

^{13}C NMR (75 MHz, $CDCl_3$)

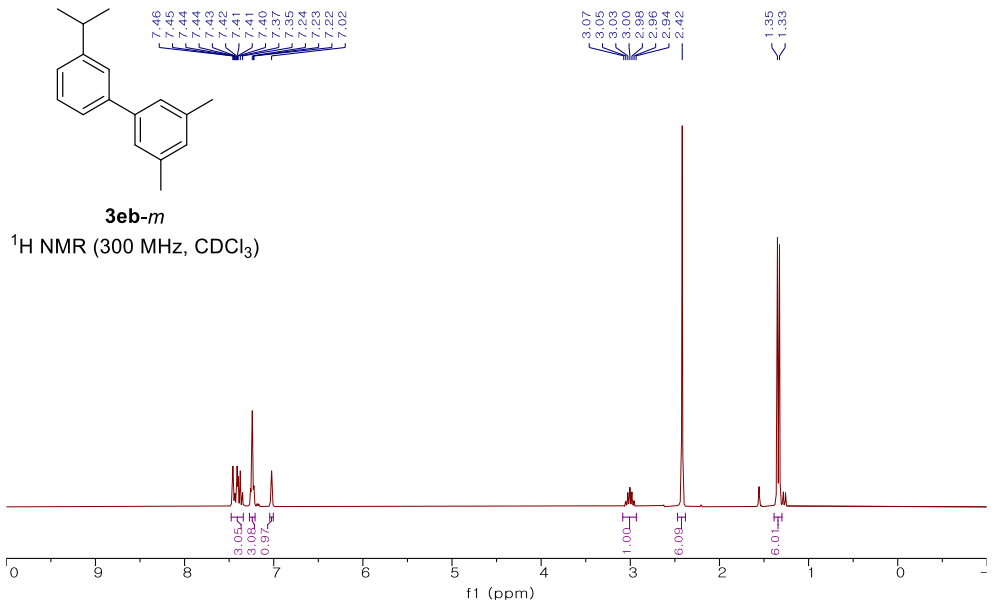

3eb-*m*

^{1}H NMR (300 MHz, $CDCl_3$)

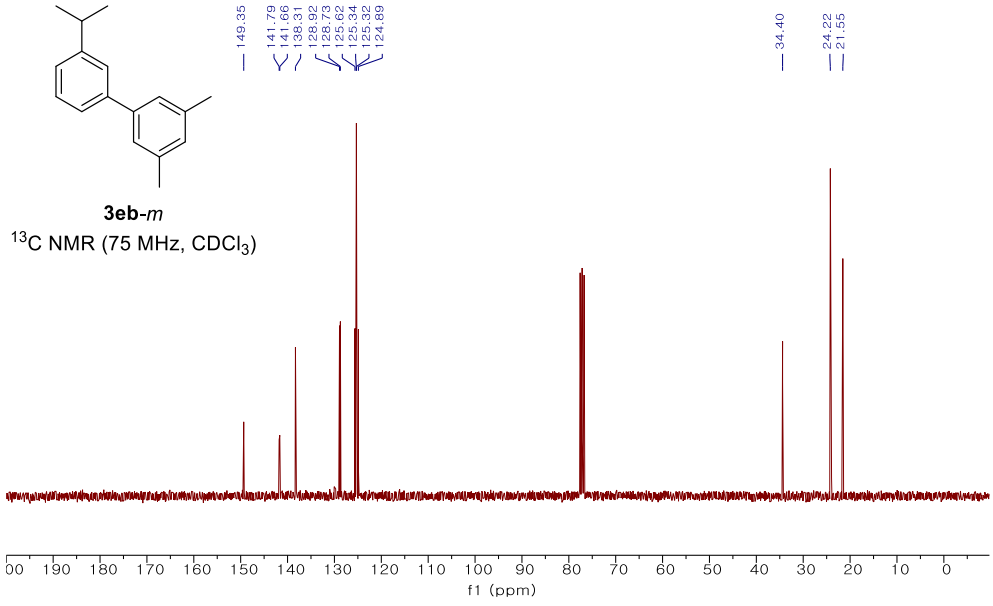

3eb-*m*

^{13}C NMR (75 MHz, $CDCl_3$)

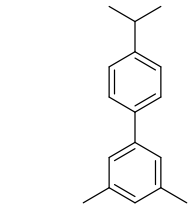

3eb-*p*

^{1}H NMR (300 MHz, $CDCl_3$)

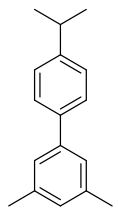

3eb-*p*

^{13}C NMR (75 MHz, $CDCl_3$)

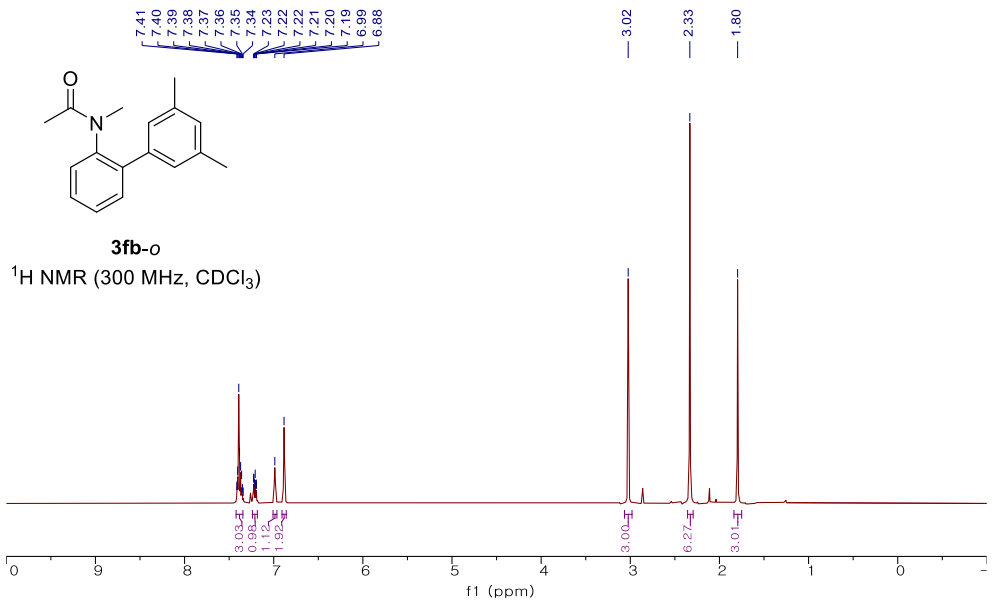
7.41
7.40
7.39
7.38
7.37
7.36
7.35
7.34
7.23
7.22
7.22
7.21
7.20
7.19
6.99
6.88
3.02
2.33
1.80
O
N
3fb-o
1H NMR (300 MHz, CDCl3)
3.03
0.98
1.12
1.92
3.00
6.27
3.01
f1 (ppm)

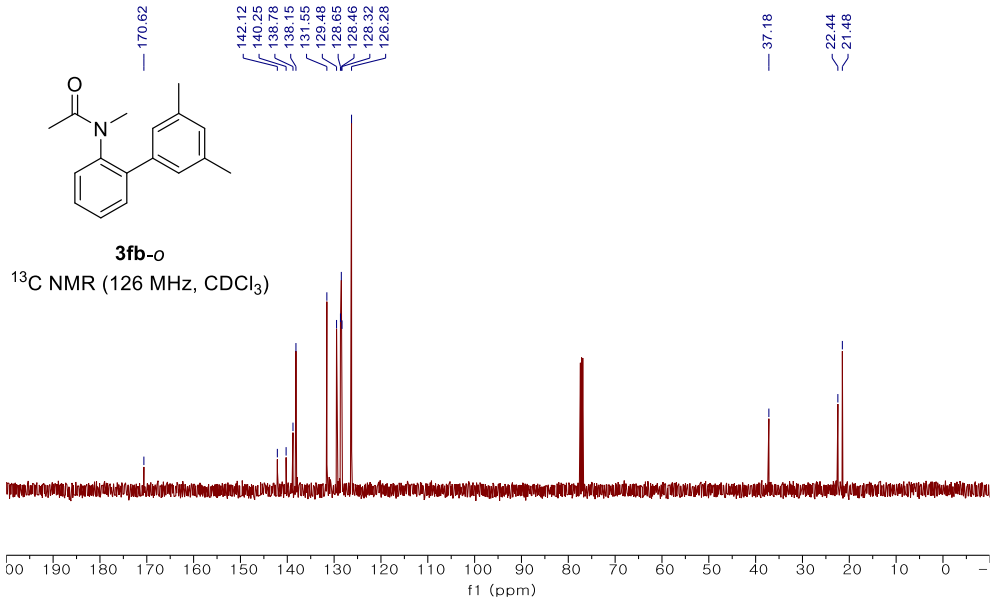
170.62
142.12
140.25
138.78
138.15
131.55
129.48
128.65
128.46
128.32
126.28
37.18
22.44
21.48
O
N
3fb-o
13C NMR (126 MHz, CDCl3)
f1 (ppm)

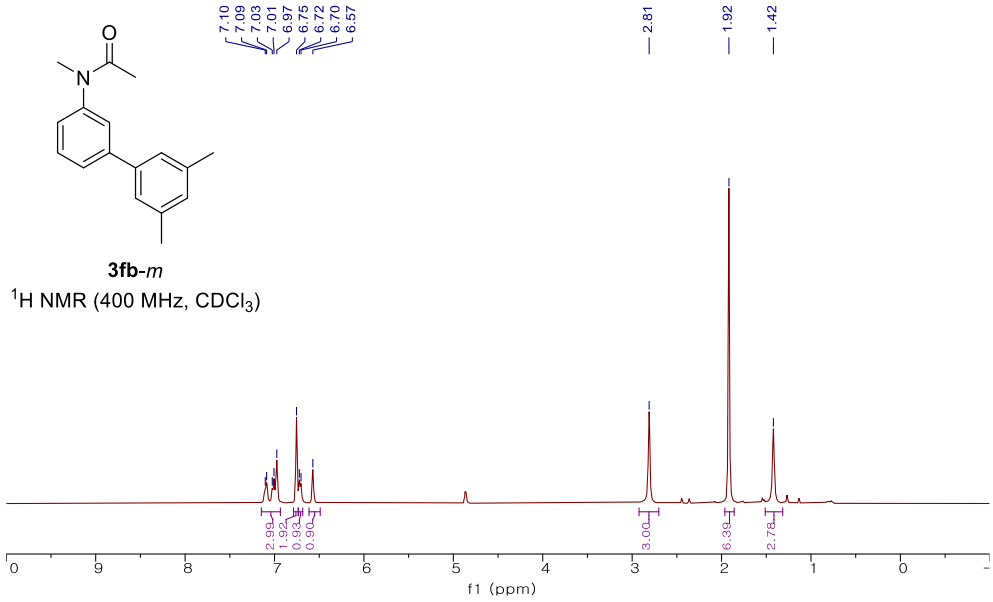

3fb-*m*

^{1}H NMR (400 MHz, $CDCl_3$)

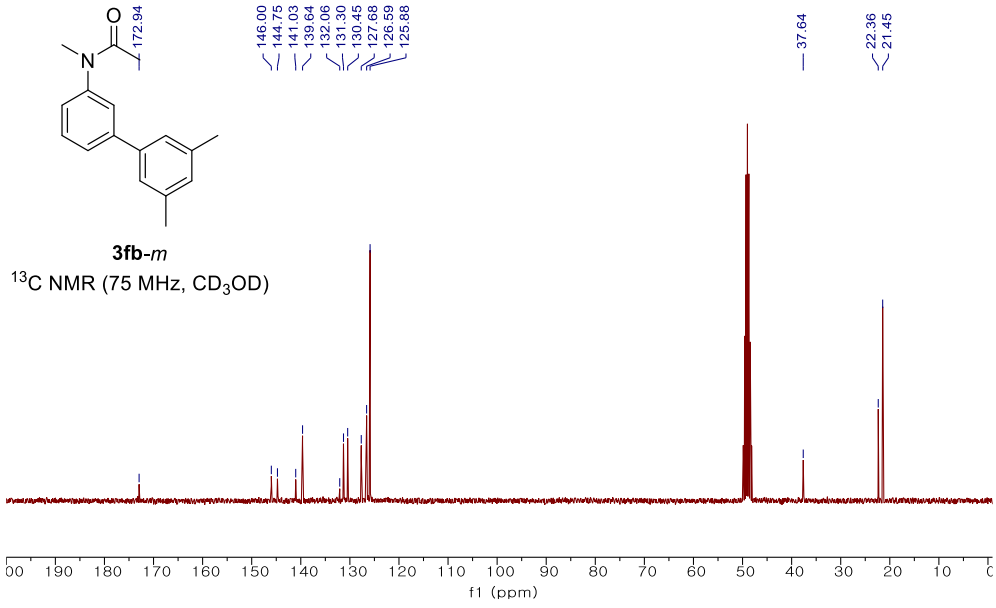

3fb-*m*

^{13}C NMR (75 MHz, CD_3OD)

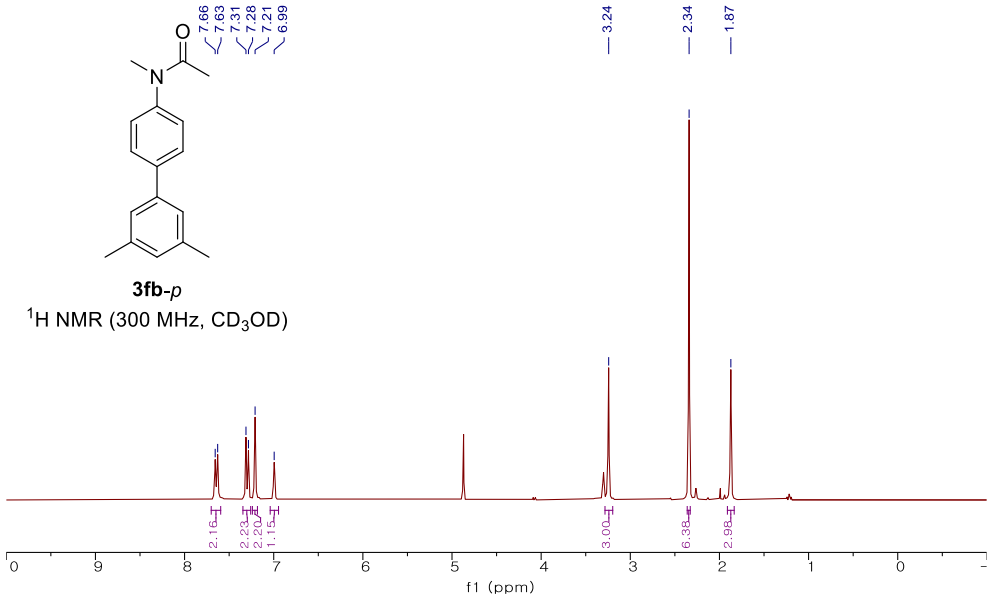

3fb-*p*

^{1}H NMR (300 MHz, CD_3OD)

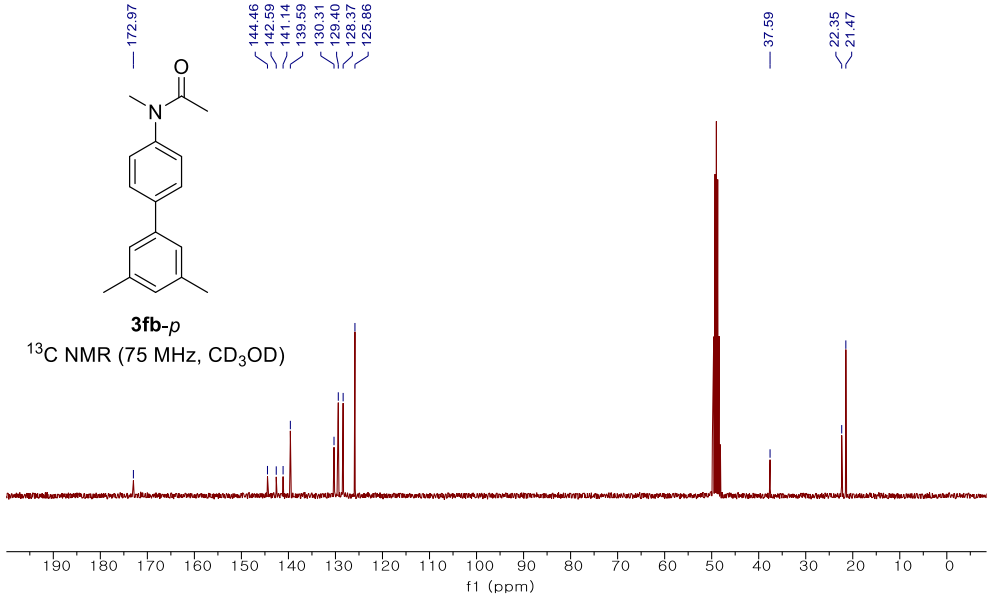

3fb-*p*

^{13}C NMR (75 MHz, CD_3OD)

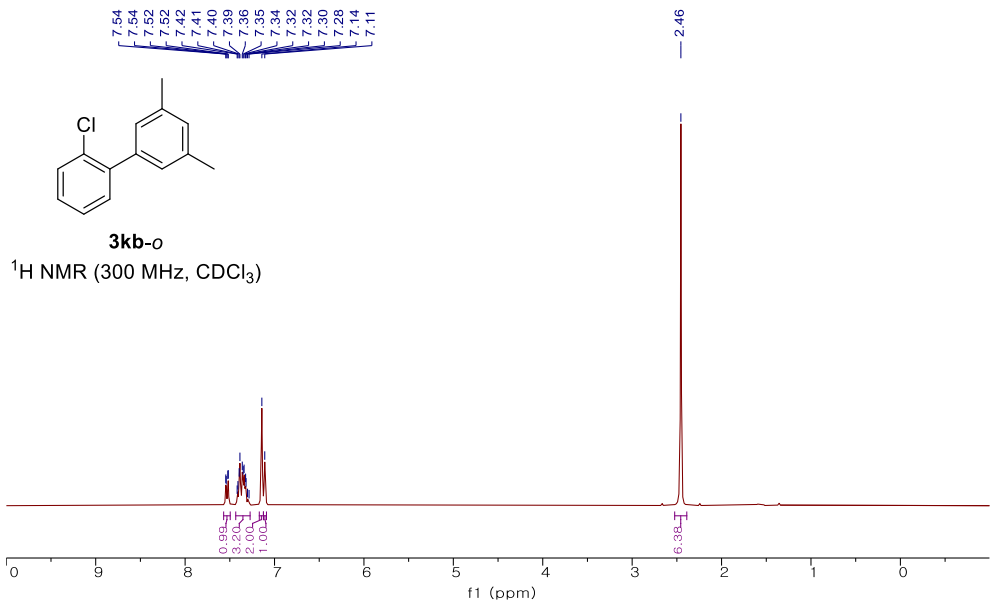

3kb-*o*

^{1}H NMR (300 MHz, $CDCl_3$)

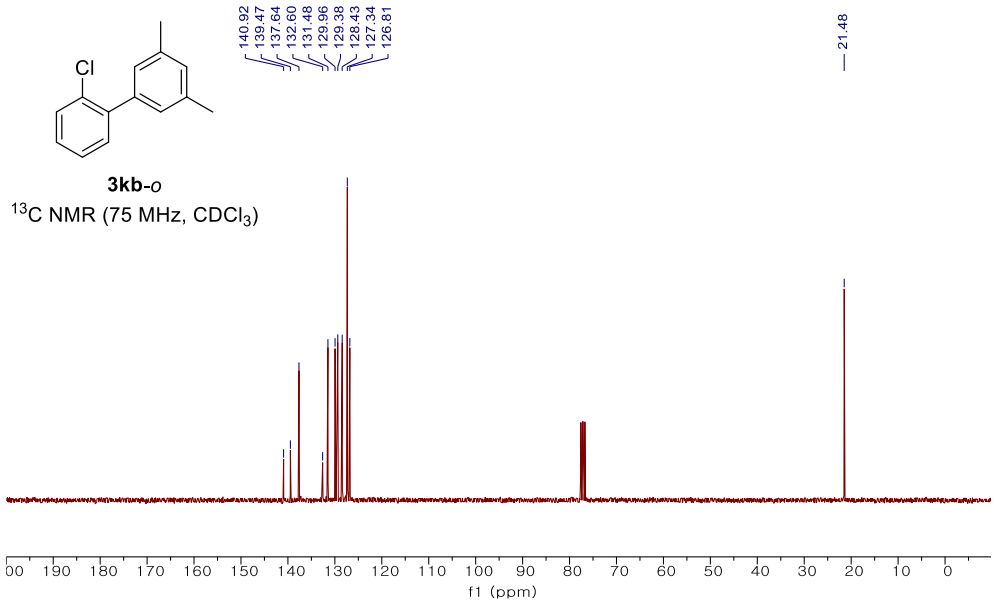

3kb-*o*

^{13}C NMR (75 MHz, $CDCl_3$)

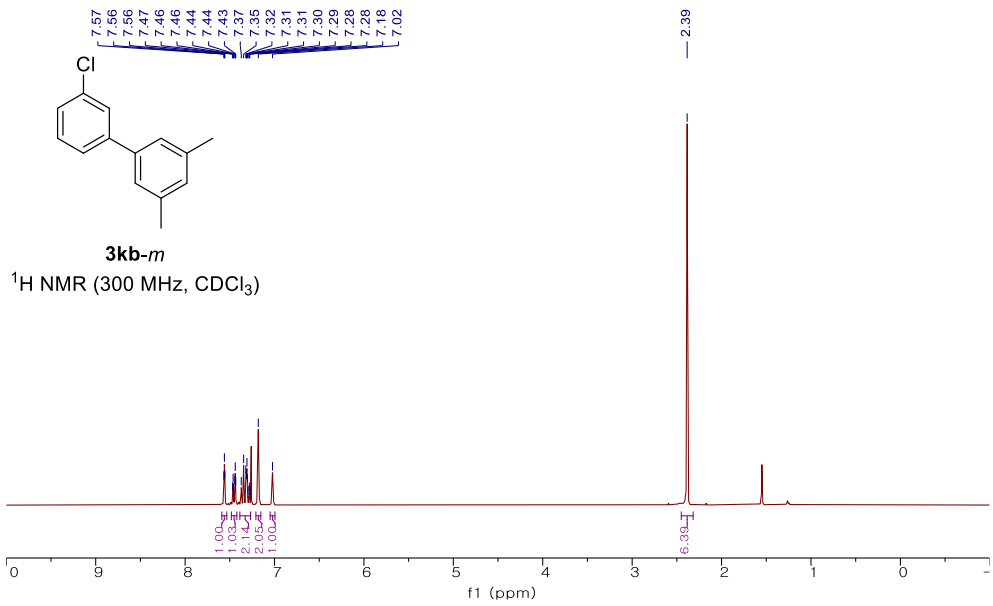

3kb-*m*

^{1}H NMR (300 MHz, $CDCl_3$)

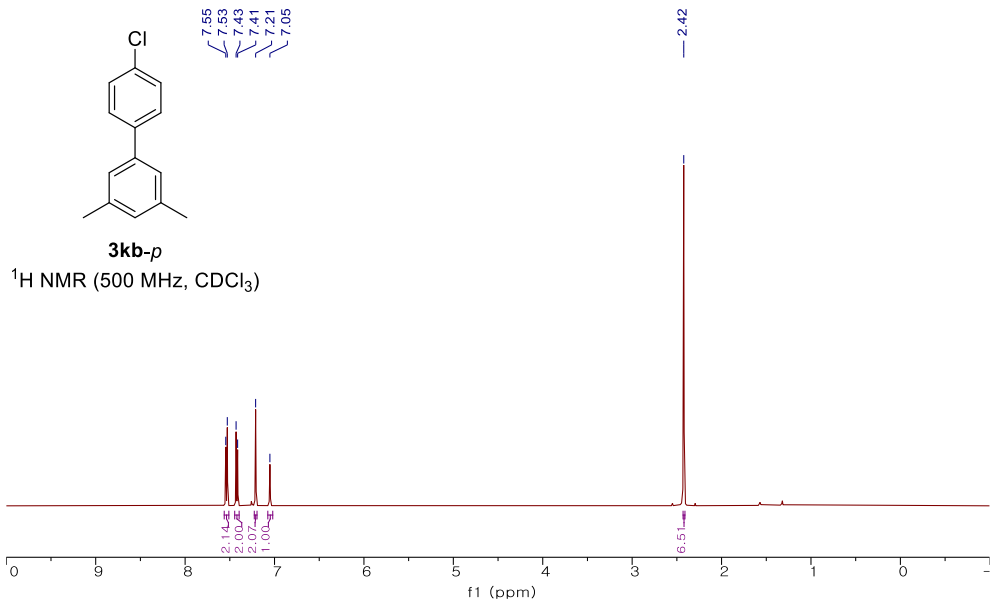

3kb-*p*

^{1}H NMR (500 MHz, $CDCl_3$)

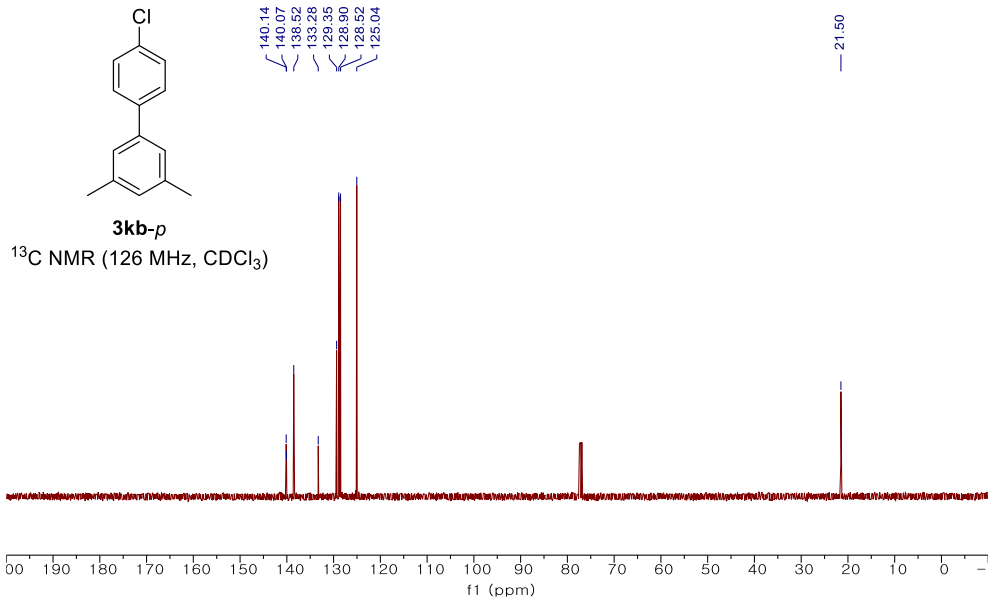

3kb-*p*

^{13}C NMR (126 MHz, $CDCl_3$)

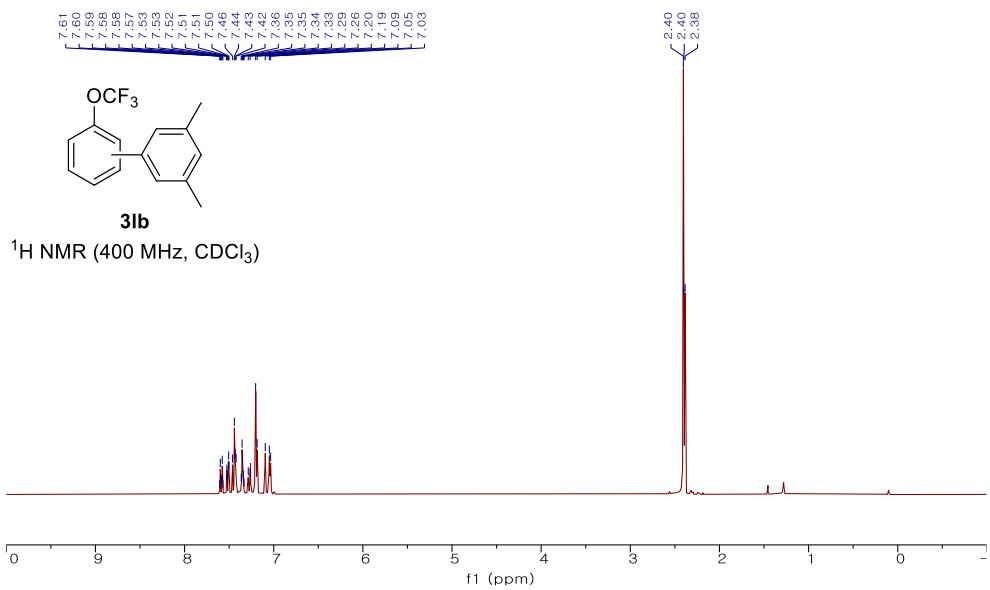

3lb

^{1}H NMR (400 MHz, $CDCl_3$)

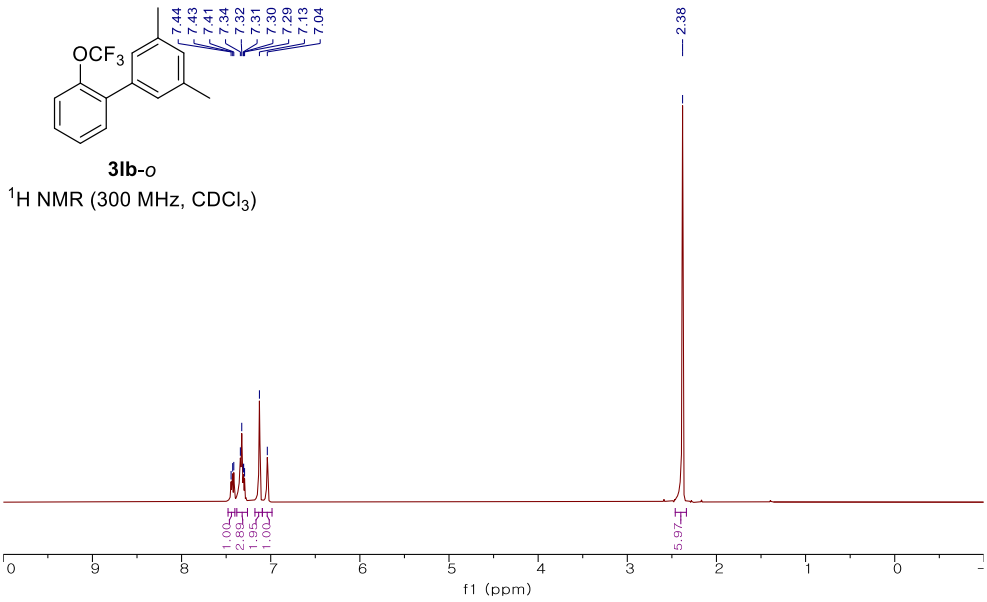

3lb-*o*

^{1}H NMR (300 MHz, $CDCl_3$)

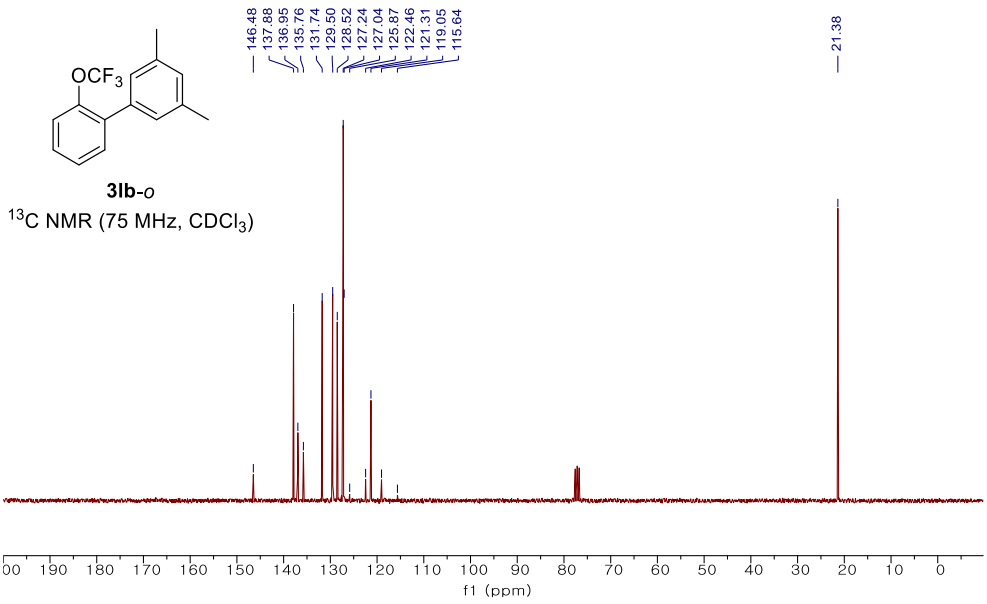

3lb-*o*

^{13}C NMR (75 MHz, $CDCl_3$)

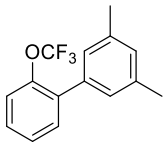

3lb-*o*

^{19}F NMR (376 MHz, $CDCl_3$)

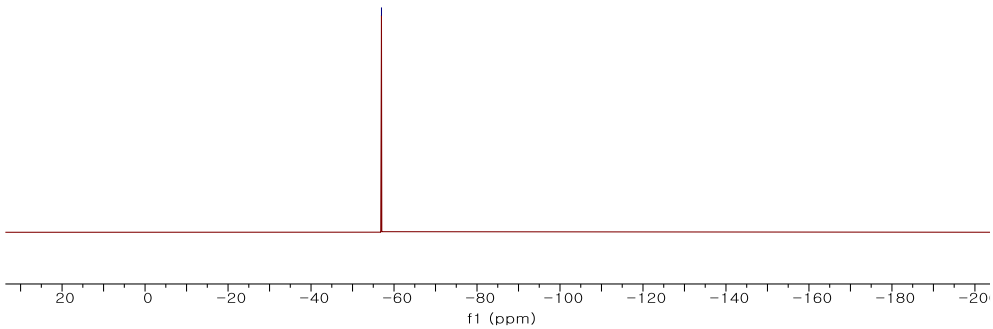

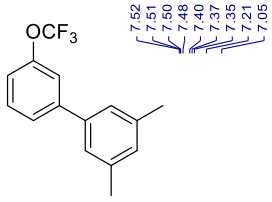

3lb-*m*

^{1}H NMR (300 MHz, $CDCl_3$)

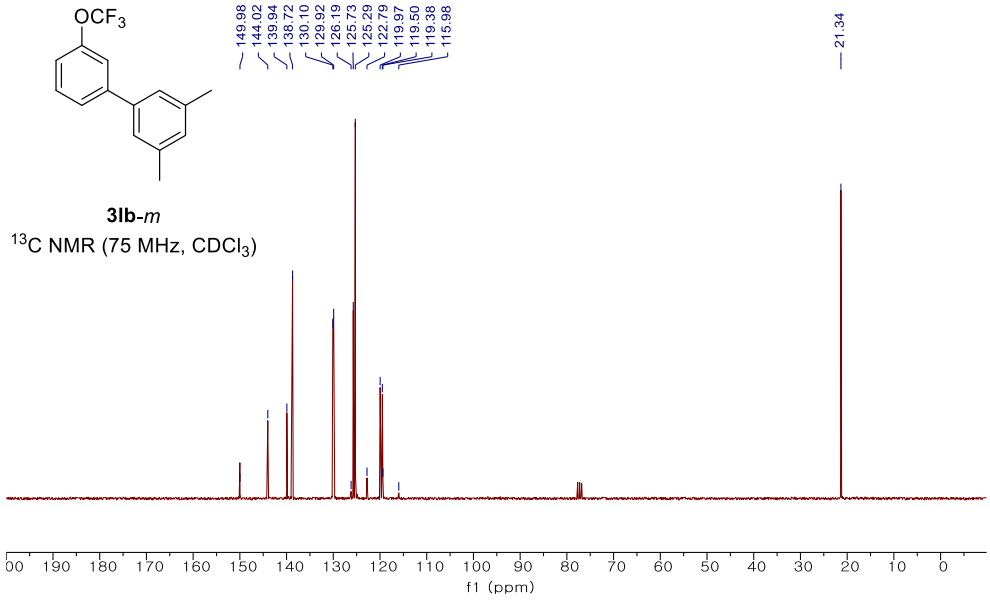

3lb-*m*

^{13}C NMR (75 MHz, $CDCl_3$)

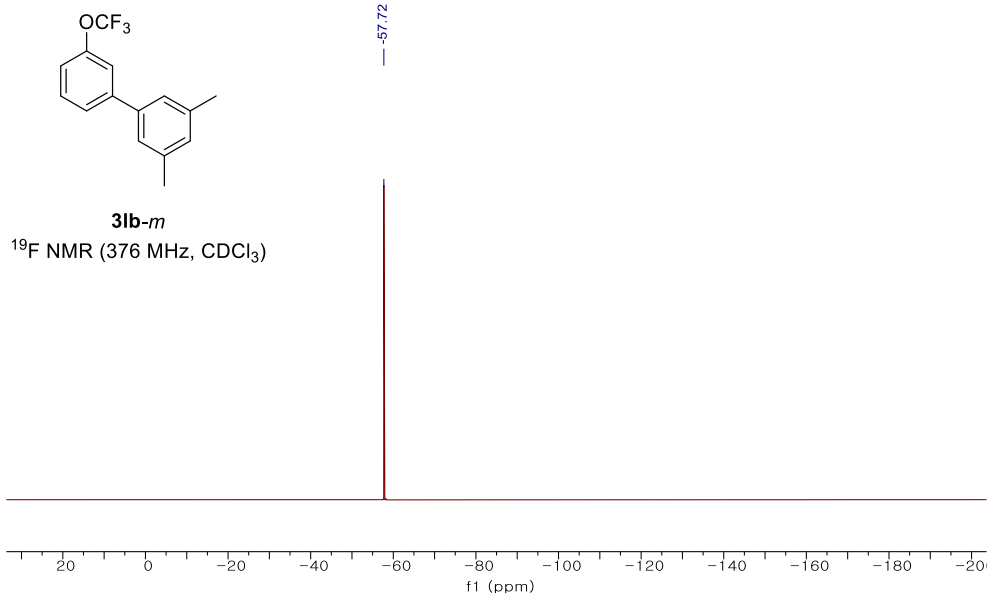

3lb-*m*

^{19}F NMR (376 MHz, $CDCl_3$)

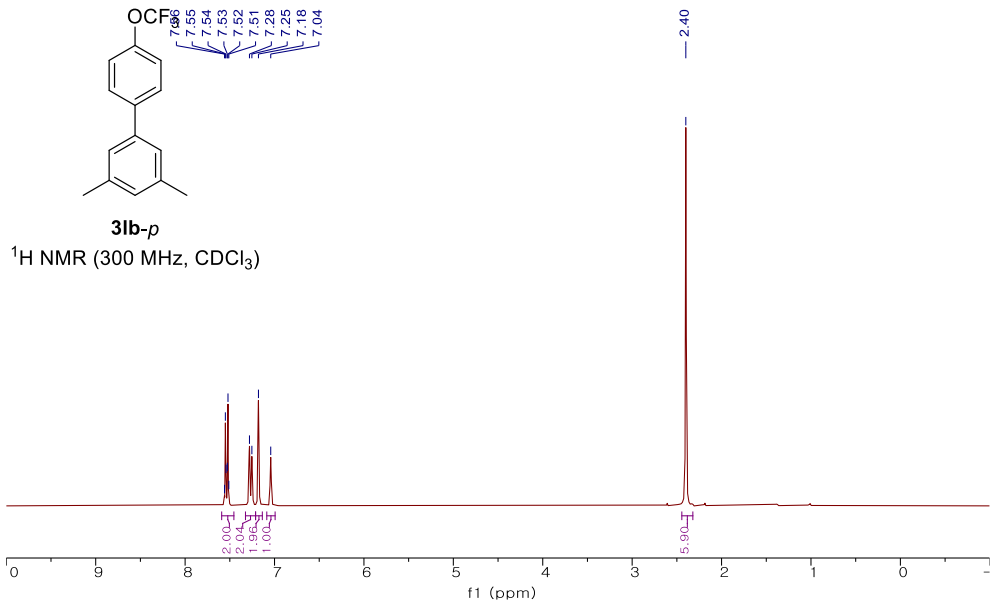

3Ib-*p*

^{1}H NMR (300 MHz, $CDCl_3$)

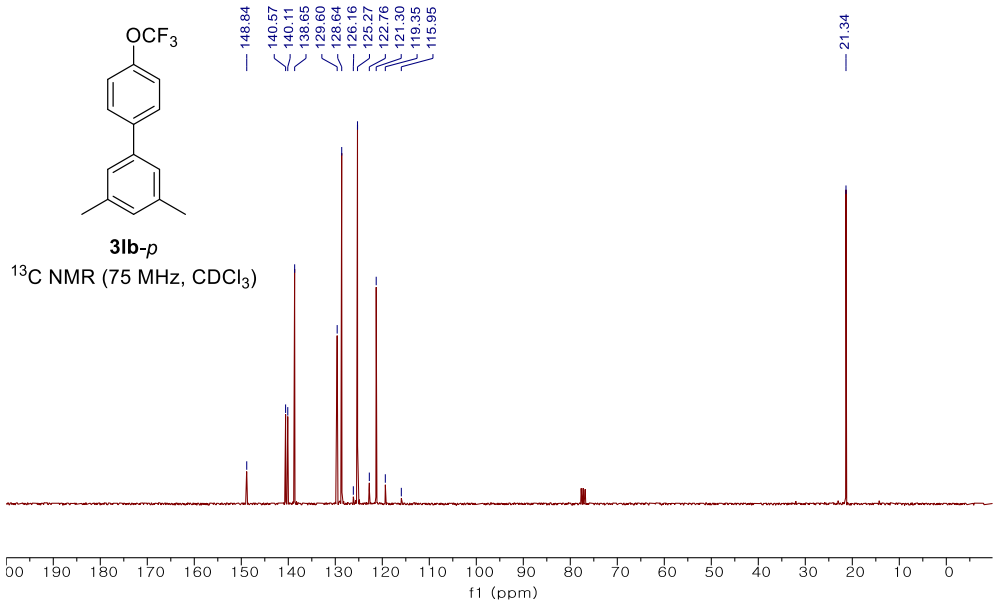

3Ib-*p*

^{13}C NMR (75 MHz, $CDCl_3$)

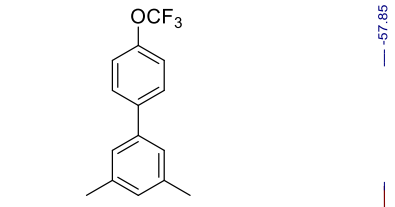

3lb-*p*

^{19}F NMR (376 MHz, $CDCl_3$)

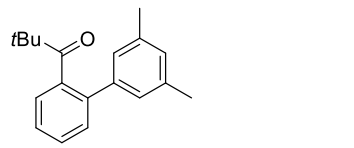

3nb-*o*

^{1}H NMR (300 MHz, $CDCl_3$)

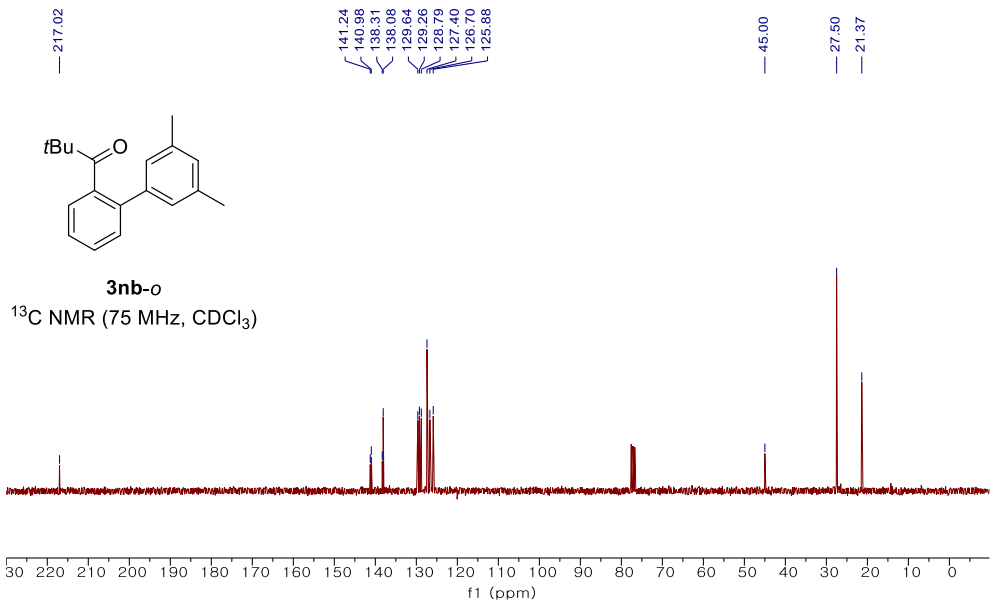

3nb-*o*

^{13}C NMR (75 MHz, $CDCl_3$)

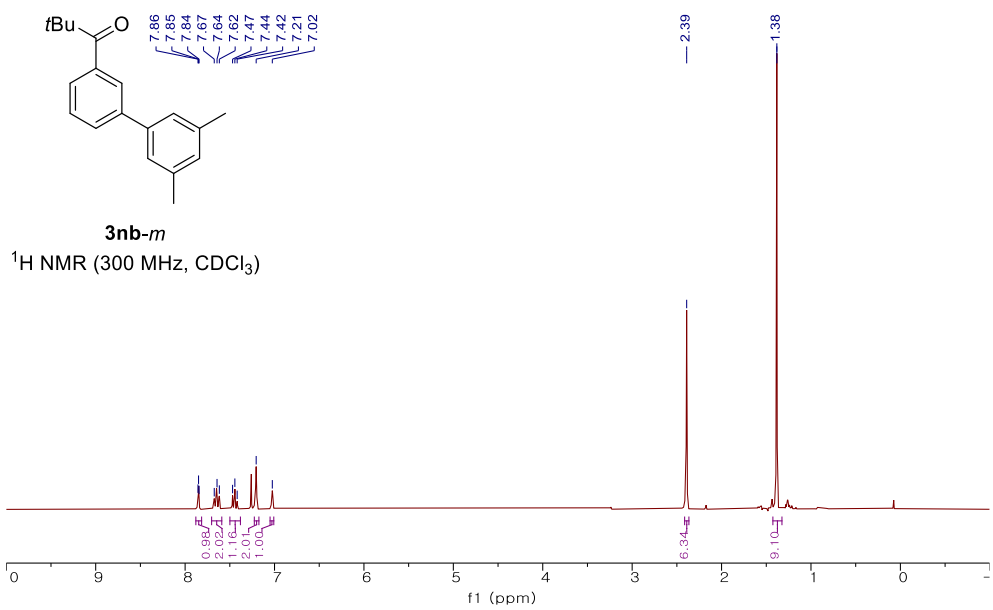

3nb-*m*

^{1}H NMR (300 MHz, $CDCl_3$)

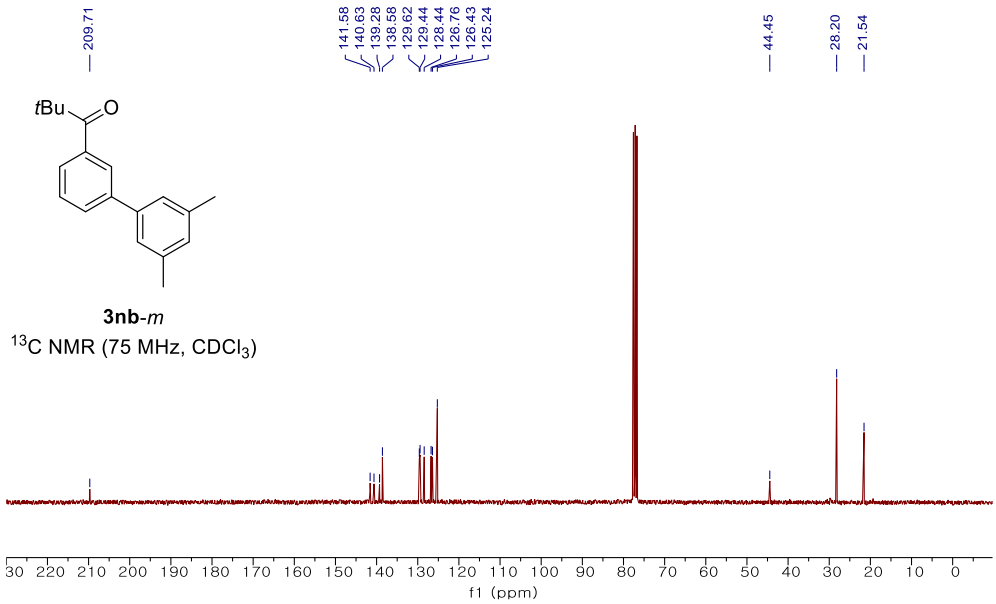

3nb-*m*

^{13}C NMR (75 MHz, $CDCl_3$)

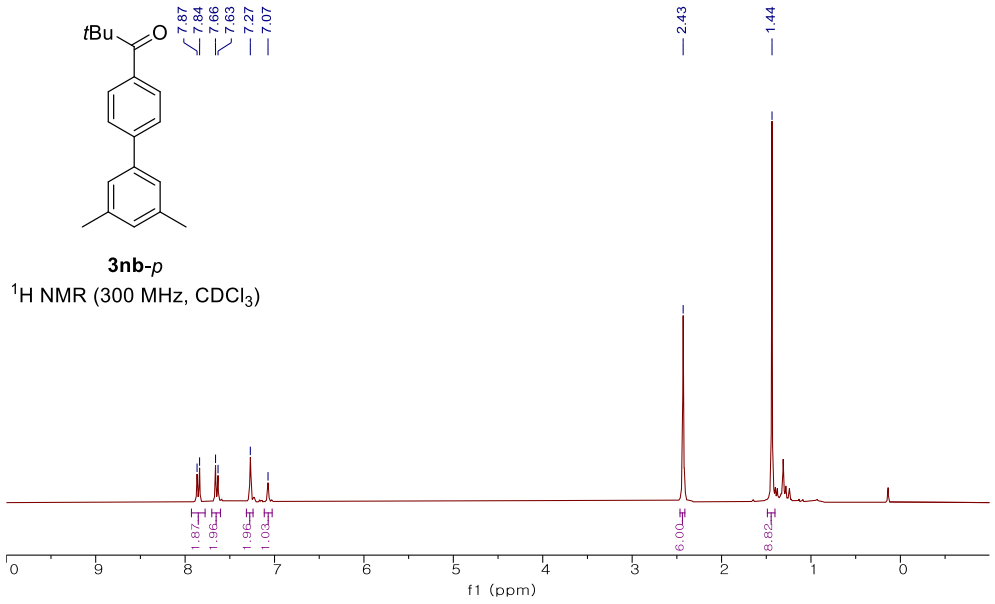

3nb-*p*

^{1}H NMR (300 MHz, $CDCl_3$)

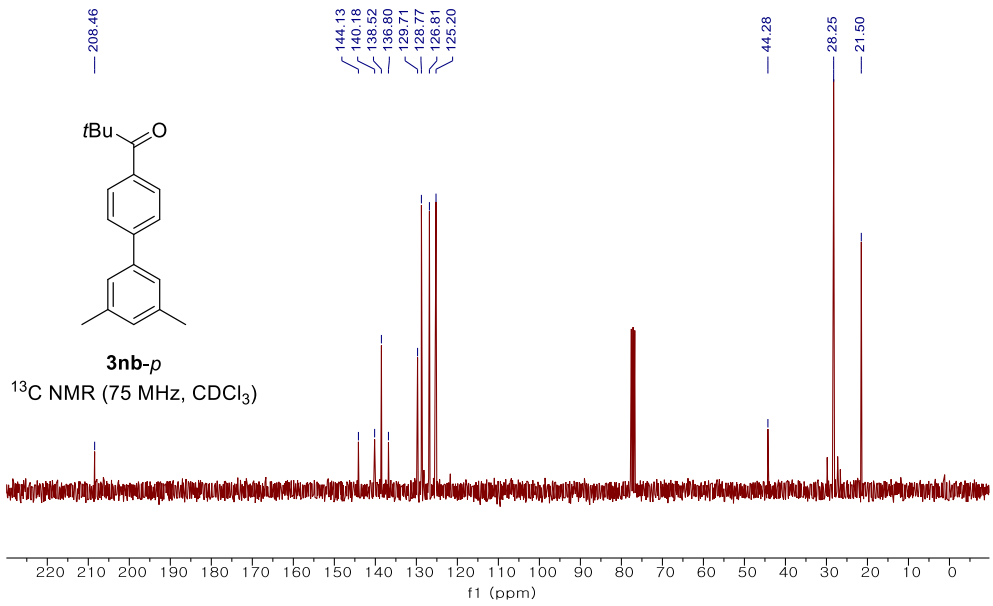

3nb-*p*

^{13}C NMR (75 MHz, $CDCl_3$)

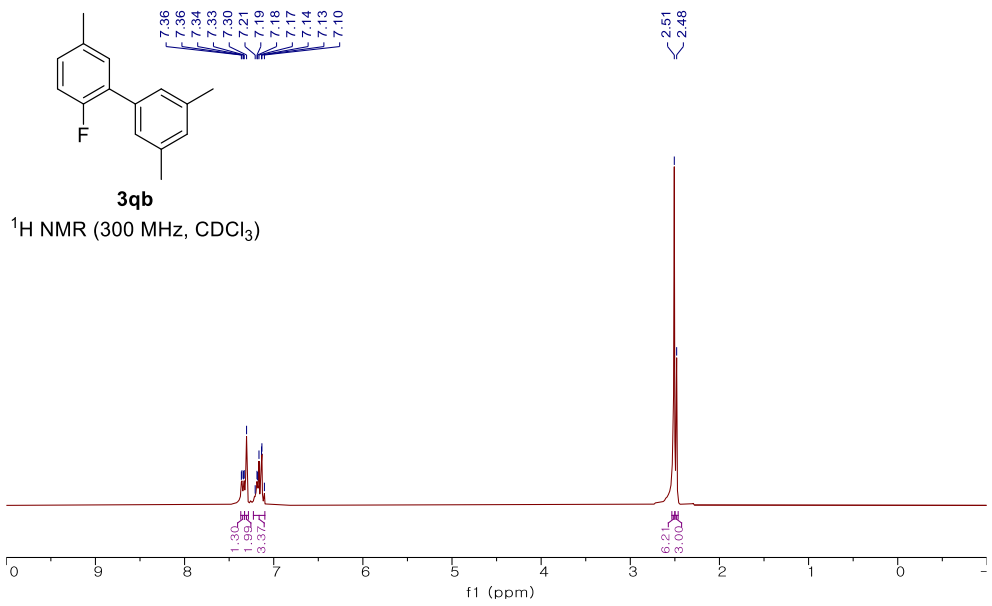

3qb

^{1}H NMR (300 MHz, $CDCl_3$)

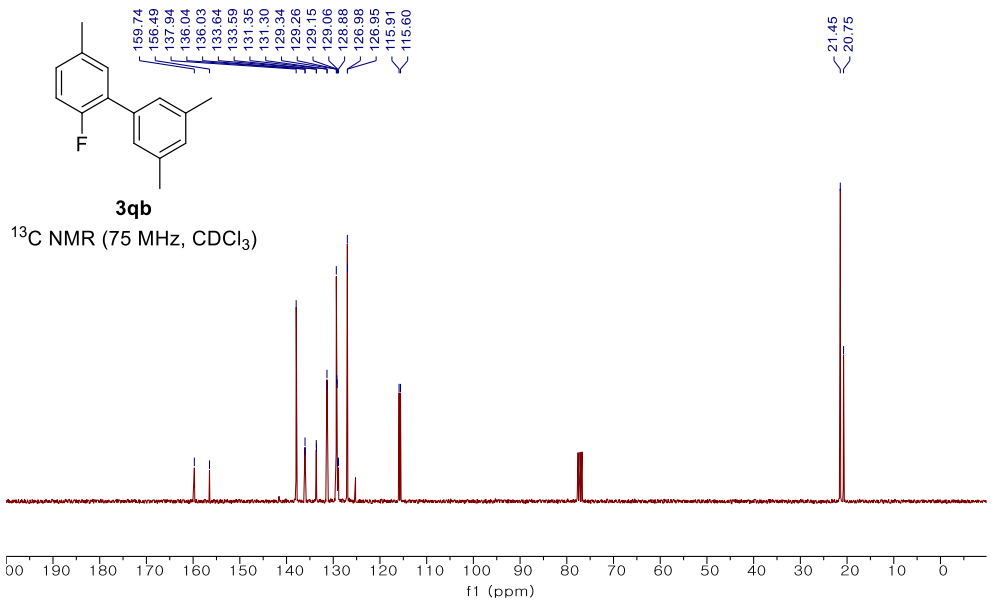

3qb

^{13}C NMR (75 MHz, $CDCl_3$)

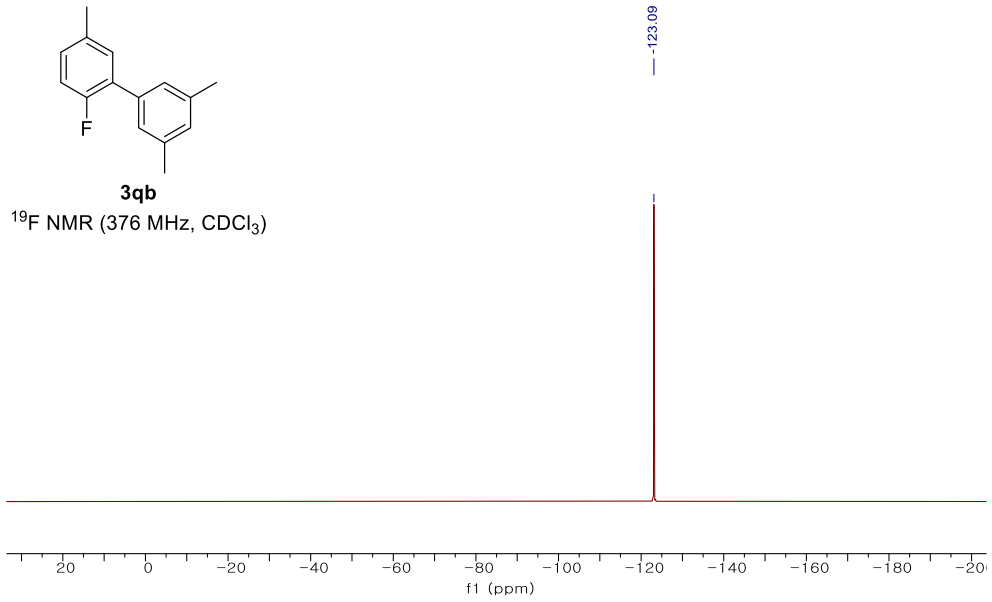

3qb

^{19}F NMR (376 MHz, $CDCl_3$)

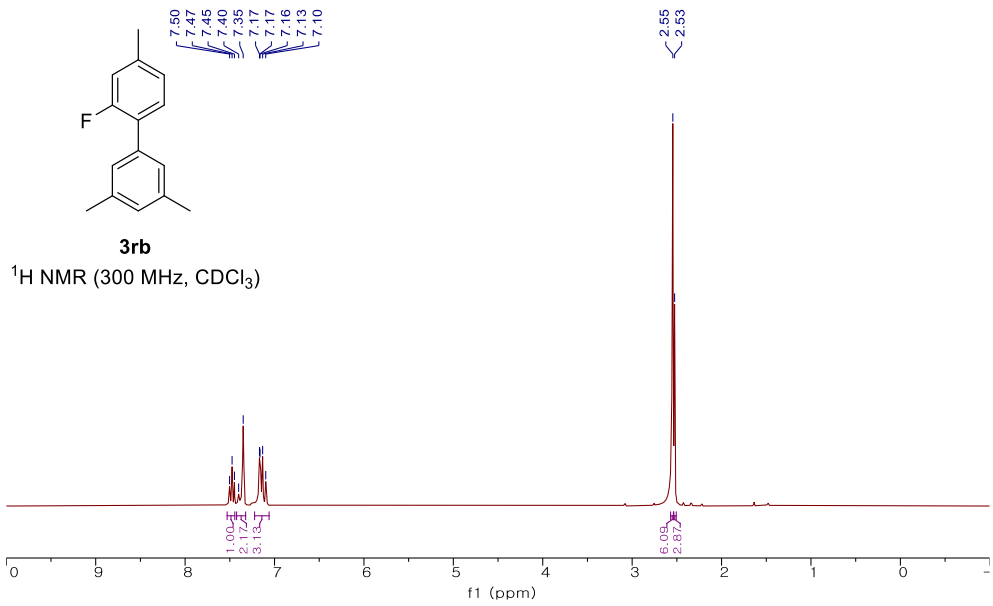

3rb

^{1}H NMR (300 MHz, $CDCl_3$)

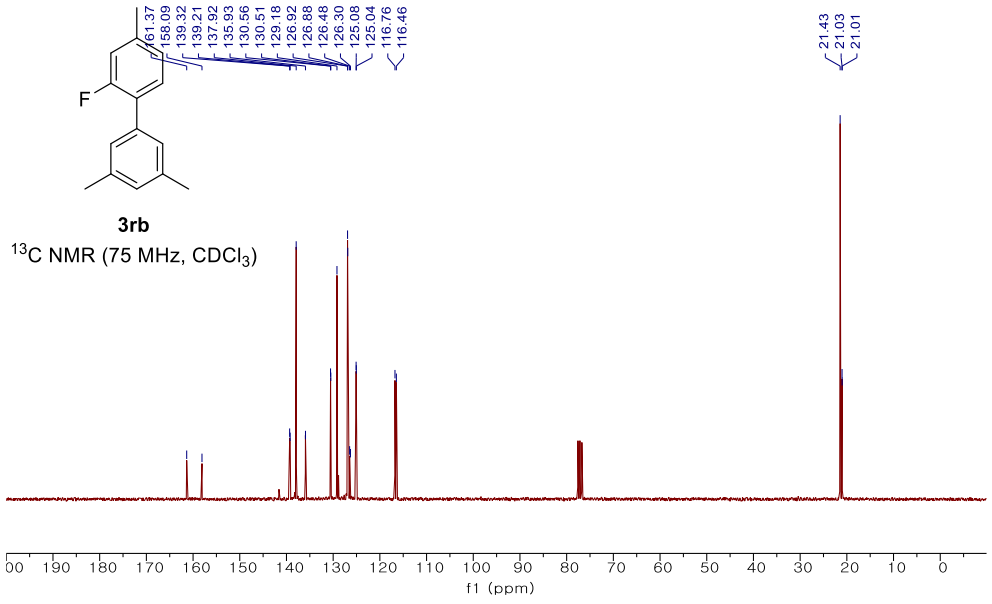

3rb

^{13}C NMR (75 MHz, $CDCl_3$)

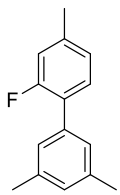

3rb

^{19}F NMR (376 MHz, $CDCl_3$)

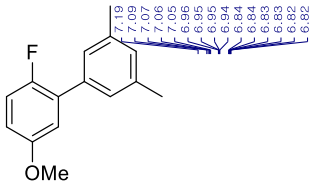

3sb

^{1}H NMR (400 MHz, $CDCl_3$)

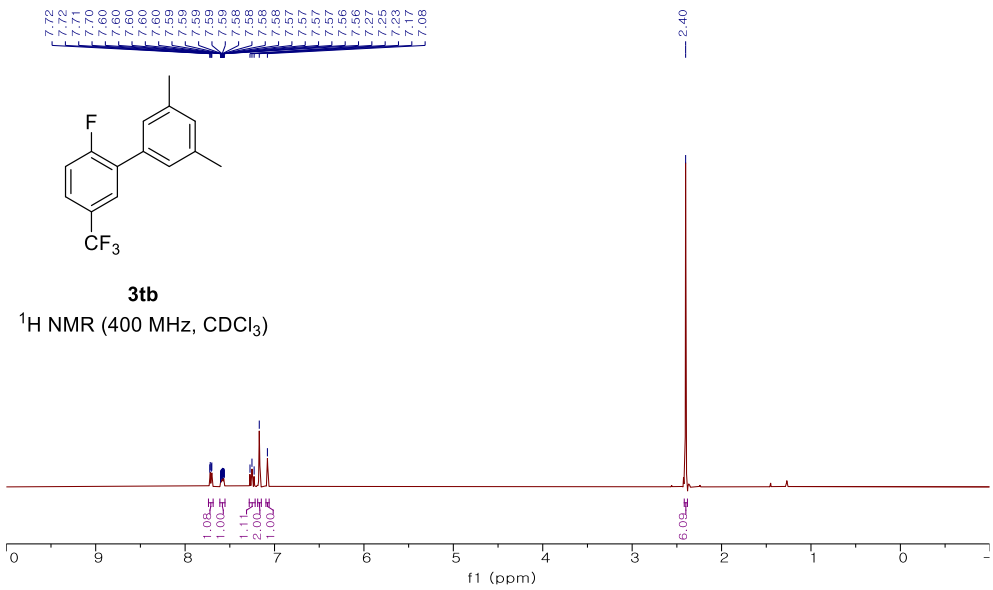

3tb

^{1}H NMR (400 MHz, $CDCl_3$)

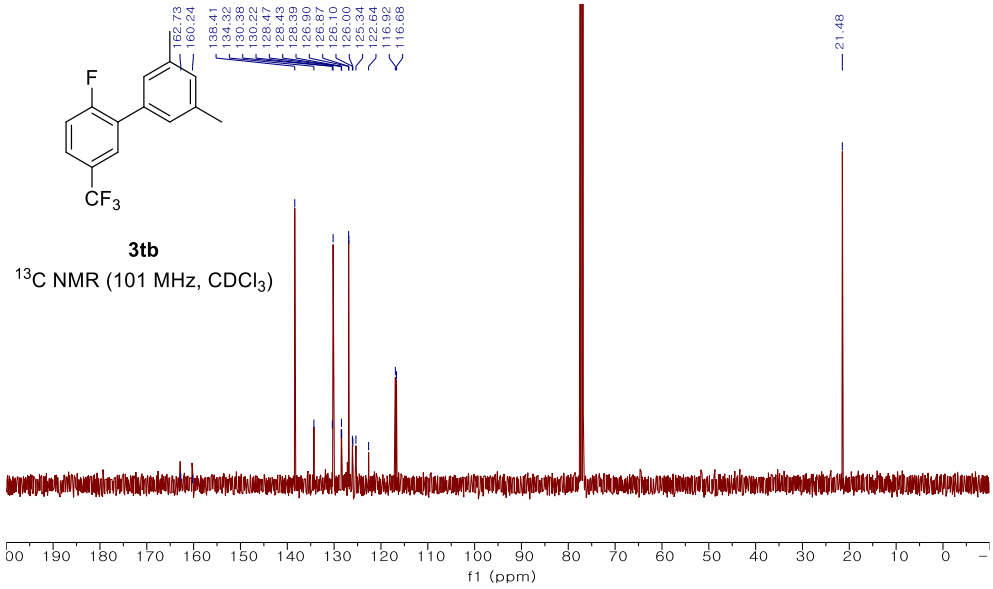

3tb

^{13}C NMR (101 MHz, $CDCl_3$)

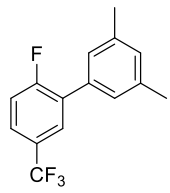

3tb

^{19}F NMR (376 MHz, $CDCl_3$)

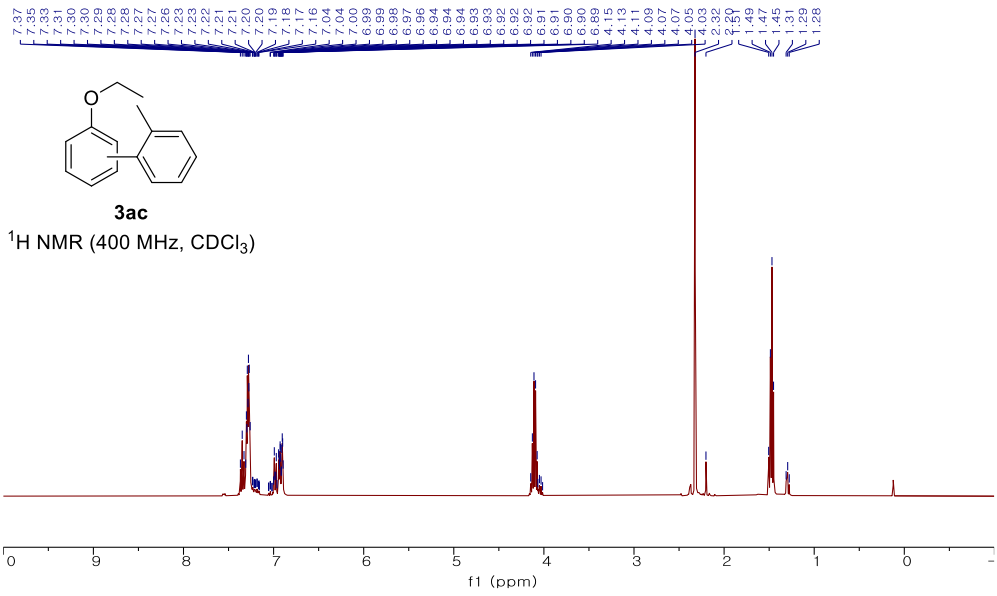

3ac

^{1}H NMR (400 MHz, $CDCl_3$)

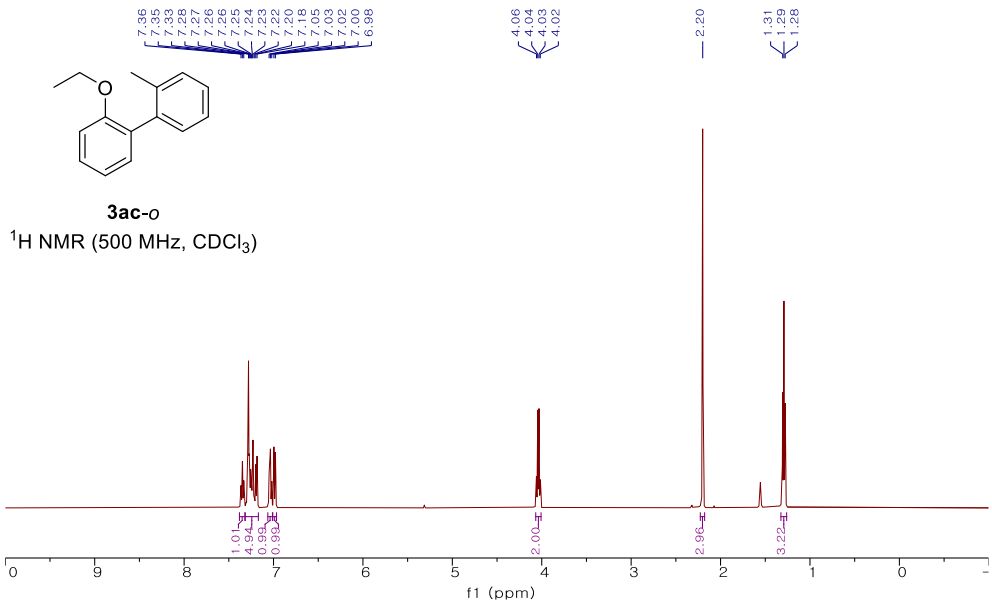

3ac-*o*

^{1}H NMR (500 MHz, $CDCl_3$)

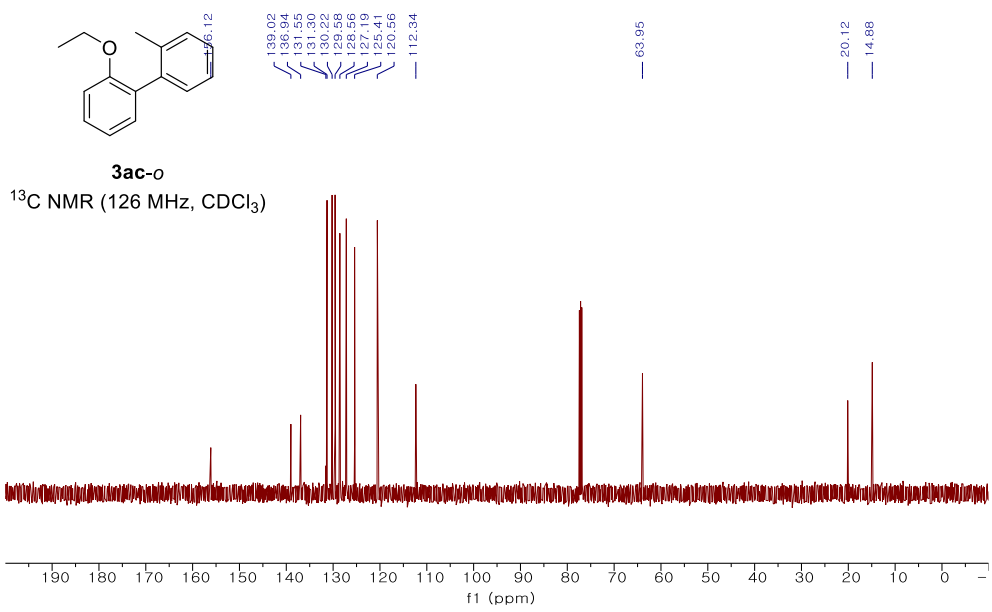

3ac-*o*

^{13}C NMR (126 MHz, $CDCl_3$)

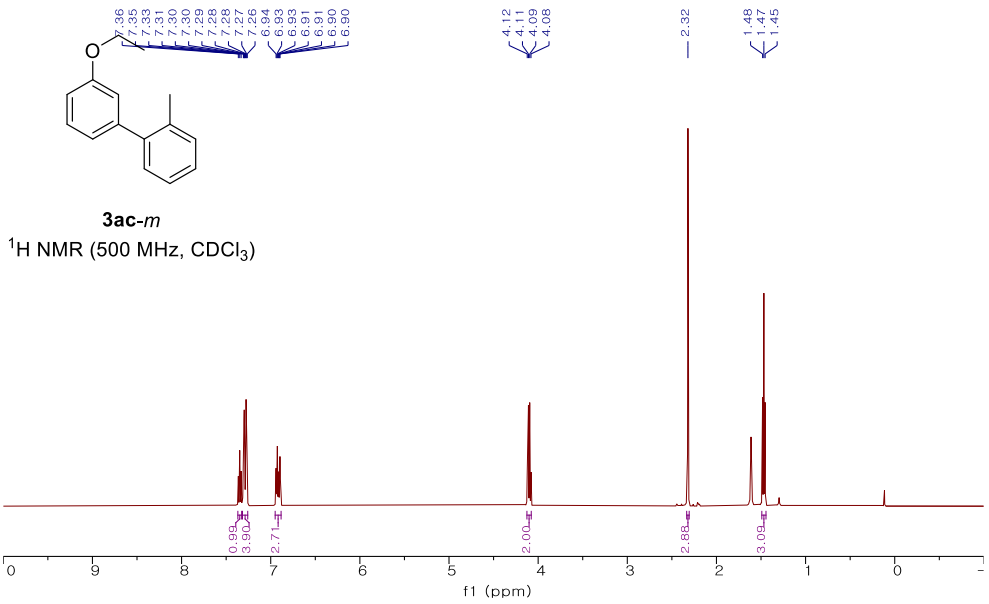

3ac-*m*

^{1}H NMR (500 MHz, $CDCl_3$)

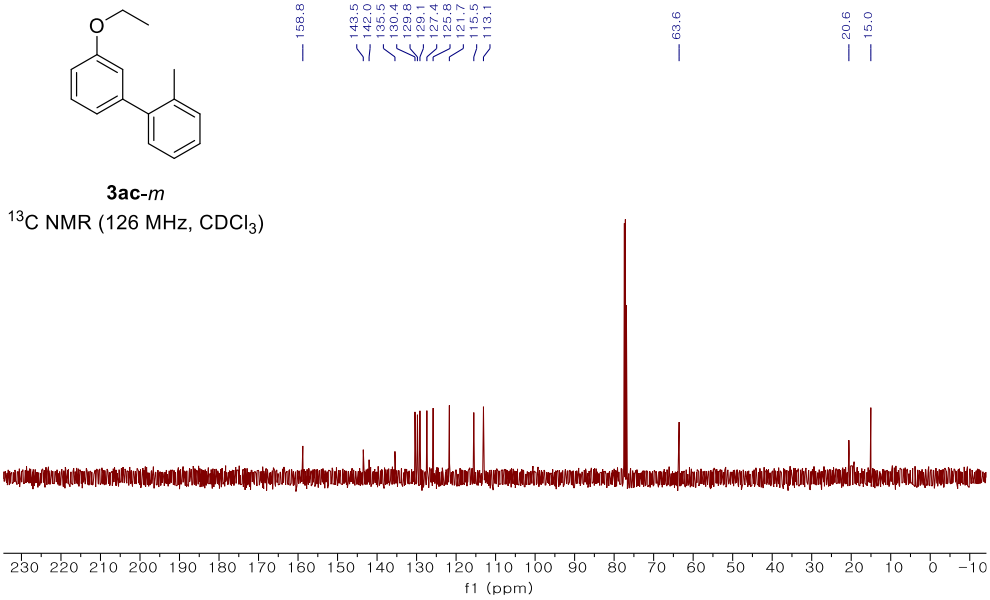

3ac-*m*

^{13}C NMR (126 MHz, $CDCl_3$)

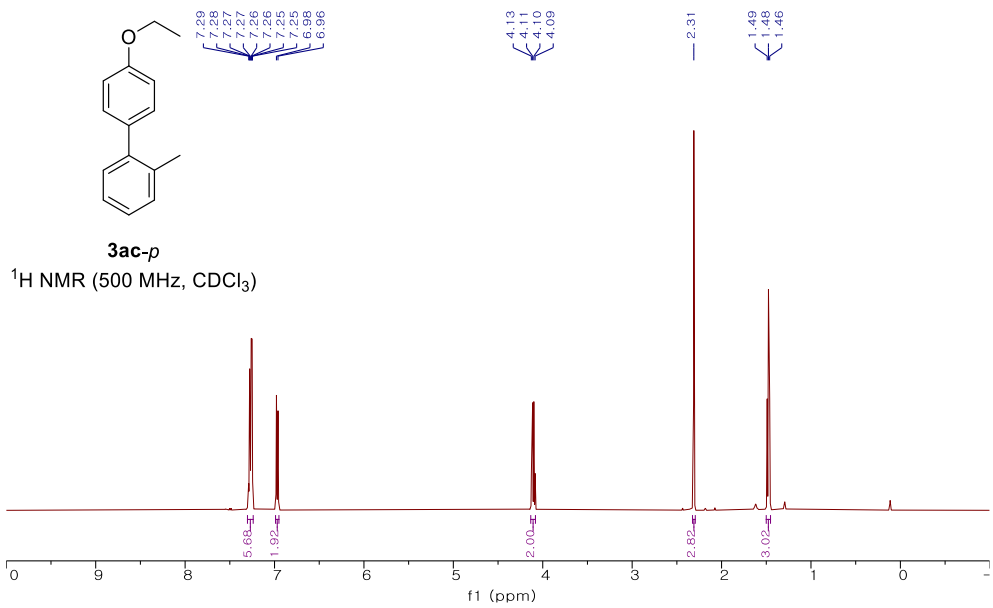

3ac-*p*

^{1}H NMR (500 MHz, $CDCl_3$)

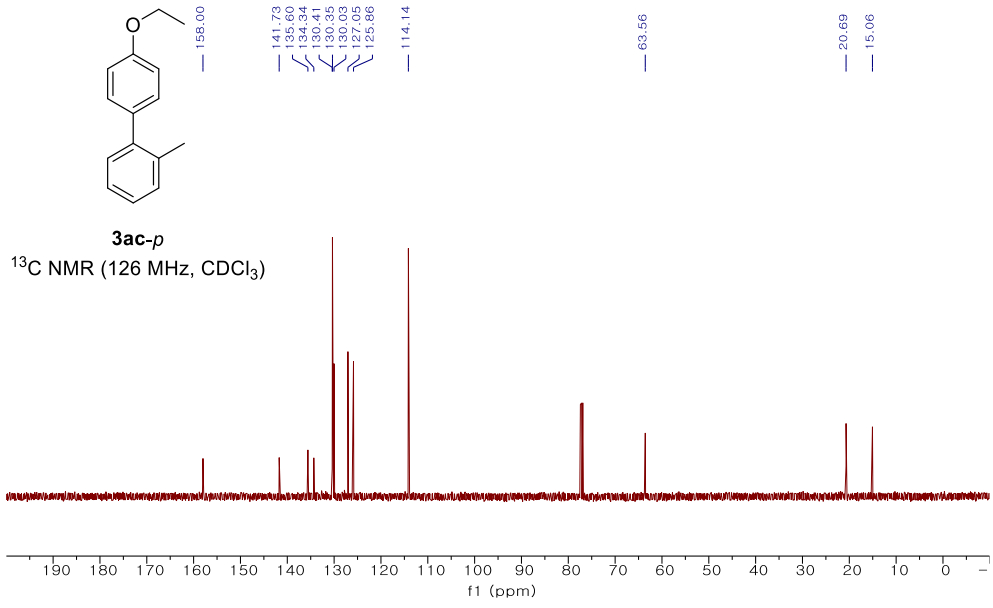

3ac-*p*

^{13}C NMR (126 MHz, $CDCl_3$)

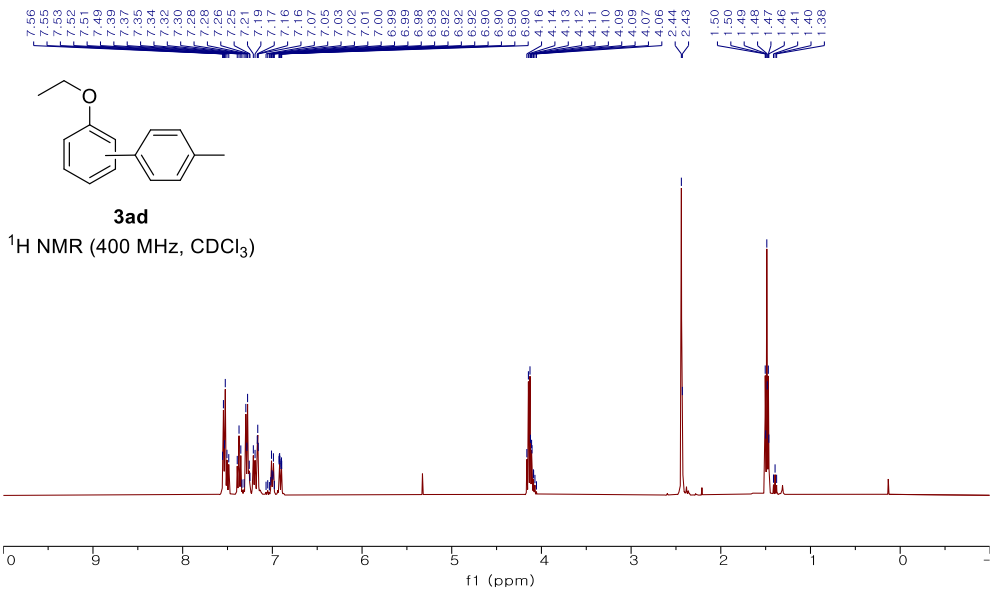
7.56 7.55 7.53 7.52 7.51 7.49 7.39 7.37 7.35 7.34 7.32 7.30 7.28 7.28 7.26 7.25 7.21 7.19 7.17 7.16 7.16 7.07 7.05 7.03 7.02 7.01 7.00 6.99 6.98 6.93 6.92 6.92 6.92 6.90 6.90 6.90 6.90 4.16 4.14 4.13 4.12 4.11 4.10 4.09 4.09 4.07 4.06 2.44 2.43 1.50 1.50 1.49 1.48 1.47 1.46 1.41 1.40 1.38
O
3ad
^{1}H NMR (400 MHz, $CDCl_3$)
0 9 8 7 6 5 4 3 2 1 0
f1 (ppm)

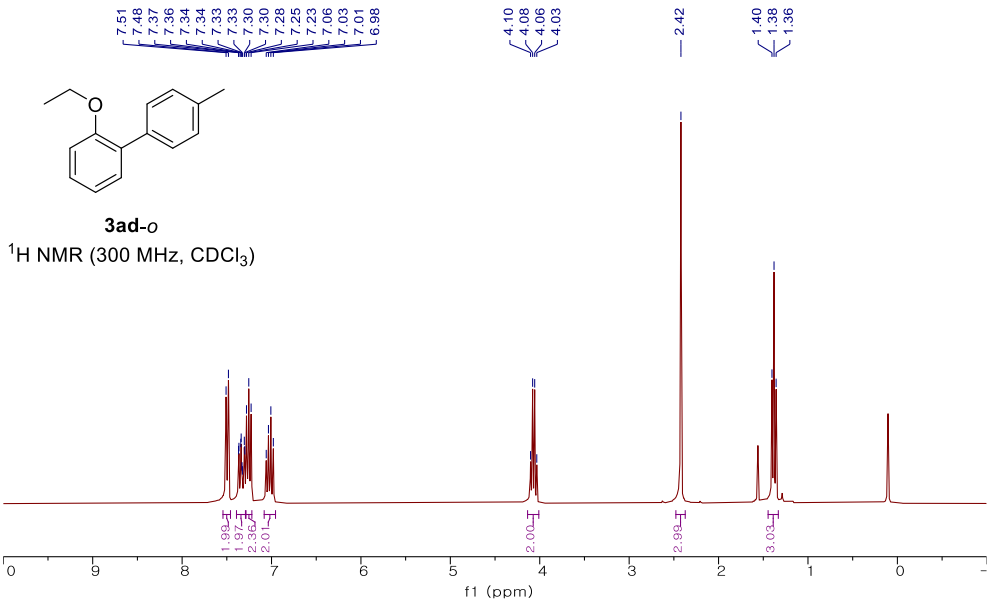
7.51 7.48 7.37 7.36 7.34 7.34 7.33 7.33 7.30 7.30 7.28 7.25 7.23 7.06 7.03 7.01 6.98 4.10 4.08 4.06 4.03 2.42 1.40 1.38 1.36
O
3ad-*o*
^{1}H NMR (300 MHz, $CDCl_3$)
1.99 1.97 2.36 2.01 2.00 2.98 3.03
0 9 8 7 6 5 4 3 2 1 0
f1 (ppm)

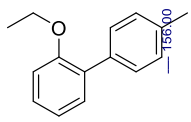

3ad-*o*

^{13}C NMR (126 MHz, $CDCl_3$)

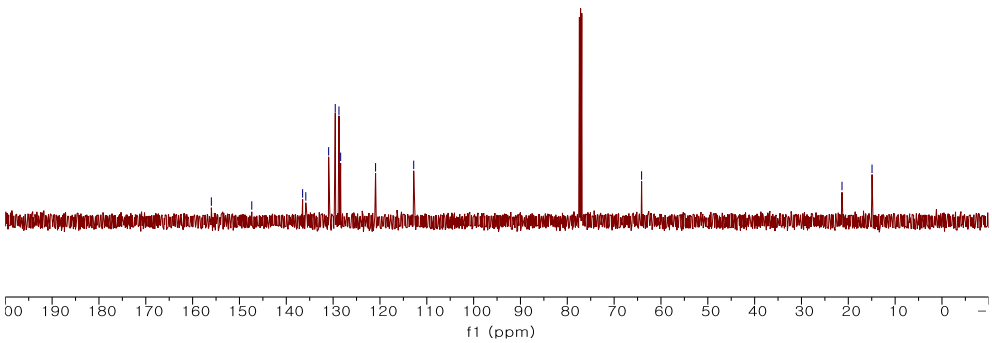

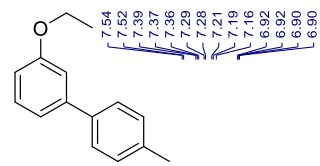

3ad-*m*

^{1}H NMR (500 MHz, $CDCl_3$)

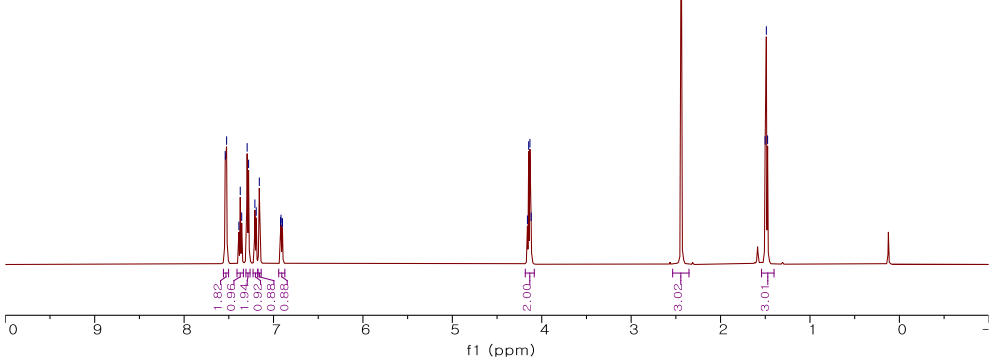

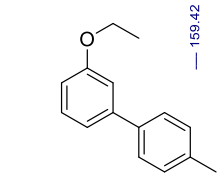

3ad-*m*

^{13}C NMR (126 MHz, $CDCl_3$)

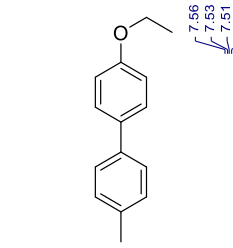

3ad-*p*

^{1}H NMR (300 MHz, $CDCl_3$)

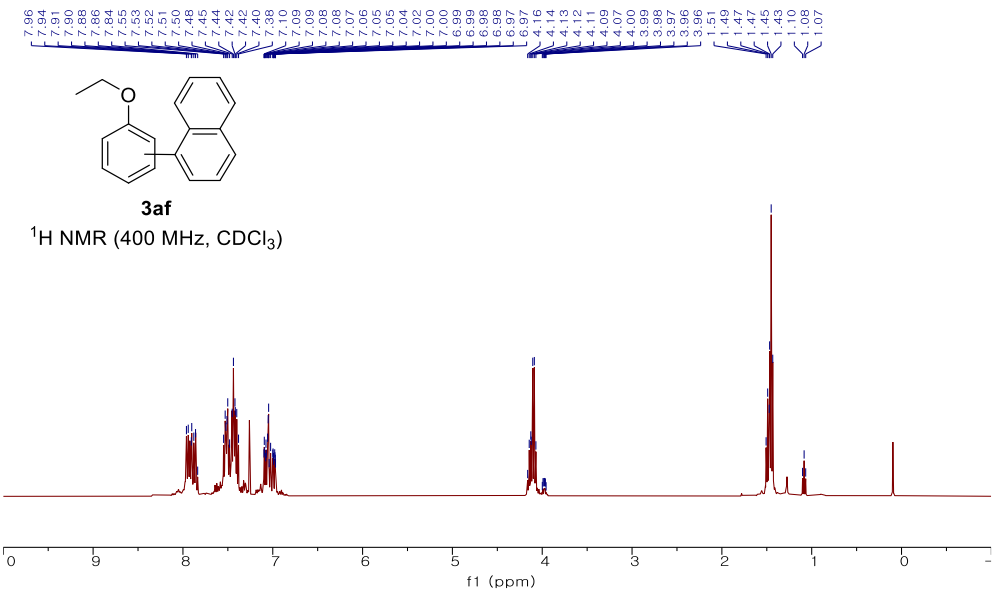

3af

^{1}H NMR (400 MHz, $CDCl_3$)

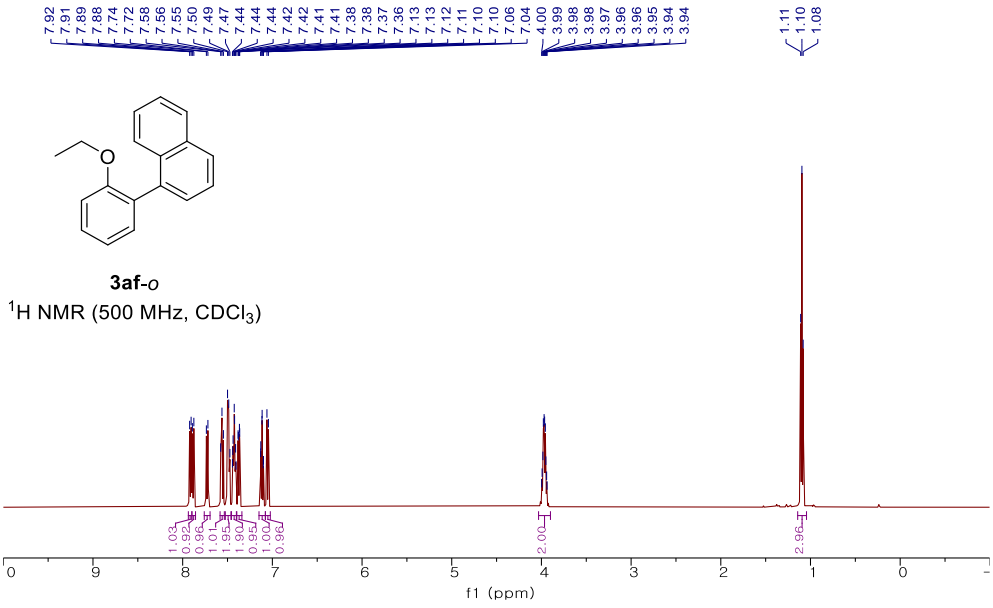

3af-*o*

^{1}H NMR (500 MHz, $CDCl_3$)

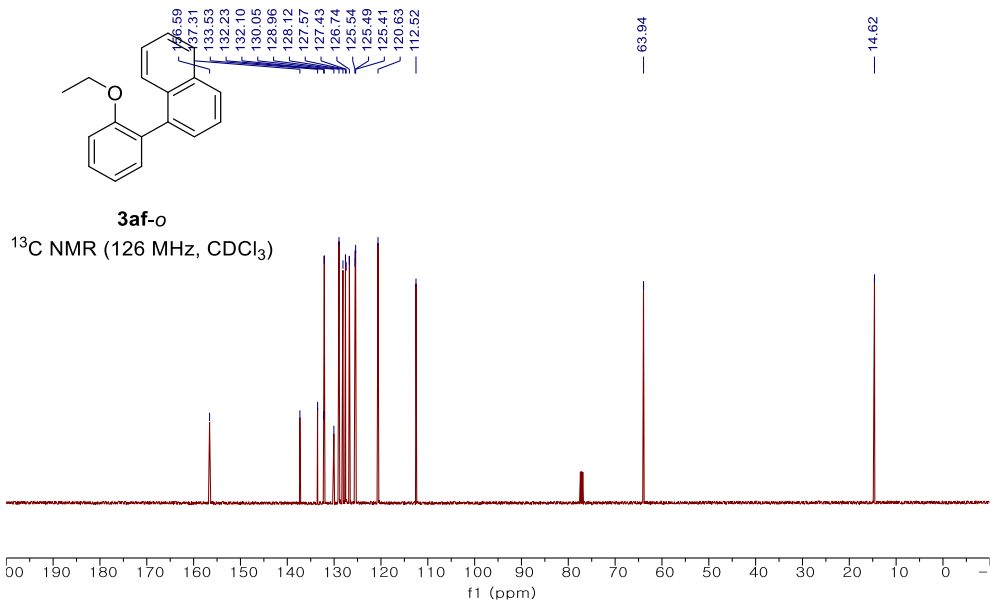
156.59
137.31
133.53
132.23
132.10
130.05
128.96
128.12
127.57
127.43
126.74
125.54
125.49
125.41
120.63
112.52
63.94
14.62
O
3af-o
13C NMR (126 MHz, CDCl3)
00 190 180 170 160 150 140 130 120 110 100 90 80 70 60 50 40 30 20 10 0
f1 (ppm)

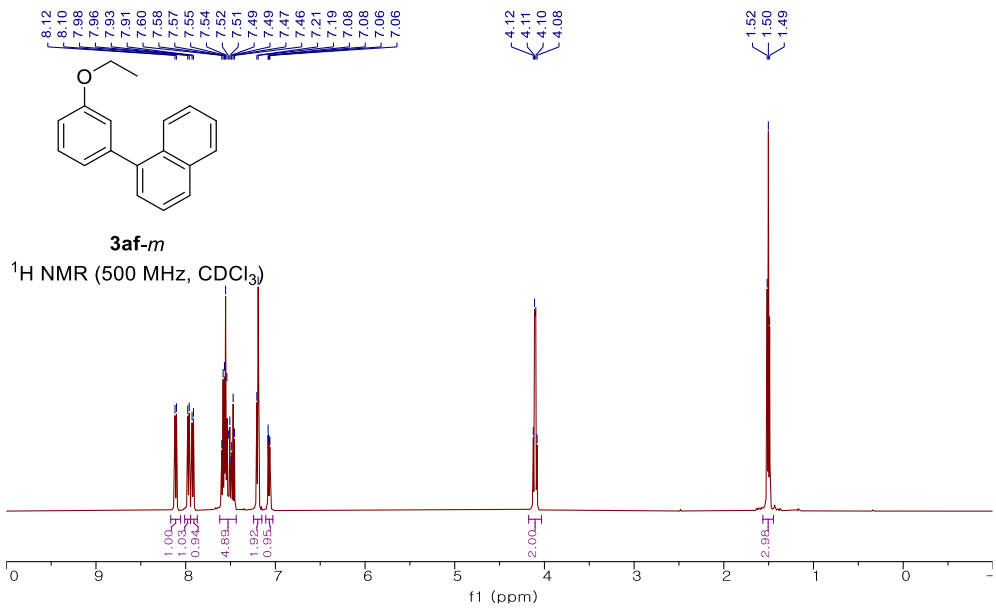
8.12
8.10
7.98
7.96
7.93
7.91
7.60
7.58
7.57
7.55
7.54
7.52
7.51
7.49
7.49
7.47
7.46
7.21
7.19
7.08
7.08
7.06
7.06
4.12
4.11
4.10
4.08
1.52
1.50
1.49
O
3af-m
1H NMR (500 MHz, CDCl3)
1.00
1.03
0.94
4.89
1.92
0.95
2.00
2.98
0 9 8 7 6 5 4 3 2 1 0
f1 (ppm)

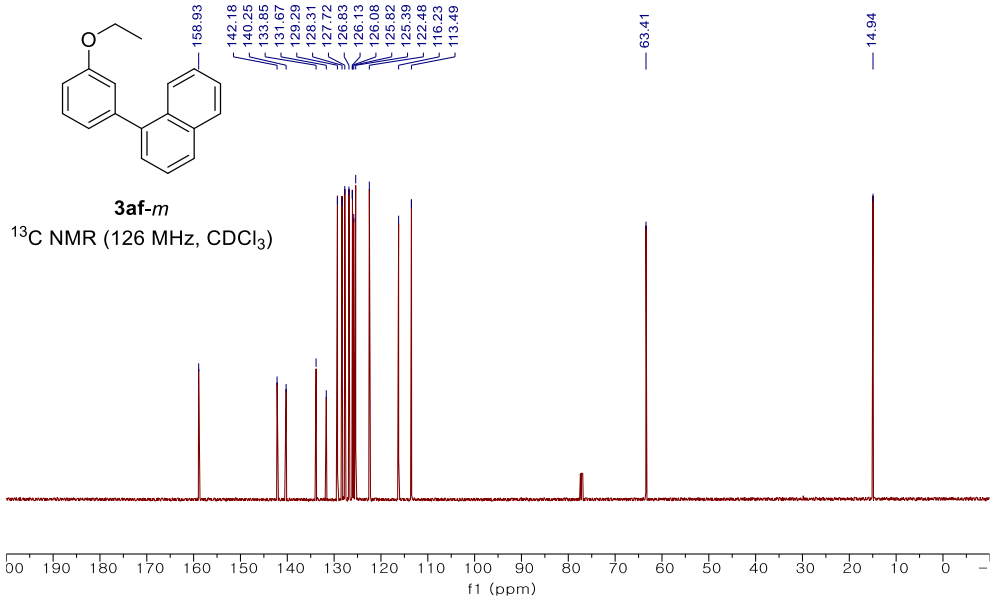

3af-*m*

^{13}C NMR (126 MHz, $CDCl_3$)

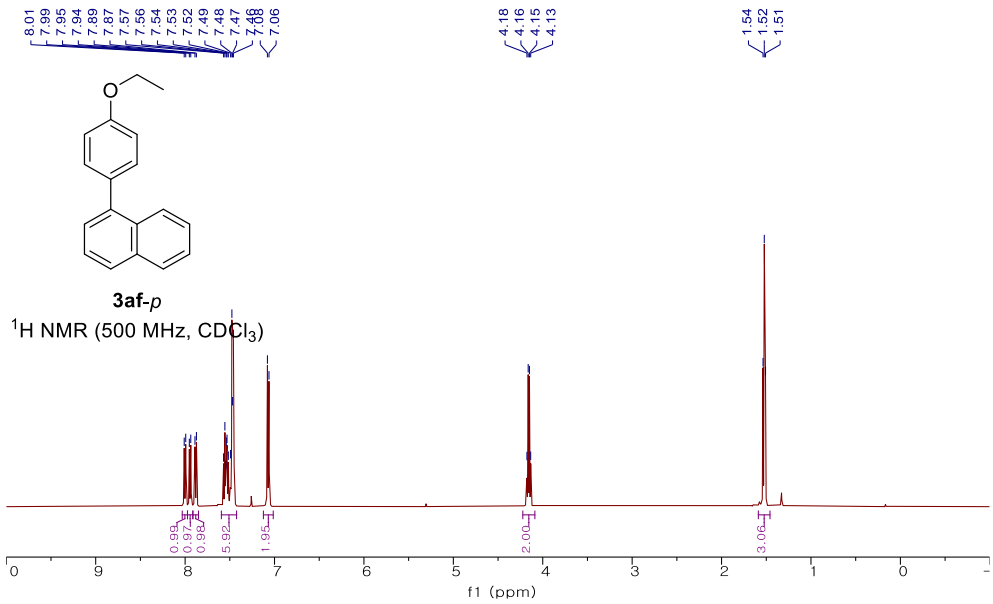

3af-*p*

^{1}H NMR (500 MHz, $CDCl_3$)

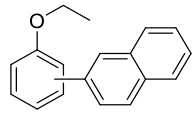

3ag

^{1}H NMR (300 MHz, $CDCl_3$)

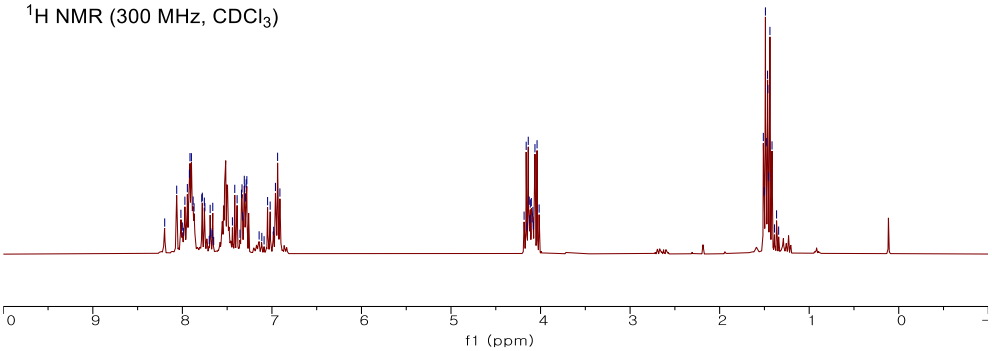

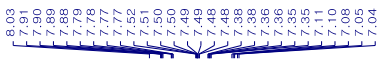

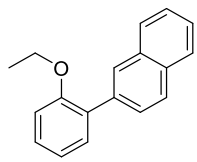

3ag-*o*

^{1}H NMR (300 MHz, $CDCl_3$)

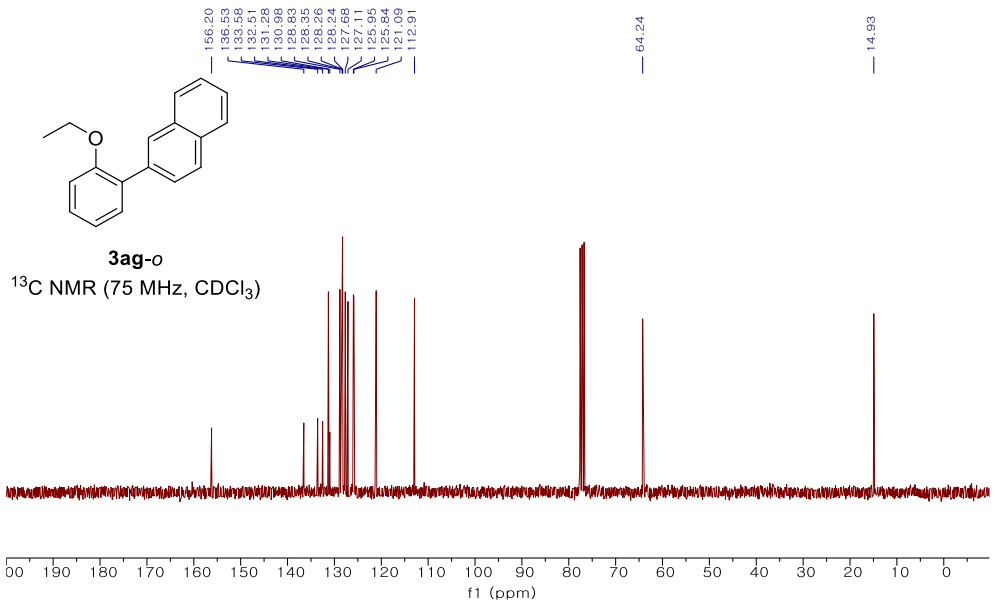

3ag-*o*

^{13}C NMR (75 MHz, $CDCl_3$)

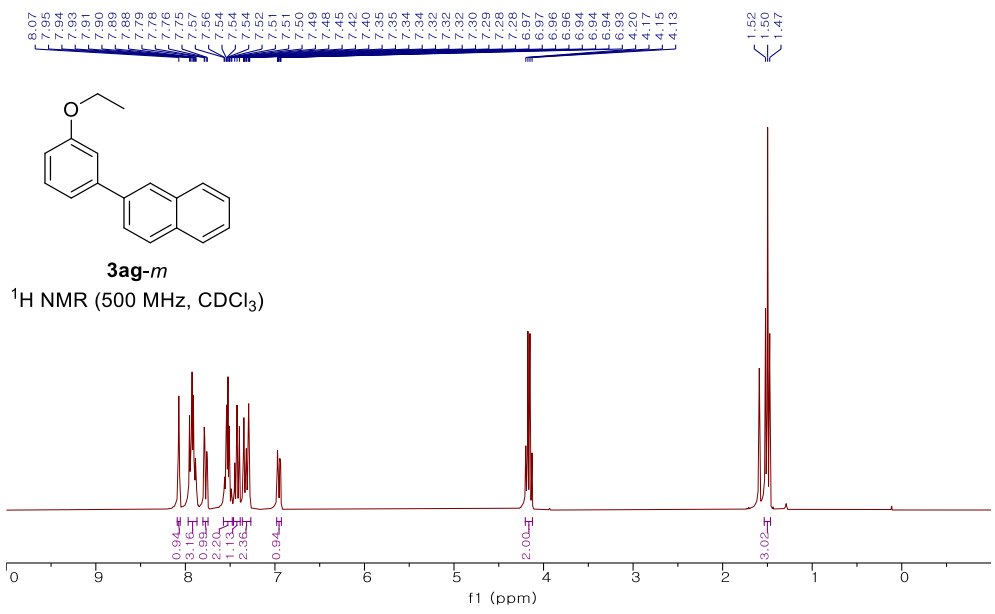

3ag-*m*

^{1}H NMR (500 MHz, $CDCl_3$)

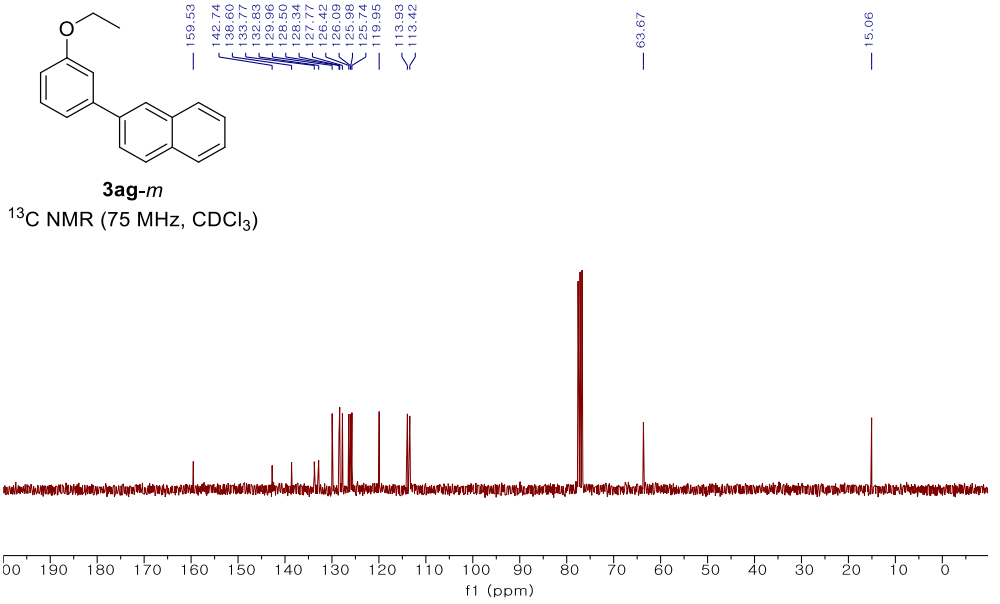

3ag-*m*

^{13}C NMR (75 MHz, $CDCl_3$)

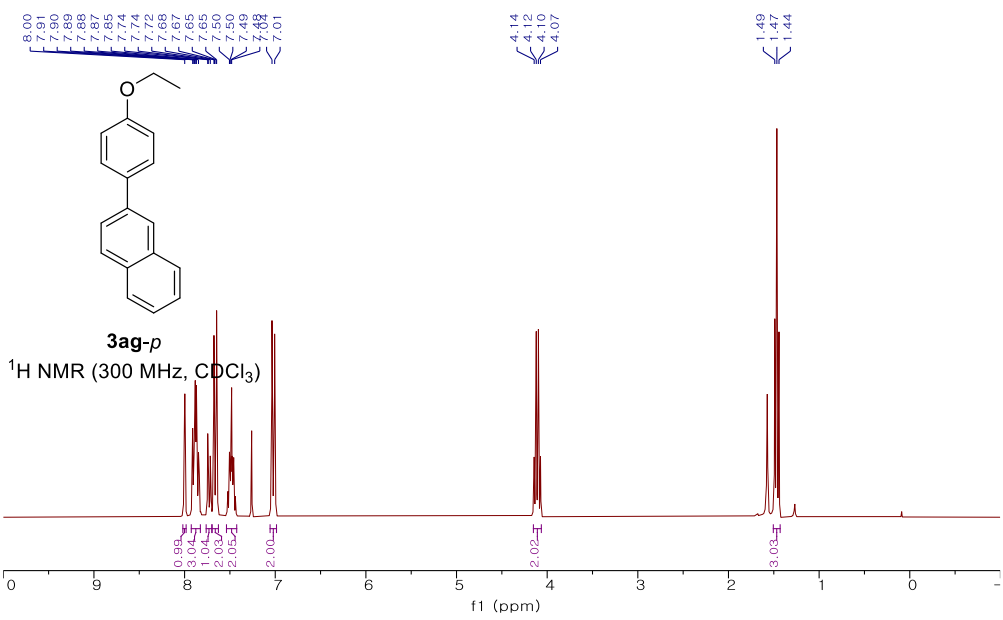

3ag-*p*

^{1}H NMR (300 MHz, $CDCl_3$)

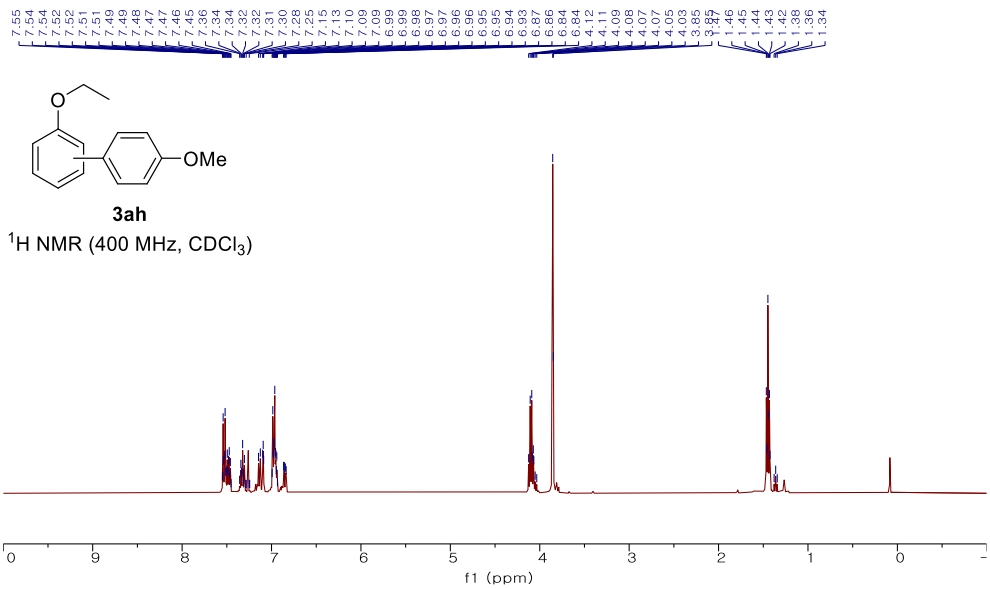
7.55 7.54 7.54 7.52 7.52 7.51 7.51 7.49 7.49 7.48 7.47 7.47 7.46 7.45 7.36 7.34 7.34 7.32 7.31 7.30 7.28 7.25 7.15 7.13 7.10 7.09 7.09 6.99 6.99 6.98 6.97 6.97 6.96 6.96 6.96 6.95 6.95 6.94 6.93 6.87 6.86 6.84 6.84 4.12 4.11 4.09 4.08 4.07 4.07 4.05 4.03 3.85 3.85 1.47 1.46 1.45 1.44 1.43 1.42 1.38 1.36 1.34
O
OMe
3ah
1H NMR (400 MHz, CDCl3)
0 9 8 7 6 5 4 3 2 1 0
f1 (ppm)

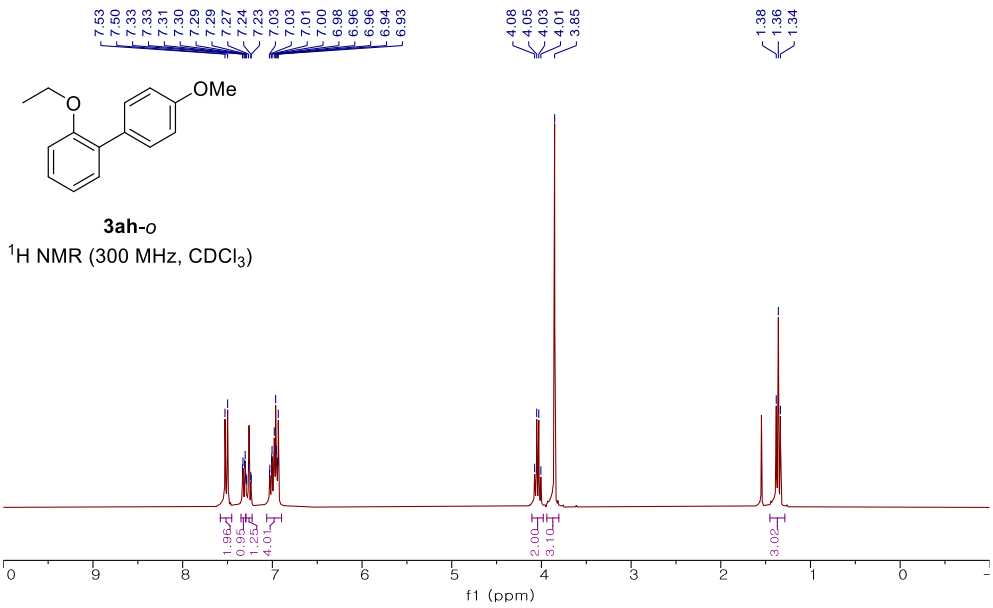
7.53 7.50 7.33 7.33 7.31 7.30 7.29 7.29 7.27 7.24 7.23 7.03 7.03 7.01 7.00 6.98 6.96 6.96 6.94 6.93 4.08 4.05 4.03 4.01 3.85 1.38 1.36 1.34
O
OMe
3ah-o
1H NMR (300 MHz, CDCl3)
1.96 0.96 1.25 4.01 2.00 3.10 3.02
0 9 8 7 6 5 4 3 2 1 0
f1 (ppm)

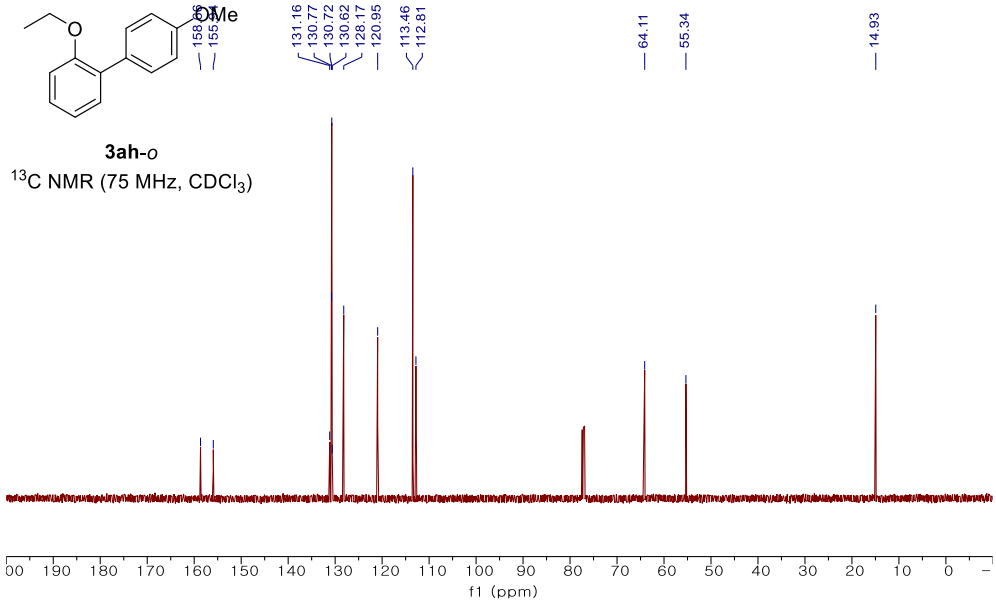

3ah-*o*

^{13}C NMR (75 MHz, $CDCl_3$)

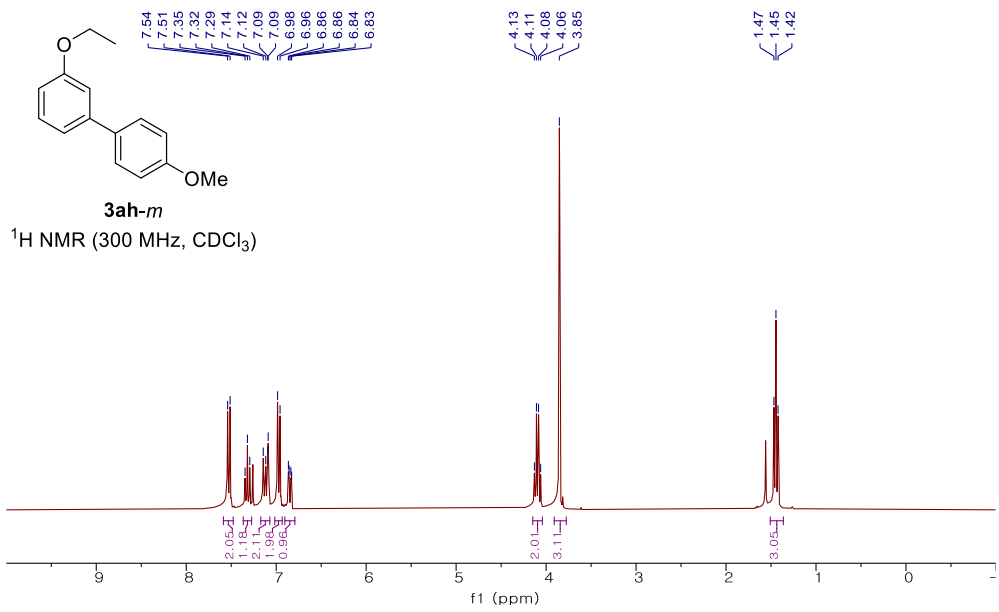

3ah-*m*

^{1}H NMR (300 MHz, $CDCl_3$)

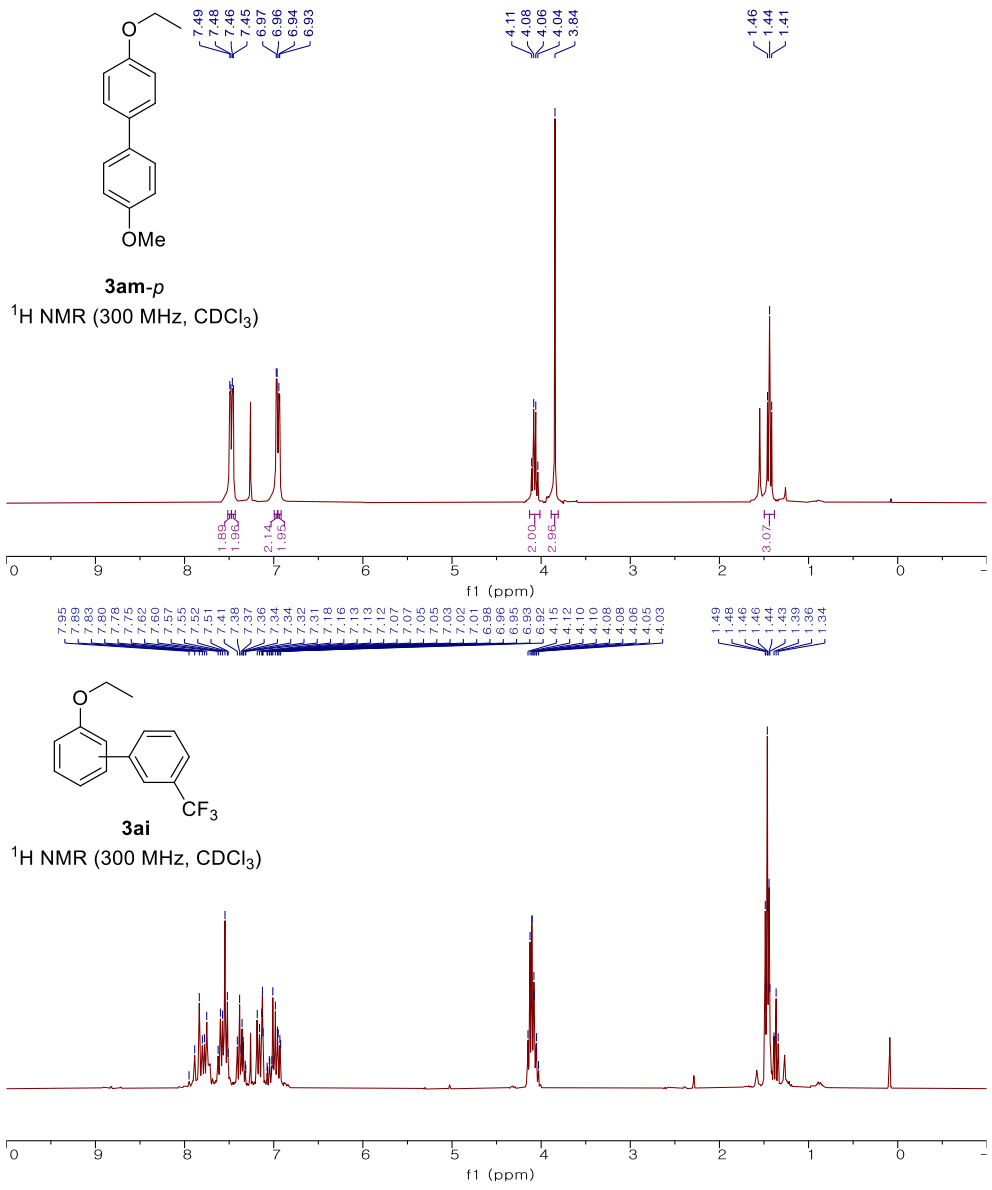

3am-*p*

^{1}H NMR (300 MHz, $CDCl_3$)

3ai

^{1}H NMR (300 MHz, $CDCl_3$)

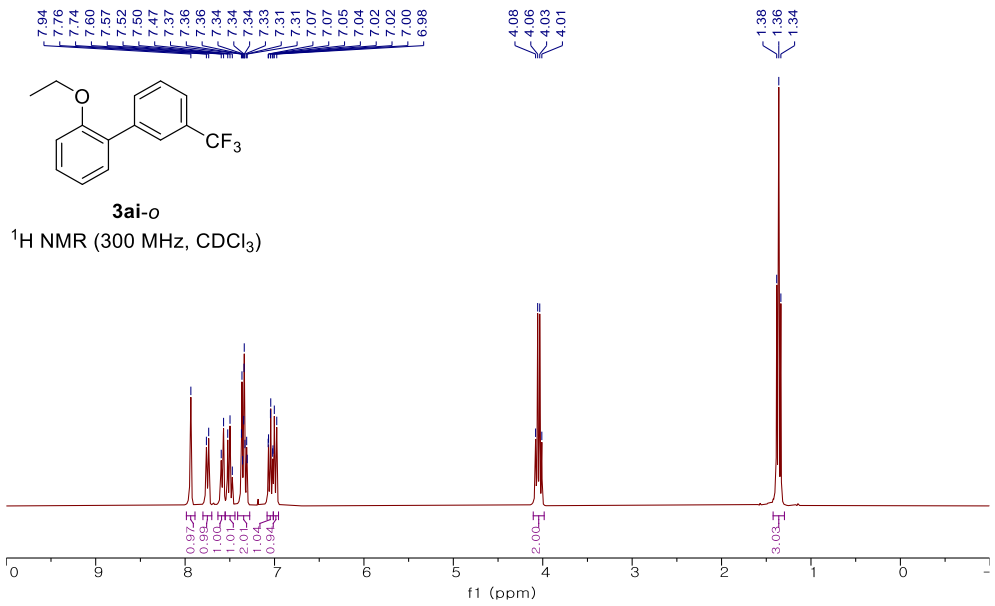

3ai-*o*

^{1}H NMR (300 MHz, $CDCl_3$)

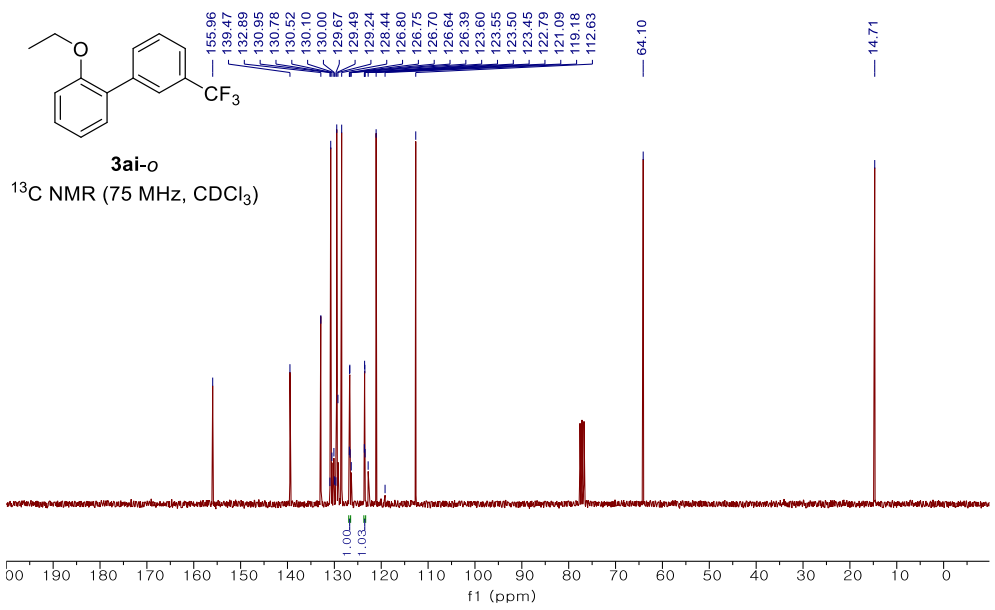

3ai-*o*

^{13}C NMR (75 MHz, $CDCl_3$)

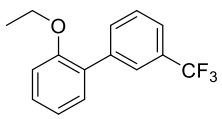

3ai-*o*

^{19}F NMR (376 MHz, $CDCl_3$)

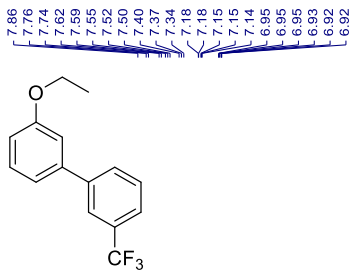

3ai-*m*

^{1}H NMR (300 MHz, $CDCl_3$)

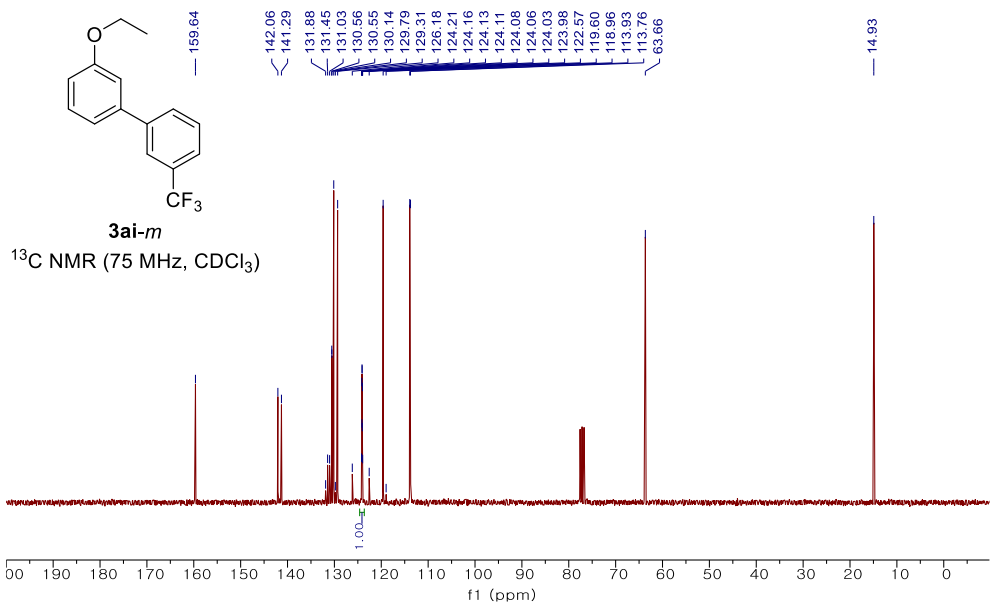

3ai-*m*

^{13}C NMR (75 MHz, $CDCl_3$)

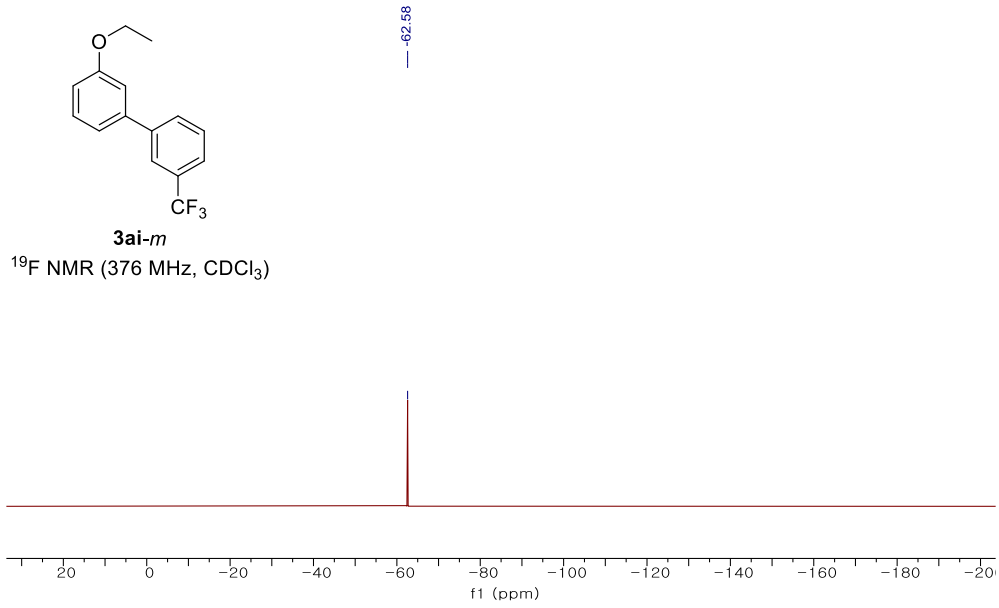

3ai-*m*

^{19}F NMR (376 MHz, $CDCl_3$)

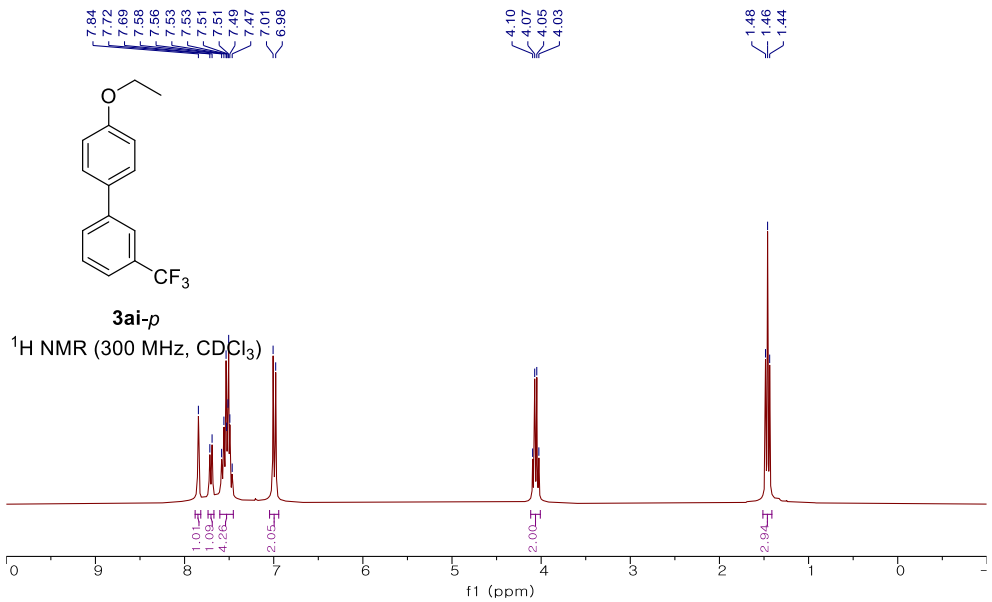

3ai-*p*

^{1}H NMR (300 MHz, $CDCl_3$)

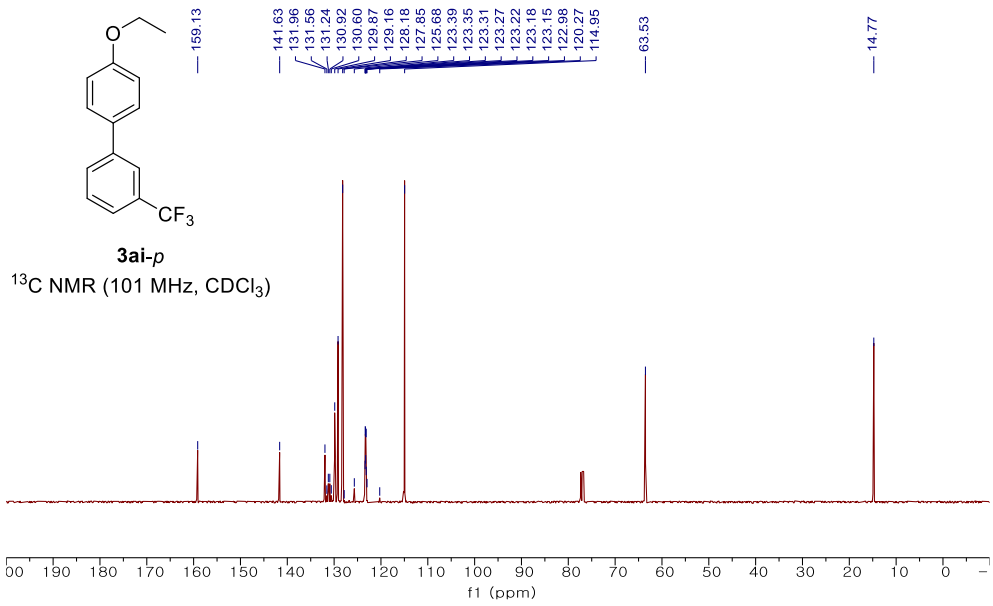

3ai-*p*

^{13}C NMR (101 MHz, $CDCl_3$)

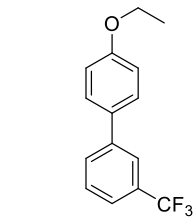

3ai-*p*

^{19}F NMR (376 MHz, $CDCl_3$)

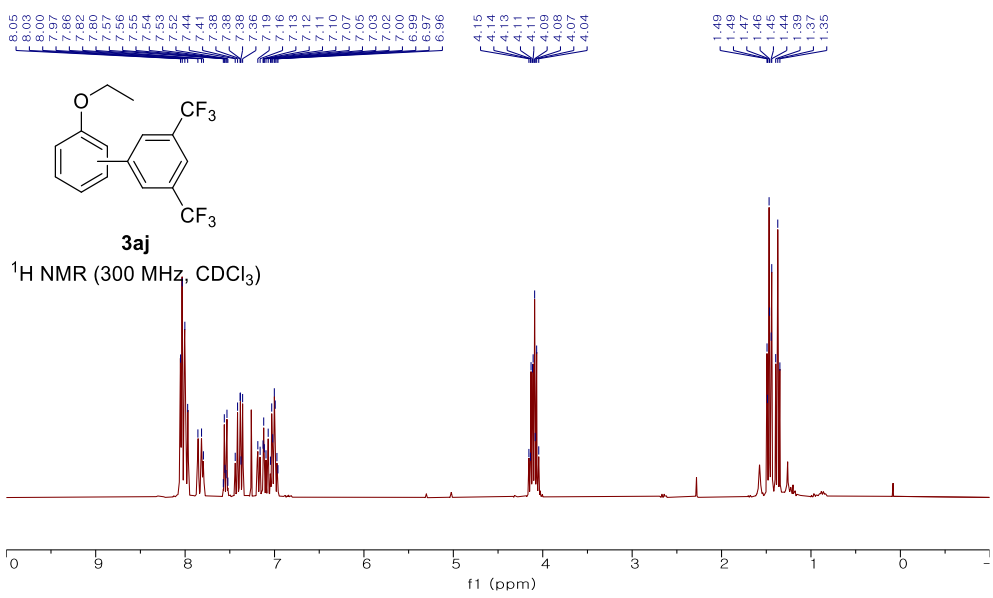

3aj

^{1}H NMR (300 MHz, $CDCl_3$)

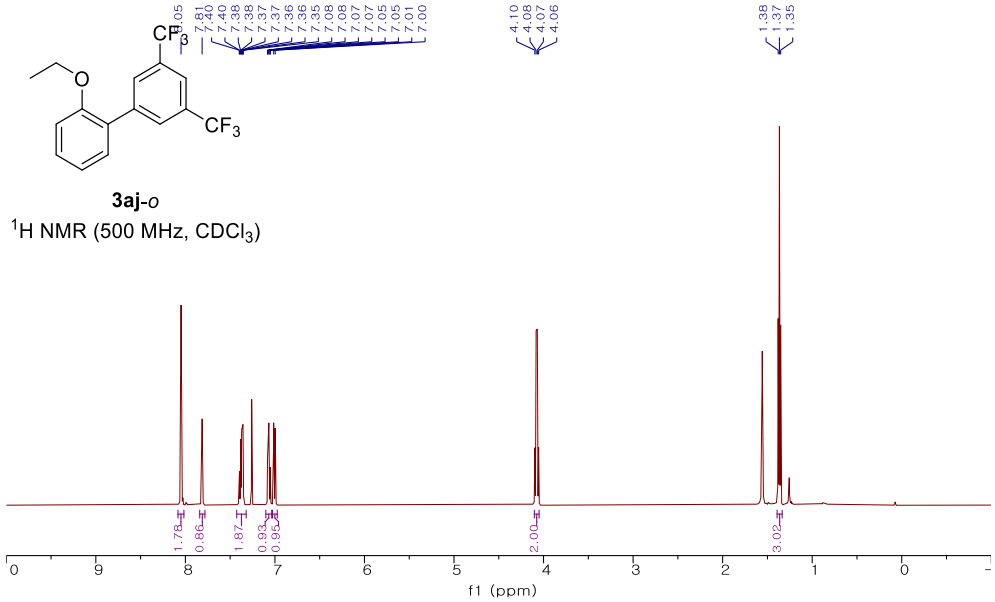

3aj-*o*

^{1}H NMR (500 MHz, $CDCl_3$)

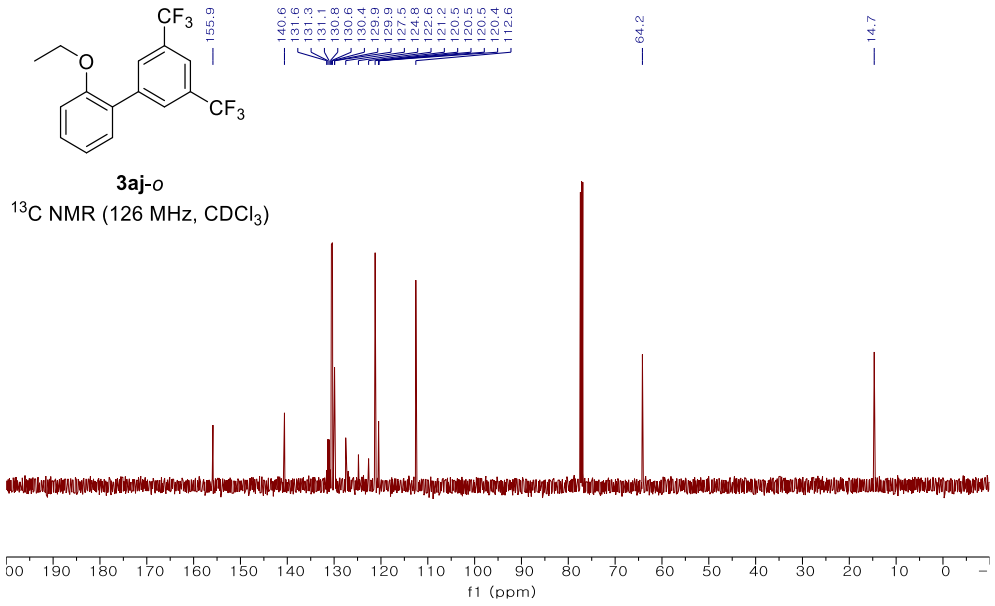

3aj-*o*

^{13}C NMR (126 MHz, $CDCl_3$)

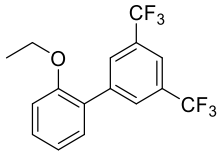

3aj-*o*

^{19}F NMR (376 MHz, $CDCl_3$)

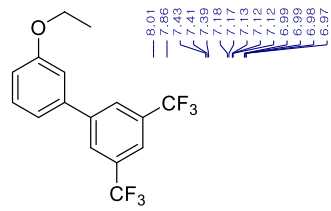

3aj-*m*

^{1}H NMR (500 MHz, $CDCl_3$)

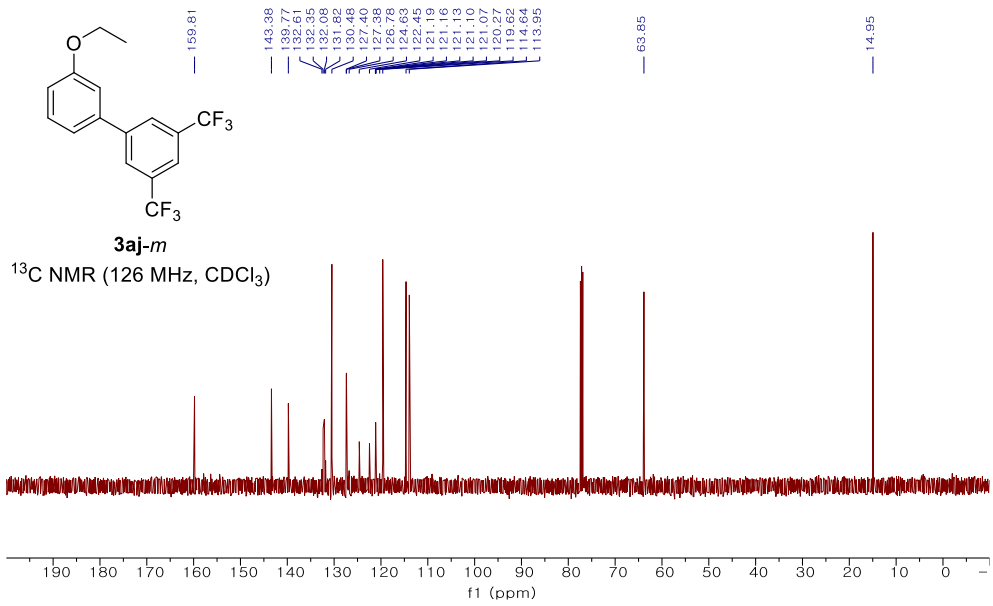

3aj-*m*

^{13}C NMR (126 MHz, $CDCl_3$)

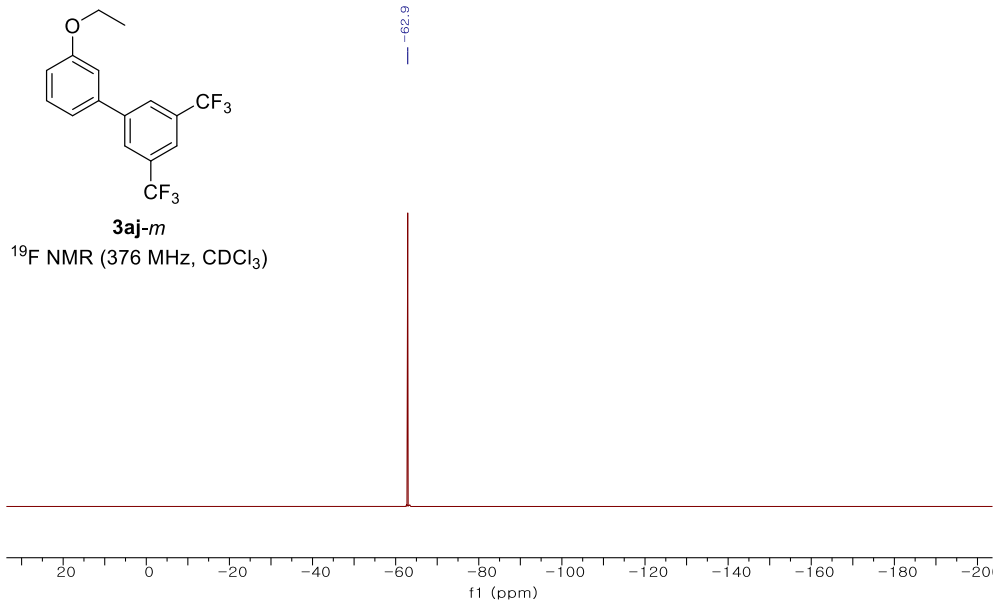

3aj-*m*

^{19}F NMR (376 MHz, $CDCl_3$)

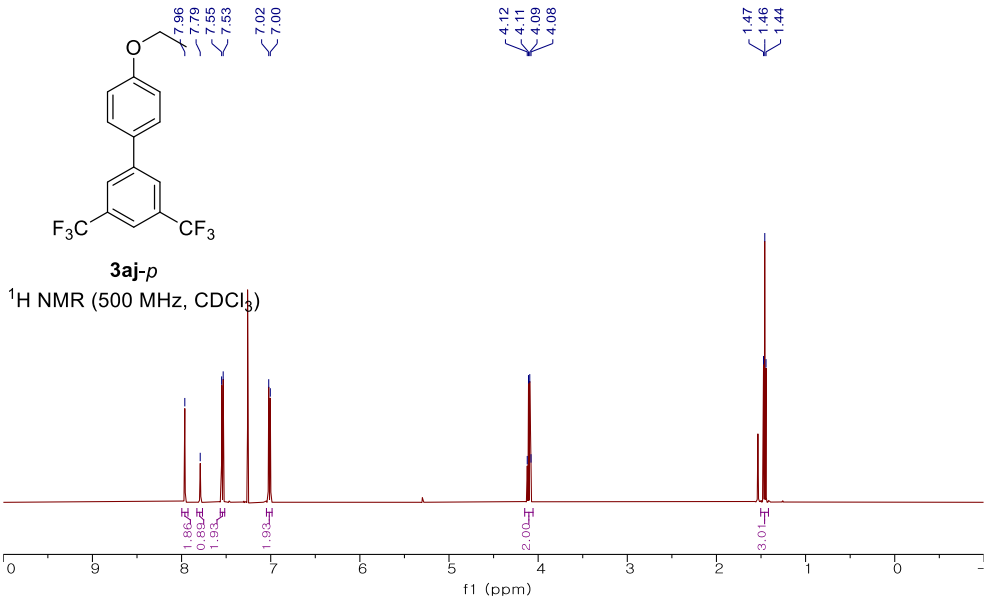

3aj-*p*

^{1}H NMR (500 MHz, $CDCl_3$)

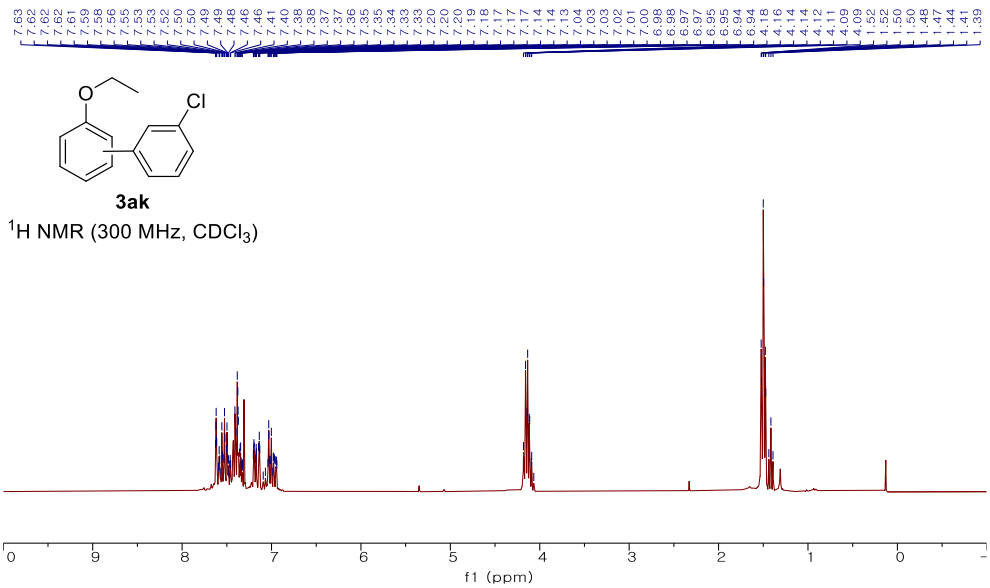

3ak

^{1}H NMR (300 MHz, $CDCl_3$)

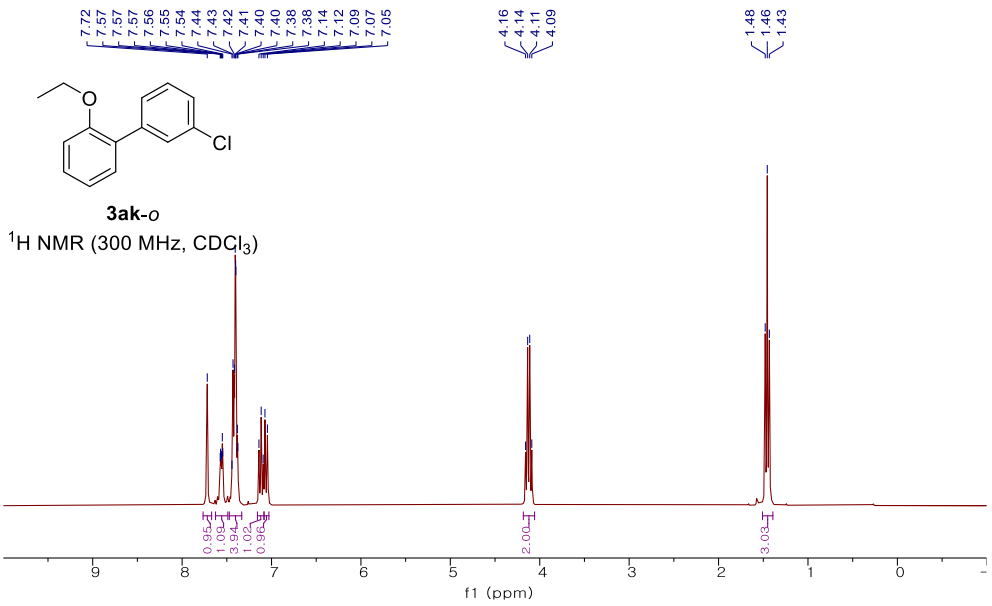

3ak-*o*

^{1}H NMR (300 MHz, $CDCl_3$)

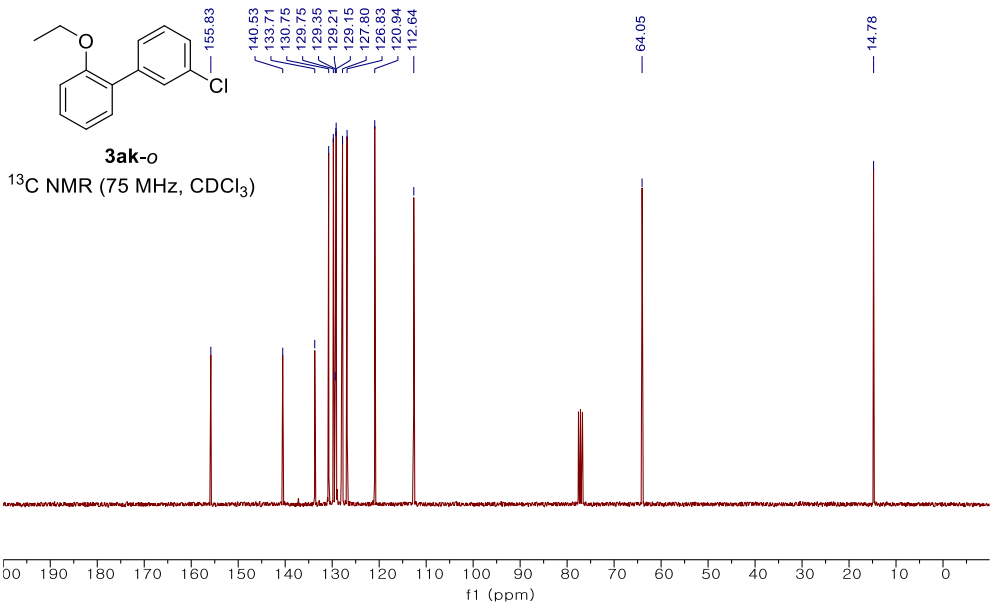

3ak-*o*

^{13}C NMR (75 MHz, $CDCl_3$)

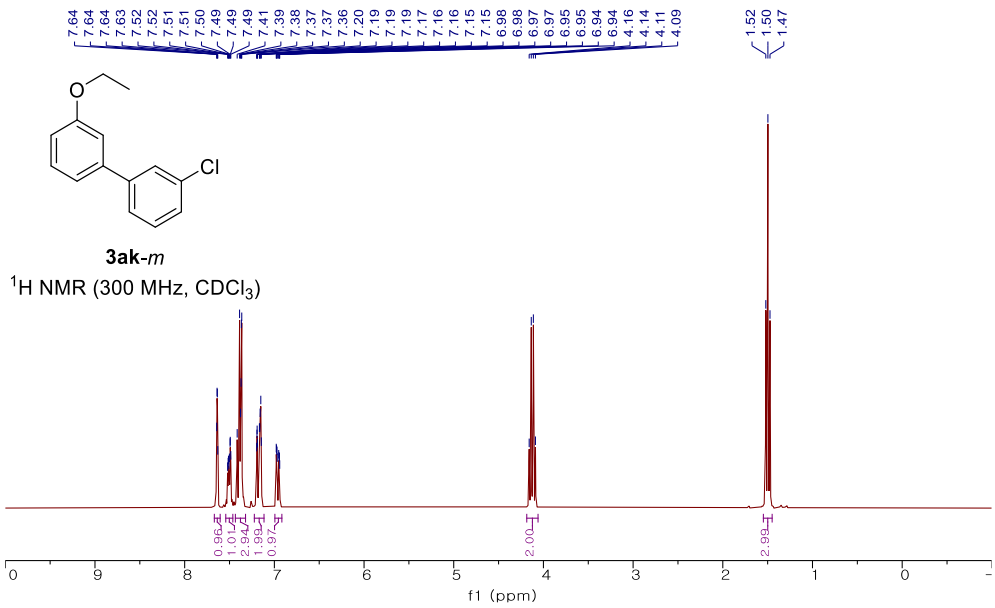

3ak-*m*

^{1}H NMR (300 MHz, $CDCl_3$)

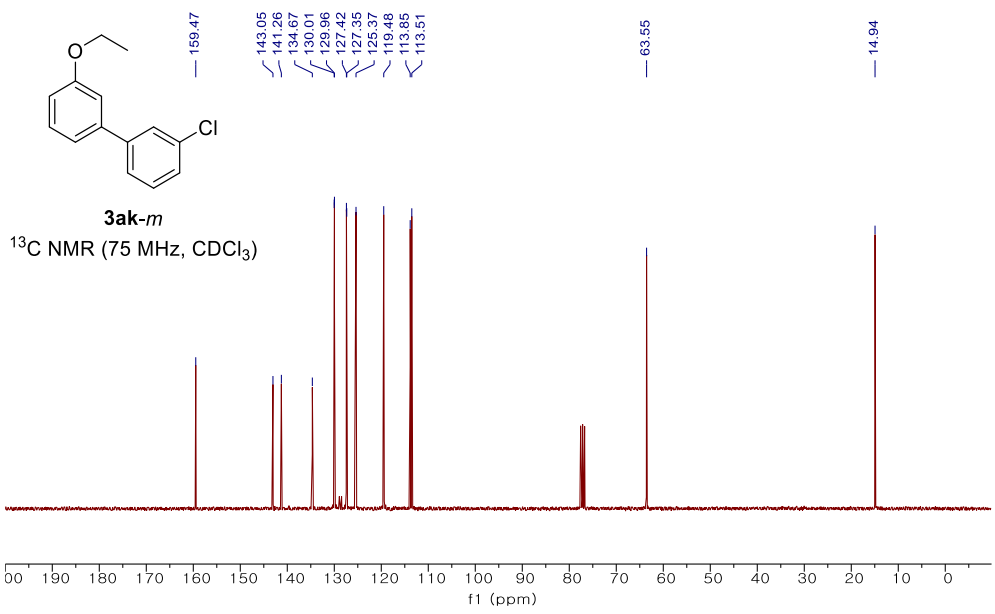

3ak-*m*

^{13}C NMR (75 MHz, $CDCl_3$)

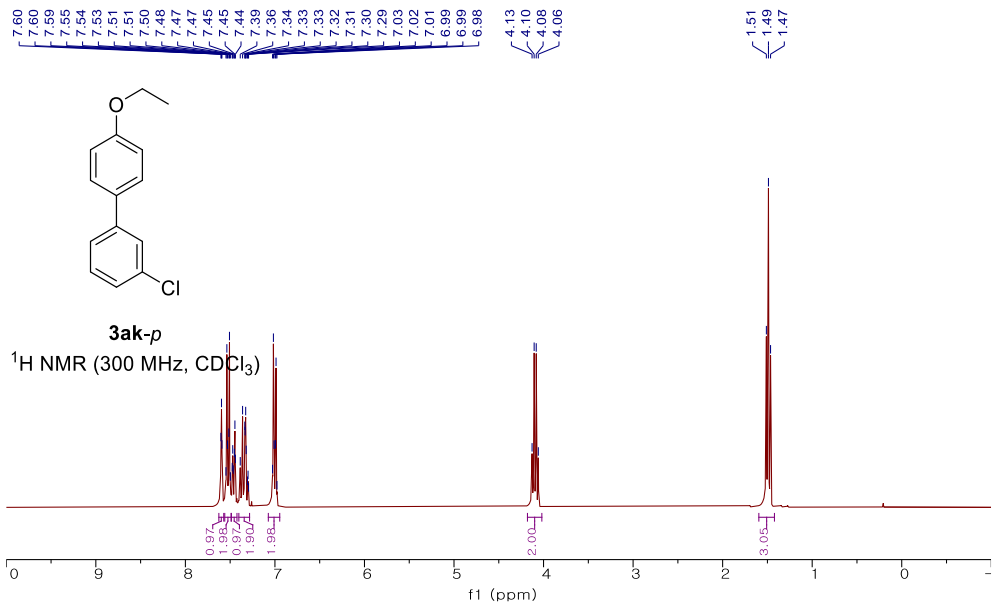

3ak-*p*

^{1}H NMR (300 MHz, $CDCl_3$)

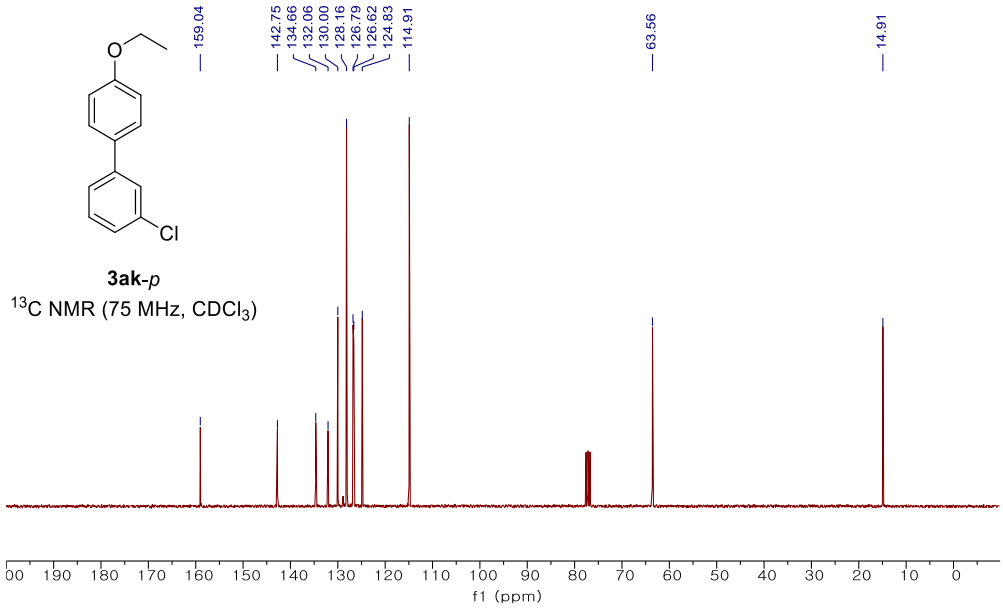

3ak-*p*

^{13}C NMR (75 MHz, $CDCl_3$)

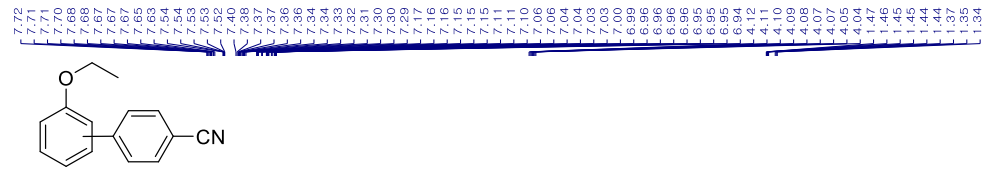

3al

^{1}H NMR (600 MHz, $CDCl_3$)

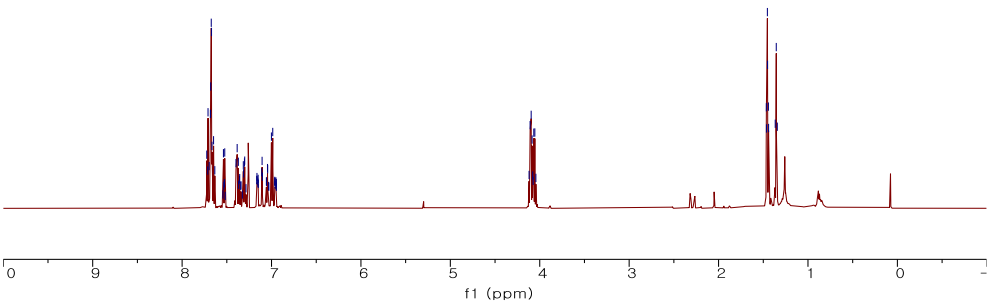

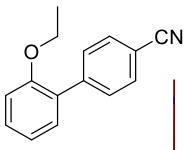

3al-*o*

^{1}H NMR (400 MHz, $CDCl_3$)

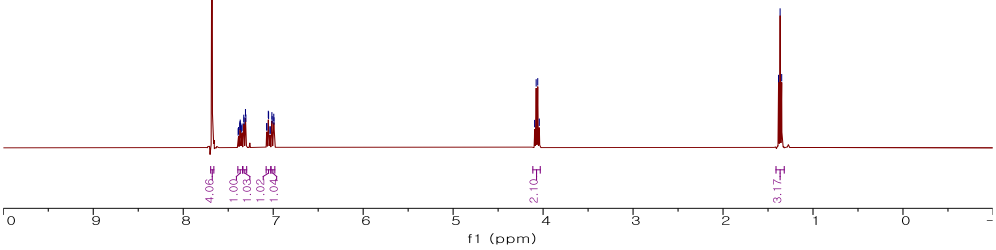

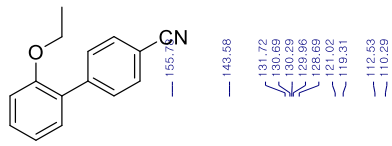

3al-*o*

^{13}C NMR (101 MHz, $CDCl_3$)

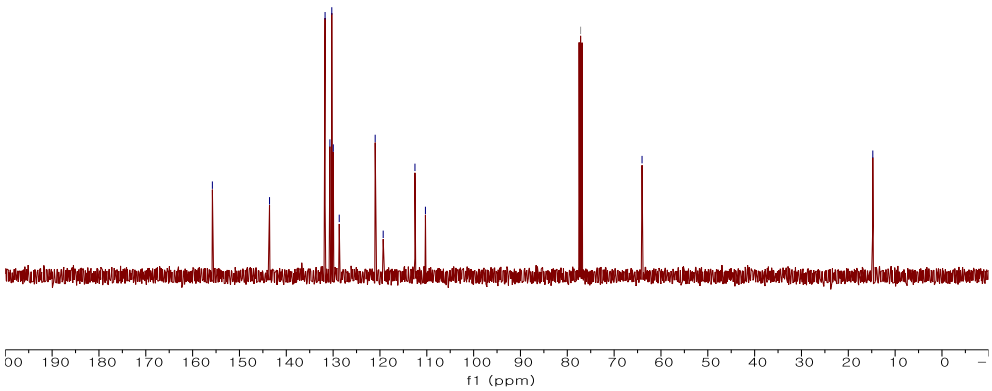

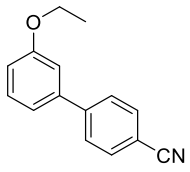

3al-*m*

^{1}H NMR (400 MHz, $CDCl_3$)

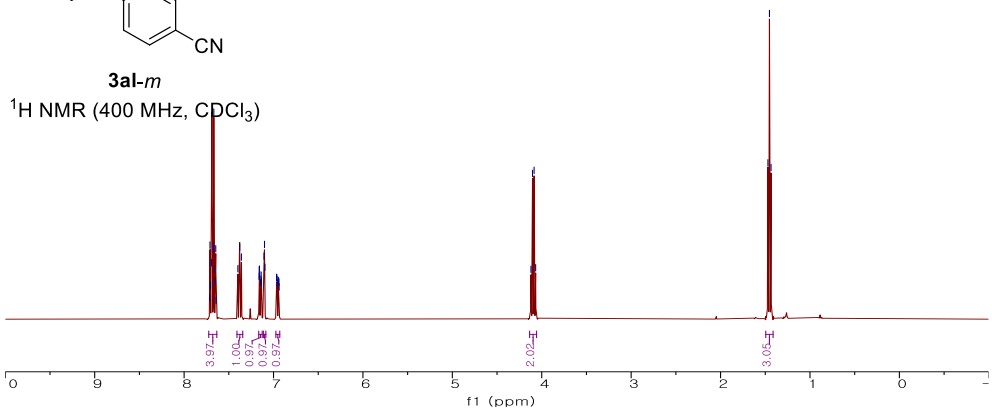

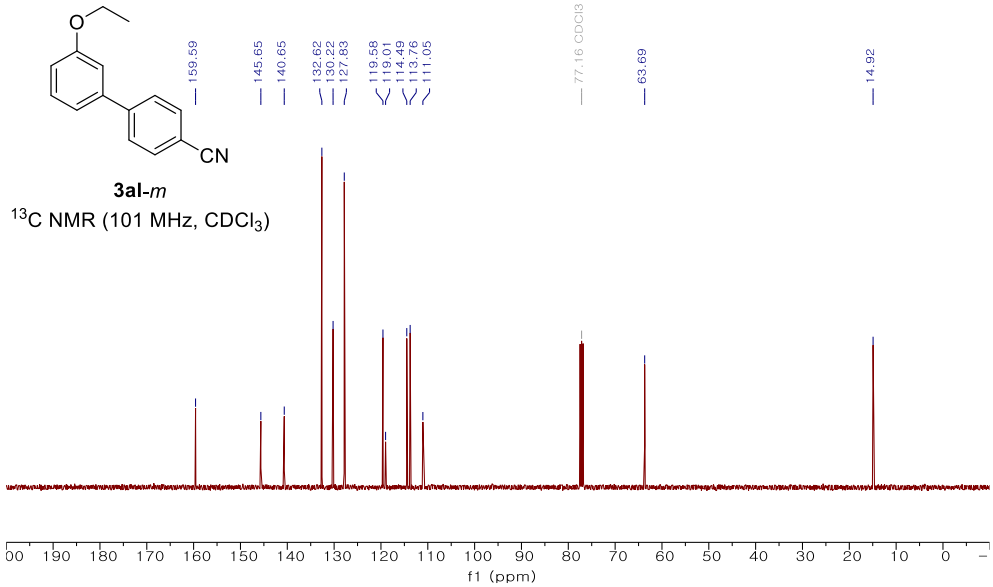

3al-*m*

^{13}C NMR (101 MHz, $CDCl_3$)

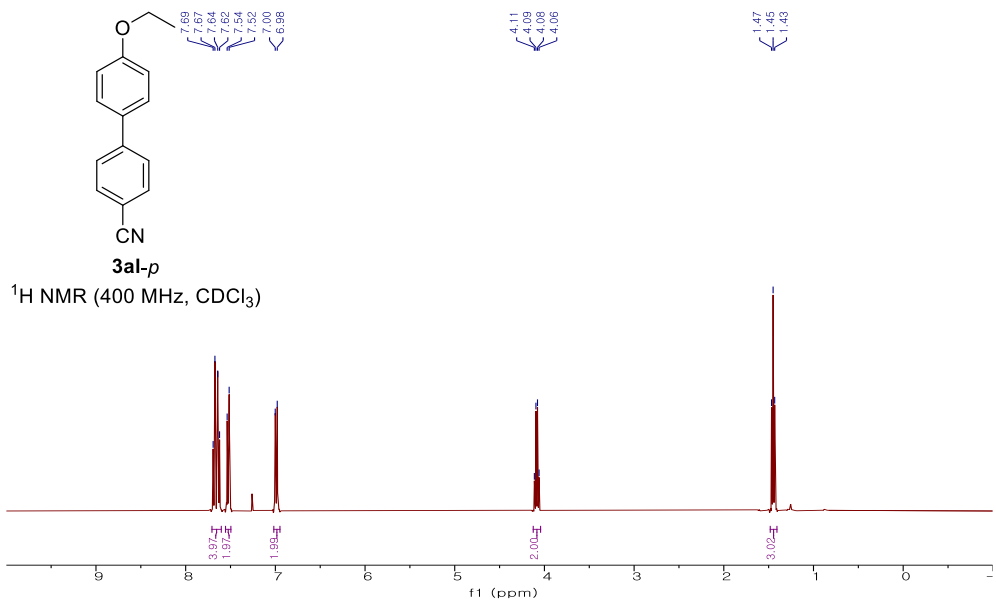

3al-*p*

^{1}H NMR (400 MHz, $CDCl_3$)

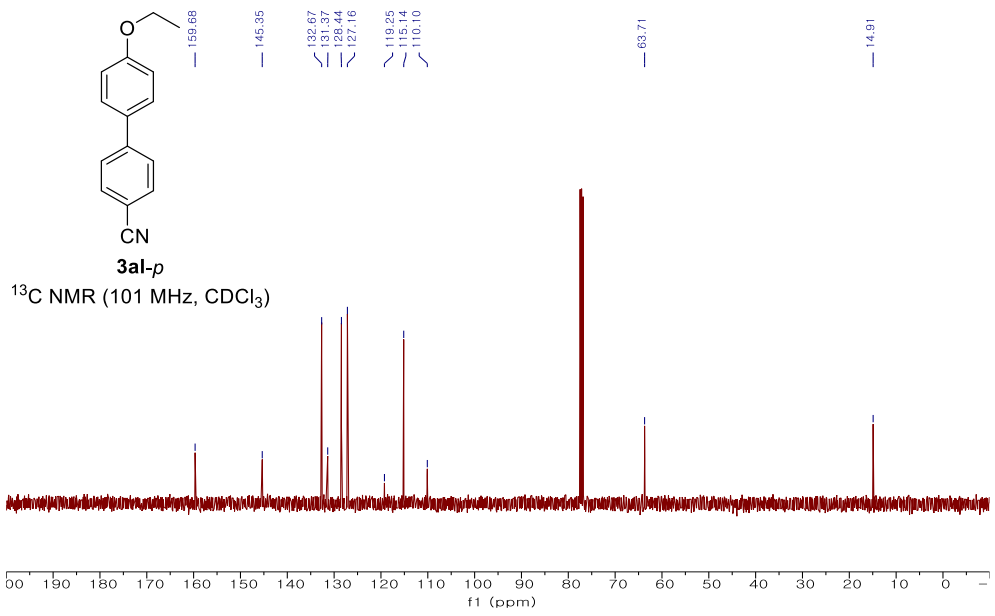

3al-*p*

^{13}C NMR (101 MHz, $CDCl_3$)

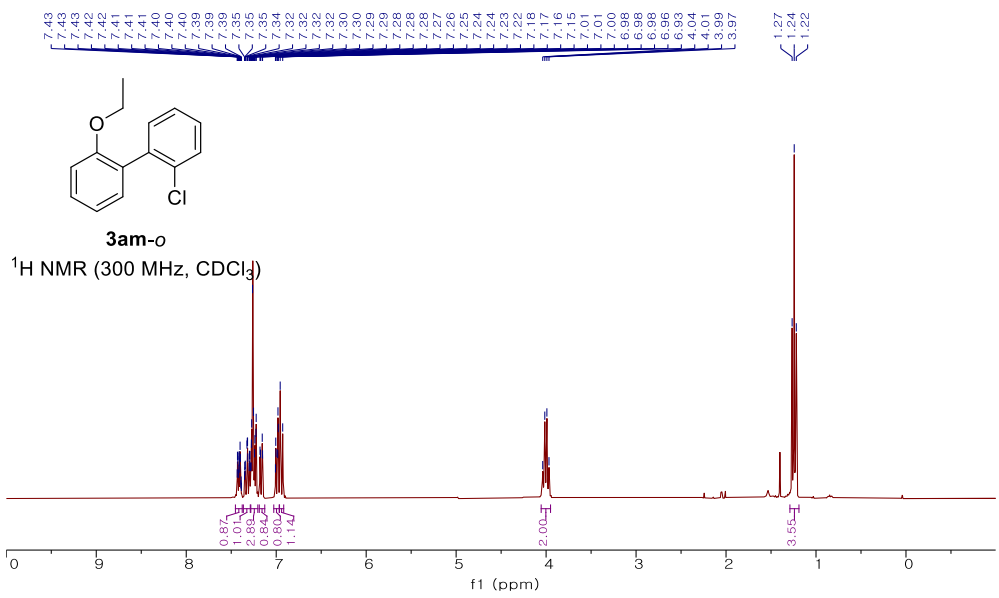

3am-*o*

^{1}H NMR (300 MHz, $CDCl_3$)

3am-*o*

^{13}C NMR (101 MHz, $CDCl_3$)

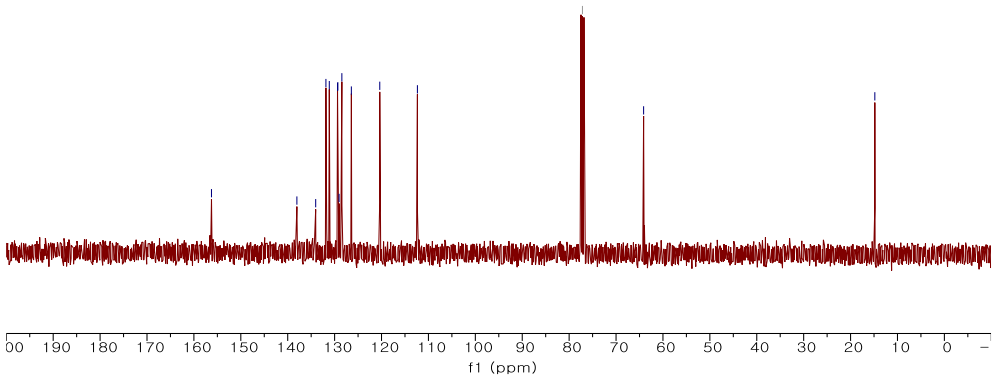

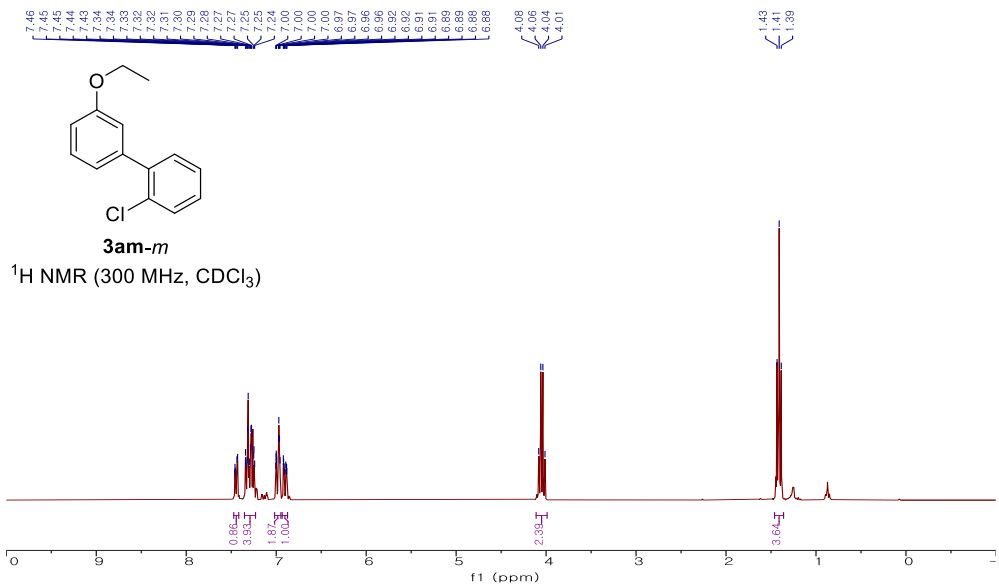

3am-*m*

^{1}H NMR (300 MHz, $CDCl_3$)

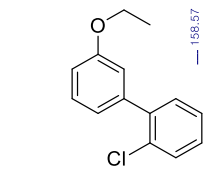

3am-*m*

^{13}C NMR (101 MHz, $CDCl_3$)

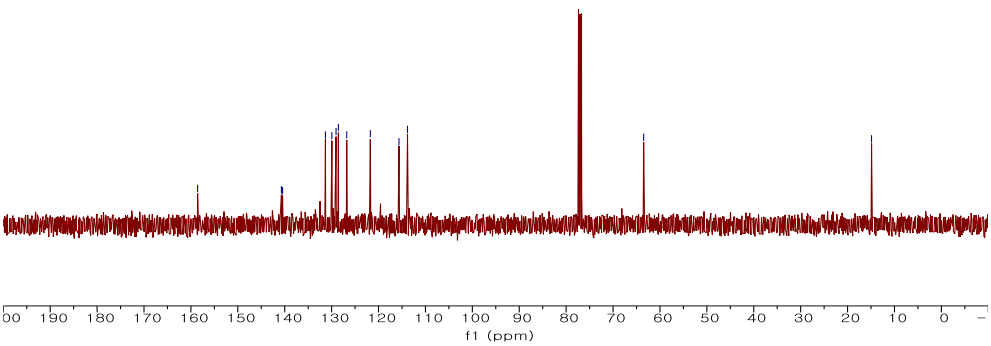

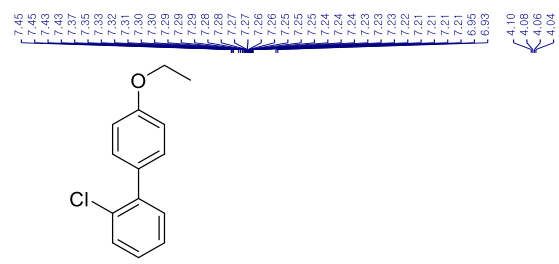

3am-*p*

^{1}H NMR (400 MHz, $CDCl_3$)

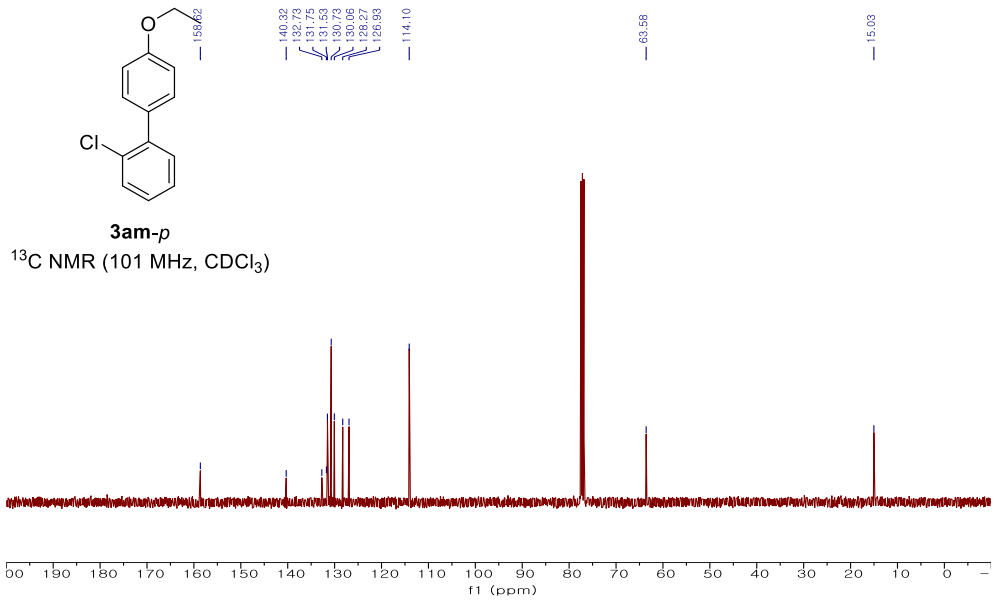

3am-*p*

^{13}C NMR (101 MHz, $CDCl_3$)

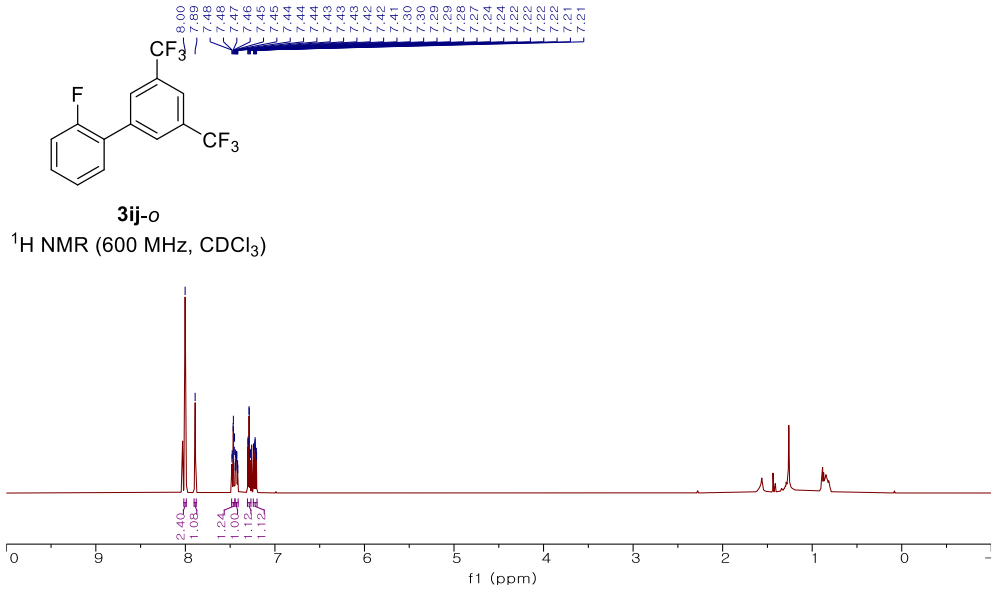

3ij-*o*

^{1}H NMR (600 MHz, $CDCl_3$)

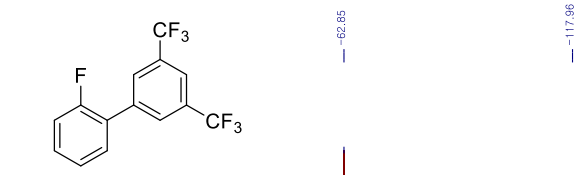

3ij-*o*

^{19}F NMR (376 MHz, $CDCl_3$)

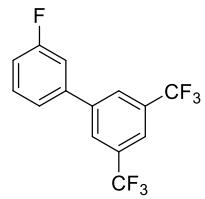

3ij-*m*

^{1}H NMR (400 MHz, $CDCl_3$)

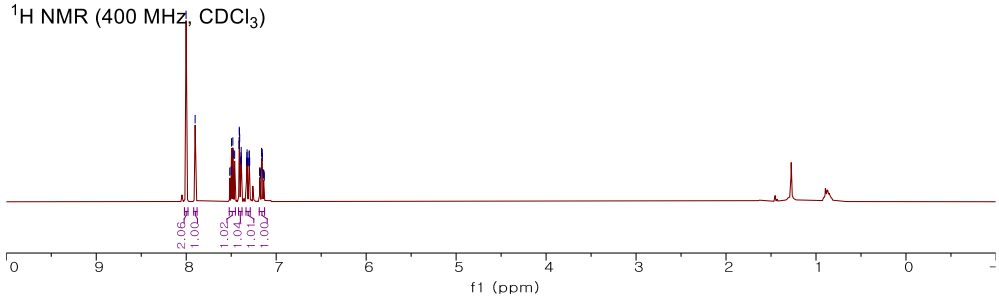

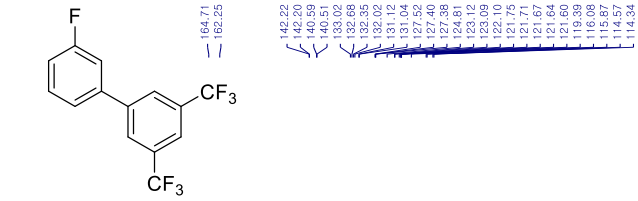

3ij-*m*

^{13}C NMR (101 MHz, $CDCl_3$)

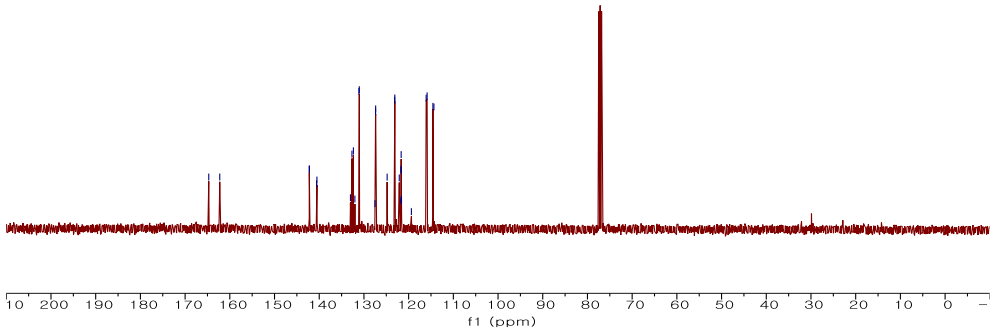

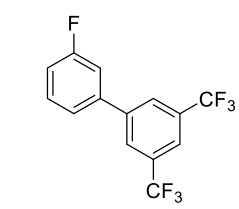

3ij-*m*

^{19}F NMR (376 MHz, $CDCl_3$)

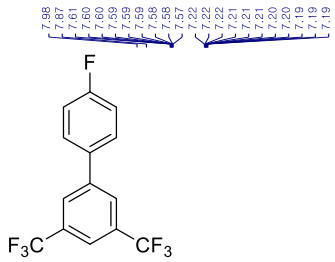

3ij-*p*

^{19}F NMR (376 MHz, $CDCl_3$)

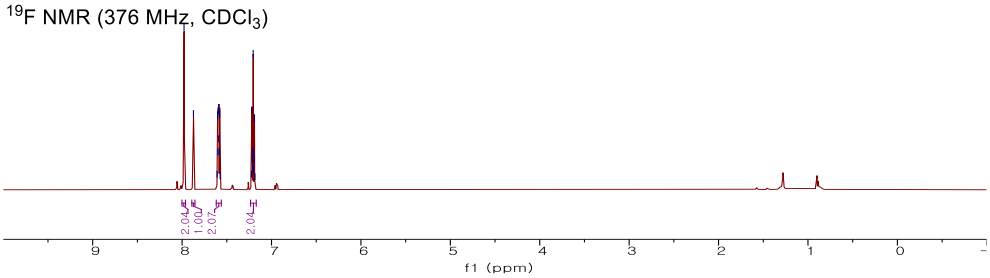

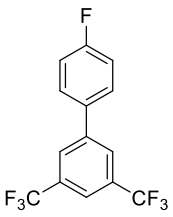

3ij-*p*

^{1}H NMR (600 MHz, $CDCl_3$)

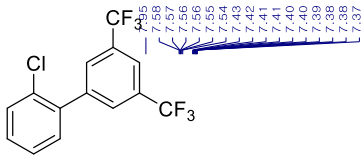

3kj-*o*

^{1}H NMR (400 MHz, $CDCl_3$)

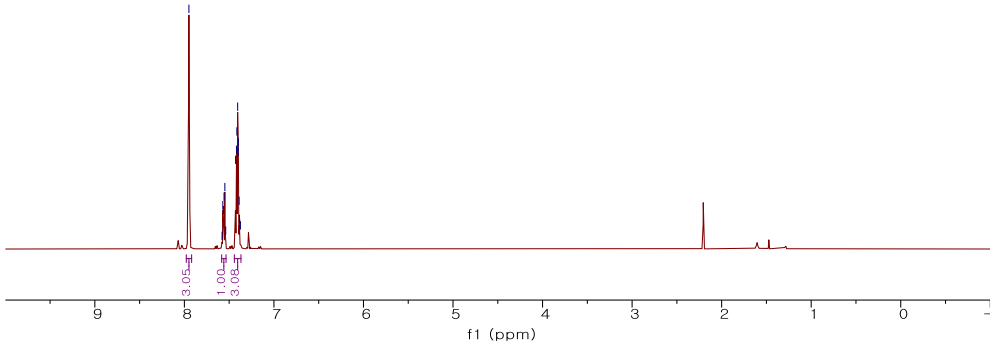

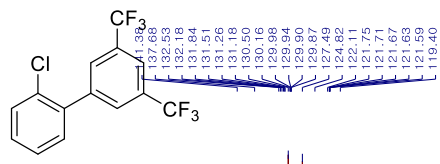

3kj-*o*

^{13}C NMR (101 MHz, $CDCl_3$)

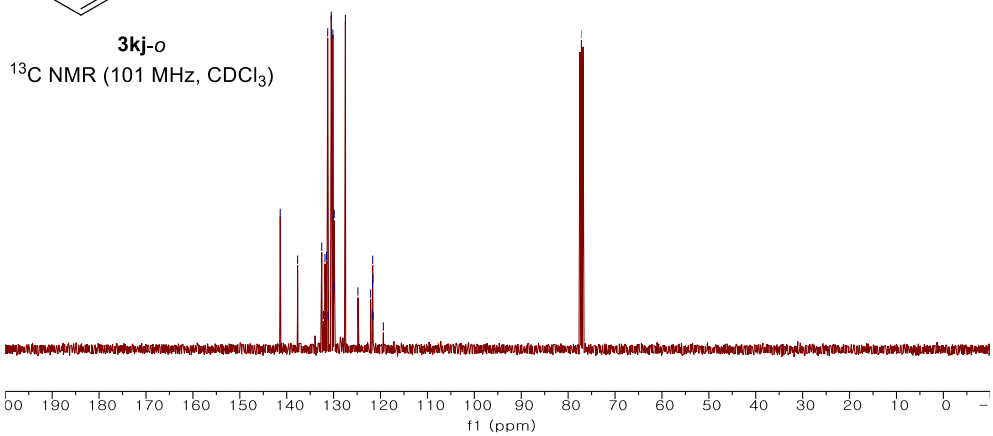

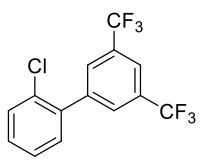

3kj-*o*

^{19}F NMR (376 MHz, $CDCl_3$)

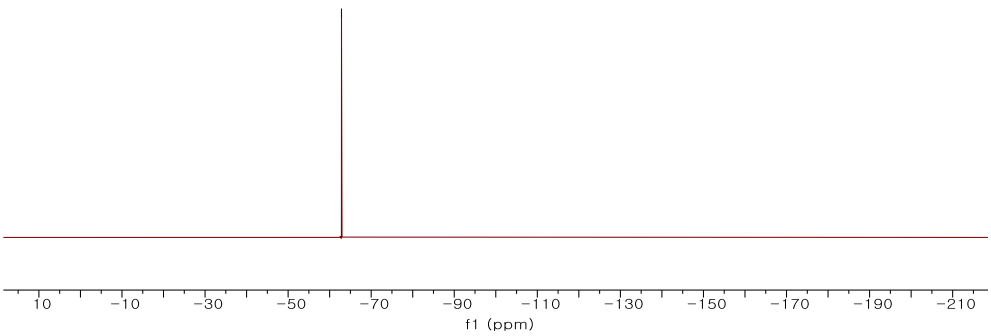

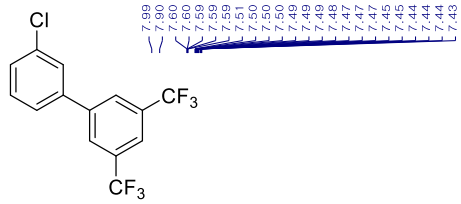

3kj-*m*

^{1}H NMR (400 MHz, $CDCl_3$)

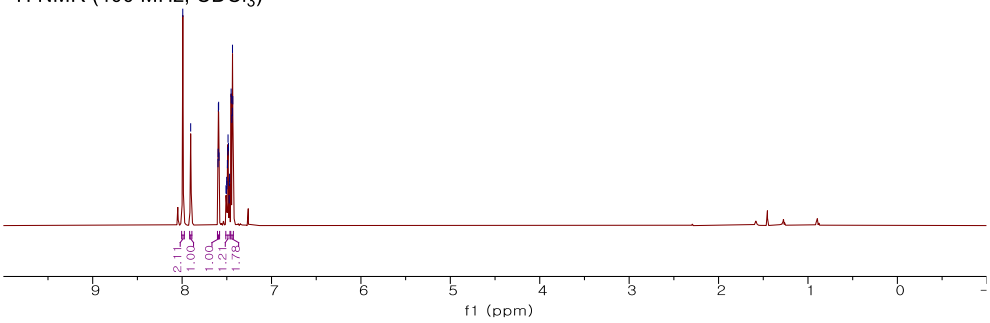

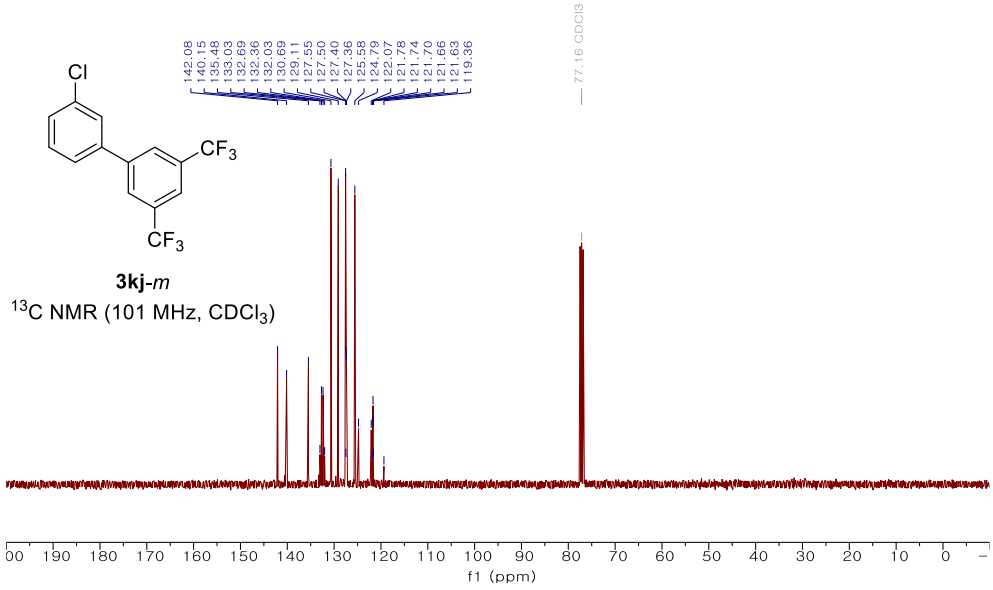

3kj-*m*

^{13}C NMR (101 MHz, $CDCl_3$)

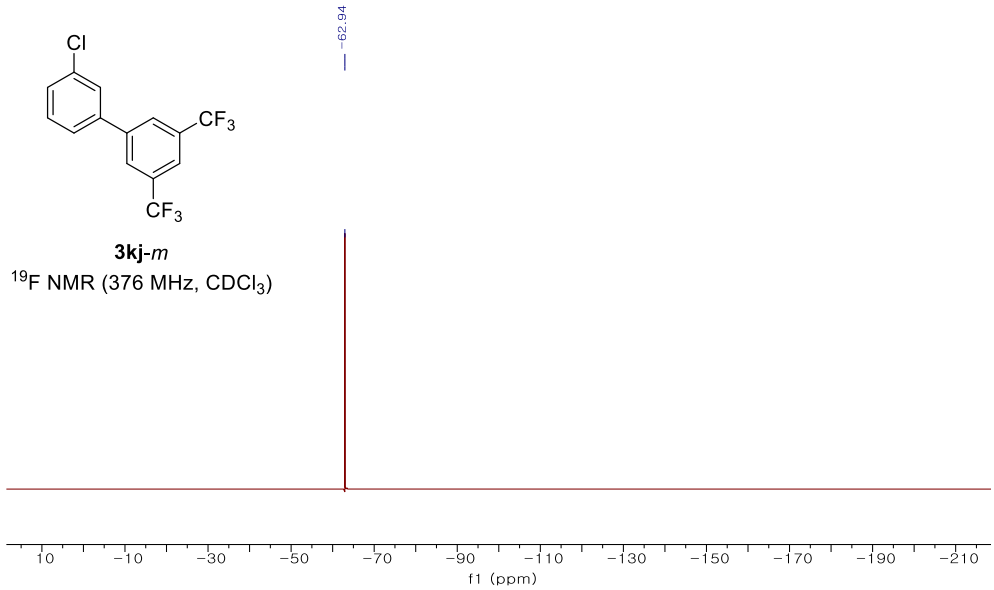

3kj-*m*

^{19}F NMR (376 MHz, $CDCl_3$)

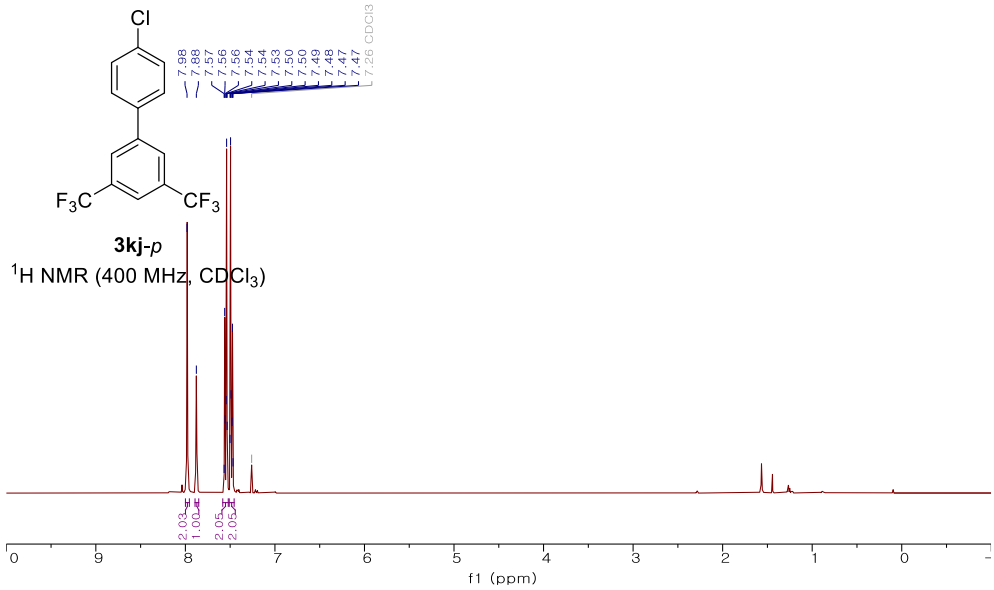

3kj-*p*

^{1}H NMR (400 MHz, $CDCl_3$)

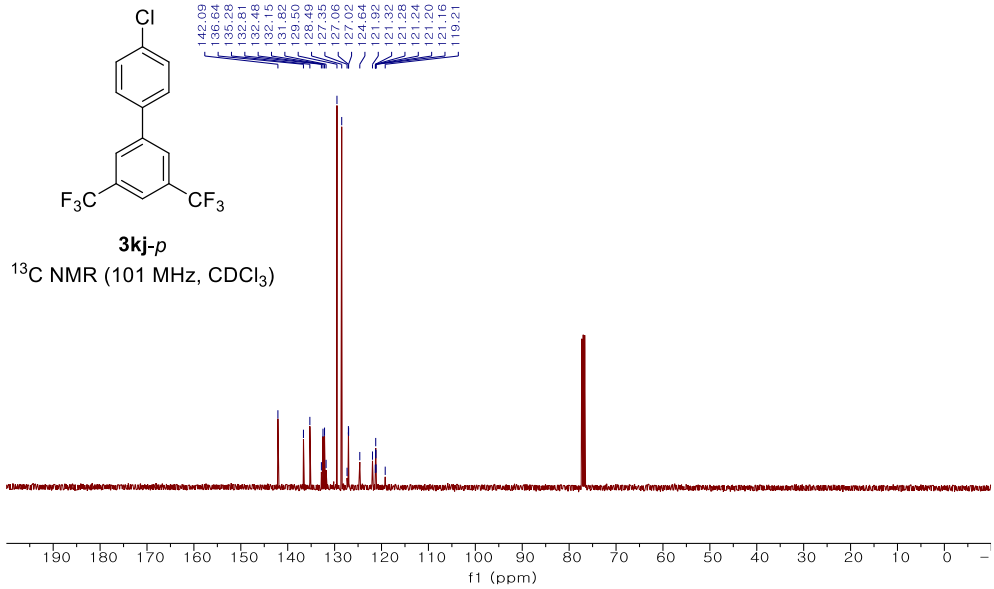

3kj-*p*

^{13}C NMR (101 MHz, $CDCl_3$)

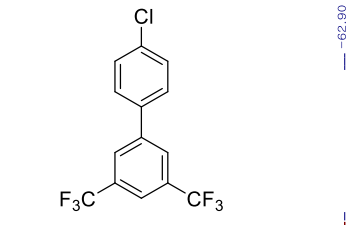

3kj-*p*

^{19}F NMR (376 MHz, $CDCl_3$)

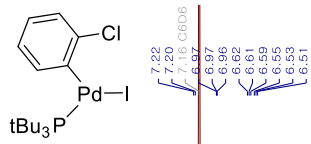

4b

^{1}H NMR (400 MHz, C_6D_6)

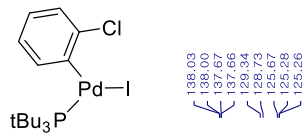

4b

^{13}C NMR (151 MHz, CD_2Cl_2)

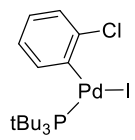

4b

^{31}P NMR (162 MHz, C_6D_6)

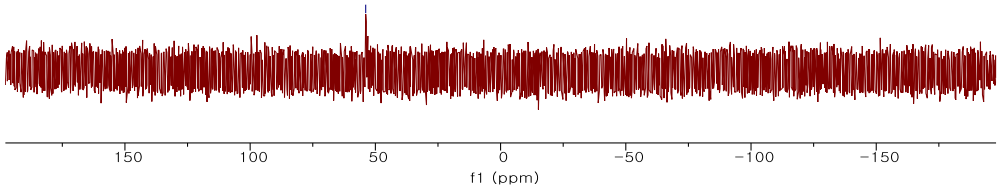

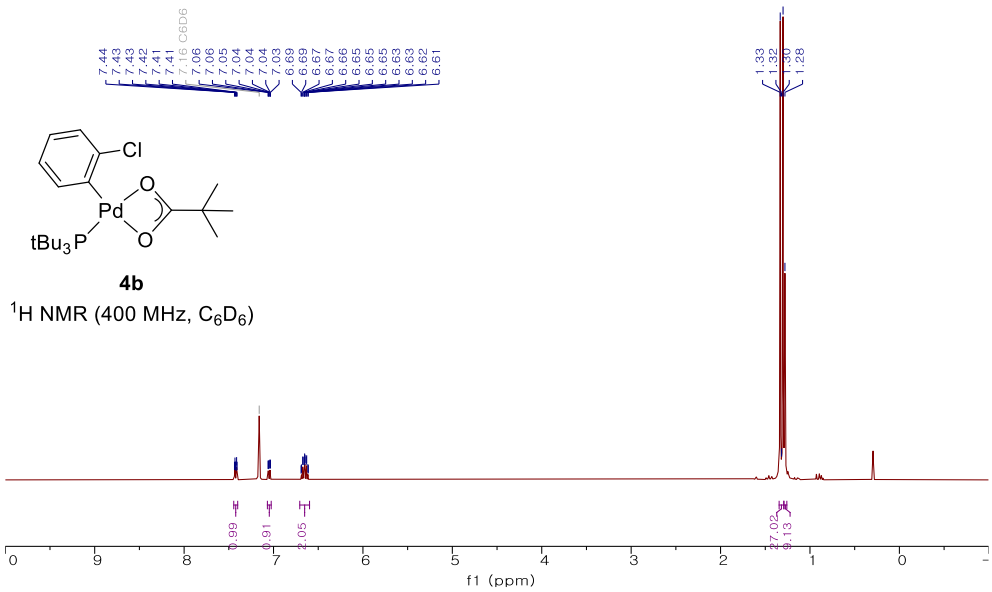

4b

^{1}H NMR (400 MHz, C_6D_6)

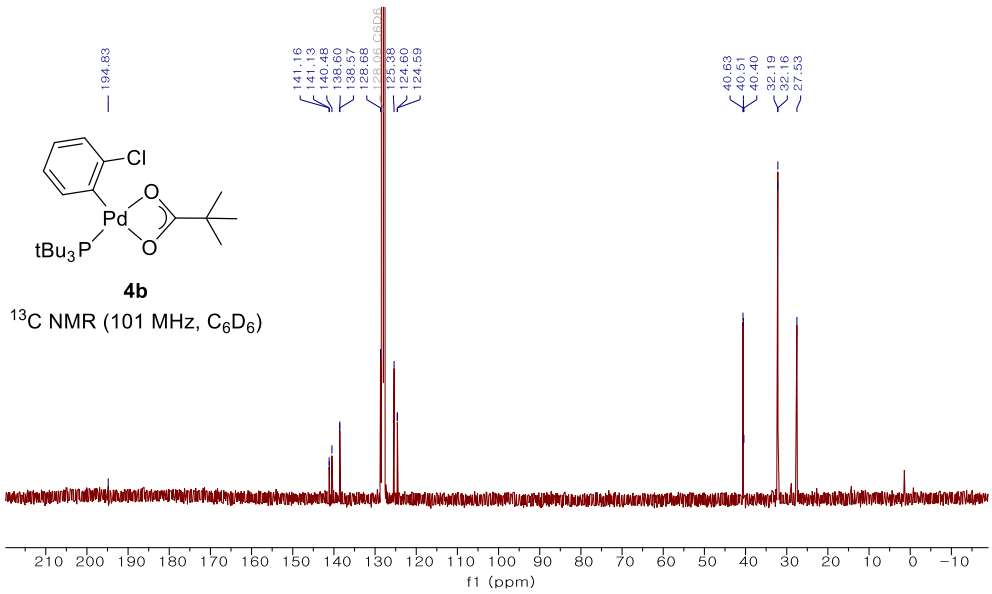

4b

^{13}C NMR (101 MHz, C_6D_6)

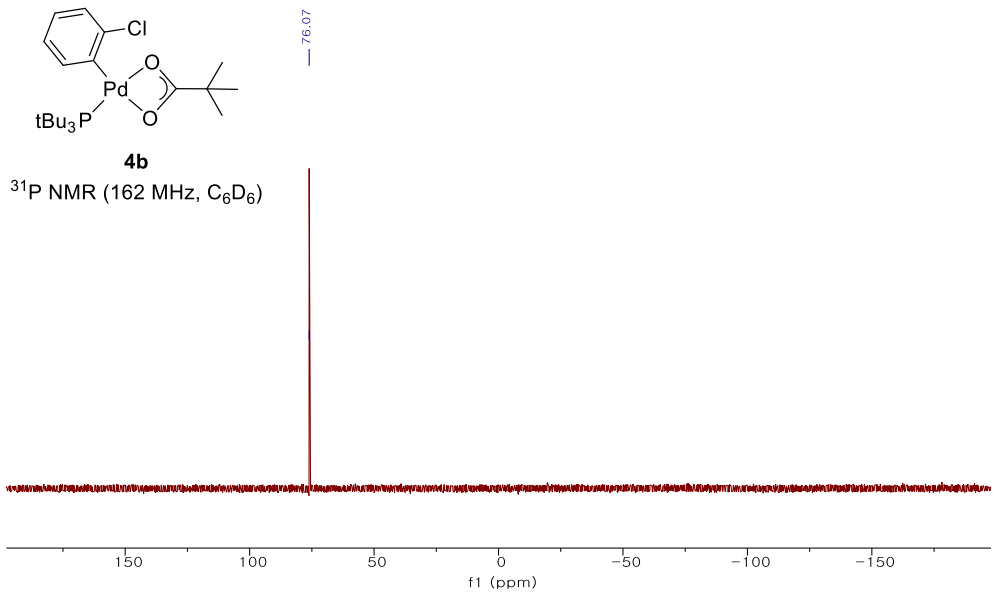

4b

^{31}P NMR (162 MHz, C_6D_6)

Chapter 6

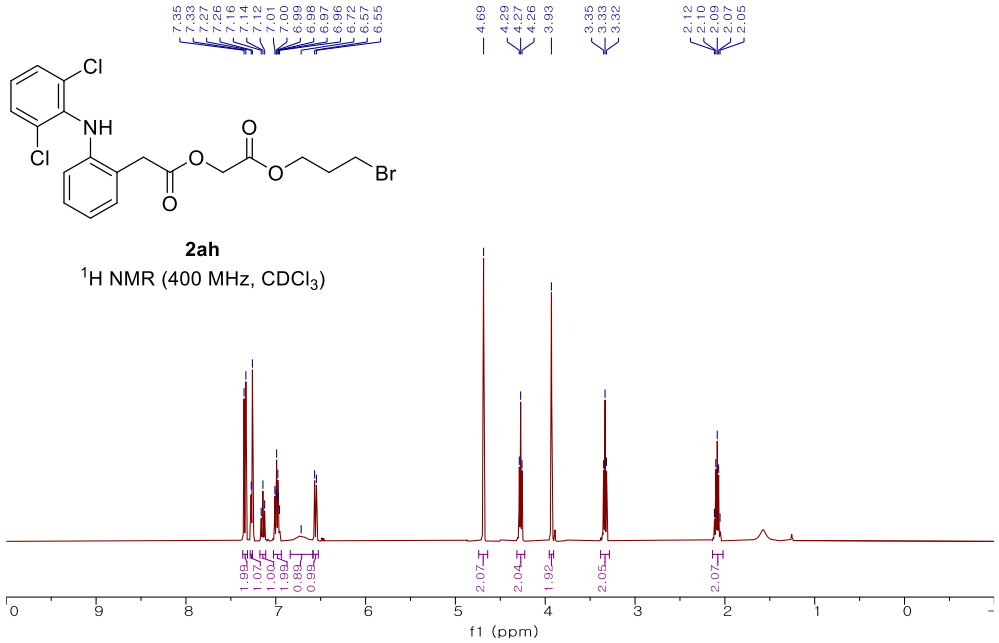

2ah

^{1}H NMR (400 MHz, $CDCl_3$)

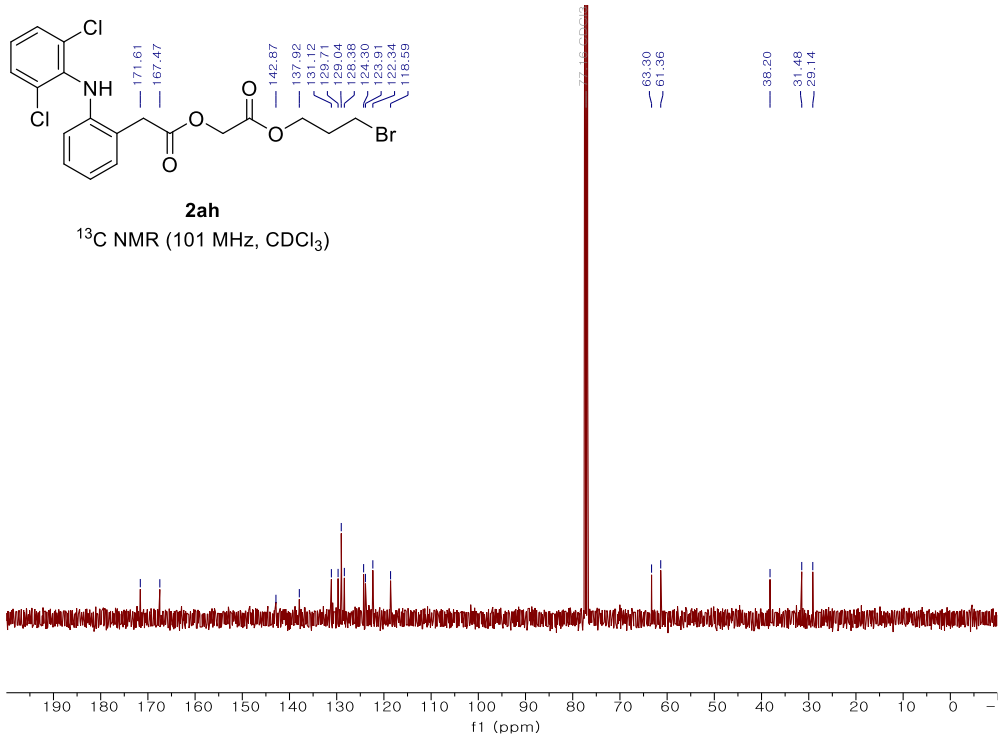

2ah

^{13}C NMR (101 MHz, $CDCl_3$)

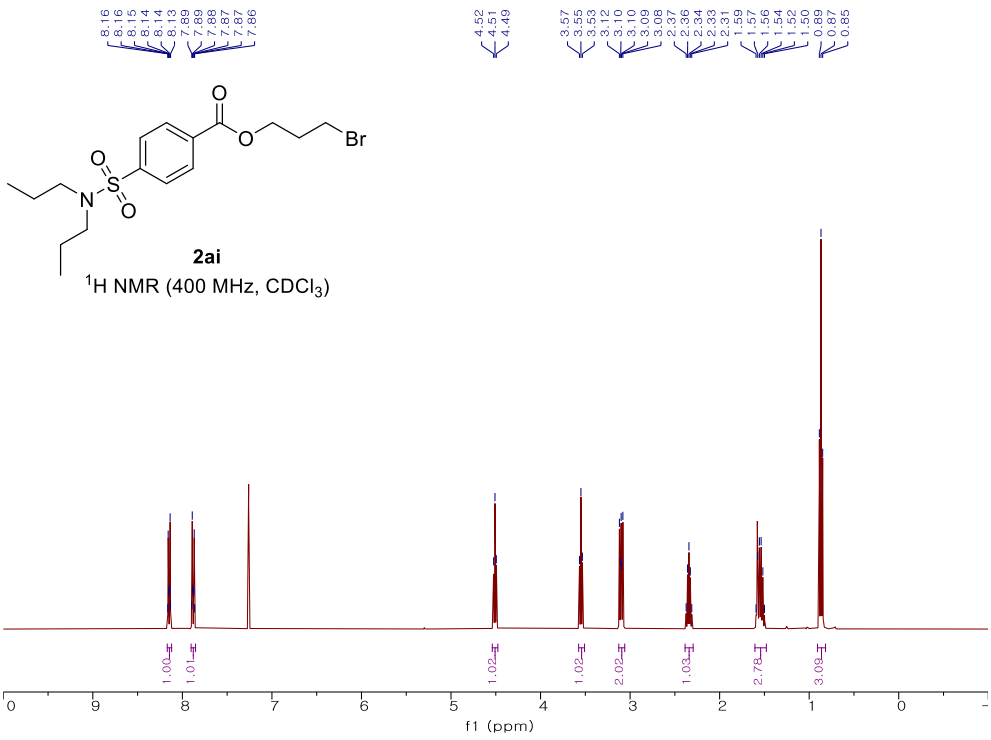
8.16
8.16
8.15
8.14
8.14
8.13
7.89
7.88
7.87
7.87
7.86
4.52
4.51
4.49
3.57
3.55
3.53
3.12
3.10
3.10
3.09
3.08
2.37
2.36
2.34
2.33
2.31
1.59
1.57
1.56
1.54
1.52
1.50
0.89
0.87
0.85
O
O
Br
O
S
O
N
2ai
1H NMR (400 MHz, CDCl3)
1.00
1.01
1.02
1.02
2.02
1.03
2.78
3.09
0
9
8
7
6
5
4
3
2
1
0
f1 (ppm)

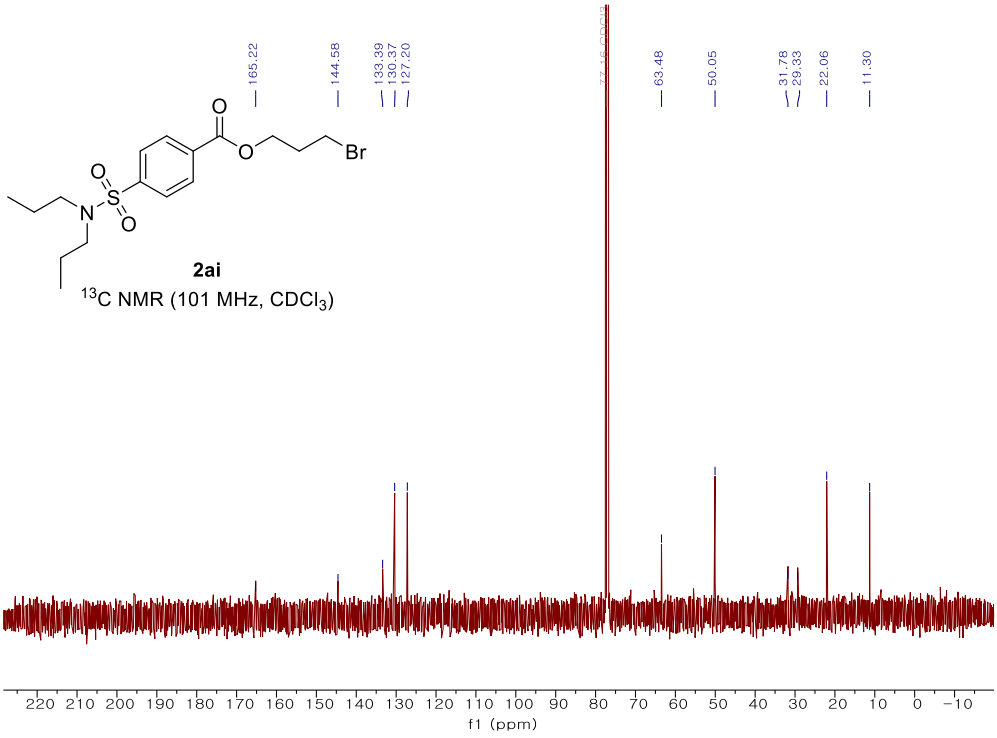
165.22
144.58
133.39
130.37
127.20
77.16 CDCl3
63.48
50.05
31.78
29.33
22.06
11.30
O
O
Br
O
S
O
N
2ai
13C NMR (101 MHz, CDCl3)
220 210 200 190 180 170 160 150 140 130 120 110 100 90 80 70 60 50 40 30 20 10 0 −10
f1 (ppm)

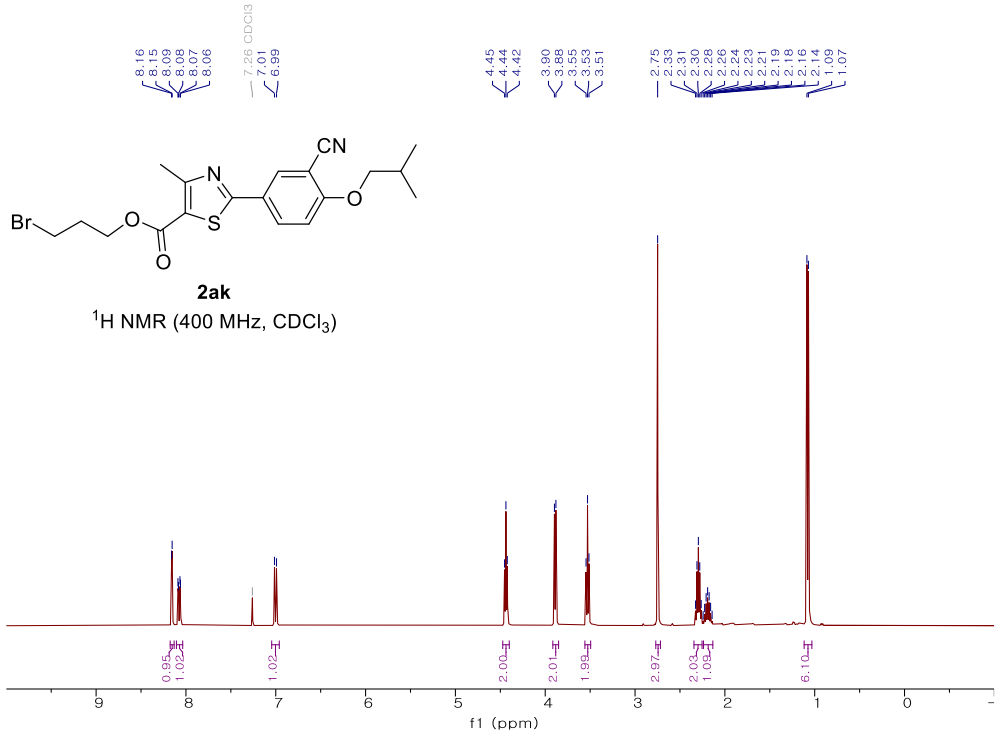

2ak

^{1}H NMR (400 MHz, $CDCl_3$)

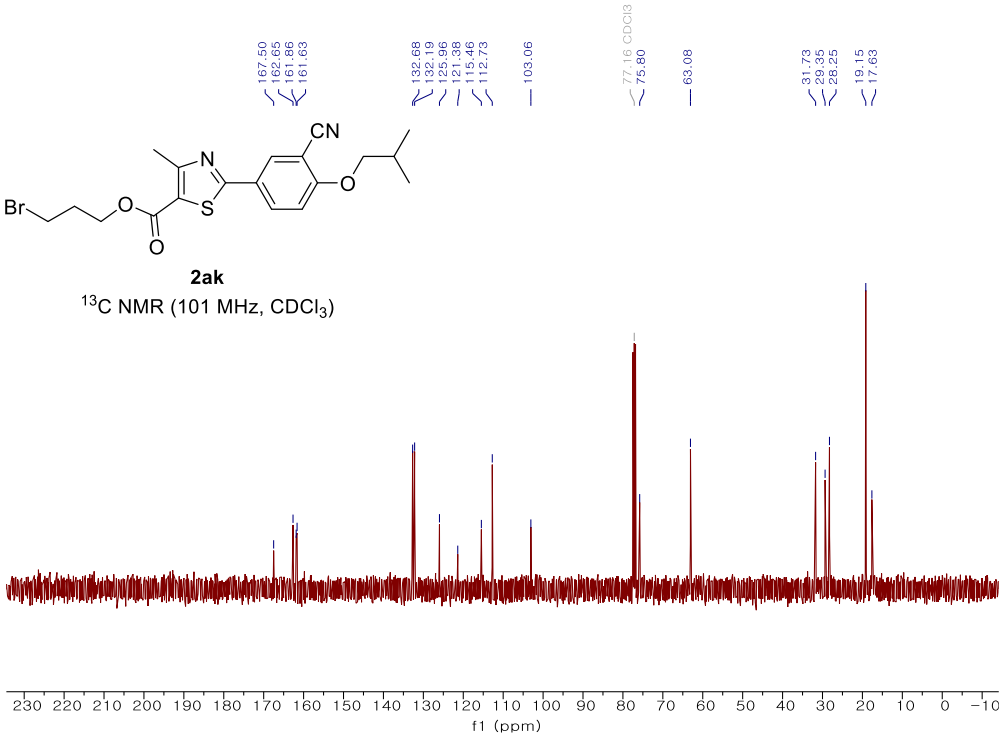

2ak

^{13}C NMR (101 MHz, $CDCl_3$)

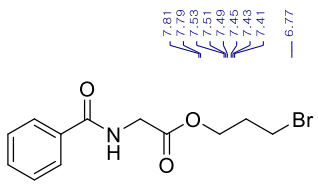

2al

^{1}H NMR (400 MHz, $CDCl_3$)

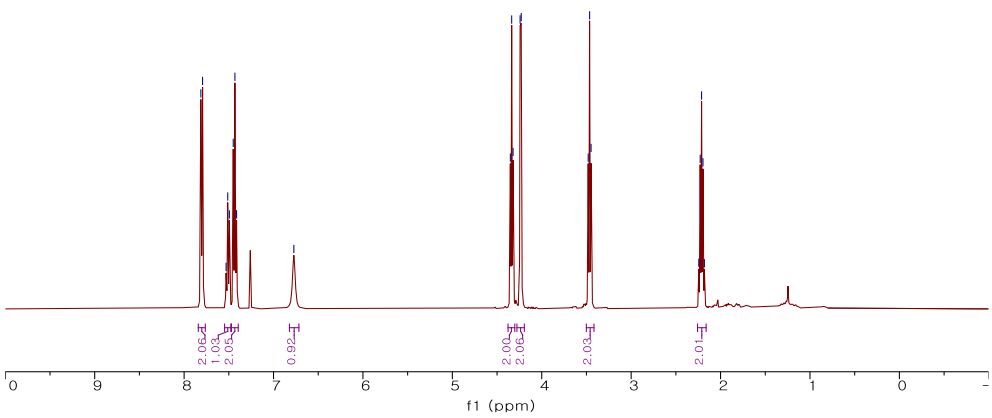

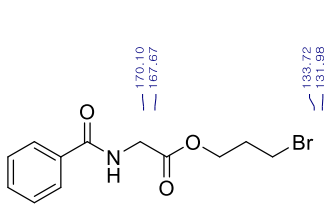

2al

^{13}C NMR (101 MHz, $CDCl_3$)

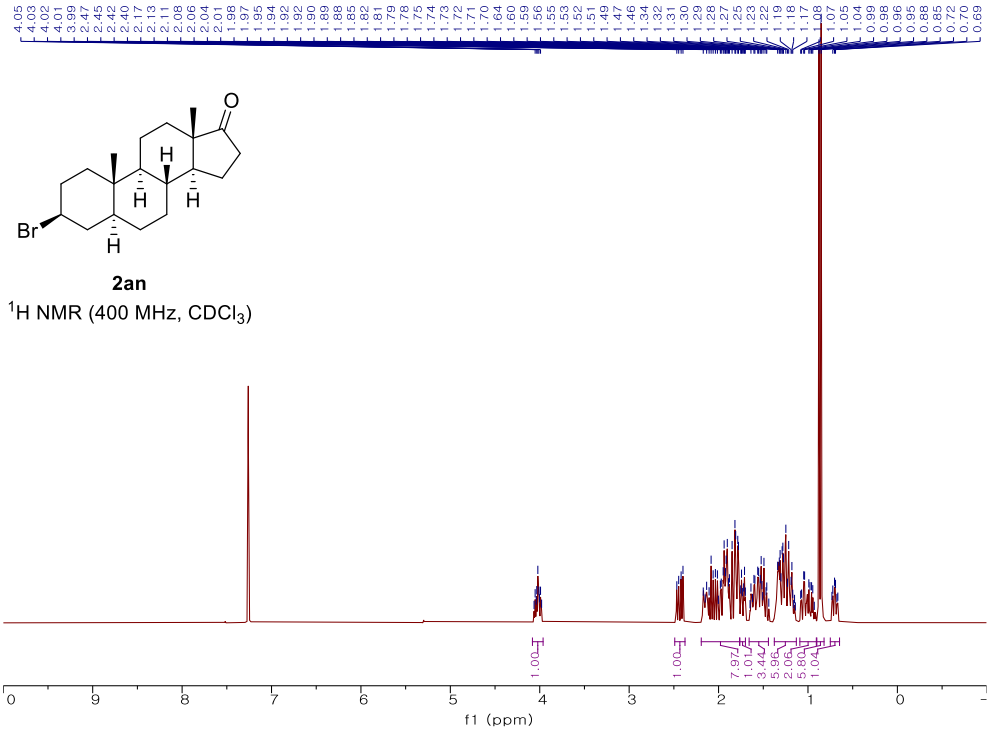

2an

^{1}H NMR (400 MHz, $CDCl_3$)

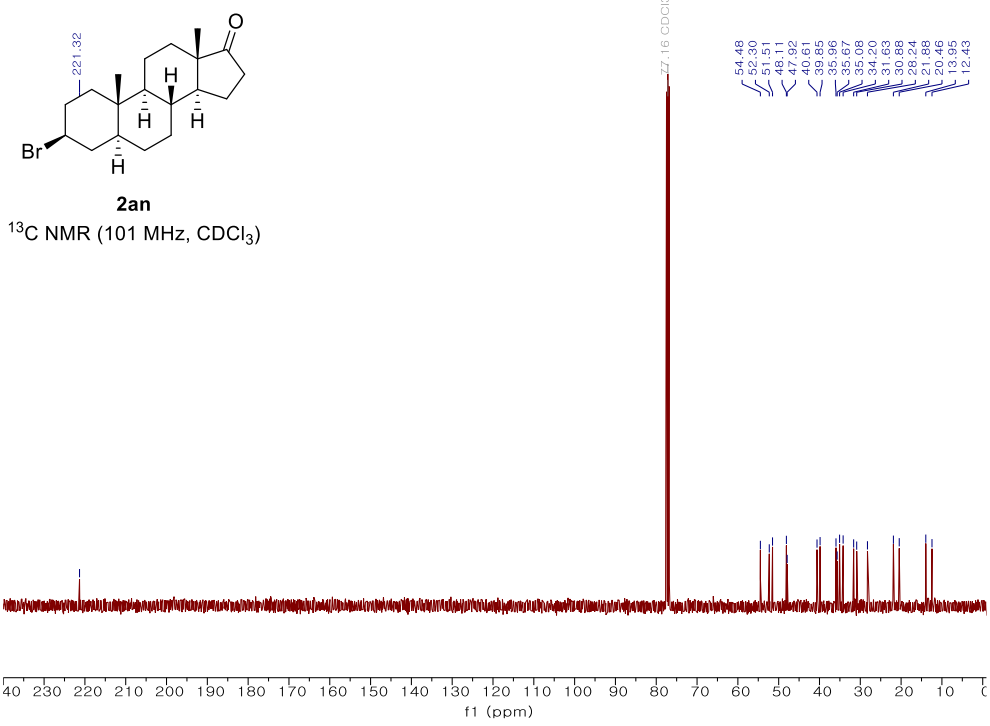

2an

^{13}C NMR (101 MHz, $CDCl_3$)

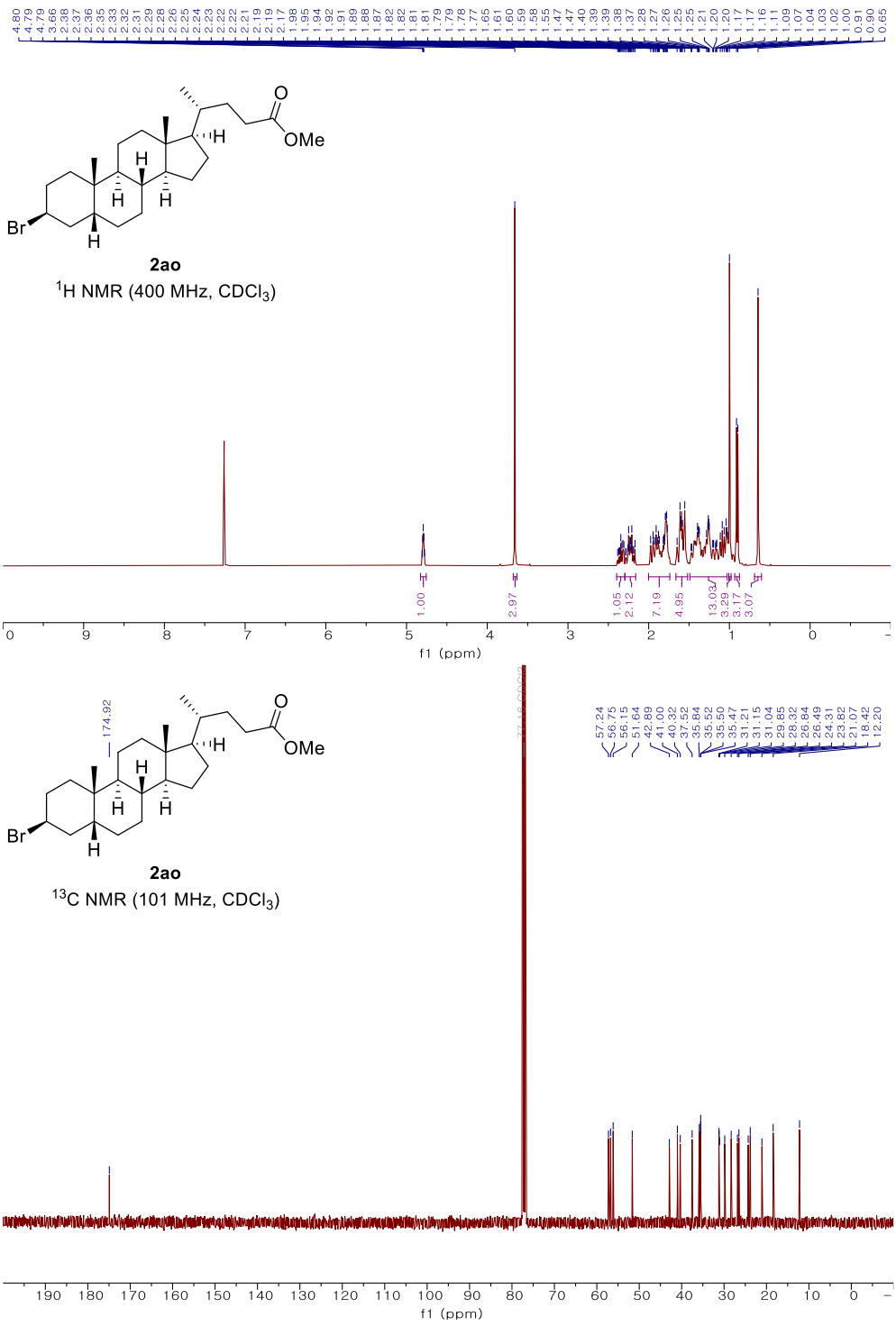
4.80 4.79 4.79 3.66 2.38 2.37 2.36 2.35 2.33 2.32 2.31 2.29 2.28 2.26 2.25 2.24 2.23 2.22 2.22 2.21 2.19 2.19 2.17 1.98 1.95 1.94 1.92 1.91 1.89 1.88 1.87 1.82 1.82 1.81 1.81 1.79 1.79 1.78 1.77 1.65 1.61 1.60 1.59 1.58 1.55 1.47 1.47 1.40 1.39 1.38 1.37 1.28 1.27 1.26 1.25 1.25 1.21 1.20 1.20 1.17 1.17 1.16 1.11 1.09 1.07 1.04 1.03 1.02 1.00 0.91 0.90 0.65
O
OMe
H
H
H
H
Br
H
2ao
1H NMR (400 MHz, CDCl3)
1.00
2.97
1.05
2.12
7.19
4.95
13.03
3.29
3.17
3.07
f1 (ppm)
174.92
77.16 CDCl3
57.24
56.75
56.15
51.64
42.89
41.00
40.32
37.52
35.84
35.52
35.50
35.47
31.21
31.15
31.04
29.85
28.32
26.84
26.49
24.31
23.82
21.07
18.42
12.20
2ao
13C NMR (101 MHz, CDCl3)
f1 (ppm)

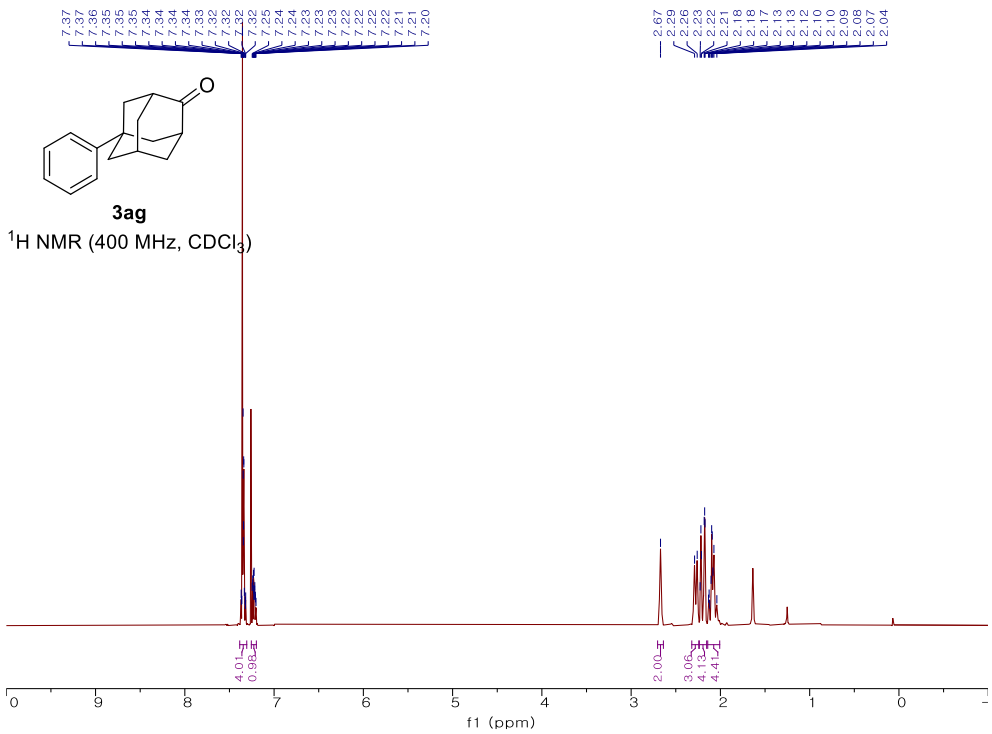

3ag

^{1}H NMR (400 MHz, $CDCl_3$)

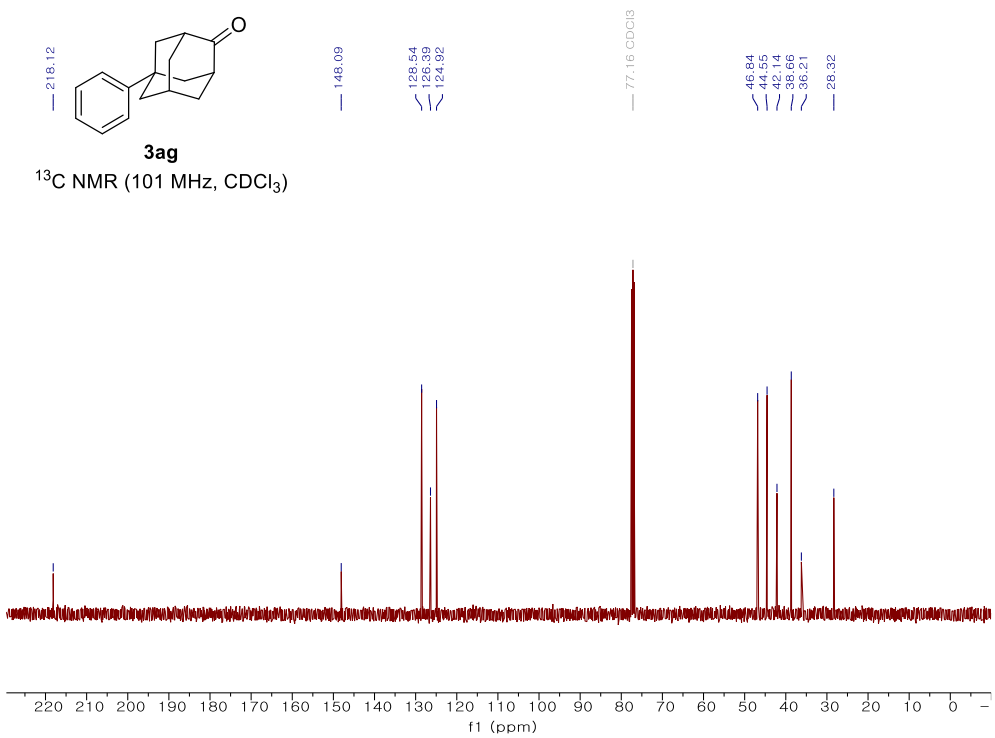

3ag

^{13}C NMR (101 MHz, $CDCl_3$)

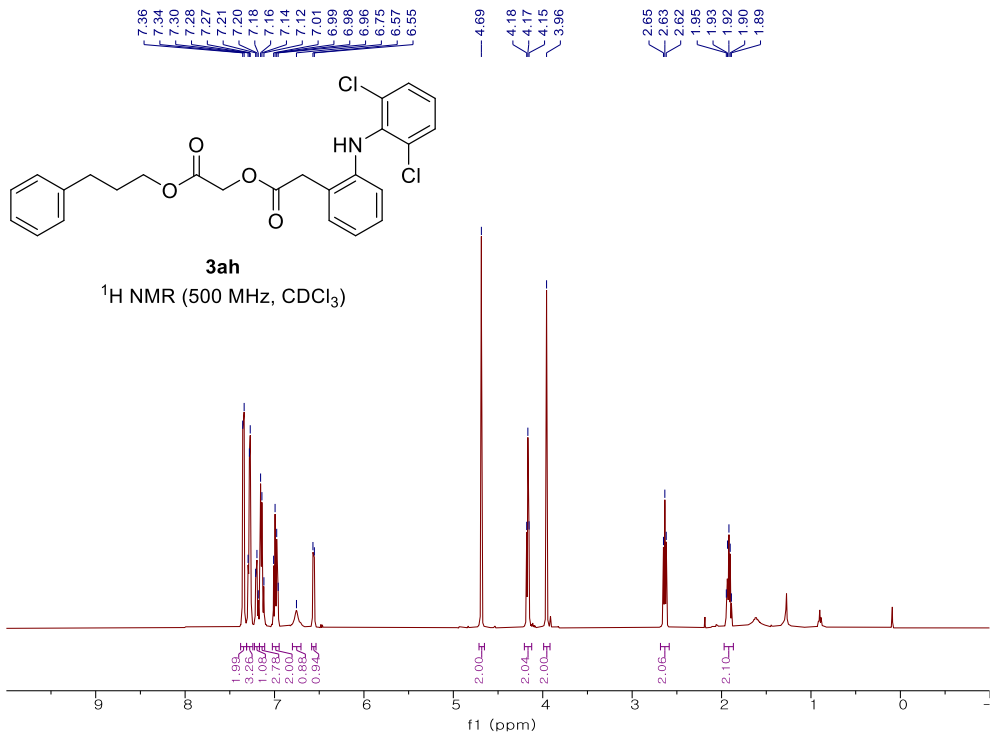

3ah

^{1}H NMR (500 MHz, $CDCl_3$)

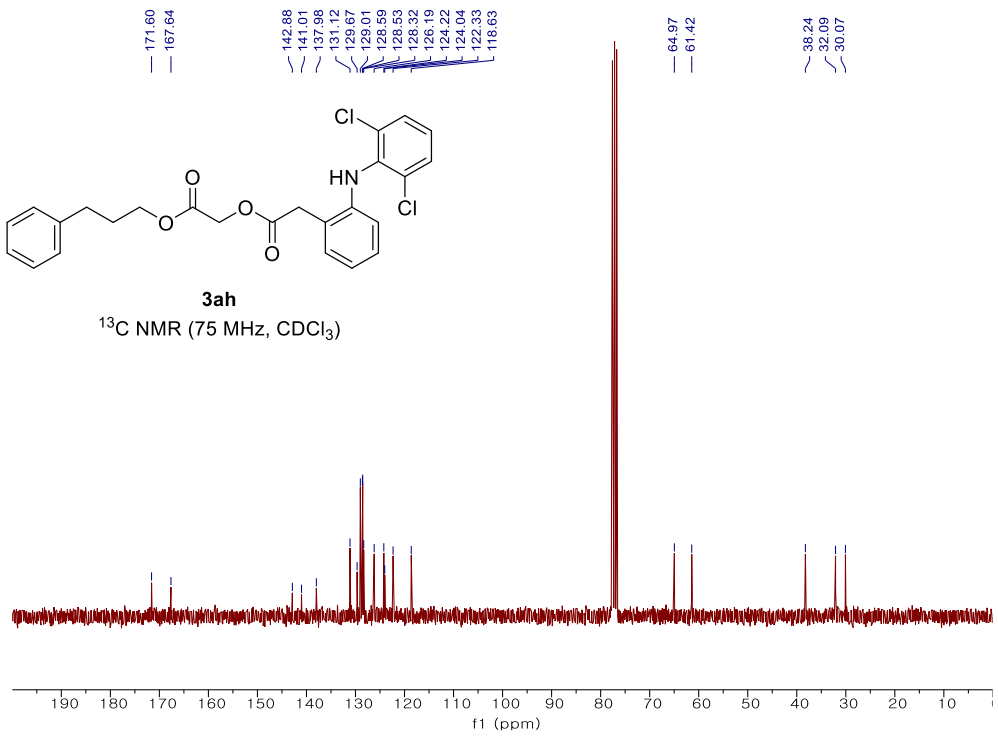

3ah

^{13}C NMR (75 MHz, $CDCl_3$)

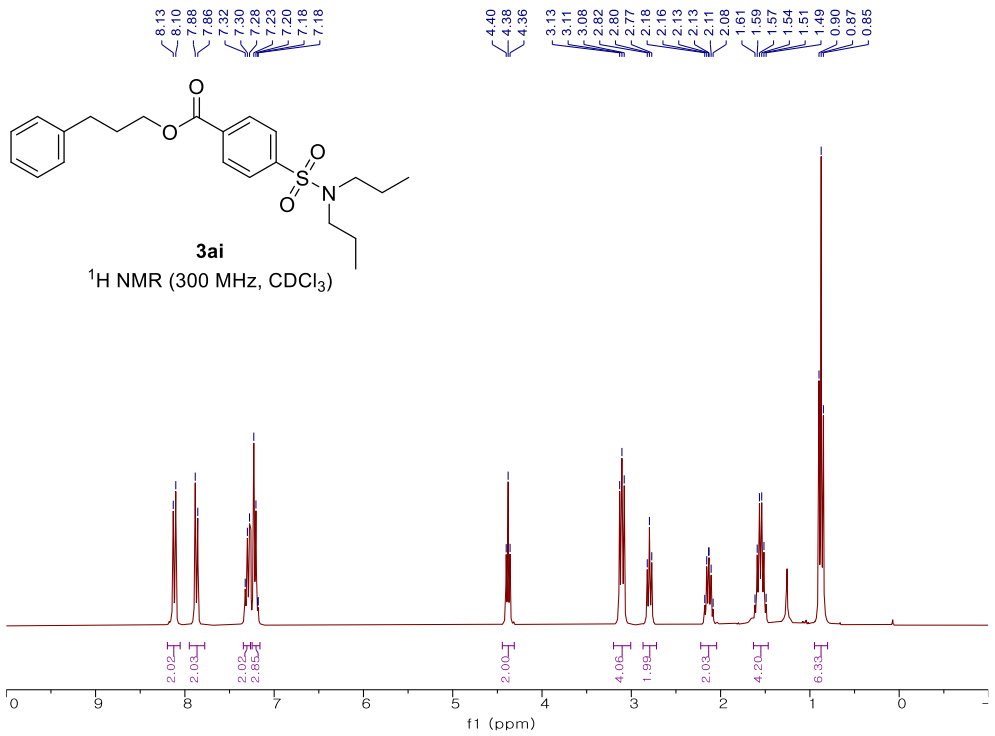

3ai

^{1}H NMR (300 MHz, $CDCl_3$)

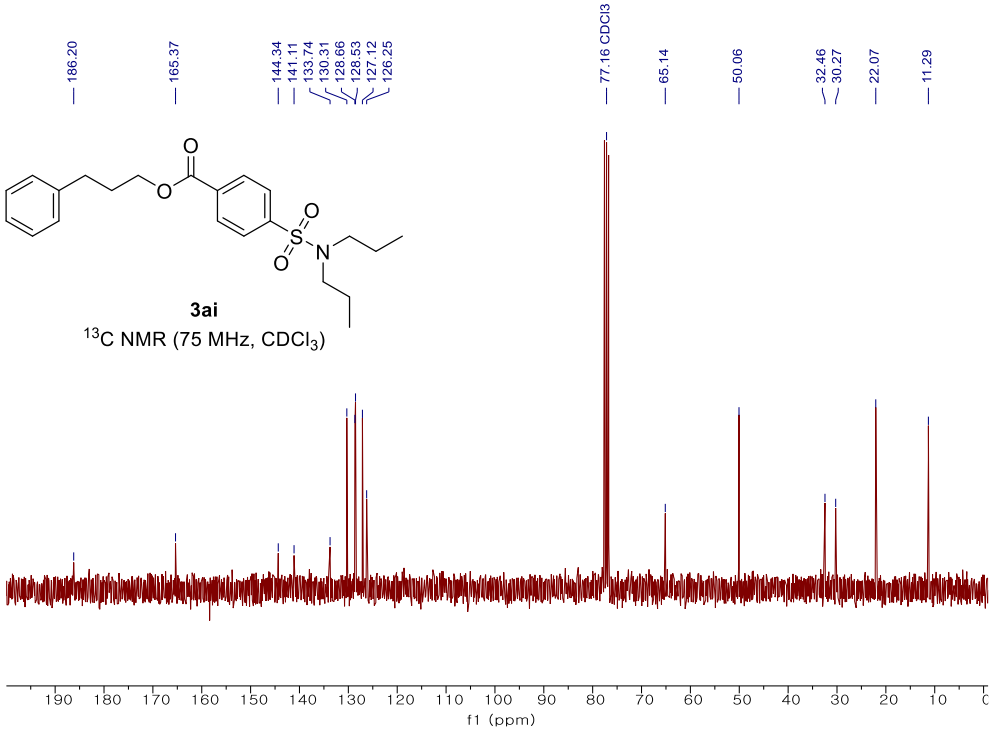

3ai

^{13}C NMR (75 MHz, $CDCl_3$)

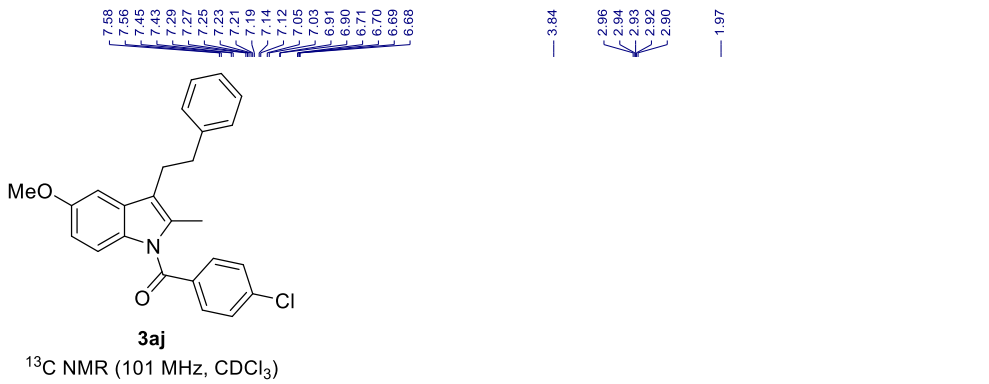

3aj

^{13}C NMR (101 MHz, $CDCl_3$)

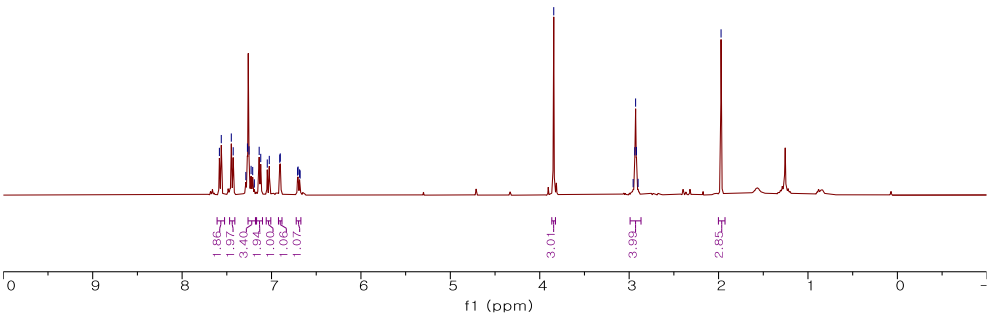

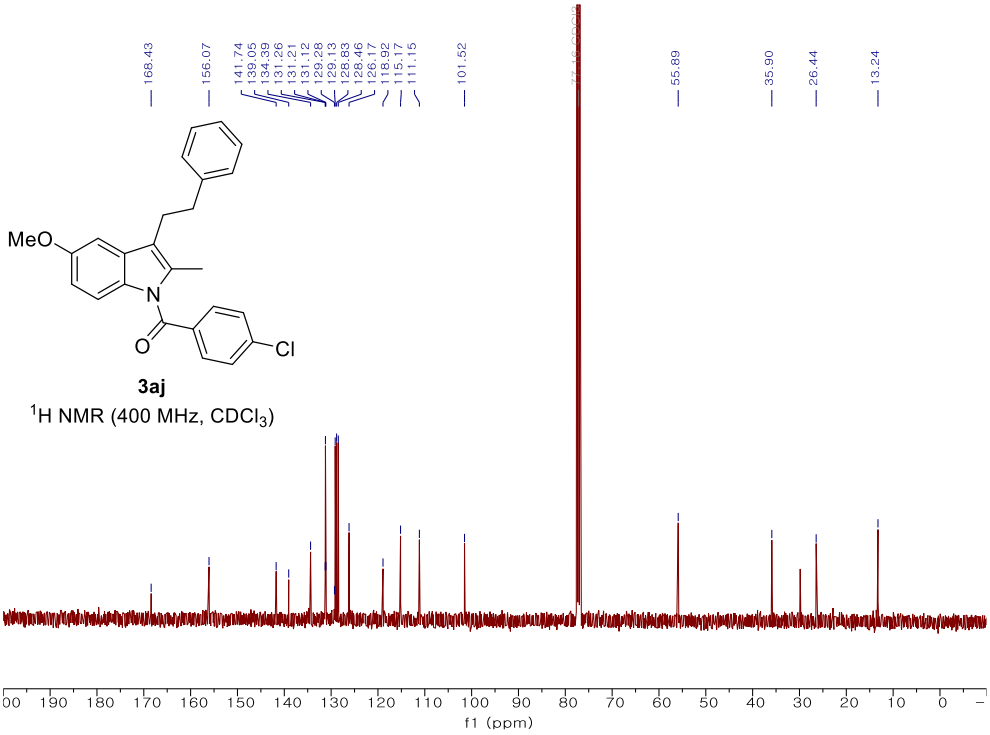

3aj

^{1}H NMR (400 MHz, $CDCl_3$)

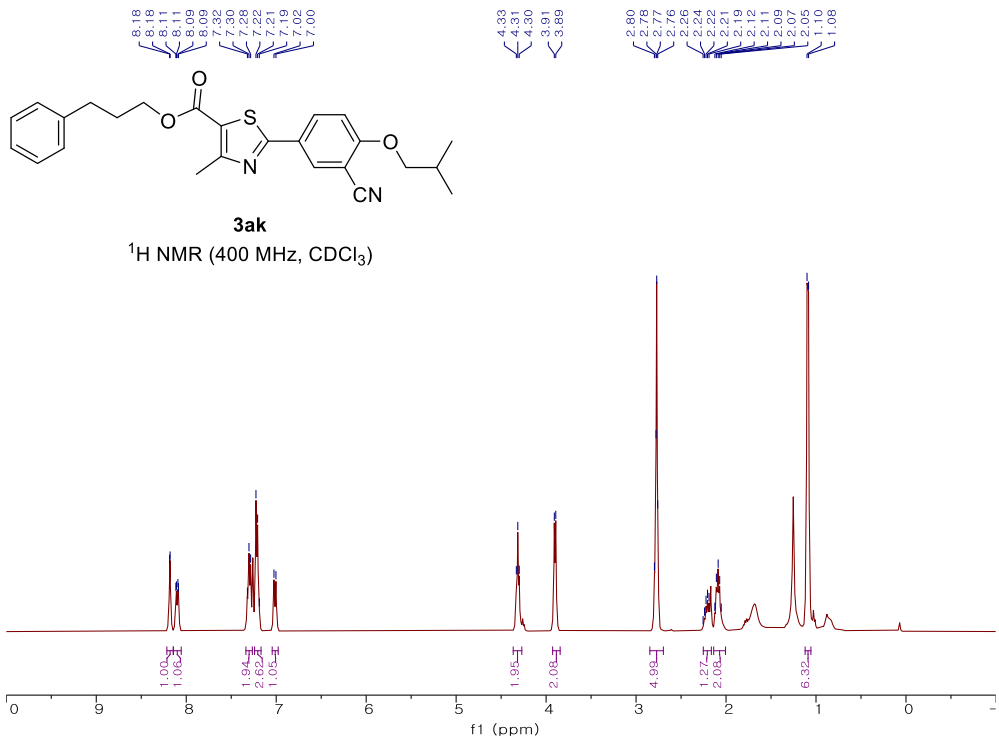

3ak

^{1}H NMR (400 MHz, $CDCl_3$)

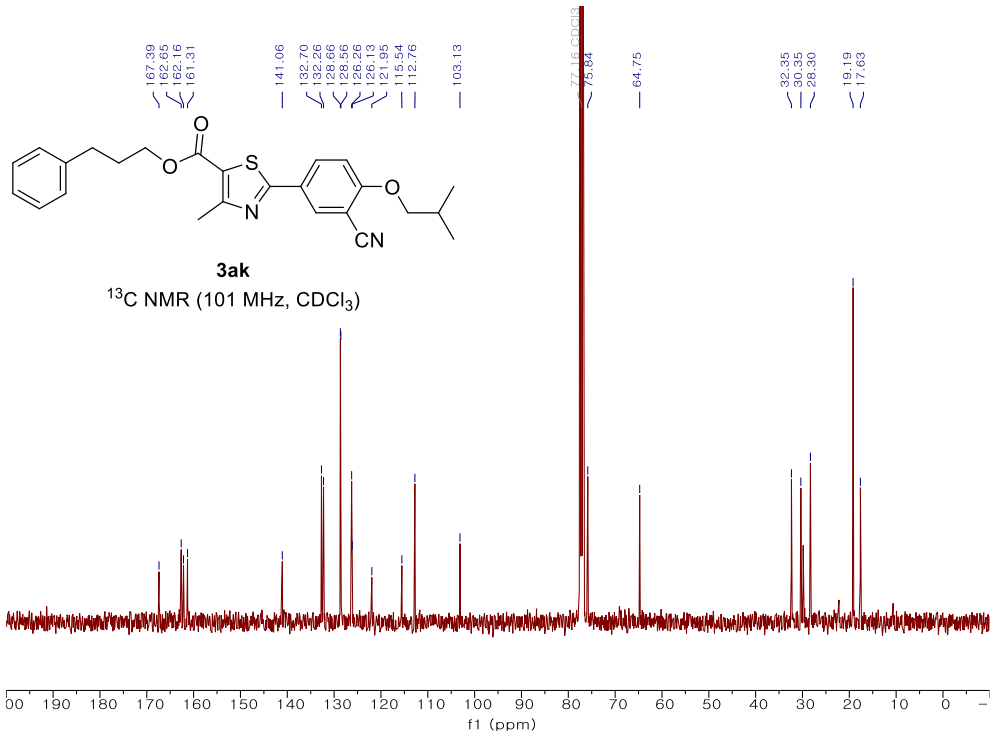

3ak

^{13}C NMR (101 MHz, $CDCl_3$)

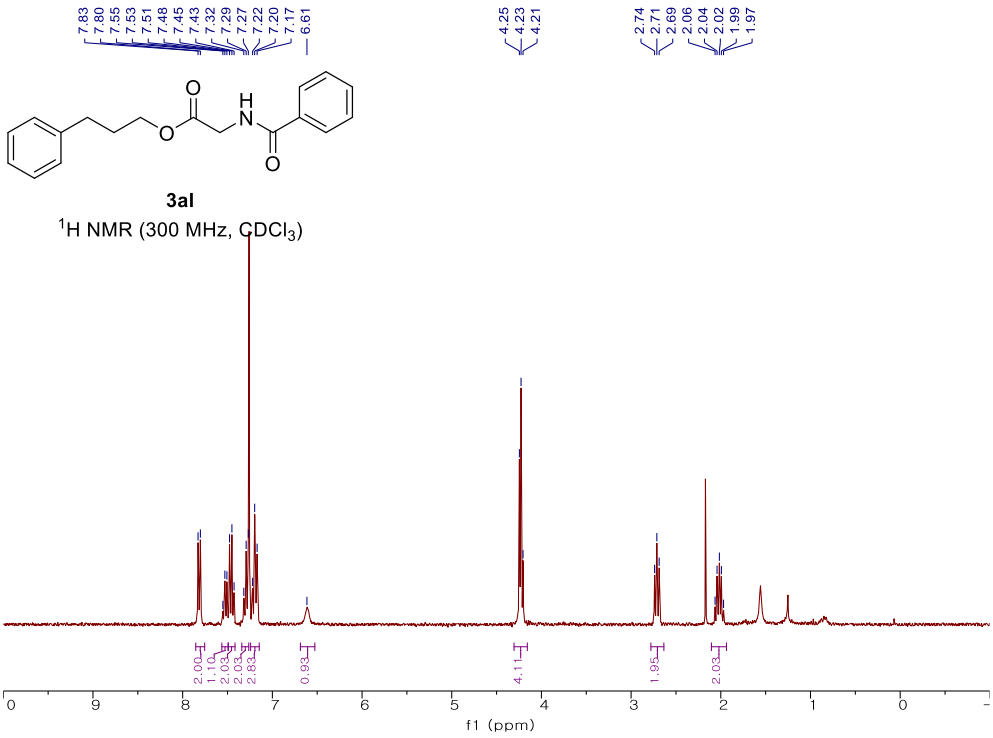

3al

^{1}H NMR (300 MHz, $CDCl_3$)

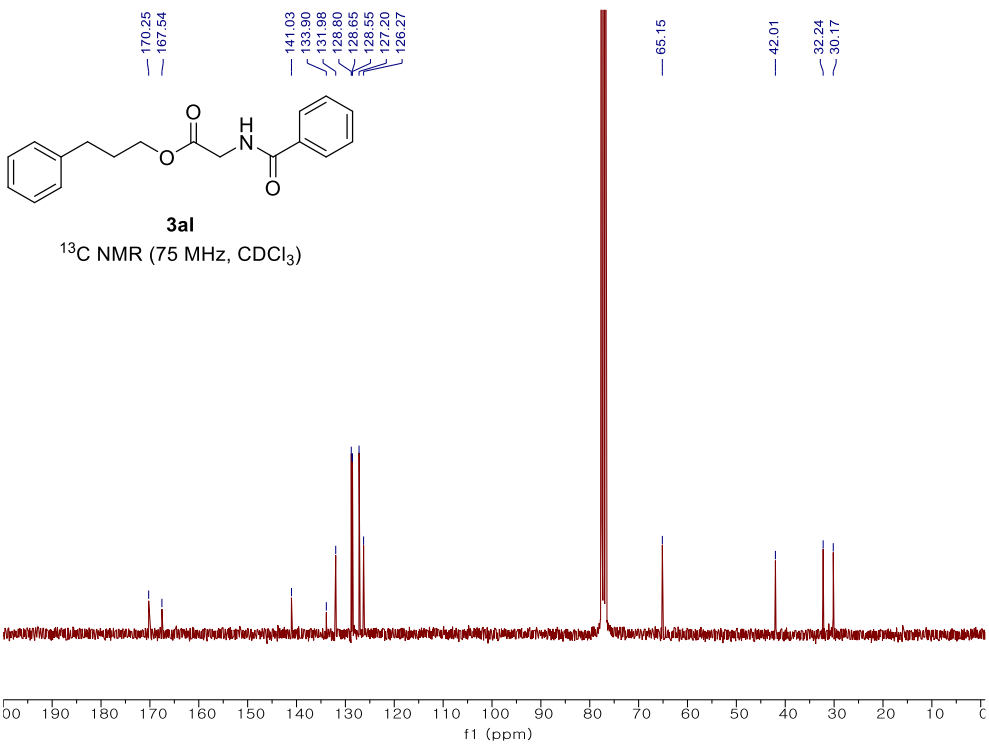

3al

^{13}C NMR (75 MHz, $CDCl_3$)

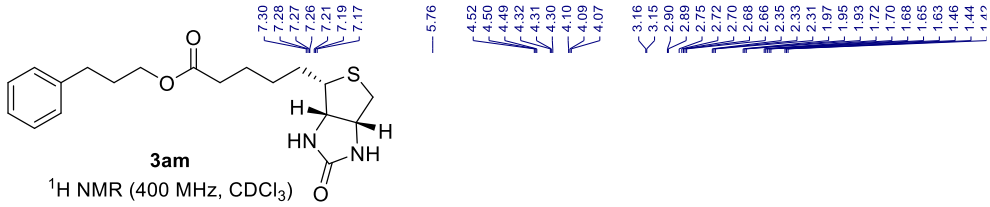

3am

^{1}H NMR (400 MHz, $CDCl_3$)

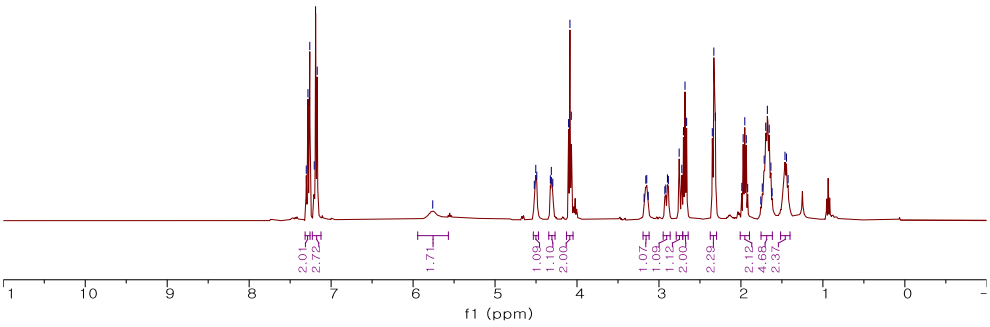

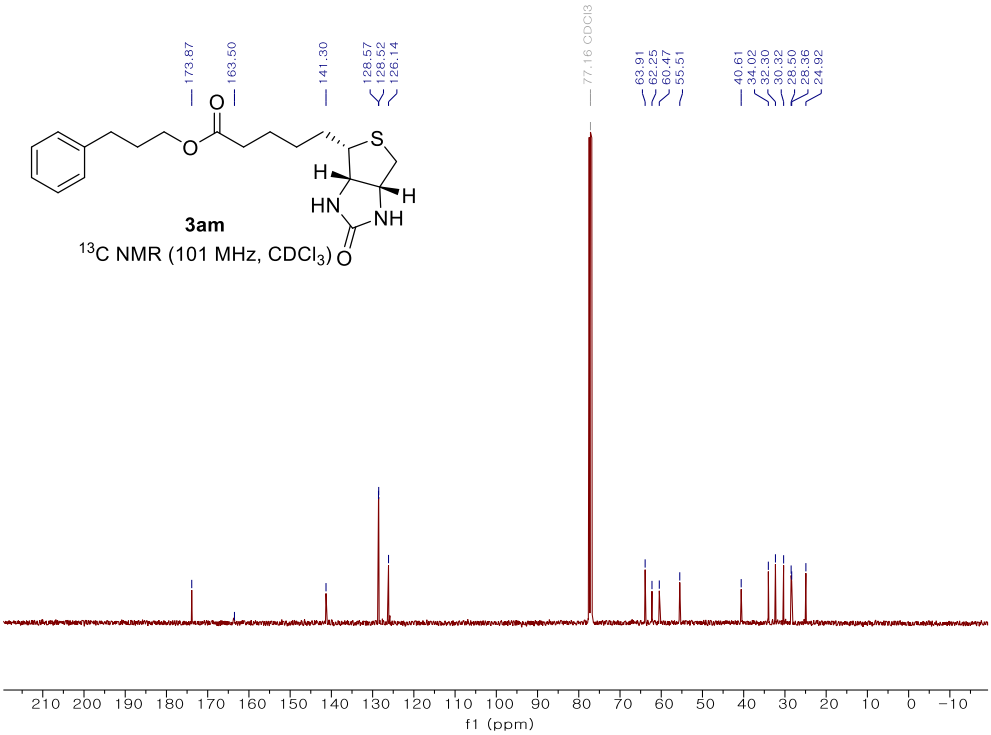

3am

^{13}C NMR (101 MHz, $CDCl_3$)

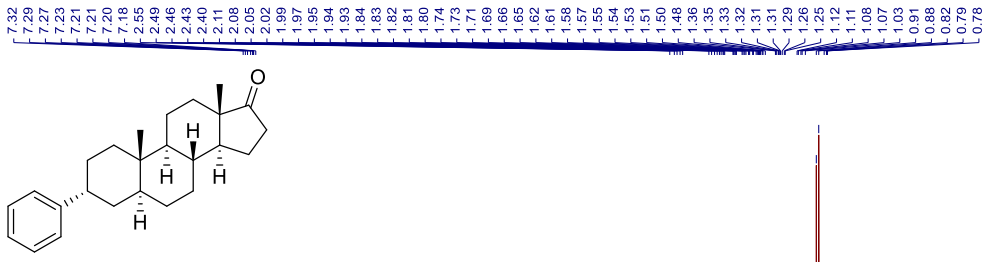

3an

^{1}H NMR (300 MHz, $CDCl_3$)

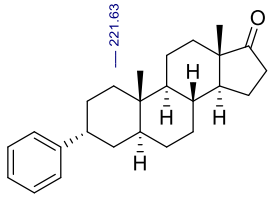

3an

^{13}C NMR (75 MHz, $CDCl_3$)

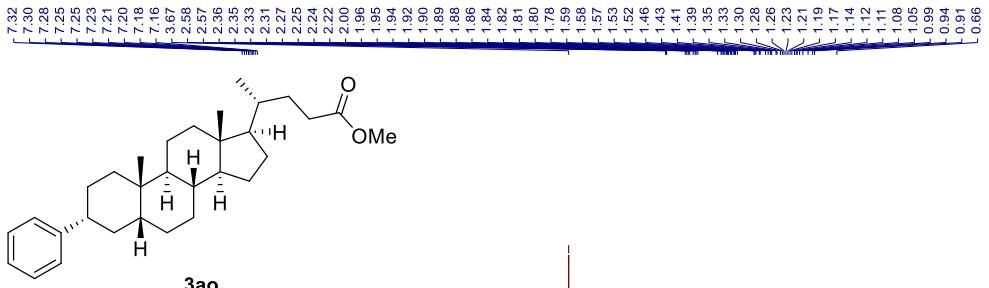

3ao

^{1}H NMR (300 MHz, $CDCl_3$)

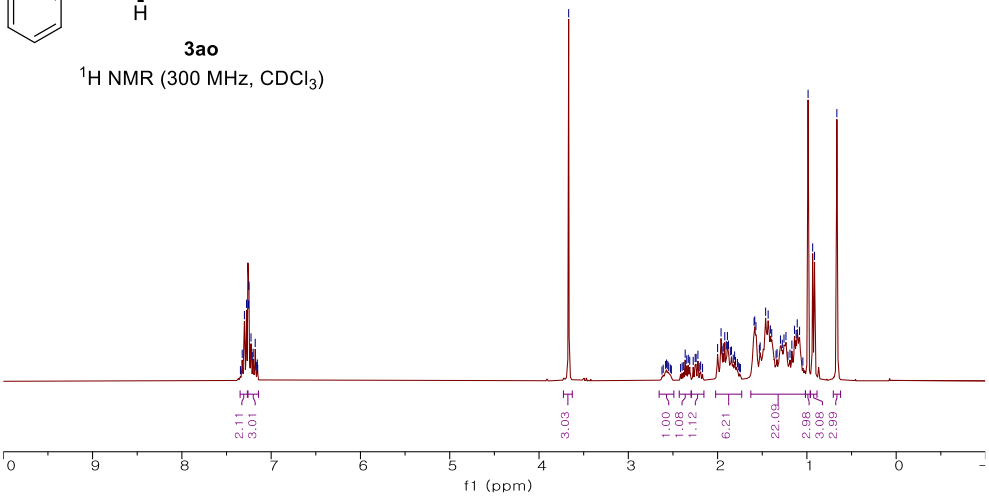

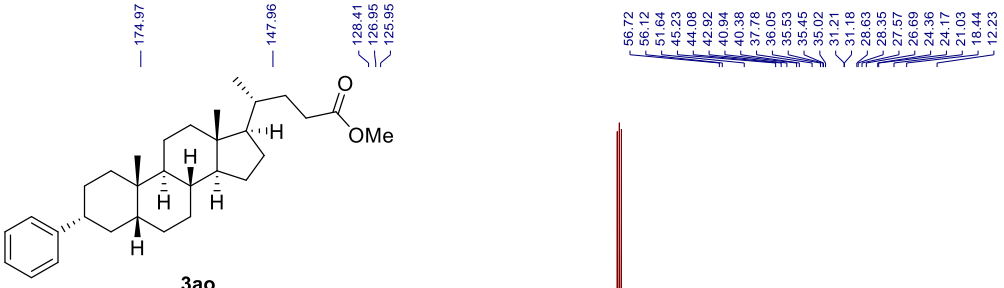

3ao

^{13}C NMR (75 MHz, $CDCl_3$)

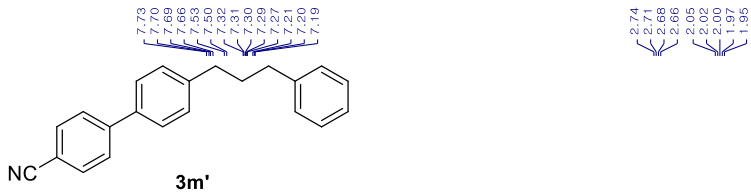

3m'

^{1}H NMR (300 MHz, $CDCl_3$)

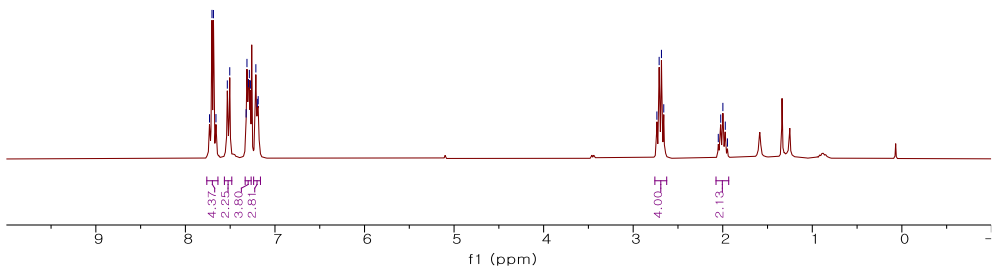

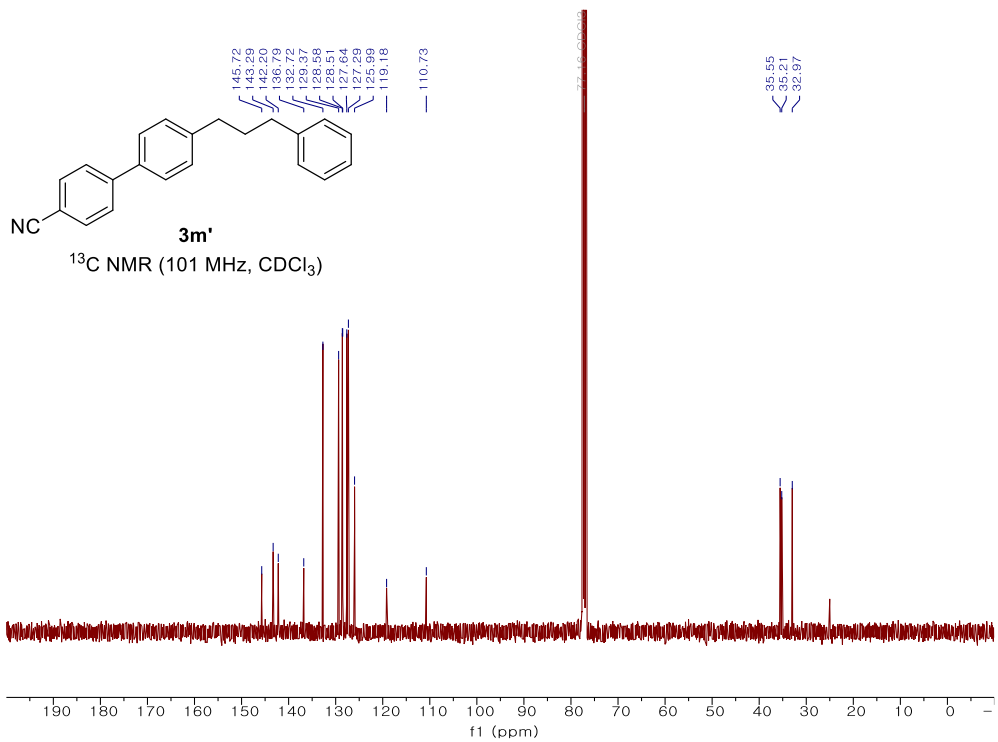

3m'

^{13}C NMR (101 MHz, $CDCl_3$)

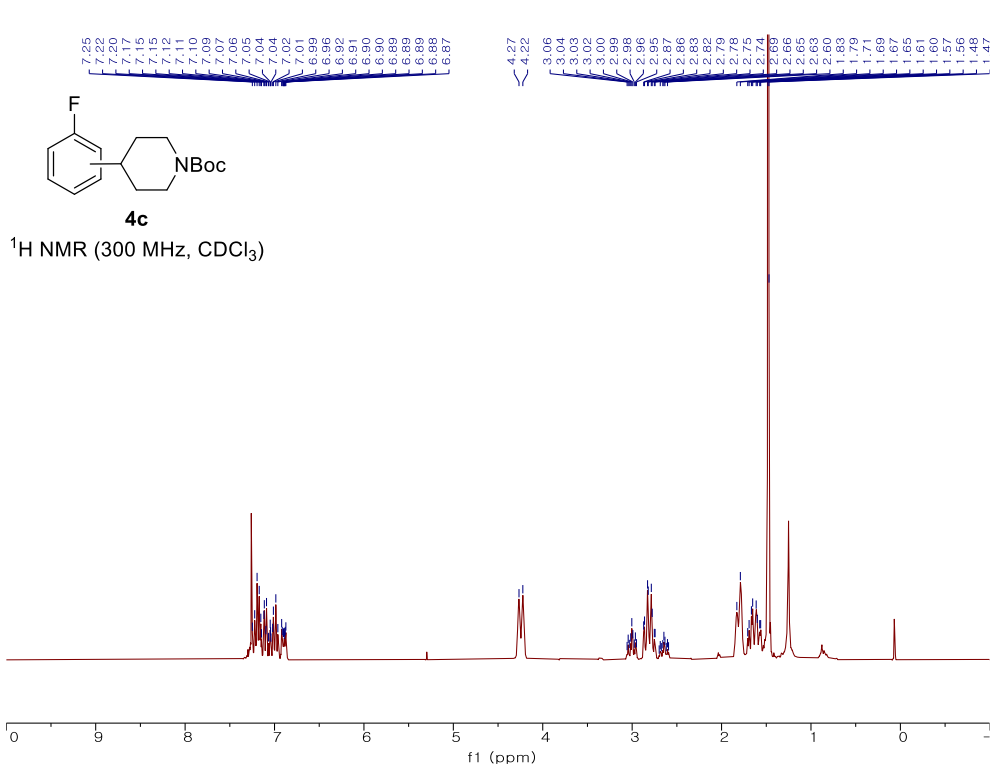

4c

^{1}H NMR (300 MHz, $CDCl_3$)

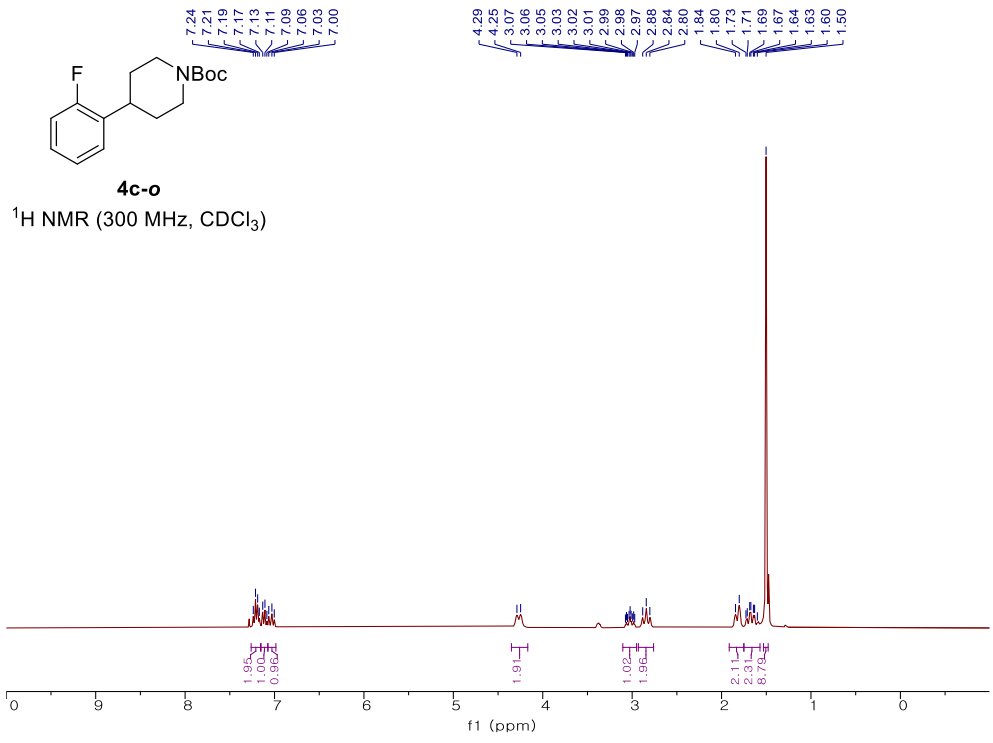

4c-*o*

^{1}H NMR (300 MHz, $CDCl_3$)

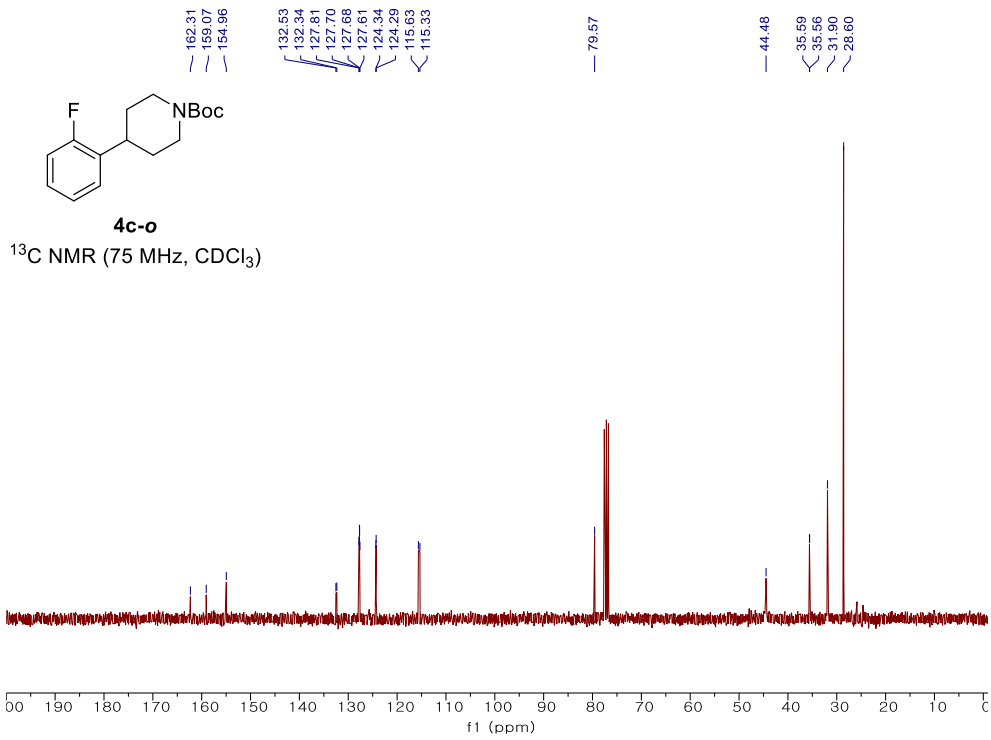

4c-*o*

^{13}C NMR (75 MHz, $CDCl_3$)

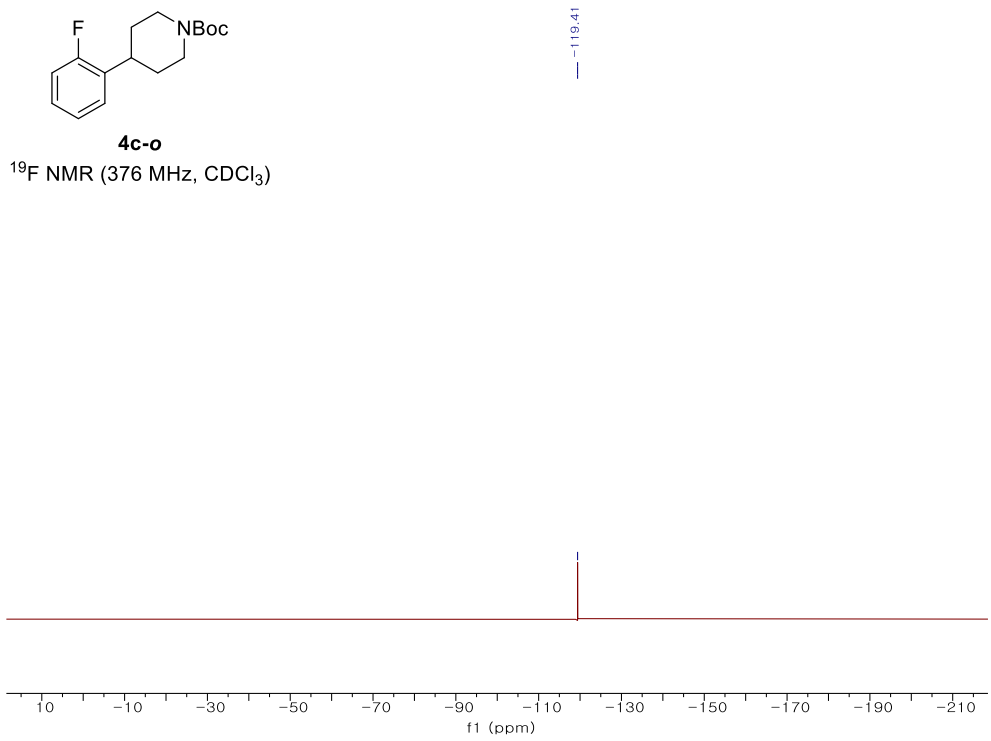

4c-*o*

^{19}F NMR (376 MHz, $CDCl_3$)

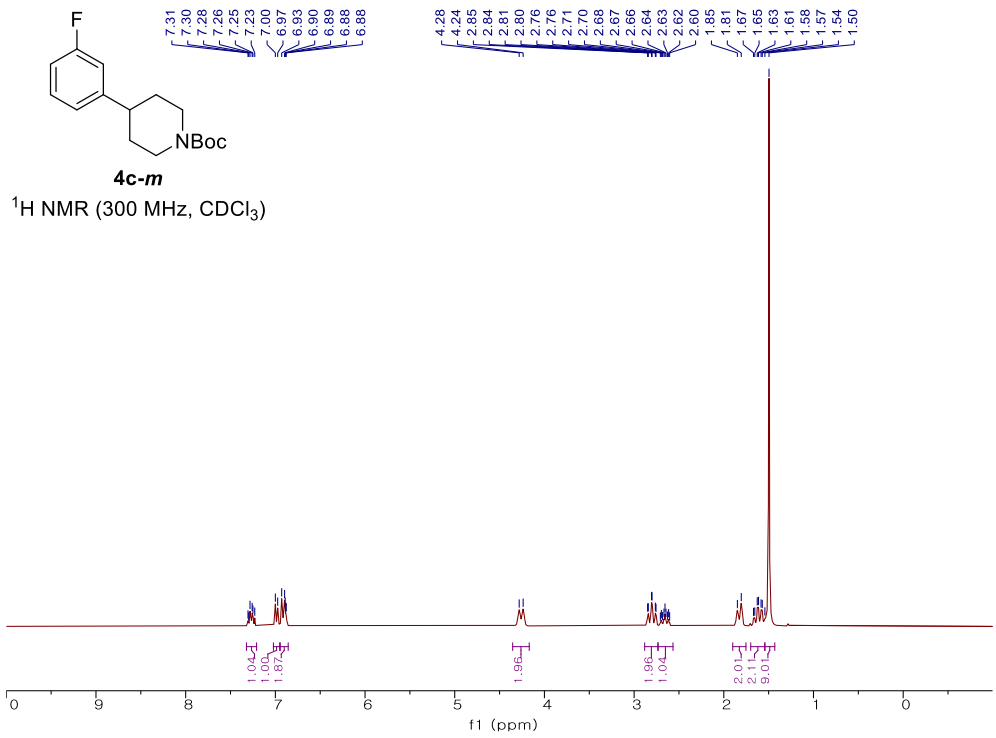

4c-*m*

^{1}H NMR (300 MHz, $CDCl_3$)

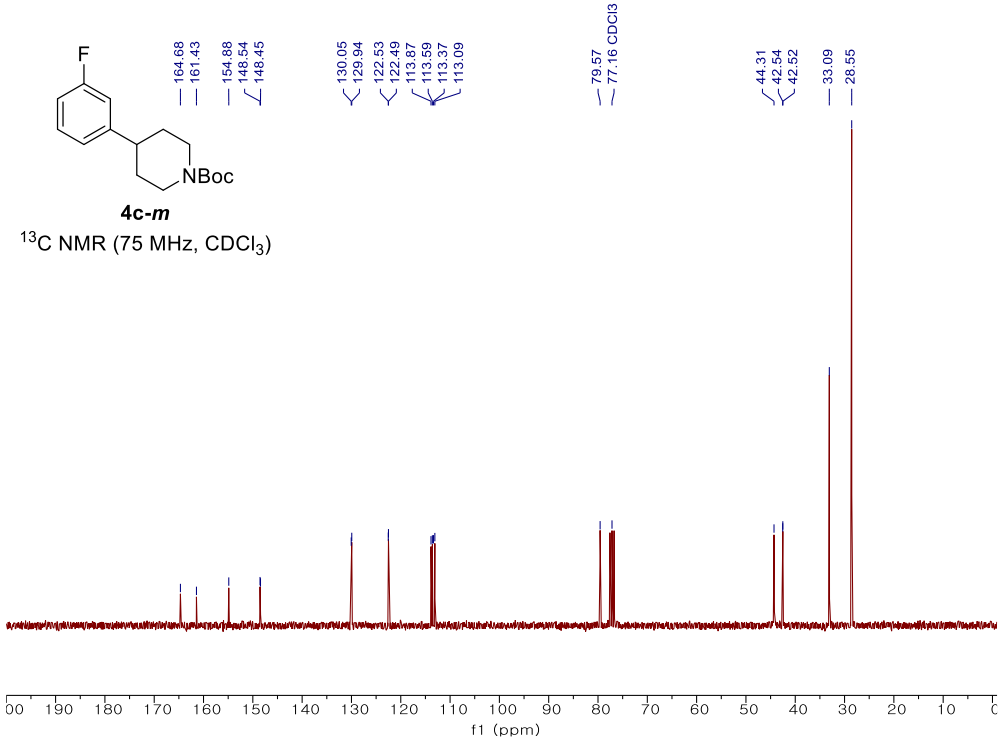

4c-*m*

^{13}C NMR (75 MHz, $CDCl_3$)

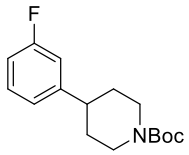

4c-*m*

^{19}F NMR (376 MHz, $CDCl_3$)

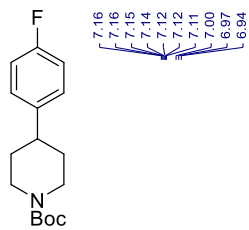

4c-*p*

^{1}H NMR (300 MHz, $CDCl_3$)

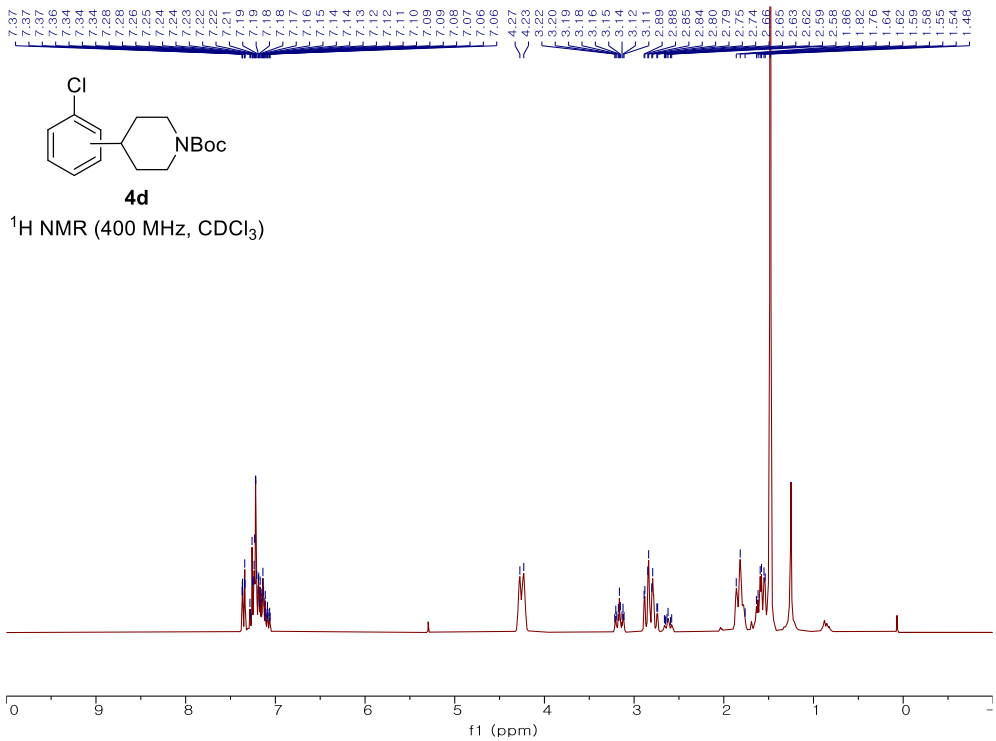

4d

^{1}H NMR (400 MHz, $CDCl_3$)

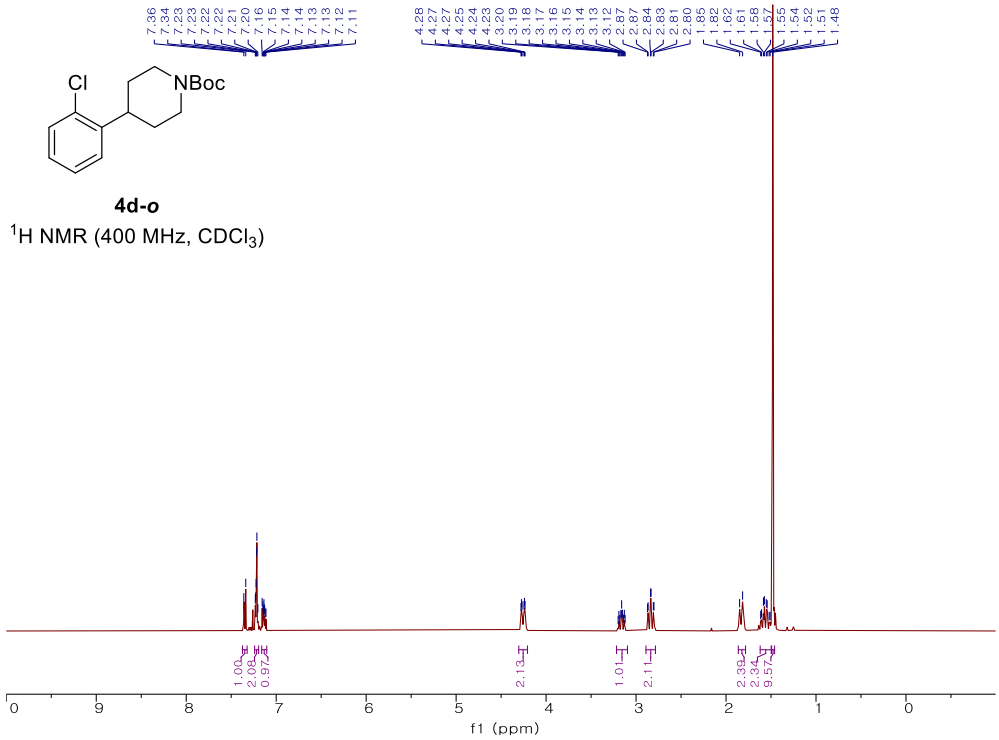

4d-*o*

^{1}H NMR (400 MHz, $CDCl_3$)

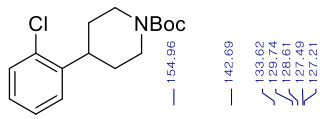

4d-*o*

^{13}C NMR (101 MHz, $CDCl_3$)

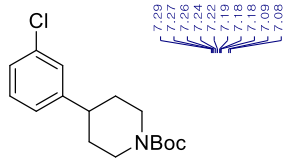

4d-*m*

^{1}H NMR (400 MHz, $CDCl_3$)

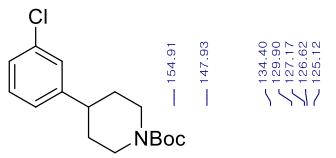

4d-*m*

^{13}C NMR (101 MHz, $CDCl_3$)

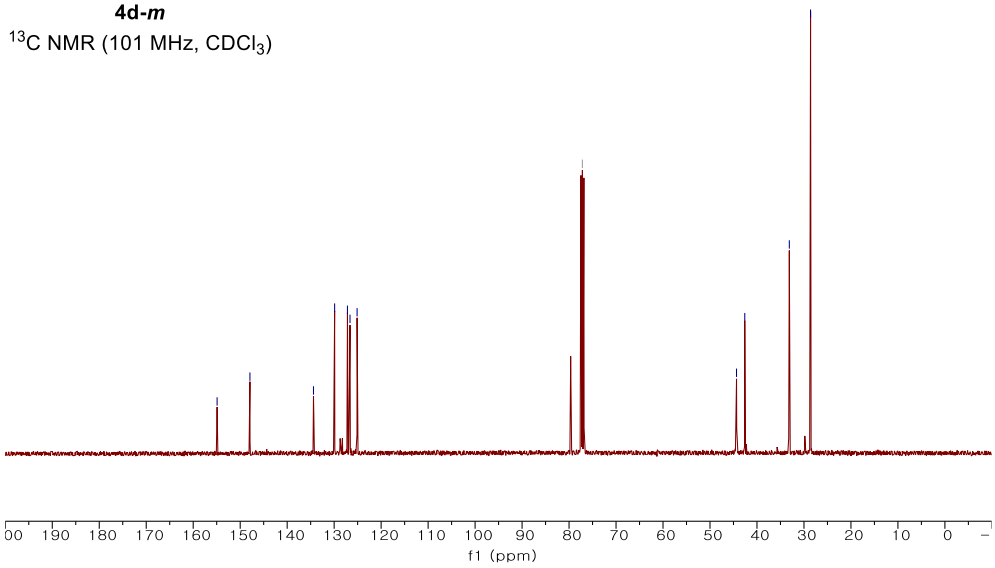

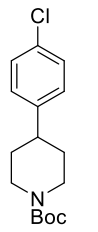

4d-*p*

^{1}H NMR (400 MHz, $CDCl_3$)

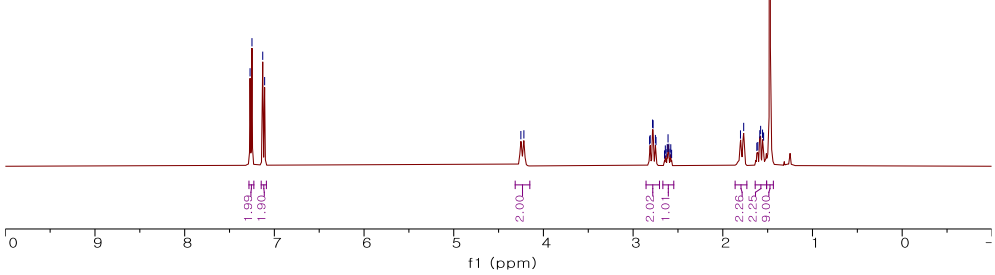

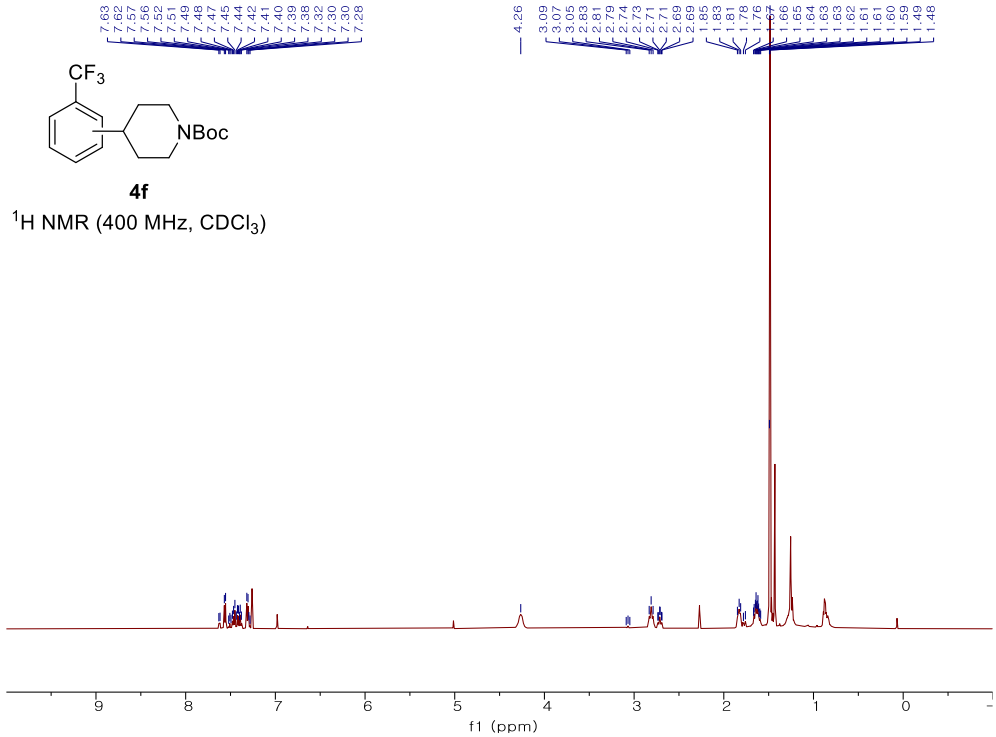

4f

^{1}H NMR (400 MHz, $CDCl_3$)

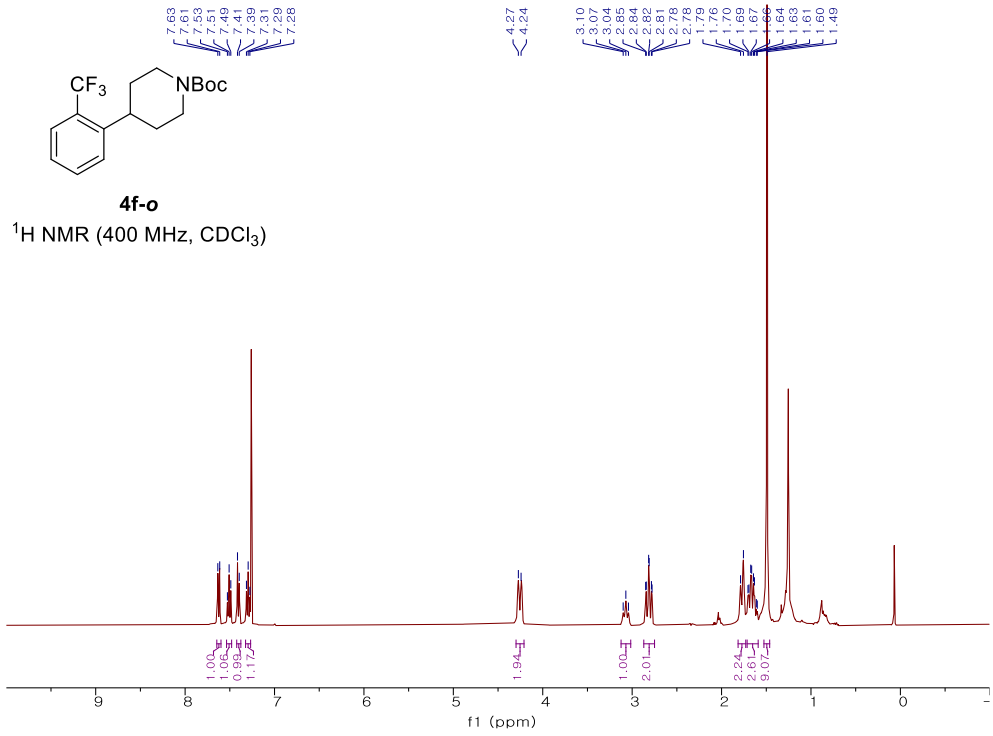

4f-*o*

^{1}H NMR (400 MHz, $CDCl_3$)

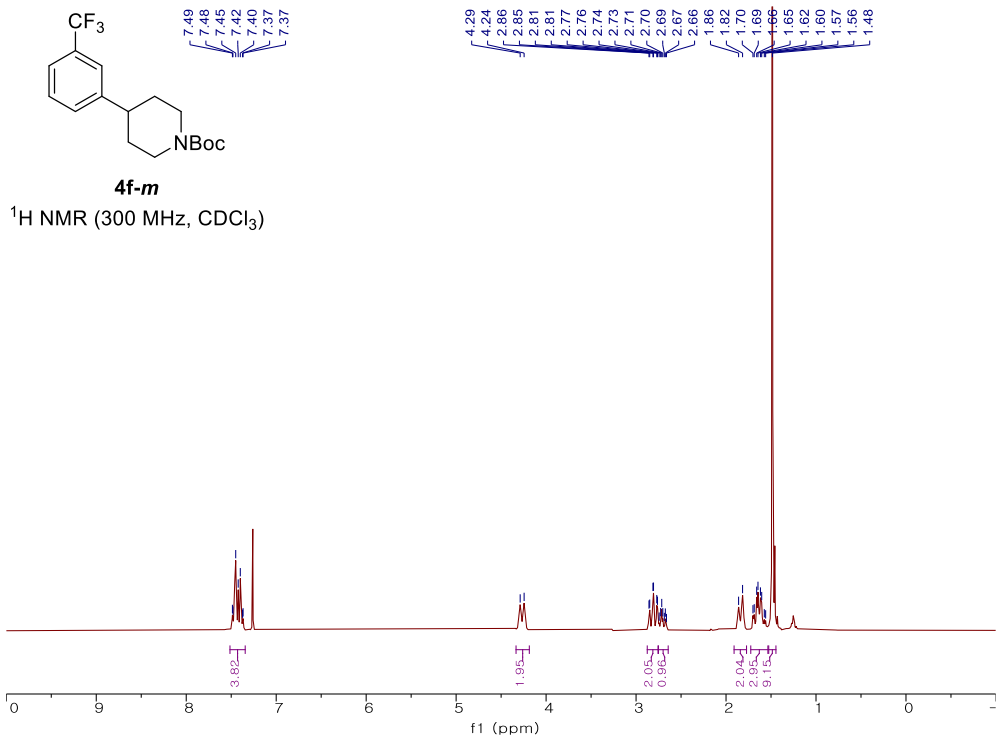

4f-*m*

^{1}H NMR (300 MHz, $CDCl_3$)

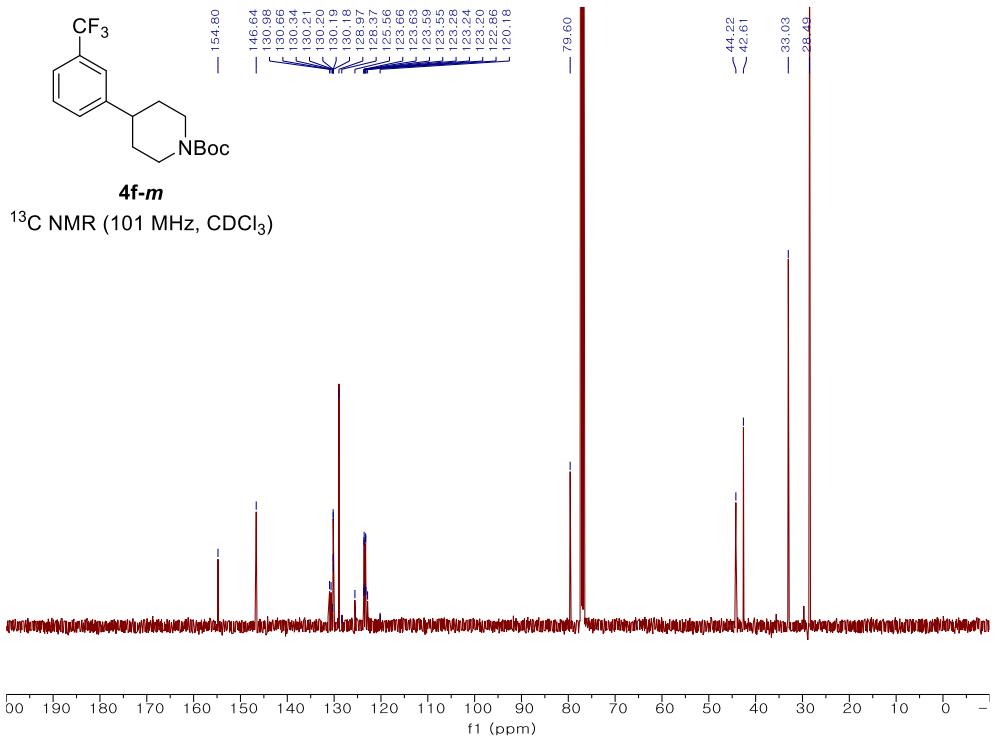

4f-*m*

^{13}C NMR (101 MHz, $CDCl_3$)

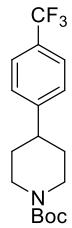

4f-*p*

^{1}H NMR (300 MHz, $CDCl_3$)

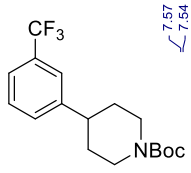

4f-*m*

^{19}F NMR (376 MHz, $CDCl_3$)

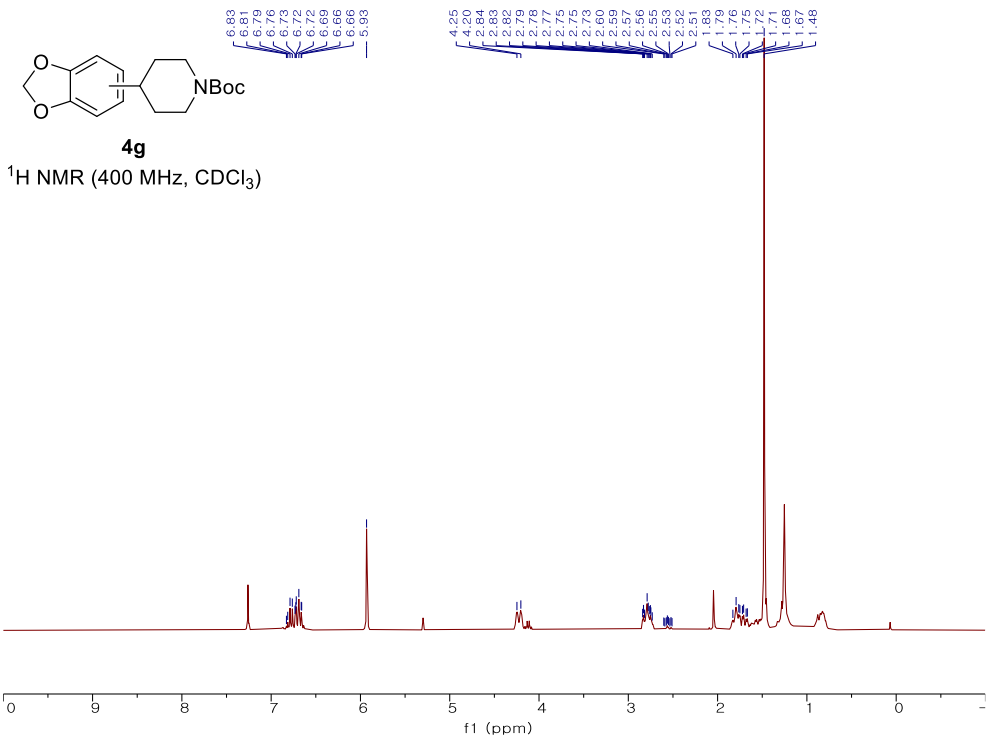

4g

^{1}H NMR (400 MHz, $CDCl_3$)

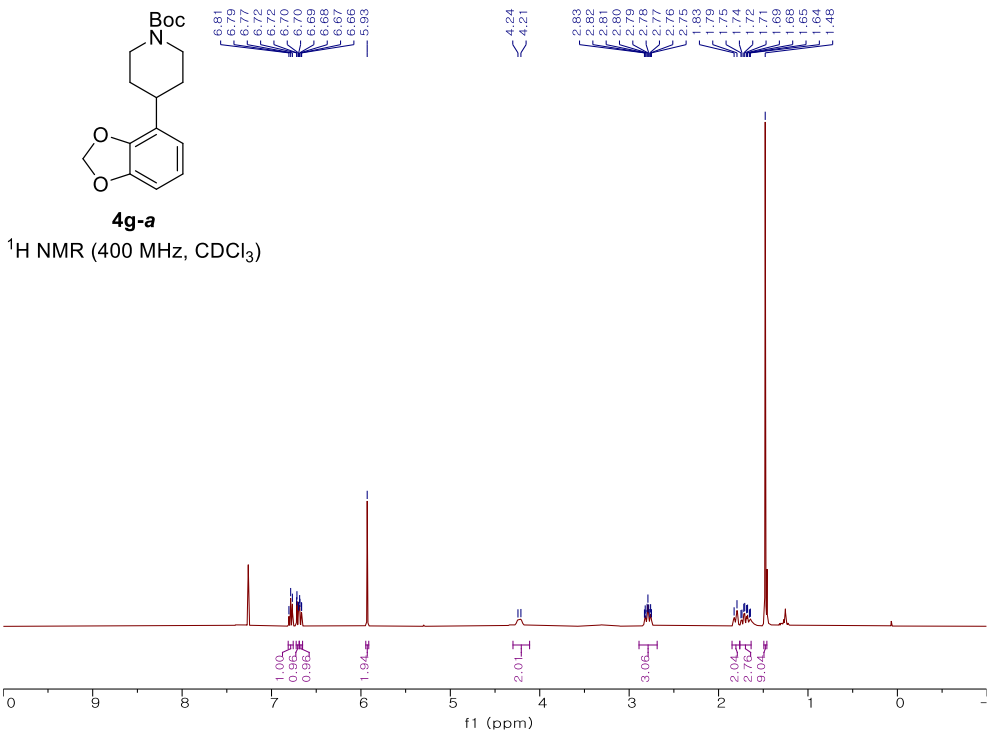

4g-*a*

^{1}H NMR (400 MHz, $CDCl_3$)

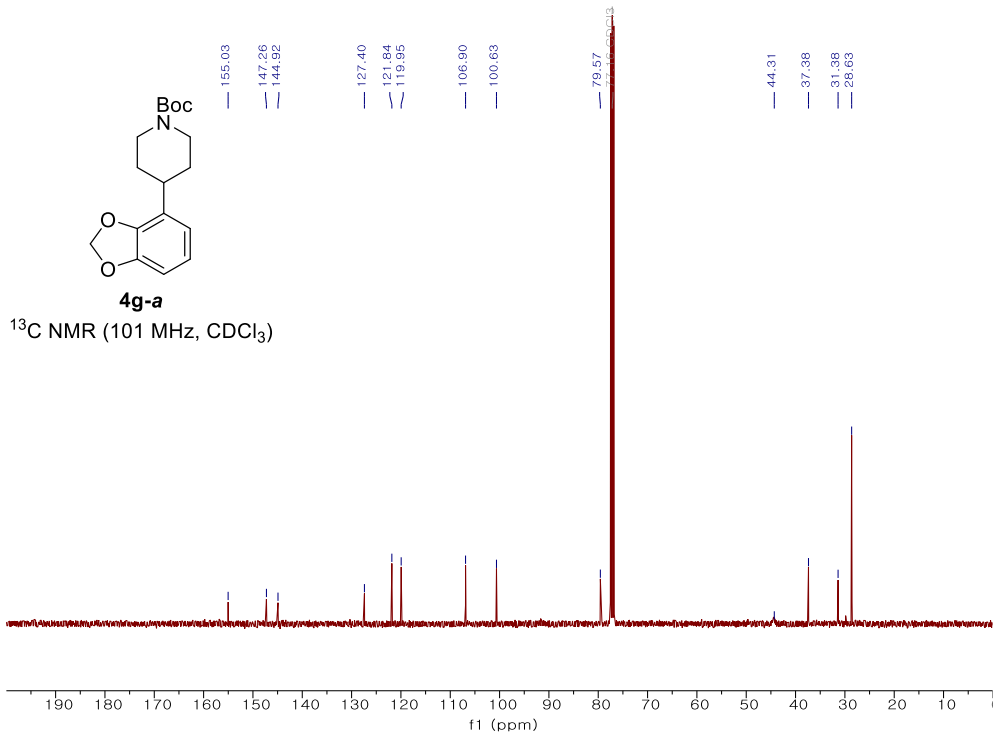

4g-*a*

^{13}C NMR (101 MHz, $CDCl_3$)

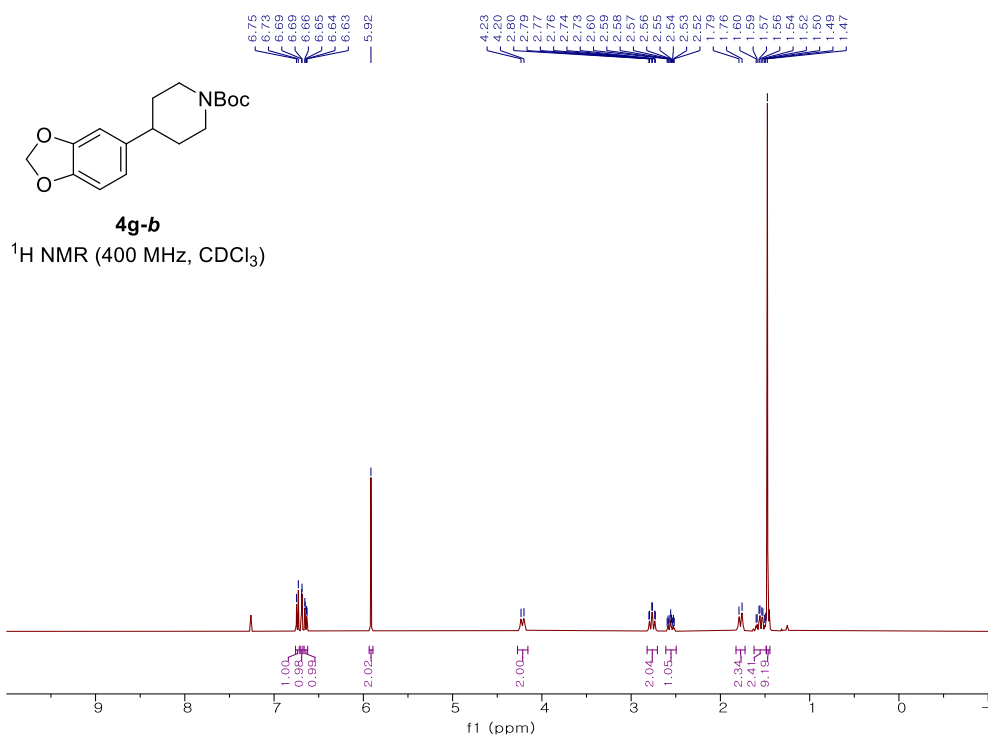

4g-*b*

^{1}H NMR (400 MHz, $CDCl_3$)

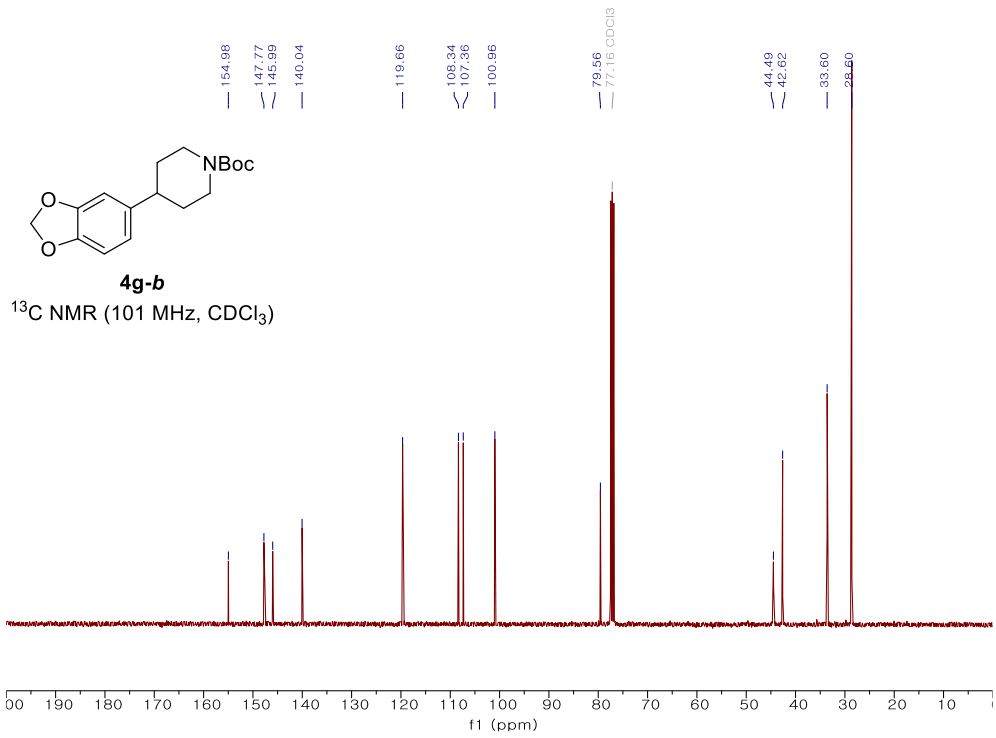

4g-*b*

^{13}C NMR (101 MHz, $CDCl_3$)

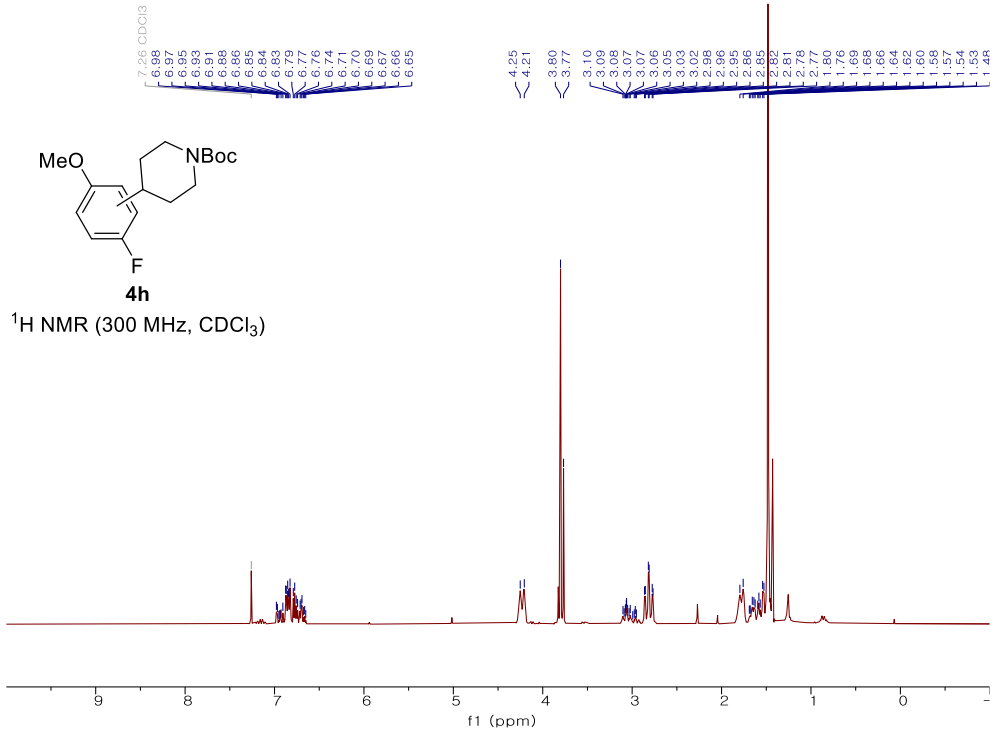

4h

^{1}H NMR (300 MHz, $CDCl_3$)

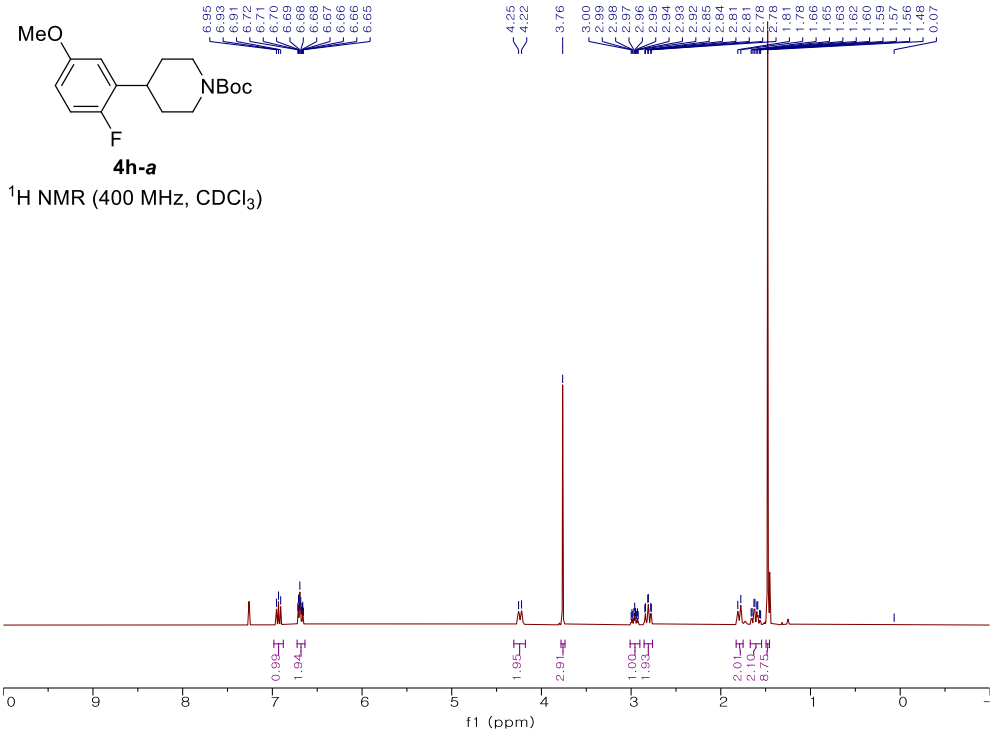

4h-*a*

^{1}H NMR (400 MHz, $CDCl_3$)

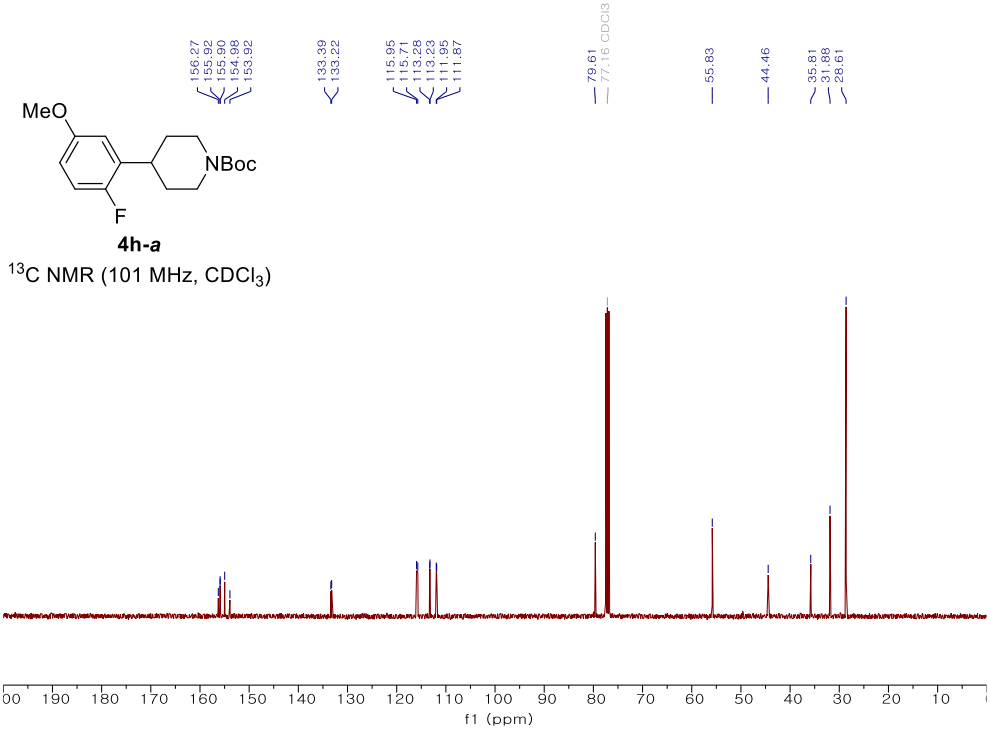

4h-*a*

^{13}C NMR (101 MHz, $CDCl_3$)

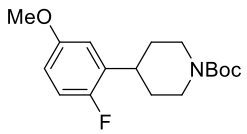

4h-*a*

^{19}F NMR (376 MHz, $CDCl_3$)

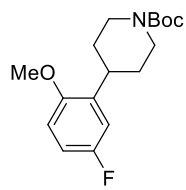

4h-*b*

^{1}H NMR (400 MHz, $CDCl_3$)

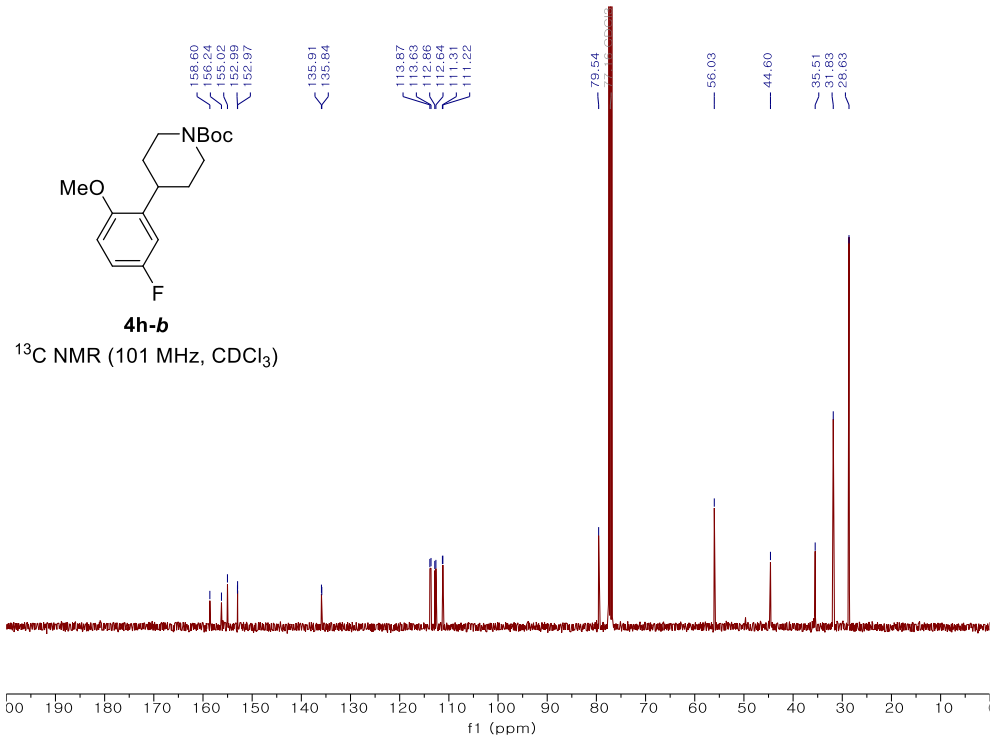

4h-*b*

^{13}C NMR (101 MHz, $CDCl_3$)

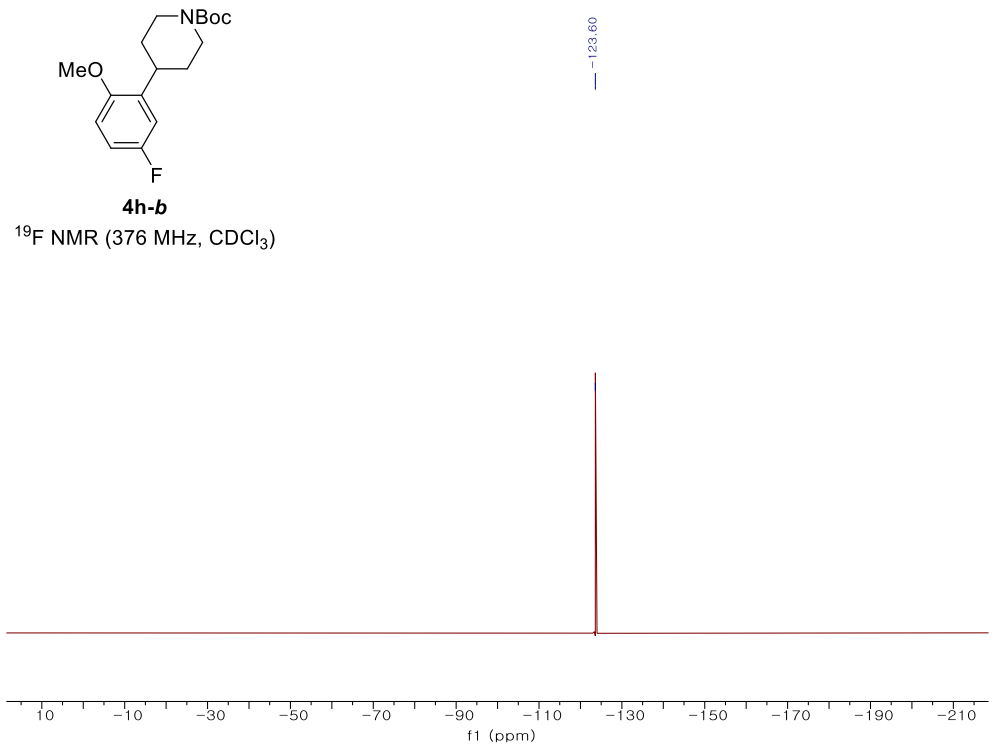

4h-*b*

^{19}F NMR (376 MHz, $CDCl_3$)

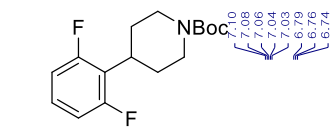

4i-*a*

^{1}H NMR (400 MHz, $CDCl_3$)

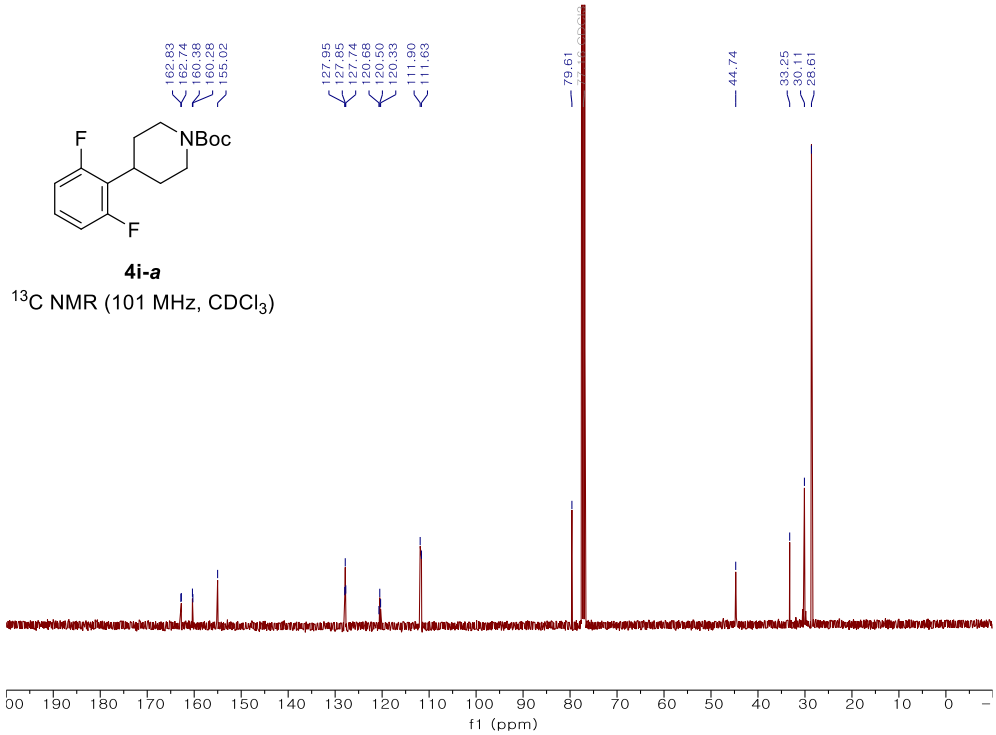

4i-*a*

^{13}C NMR (101 MHz, $CDCl_3$)

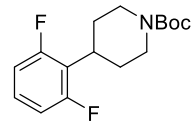

4i-*a*

^{19}F NMR (376 MHz, $CDCl_3$)

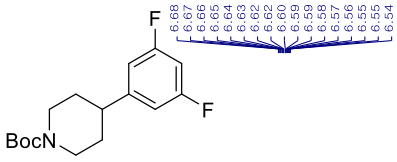

4i-*b*

^{1}H NMR (400 MHz, $CDCl_3$)

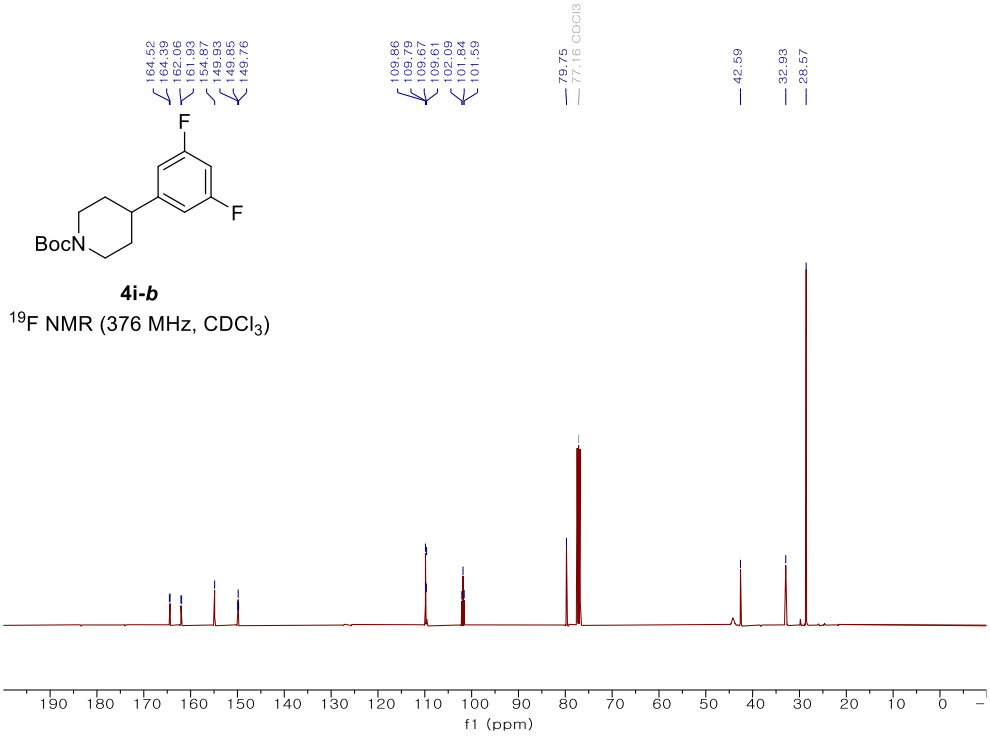

4i-*b*

^{19}F NMR (376 MHz, $CDCl_3$)

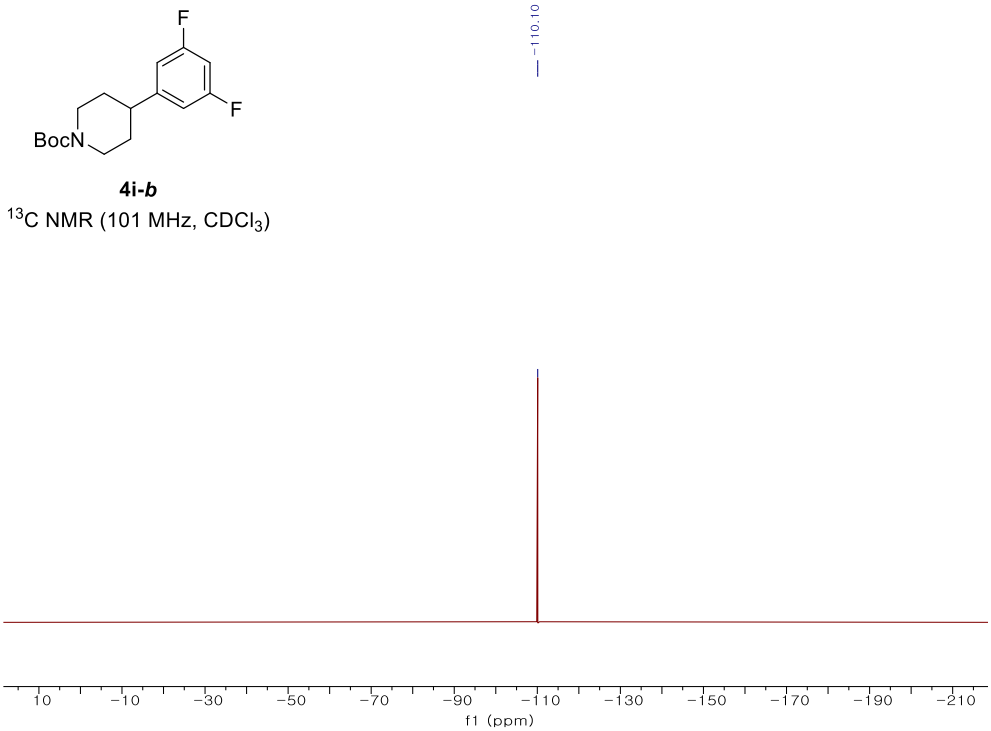

4i-*b*

^{13}C NMR (101 MHz, $CDCl_3$)

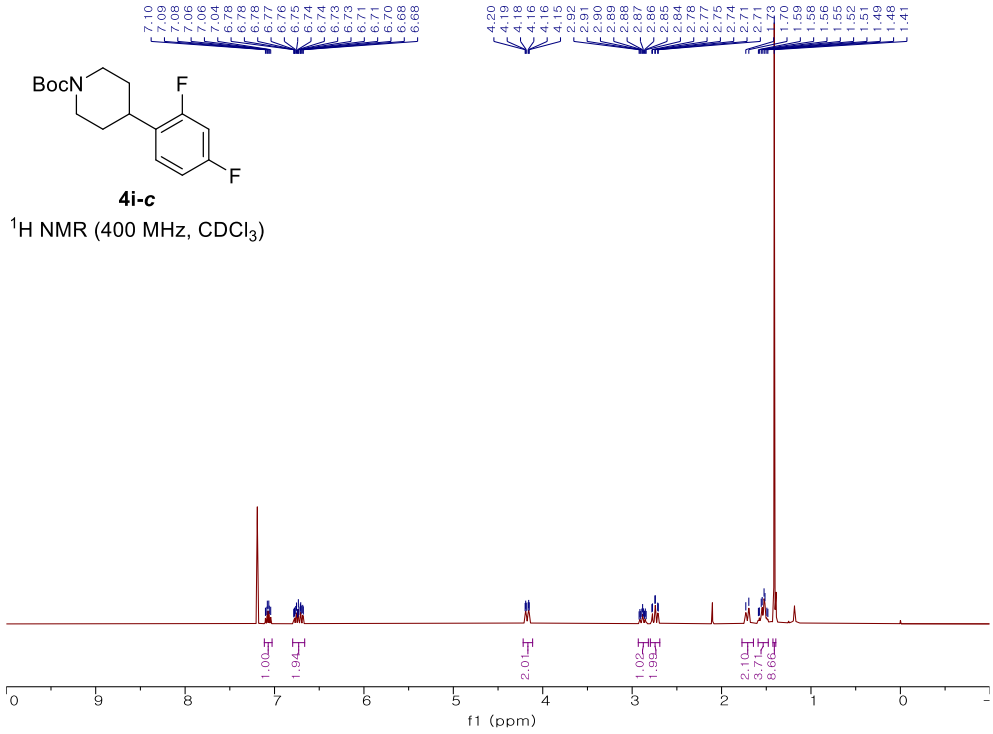

4i-*c*

^{1}H NMR (400 MHz, $CDCl_3$)

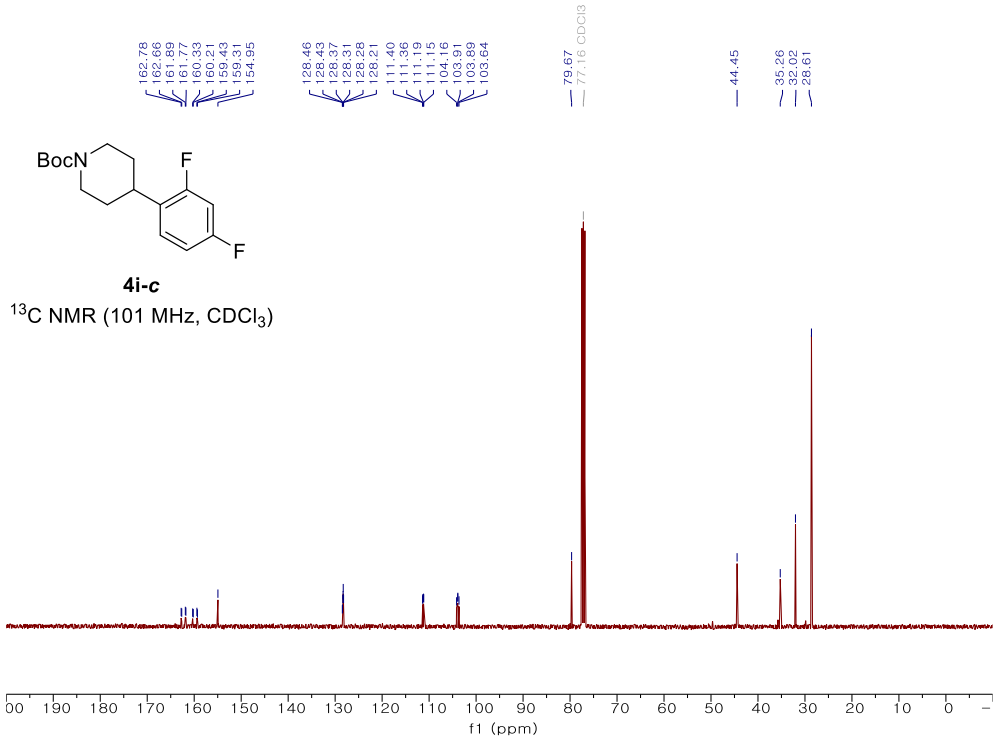

4i-*c*

^{13}C NMR (101 MHz, $CDCl_3$)

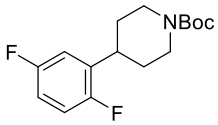

4j

^{1}H NMR (400 MHz, $CDCl_3$)

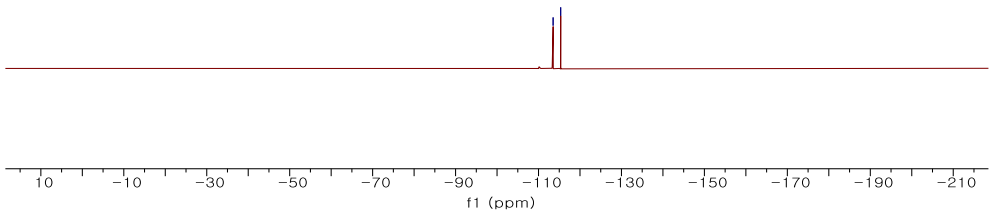

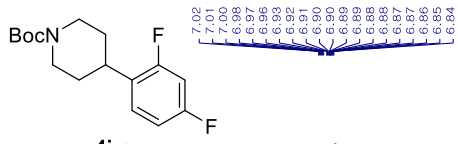

4i-*c*

^{19}F NMR (376 MHz, $CDCl_3$)

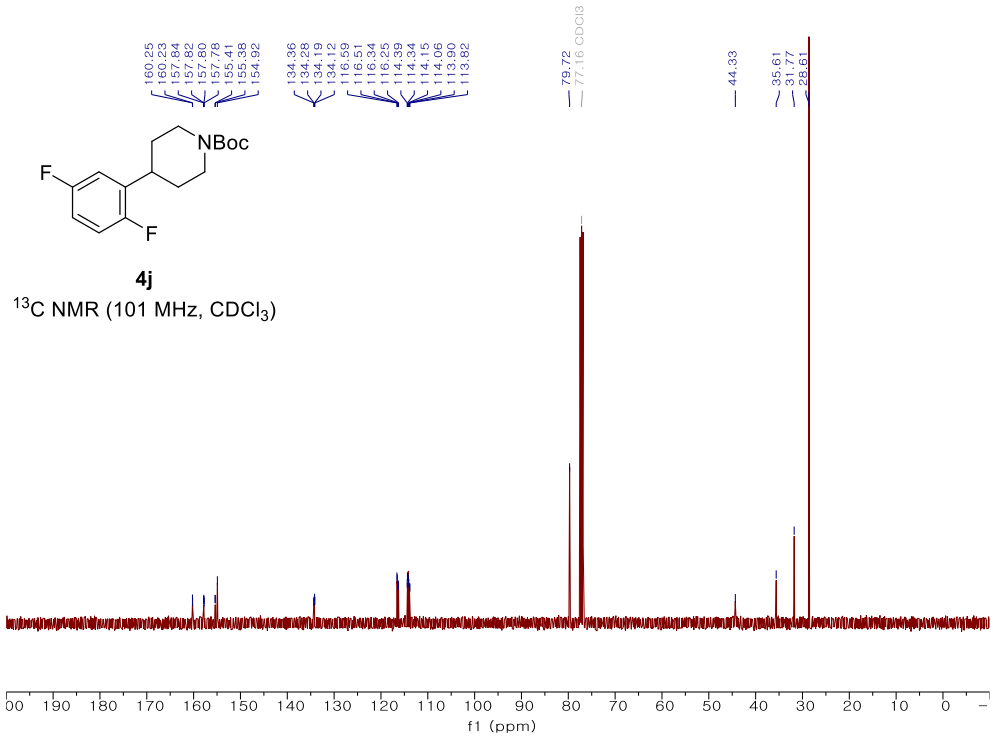

4j

^{13}C NMR (101 MHz, $CDCl_3$)

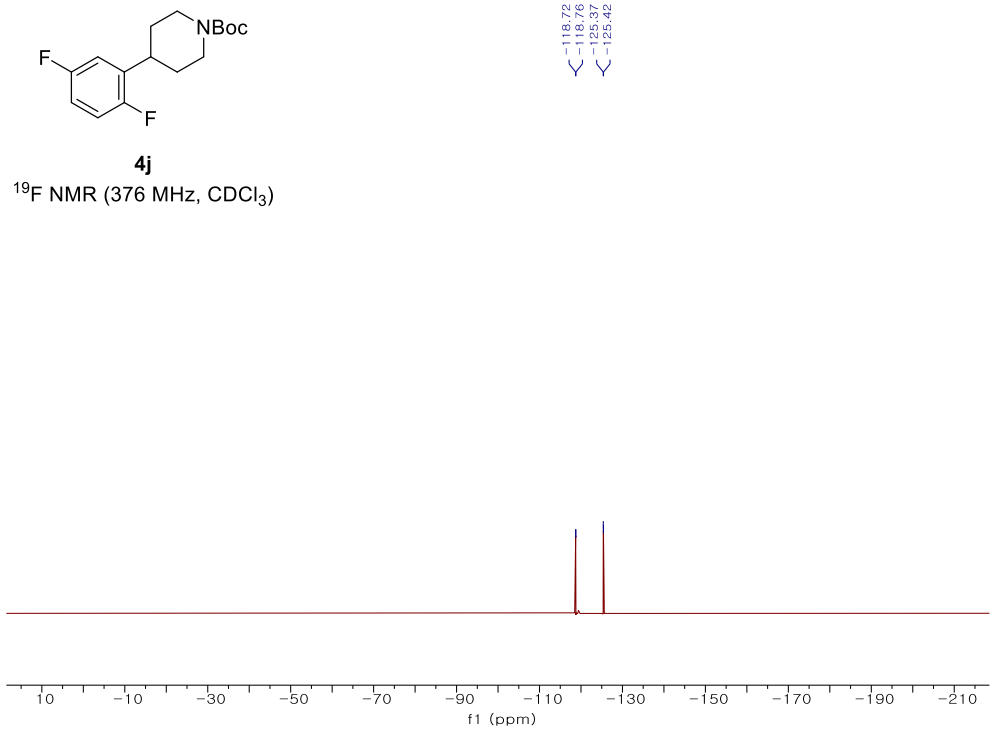

4j

^{19}F NMR (376 MHz, $CDCl_3$)

국문초록

루테늄 촉매의 이동 수소화를 통한 이민 합성 및 팔라듐 촉매를 이용한 비활성 방향족 화합물의 C-H 결합 기능화

본 연구는 전이금속 촉매를 이용한 탄소-질소 및 탄소-탄소 결합 형성 반응 개발에 대한 것이다. 진행된 연구는 결합 형성 반응에 따라 크게 두 부분으로 나누어진다.

첫 부분에서는 알코올 탈수소화 기반 촉매적 이민 합성법에 관한 연구를 소개한다. 이민의 합성적으로 유용하여, 많은 이민 합성법이 개발되었다. 1장에서는 이민 합성 전략과 대표적인 예들을 소개한다. 루테늄-이중하이드라이드 촉매를 이용한 나이트릴과 알코올로부터의 화학선택적 이민 합성법을 개발하였다 (2장). 개발된 반응은 수소-이동화 전략을 적용하여 간단하고, 편리하며, 친환경적인 이민 합성법을 제공한다.

두번째 부분에서는 전이금속 촉매반응을 이용한 탄소-수소 결합 기능화에 관한 연구를 소개한다. 방향족 화합물의 직접적인 탄소-수소 결합 기능화 반응은 유기화학 분야에서 가장 큰 화두이다. 최근 전이금속 촉매반응을 이용한 연구에서는 선택적이고 효율적으로 비활성화된 탄

소-수소 결합을 변환할 수 있다. 3장에서는 탄소-수소 결합 기능화 전략과 탄소-수소 결합 아릴화 및 알킬화 반응을 이용한 탄소-탄소 결합 형성 반응의 대표적인 예들을 소개한다. 4장에서는 빛에 의한 팔라듐 촉매반응 연구와 이의 메커니즘 관점이 논의되었다. 광활성화된 Pd(0)의 독특한 촉매적 특성을 통하여 새로운 탄소-탄소 결합 형성 반응이 개발되었다. 5장에서는 팔라듐 촉매를 이용한 간단한 방향족 화합물의 탄소-수소 결합 아릴화 반응에서 선택성과 메커니즘 연구에 대해 다룬다. 반응속도 측정과 당량 실험을 포함한 종합적인 메커니즘 연구 수행을 기반으로 협동적 이금속 메커니즘을 구체적으로 제안하였다. 개발된 반응에서는 탄소-수소 결합 활성화 단계가 아닌 금속교환 단계가 선택성-결정 단계로 규명되었다. 마지막으로, 6장에서는 빛에 의한 팔라듐 촉매반응을 이용한 간단한 방향족 화합물과 알킬브롬으로부터 촉매적 탄소-수소 결합 알킬화 반응 개발에 대해 소개한다. 메커니즘 연구를 통하여 브롬 원자 이동을 매개로한 Pd(0)/Pd(I) 산화환원 촉매 반응 과정을 규명하였다. 알킬 할라이드 간의 다른 반응성은 포메이트 염기 의한 영향성으로 나타난다. 이는 비활성화된 $Pd(PPh_3)_2Br_2$ 촉매를 활성화된 Pd(0) 촉매종으로 환원하는 역할을 수행한다.

주요어 : 이민 합성, 알코올 활성화, 이동 수소화, C-H 아릴화, 메탈화-탈양성자화, C-H 알킬화, 팔라듐 광화학

학 번 : 2015-20372